STATIC, DYNAMIC AND AEROELASTIC BEHAVIOUR OF THIN-WALLED COMPOSITE STRUCTURES WITH APPLICATION TO AIRCRAFT WINGS

by

Jehan Zeb Khan

Thesis submitted for the Degree of Doctor of Philosophy

City University

Department of Mechanical Engineering and Aeronautics

December 1992

CONTAINS DISKETTE

CONTENTS

CONTENTS

CONTENTS

LIST OF TABLES

LIST OF FIGURES

LIST OF FIGURES

LIST OF PHOTOGRAPHS

ACKNOWLEDGEMENTS

I am thankful to God Almighty who has given me the courage and strength to complete my thesis.

I would like to thank the Department of Mechanical Engineering and Aeronautics and Ministry of Science and Technology, Government of Pakistan for giving me the opportunity to carry out the research which is reported in this thesis.

I would especially like to thank my supervisors Dr. J.R. Banerjee and Mr. G.N. Sage for their invaluable help during the course of this project.

I would also like to thank the technical staff in the Department for their kind co-operation in preparing various jigs and conducting wind tunnel tests.

I would also like to thank Dr. R. Harrison for his invaluable help in doing modal analysis and providing me with necessary hardware and computer software.

I would also like to thank my dear family and colleagues in supporting me at all times.

DECLARATION

I hereby grant powers of discretion to the University Librarian to allow this thesis to be copied in whole or in part without further reference to me. This permission covers only single copies made for study purposes, subject to normal conditions of acknowledgement.

ABSTRACT

Theoretical and experimental investigations of the static and dynamic behaviour of thin-walled structures are carried out with the ultimate aim of improving prediction procedures for various aeroelastic phenomena. The dynamic stiffness matrix approach is used for structural idealization, while strip theory and Theodorsen's function C(k) are used for the aerodynamic idealization.

The dynamic stiffness matrix for a thin-walled composite beam with geometric and material coupling together with an axial load (compressive or tensile) applied at the centroid, has been developed. An exact analysis was then carried out using the derived dynamic stiffness matrix. Special cases, that are derivatives of the general case have been identified and discussed.

A three stage program was developed to compute various static and dynamic properties of thin-walled closed or open section composite beams. In the first stage, equivalent elastic constants (overall laminate moduli) were evaluated for a given stacking sequence and material properties. In the second stage, various sectional properties were computed. When the outputs from these two stages were combined, valuable data on sectional rigidities, mass per unit length, polar mass moment of inertia, and shear centre location from the centroid were obtained. In the third stage of the program, all these properties were used to compute the natural frequencies and normal mode shapes of thin-walled composite structures. These programs can be used individually as well as in a combined manner.

An experimental investigation of composite thin plates with varying degrees of bending-torsion coupling was conducted. Flexural and torsional rigidities, natural frequencies, normal mode shapes and flutter speed and frequency were experimentally determined. The results obtained were in close agreement with the theoretical predictions.

Various open composite sections were experimentally studied for their static and dynamic properties. The results demanded a more refined investigation of the theory. In addition to the experimental study of composite open sections, a parametric study of uncoupled and coupled frequencies of such sections with common boundary conditions was also conducted.

Thin-walled closed aerofoil shaped cantilevered

structures were tested to establish flexural and torsional rigidities, shear centre, and the polar-mass-moment of inertia. Natural frequencies and normal mode shapes were also determined. The aeroelastic behaviour of these sections was investigated to establish divergence and flutter characteristics.

Comparisons of the experimental results with theoretical predictions of flutter speed and frequency were in general satisfactory and the results provided an insight into the aeroelastic behaviour of thin-walled composite beams. The results are discussed and commented on.

NOTATIONS

A	Area
A_{ij}	Extensional stiffness
a_o	Lift-curve slope value
B_{ij}	Coupling stiffness
b	Semi-chord length
C(k)	Theodorsen's function
c	(i) Chord length
	(ii) Speed of sound
	(iii) Distance from root to the application of load
c_l	Coefficient of lift
c_m	Coefficient of pitching moment
c_β	Control surface chord
D_{ij}	Bending stiffness
E	(i) Young's modulus of elasticity
	(ii) Elastic forces (Structural)
E_1, E_2	Young's modulus of elasticity in the fibre and transverse directions
E_x, E_y, G_{xy}	Equivalent elastic constants
EI	Bending/flexural rigidity
EI_o	Bending rigidity near the root
e	Distance between the centroid and shear centre
G	Shear modulus of rigidity
G_{12}	Shear modulus of rigidity in the 12 - plane
GJ	Torsional rigidity
h	Vertical deflection (heave motion)
I	Inertial forces
I_r	Reference moment of inertia
K	(i) Küssner kernel function
	(ii) Bending/torsion coupled rigidity
K_x, K_y, K_{xy}	Curvatures corresponding to moments M_x, M_y and M_{xy}
K_h	Stiffness of the support in bending
L	(i) Lift force

	(ii) Lagrangian
ℓ	Length (span)
M	Pitching moment
m	Mass per unit length
M_x, M_y	Bending moments per unit length
M_{xy}	Twisting moment per unit length
N_x, N_y	Normal forces per unit length in x and y directions
N_{xy}	shear force per unit length in xy plane
P	Axial force
p	Load
Q_i	Generalised forces corresponding to externally applied forces
q	Shear flow
q_b	Basic shear flow
q_i	Generalized coordinates
r	Radius of gyration
S	(i) Area of the lifting surface
	(ii) Shear force
s	Span of the lifting surface (wing)
T	Total kinetic energy of the system
t	(i) Time
	(ii) Thickness
U	Speed of the flow
u	Speed of air over the moving aerofoil
V	Potential or elastic strain energy of the system
w	Down-wash
u,v,w	Displacement components in x, y, z directions
x_α, ξ_E	Distance of shear centre from the centroid

GREEK SYMBOLS

α	(i) Torsional deformation (pitching motion)
	(ii) Angle of attack of the aerofoil to the flow of air
β	Angle of attack of the control surface
δ	Length of side walls in a multi-cell section
Φ	Wagner's function
ϕ_{xi}, ϕ_{yi}, ϕ_{zi}	Generalized displacements
ϕ_h , ϕ_α	Generalized displacements of h and α
$\varepsilon_x, \varepsilon_y, \varepsilon_z$	Normal strains in x, y, and z directions
ξ_E	Shear centre location from a reference point
$\gamma_{xy}, \gamma_{yz}, \gamma_{xz}$	Shear strains in xy, yz, and xz planes
λ	Lame's constant
μ	Viscosity of the fluid
ν	Poisson's ratio
ρ	Density (air, composite material, etc.)
σ	Stress
θ	(i) Ply orientation angle
	(ii) Angle of twist
ω	(i) Frequency of oscillation
ω	(ii) Eigen value
ω_β	Control Surface Frequency
τ	Non-dimensional time

MATRICES

[A]	Aerodynamic matrix
[F]	Force matrix
[K]	Generalized stiffness matrix
{K}	Bending and twisting curvatures
$[K_f]$	Dynamic stiffness matrix
{M}	Bending and twisting moments
[M]	Generalized mass matrix
{N}	Inplane forces
{q}	Modal coordinates (column matrix)
[QF]	Generalized aerodynamic matrix
[QA]	Flutter matrix

GENERAL INTRODUCTION

Historical Background

In the early days, aeroplanes were designed by making use of materials that usually provide a rigid structure, but as the need for lighter weight and higher performance increased, composite materials were introduced. The usual design procedures have changed with these new materials yielding lighter and stronger structures. However, this has led to flexible structures which are more susceptible to aeroelastic problems, so that in modern aircraft design procedures, aeroelastic constraints play a vital role.

Flutter, an aeroelastic phenomenon in which the external source of energy is the air stream, was known to aircraft engineers as early as 1916. It is not necessary for aircraft to be accelerated intentionally beyond the flutter free air speed in order to experience flutter. For example an excessive air speed may result when a phugoid is experienced or an unwanted dive is made. A slight disturbance at this stage may set up dangerously diverging vibrations, often called self-excited oscillations or flutter, causing failure of the structure. Thus investigation of flutter has become a serious factor in the design process.

In the early days, problems relating to flutter were overcome by means of mass balancing of the structure. The design of aircraft structures using conventional isotropic materials has been securely based on vast experimental experience, and further does not require anything but straightforward theories such as the Engineer's bending theory, St. Venant theory or Bredt-Batho's theory. All design practice for low/medium speed aircraft has been based on such ideas. For various reasons, such as high specific strength and stiffness, the prospect of high

fatigue life and low maintenance cost, composite materials were first introduced in 70's in primary structures, particularly in helicopter blades where these properties were exploited. Initially fibre reinforced composite materials were introduced to simulate the behaviour of isotropic ones, so the analysis of early fibre reinforced composite structures was straightforward. Then the possibility of using the fibre reinforced composite materials in a more adventurous way brought a need for a new mechanics.

Nowadays, new materials, particularly fibre reinforced composites, have given new dimensions to the flutter control problem. Due to the directional properties of fibre reinforced materials, the capability of achieving an improved design has been enhanced tremendously, and this whole exercise has been named as **AEROELASTIC TAILORING**. Lifting surfaces of an aircraft are prime subjects of this relatively new field, particularly when aspect ratios are high and the structure is comparatively more flexible. Several types of aeroelastic problems, both static and dynamic when coupled with composite materials such as fibre reinforced composites, make this an extremely fertile field for research.

Various approximate and analytical techniques have been developed in this work for predicting aeroelastic behaviour of an aircraft. To maintain accurate predictions it is necessary to increase the complexity of the mathematical modelling of the structure. The work has been carried out in particular in the context of composite materials.

The introduction of composite materials in the manufacture of lifting surfaces has renewed interest in thin-walled structures. These structures not only perform the job of retaining the profile but also act as main

bending and torsional members compared to wing-box structures with ribs often used in wings made of conventional materials. The unsymmetrical geometry of the cross section introduces the problem of elastic coupling due to non-coaxial elastic and centroidal axes. The complexity of the structure is enhanced by the material bending-torsion and extension/torsional coupling due to symmetric and anti-symmetric laminate stacking sequence. The novelty and little known behaviour of these structures made them very attractive candidates for research.

Aims and Objectives

Because we lack authority in the design of lighter thin-walled fibre composite structures compared with that which underpins the design of light alloy ones, the primary aim of the work reported here is to secure a comparable design base. This has been attempted by means of a series of technical tasks which are listed below. Each of these tasks has been confirmed by appropriate experiments thus consolidating the theory before proceeding to the next tasks.

(i) To assess the reliability of available means of estimating static and dynamic structural properties of composite structures, such as beams, plates, and thin-walled open and closed sections including wing sections.

(ii) To develop a computer program to calculate static structural properties for composite structures.

(iii) To develop an exact solution for free vibration analysis of thin-walled composite sections with

elastic and material bending-torsion coupling with an axial load present using a dynamic stiffness matrix approach.

(iv) To develop a computer program to predict critical buckling loads, natural frequencies and normal mode shapes of composite thin-walled structures with elastic and material bending-torsion coupling and axial load.

(v) To investigate the effect of the bending-torsion coupling stiffness of symmetrically laminated thin-walled structures on the predominantly bending and predominantly torsional natural frequencies and normal mode shapes.

(vi) To develop a computer program to predict flutter speed and frequency of a composite lifting surface with the bending-torsion coupling stiffness.

(vii) To investigate the effect of the bending-torsion coupling stiffness on the flutter speed and frequency of thin-walled composite structures.

(viii) To carry out an experimental investigation into the static, dynamic, and aeroelastic characteristics of composite beam, plate, and thin-walled closed and open section structures including an aircraft wing.

Brief Outlines and Layout of the work

The prediction of aeroelastic properties depends upon static and dynamic characteristics of the structure.

Therefore, the investigation was split into three main stages namely, static, dynamic, and aeroelastic. Each stage had two major aspects to be investigated: one theoretical and one experimental. An initial update of the present status of each stage of investigation was a common exercise that was strictly followed throughout the reported work. It was noticed that each stage proved to be an important research exercise in itself.

The experimental investigation started with the establishment of the material properties. An initial parametric study with these material properties helped in making a choice of the feasible geometrical details of various structures to be investigated. Various computer programs were developed which helped in conducting these initial studies.

The test techniques were validated by conducting similar tests on structures made of conventional (isotropic) materials, prior to any test on composite structures. This practice helped in isolating the errors caused by the test setup, etc.

In order to obtain reliable estimates of the structural static properties such as rigidities, etc., a summary of the available work was prepared. A programme of experimental investigation of static structural properties of various different types of structure was conducted. The results were compared with the theoretical predictions and the reliability of available means of estimating static structural properties was evaluated.

In the second stage of investigation, an exact solution for vibration analysis was obtained for thin-walled composite sections with both elastic and material coupling present. The evaluated dynamic stiffness matrix is used to analyse the structure statically and estimate its critical buckling load. It is also used in

dynamic analysis to investigate the natural frequencies and mode shapes of the structure. In other degenerated cases such as with material coupling only, explicit equations were obtained. The advantage of these explicit equations over the numerical methods is appreciated due to a large saving in computer time.

The composite structures already tested for their static structural properties in the first stage were further tested to establish their natural frequencies and mode shapes. Experimental results were compared with the theoretical predictions to assess the reliability of the theoretical model selected.

In the final stage of experimental investigations, structures such as plates and thin-walled closed sections with aerodynamic profiles were tested in the wind tunnel to study their sub-critical and critical flutter behaviour. Experimental results were compared with computer program predictions for flutter speed and frequency.

Each chapter of the thesis is self-contained and can be treated individually. After giving a brief introduction to the chapter contents, a historical review of the subject is presented. This is followed by the theoretical background. In reporting the experimental results validation of the test technique is first discussed, and then the tests performed on composite structures are described. The test results are corroborated by discussion of results and conclusions.

CHAPTER 1

AEROELASTICITY

1.1 INTRODUCTION

The design of aircraft often aims at lighter components, resulting in flexible structures prone to distortion due to loads. Aerodynamic loads are essentially due to the geometry of the lifting surface structures. If somehow these loads cause deformations in the structure and vary the geometry, they will give rise to totally different aerodynamic loads. These loads will produce further distortions in the shape of the lifting surface and so on. This interaction between aerodynamic, elastic and inertia forces is classified as the subject of **AEROELASTICITY.**

Although the aircraft on many occasions is idealised to be rigid, its structural flexibility is fundamentally responsible for a variety of complicated aeroelastic phenomena. Aeroelastic effects are due to the mutual interaction of inertial, elastic (structural), and aerodynamic forces induced by static or dynamic disturbing forces. In the absence of external disturbing forces, one has to deal with aeroelastic stability problems, the most serious of which is the dynamic instability known as flutter. Aeroelastic phenomena are often restricted to the physical lifting surfaces of an aircraft, such as wings, stabilizers, controls, etc., because their mutual coupling via the relatively heavy and stiff fuselage may be comparatively small.

The various aeroelastic phenomena can be classified by means of Collar's [1] well known triangle of forces, shown in Figure (1.1). Three types of force, namely (i) aerodynamic, (ii) elastic, and (iii) inertial are placed at the vertices of a triangle. Then every aeroelastic

phenomenon can be located according to its relation to the three vertices. Static aeroelastic phenomena due to interaction of aerodynamic and elastic forces (such as lifting surface divergence or control surface efficiency) lie outside the triangle on the upper left side, whereas dynamic aeroelastic phenomena (such as flutter, dynamic response and buffeting) lie within the triangle, since they involve all three kinds of force. The interaction of elastic and inertial forces give rise to mechanical vibrations, being important for the analytical treatment of dynamic aeroelastic problems, whereas the interaction between aerodynamic and inertial forces will introduce rigid body dynamics.

Static aeroelastic phenomena are associated with static structural deformations and steady-flow aerodynamic forces which are easy to predict by conventional steady-flow aerodynamics. However, the prediction of unsteady aerodynamic inputs for problems in high-frequency aircraft dynamics makes it complicated.

1.2 FLUTTER

Flutter is a closed loop structural vibration problem. Aeroelastic flutter is a self-excited type of vibration, where in a linear system the motion-induced unsteady air loads give rise to oscillatory amplitudes of increasing magnitude, as shown in Figure (1.2). Flutter is different from forced or resonant oscillations since the flutter occurs in the absence of any periodic external excitation. A lifting surface in flutter acts as an air-engine which extracts energy from the air. Therefore, flutter may be defined as an oscillatory instability occurring in an aircraft in flight, where the structural flexibility plays an important role in the instability.

1.3 A BRIEF HISTORY OF FLUTTER

The history of flutter can be dated back to the early days of flight. The Wright Brothers in their historical flight made beneficial use of aeroelastic effects for roll control of their biplane by the use of wing warping in place of ailerons. They were also aware of the adverse aeroelastic effects of the loss of thrust of a propeller, due to twisting of the blades, by their experiments on the performance of thin propellers having broad blades. They noticed that the propeller tip under heavy thrust loads twisted to partially unload by itself [z].

On December 8, 1903, Prof. Samuel P. Langley failed for the second time, in an attempted launch of his powered flying machine. The collapse of the rear wing and tail seems to be a less certain cause of failure. Hill [a] suggested that insufficient wing-tip stiffness could have been resulted in wing torsional divergence i.e. aeroelasticity might have played an important role in it. Collar in his survey papers [4,5] and Garrick and Reed [6] shared the same view with Hill's investigations.

While investigating violent antisymmetrical torsional oscillations in the Handley-Page 0/400 biplane bomber during World War I, Lanchester distinguished between flutter and resonance and suggested an increase in torsional stiffness as a remedy. A similar solution was suggested for the tail flutter experienced by the de Havilland DH-9 aircraft. Bairstow, and Fage [7] provided the analytical background for Lanchester's investigations.

Bryan [a] derived dynamic equations of motion for the stability of rigid-body aircraft using small disturbance method. The aerodynamic derivatives by Bairstow and Fage [7] were termed aerodynamic coefficients of stability. The determinant of these coefficients gives a quartic polynomial for the determination of roots (i.e. eigenvalues

and eigenvectors) and predicts the stability of the system using Routh's criteria [9].

In 1922, Baumhauer and Koning [10] introduced the technique of mass balance of the control surfaces to uncouple dynamic interaction between modes. This approach was adopted by Fokker [11] in trouble shooting of mono-plane D-VIII and in the initial study conducted by Blasius [11] on the Albatross which was followed by a detailed analysis of Reissner in 1926 [12].

The technical word of FLUTTER was first introduced in the 1924-25 year book of British Aeronautical Research Committee (ARC). In 1925, the ARC Accident Investigation Subcommittee reported five incidences of flutter with similar reports from Holland and the U.S.A. [13]. In 1936, more than fifty cases of wing, rudder and elevator flutter were reported.

The development of nonstationary aerofoil theory led to the progress of flutter analysis. In 1922, Birnbaum extended Ackerman's concept to nonstationary aerofoils on Prandtl's suggestions [14,15] to obtain numerical results for reduced frequency, k, up to 0.12. (Note that $k = \frac{\omega b}{U}$ where ω is the circular frequency of sinusoidal motion, b is an arbitrary reference length and U is the airspeed.) In 1929, Glauert [16,17] obtained results for k = 0.5 using Wagner's method [18] and Küssner [19] used Birnbaum's method to yield results for k = 1.5. Finally, Theodorsen in 1934 [20], published an exact solution of a harmonically oscillating wing for an unlimited value of k.

Frazer and Duncan [21] and Perring [22] used simple and scaled wind tunnel models to study and identify the phenomena of flutter which resulted in design recommendations and indicated the need for measurements of aerodynamic derivatives. These tests also demonstrated the efficacy of the aeroelastically scaled models for

prediction of critical flutter speed of a full scale prototype. The scaling laws for dynamic similarity between a model and a full-scale were developed by Wood and Lamb [23] in 1927.

Similar to British progress in aeroelasticity, Zham and Bear [24], Newell, Younger and Greene [25] in the United States, analysed flutter by attributing the phenomenon to the wake of the main wing and suggested an increase in torsional rigidity and moving the mass centre forward. Wind tunnel flutter tests were carried out by Rauscher, Grady and MeVay [26].

Duncan and Collar [27] extended Glauert's theory to cater for wing translation and rotation obtaining results through numerical integration. Theodorsen gave a theory [20] for the two dimensional oscillating flat plate undergoing translation, rotation and aileron motions. The total lift developed was divided into circulatory and non-circulatory parts of the velocity potential. The trailing edge flow condition provided a relation between the two parts. The solution leads to a combination of Bessel (or Hankel) functions designated by C(k), commonly known as Theodorsen's (circulation) function, where k is the reduced frequency. Silverstein and Joyner [28] experimentally confirmed the oscillating lift of an aerofoil in pitching motion. In the case of flutter stability, Theodorsen took a different course of action by defining eigenvalues to be complex quantities for a sinusoidal aerodynamics. For the flutter condition, both real and imaginary parts should vanish simultaneously.

Parametric studies of flutter calculations were conducted by Theodorsen and Garrick [29] which provided a valuable insight in their individual behaviour.

Burgers [30] applied Birnbaum's theory to calculate the horizontal forces on a flapping wing and developed the

theory of the propulsive forces on a flat plate aerofoil including the effect of the suction force at the sharp leading edge. Garrick extended the analysis to include aileron motion [31] using the concept of aerodynamic energy as described in relation to Duncan's "flutter engine" [32].

Garrick [33] found an analogy between oscillatory and indicial aerodynamics. In the case of a simple flat plate, the Fourier integral or Laplace transform establishes the relation between the indicial lift function of Wagner $K_1(s)$ and the frequency response function of Theodorsen C(k). Similarly, Von Kármán and Sears [34] developed the frequency response function known as Sear's gust function from the indicial lift function of Küssner [35].

Walker and Farren [36] found that the lift coefficient was greater than the usual maximum value for a static case, leading to a complex nonlinear hysteresis effect for an oscillating aerofoil, being a function of Reynold's number. This will occur in stall flutter and also in the case of high angle of attack buffeting.

In 1933 Roxbee Cox [37] gave an empirical formula for flutter calculations based on wing torsional stiffness and Küssner [35] in 1935 developed a similar expression based on reduced torsional frequency. Both attempts showed that the German approach of Küssner [35] and Theodorsen [20] considered flutter as a sinusoidal motion expressed in terms of natural frequency. In contrast, the British approach along Bryan's stability theory [8] and Routh's discriminants [9] was based on stiffness, inertia, and damping coefficients which ignored a direct relationship between natural vibration modes and flutter.

In 1935, Von Schlippe in Germany used the inflight resonance technique [38], to substitute actually flying the aircraft to critical flutter speed. Flutter speed would be an asymptote to the curve obtained by plotting resonant

damping against air speed. The estimated flutter speed can thus be deduced from the pre-critical flutter speed observations. However, Frazer and Jones [39] cautioned that the damping may suddenly diminish for very small changes of air speed. This technique was in service successfully until 1938 when a Junkers JU90 fluttered unexpectedly during the flight test and crashed.

Bratt, Wight and Tilley [40] applied an electrical technique to measure the aerodynamic damping for pitching oscillations using a Wattmeter harmonic analyser. The electronic Wattmeter analysed the rectified and modulated output from the stress indicator and measured the damping coefficient directly. The Vector Method of vibration measurement developed by Kennedy and Pancu [41] along with the Wattmeter analyser played an important role in aircraft ground and flight resonance testing.

Survey papers, NASA SP-285 and 415, published in 1975 give an account of the contributions made by ground based and inflight digital computers, real time analysis and a variety of excitation methods (steady-state, transient, pulsed, and random) to make the tests possible and safe.

Wasserman and Mykytow [42] used polyvinyl-chloride wind tunnel models to match the all metal and fast aeroplane characteristics. Other examples are the 1/4-scale model of a PBM-1 seaplane tested in the NACA Propeller Research Tunnel by Nagel, Bergen, Miller and Hartman in 1938 and the Vultee XP-54 tested in 1942, resulting in elevator flutter and in 1944, a complete aeroelastic model of a Junkers JU-288, tested in Germany. The designs of B-47 and B-52 jet transports benefited from such model studies.

In 1946 a special 4-ft wind tunnel was designed to provide flutter test research facility by running it at high subsonic Mach numbers, i.e. up to 0.8, at the Langley Laboratory in the United States of America. The tunnel test

medium can be air or a high density fluid such as Freon to achieve a considerably lower speed of sound (the density of Freon being four times than that of air, the speed of sound can thus be reduced to half when compared to its value in air). Later it was changed into a 2-ft slotted throat continuous flow transonic tunnel. Another 26-inch transonic blowdown tunnel was particularly useful in testing small wing and tail flutter test models.

Flutter tests in the transonic region were conducted by means of dropping models from a high flying aircraft, ground-launched rocket propelled models, models mounted on aeroplane wings flying in a uniform transonic flow region, models and full-scale components mounted on rocket sleds capable of accelerating to transonic speeds.

In 1938, Possio in Italy [43] applied the concept of acceleration potential introduced by Prandtl [44] to the two-dimensional nonstationary problem. The solution of Possio's integral equation measured the loading over a flat plate aerofoil for a known displacement i.e. for a given downwash. He also gave a numerical procedure to the problem in a supersonic mainstream [45].

Lifting-line theory was developed by Cicala (1937) [46], Jones (1940) [47], Küssner (1943) [48] and Reissner (1944) [49] by generalizing Prandtl's integral equation [44] (of induced drag and spanload distribution) for unsteady flows. The lifting-line and multiple lifting-line methods played a vital role until computational methods for lifting-surface theory were developed by Jones [50] with indicial aerodynamic aspects. A substitute expression for the Wagner function was given which was useful in applications to transfer functions.

Küssner [51], provided the basis for a general lifting surface theory for finite wings, making use of Prandtl's acceleration potential and the effect of a uniform moving

doublet. The unknown aerodynamic load distribution is related to the downwash by means of Küssner's kernel function K. In two dimensions, the integral reduces to the kernel of Possio's equation. In 1954, a general explicit expression for K was developed by Watkins, Runyan and Wollston [52].

Numerical lifting surface methods, initially developed by Falkner [53] using the velocity potential were extended to oscillating flows by Jones [54] and Morino [55].

By World War II, the need for faster, all metal aeroplanes with a variety of performance requirements introduced new kinds of aeroelastic problems such as the tip-tank flutter and aileron buzz experienced in the case of P-80 aeroplane [56], transonic flutter of thin wings of high speed aircraft, panel flutter at supersonic speeds and unique problems arising from battle-field damage, etc.

A survey of flutter incidents during 1945-55 [57] showed a total figure of 54 alone on US military aircraft which included transonic control-surface buzz and wing flutter. A fighter aeroplane was lost in a test flight in the 1950's due to flutter of a hydraulic line. In another incident panel flutter caused serious cockpit noise. In the 1960's panel flutter on the Saturn V Apollo launch vehicle ended in a costly investigation of the vehicle [57].

In 1941, Loring [58] outlined a general approach to flutter analysis making use of the examples given by Frazer, Duncan and Collar in their book on matrices [59].

Smilg and Wasserman [60] in 1942 prepared comprehensive tables for unsteady aerodynamic coefficients based on Theodorsen theory and made an addition to the work of Küssner and Schwarz (1940) on control-surface aerodynamic balance. The procedure, commonly known as V-g method, adopted for flutter computation was based on structural damping involving the parameter g (damping

factor). The modal damping coefficient is plotted against the air speed. The flutter condition is achieved when one of the modal damping coefficients vanishes.

Lappert [61], Bell [62], Winson [63] and Baird [64] introduced computers in flutter analysis in the fifties. MacNeal, McCann and Wilts [65], developed a flutter analysis technique on an analogue computer. Others used multi-degree of freedom flutter simulators and electrical analogies for flow solutions.

A survey of aeroelasticity with reference to flutter shows that from 1936 to the late sixties ground vibration tests were used to measure the natural frequencies and normal mode shapes of the structure [66-69]. A very simple two dimensional unsteady aerodynamic theory was used to predict the flutter speed [70,10]. The notable contributions made during that period were due to Loring [71] and Barton [72]. Loring's work was based on generalized coordinates whereas Barton relied on a coefficient method. Sherman, Dipola and Frissel [73] used a simplified version of the Routh-Hurwitz discriminant and Ruggiero [74] made a comparative investigation of various methods. These earlier works eventually led to the application of IBM machines to the solution of the flutter determinant for example, see Leppert [61].

A significant contribution to computer aeroelastic analysis programmes was the development of NASTRAN [75]. The structural idealization used in NASTRAN is based on the finite element method and the program uses the vortex lattice theory in the aerodynamic idealization.

The capacity of the finite element method is indisputable but its huge memory size requirement and high cost have attracted other means of solving structural engineering problems. The development of thin-walled structure theory has been a great step in this direction.

CALFUN, a program for CAlculation of Flutter speed Using Normal modes has been developed by Banerjee [76,77] and is based on Loring's work [71]. The program can run even on a PC which clearly shows its advantage over its rival software in the market such as NASTRAN, etc. However, this does not make the well established packages like NASTRAN (which has detailed modelling capability) redundant. In the usual design procedure there are many phases and at the initial stage it is advisable to avoid costly programs like NASTRAN. However, it is ideal to analyse an aircraft wing using a relatively cheaper but sufficiently accurate computer program in the early stages of the design. The analysis can then be refined by repeating the exercise on an established finite element package.

The introduction of composites, super critical wings, and active control techniques are the challenges that aeroelasticity has to face today. The last twenty years have been remarkable for the advent of finite element calculations and, more recently, for the development of optimization methods and proposals for new ground vibration test techniques. Composite materials are opening several new possibilities, but are raising difficult problems that are still under investigation.

Progress in the field of aeroelasticity with special reference to flutter analysis can be divided into two branches. Firstly, optimised structures are designed using already known analysis procedures and composite materials to improve the performance of the aircraft by passively controlling deformation in aerodynamically loaded lifting surfaces.

Secondly, the analysis techniques are undergoing constant modification such as improved macromechanics for composite materials, structural elements to cater for more degrees of freedom and better aerodynamic codes based on

three-dimensional and unsteady aerodynamics. For example computational fluid dynamics has been recently employed in wing flutter analysis using generalized aerodynamic forces. A transonic small-disturbance computer code called CAP-TSD [78] for flutter prediction has been developed which has the capability of the aeroelastic analysis of a complete aircraft configuration. The program can also predict steady and unsteady aerodynamic pressure distributions.

The notable research work done on the subject of aeroelasticity in the late sixties has been reported by Fung [79], Scanlan and Rosenbaum [80], Bisplinghoff, Ashley and Halfman [87]. A five-volume manual was prepared by the NATO Advisory Group for Aeronautical Research and Development under the editorship of Jones [81]. Other useful books are by Duncan [82] on the treatment of dynamic stability of aeroplanes and by Templeton [83] on the explanation and avoidance of control surface flutter at subsonic speeds. An excellent monograph on the practical engineering aspect was given by Broadbent [84]. Other notable contributors in the field during this period are Abramson [85], Myklestad [86], Freberg and Kemler [87], Von Kármán and Biot [88], and the translation from Russian of Grossman's report [89]. More recent contributions to the subject of the aeroelastic behaviour of lifting surfaces are amongst others by Bisplinghoff and Ashley [90] and Dowell [91].

1.4. FLUTTER ANALYSIS USING GENERALIZED COORDINATES AND NORMAL MODES

A complete flutter analysis using generalized coordinates and various techniques of solving the flutter determinant can be found in references [79,80,90,91]. A brief summary of flutter analysis using generalized coordinates and normal modes will be presented here.

SUMMARY OF THE METHOD:

1. Determination of natural frequencies and normal mode shapes.
2. Selection of modes (normal modes) for flutter analysis.
3. Reduction of mass and stiffness matrices to diagonal form to give generalized mass and stiffness matrices respectively.
4. Expression of the aerodynamic matrix in modal coordinates to give the generalized aerodynamic matrix.
5. Formation of the flutter matrix by algebraically summing generalized mass, stiffness and aerodynamic matrices.
6. Solution of the flutter determinant.

THE AERODYNAMIC MATRIX IN MODAL COORDINATES (ASSUMPTIONS):

(i) Lift and moments are linear functions of h and α.

(ii) Airflow is two dimensional (infinite aspect ratio, the strip theory assumption).

(iii) Aerodynamic coefficients are computed for a flat plate aerofoil at zero mean angle of attack.

TORSION-BENDING AERODYNAMIC FORCES:

The aerodynamic lift and moment of the wing induced by a bending deflection h (positive downward measured at the elastic axis) and a pitching rotation α (positive nose-up) about the elastic axis are given in terms of Theodorsen's function C(k) [20] as follows :

$$\frac{L}{\rho\pi b U^2} = -k^2\left(\frac{h}{b} - a_h\alpha\right) + ik\alpha + 2C(k)\left[\alpha + \frac{ihk}{b} + \left(\frac{1}{2} - a_h\right)ik\alpha\right] \qquad (1.4.1a)$$

$$\frac{M}{\rho\pi b^2 U^2} = \left(\frac{1}{2} + a_h\right)2C(k)\left[\alpha + \frac{ihk}{b} + \left(\frac{1}{2} - a_h\right)ik\alpha\right] - k^2 a_h\left(\frac{h}{b} - a_h\alpha\right) - \left(\frac{1}{2} + a_h\right)ik\alpha + \frac{k^2}{8}\alpha \qquad (1.4.1b)$$

where $k = \frac{\omega b}{U}$ = reduced frequency parameter

L = lift, positive upwards

h = heave, positive downwards

M = moment, positive nose-up

α = angle of attack, positive leading edge up

The lift and moment given above can be expressed in matrix form as follows

$$\begin{Bmatrix} L \\ M \end{Bmatrix} = \begin{bmatrix} A_{11} & A_{12} \\ A_{12} & A_{22} \end{bmatrix} \begin{Bmatrix} h \\ \alpha \end{Bmatrix} \qquad (1.4.2)$$

where

$$A_{11} = \pi\rho U^2 \left[-k^2 + 2C(k)ik\right]$$

$$A_{12} = \pi\rho U^2 b \left[(a_h k^2 + ik) + 2C(k)[1 + ik(\tfrac{1}{2} - a_h)\right]$$

$$A_{21} = \pi\rho U^2 b \left[2C(k)ik(\tfrac{1}{2} + a_h) - k^2 a_h\right]$$

$$A_{22} = \pi\rho U^2 b^2 \left[2C(k)(\tfrac{1}{2} + a_h)\,[1 + ik\,(\tfrac{1}{2} - a_h)] + \frac{k^2}{8} + k^2 a_h^2 - (\tfrac{1}{2} - a_h)ik\right]$$

Assuming only three modes for simplicity, the aerodynamic matrix in terms of generalized coordinates (q_1, q_2, q_3) can be derived as follows:

$$\begin{Bmatrix} h(x,t) \\ \alpha(x,t) \end{Bmatrix} = \begin{bmatrix} h_1(x) & h_2(x) & h_3(x) \\ \alpha_1(x) & \alpha_2(x) & \alpha_3(x) \end{bmatrix} \begin{Bmatrix} q_1(t) \\ q_2(t) \\ q_3(t) \end{Bmatrix} \qquad (1.4.3)$$

or expressed in summation signs

$$\left.\begin{aligned} h(x,t) &= \sum h_i(x)\, q_i(t) \\ \alpha(x,t) &= \sum \alpha_i(t)\, q_i(t) \end{aligned}\right\} \qquad (1.4.4)$$

The generalized aerodynamic forces Q_i corresponding to the generalized coordinates q_i are found by calculating the virtual work done δW by the airforces in varying q_i to $q_i + \delta q_i$

$$\delta W_i = \delta q_i \int_0^{\ell} \left[L(x)h_i(x) + M(x)\alpha_i(x)\right] dx \qquad (1.4.5)$$

In matrix form

$$\begin{bmatrix} \frac{\delta W_1}{\delta q_1} \\ \frac{\delta W_2}{\delta q_2} \\ \frac{\delta W_3}{\delta q_3} \end{bmatrix} = \int_0^{\ell} \begin{bmatrix} h_1 & \alpha_1 \\ h_2 & \alpha_2 \\ h_3 & \alpha_3 \end{bmatrix} \begin{bmatrix} L \\ M \end{bmatrix} dx \qquad (1.4.6)$$

Then substituting expression of $\begin{bmatrix} L \\ M \end{bmatrix}$ from equation (1.4.2)

$$\begin{bmatrix} \frac{\delta W_1}{\delta q_1} \\ \frac{\delta W_2}{\delta q_2} \\ \frac{\delta W_3}{\delta q_3} \end{bmatrix} = \int_0^{\ell} \begin{bmatrix} h_1 & \alpha_1 \\ h_2 & \alpha_2 \\ h_3 & \alpha_3 \end{bmatrix} \begin{bmatrix} A_{11} & A_{12} \\ A_{12} & A_{22} \end{bmatrix} \begin{bmatrix} h \\ \alpha \end{bmatrix} dx$$

$$= \int_0^{\ell} \begin{bmatrix} h_1 & \alpha_1 \\ h_2 & \alpha_2 \\ h_3 & \alpha_3 \end{bmatrix} \begin{bmatrix} A_{11} & A_{12} \\ A_{12} & A_{22} \end{bmatrix} \begin{bmatrix} h_1(x) & h_2(x) & h_3(x) \\ \alpha_1(x) & \alpha_2(x) & \alpha_3(x) \end{bmatrix}$$

$$\begin{Bmatrix} q_1(t) \\ q_2(t) \\ q_3(t) \end{Bmatrix}$$

$$= \begin{bmatrix} QF_{11} & QF_{12} & QF_{13} \\ QF_{21} & QF_{22} & QF_{23} \\ QF_{31} & QF_{32} & QF_{33} \end{bmatrix} \begin{bmatrix} q_1 \\ q_2 \\ q_3 \end{bmatrix} \qquad (1.4.7)$$

where

$$QF_{ij} = \int_0^{\ell} (A_{11} h_i h_j + A_{21} h_j \alpha_i + A_{12} h_i \alpha_j + A_{22} \alpha_i \alpha_j) dx$$

[QF] = generalized aerodynamic matrix

FORMATION AND SOLUTION OF FLUTTER DETERMINANT:

The flutter matrix is formed by summing the generalized mass, stiffness and aerodynamic matrices.

$$[QA] = [-\omega^2 [M] + [K] - [QF]]\{q\} \qquad (1.4.8)$$

where

[QA] = flutter matrix

[M] = generalized mass matrix

= $[\phi]^T[M]\ [\phi]$

[K] = generalized stiffness matrix

= $[\phi]^T[K]\ [\phi]$

[QF] = generalized aerodynamic matrix and is complex

{q} = generalized coordinate vector

$[\phi]^T$ = transpose of $[\phi]$

FLUTTER DETERMINANT:

$$\left|-\omega^2[M] + [K] - [QF]\right| = 0 \qquad (1.4.9)$$

This complex flutter determinant is a function of airspeed and frequency. At the flutter speed both the real and imaginary parts of the determinant, Δ_R and Δ_I respectively, must vanish. In the solution procedure used in this work, first an airspeed was chosen and the real and the imaginary parts of the flutter determinant were calculated for a range of frequency. The process was repeated for a range of airspeeds until both the real and the imaginary parts of the flutter determinant (hence the whole flutter determinant) vanish completely. This method is often referred to as Theodorsen's method [20].

A direct solution procedure for computing the flutter speed and frequency can be applied to the aeroelastic analysis. Reference [02] provides a procedure to calculate the flutter speed and frequency of a finite element structural model and an unsteady aerodynamic model based on three-dimensional subsonic compressible lifting-surface theory. The efficiency of the iterative process of automatic search for the flutter speed and frequency is improved by the use of an approximated Jacobian matrix.

1.5 CONCLUSIONS

This chapter presents a glimpse of the historical development of aeroelasticity and the problems experienced by the early research workers with special reference to aircraft flutter and how these problems were solved by the pioneers of aeroelasticity and their successors. The survey covers a period from the earlier days of flight to the late eighties. During this period, aeroelasticity has made considerable progress in overcoming adverse aeroelastic effects. The attitude that a statically designed aircraft may be considered perfectly safe without going into cumbersome aeroelastic analysis has changed. Now aeroelastic considerations not only influence the performance of an aircraft but also play an important role in the overall design.

The complex and iterative nature of the aeroelastic problems always posed an obstacle to earlier investigators. The introduction of computers and techniques such as finite element analysis methods has drastically reduced computation time and effort. Complicated and large structures can be modelled with a great number of degrees of freedom. Computer software that can handle symbolic computation has even made explicit analysis with a high degree of complexity possible.

The explicit methods now adopted are definitely faster techniques as compared to finite element analysis. In the former approach the cross-sectional properties are presented as a single block of information whereas in the finite element analysis the structure is divided into several elements both chordwise and spanwise. The highly iterative nature of the problem demands the need for explicit methods of computation to save labour and computer time. This is particularly true when high accuracies are required.

The introduction of unconventional materials in the manufacture of modern aeroplanes necessitates considerable investigation into the aeroelastic behaviour of aircraft structures made of these materials. The use of fibrous materials for achieving passive means of overcoming aeroelastic problems is still another fertile area of research. Active control technology in the suppression of flutter and divergence and in load alleviation also poses an important challenge. Other research areas such as helicopter and propeller aeroelasticity, where the basic phenomenon is no longer linear, provide opportunities for further research. The progress in this field depends on the derivation of relatively simple nonlinear models and on the proposal for new algorithms for the calculation of the coupling between flow and structure.

REFERENCES

1. Collar, A.R., "The Expanding Domain of Aeroelasticity," Journal of the Royal Aeronautical Society, Vol. (50), August 1946, pp. 613-636.

2. McFarland, M.W., ed., The Papers of Wilbur and Orville Wright, McGraw-Hill, New York, 1953, p.510 (Kelly, F.C., The Wright Brothers, Ballantine Books, Inc., New York, 1956, p.80).

3. Hill, G.T.R., "Advances in Aircraft Structural Design," Anglo American Aeronautical conference, The Royal Aeronautical Society, Brighton, Sept. 1951.

4. Collar, A.R., "Aeroelasticity-Retrospect and Prospect," The Second Lanchester Memorial Lecture, Journal of the Royal Aeronautical Society, Vol.63, Jan.1959, pp.1-15.

5. Collar, A.R., "The First Fifty Years of Aeroelasticity," Aerospace, Vol.5, (paper No. 545), Feb. 1978, pp. 12-20.

6. Garrick, I.E. and Wilmer H. Reed III, "Historical Development of Aircraft Flutter," Journal of Aircraft, Vol.18, No.11, November 1981, pp. 897-912.

7. Bairstow, L.,and A. Fage, "Oscillations of the Tail Plane and Body of an Aeroplane in Flight. Aeronautical Research Com. R.& M. 276, part ii, July 1916.

8. Bryan, G.H., Stability in Aviation, MacMillan, London, 1911.

9. Routh, E.J., Treatise on Rigid Dynamics, MacMillan, New

York, 1905.

10. Birnbaum, W.: Die tragende Wirbelfläche als Hilfsmittel zur Behandlung des ebenen Problems der Tragflügeltheorie. Z. angew. Math. u. Mech. 3, 290-297, 1923.

11. Blasius, H. : Über Schwingungserscheinungen an Einholmigen Unterflügeln. Z. Flugtech. u. Motorluftschef. 16, 39-42, 1925.

12. Reissner, H., "Neurere Probleme aus der Flugzeugstalik"(New static structural problems of wings), Zeitschrift fuer Flugtechnik und Motorluft schiffahrt, vol.17, April 1926, pp.137-146.

13. Accidents Investigation Subcommittee, "Accidents to Aeroplanes Involving flutter of the wings," R & M 1041, 1925.

14. Birnbaum, W. : Die tragende Wirbelfläche als Hilfsmittel zur Behandlung des ebenen Problems der Tragflügeltheorie. z. angew. Math. u. Mech. 3, 290-297, 1923.

15. Birnbaum, W. : Das ebene Problem des schlagenden Flügels. Z.angew. Math. u. Mech. 4, 277-292, 1924.

16. Glauert, H., "The Accelerated Motion of a Cylindrical Body through a Fluid," Aeronaut. Research Com. R.& M. 1215, 1929.

17. Glauert, H., "The Force and Moment of an Oscillating Aerofoil," Aeronaut. Research Com. R.& M. 1242, 1929.

18. Glauert, H., "The Accelerated Motion of a Cylind rical Body through a Fluid," Aeronaut. Research Com. R.& M. 1215, 1929.

19. Glauert, H., "The Force and Moment of an Oscillating aerofoil," Aeronaut. Research Com. R.& M. 1242, 1929.

20. Küssner, H.G., "Schwingungen von Flugzeugflügeln," Luftfahrt- Forsch, Vol. 4, No. 2, 1929, pp. 41-62.

21. Theodorsen, Th., "General Theory of Aerodynamic Instability and the Mechanism of flutter," NACA Rept. 496, 1934.

22. Frazer, R.A. and Duncan, D.J., "The Flutter of Aeroplane Wings," R & M 1155, 1929.

23. Perring, W.G.A., "Wing Flutter Experiments Upon a Model of a Single Seater Biplane," R & M 1197, 1928.

24. Zahm, A.F. and Bear, R. M., "A Study of Wing Flutter," NACA Rept. 285, 1926.

25. Greene, C.F., "An Introduction to the Problem of Wing Flutter," Transactions of the American Society of Mechanical Engineers, AER-50-10, vol. 49-50, Part I, 1927-28.

26. Rauscher, M., "Uber die Schwingungen freitragen der Flüel (On the Flutter of a Wing), Luftfahrtforschung, Vol. 4, July 1929, pp. 94-106.

27. Accidents Investigation Subcommittee, "Report on Puss Moth Accidents," R & M 1699, 1936.

28. Duncan, W.J. and Collar, A.R., "Calculation of the Resistance Derivatives of Flutter theory," R & M 1500, 1932.

29. Theodorsen, T. and Garrick, I.E., "Mechanism of Flutter - A Theoretical and Experimental Investigation of the Flutter Problem," NACA TR-685, 1940 (issued in 1938 as a memorandum report).

30. Silverstein, A. and Joyner, U.T., "Experimental Verification of the Theory of Oscillating Airfoils," NACA Rept. 673, 1939.

31. Küssner, H.G., "Zusammenfassenden Bericht Über den instationaren Auftrieb von Flügeln" (Comprehensive Report on the Nonstationary Lift of Wings), Luftfahrtforschung, Vol. 13, December 1936, pp. 410-424.

32. Bugers, J.M., Aerodynamic Theory, Vol. II, edited by W.F. Durand, Julius Springer, Berlin, 1934, pp. 380-410, (reprinted 1943).

33. Garrick, I.E., "Propulsion of a Flapping and Oscillating Airfoil," NACA Rept. 567, 1936.

34. Duncan, W.J., "The Fundamentals of Flutter," Aircraft Engineering, parts I and II, January 1945.

35. Garrick, I.E., "On Some Fourier Tranforms in the Theory of Nonstationary Flows," Proceedings of the Fifth International Congress on Applied Mechanics, Cambridge, Mass.,Sept. 1938, pp. 590-593.

36. Von Karman, Th. and Sears, W.R., "Airfoil Theory for

Non-Uniform motion," Journal of the Franklin Institute, Vol. 5, 1938.

37. Walker, P.B., "Growth of Circulation about a Wing and an Apparatus for Measuring Fluid Motion," R. & M. 1402, 1931.

38. Cox, H.R., "A Statistical Method of Investigating the Relations between the Elastic Stiffness of Aeroplane Wings and Wing-Aileron Flutter," Aeronautical Research Com. R. & M. 1505, 1932.

39. Von Schlippe, B., "Zur Frage der selbsterregten Flügelschwingungen," Luftfahrtforschung, Vol. 13, Feb. 1936; also, NACA TM-806, 1936.

40. Frazer, R.A. and Jones, W.P., "Forced Oscillations of Aeroplanes, with Special Reference to Von Schlippe's Method of Predicting Critical Speeds for Flutter," R. & M. 1795, 1937.

41. Frazer, R.A., Duncan, W.J. and Collar, A.R., Elementary Matrices, Cambridge University Press, Cambridge, England, 1938.

42. Loring, S.J., "Outline of General Approach to the Flutter Problem," Society of Automotive Engineering Journal, Aug. 1941, pp. 345-356.

43. Prandtl, L.,"Wing Theory in a Compressible Medium," Luftfahrtforschung, Vol. 13, Oct. 1936, pp. 313-319.

44. Possio, C., "Aerodynamic Forces on an Oscillating Profile in a Compressible Fluid at Subsonic Speeds,"

Aerotecnica, Vol. 18, 1938, pp. 441-458.

45. Possio, C., "Aerodynamic Forces on an Oscillating Profile at Supersonic Speeds," Pontificia Accademia Scientiarum Acta, Vol. 1, No. 14, 1937, pp. 93-106.

46. Cicala, P., "Nonstationary Motion of a Wing of Finite Span," Rendiconti Accademia Nazionale Lincei, Romè, Vol. 25, Ser. 6a, 1937, pp. 97-102.

47. Jones, W. P. and Skan, S.W., "Calculation of Derivatives for Rectangular Wings of finite Span by Cicala's Method," R & M 1920, 1940.

48. Dingel, M. and Küssner, H.G., Contributions to Nonstationary Theory of Wings, Part VIII, "The Oscillating Wing of Large Span," ZWB, FB, 1774, 1943. Air Material Command, USAF Transl. F-TS-935 -RE, 1947.

49. Reissner,E., "On the General Theory of Thin Airfoils for Non-uniform Motion," NACA TN-946, 1944: also TN-1194, 1947.

50. Jones, R.T., "The Unsteady Lift of a Wing of Finite Aspect Ratio," NACA Rept. 681, 1940.

51. Watkins, C.E., Runyan, H.L., and Woolston, D.S., "On the Kernel Function of the Integral Equation Relating the Lift and Downwash Distributions of Oscillating Finite Wings in Subsonic Flow," NACA TN-3131, 1954; also, NACA TR 1234, 1955.

52. Falkner, V.M., "The Calcultion of Aerodynamic Loading on Surfaces of Any Shape," R & M 1910, 1943.

53. Jones, W. P., "Aerodynamic Forces on Wings in Non-uniform Motion," R & M 2117, 1945.

54. Morino, L.,"A General Theory of Unsteady Compressible Potential Aerodynamics," NASA CR-2464, Dec. 1974.

55. Smilg, B. and Wesserman, L.S., "Application of Three Dimensional Flutter Theory of Aircraft Structures," Air Corps Technical Rept. 4798, 1942.

56. Bratt, J.B., Wight, K.C., and Tilly, V.J., "The Application of the 'Wattmeter' Harmonic Analyser to the Measurement of Aerodynamic Damping for Pitching Oscillations," R. & M. 2063, 1942.

57. Kennedy, C.C. and Pancu, C.D.P., "Use of Vectors in Vibration Measurement and Analysis," Journal of The Aeronautical Sciences, Vol. 14, November 1947, pp. 603-625.

58. Wasserman, L.S. and Mykytow, W.S., "Model Construction," AGARD Mannual on Aeroelasticity, Vol. 4, Chap. 7, 1961.

59. Erickson, A.L. and Stephenson, J.D., "Transonic Flutter of Control Surfaces," NACA RM No. AT F 30, 1947.

60. Lighthill, M.J., "Oscillating Airfoils at High Mach Number," Journal of the Aeronautical Sci., Vol. 20, June 1953, pp. 402-406.

61. NACA Subcommittee on Vibration and Flutter, "A Survey and Evaluation of Flutter Research and Engineering," NACA RM-56112, 1956.

62. Leppert, E.L.Jr., "An Introduction of IBM Machines to the Solution of the Flutter Determinant," Journal of Aeronautical Sci., March 1947, pp. 171-174.

63. Bell, Wm.D., "A Simplified Punch Card Approach to the Solution of the Flutter Determinant," Journal of Aeronautical Sci., February 1948.

64. Winson, J., "The Solution of Aeroelastic Problems by Electronic Analog Computation," Journal of Aeronautical Sci., July 1950.

65. Baird, E.F. and Kelley, H.J., "Formulation of the Flutter Problem for Solution on an Electronic Analog Computer," Reader's Forum, Journal of Aeronautical Sci., Vol. 17, March 1950.

66. MacNeal, R.H., McCann, G.D., and Wilts, C.H., Reader's Forum, Journal of Aeronautical Sci., January 1951, p.71.

67. Turner, M.J., Clough, R.W., Martin, H.C., and Topp, L.J., "Stiffness and Deflection Analysis of Complex Structures," Journal of the Aeronautical Sciences, Vol. 23, September 1956, p. 805.

68. Bisplinghoff, B.L., Ashley, H., and Halfman, R.L., Aeroelasticity, Addison-Wesley, Cambridge, 1955.

69. Williams, D., "Recent Developments in the Structural Approach to Aeroelastic Problems," Journal of the Royal Aeronautical Society, Vol. 58, June 1954, pp. 403-428.

70. De Vries, G., "Determination Experimentale des masses généralisées," La Recherche Aéronautique No. 60, 1957.

71. Küssner, H.G., "Augenblicklicher Eutwicklungstand der Frage des Flügel-flatterns," Luftfahrt forschung, Vol. 12, 1935.

72. Loaring, S.J., "Use of Generalised Co-ordinates in Flutter Analysis," SAE Journal (Transaction) Vol. 52, April 1944, pp. 113-132.

73. Barton, M.V., "Coefficient Method for Solving the Flutter Frequency Equation," Journal of the Aeronautical Sciences, April 1945, pp. 164-168.

74. Many Authors, Manual on Aeroelasticity, published in five parts by NATO Advisory Group for Aeronautical Research and Development, 1959.

75. Sherman, S., Dipaola, J., and Frissel, H.F., "The Simplification of Flutter Calculations by Use of an Extended Form of the Routh-Hurwitz Discriminant," Journal of the Aeronautical Sciences, October 1945, pp. 385-392.

76. Ruggiero, R.J., "Investigation of Three Methods for Solving the Flutter Equations and their Relative Merits," Journal of the Aeronautical Sciences, Vol. 13, No. 1, January 1946, pp. 3-22.

77. Tischler, V.A. and Venkayya, V.B., "Sensitivity Analysis and Optimization Issues in NASTRAN," 19th NASTRAN User's Colloquium, Vol. 3111, Chapter 13, 1991.

78. Banerjee, J.R., "User's Guide to the Computer Program-CALFUN (CALculation of Flutter Speed Using Normal Modes)", Unpublished Report.

79. Banerjee, J.R., "Use and Capability of CALFUN : A Program for CALculation of Flutter Speed Using Normal modes," Proceedings Int. AMSE Conf. "Modelling and Simulation", Athens, June 27-29, 1984, Vol. 3.1, pp. 121-131.

80. Fung, Y.C., An Introduction to the Theory of Aeroelasticity, John Wiley and Sons, New York, 1955.

81. Scanlan, R.H. and Rosenbaum, R., Introduction to the Study of Aircraft Vibration and Flutter, The Macmillan Company, New York, 1951.

82. Duncan, W.J., Control and Stability of Aircraft, Cambridge University Press, Cambridge, 1952.

83. Templeton, H., Mass Balanceing of Aircraft Control Surfaces, Chapman and Hall Ltd., London, 1954.

84. Broadbent, E.G., The Elementary Theory of Aeroelasticity, "Aircraft Engineering" Monograph, Bunhill Publications Ltd., London, 1954.

85. Abramson, H.N., An Introduction to the Dynamics of Airplanes, The Ronald Press Company, New York, 1958.

86. Myklestad, N.O., Vibration Analysis, McGraw-Hill Book Company, New York, 1944.

87. Freberg, C.R. and Kemler, E.N., Aircraft Vibration and Flutter, John Wiley and Sons, New York, 1944.

88. von Kármán, T. and Biot, M.A., Mathematical Methods in Engineering, McGraw-Hill Book Company, New York, 1940.

89. Küssner, H.G., "General Airfoil Theory," Luftfahrtforschung, Vol. 17, 1940, pp. 470-478; also, NACA TM-979, Dec. 1941.

90. Grossman, E.P., Flutter, Joukowsky Mem. Central Aero-Hydrodynamic Institute Report 186, 1935, translated as Air Force Translation F-TS-1225-1A(GDAM-A9-T-44).

91. Bisplinghoff, R.L. and Ashley, H., Principles of Aeroelasticity, Dover Publications, Inc. New York, 1962.

92. Dowell, E.H., Curtiss,Jr., H.C., Scanlan, R.H., and Sisto, F., A Modern Course in Aeroelasticity, Kluwer Academic Publishers, 2nd Edt., 1989.

93. Cunningham, H.J., Batina, J.T., and Bennett, R.M., "Modern Wing Flutter Analysis by Computational Fluid Dynamics Methods," Journal of Aircraft, Vol. 25, No. 10, October 1988, pp. 962-968.

94. Murthy, D.V. and Kaza, K.R.V., "A Computational Procedure for Automated Flutter Analysis," Communications in Applied Numerical Methods, Vol. 5, 1989, pp. 29-37.

95. Dally, J.W. and Riley, W.F., Experimental Stress Analysis, McGraw-Hill Book Company, 1965.

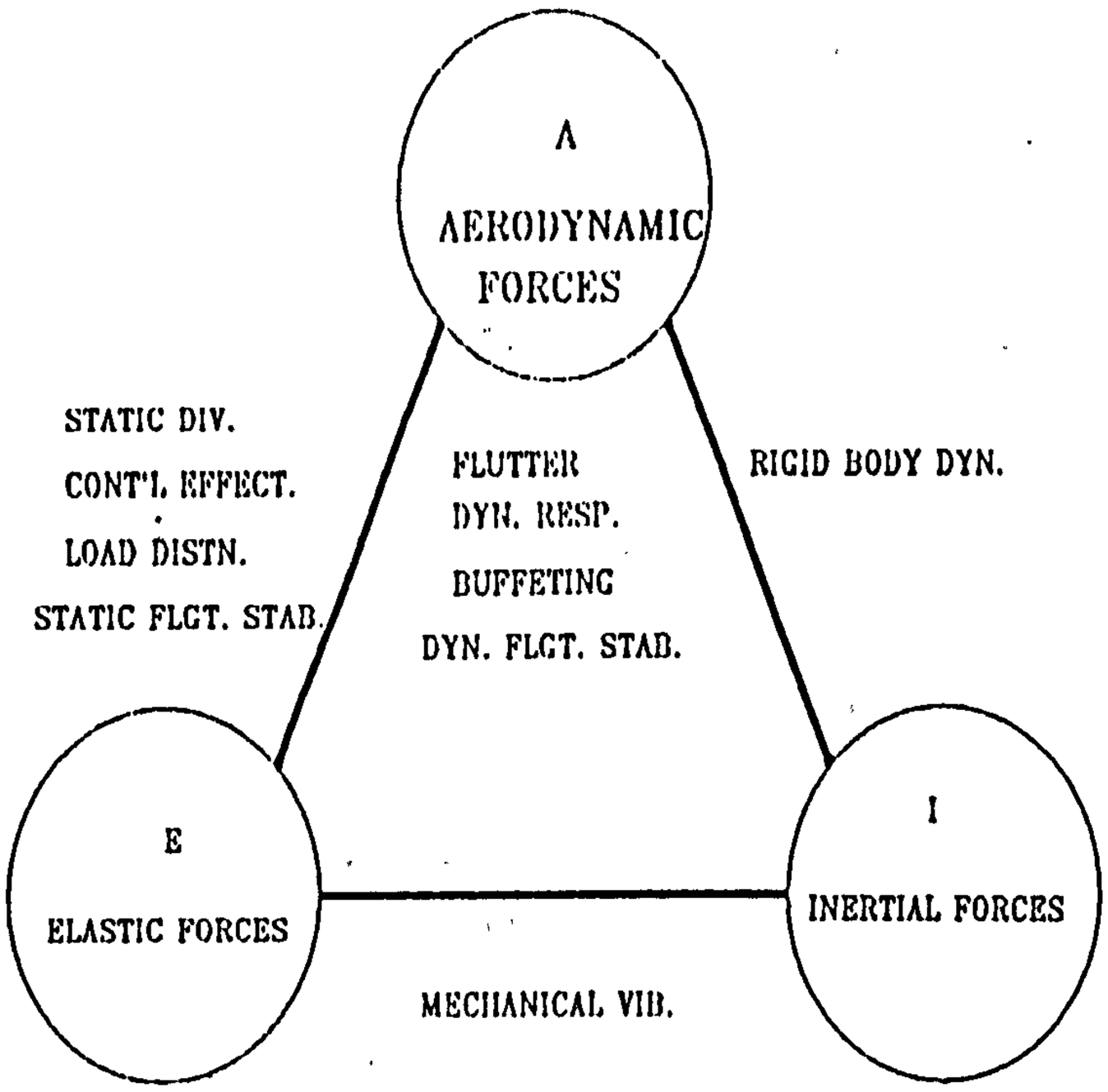

Figure 1.1 Collar's triangle of forces

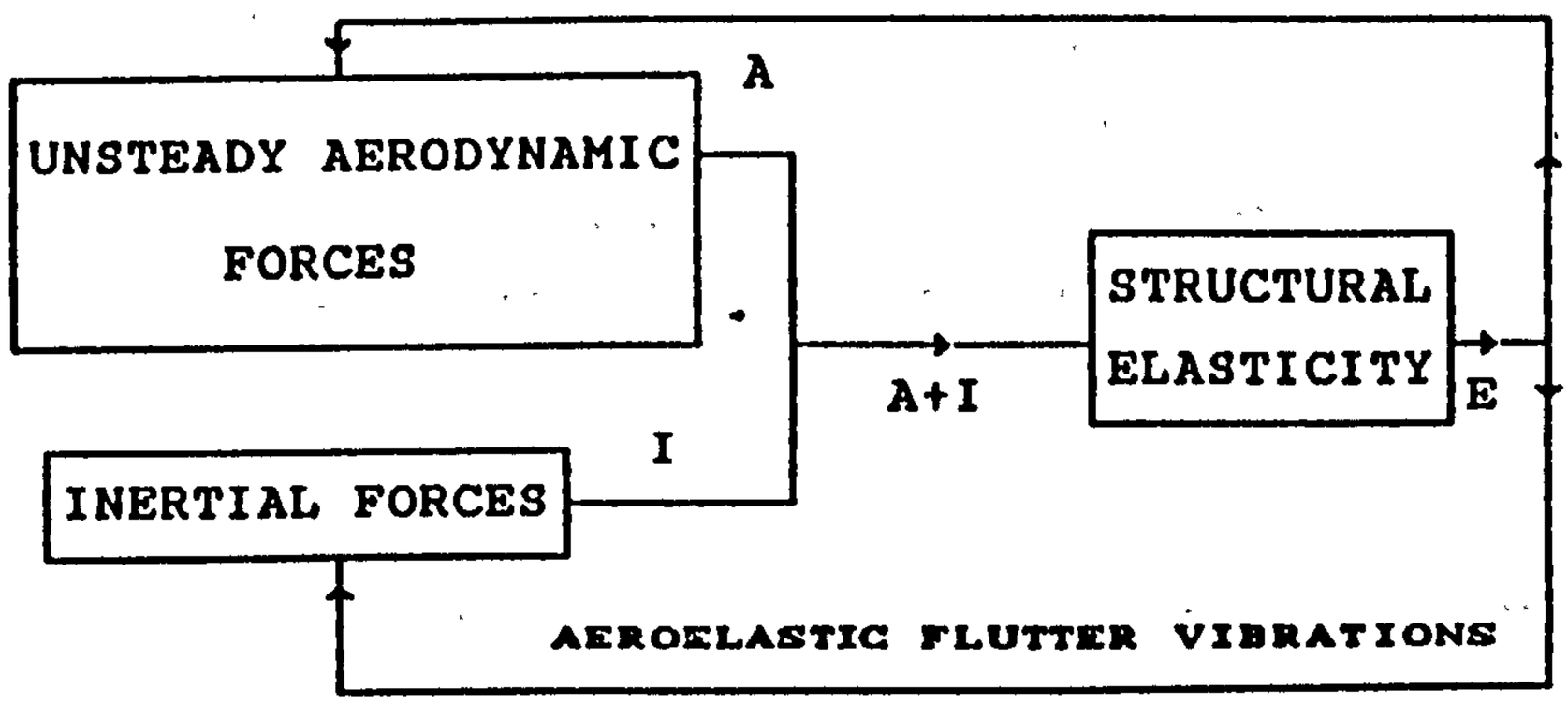

Figure 1.2 Closed loop flutter instability

CHAPTER : 2
AEROELASTIC TAILORING

2.1 INTRODUCTION

Aeroelastic tailoring refers to a design process in which minimum weight is an objective. It also involves the use of structural deformation of a lifting surface to achieve aircraft performance which is usually not associated with structural design. Other objectives include maximizing the lift to drag ratio of a flexible surface, expanding the flight envelope, and improving the ride quality and aircraft manœuvrability. The effectiveness of aeroelastic tailoring depends on the creation of external aerodynamic loads within the desirable limits through controlled deformation.

Therefore, in a way, similarity exists between active control and aeroelastic tailoring. The only difference is that aeroelastic tailoring is a passive means of achieving the required aerodynamic distribution.

2.2 DEFINITION

Aeroelastic tailoring is the embodiment of directional stiffness into an aircraft structural design to control aeroelastic deformation, static or dynamic, in such a fashion as to affect the aerodynamic and structural performance of the aircraft in a beneficial way.

In other words, aeroelastic tailoring is a particular application in the general field of structural optimization under aeroelastic constraints.

2.3 HISTORICAL REVIEW

The earlier investigations such as Voigt [1], Brown [2], and Hearmon [3] indicated the existence of elastic coupling between bending and torsional degrees of freedom in materials such as crystalline substances and plywood.

In 1949, Munk [4] suggested propellers containing diagonally disposed fibrous material based on this concept.

The purpose of this invention was to provide a fixed pitch propeller, the blade of which twisted elastically and favourably as the thrust varied.

In 1953, a novel wing design, known as the AERO-ISOCLINIC wing, was incorporated into the design of the Short S.B.4 or Sherpa prototype invented by Hill [5]. The unique design feature of the wing allowed a constant spanwise angle of attack despite flexural distortions due to aerodynamic pressure distribution.

The aeroelastic characteristics of the aero-isoclinic wing were achieved in part by placing the torsion-box well back in the wing [6]. It satisfies the definition given of aeroelastic tailoring, wherein aircraft performance is the driving goal.

In 1969, as part of a programme to improve transonic performance, General Dynamics submitted a proposal to the Air Force Flight Dynamics Laboratory to apply advanced filamentary composite materials to the design of a super-critical wing [7]. The objective of the programme was to provide the best wing shape (primarily twist distribution) at both cruise and a design manœuvre condition.

At General Dynamics, Waddoups, McCullers, and Naberhaus [64], had been pursuing the application of advanced composites for design improvements other than the obvious weight savings. Maske's [8] work encouraged them to show that the directional properties of composites can provide a significant level of anisotropy to create coupling between bending and twisting deformations in order to produce the desired shape control for the super critical wing. At that time the name "aeroelastic tailoring" [8] was coined.

A contract [9] was given by AFFDL to General Dynamics to prepare proposals for the development of a pilot computer programme for the aeroelastic and strength optimization of aircraft lifting surfaces using the unique properties of filamentary composite materials. The most significant

development of this contract was the Wing Aeroelastic Synthesis Procedure (WASP), later simply called TSO [10]. It was a mathematical programming penalty method approach with the Davidson-Fletcher-Powell algorithm [11] for unconstrained minimization.

The program was developed for the preliminary design of lifting surfaces. The structure was idealised as a simple plate model. The TSO is a powerful design tool with good aerodynamic representation and comprises various aeroelastic analysis procedures. The project was completed in 1972 with the theoretical background provided by Dong [12], Young [13], Barton [14], Waddoups [15,16], and Ashton [17,18].

Rockwell was selected in 1975 [19] to design and build a half-scale remotely piloted research vehicle of a Highly Manoeuvrable Advanced Technology (HiMAT) aircraft for NASA. In February 1978, the aeroelastically tailored wing aircraft was ready for flight tests [19]. The wings were designed with a jig shape (a jig is a type of frame, very accurately planned and constructed, used in aeroplane assembly) such that the aeroelastic deformation in cruising flight optimise the cruise, and the canards were aeroelastically tailored to allow the desired 8-g manoeuvre to be sustained.

The contributions made by AFFDL and General Dynamics were mainly due to exploitation of the high specific strength (ultimate tensile strength/density of the material) and specific stiffness (modulus/density) properties of composite materials. Figures (2.1) and (2.2) give a summary of these properties for Aluminium, Titanium, Steel and composite materials with a 60% fibre volume fraction.

The forward swept wing aircraft X-29 is one of the most recent demonstrators of aeroelastic tailoring. The benefits of forward swept wings were known as early as 1935 [20]. By the 1940's, designers made use of swept wings, both forwards and backwards to reduce transonic drag. A swept forward wing involved the additional problem of divergence. The solution

to this was to stiffen the wing which resulted in a weight penalty. In 1974, Krone [21] showed that, with little or no weight penalty, tailored composite lifting surfaces were possible which avoided divergence in forward swept wing aircraft. Grumman further investigated forward sweep for improved transonic manoeuvering performance on the same lines [22]. The Defence Advanced Research Projects Agency (DARPA) in 1977, began verification of divergence avoidance with aeroelastically tailored composites along with performance evaluation of forward swept wing designs [23]. General Dynamics, Grumman, and Rockwell carried out these in depth studies under the technical direction of AFFDL. In the end DARPA selected Grumman to design and build the X-29. In December 1984, the first flight took place.

During the period 1971-1986, research studies in the field of aeroelastic tailoring were focused on two major issues:

1. General studies of composite mechanics, in order to comprehend the phenomena, evaluate the theory and carry out parametric trend studies.
2. Specific application of the technology to particular designs.

Aeroelastic tailoring has reached this stage through developments in fibrous composite materials and mathematical programming methods. The former increased aircraft structural design options, while the latter allowed the designer efficiently to use the numerous design variables.

Tsai and Hahn [24] and others provided the theory of the mechanics that helped to predict and design structures using composite directional stiffness and strength characteristics with better stiffness-to-weight ratios. The work of Shirk and Griffin [25], demonstrated deformation control with laminate design.

In order to comprehend the complexity of structural design with fibrous composites, a quotation from McCullers

[26] is appropriate: "Advantageous utilization of the anisotropic properties of composites requires consideration of additional design variables and use of complex behaviour and failure mode analysis techniques. Many metal design problems can be reduced to the determination of a single thickness for each member. A composite laminate, however, requires the determination of the number of plies and the orientation of each ply for the material(s) selected, which increases the magnitude and complexity of the design problem. Therefore, although optimization techniques are very useful in metal design problems, they are almost essential for the efficient design of composite structures." Survey papers by Schmit [27], Ashley [28], and Lansing et al. [29] are useful contributions relating work done on optimization.

There are usually two major levels of research effort. The first one make use of sophisticated numerical methods to perform the design work. The wing aeroelastic synthesis procedure (TSO) [10], and the Flutter And Strength Optimization Procedure (FASTOP) [30] are excellent examples of this level of activity.

The second level of research effort is less sophisticated but more academic and thereby enables one to understand the mysteries and consequences of the new technology as well as to assess the limits and problems associated with its application. This level of research concentrates on the mathematical modelling of structures. As a result problems have been analysed with various degrees of complexity and their merits have been observed in detail. For example, many references proposed a beam-like model for the structural deformation of the wing, since the tailoring was focused on bending-twisting deformation coupling. While in others, more complicated models were used to observe the various aspects of aeroelastic tailoring. But in general, they all concentrated on stability of the aircraft in

divergence and flutter, lateral control effectiveness, and load redistribution for unswept, swept-back, and swept-forward wings.

Ashton [31], developed anisotropic plate theory, while Ashton and Love [32], in a series of experiments demonstrated the effect of laminated composite design on the natural frequencies, ultimate strength, and critical buckling load of rectangular boron-epoxy plates. This eventually contributed to the development of TSO.

Similarly, the effect of ply orientation of a symmetrical cross-ply laminate on flutter of a beam like wing was studied by Housner and Stein [33]. They demonstrated that flutter speed was dependent upon the bending and torsional stiffnesses with variation in ply orientation.

Bakthavatsalam [34] examined the effect on flutter speed of an aeroelastically tailored wing and tail surfaces of a wing-tail flutter model.

McCullers et al [35] performed detailed experiments on anisotropic plates to obtain the static and dynamic responses of a wing structure by varying anisotropy, planform shape (i.e. leading-edge angle, taper ratio, and aspect ratio), curvature, shear modulus, and tapered cores.

Shirk and Griffin [25], used TSO to design three similar wings to achieve different flutter and control reversal requirements. Their work also shows that how wings can be designed for minimum weight, maximum washin, and maximum washout characteristics as well as wing with a desired centre of pressure location either from a load relief standpoint or increased flexible lift requirements.

Weisshaar [36-40] moved the boundaries of the work done by Housner and Stein [33], by demonstrating the use of laminates with bending/torsional cross-coupling to increase the divergence speed of swept-forward wings. He also mentioned the effects of cross-coupling on the spanwise

centre-of-pressure position and lateral control effectiveness of swept-back and swept-forward wings. Laminate design can also be used for increasing the aileron reversal dynamic pressures [41].

Lerner and Markowitz [42] made use of a modified version of FASTOP in their initial studies on the X-29. The Air Force Flight Dynamics Laboratories, U.S.A.,experimentally demonstrated the effect of ply rotation on the divergence speed. Sherrer et al [43] showed how a simple rotation of a $0\pm45^{\circ}$ graphite-epoxy laminated wing can be used to increase the divergence speed with various angles of leading edge sweep. Schneider developed a routine for FASTOP to examine the effect of ply angle on divergence speed with variation of optimized wing weight and wing-box sweep [44].

Austin et al [45] gave details of a stiffness model that can be used to describe a laminated box-beam with spars. Gimmestad [46] used an identical model to study the effect of laminate design on load redistribution, flutter speed, and structural weight.

Gimmestad [46], Williams [47], and Gratke and Williams [48] made use of a spar and rib stiffening arrangement to control directional stiffness and bending/twisting cross-coupling, based on Hill's aero-isoclinic wing approach [7]. This proved that aeroelastic tailoring is not limited to composite materials.

Dwyer and Rogers [49] and Rogers [50] made use of coupling between centrifugal force and shearing strain in the plane of the blade cross-section to passively control the angle of attack of a propeller. An idealized thin-walled tube model was used to examine the variation of stress-strain coupling and allowable stress with property axis and composite fibre orientation.

At the Royal Aeronautical Establishment (RAE) Mansfield and Sobey [51] discussed an analytical model of an anisotropic, single cell tube that they used for tailoring

studies. This study indicated the use of extension-torsion coupling in the design of rotor blade. They also discussed the likely effects of laminate design upon structural dynamic properties of beam-like structures.

Niblett [52], in addition to his major work on flutter and divergence of laminated swept-forward wings, introduced the bending/twist "cross-coupling" concept and defined a non-dimensional parameter so as to distinguish tailoring studies from normal laminate problems. This non-dimensional parameter was also recognized by Austin et al. [43] and Weisshaar [36], except that Weisshaar and Niblett defined it as a bounded cross-flexibility parameter.

The work of Weisshaar [33], Weisshaar and Foist [34], Hollowell and Dugundji [35], Crawley and Dugundji [36], and Jensen et al. [37] pointed out interesting facts about the assumption of chordwise rigidity. The chordwise bending mode can bring about substantial changes in natural frequencies and mode shapes of highly coupled laminates; eventually poor correlation will exist between theoretical and experimental flutter velocities.

The stiffness predictions [38], based on a beam model [31] and on a plate model [24] show considerable disagreement. The differences may be negligible for slender metallic plates but are important with plated structures with off-axis plies.

Lynch et al [39] used an improved version of TSO [10] analytically to study the amount of camber and twist achievable by aeroelastic tailoring. Furthermore, the effect of these orientations on roll effectiveness, flutter speed, flexibility to rigidity ratio, and tip deflection were studied. The possibility of enhancing the performance benefits by increasing span or decreasing wing depth due to strength and stiffness characteristics of composites was also demonstrated.

Foist [∞] and Weisshaar and Foist [54,61] looked into the potential effects of boundary conditions (of the wing root) on flutter and divergence. During their investigation "body-freedom" flutter was found wherein the wing root is allowed the freedom to move with the fuselage. Hence inclusion of rigid-body modes in a comprehensive flutter analysis during the design process is an important factor.

Following the work of Niblett [52], Weisshaar and Foist [54] developed a cross-coupling parameter ψ in terms of the bending, torsional, and bending/torsional cross-coupling stiffnesses used by Weisshaar [56] which are EI, GJ, and K, respectively. In the case of beam analysis:

$$\psi^2 = \frac{K^2}{EI\ GJ} < 1 \qquad (2.1)$$

The parameter ψ is very useful in the tailoring studies, since it is bounded by ± 1. In the case of plates, there are three parameters instead of one as given below:

$$\psi_1 = \frac{D_{16}}{\sqrt{D_{11}D_{66}}} \quad , \quad \psi_2 = \frac{D_{26}}{\sqrt{D_{22}D_{66}}} \quad , \quad \bar{\nu} = \frac{D_{12}}{\sqrt{D_{11}D_{22}}} \qquad (2.2)$$

and the above parameters must satisfy the relation [54]:

$$1 - \psi_1^2 - \psi_2^2 - \bar{\nu}\ (\ \bar{\nu} - 2\ \psi_1\ \psi_2) > 0 \qquad (2.3)$$

where

ψ_1 , ψ_2 = primary aeroelastic tailoring parameters that control coupling between bending and twisting curvatures

and $\bar{\nu}$ = reduces to Poisson's ratio for isotropic structures

Use of the stiffness cross-coupling parameter to examine the aeroelastic stability of beam-like structures

was studied in references [61-63]. For instance, structural dynamic response and flutter is controlled through tailoring such that the normal mode shapes are changed by stiffness cross-coupling [62]. Also, for example, it has been shown that a pure torsional mode at zero degree fibre orientation can change that to the second bending mode when the plies are oriented perpendicular to the reference axis [62]. The effects of cross-coupling stiffness on flutter and divergence speeds have been studied in reference [63]. A similar study was conducted by Austin et al. [45] with different nondimensional parameters. The effect is similar to sweeping a wing while keeping the aspect ratio the same. The positive cross-coupling stiffness gives a wash-in characteristic and negative cross-coupling stiffness yields a wash-out characteristic similar to the effect experienced in swept forward and aft-sweep configurations respectively.

The Transonic Aircraft Technology (TACT) programme demonstrated the application of aeroelastic tailoring with advanced composites by designing an aerodynamically efficient jig shaped wing for both cruise flight and high g manoeuvres where washout (incidence decreasing from root to tip) is an important characteristic [64,65]. The design constraints were pivot and wing loads, flutter speed, and panel buckling. A parametric study [64] demonstrated that material bending-twisting coupling has a comparatively greater effect than that of box chord dimension in shape control. The twist of the composite wing was found to be double of an aluminium wing and a reduction of 4% in pivot load was obtained. The flutter speed requirement was achieved without any weight penalty. These studies were later on confirmed on a 1/24 scale model in the wind tunnel [66].

In 1975, Grumman was contracted by the Air Force Flight Dynamics Laboratory (AFFDL) to define the benefits of

applying composite material technology to an Advanced Design Composite Aircraft (ADCA) [66,67]. It was hoped that the aircraft would be smaller, lighter, and less costly than its metallic counterpart but capable of performing a supersonic penetration interdiction fighter mission at lower life cycle costs. As a result of the ADCA program, aeroelastic tailoring technology of the wing and vertical stabilizer was developed [66].

The important characteristics of the wing were mission performance, take-off gross weight, transonic manœuvre condition, and wing shape at supersonic cruise. A comparison of tailored and untailored aeroelastic wings for twist characteristics subject to minimum structural weight and strength at ultimate load constraints showed that the tailored design fulfilled supersonic cruise requirements with negligible improvements in transonic manoeuverability.

The plies were rotated through fifteen degrees aft of the main load-carrying axis in the case of the fin which improved the flutter speed and increased effectiveness in generating yawing moments. The effectiveness of the fin can be utilised in two ways. Firstly, by maintaining the fin size, the lateral directional stability and rolling performance can be improved and lateral manœuvre loads can be decreased. Also the response requirements of the control system may be relaxed. Secondly, without making any change in the lateral stability performance of the aircraft the fin size can be reduced. This in turn will reduce the fin weight and drag relating to the fin surface.

General Dynamics also conducted further studies through several contracts with the AFFDL. The first study [67] resulted in the TSO program and a 3/8 scale component of a conceptual fighter wing with an ultimate objective of increasing the aerodynamic effectiveness by elastic camber and twist. A parametric study was conducted on ten minimum

weight graphite-epoxy skin designs with two different objectives, namely maximum static aeroelastic lift and maximum load relief. The design objective was to achieve maximum flexibility-to-rigidity lift ratio through camber and twist control while maintaining an uninterrupted tip-to-tip spanwise ply orientation. The materials used were graphite-epoxy for the skin with a full-depth aluminium honeycomb core, and fibre glass spars. The structure was analysed both by TSO and ,a finite element package with influence coefficient and vibration tests. The tests agreed both in static deflections and resonance frequencies with the predictions within 5% . The eventual output of this study was a build-up of confidence in the analytical procedures adopted in the design process [∞].

In a second study [∞], the TSO computer program code was improved to study performance benefits through shape control. The investigation concentrated on a low aspect ratio fighter wing and a high aspect ratio bomber wing. The findings were as follows:

1. A composite wing should be aeroelastically tailored to provide acceptable aerodynamic characteristics with minimum weight, otherwise the weight penalty will result in an undesirable aerodynamic centre shift.
2. Maximizing camber while obtaining high negative twist should be utilised to obtain the best drag polar break lift coefficient.
3. The planform geometry can be improved by the weight saving feature of the composites. For example an extension in the wing span gives 5.8 % greater sustained turn rate than a wing with a usual leading-edge flap at Mach number 0.9 and a 2.3 % increase at Mach number 1.2.
4. In the case of the bomber wing, a 13.6 % increase in ferrying range and 15.6 % increase in refuel altitude were achieved.

In a third contract [68-71], wind tunnel data for a tailored wing design were obtained, demonstrating the range of beneficial aeroelastic response attainable. For this study a wing/body-of-revolution/strake configuration was selected. The wing planform was the product of another research and development program on a similar planform of extended-span fighter wing, which provided good transonic manoeuverability without losing supersonic performance.

The design study considered three aeroelastically tailored wings and a rigid steel wing [71]. They are discussed briefly below :

1. The first wing was designed to reduce drag at transonic manoeuvre conditions by aeroelastic camber and negative twist i.e. washout. The analysis indicated that the flutter speed was unexpectedly higher than that of the F-16 metal wing, because the aeroelastically tailored wings have greater areas and aspect ratios and thinner aerofoil sections than the F-16 wing.
2. The second wing was designed to increase lift-curve slope through positive twist i.e. washin and camber. The application is a fin, where in the case of conventional designs the effectiveness of the surface is lost due to aeroelastic effects. Hence the washin and washout capabilities of composite wings gave the concept of deformation control in these fibrous materials.
3. The third wing was an untailored design, having a balanced composite wing laminated with equal amounts of cross plies.
4. The steel wing provided a conventional model data base.

The datum was provided by the untailored design and was compared with the tailored wings to establish the benefits of aeroelastic tailoring.

General Dynamics also worked on the preliminary design of the Wing/Inlet Composite Advanced Development (WICAD) program [72] to :

1. Provide a flight-worthy wing and winglet for the F-16
2. Develop and demonstrate advanced composite conceptual design technology to manufacture low-cost, lightweight, and durable fighter wing and winglet structures.

The study using TSO defined a wing skin with a laminate weighing 67.5% of an aluminum alloy skin, a flexible-to-rigid lift ratio of 1.116, and a flutter speed 12.7% higher than the aluminium skin design. This programme of investigation was terminated after a period of only seven months preventing validation of the aeroelastically tailored design through ground or flight testing.

HiMAT was the first modern, aeroelastically tailored remotely piloted research vehicle, designed and constructed by Rockwell for the NASA Dryden Flight Research Centre [73-76]. The outboard wing and the canard were aeroelastically tailored in such a way that the aircraft was capable of performing a sustained 9-g turn at Mach 0.9 at an altitude of 25,000 feet. This was an additional transonic manoeuvre requirement while maintaining the aircraft's subsonic cruise performance. The flight tests were carried out in 1979.

The wing and canard were aeroelastically tailored by a two phase iterative process. First, a preliminary sizing was obtained by using the computer programs AC87 and AC89. These two computer codes initially developed by Rockwell [74] were based on advanced composite beam theory. The results were verified later by NASTRAN. The process was iterated until twist and strength requirements were satisfied. The HiMAT programme demonstrated the feasibility of using unbalanced,

graphite-epoxy laminates to control aeroelastic twist, except results obtained at 110 % limit load at 8-g maneuver test conducted on wing and canard did not agree well with the analytical predictions. This was due to the nonlinear behaviour of composite properties in the transverse direction to the fibres.

DARPA funded General Dynamics, Grumman, and Rockwell to prepare a feasibility study for a forward-swept wing, small fighter class aircraft flight demonstrator, the X-29 [77]. These studies followed experimental investigation by Grumman [78] and Rockwell [79] to assess the accuracy of predicting the wing divergence speed. Other aspects of these experiments were focused on the understanding of the static aeroelastic phenomena i.e. divergence of a fixed-root forward-swept wing, model design and fabrication processes for the simulation of aeroelastic properties and sub-critical divergence test techniques. Despite the different approaches adopted by the two companies the ultimate results were similar.

Grumman used FASTOP and found that rotating a conventional $[0,\pm45^{\circ},90^{\circ}]$ laminate, so that the primary bending plies are 9 degrees forward of the reference structural axis, added the desirable bending-torsional coupling necessary to minimize the wing washin tendencies. On the other hand, Rockwell used TSO to design with the cross plies oriented 30 degrees forward of and 51 degrees aft of the reference axis along with the primary bending plies oriented at 9 degrees forward of the reference axis. The models were tested in the NASA Langley Research Centre 16-ft transonic dynamics tunnel. Experimental results showed that wing divergence could be avoided by the application of aeroelastic shape control possible due to tailoring of the advanced composites.

Gimmestad [46] performed a study of a cargo transport

aeroplane to show the effect of composites on the aeroelasticity of a high aspect ratio wing with an aft sweep of 35 degrees. Effects of flexibility, anisotropy and so-called "jig twisting" (jig twisting is a deformation introduced into the built shape of the wing such that the optimum span loading, and hence minimum drag is achieved in cruising flight) on a composite and a conventional aluminium alloy wing were explored. Gimmestad's conclusions were :

1. An explanation for aeroelastic effects and jig twisting in preliminary design for performance enhancement is essential.
2. Anisotropy can have effects on the stability and control of the aircraft.
3. The anisotropic effects witnessed in composites are also found in conventional materials but to a much lesser extent.

In another study, Gimmestad [80] showed on a composite winglet of the KC-135 using TSO that it can be designed for substantially larger aeroelastic washout losses in order to reduce wing bending moments.

In another study, TSO was used by Triplett [81] to re-design a wing for the fighter aircraft F-15 resulting in the saving of 55 lbs in weight and a reduction in drag with an improvement in the roll effectiveness. The other parts of the study covered the preliminary design of a tail plane, a prototype aircraft movable outer wing panel, and a conceptual aircraft wing. In the case of the conceptual aircraft wing a 3 % weight saving was achieved, but with 4.6 degrees of washout twist there was a weight penalty of 2.5%.

Triplett [82] also pointed out in another study that there can be no weight penalty while dealing with the problem of divergence in case of forward-swept wings.

However it was shown that the induced drag will increase with the forward-swept configuration.

The work of Sensburg et al. [83] on the Airbus A300 for gust load alleviation on an extended wing resulted in 1.7% increase in root bending moment with aeroelastic tailoring as compared to 7% with a conventional material.

Schweiger et al. [84] studied the potential of aeroelastic tailoring on a high aspect ratio glider to control wing/body flutter due to the interaction between the swept wing bending mode and the short period mode.

The Lavi fighter developed by Grumman for Israel Aircraft Industries, has utilised FASTOP to optimize the advanced composite structures for improved control effectiveness of the wing elevons and the overall performance of the fin [85].

Librescu and Simovich [86] formulated a simple algorithm that allows for the determination, in a closed form, of the divergence instability of advanced composite swept forward and aft-swept wing structures. The analysis includes the warping restraint effects and its influence on the static instability is discussed. Although in the case of metallic wings warping restraint has a stabilizing effect (more pronounced with small aspect ratio and diminishing effect with moderate aspect ratio wings), its effect is more complex in the case of composite wings.

Another aspect of aeroelastic tailoring which has rapidly attracted the attention of many researchers in the field, is the development of optimization techniques. Aeroelastic tailoring is considered to be a particular application of the general field of structural optimization under aeroelastic constraints such as flutter and divergence, etc. Some excellent survey papers on the subject can be seen in references [28,29,87] along with a comprehensive survey on aeroelastic tailoring by Shirk,

Hertz, and Weisshaar [88].

At the Air Force Flight Dynamics Laboratory, the TSO [10] (aeroelastic Tailoring and Structural Optimization) was the first attempt to develop an optimization program with special reference to aeroelastic tailoring. Its scope of application and limitations have already been discussed in detail. Then FASTOP [20] (Flutter And Strength Optimization Program) appeared with finite element idealization of an aircraft wing but aeroelastic loads were not included in the optimization process. Other similar approaches made in the area were COMBO [43] and SWEEP [80] (Structural WEight Estimation Program).

A very recent addition to aeroelastic optimization programmes is the development of the computer program ADOP [00] (Aeroelastic Design Optimization Program) by McDonnell Douglas Corporation. This program resulted from considerable improvements and modification of an existing aeroelastic analysis program called ASTROS [01] (Automated STructural Optimization System). Although ADOP is now capable of handling a complete aircraft configuration with up to 250,000 degrees of freedom it appears to be a very expensive tool for performing design optimization. Such a programming tool inevitably makes extensive use of computer time and is also beyond the scope of most designers. Thus the development of an aeroelastic computer program which is short, compact, completely self contained and portable is of great value.

2.4 THE FUTURE OF AEROELASTIC TAILORING

As has been pointed out in the historical review the concept of aeroelastic tailoring existed well before the introduction of composite materials, hence it will be very unjust to limit our attention to glass, carbon, and Kevlar reinforced fibre plastics, etc. A new category of materials

has already been introduced known as MMC i.e. the Metal Matrix Composite. A typical MMC may constitute boron fibres in aluminium matrix. The macromechanics of a generally orthotropic laminate is equally applicable to structures made of MMC. The high temperature metal constituents and minimum degradation of properties due to environmental changes are distinguishing features of MMC which make it very popular in the aircraft industry.

Aeroelastic tailoring has been concerned with the advanced filamentary composites and mathematical programming techniques, though procedures for the efficient utilization of advanced composite materials in aircraft design have not yet been fully developed. The performance and durability of a particular design depends on the structural dynamic behaviour and flexibility of an aircraft. Hence these characteristics are expected to be taken into account in the development of aeroelastic tailoring strategies. It has been mentioned that directional stiffness and the resulting aerodynamic coupling influence a number of areas of aircraft performance. Thus a comprehensive approach in the design procedure is required to fulfill all the requirements simultaneously.

Large space structures represent another potential area of aeroelastic tailoring research. The repetitive lattice arrangement of a number of space structures forms an anisotropic design. The active control system of these space structures can be enhanced by achieving passive modal control through tailoring the orientation of the structural members.

Aeroelastic tailoring is also playing an important role in the design procedures of aerospace structures and is becoming a component of such procedures.

REFERENCES

1. Voigt, W.,"Lehrbuch der Kristallphysik," Teuber, 1928.

2. Brown, W.F. Jr., "Interpretation of Torsional Frequencies of Crystal Specimens," Physical Review, Vol. 58, Dec. 1, 1940, pp. 998-1001.

3. Hearmon, R.F.S., "The significance of Coupling between Shear and Extension in the Elastic Behavior of Wood and Plywood," Proceedings of the Physical Society, Vol. 55, 1943, pp. 67-80.

4. Munk, M.M., "Propeller Containing Diagonally Disposed Fibrous Material," U.S. Patent 2,484,308,1111, Oct. 1949.

5. "Sherpa Takes the Air," Flight and Aircraft Engineer, No. 2334, Vol. LXIV, Oct. 16, 1953, PP. 535.

6. "Pterodactyl to Sherpa," Flight and Aircraft Engineer, No. 2339 Vol. LXIV, Nov. 20, 1953, pp. 680-681.

7. Waddoups, M.E., Smith, C.B., and McMickle, R.W., "Composite Wing for Transonic Improvement, Composite Wing Aeroelastic Response Study," AFFDL-TR-71-24, Vol. 1, Dec. 1972.

8. Waddoups, M.E., Private communication with Weisshaar, General Dynamics, Ft. Worth Div., Ft. Worth, TX, July 14, 1983.

9. "Dynamic Characteristics of Advanced filamentary Composite Structures," USAF Contract F33645-70-C-1837, Sept. 1970.

10.McCullers, L.A. and Lynch, R.W.,"Dynamic Characteristics of Advanced Filamentary Structures, Vol. II - Aeroelastic Synthesis Procedure Development," AFFDL-TR-73-111, Sept. 1974.

11. Fletcher, R. and Powell, M.J.D., "A rapidly convergent descent method for minimization," The Comp. Journal, Vol. 6, 1963, pp. 163-168.

12.Dong, S.B., Matthiesen, R.B., Pister, K.S., and Taylor, R.L., "Analysis of Structural Laminates," Aeronautical Research Laboratory, University of California, Los Angeles, Rept. 76, 1961.

13.Young, D., "Vibration of Rectangular Plates by the Ritz Method," Journal of Applied Mechanics, Vol. 17, Dec. 1950, pp. 448-453.

14.Barton, M.V., "Vibration of Rectangular and Skew Cantilevered Plates Representing idealised Missile fins," Defence Research Laboratory, University of Texas, Austin, Rept. 222, Dec. 1949.

15.Waddoups, M.E., "The Vibration Response of Laminated Orthotropic Plates," M.S. Thesis, Dept. of Mechanical Engineering, Brigham Young University, Provo, UT, Aug. 1965.

16.Waddoups, M.E. and McCullers, L.A., "Structural Synthesis of Anisotropic Plates," presented at the AIAA/ASME Structures, Structural Dynamics and Materials Conference, April 1970.

17.Ashton, J.E. and Waddoups, M.E., "Analysis of Anisotropic Plates," Journal of Composite Materials, Vol. 3, Jan. 1969, pp. 148-165.

18.Ashton, J.E., "Analysis of Anisotropic Plates II," Journal of Composite Materials, Vol. 3, July 1969, pp. 470-479.

19.Price, M.A., "HiMAT Structural Development Design Methodology," NASA CR-144886, Oct. 1979.

20.Busemann, A., 5th Volta Congress on High Speeds in Aviation, Compedoglio, Italy, Oct. 1935.

21.Krone, N.J., "Divergence Elimination with Advanced Composites," Ph.D. Thesis, University of Maryland, College Park, MD, Dec. 1974.

22.Krone, N.J., "Divergence Elimination with Advanced Composites," AIAA Paper 75-1009, Aug. 1975.

23.Krone, N.J., "Forward Swept Wing Flight Demonstrator," AIAA Paper 80-1882, Aug. 1980.

24.Tsai, S.W. and Hahn, H.T., Introduction to Composite Materials, Technomic, Westport, CT. 1980.

25.Shirk, M.H. and Griffin, K.E., "The Role of Aeroelasticity in Aircraft Design with Advanced Filamentary Composite Materials," Proceedings of the 2nd Conference on Fibrous Composites in Flight Vehicle Design, AFFDL-TR-74-103, May 1974, pp. 405-438.

26.McCullers, L.A., "Automated Design of Advanced Composite Structures," Proceedings of the ASME Structural Optimization Symposium, AMD-Vol. 7, Nov. 1974, pp. 119-133.

27.Schmit, L.A., "Structural Synthesis - its Genesis and Development," AIAA Journal, Vol. 19, Oct. 1981, pp.

1249-1263.

28.Ashley, H., "On Making Things the Best - Aeronautical uses of Optimization," Journal of Aircraft, Vol. 19, Jan. 1982, pp. 5-28.

29.Lansing, W., Lerner, E., and Taylor, R.F., "Applications of Structural Optimization for Strength and Aeroelastic Design Requirements," AGARD-R-664, Sept. 1977.

30.Wilkinson, K., Markowitz, J., Lerner, E., George, D., and Batill, S.M., "FASTOP : A Flutter and Strength Optimization Programme for Lifting Surface Structures," Journal of Aircraft, Vol. 14, June 1977, pp. 581-587.

31.Ashton, J.E., "Anisotropic Plate Analysis," Fort Worth Division, General Dynamics, Fort Worth, TX, R&D Rept. FZM-4899, Oct. 1967.

32.Ashton, J.E. and Love, T.S., "Stability of Anisotropic Plates," Fort Worth Div., General Dynamics, Forth Worth, TX, R&D Rept. FZM-4992, Feb. 1968.

33.Housner, J.M. and Stein, M., "Flutter Analysis of Swept-Wing Subsonic Aircraft with Parameter Studies of Composite Wings," NASA TN-D7539, Sept. 1974.

34.Bakthavatsalam, T.N., "Suppression of Interference Flutter by Composite Tailoring," Ph.D. Thesis, University of Texas, Austin, May 1983.

35.McCullers, L.A., Naberhaus, J.D., and Bensinger, C.T.,"Dynamic Characteristics of Advanced Filamentary Composite Structures, Volume I - Test Specimen Program," AFFDL TR-73-111, Sept. 1974.

36.Weisshaar, T.A., "Aeroelastic Stability and Performance Characteristics on Aircraft with Advanced Composite Sweptforward Wing Structures," AFFDL-TR-78-116, Sept. 1978.

37.Weisshaar, T.A., "Divergence of Forward Swept Composite Wings," Journal of Aircraft, Vol. 17, June 1980, pp. 442-448.

38.Weisshaar, T.A., "Forward Swept Wing Static Aeroelasticity," AFFDL-TR-79-3087, June 1979.

39.Weisshaar, T.A., "Aeroelastic Tailoring of Forward Swept Composite Wings," Journal of Aircraft, Vol. 18, Aug. 1981, pp. 669-676.

40.Weisshaar, T.A., "The Influence of Aeroelasticity on Swept Composite Wings," AFWAL-TR-80-3137, Nov. 1980.

41.Weisshaar, T.A., "Aeroelastic Stability of Forward Swept Composite Wing Aircraft," Proceedings of the Bristol International Conference on Forward Swept Wing Aircraft, No. II-5, Bristol, UK, March 1982, pp. II.5.1-II.5.13.

42.Lerner, E. and Markowitz, J., "An Efficient Structural Resizing Procedure for Meeting Static Aeroelastic Design Objectives," Journal of Aircraft, Vol. 16, Feb. 1979, pp. 65-71.

43.Sherrer, V.C., Hertz, T.J., and Shirk, M.H., "Wind Tunnel Demonstration of Aeroelastic Tailoring Applied to Forward Swept Wings," Journal of Aircraft, Vol. 18, Nov. 1981, pp. 976-983.

44.Schneider, G., Gödel, H., and Sensburg, O., "Structural Optimization of Advanced Aircraft Structures," presented at

the 12th Congress of the International Council of the Aeronautical Sciences, Oct. 1980.

45.Austin, F., Hadcock, R., Hutchings, D., Sharp, D., Tang, S., and Waters, C., "Aeroelastic Tailoring of Advanced Composite Lifting Surfaces in Preliminary Design," Proceedings of the AIAA/ASME/SAE 17th Structures, Structural Dynamics and Materials Conference, May 1976, pp. 69-79.

46.Gimmestad, D., "An Aeroelastic Optimization Procedure for Composite High Aspect Ratio Wings," AIAA Paper 79-0726, 1979.

47.Williams, J.G., "Analysis/Theory of Controlled Configurated Structures," AFFDL-TR-74-137, 1974.

48.Gratke, S.D. and Williams, J.G., "Analysis/Theory of Controlled Configured Structures (CCS)," AIAA Paper 77-1212, Aug. 1977.

49.Dwyer, W.J. and Rogers, J.B., "Aeroelastically Tailored Propellers," SAE Paper 770455, March 1977.

50.Rogers, J.B., "Aeroelastically Tailored Propellers," M.S. Thesis, University of Texas, May 1976.

51.Mansfield, E.H. and Sobey, A.J., "The Fibre Composite Helicopter Blade," Aeronautical Quarterly, Vol. 30, May 1979, pp. 413-449.

52.Niblett, Li.T., "Divergence and Flutter of Sweptforward Wings with Cross-flexibilities," RAE-TR-80047, April 1980.

53.Weisshaar, T.A., "Structural Dynamic Tailoring of Advanced Composite Lifting Surfaces," Purdue University,

West Lafayette,IN, AAE-82-1, June 1982.

54.Weisshaar, T.A. and Foist, B.L., "Vibration and Flutter of Advanced Composite Lifting Surfaces," Proceedings of the AIAA/ASME 24th Structures, Structural Dynamics and Materials Conference, May 1983, pp. 498-508.

55.Hollowell, S.J. and Dugundji, J., "Aeroelastic Flutter and Divergence of Stiffness Coupled, Graphite/Epoxy, Cantilevered Plates," presented at the 23rd AIAA/ASME/ASCE/AHS Structures, Structural Dynamics and Materials Conference, AIAA Paper 82-0722, May 1982.

56.Crawley, E.F. and Dugunji, J., "Frequency Determination and Non-dimensionalization for Composite Cantilevered Plates," Journal of Sound and Vibration, Vol. 72, No. 1, 1980, pp. 1-10.

57.Jensen, D.W., Crawley, E.F., and Dugundji, Jr., "Vibration of Cantilevered Graphite/Epoxy Plates with Bending-Torsion Coupling," Journal of Reinforced Plastics and Composites, Vol. 1, July 1982, pp. 254-269.

58.Weisshaar, T.A. and Foist, B.L., "Vibration Tailoring of Advanced Composite Lifting Surfaces," Journal of Aircraft, Vol. 22, Feb. 1985, pp. 141-147.

59.Lynch, R.W., Rogers, W.A., and Braymen, W.W., "Aeroelstic Tailoring of Advanced Composite Structures for Military Aircraft, Volume I - General study," AFFDL-TR-76-100, April 1977.

60.Foist, B.L., "Aeroelastic Stability of Aircraft with Advanced Composite Wings," M.S. Thesis, School of Aeronautics and Astronautics, Purdue University, West

Lafayette, IN, August 1982.

61.Weisshaar, T.A. and Foist, B.L., "Aeroelastic Tailoring of Aircraft subject to Body Freedom Flutter," AFWAL-TR-83-3137, November 1983.

62.Stukel, S.P., "Aeroelastic Tailoring for Passive Flutter Suppression," M.S. Thesis, School of Aeronautics and Astronautics, Purdue University, West Lafayette, IN, December 1982.

63.Ryan, R.J.,"The effect of Aeroelastic Tailoring in the Passive Control of Flutter and Divergence of Aircraft Wings," M.S. Thesis, School of Aeronautics and Astronautics, Purdue University, West Lafayette, IN, December 1983.

64.Waddoups, M.E., Smith, C.B., and McMickle, R.W., "Composite Wing for Transonic Improvement, Volume I - Composite Wing Aeroelastic Response Study," AFFDL-TR-71-24, December 1972.

65.Waddoups, M.E., McCullers, L.A., and Naberhaus, J.D., "Composite Wing for Transonic Improvement, Volume II, Advanced Analysis Evaluation," AFFDL-TR-71-24, November 1971.

66.Forsch, H., "Advanced Design Composite Aircraft (ADCA) Study," AFFDL-TR-76-97, Vol. I, November 1976.

67.Naberhaus, J.D. and Waddoups, M.E., "Dynamic Characteristics of Advanced Filamentary Composite Structures, Vol. III - Demonstration Component Program," AFFDL-TR-73-111, September 1974.

68.Lynch, R.W., Rogers, W.A., and Brayman, W.W.,

"Aeroelastic Tailoring of Advanced Composite Structures for Military Aircraft," AFFDL-TR-76-100, April 1977.

69.Rogers, W.A., Brayman, W.W., Murphy, A.C., Graham, D.H., and Love, M.H., "Validation of Aeroelastic Tailoring by Static Aeroelastic and Flutter Tests," AFWAL-TR-81-3160, September 1982.

70.Rogers, W.A., Brayman, W.W., and Shirk, M.H., "Design Analysis and Model Tests of an Aeroelastically Tailored Lifting Surface," AIAA Paper 81-1673, August 1981.

71.Brayman, W.W., Rogers, W.A., and Shirk, M.H., "Wind Tunnel Test and Aerodynamic Analysis of Three Aeroelastically Tailored Wings," presented at the 13th Congress of the International Council of the Aeronautical Sciences and AIAA Aircraft Systems and Technology Conference, ICAS-82-5.7.3, August 1982.

72.Maske, E.B., "Wing/Inlet Composite Advanced Development," AFFDL-TR-76-88, September 1976.

73.Lockenhauer, J.L. and Layton, G.P., "RPRV Research Focus on HiMAT," Astronautics and Aeronautics, Vol. 14, April 1976, pp. 36-41.

74.Price, M.A., "HiMAT Structural Development Design Methodology," NASA CR-144886, October 1979.

75.Brown, L.E. Jr., Price, M.A., and Genyrich, P.B., "Aeroelastically Tailored Wing Design," Proceedings of Evolution of Aircraft Wing Design Symposium, Dayton, Ohio, March 1980, pp. 141-146.

76.Lokos, W., "HiMAT Aeroelastic Analysis," Research and

Technology Annual Report 1983, NASA TM-85865, November 1983.

77.Hertz, T.J., Shirk, M.H., Ricketts, R.H., and Weisshaar, T.A., "On the Track of Practical Forward-Swept Wings," Astronautics and Aeronautics, Vol. 20, January 1982, pp. 40-52.

78.Wilkinson, K. and Rauch, F., "Predicted and Measured Divergence Speeds of an Advanced Composite Forward Swept Wing Model," AFWAL-TR-80-3059, July 1980.

79.Ellis, J.W., Dobbs, S.K., and Miller, G.D., "Structural Design and Wind Tunnel Testing of a Forward Swept Fighter Wing," AFWAL-TR-80-3073, July 1980.

80.Gimmestad, D., "Aeroelastic Tailoring of a Composite Winglet for KC-135," Proceedings of the 22nd Structures, Structural Dynamics and Materials Conference, April 1981, pp. 373-376.

81.Triplett, W.E., "Aeroelastic Tailoring Studies in Fighter Aircraft Design," Proceedings of the 20th Structures, Structural Dynamics and Materials Conference, April 1979, pp. 72-78.

82.Tripplet, W.E., "Aeroelastic Tailoring of a Forward Swept Wing and Comparisons with Three Equivalent Aft Swept Wings," Proceedings of the AIAA/ASME/ASCE/AHS 21st Structures, Structural Dynamics and Materials Conference, May 1980, pp. 754-760.

83.Sensburg, O., Becker, J., Lusebrink, H., and Weiss, F., "Gust Load Allevation on Airbus A-300," presented at 13th Congress of the International Council of the Aeronautical Sciences, August 1982.

84.Schweiger, J., Sensburg, O., and Berns, H.J., "Aeroelastic Problems and Structural Design of a Tailless CFC-Sailplane," presented at the Second International Symposium on Aeroelasticity and Structural Dynamics, Aachen, FRG, April 1985.

85. Shirk, M.H., Hertz, T.J., and Weisshaar, T.A., "Aeroelastic Tailoring - Theory, Practice, and Promise," Journal of Aircraft, Vol. 23, No. 1, January, 1986. (Reply by Lerner, E. in response to AFWAL/FIBR survey letter, March 8, 1983).

86. Librescu, L. and Simovich, J., "General Formulation for the Aeroelastic Divergence of Composite Swept-Forward Wing Structures," Journal of Aircraft, Vol. 25, No. 4, April, 1988, pp.364-371.

87. Coupry, G., "Aeroelasticity today and tomorrow," AIAA and ICAS-86-0.2, 1986.

88. Shirk, M.H., Hertz, T.J., and Weisshaar, T.A., "Aeroelastic Tailoring - Theory, Practice, and Promise," Journal of Aircraft, Vol. 23, No. 1, January, 1986.

89. Asceni, L., et al., "A Structural Weight Estimation Programme (SWEEP) for Aircraft," ASD/XR 74-10, June 1974.

90. Dodd, A.J. and et al., "Aeroelastic Design Optimization Program," Journal of Aircraft, Vol. 27, No. 12, December 1990.

91. Herendeen, D.L., Hoesly, R.L., Johnson, E.H., and Venkayya, V.B., "ASTROS - An Advanced Software Environment for Automated Design," AIAA Paper 86-0856, May 1986.

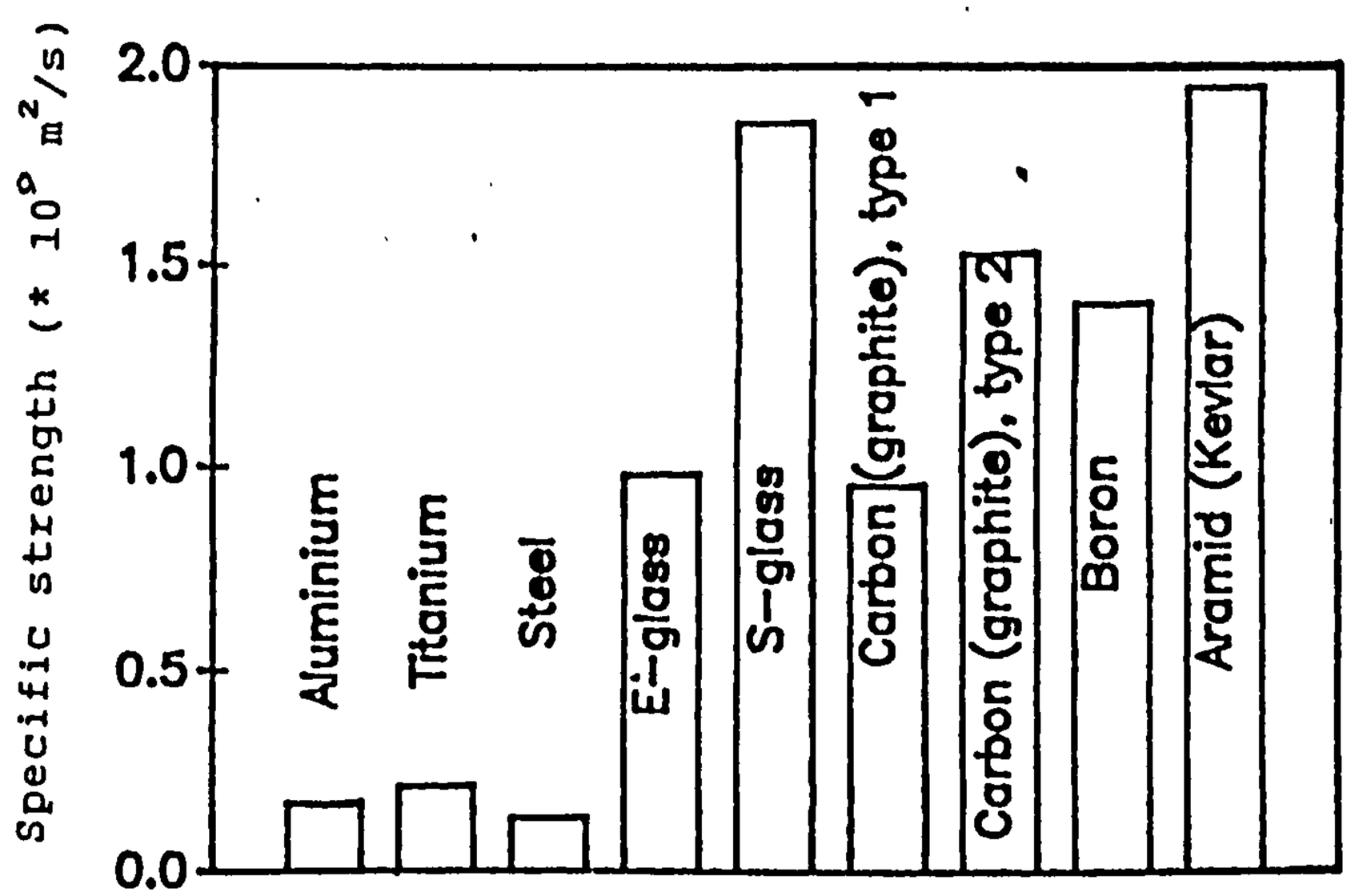

Figure 2.1 A comparison of composites with 60% fibre volume fraction and metals by specific strength (ultimate strength/density)

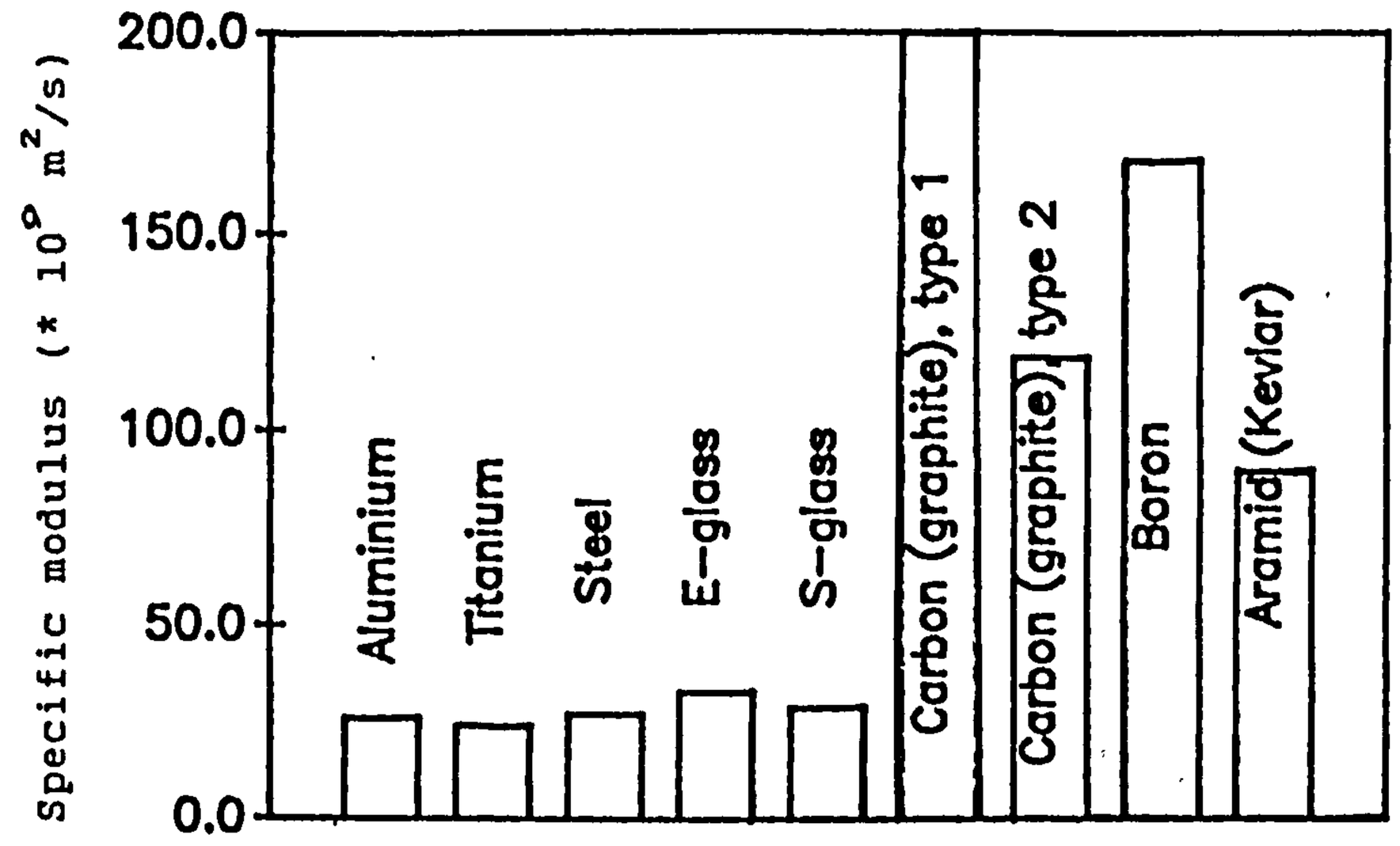

Figure 2.2 A comparison of composites with 60% fibre volume fraction and metals by specific stiffness (material elastic modulus/density)

CHAPTER : 3

COMPOSITES

3.1 INTRODUCTION

The orthotropic properties of composite materials, particularly the directional stiffness and strength characteristics provide new dimensions to the design of structures that are not possible when using conventional materials. These directional attributes can be incorporated in a structure by controlling the stacking sequence of the orthotropic layers. The high specific strength and specific stiffness (ratios of ultimate tensile strength and modulus respectively to the density) qualities of composites have special significance in designing aircraft structures.

3.2 LAMINATE EQUIVALENT ELASTIC CONSTANTS

The laminate macro-mechanics can be found in Tsai and Hahn [1], Jones [2] or in other standard texts on composite materials. Composites can be categorised into several different types depending upon ply thickness, fibre orientation and number of layers as shown in Figure (3.1).

The general laminate constitutive equations for load-deformation relationships as given in reference [2] are as follows :

$$\begin{Bmatrix} N_x \\ N_y \\ N_{xy} \end{Bmatrix} = \begin{bmatrix} A_{11} & A_{12} & A_{16} \\ A_{12} & A_{22} & A_{26} \\ A_{16} & A_{26} & A_{66} \end{bmatrix} \begin{Bmatrix} \varepsilon^{o}_{x} \\ \varepsilon^{o}_{y} \\ \gamma^{o}_{xy} \end{Bmatrix} + \begin{bmatrix} B_{11} & B_{12} & B_{16} \\ B_{12} & B_{22} & B_{26} \\ B_{16} & B_{26} & B_{66} \end{bmatrix} \begin{Bmatrix} k_x \\ k_y \\ k_{xy} \end{Bmatrix} \quad (3.1a)$$

and

$$\begin{Bmatrix} M_x \\ M_y \\ M_{xy} \end{Bmatrix} = \begin{bmatrix} B_{11} & B_{12} & B_{16} \\ B_{12} & B_{22} & B_{26} \\ B_{16} & B_{26} & B_{66} \end{bmatrix} \begin{Bmatrix} \varepsilon^o_x \\ \varepsilon^o_y \\ \gamma^o_{xy} \end{Bmatrix} + \begin{bmatrix} D_{11} & D_{12} & D_{16} \\ D_{12} & D_{22} & D_{26} \\ D_{16} & D_{26} & D_{66} \end{bmatrix} \begin{Bmatrix} k_x \\ k_y \\ k_{xy} \end{Bmatrix} \quad (3.1b)$$

where

N_x, N_y = normal forces per unit length in x and y directions respectively

N_{xy} = shear force per unit length

ε_x, ε_y = normal strains in x and y directions

γ_{xy} = shear strain

M_x, M_y, M_{xy} = moments per unit length

k_x, k_y, k_{xy} = twist curvatures of the middle surface

A_{ij} = extensional stiffness

B_{ij} = coupling stiffness

D_{ij} = bending stiffness

In the case of symmetric laminates with multiple generally orthotropic layers, the coupling B matrix will vanish and equations (3.1a) and (3.1b) will uncouple to give the following load-deformation relationships.

$$\begin{Bmatrix} N_x \\ N_y \\ N_{xy} \end{Bmatrix} = \begin{bmatrix} A_{11} & A_{12} & A_{16} \\ A_{12} & A_{22} & A_{26} \\ A_{16} & A_{26} & A_{66} \end{bmatrix} \begin{Bmatrix} \varepsilon^o_x \\ \varepsilon^o_y \\ \gamma^o_{xy} \end{Bmatrix} \quad (3.2a)$$

$$\begin{Bmatrix} M_x \\ M_y \\ M_{xy} \end{Bmatrix} = \begin{bmatrix} D_{11} & D_{12} & D_{16} \\ D_{12} & D_{22} & D_{26} \\ D_{16} & D_{26} & D_{66} \end{bmatrix} \begin{Bmatrix} k_x \\ k_y \\ k_{xy} \end{Bmatrix} \quad (3.2b)$$

The presence of some elements in the A and D matrices will cause coupling between various deformations. For example A_{16}, A_{26}, D_{16}, and D_{26} will cause coupling between normal forces and shearing strain, shearing force and normal strains, normal moments and twist, and twisting moment and normal curvatures respectively.

3.2.1 EQUIVALENT ELASTIC CONSTANTS IN MEMBRANE MODE

Let us assume that only a normal load N_x per unit length is applied along the x-axis and N_y, and N_{xy} are absent. Re-arranging equation (3.2a) and substituting the above mentioned assumptions:

$$\begin{Bmatrix} \varepsilon_x^\circ \\ \varepsilon_x^\circ \\ \gamma_{xy}^\circ \end{Bmatrix} = \begin{bmatrix} A_{11} & A_{12} & A_{16} \\ A_{12} & A_{22} & A_{26} \\ A_{16} & A_{26} & A_{66} \end{bmatrix}^{-1} \begin{Bmatrix} N_x \\ 0 \\ 0 \end{Bmatrix} \qquad (3.3)$$

therefore,

$$\varepsilon_x^\circ = A_{11}^* N_x \qquad (3.4)$$

where A_{11}^* = element of the inverted A-matrix

and $\varepsilon_x = \varepsilon_x^\circ$ due to zero curvatures

but $\sigma_x = E_x \varepsilon_x$

and $$\sigma_x = \frac{P}{A} = \frac{P}{b\ t} = \frac{N_x}{t}$$

where $$N_x = \frac{P}{b}$$

therefore, $$\frac{N_x}{t} = E_x \varepsilon_x$$

or

$$N_x = E_x \ \varepsilon_x \ t \qquad (3.5)$$

Replacing eq. (3.5) in eq. (3.4), we get

$$\varepsilon_x^\circ = A_{11}^* E_x \ \varepsilon_x \ t$$

Therefore, the equivalent Young's modulus in the x-direction of the laminate lay-up is given by

$$E_x = \frac{1}{t . A_{11}^*} \qquad (3.6)$$

The expression for Young's modulus in the y-direction can be obtained in a similar way. Thus

$$E_y = \frac{1}{t\, A^*_{22}} \qquad (3.7)$$

$$G_{xy} = \frac{1}{t\, A^*_{66}} \qquad (3.8)$$

3.2.2 EQUIVALENT ELASTIC CONSTANTS IN A BENDING MODE

Similarly from equation (3.2b) one can arrive at the following relationships for the equivalent elastic constants in the bending mode :

$$E_x = \frac{12}{t^3 D^*_{11}} \qquad (3.9)$$

$$E_y = \frac{12}{t^3 D^*_{22}} \qquad (3.10)$$

$$G_{xy} = \frac{12}{t^3 D^*_{66}} \qquad (3.11)$$

3.3 LAMINATE - Computer Program

Two computer programs, one in BASIC and the other in FORTRAN (computer languages) were written to perform the composite analysis for a given lay-up (see Appendix (C)). The flow diagram for both of the programs is shown in Figure (3.2) describing the general procedure adopted to analyse the laminate. Both programs can handle up to five different materials and twenty plies in a particular laminate.

The instructions to run the LAMINATE program are given in Appendix (H) along with an illustrative example.

3.4 PARAMETRIC STUDY ON PLY ORIENTATION OF A SINGLE LAYER LAMINATE

A parametric study of the effect of ply orientation on the laminate equivalent elastic constants of a single layer configuration was conducted. The subscripts 1 and 2 are adopted for the composite along the fibre and transverse to the fibre directions respectively whereas the subscripts x and y are used along the chord and spanwise directions of the laminate. If the y-axis is aligned with the composite fibre direction then the material elastic constants will be the same as the laminate equivalent elastic constants. However, when the fibres are oriented at an angle to the y-axis then the laminate equivalent elastic constants will vary in their magnitude as given by equations (3.6) to (3.11).

A computer program based on existing laminate theory [1,2] was written (see Appendix (C)) and initially the effect of fibre orientation on the laminate equivalent elastic constants was studied with hypothetical laminate material properties. The ratio of Young's modulus along the fibres, E_ℓ to the shear modulus G was varied and the results were plotted as shown in Figure (3.3). The plots suggest that a higher E_ℓ to G ratio will bring sharp changes in the laminate equivalent elastic constants as the ply orientation is changed from 0° to 45°. In the case of an E_ℓ to G ratio of 2 the changes are almost negligible.

The calculations were then carried out for the typical composite materials. The elastic properties were based on fibres in epoxy resin matrix at a nominal 60% fibre volume fraction. The corresponding E_ℓ to G ratios are given below :

1. Unidirectional E glass	10.0
2. Woven E Glass	5.0
3. Woven Glass (hand-lay-up)	14.0
4. Unidirectional Kevlar	40.0
5. Woven Kevlar	8.5

6. Unidirectional Xas Carbon	27.0
7. Woven Xas	12.5
8. Unidirectional H.M. Carbon	40.6
9. Unidirectional Boron	37.0

The laminate equivalent elastic constants were plotted against the ply orientation angle as shown in Figures (3.4) - (3.6). The study showed that the E/G ratio determines the sensitivity of the laminate equivalent elastic constants to the ply orientation. In the case of materials with higher ratios, change in ply orientation will produce greater effects on the laminate equivalent elastic constants as compared to materials with smaller ratios. These results provide a sensitivity analysis for optimization procedures.

3.5 CONCLUSION

A laminate can be designed to exhibit a desired set of deformations as shown in Figure (3.7). The plate bending stiffness matrix [D] plays a vital role as indicated. The bending and torsional deformations are elastically uncoupled if members in the third row and column of the D-matrix are absent. But if the D-matrix is fully populated, then coupling will exist. The magnitudes and signs of D_{16} and D_{66} determine the direction and the extent of this coupling. A symmetric laminate subjected to bending moments or torques can display coupled transverse displacement and twist, while an antisymmetric laminate subjected to torque or normal loads in tension or compression can exhibit coupled deformations by twisting as well as longitudinal displacement.

The ratio of Young's modulus to the shear modulus, (E/G) plays an important role in the variation of these properties when the orientations of the fibres are changed. Materials with larger ratios will give greater manœuvreability. This quality will eventually help in making the choice of the material for a particular application.

REFERENCES

1. Tsai, S.W. and Hahn, H.T., Introduction of Composite Materials, Technomic, Westport, CT. 1980.

2. Jones, R.M., Mechanics of Composite Materials, Scripta Book Company, Washington, D.C., 1975.

3. Shirk, M.H. and Griffin, K.E., "The Role of Aeroelasticity in Aircraft Design with Advanced Filamentary Composite Materials," Proceedings of the 2nd Conference on Fibrous Composites in Flight Vehicle Design, AFFDL-TR-74-103, May 1974, pp. 405-438.

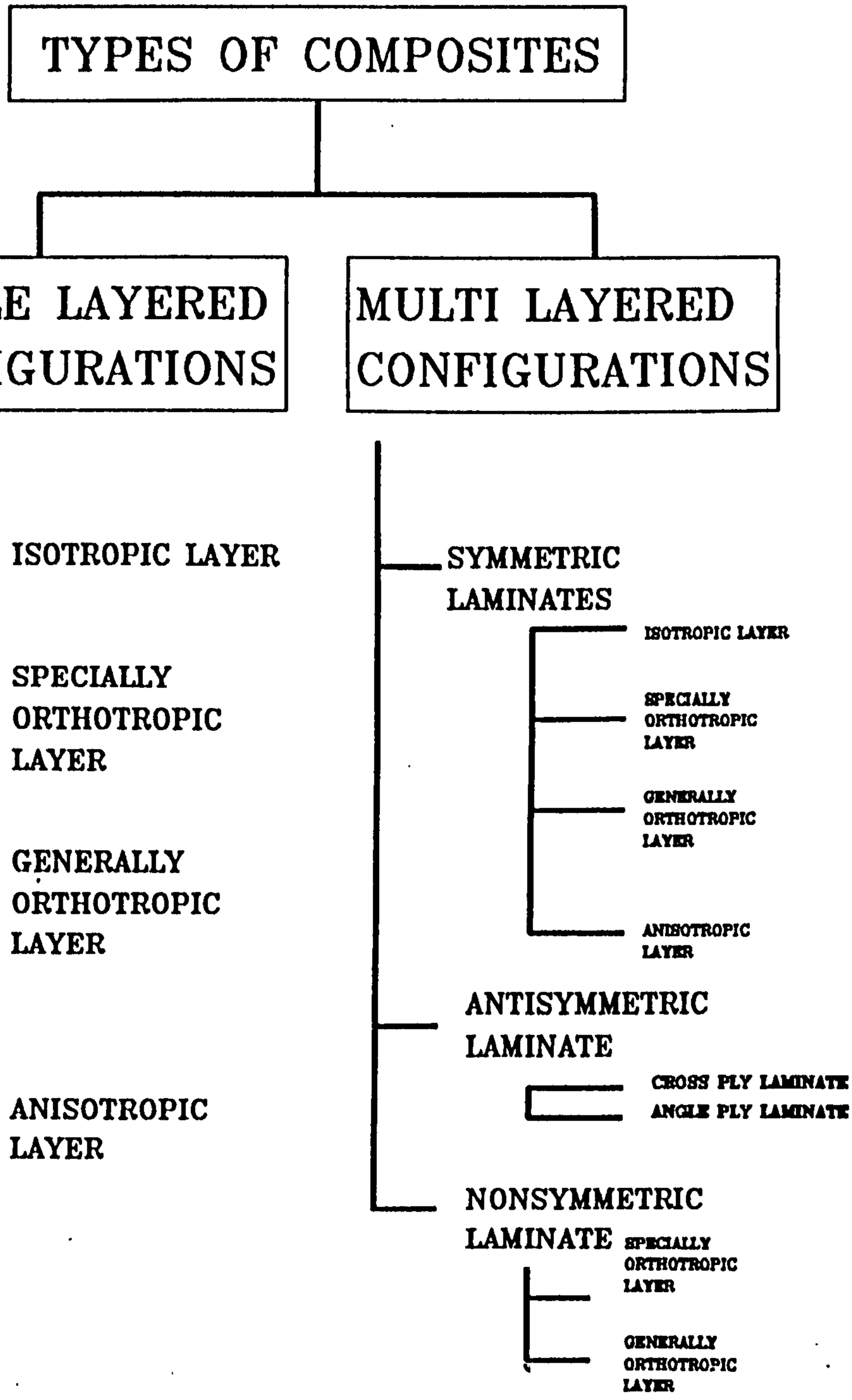

Figure 3.1 Types of composites

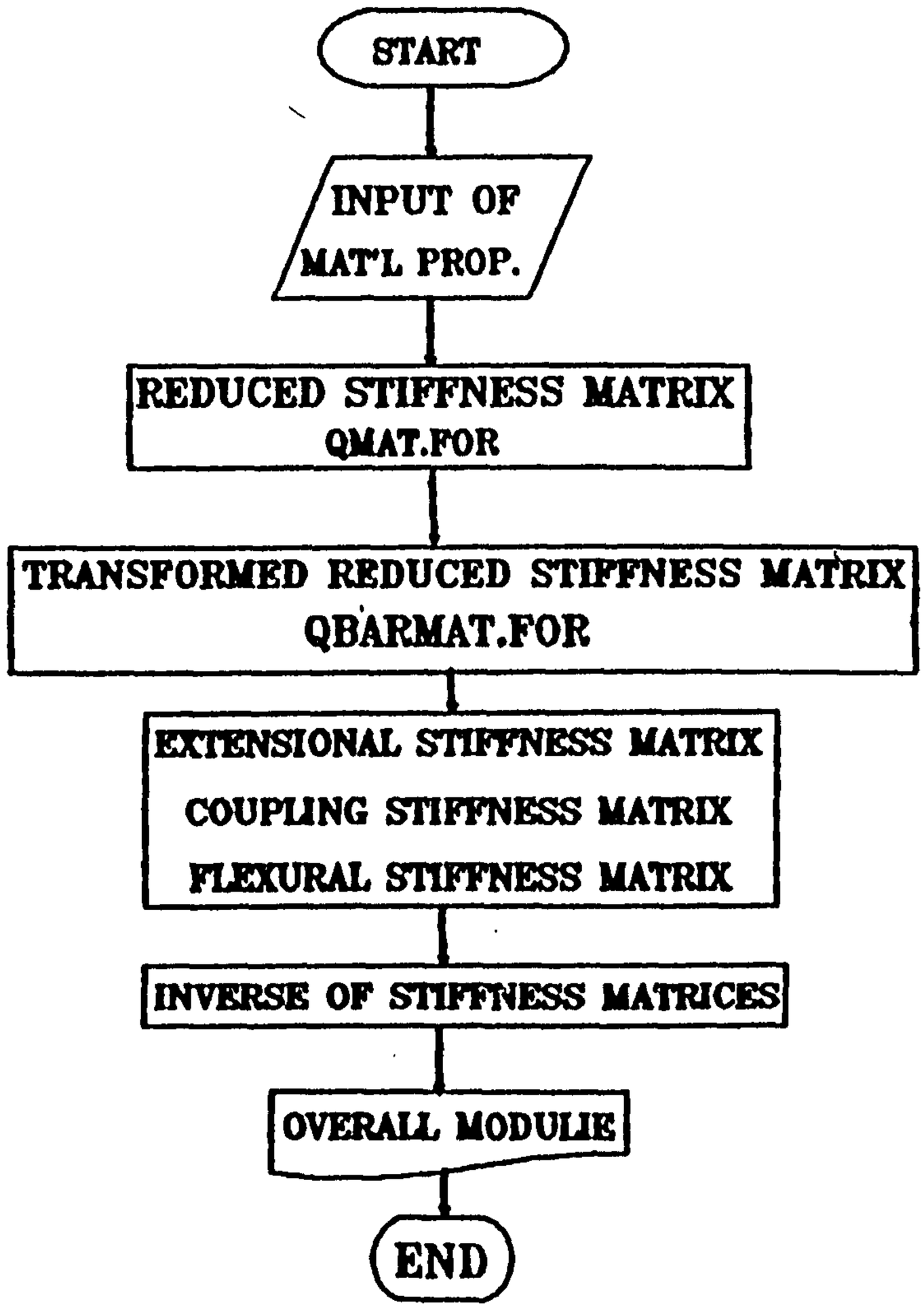

Figure 3.2 Flow Chart for LAMINATE Computer Program

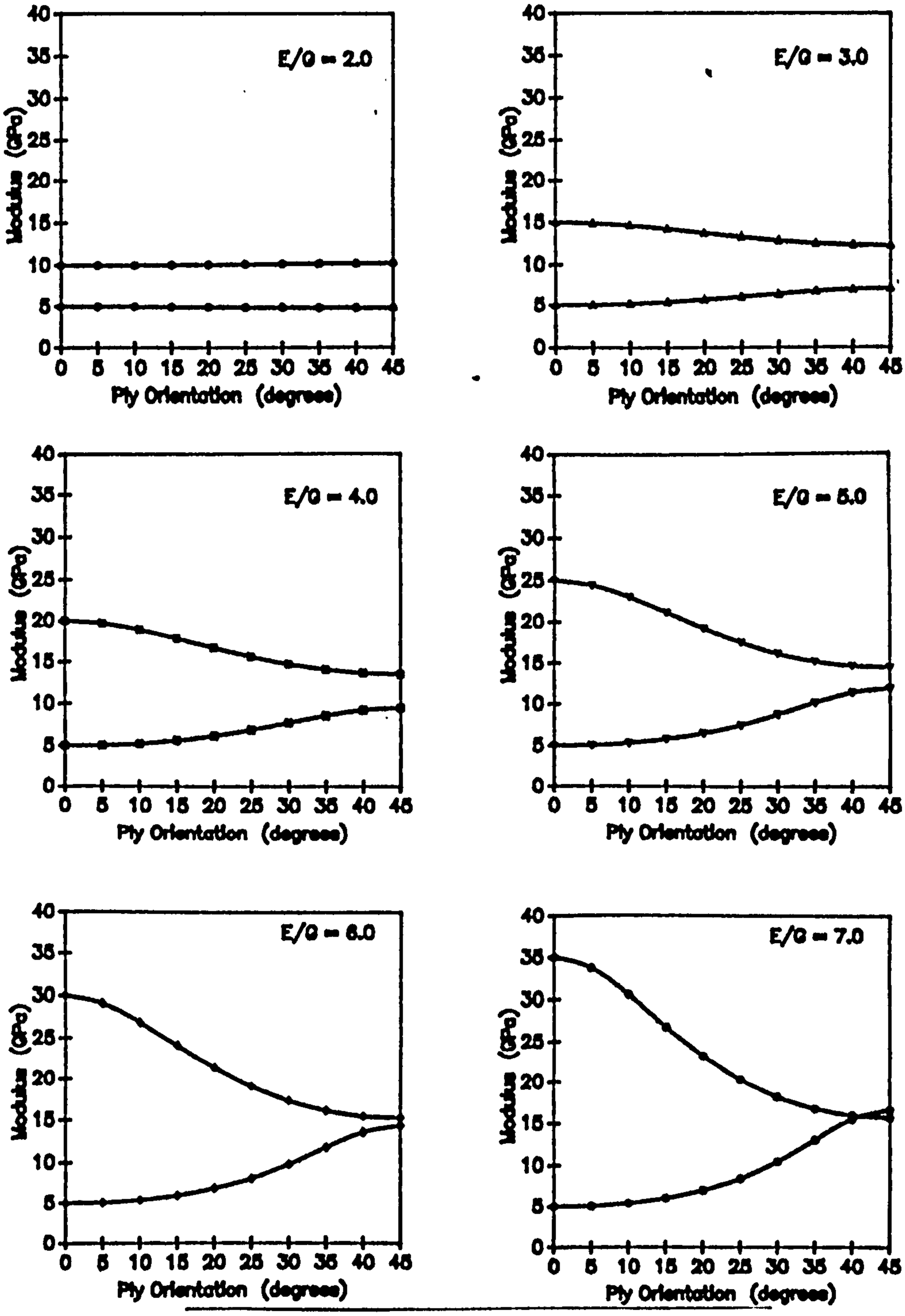

Figure 3.3 Effect of ply orientation on the laminate equivalent elastic constants (fibre volume fraction 60%)

□ – Young's modulus of elasticity (GPa)
■ – Shear modulus of rigidity (GPa)

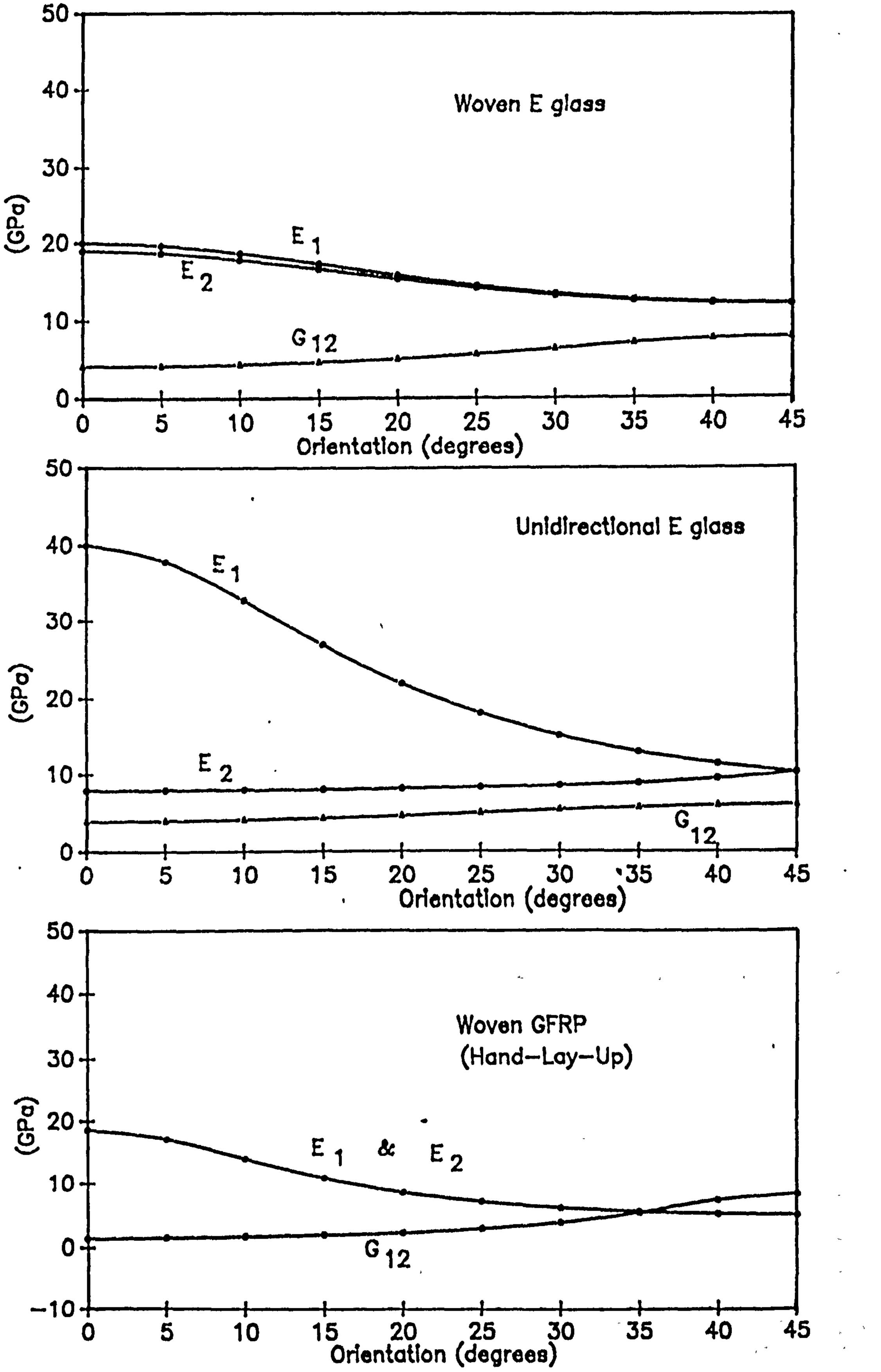

Figure 3.4 Effect of ply orientation on the laminate equivalent elastic constants of a single ply glass/epoxy laminate with 60% fibre volume fraction

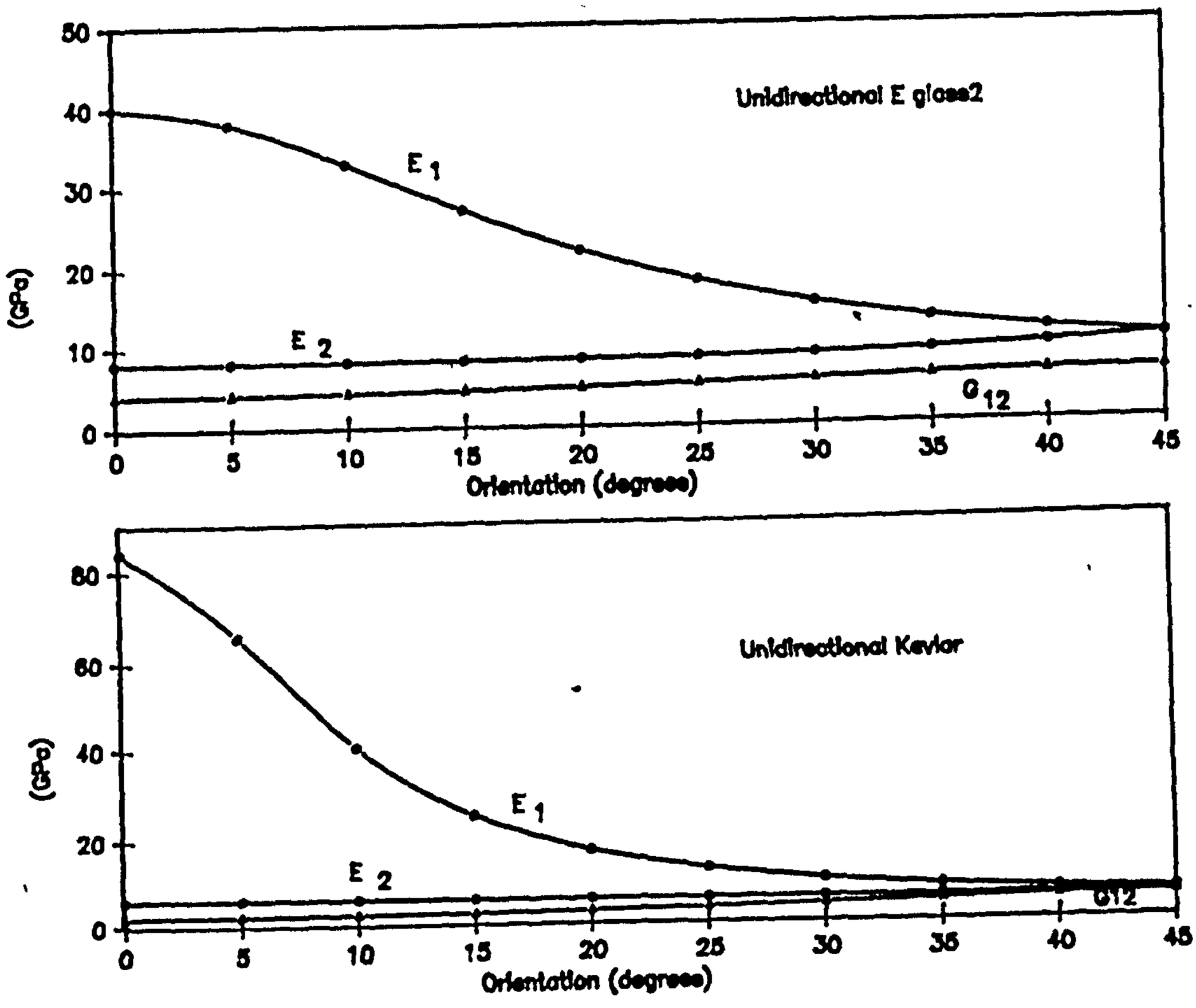

Figure 3.5 Effect of ply orientation on the laminate equivalent elastic constants of unidirectional composites with 60% fibre volume fraction

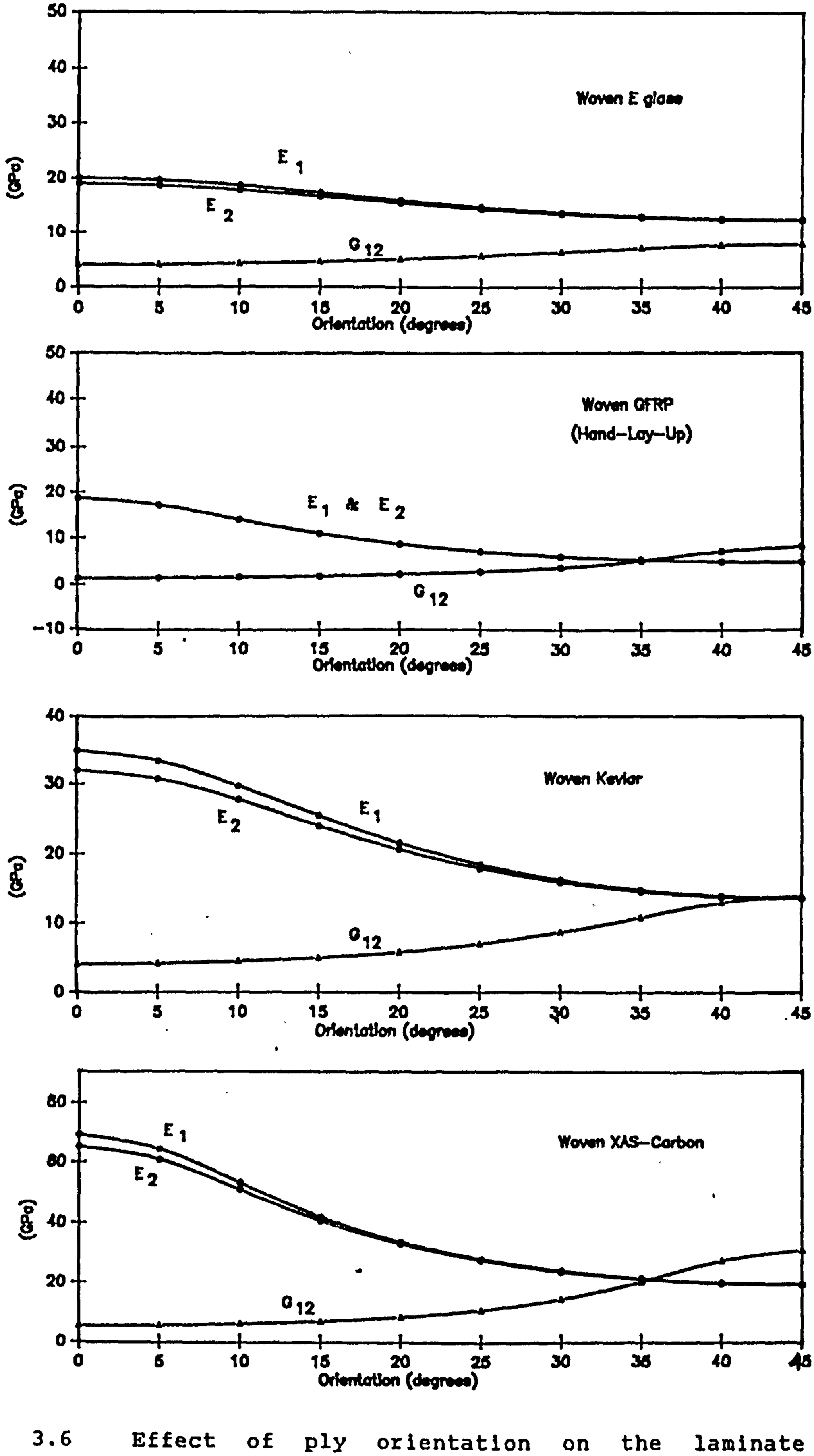

Figure 3.6 Effect of ply orientation on the laminate equivalent elastic constants of woven composites with 60% fibre volume fraction

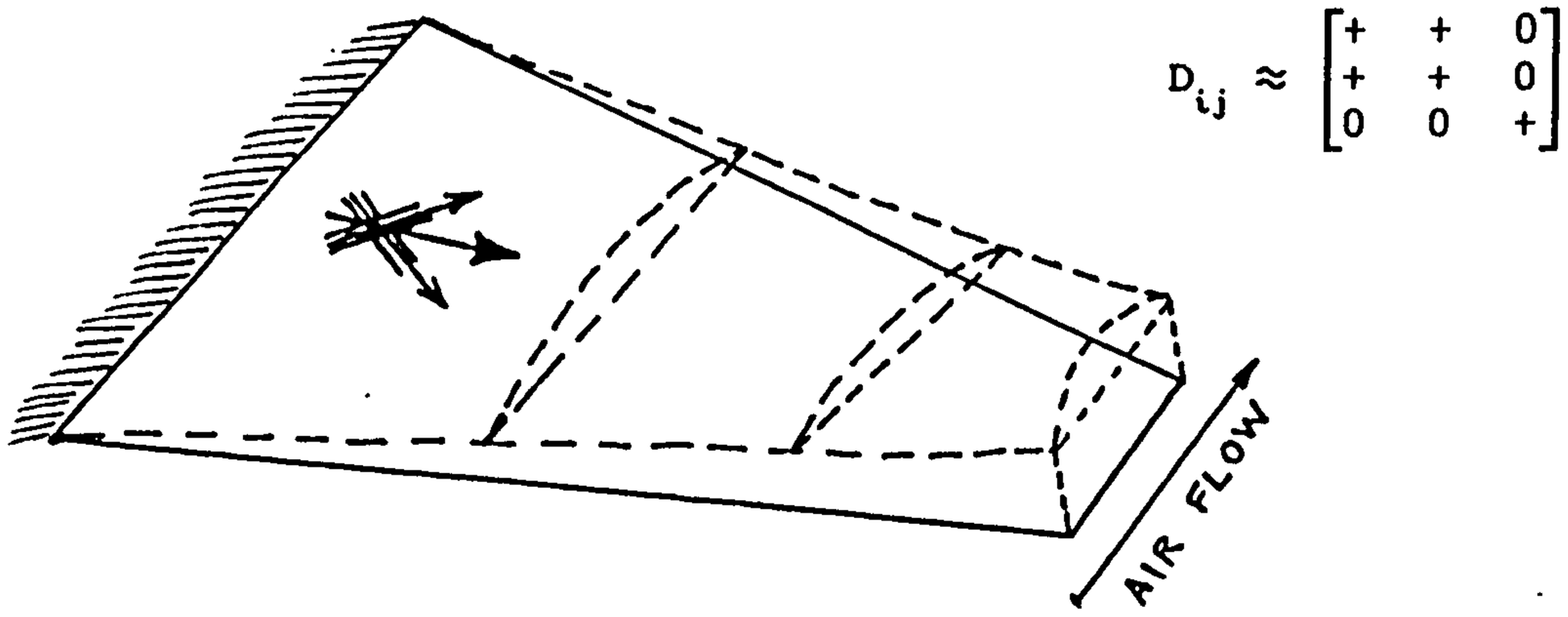

ORTHOTROPIC CHORD-SPAN BENDING COUPLING

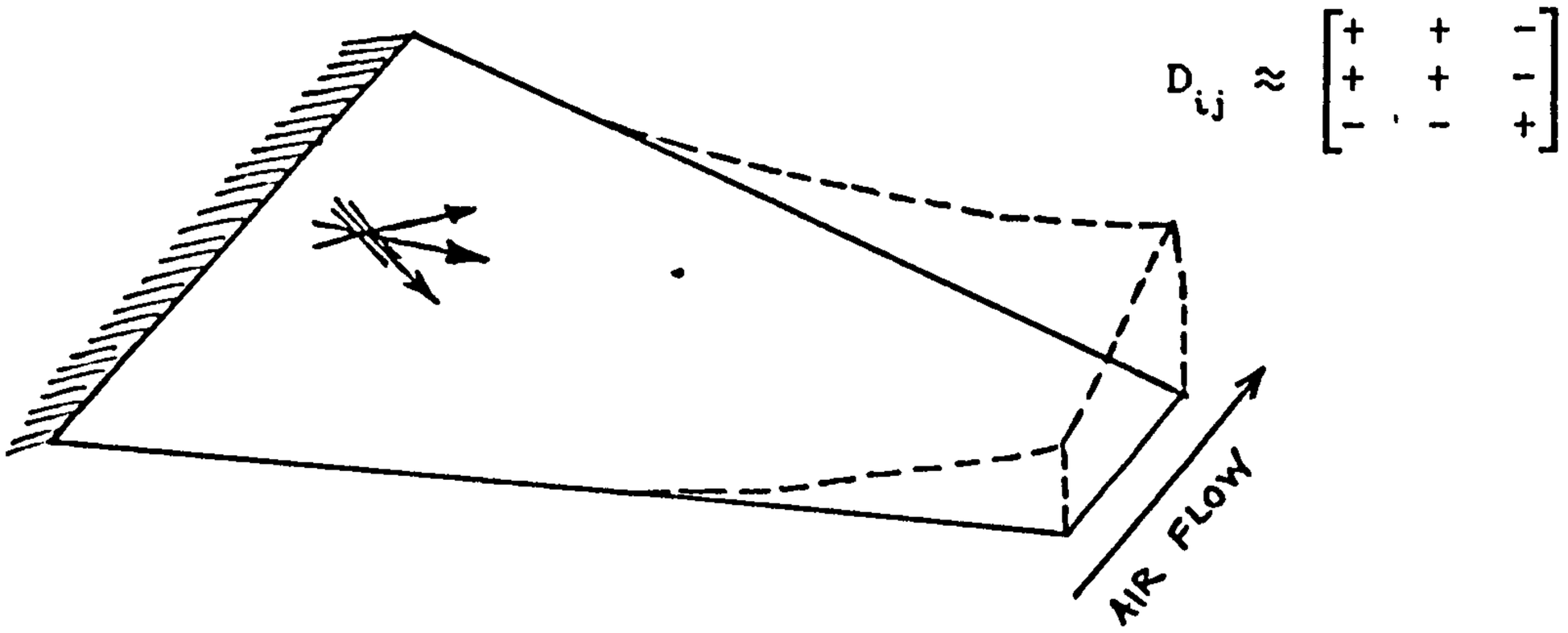

ANISOTROPIC BENDING-TWIST COUPLING (WASH-OUT)

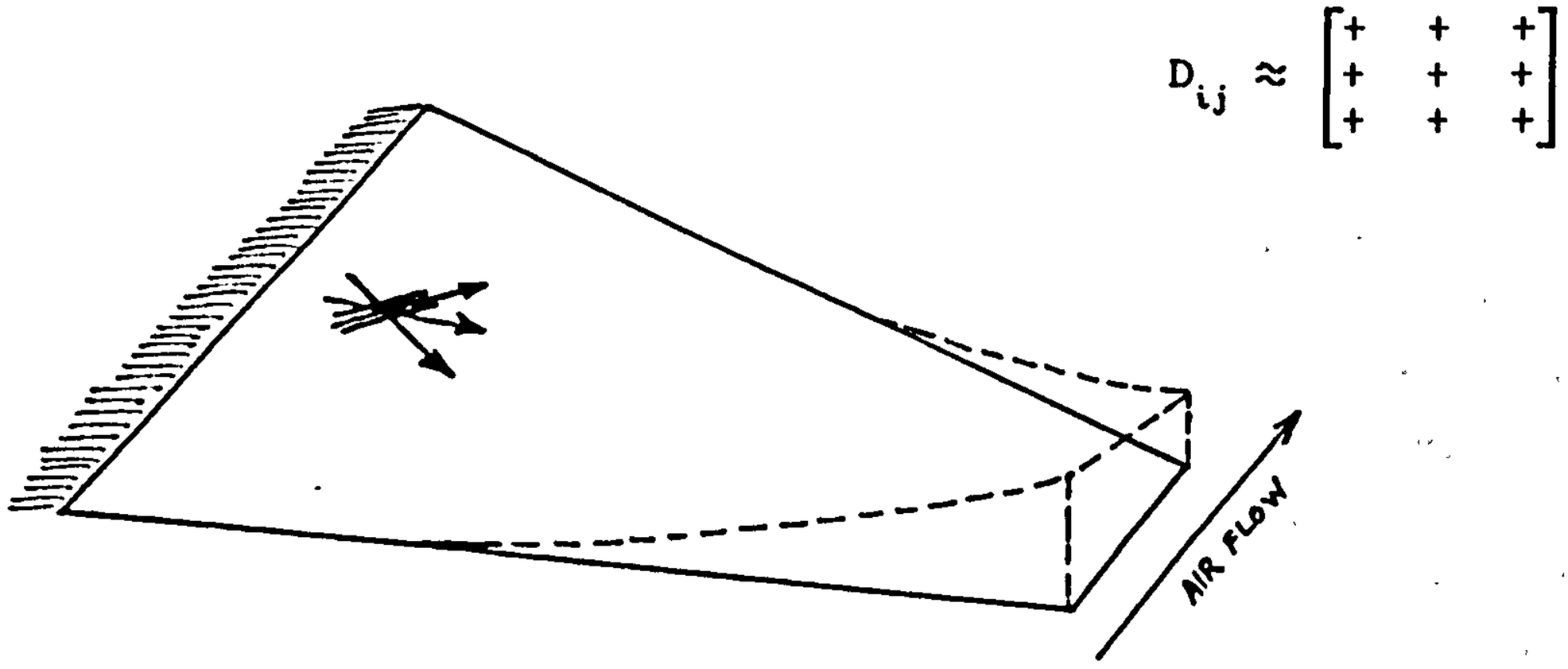

ANISOTROPIC BENDING-TWIST COUPLING (WASH-IN)

Figure 3.7 Coupled deflection shapes

CHAPTER : 4

STRUCTURAL PROPERTIES OF COMPOSITE BEAMS AND PLATES

4.1 INTRODUCTION

The successful prediction of dynamic characteristics of a structure like an aircraft wing depends on adequate knowledge of the static structural properties such as bending and torsional stiffnesses, and the shear centre location. The mass per unit length and polar mass moment of inertia of the structure are also important parameters which influence the dynamic behaviour of the structure. For isotropic materials, theoretical models for the prediction of these properties and experimental procedures have already been established and in the past two decades considerable efforts have been made in obtaining estimates of structural properties of composite structures. A summary of some of these works is given in the next section.

In the case of isotropic materials, the properties such as Young's modulus and shear modulus are independent of the cross-section of the structure and the loading conditions. But for composite materials, due to the fibrous nature of its make-up, the material characteristics will vary with the orientation of the fibres, the stacking sequence of the plies, the cross-section of the structure, and the loading conditions. The cross-section of the structure and the loading conditions will affect the mode of deformation and eventually the stress-strain conditions in the structure, thus requiring a completely different set of equations to calculate the material properties. (The laminate equivalent elastic constants based on membrane mode and bending mode deformations have been discussed in Chapter (3).)

Once the material properties are evaluated then sectional characteristics can be investigated. For instance, the shear centre location for a cross-section is purely a sectional property depending on the geometry of the section. But in the case of composite materials the location of the shear centre is also influenced by the laminate material properties which again depend on the laminate stacking sequence.

4.2 REVIEW OF THE LITERATURE

In the case of infinitely long beams made of conventional materials, effects of shear lag and shear deformation are small enough to be neglected and the bending stiffness will be simply the product of Young's modulus of elasticity and the second moment of the area of cross-section. But in the case of thin-walled beams, these effects cannot be ignored. Mansfield's analysis [1] of a thin-walled cylindrical rectangular cross-section with significant shear lag and shear deflection effects (see Appendix (A)) is a good example.

Introduction of composite materials in aircraft structures has added the material coupling stiffness term to the complexity of the problem. Housner and Stein [2], provided the model for balanced ply i.e. symmetrical laminates. The bending and torsional stiffnesses were assumed to arise solely from thin laminated composite cover-sheets forming the upper and lower surfaces of the wing. The equivalent bending and torsional stiffnesses of the resulting box beam were computed by using classical Euler-Bernoulli beam deformation assumptions (see Appendix (A)).

The same structural idealization was used by Weisshaar [3,4] when he investigated the divergence behaviour of forward swept composite wings. He also conducted a systematic study of bending-twisting and

extension-twisting stiffness coupling terms for linear displacements [3,4].

Mansfield and Sobey [3] treated the composite thin cylindrical tube (beam) composed of an arbitrary lay-up of fibre composite plies. Expressions were derived for the coupled torsional, extensional and bending stiffnesses for linear displacements (see Appendix (B)). Libove [6], presented more or less the same theory in later years and admitted that at the time of his investigations he was not aware of Mansfield and Sobey's contributions to the subject [3].

Hong and Chopra [7,8] developed a non-linear analysis for thin-walled composite beams undergoing transverse bending (flap and lag), torsion and axial deflections, based on nonlinear strain displacement relations of Hodges and Dowell [9]. A simple analytical expression was given for the cross-sectional warping, while effects of transverse shear were neglected. Later extensive investigations of the behaviour of structural coupling terms due to ply orientations were made by Chandra, Stemple, and Chopra [10] and Smith and Chopra [11]. A direct analytical method for the prediction of the effective elastic stiffnesses and corresponding load-deformation behaviour of composite symmetric and anti-symmetric box-beam structures was developed (see Appendix (B)).

The concept of the shear centre can be dated back as early as 1920 when Eggensschwyler and Maillart [12] for the first time defined the concept of the shear centre and advocated the idea that the centroid is not the only characteristic point of the cross-section. In the case of thin-walled beams made of isotropic materials, a single point i.e. the shear centre can be located in the cross-section through which shear loads produce no twisting. This point is a geometric property

of the cross-section and is independent of the loading. In the case of thin-walled composite beams, the local rate of twist not only depends on the torque and the shear forces but also varies with the axial load applied and moments about chordwise and spanwise axes [σ].

The estimation of structural properties of isotropic/conventional material structures will be discussed briefly in this Chapter. Composite structures with various cross-sections will be analysed for the estimation of structural properties by means of a variety of theoretical models which represent the actual structure. The procedures for the experimental determination of bending-torsion coupling stiffness for symmetric laminates and extension-torsion coupling stiffness for the antisymmetric laminates are evaluated.

The effect of shear deformation on the resulting bending deformation is studied with special reference to composite structures. The effect of the warping inertia term on open sections which causes substantial differences between the predicted and experimental results are also discussed.

4.3 STRUCTURAL STIFFNESS

The stiffness of a structure is its resistance to deformation as the structure comes in contact with an unbalanced system of forces and moments. It primarily depends on the material property and the geometry of the cross-section. Therefore, a desired magnitude of stiffness can be achieved by selecting from a range of materials and varying the geometrical parameters such as size and shape of the cross-section. In the case of composite materials the fibre orientation and the laminate stacking sequence gives a wide number of possibilities of achieving certain values of stiffness.

In the case of thin-walled beams, bending or

bending stiffness EI, torsional stiffness GJ, extensional stiffness EA, and warping stiffness EΓ are often considered. In the case of composite materials the bending-torsion coupling stiffness K_b for symmetric laminates and the extension-torsion coupling stiffness K_a for antisymmetric laminates are further added to the above list of stiffnesses. The accurate determination of these stiffnesses ensures a correct prediction of natural frequencies of the structure.

In the case of isotropic materials the task of calculating the stiffnesses mainly involves the computation of the geometrical properties i.e. area of the section, second area moment, warping inertia term, etc. Once these properties are computed, the stiffnesses are then the product of the moduli of the material and the geometric properties of the section. But in the case of anisotropic materials like composites, the task is not straightforward and is two-fold. Firstly the laminate equivalent elastic constants are evaluated and secondly the sectional properties are determined. Another approach can be followed is that of the macro-mechanics of the composites, where the overall stiffness estimation can be obtained by developing the stiffness matrix that will relate the stresses to the strains. In the latter approach, material and sectional details both go into the analysis together. Both methods will be discussed after a brief account is given concerning isotropic materials.

4.3.1 STIFFNESS ESTIMATION OF ISOTROPIC STRUCTURES

In the case of conventional isotropic materials, the material moduli are independent of the cross-sectional details and the boundary conditions of the structure. The cross-sectional area, second area moment, warping inertia, and Saint Venant torsion constant for various

shapes are well known quantities. A comprehensive list of these properties can be found in reference [19]. The product of appropriate quantities such as Young's modulus of elasticity multiplied with the second area moment will give the bending or flexural stiffness and similarly, the Saint Venant torsion constant times the shear modulus of stiffness will give the measure of the torsional stiffness of the structure, etc.

4.3.2 STIFFNESS ESTIMATION OF COMPOSITE STRUCTURES

In the case of composite structures, the material moduli and cross-sectional details can both vary. The geometry along with the loading conditions will influence the procedures through which the moduli of the material are to be obtained. Thus, for example, at times, laminate equivalent elastic constants based on longitudinal modes may be required while in other cases laminate elastic constants based on bending modes will be desired. For some geometries it may be possible to compute laminate equivalent elastic constants and sectional properties separately and the product of both will give the stiffness; but in other cases it will be desirable to approach the problem in a unified manner i.e. the stiffnesses are computed directly.

THEORY

The right-handed Cartesian axes in the discussion to follow are assigned in such a way that x, y, and z - axes refers to the chordwise and spanwise (along the flexural axis of the structure) direction and that orthogonal to both x and y-axes respectively. The composite fibre axes 1, 2, and 3 refers to longitudinal, transverse and out of the plane of the lamina respectively. The macro-mechanics of composite materials assume that if the laminate is

specially orthotropic then the fibre axis 1 is along the x-axis of the structure. Thus in case of generally orthotropic laminates the fibre angle is measured from the x-axis as shown in Figure (4.1a). However, in this work the fibre axis is usually at an angle with the y-axis and in the case of specially orthotropic laminates, the fibres will be aligned with the y-axis.

A summary of the theoretical prediction of bending, torsional, and bending/torsional material coupling stiffnesses will be discussed for various structural elements (in the order of their degree of complexity) as follows :

(i) BEAM ELEMENT :

The moment-curvature and inplane stress-strain relations for the general case of a laminate are (given by equations (3.1a) and (3.1b) of Chapter (3)) as follows:

$$\begin{Bmatrix} N \\ M \end{Bmatrix} = \begin{bmatrix} A & B \\ B & D \end{bmatrix} \begin{Bmatrix} \varepsilon \\ K \end{Bmatrix} \qquad (4.1)$$

where $N = \begin{Bmatrix} N_x \\ N_y \\ N_{xy} \end{Bmatrix}$ = inplane forces

$M = \begin{Bmatrix} M_x \\ M_y \\ M_{xy} \end{Bmatrix}$ = bending and twisting moments

$K = \begin{Bmatrix} K_x \\ K_y \\ K_{xy} \end{Bmatrix}$ = bending and twisting curvatures

where

A_{ij}, B_{ij}, D_{ij} = inplane, coupled and flexural moduli respectively

For a symmetric laminate B_{ij} will vanish. Therefore, flexural and longitudinal modes will uncouple. If a beam as shown in Figure (4.1b) has bending moment M_x and an end torque M_{xy} but no chordwise bending moment M_y, then the equation (4.1) will reduce to :

$$\begin{Bmatrix} M_x \\ 0 \\ M_{xy} \end{Bmatrix} = \begin{bmatrix} D_{11} & D_{12} & D_{16} \\ D_{21} & D_{22} & D_{26} \\ D_{61} & D_{62} & D_{66} \end{bmatrix} \begin{Bmatrix} K_x \\ K_y \\ K_{xy} \end{Bmatrix} \qquad (4.2)$$

or

$$M_x = D_{11} K_x + D_{12} K_y + D_{16} K_{xy} \qquad (4.3a)$$

$$0 = D_{21} K_x + D_{22} K_y + D_{26} K_{xy} \qquad (4.3b)$$

$$M_{xy} = D_{61} K_x + D_{62} K_y + D_{66} K_{xy} \qquad (4.3c)$$

The second equation will yield

$$K_y = - (D_{21} K_x + D_{26} K_{xy}) / D_{22} \qquad (4.4)$$

Therefore,

$$M_x = \left(D_{11} - \frac{D_{12}^2}{D_{22}}\right) K_x + \left(D_{16} - \frac{D_{12} D_{26}}{D_{22}}\right) K_{xy} \qquad (4.5)$$

and similarly

$$M_{xy} = \left(D_{16} - \frac{D_{12} D_{26}}{D_{22}}\right) K_x + \left(D_{66} - \frac{D_{26}^2}{D_{22}}\right) K_{xy} \qquad (4.6)$$

Therefore, in matrix form

$$\begin{Bmatrix} M_x \\ M_{xy} \end{Bmatrix} = \begin{bmatrix} \left(D_{11} - \frac{D_{12}^2}{D_{22}}\right) & \left(D_{16} - \frac{D_{12}D_{26}}{D_{22}}\right) \\ \left(D_{16} - \frac{D_{12}D_{26}}{D_{22}}\right) & \left(D_{66} - \frac{D_{26}^2}{D_{22}}\right) \end{bmatrix} \begin{Bmatrix} K_x \\ K_{xy} \end{Bmatrix}$$

or

$$\begin{Bmatrix} M_x \\ M_{xy} \end{Bmatrix} = \begin{bmatrix} K_{11} & K_{16} \\ K_{16} & K_{66} \end{bmatrix} \begin{Bmatrix} K_x \\ K_{xy} \end{Bmatrix} \qquad (4.7)$$

where K_{11} = corresponds to bending stiffness EI

K_{66} = corresponds to torsional stiffness GJ

K_{16} = bending/torsional coupling stiffness K_s

(ii) THIN PLATE ELEMENT :

A plate is a three dimensional sheet of elastic material which lies in a plane. Plates possess bending stiffness as a result of their thickness and the elasticity of the plate material. As the plate deflects, the mid-surface of the plate (half way between the top and bottom surfaces i.e. neutral surface) remains unstressed. At all other points there is a biaxial state of stress. Normals to the mid-surface remain normal as the plate deflects. The stresses and strains are proportional to the distance from the mid-surface. The maximum stresses and strains are thus at the surface of the plate. For an isotropic plate lying in the x-y plane, the normal strains (ε_x and ε_y) and shear strain (ε_{xy}) in the plane of the plate are

$$\varepsilon_x = - z \frac{\partial^2 w}{\partial x^2}$$

$$\varepsilon_y = - z \frac{\partial^2 w}{\partial y^2} \qquad (4.8)$$

$$\varepsilon_{xy} = - 2 z \frac{\partial^2 w}{\partial x \partial y}$$

If the out-of-plane strains are absent, then

$$\varepsilon_{xz} = \varepsilon_{yz} = \varepsilon_{zz} = 0$$

where z is the distance perpendicular to the plate mid-surface and w is the transverse deflection of the plate mid-surface. These strains are associated with the following stresses for a homogeneous isbtropic material:

$$\sigma_{xx} = \frac{E}{(1-\nu^2)} (\varepsilon_x + \nu \varepsilon_y)$$

$$\sigma_{yy} = \frac{E}{(1-\nu^2)} (\varepsilon_y + \nu \varepsilon_x) \qquad (4.9a)$$

$$\sigma_{xy} = G \varepsilon_{xy} \quad , \quad \sigma_{xz} = \sigma_{yz} = \sigma_{zz} = 0 \qquad (4.9b)$$

where E = Young's modulus

G = shear modulus

ν = Poisson's ratio

For anisotropic (composite) materials:

$$\begin{Bmatrix} \sigma_{xx} \\ \sigma_{yy} \\ \sigma_{xy} \end{Bmatrix} = \begin{bmatrix} \bar{Q}_{11} & \bar{Q}_{12} & \bar{Q}_{16} \\ \bar{Q}_{21} & \bar{Q}_{22} & \bar{Q}_{26} \\ \bar{Q}_{16} & \bar{Q}_{26} & \bar{Q}_{66} \end{bmatrix} \begin{Bmatrix} \varepsilon_{xx} \\ \varepsilon_{yy} \\ \varepsilon_{xy} \end{Bmatrix} \qquad (4.10)$$

where the first subscript refers to the normal to the face on which the stress acts; the second subscript is the direction of the stress. Thus in equation (4.10) σ_{xx} and σ_{yy} are the normal stresses and σ_{xy} is the shear stress. These stresses are shown schematically in Figure (4.2). (Note that σ_{zz} is ignored in the thin plate theory).

$\left.\begin{matrix} M_x \\ M_y \end{matrix}\right\}$ = bending moment , M_{xy} = twisting moment

For an isotropic plate

$$M_x = -\int_{-h/2}^{h/2} \sigma_{xx}\, z\, dz = \frac{E\, h^3}{12\,(1-\nu^2)} \left[\frac{\partial^2 z}{\partial x^2} + \nu \frac{\partial^2 z}{\partial y^2}\right] \qquad (4.11a)$$

$$M_y = -\int_{-h/2}^{h/2} \sigma_{yy}\, z\, dz = \frac{E\, h^3}{12\,(1-\nu^2)} \left[\frac{\partial^2 z}{\partial y^2} + \nu \frac{\partial^2 z}{\partial x^2}\right] \qquad (4.11b)$$

$$M_{xy} = -\int_{-h/2}^{h/2} \sigma_{xy}\, z\, dz = \frac{E\, h^3}{12\,(1+\nu)} \frac{\partial^2 z}{\partial x \partial y} \qquad (4.11c)$$

The integrals are taken through the thickness of the plate. However in case of an anisotropic (composite) plate :

$$\begin{Bmatrix} M_x \\ M_y \\ M_{xy} \end{Bmatrix} = \begin{bmatrix} D_{11} & D_{12} & D_{16} \\ D_{21} & D_{22} & D_{26} \\ D_{16} & D_{26} & D_{66} \end{bmatrix} \begin{Bmatrix} K_{xx} \\ K_{yy} \\ K_{xy} \end{Bmatrix} \qquad (4.12)$$

where

$$K_{xx} = -\frac{\partial^2 w}{\partial x^2} \quad ; \quad K_{yy} = -\frac{\partial^2 w}{\partial y^2} \quad ; \quad K_{xy} = -2\frac{\partial^2 w}{\partial x \partial y}$$

Re-arranging equation (4.12) :

$$\begin{Bmatrix} K_{xx} \\ K_{yy} \\ K_{xy} \end{Bmatrix} = \begin{bmatrix} D_{11} & D_{12} & D_{16} \\ D_{21} & D_{22} & D_{26} \\ D_{16} & D_{26} & D_{66} \end{bmatrix}^{-1} \begin{Bmatrix} M_x \\ M_y \\ M_{xy} \end{Bmatrix} \qquad (4.13)$$

In the absence of chordwise moment and torque, the following relation between spanwise curvature and bending moment is obtained :

$$K_{xx} = D^*_{11}\, M_x \qquad (4.14)$$

where D^*_{11} is the element of the inverse matrix.

Comparing equation (4.14) with the bending moment and curvature relationship for a beam made of isotropic material $EI \frac{\partial^2 w}{\partial x^2} = - M$, an expression is obtained for the bending stiffness of the anisotropic plates

$$EI = c / D^*_{11} \qquad (4.15)$$

where c is the chord of the plate. Note that moments in equation (4.13) are per unit width of the plate. Similarly, assuming the presence of only torsional load on the plate will give the following relation :

$$K_{xy} = D^*_{\sigma\sigma} M_{xy} \qquad (4.16)$$

Further comparison with the similar relation in the case of isotropic materials $\tau = GJ \frac{\partial \theta}{\partial x}$; where τ is the applied torque and $\theta = \frac{\partial w}{\partial y}$ is the angle of twist, will give the following expression for the torsional stiffness of the plate :

$$GJ = 2 c / D^*_{\sigma\sigma} \qquad (4:17)$$

Structural properties obtained in equations (4.15) and (4.17) are very useful when a plate due to its large aspect ratio can be idealized as a beam structure. These properties can then be entered in dynamic analyses which will be discussed in Chapters (7), (8) and (9) respectively.

For composite symmetrically laminated plates, reference [10] suggests the following expressions for the estimation of bending, torsional, and bending/torsional stiffnesses.

$$K_{22} = c\, D_{11}$$

$$K_{24} = 2\, c\, D_{22} \qquad (4.18)$$

$$K_{44} = 4\, c\, D_{66}$$

where K_{22} = EI = Bending stiffness

K_{24} = K = Bending/torsional coupling stiffness

K_{44} = GJ = Torsional stiffness

c = Chord length or width of the plate

(iii) THIN-WALLED BEAM ELEMENT :

Thin-walled composite cylindrical structures can be divided into two major categories, namely symmetric and antisymmetric. In a symmetric configuration, the ply lay-ups on opposite sides are mirror images with respect to the mid-axis. But in case of the antisymmetric configuration, the ply lay-ups on opposite sides are in reverse order.

For a symmetric laminate, the coupling moduli, B_{ij} will vanish. Therefore, the bending and longitudinal modes of deformation will uncouple.

Furthermore, thin-walled beams can be divided into closed sections and open sections. First the stiffness estimation for closed sections will be discussed. The discussion on open sections will follow.

(a) CLOSED SECTIONS :

(a1) GENERAL CASE WITH ARBITRARY CROSS SECTION

A cylindrical tube subjected to torsion, bending and longitudinal tension using cylindrical coordinates as shown in Figure (4.5) and in the absence of circumferencial stresses and strains has been analysed by

Mansfield and Sobey [5] (see Appendix (B)). Equations (B.1.4) to (B.1.7) of Appendix (B) give relationships between the longitudinal tension, spanwise and chordwise bending moments and torque to their respective rate of deformations respectively. A global stiffness matrix can be obtained by writing these equations in a matrix form as follows :

$$\begin{Bmatrix} P \\ M_x \\ M_z \\ M_y \end{Bmatrix} = \begin{bmatrix} \oint H_{11}ds & -\oint H_{21}ds & & 0 \\ 0 & -\oint z\, H_{21}ds & \oint z^2 H_{11}ds & 0 \\ 0 & \oint x\, H_{21}ds & 0 & \oint x^2 H_{11}ds \\ 0 & 2\,A & 0 & \end{bmatrix} \begin{Bmatrix} \varepsilon_o \\ N_{ys} \\ K_x \\ K_z \end{Bmatrix} \tag{4.19}$$

All the terms in equation (4.19) are in the usual notation that have been defined in Appendix (B) (also see list of notation). Substitution of normal strains, curvatures and twist for the shear flow N_{ys} in the structure will result in a fully populated stiffness matrix. A simplified stiffness matrix for a mirror-wise, symmetrically laminated composite tube is obtained as follows [5].

$$\begin{Bmatrix} M_x \\ M_y \end{Bmatrix} = \begin{bmatrix} \oint z^2 H_{11}ds + \dfrac{\left[\oint z\, H_{21}ds\right]^2}{\oint H_{22}ds} & -2A\,\dfrac{\oint z\, H_{21}ds}{\oint H_{22}ds} \\ -2A\,\dfrac{\oint z\, H_{21}ds}{\oint H_{22}ds} & \dfrac{4\,A^2}{\oint H_{22}ds} \end{bmatrix} \begin{Bmatrix} K_x \\ \dfrac{d\theta}{dy} \end{Bmatrix} \tag{4.20}$$

Equation (4.20) give following expressions for the

bending, torsional and coupled (bending/torsional) stiffnesses of a symmetrically laminated mirror-wise thin-walled composite tube.

$$EI = \oint z^2 H_{11} ds + \frac{\left[\oint z H_{21} ds\right]}{\oint H_{22} ds} \qquad (4.21)$$

$$GJ = \frac{4 A^2}{\oint H_{22} ds} \qquad (4.22)$$

$$K = -2A \frac{\oint z H_{21} ds}{\oint H_{22} ds} \qquad (4.23)$$

Equation (4.21) suggests that calculation of bending stiffness by means of multiplying the laminate equivalent elastic constant E_x (in the longitudinal direction) with the second area moment of the cross-section will give under estimated results when the fibres are at angles other than 0 and 45 degrees. The estimation of torsional stiffness will produce similar results with both techniques.

(a2) BOX BEAM CROSS SECTION

A similar analysis for the prediction of stiffnesses applicable to box-beam structures has been given by Chopra et al [9] (see Appendix (B)). The circumferencial strains are not assumed to be zero as compared with Mansfield and Sobey's approach [5]. The theory is initially developed for a box beam geometry but with a few substitutions the analysis can be adopted for any arbitrary cross-section.

The x and y axes are aligned with the chordwise and spanwise (flexural axis) axes of the structure respectively. The deformed structure is represented by the orthogonal coordinate system ξ, ζ and η as shown in Figure (4.3a).

The stress-strain relationship for the top and bottom flanges of a box beam shown in Figure (4.3b) is given by the following expression :-

$$\begin{Bmatrix} \sigma_{\xi\xi} \\ \sigma_{\eta\eta} \\ \tau_{\xi\eta} \end{Bmatrix} = \begin{bmatrix} \bar{Q}_{11} & \bar{Q}_{12} & \bar{Q}_{16} \\ \bar{Q}_{12} & \bar{Q}_{22} & \bar{Q}_{26} \\ \bar{Q}_{16} & \bar{Q}_{26} & \bar{Q}_{66} \end{bmatrix} \begin{Bmatrix} \varepsilon_{\xi\xi} \\ \varepsilon_{\eta\eta} \\ \gamma_{\xi\eta} \end{Bmatrix} \qquad (4.24)$$

where $\bar{Q}$ = transformed reduced stiffness matrix of the kth lamina in the ξ-η (or ξ-ζ) plane. Since $\sigma_{\eta\eta} = 0$ equation (4.24) can be simplified by solving for $\varepsilon_{\eta\eta}$ as shown below:

$$\begin{Bmatrix} \sigma_{\xi\xi} \\ \\ \tau_{\xi\eta} \end{Bmatrix} = \begin{bmatrix} \bar{C}_{11} & \bar{C}_{16} \\ \\ \bar{C}_{16} & \bar{C}_{66} \end{bmatrix} \begin{Bmatrix} \varepsilon_{\xi\xi} \\ \\ \gamma_{\xi\eta} \end{Bmatrix}, \qquad (4.25)$$

where

$$\bar{C}_{11} = \bar{Q}_{11} - \frac{\bar{Q}_{12}^2}{\bar{Q}_{22}}$$

$$\bar{C}_{16} = \bar{Q}_{16} - \frac{\bar{Q}_{12}\bar{Q}_{26}}{\bar{Q}_{22}}$$

$$\bar{C}_{66} = \bar{Q}_{66} - \frac{\bar{Q}_{26}^2}{\bar{Q}_{22}}$$

Similarly for left and right flanges with $\sigma_{\zeta\zeta} = 0$, the following relationship can be obtained :

$$\begin{Bmatrix} \sigma_{\xi\xi} \\ \\ \tau_{\xi\zeta} \end{Bmatrix} = \begin{bmatrix} \bar{C}_{11} & \bar{C}_{16} \\ \\ \bar{C}_{16} & \bar{C}_{66} \end{bmatrix} \begin{Bmatrix} \varepsilon_{\xi\xi} \\ \\ \gamma_{\xi\zeta} \end{Bmatrix} \qquad (4.26)$$

A simplified linear analysis is presented for bending and torsion of thin-walled symmetric composite beams based on the coupled nonlinear analysis of Hong and Chopra [9] for a composite helicopter rotor blade subjected to flap bending, lag bending (i.e. chordwise bending), elastic twist, and axial deflections.

$$\begin{Bmatrix} M \\ T \end{Bmatrix} = \begin{bmatrix} EI & K_{PS} \\ K_{PS} & GJ \end{bmatrix} \begin{Bmatrix} \frac{d^2w}{dy^2} \\ \frac{d\phi}{dy} \end{Bmatrix} \qquad (4.27)$$

where

$$EI = \sum_{K=1}^{N} \int\int_{1,2} \bar{C}_{11}^{(K)} \zeta^2 \, d\eta \, d\zeta + \sum_{\ell=1}^{M} \int\int_{3,4} \bar{C}_{11}^{(K)} \zeta^2 \, d\eta \, d\zeta \qquad (4.28a)$$

$$GJ = \sum_{K=1}^{N} \int\int_{1,2} \bar{C}_{\sigma\sigma}^{(K)} \zeta^2 \, d\eta \, d\zeta + \sum_{\ell=1}^{M} \int\int_{3,4} \bar{C}_{\sigma\sigma}^{(K)} \hat{\eta}^2 \, d\eta \, d\zeta \qquad (4.28b)$$

$$K_{P\theta} = \sum_{K=1}^{N} \int\int_{1,2} \bar{C}_{1\sigma}^{(K)} \hat{\zeta} \, \zeta \, d\eta \, d\zeta \qquad (4.28c)$$

Subscripts 1,2 represent the top and bottom of the box and 3,4 represent the left and right sides of the laminated box beam.

N = number of layers in laminate 1 or 2
M = number of layers in laminate 3 or 4

and

$$\hat{\eta} = \eta - \lambda,\zeta \quad \text{and} \quad \hat{\zeta} = \zeta - \lambda,\eta \qquad (4.29)$$

$$\lambda = \text{warping function} = \beta \, \zeta \, \eta = \frac{(c - d)}{(c + d)} \zeta \, \eta \qquad (4.30)$$

(b) OPEN SECTIONS

In the case of open sections, laminate equivalent elastic constants in the bending mode are computed and the sectional constants are calculated assuming that the structure is made of isotropic material. The product of the elastic constants and appropriate cross-sectional constants will give flexural and torsional rigidity values.The last two unified approaches discussed are not applicable due to the reason that the analysis based on equations of equilibrium is valid only for open sections supporting shearing loads and not torsional loads. A complete analysis of the estimation of stiffnesses for open cross-sections is beyond the scope of this work even though some progress has been made. Tests carried out on open sections (reported in Chapter 5) gave large discrepancies between predictions and experimental results which clearly demand a more rigorous analysis of this subject.

4.4 TORSIONAL RIGIDITY OF MULTI-CELL SECTIONS

The torsional rigidity of a single cell structure made of isotropic material is given by the following expression (see Appendix B) :

$$GJ = T \frac{\ell}{\Theta} \qquad (4.31)$$

where J = torsion constant of the cross-section
G = shear modulus of rigidity of the material.

The computation of torsional rigidity of a structure mainly involves the effort of calculating the J value for the cross-section. For a circular cross-section, the torsion constant J is simply equal to the polar second moment of area about the centre. In the case of an open section of thickness t, the torsion constant J is given by [15]:

$$J = \frac{1}{3} \int_0^{\infty} t^3 \, ds \qquad (4.32)$$

and for a single cell thin-walled closed section :

$$J = \frac{4 A^2}{\oint \frac{ds}{t}} \qquad (4.33)$$

In this section of the chapter, an analysis to determine the torsional rigidity of multi-cell structures will be discussed. For the sake of brevity only the two cell section will be discussed in detail. This will be followed by an attempt to generalize the procedure to determine the torsional stiffness for a multi-cell structure with any number of cells.

4.4.1 TWO CELLS

Consider a two-cell section as shown in Figure (4.4a), subjected to a torque T about the shear centre. Assuming that the Bredt-Batho theory of torsion is applicable, the total torque is therefore the sum of the individual torques from each cell, i.e. :

$$T = 2 A_1 q_1 + 2 A_2 q_2 \qquad (4.34)$$

where A_1 and A_2 are cell areas of cell I and II respectively and q_1 and q_2 are shear flows as shown in Figure (4.4). The shear flows in the walls of each cell are in equilibrium at any junction. The rate of twist in each cell is given by

$$\frac{d\theta}{dy} = \frac{1}{2AG} \oint q \frac{ds}{t} \qquad (4.35)$$

The rate of twist in every cell must be equal. Thus

$$\left(\frac{d\theta}{dy} \right)_1 = \left(\frac{d\theta}{dy} \right)_2 = \left(\frac{d\theta}{dy} \right)_{overall} \qquad (4.36)$$

Hence using the right side of equation (4.35)

$$\frac{1}{2A_1G}\left[q_1\left(\frac{b_1}{t_1}+\frac{a}{t_2}+\frac{b_1}{t_2}\right)+\frac{a}{t_4}\left(q_1-q_2\right)\right]=$$

$$\frac{1}{2A_2G}\left[q_2\left(\frac{b_2}{t_5}+\frac{a}{t_6}+\frac{b_2}{t_7}\right)+\frac{a}{t_4}\left(q_2-q_1\right)\right]$$

Substituting $\delta_{10}=\left(\frac{b_1}{t_1}+\frac{a}{t_2}+\frac{b_1}{t_2}\right)$

$$\delta_{12}=\frac{a}{t_4}$$

$$\delta_{20}=\left(\frac{b_2}{t_5}+\frac{a}{t_6}+\frac{b_2}{t_7}\right)$$

the expression simplifies to

$$q_1\left[\delta_{10}+\delta_{12}+\frac{A_1}{A_2}\delta_{12}\right]=q_2\left[\delta_{12}+\frac{A_1}{A_2}\left(\delta_{20}+\delta_{12}\right)\right] \qquad (4.37)$$

Now by considering the first and the last quantities in equation (4.36)

$$\left(\frac{d\theta}{dy}\right)_1=\left(\frac{d\theta}{dy}\right)_{overall}$$

which results after necessary substitution

$$\frac{1}{2A_1G}\left(q_1\delta_{10}+\left(q_1-q_2\right)\delta_{12}\right)=\frac{d\theta}{dy}$$

and further simplification gives

$$\left(\delta_{10}+\delta_{12}\right)q_1-\delta_{12}q_2-2A_1\frac{d\theta}{dy}=0 \qquad (4.38)$$

Rewriting equations (4.34),(4.37) and (4.38) in matrix form :

$$\begin{bmatrix} 2A_1 & 2A_2 & 0 \\ \left(\delta_{10}+\delta_{12}+\frac{A_1}{A_2}\delta_{12}\right) & -\left[\delta_{12}+\frac{A_1}{A_2}\left(\delta_{20}+\delta_{12}\right)\right] & 0 \\ \left(\delta_{10}+\delta_{12}\right) & -\delta_{12} & -2A_1 \end{bmatrix}\begin{bmatrix} q_1 \\ q_2 \\ \frac{d\theta}{dy} \end{bmatrix}=\begin{bmatrix} T \\ 0 \\ 0 \end{bmatrix}$$

or simply

$$[\Delta]\ [q] = [T] \qquad (4.39)$$

Therefore,

$$[q] = [\Delta]^{-1}\ [T]$$

or

$$\begin{bmatrix} q_1 \\ q_2 \\ \frac{d\theta}{dy} \end{bmatrix} = \begin{bmatrix} \Delta^*_{11} & \Delta^*_{12} & \Delta^*_{13} \\ \Delta^*_{21} & \Delta^*_{22} & \Delta^*_{23} \\ \Delta^*_{31} & \Delta^*_{32} & \Delta^*_{33} \end{bmatrix} \begin{bmatrix} T \\ 0 \\ 0 \end{bmatrix} \qquad (4.40)$$

Therefore,

$$\frac{d\theta}{dy} = \Delta^*_{31} T \qquad (4.41)$$

or

$$GJ = \frac{T}{\left[\frac{d\theta}{dy}\right]} = \frac{1}{\Delta^*_{31}} \qquad (4.42)$$

which comes out to be

$$GJ = \left[\frac{\delta_{20} A_1^2 + \delta_{12} A^2 + \delta_{10} A_2^2}{\delta_{12}\delta_{20} + \delta_{10}\delta_{20} + \delta_{10}\delta_{12}} \right] \qquad (4.43)$$

4.4.2 GENERAL EXPRESSION FOR MULTI-CELL STRUCTURES

The application of Bredt-Batho's theory of torsion to n cells will give the following concise expressions :

$$T = 2 \sum_{i=1}^{n} A_i\ q_i \qquad (4.44)$$

$$\left(\frac{d\theta}{dy}\right)_1 = \left(\frac{d\theta}{dy}\right)_2 = \cdots\cdots = \left(\frac{d\theta}{dy}\right)_n = \left(\frac{d\theta}{dy}\right)_{overall} \qquad (4.45)$$

These equations will form (n + 1) number of simultaneous equations and their coefficients will give a matrix of order (n + 1). The reciprocal of the $((n+1),1)$ element of the inverse matrix will be the torsional rigidity of the section.

$$GJ = \frac{1}{\Delta^*_{(n+1),1}} \qquad (4.46)$$

4.5 SHEAR CENTRE

The position of a shear centre is defined as that point in the cross-section through which shear loads produce no twisting. It may be shown by use of the reciprocal theorem that this point is also the centre of twist of sections subjected to torsion.

The centre of twist is a point in a cross-section that remains stationary when a torque is applied to that section. If the supporting constraint of the beam is perfectly rigid, the flexural centre coincides with the centre of twist or the shear centre.

4.5.1 CLOSED SECTIONS MADE OF ISOTROPIC MATERIALS

General stress, strain and displacement relationships for an element ($\delta s \times \delta y \times t$) of a closed or open section are deduced by considering that the element is maintained in equilibrium by a system of direct and shear stresses as shown in the Figure [4.5]. The direct stress σ_y is produced by bending moments or by bending action of shear loads. The shear stresses τ_{sy}, τ_{ys} are due to shear and/or torsion of a closed section or shear of an open section. The hoop stress σ_s is usually zero but may be present in closed sections due to internal pressure. If t is assumed to be constant over the length δs then $\tau_{ys} = \tau_{sy} = \tau$. It is convenient to work in terms of shear flow q, i.e. shear force per unit length. The theory for computation of a shear centre of a closed section is well known and is given for convenience in Appendix (G.3).

For analysis on a computer, the section is divided into several small straight segments. The co-ordinates of the segments are entered along with the thickness and material properties such as the moduli of elasticity and rigidity. The thickness "t" in the equation refers to the direct stress carrying thickness of the skin.

$$x_i \ , \ z_i \qquad i=0,1,2,\ldots\ldots,n$$

where x_o, z_o = initial node of the first segment

x_n, z_n = last node of the last segment

x_i, z_i = the end node of the i-th segment

Computation of I_{xx}, I_{zz}, I_{xz} is carried out as usual. The x and z quantities as given in equations (G.28) and (G.30) (see Appendix G.3) for shear flow in the section can be expressed in terms of s as shown in Figure (4.6).

$$z = z_o + s \sin\theta = z_{i-1} + \left\{\frac{z_i - z_{i-1}}{\ell_i}\right\} s \qquad (4.47a)$$

$$x = x_o + s \sin\theta = x_{i-1} + \left\{\frac{x_i - x_{i-1}}{\ell_i}\right\} s \qquad (4.47b)$$

Substituting the above values of x and z in equations (G.28) or (G.30):

$$q_b = -\frac{\bar{S}_z}{I_{xx}} \int_o^{\ell_i} t_i \left[z_{i-1} + \left\{\frac{z_i - z_{i-1}}{\ell_i}\right\} s \right] ds - \frac{\bar{S}_x}{I_{zz}} \int_o^{\ell_i} t_i \left[x_{i-1} + \left\{\frac{x_i - x_{i-1}}{\ell_i}\right\} s \right] ds$$

$$= -\frac{\bar{S}_z}{I_{xx}} t_i \left| z_{i-1}s + \left\{\frac{z_i - z_{i-1}}{\ell_i}\right\} \frac{s^2}{2} \right|_o^{\ell_i} - \frac{\bar{S}_x}{I_{zz}} t_i \left| x_{i-1}s + \left\{\frac{x_i - x_{i-1}}{\ell_i}\right\} \frac{s^2}{2} \right|_o^{\ell_i} \qquad (4.48)$$

Therefore, for each segment

$$q_{bi} = -\frac{\bar{S}_z}{I_{xx}} t_i \left[z_{i-1}\ell_i + \left\{\frac{z_i - z_{i-1}}{\ell_i}\right\} \frac{\ell_i^2}{2} \right] -$$

$$\frac{\bar{S}_x}{I_{zz}} t_i \left[x_{i-1} \ell_i + \left\{ \frac{x_i - x_{i-1}}{\ell_i} \right\} \frac{\ell_i^2}{2} \right]$$

or simply

$$q_{bi} = - \frac{t_i \ell_i}{2} \left\{ \frac{\bar{S}_z}{I_{xx}} (z_i + z_{i-1}) + \frac{\bar{S}_x}{I_{zz}} (x_i + x_{i-1}) \right\} \quad (4.49)$$

There will be n values of q_{bi} for a cross-section. Then q_s will be computed by adding the individual values of q_{bi} for each segment.

$$q_{si} = q_{bi} + q_{si-1} \quad (4.50)$$

Now the value of $\oint q_b ds$ as given in equation (G.31) can be computed as follows :

$$\oint q_b \, ds = \sum_{i=1}^{n} \int_o^{\ell_i} q_{bi} ds$$

$$= \int_o^{\ell_1} \left[- \frac{\bar{S}_z}{I_{xx}} t_1 \left(z_o s + \left\{ \frac{z_1 - z_o}{\ell_1} \right\} \frac{s^2}{2} \right) - \frac{\bar{S}_x}{I_{zz}} t_1 \left(x_o s + \left\{ \frac{x_1 - x_o}{\ell_1} \right\} \frac{s^2}{2} \right) \right] ds$$

$$+ \int_o^{\ell_2} q_{b1} + \left[- \frac{\bar{S}_z}{I_{xx}} t_2 \left(z_1 s + \left\{ \frac{z_2 - z_1}{\ell_2} \right\} \frac{s^2}{2} \right) - \frac{\bar{S}_x}{I_{zz}} t_2 \left(x_1 s + \left\{ \frac{x_2 - x_1}{\ell_2} \right\} \frac{s^2}{2} \right) \right] ds$$

$$+ \int_o^{\ell_3} q_{b1} + q_{b2} + \left[- \frac{\bar{S}_z}{I_{xx}} t_3 \left(z_2 s + \left\{ \frac{z_3 - z_2}{\ell_3} \right\} \frac{s^2}{2} \right) \right.$$

$$\left. - \frac{\bar{S}_x}{I_{zz}} t_3 \left(x_2 s + \left\{ \frac{x_3 - x_2}{\ell_3} \right\} \frac{s^2}{2} \right) \right] ds + \ldots\ldots\ldots\ldots$$

After further simplification :

$$\oint q_b \, ds =$$

$$= \left| - \frac{\bar{S}_z}{I_{xx}} t_1 \left(z_0 \frac{s^2}{2} + \left\{ \frac{z_1 - z_0}{\ell_1} \right\} \frac{s^3}{6} \right) - \frac{\bar{S}_x}{I_{zz}} t_1 \left(x_0 \frac{s^2}{2} + \left\{ \frac{x_1 - x_0}{\ell_1} \right\} \frac{s^3}{6} \right) \right|_0^{\ell_1}$$

$$+ \left| q_{b1} s - t_2 \left[\frac{\bar{S}_z}{I_{xx}} \left(z_1 \frac{s^2}{2} + \left\{ \frac{z_2 - z_1}{\ell_2} \right\} \frac{s^3}{6} \right) + \frac{\bar{S}_x}{I_{zz}} \left(x_1 \frac{s^2}{2} + \left\{ \frac{x_2 - x_1}{\ell_2} \right\} \frac{s^3}{6} \right) \right] \right|_0^{\ell_2}$$

$$+ \left| q_{b1} S_3 + q_{b2} S_3 - t_3 \left[\frac{\bar{S}_z}{I_{xx}} \left(z_2 \frac{s^2}{2} + \left\{ \frac{z_3 - z_2}{\ell_3} \right\} \frac{s^3}{6} \right) + \frac{\bar{S}_x}{I_{zz}} \left(x_2 \frac{s^2}{2} + \left\{ \frac{x_3 - x_2}{\ell_3} \right\} \frac{s^3}{6} \right) \right] \right|_0^{\ell_3} + \ldots\ldots\ldots$$

$$\oint q_b \, ds =$$

$$= - t_1 \left[\frac{\bar{S}_z}{I_{xx}} \left(z_0 \frac{\ell_1^2}{2} + \left\{ \frac{z_1 - z_0}{\ell_1} \right\} \frac{\ell_1^3}{6} \right) + \frac{\bar{S}_x}{I_{zz}} \left(x_0 \frac{\ell_1^2}{2} + \left\{ \frac{x_1 - x_0}{\ell_1} \right\} \frac{\ell_1^3}{6} \right) \right]$$

$$- t_2 \left[\frac{\bar{S}_z}{I_{xx}} \left(z_1 \frac{\ell_2^2}{2} + \left\{ \frac{z_2 - z_1}{\ell_2} \right\} \frac{\ell_2^3}{6} \right) + \frac{\bar{S}_x}{I_{zz}} \left(x_1 \frac{\ell_2^2}{2} + \left\{ \frac{x_2 - x_1}{\ell_2} \right\} \frac{\ell_2^3}{6} \right) \right]$$

$$- t_3 \left[\frac{\bar{S}_z}{I_{xx}} \left(z_2 \frac{\ell_3^2}{2} + \left\{ \frac{z_3 - z_2}{\ell_3} \right\} \frac{\ell_3^3}{6} \right) + \frac{\bar{S}_x}{I_{zz}} \left(x_2 \frac{\ell_3^2}{2} + \left\{ \frac{x_3 - x_2}{\ell_3} \right\} \frac{\ell_3^3}{6} \right) \right]$$

$$\ldots\ldots\ldots + q_{b1} (\ell_2 + \ell_3 + \ldots + \ell_n) + q_{b2} (\ell_3 + \ell_4 + \ldots + \ell_n) + \ldots\ldots\ldots$$

In a generalized and simplified form,

$$\oint q_b ds = \sum_{i=1}^{n} \left[- \frac{t_i \ell_i^2}{6} \left\{ \frac{\bar{S}_z}{I_{xx}} (z_i - 2 z_{i-1}) + \frac{\bar{S}_x}{I_{zz}} (x_i - 2 x_{i-1}) \right\} + q_{bi} \left(\sum_{j=1}^{n} \ell_j - \sum_{k=1}^{i} \ell_k \right) \right] \qquad (4.51)$$

Therefore,

$$q_{so} = \frac{1}{\oint ds = \sum_{i=1}^{n} \ell_i} \sum_{i=1}^{n} \left[- \frac{t_i \ell_i^2}{6} \left\{ \frac{\bar{S}_z}{I_{xx}} (z_i - 2z_{i-1}) + \frac{\bar{S}_x}{I_{zz}} (x_i - 2x_{i-1}) \right\} + q_{bi} \left(\sum_{j=1}^{n} \ell_j - \sum_{k=1}^{i} \ell_k \right) \right] \qquad (4.52)$$

Now the exact values for q_{si} can be computed from equation (4.50) by including the value for q_{so} obtained from equation (4.52).

Then equating the moments due to the internal shear flows about a reference point (for example, the centre of gravity) to the moment of applied shear load (dummy) about the same point gives the following expression.

$$S_x \zeta_E + S_z \zeta_E = \sum_{i=1}^{N} \int_0^{\ell_i} p_i \, q_{s_i} \, ds$$

$$= \sum_{i=1}^{N} p_i \int_0^{\ell_i} (q_{bi} + q_{si-1}) \, ds$$

$$= \sum_{i=1}^{N} p_i \int_0^{\ell_i} \left[- \frac{\bar{S}_z}{I_{xx}} t_i \left[z_{i-1} \, s + \left\{ \frac{z_i - z_{i-1}}{\ell_i} \right\} \frac{s^2}{2} \right] - \frac{\bar{S}_x}{I_{zz}} t_i \left[x_{i-1} \, s + \left\{ \frac{x_i - x_{i-1}}{\ell_i} \right\} \frac{s^2}{2} \right] + q_{si-1} \right] ds$$

$$= \sum_{i=1}^{N} p_i \left(- \frac{\bar{S}_z}{I_{xx}} t_i \left[z_{i-1} \frac{\ell_i^2}{2} + \left\{ \frac{z_i - z_{i-1}}{\ell_i} \right\} \frac{\ell_i^3}{6} \right] - \right.$$

$$\left. \frac{\bar{S}_x}{I_{zz}} t_i \left[x_{i-1} \frac{\ell_i^2}{2} + \left\{ \frac{x_i - x_{i-1}}{\ell_i} \right\} \frac{\ell_i^3}{6} \right] + q_{si-1} \ell_i \right)$$

$$= \sum_{i=1}^{N} p_i \left(\frac{t_i \ell_i^2}{6} \left[- \frac{\bar{S}_z}{I_{xx}} (z_i + 2 z_{i-1}) - \frac{\bar{S}_x}{I_{zz}} (x_i + 2 x_{i-1}) \right] + q_{si-1} \ell_i \right)$$

.....(4.53)

In case of one axis of symmetry, then

$$\bar{S}_x = S_x = 0 \quad \text{and} \quad \bar{S}_z = S_z \quad \text{since} \quad I_{xz} = 0$$

Therefore,

$$S_z \xi_E = \sum_{i=1}^{N} p_i \left(\frac{t_i \ell_i^2}{6} \left[- \frac{S_z}{I_{xx}} (z_i + 2 z_{i-1}) \right] + q_{si-1} \ell_i \right)$$

(4.54)

S_z will be canceled out on both sides of the equation to give

$$\xi_E = \sum_{i=1}^{N} p_i \left(- \frac{t_i \ell_i^2}{6 I_{xx}} (z_i + 2 z_{i-1}) + q_{si-1} \ell_i \right) \qquad (4.55)$$

4.5.2 OPEN SECTIONS MADE OF ISOTROPIC MATERIALS

Shear centre computation for open sections is quite similar to that for closed sections. Equation (G.28) (see Appendix G.3) refers to open sections where q_s represents the open section shear or basic shear, also denoted as q_b. Expressing x and z in terms of s will give an expression similar to (4.48) and, after simplification, equation (4.49).

For an open section, $q_{so} = 0$. Therefore, $q_{si} = q_{bi}$. Equating the moments of the internal shears about a reference point (for example the centre of gravity) to the moment of applied shear load (dummy) about the same point gives an expression similar to equation (4.53). The rest of the analysis follows the same pattern as that which has been discussed concerning a closed section. The final expression for calculating the shear centre for the open section is identical to equation (4.55) as shown below.

$$\zeta_E = \sum_{i=1}^{N} p_i \left[- \frac{t_i \ell_i^2}{6 I_{xx}} (z_i + 2 z_{i-1}) + q_{si-1} \ell_i \right] \qquad (4.56)$$

4.5.3 CLOSED SECTIONS MADE OF COMPOSITE MATERIALS

The rate of twist $\frac{d\psi}{dy}$ in uniform thin-walled elastic beams in the case of uniform torsion as suggested by Bredt [3] is given by the expression

$$\frac{d\psi}{dy} = \frac{1}{2A} \int \frac{q}{Gt} ds \qquad (4.57)$$

In order to generalize Bredt's method for combined bending and torsion, several longitudinal cuts are assumed so that the structure is considered as an open section. The basic shear flow is computed using equation (G.30) (see Appendix G.3) on which an unknown correction shear flow to compensate for the cuts is superimposed. This correction shear flow is determined by equation (G.31) which is an equation of static equivalence, where external loads acting on the cross-section must have the same moment about a longitudinal axis as the cross-section shear flows. In the case of a multi-cell structure, the above equation is supplemented by equations of compatible rates of twist of the cells.

The method described has the following shortcomings when applied to the combined bending and torsion case:

1. The strains implied by these are not necessarily compatible, though the stresses obtained may satisfy equilibrium.
2. The method assumes that the shape of the cross-section remains preserved, hence neglecting Poisson's ratio effects.
3. Moreover it is assumed that the cross-sectional normal stresses are calculated by the Engineer's theory of bending ($\sigma = \frac{My}{I}$ or its generalization in the case of unsymmetrical bending), and therefore, it is possible to ignore shear lag and bending stresses caused by torsion.
4. The assumption in the method that the walls of the cross-section are isotropic or at least specially orthotropic; that is, one of the axes of the fibres in a composite material lies parallel to the longitudinal axis of the structure.

Hence the method is inappropriate for stubby beams with non-compact cross-sections.

For a cylindrical tube subjected to torsion, bending, and longitudinal tension, cylindrical coordinates as shown in Figure (4.7a) can be used. In the absence of circumferencial stresses and strains in the structure i.e. $N_s = 0$ & $\varepsilon_s = 0$, equation (A.24) (see Appendix A) will reduce to :

$$\begin{Bmatrix} N_y \\ N_{ys} \end{Bmatrix} = \begin{bmatrix} A_{11} & A_{13} \\ A_{13} & A_{33} \end{bmatrix} \begin{Bmatrix} \varepsilon_y \\ \gamma_{ys} \end{Bmatrix} \qquad (4.58)$$

or

$$\begin{Bmatrix} \varepsilon_y \\ \gamma_{ys} \end{Bmatrix} = \begin{bmatrix} A_{11} & A_{13} \\ A_{13} & A_{33} \end{bmatrix}^{-1} \begin{Bmatrix} N_y \\ N_{ys} \end{Bmatrix} = \begin{bmatrix} A^*_{11} & A^*_{13} \\ A^*_{13} & A^*_{33} \end{bmatrix} \begin{Bmatrix} N_y \\ N_{ys} \end{Bmatrix} \quad (4.59)$$

or

$$\begin{Bmatrix} N_y \\ \gamma_{ys} \end{Bmatrix} = \begin{bmatrix} \left(H_{11} = \dfrac{1}{A^*_{11}}\right) & -\left(H_{12} = \dfrac{A^*_{13}}{A^*_{11}}\right) \\ \left(H_{12} = \dfrac{A^*_{13}}{A^*_{11}}\right) & \left(H_{22} = A^*_{33} - \dfrac{A^{*2}_{13}}{A^*_{11}}\right) \end{bmatrix} \begin{Bmatrix} \varepsilon_y \\ N_{ys} \end{Bmatrix}$$

or simply

$$\begin{Bmatrix} N_y \\ \gamma_{ys} \end{Bmatrix} = \begin{bmatrix} H_{11} & -H_{12} \\ H_{12} & H_{22} \end{bmatrix} \begin{Bmatrix} \varepsilon_y \\ N_{ys} \end{Bmatrix} \quad (4.60)$$

General stress, strain and displacement relationships for an element (δs x δy x t) of a closed or open tube are deduced from considering that the element is maintained in equilibrium by the following system of direct and shear stresses as shown in Figure (4.7b).

σ_y = Direct stress, produced by bending moments or by bending action of shear loads.

τ_{sy} and τ_{ys} = Shear stresses, due to shear and/or torsion of a closed tube or shear of an open tube. (If t is assumed to be constant over the length δs then $\tau_{ys} = \tau_{sy} = \tau$).

σ_s = Hoop stress, usually absent but may be present in closed tubes due to internal pressure.

q = Shear flow = τ t

For equilibrium of the element in the y and s directions and neglecting body forces and hoop stresses,

equations (G.20) and (G.21) are obtained. Substitution of $N_s = \sigma_s t$ will give the following expressions :

$$\frac{\partial q}{\partial s} + \frac{\partial N_y}{\partial y} = 0 \qquad (4.61)$$

$$\frac{\partial q}{\partial y} = 0 \qquad (4.62)$$

The second expression suggests that the shear flow in the y-direction is constant or that the shear flow q only depends on s. The integration of the first equation will give

$$q(s) = q_o - \int_o^s \left(\frac{\partial N_y}{\partial y}\right) ds \qquad (4.63)$$

In the case of the classical theory for thin-walled beams made of isotropic materials, the cross-sectional normal stress is assumed to vary linearly with x and z. The longitudinal strain ε_y in this case is assumed to be a linear function of x and z.

$$\varepsilon_y = \varepsilon_o - z K_x - x K_z \qquad (4.64)$$

where $\varepsilon_o(y)$ = mean axial strain in the structure
$K_x(y)$ = curvature of the structure in the xz plane
$K_z(y)$ = curvature of the structure in the yz plane

Substituting equation (4.64) into (4.60) :

$$N_y = H_{11} (\varepsilon_o - z K_x - x K_z) - H_{12} q \qquad (4.65)$$

Differentiating with respect to y and taking into account equation (4.62) gives :

$$\frac{\partial N_y}{\partial y} = H_{11} (\varepsilon_o' - z K_x' - x K_z') \qquad (4.66)$$

where the primes denote differentiation with respect to y. Substituting equation (4.66) into (4.63) gives

$$q(s) = q_o - \int_o^s \left[H_{11} (\varepsilon_o' - z K_x' - x K_z')\right] ds$$

$$= q_o - \varepsilon_o' \int_o^s H_{11} ds + K_x' \int_o^s z H_{11} ds + K_z' \int_o^s x H_{11} ds \quad (4.67)$$

Let

$$a_1(s) = \int_o^s H_{11} ds$$

$$a_2(s) = \int_o^s z H_{11} ds \quad (4.68)$$

$$a_3(s) = \int_o^s x H_{11} ds$$

and substituting equation (4.64) and (4.67) into (4.60) gives

$$\gamma_{ys} = H_{12} (\varepsilon_o - z K_x - x K_z) + H_{22} \left[q_o - \varepsilon_o' \int_o^s H_{11} ds + K_x' \int_o^s z H_{11} ds + K_z' \int_o^s x H_{11} ds\right] \quad (4.69)$$

The resultant tensile load P after substituting the expression for N_y from equation (4.65) is :-

$$P = \oint N_y ds = \oint \left[H_{11} (\varepsilon_o - z K_x - x K_z) - H_{12} q\right] ds$$

$$= \varepsilon_o \oint H_{11} ds - K_x \oint z H_{11} ds - K_z \oint x H_{11} ds - \oint H_{12} q ds \quad (4.70)$$

Similarly the bending moment about x-axis :

$$M_x = - \oint z N_y ds$$

$$= - \varepsilon_o \oint z\, H_{11} ds + K_x \oint z^2\, H_{11} ds + K_z \oint xz\, H_{11} ds + \oint z\, H_{12} q\, ds \qquad (4.71)$$

and the chordwise moment about the z-axis :

$$M_z = - \oint x\, N_y\, ds$$

$$= - \varepsilon_o \oint x\, H_{11} ds + K_x \oint x\, z\, H_{11} ds + K_z \oint x^2\, H_{11} ds + \oint x\, H_{12} q\, ds \qquad (4.72)$$

In matrix form

$$\begin{bmatrix} \oint H_{11}\, ds & -\oint z\, H_{11}\, ds & -\oint x\, H_{11}\, ds \\ -\oint z\, H_{11} ds & \oint z^2\, H_{11} ds & \oint xz\, H_{11} ds \\ -\oint x\, H_{11} ds & \oint xz\, H_{11} ds & \oint x^2\, H_{11} ds \end{bmatrix} \begin{Bmatrix} \varepsilon_o \\ K_x \\ K_z \end{Bmatrix} = \begin{Bmatrix} P + \oint H_{12}\, q\, ds \\ M_x - \oint z\, H_{12} q\, ds \\ M_z - \oint x\, H_{12} q\, ds \end{Bmatrix}$$

or

$$[b]\ \{u\} = \{F\} \qquad (4.73)$$

Let

$$\left.\begin{aligned} Q_1 &= \oint H_{12}\, q\, ds \\ Q_2 &= \oint z\, H_{12}\, q\, ds \\ Q_3 &= \oint x\, H_{12}\, q\, ds \end{aligned}\right\} \qquad (4.74)$$

or

$$\begin{Bmatrix} \varepsilon_o \\ K_x \\ K_z \end{Bmatrix} = \begin{bmatrix} a_{11} & a_{12} & a_{13} \\ a_{21} & a_{22} & a_{23} \\ a_{31} & a_{32} & a_{33} \end{bmatrix} \begin{Bmatrix} P + Q_1 \\ M_x - Q_2 \\ M_z - Q_3 \end{Bmatrix} \qquad (4.75)$$

where a_{ij} is the inverse of the b_{ij} matrix

Since M_x and M_z , ε_o, K_x, and K_z are linear functions of y, differentiation with respect to y gives

$$\begin{Bmatrix} \varepsilon_o' \\ K_x' \\ K_z' \end{Bmatrix} = \begin{bmatrix} a_{11} & a_{12} & a_{13} \\ a_{21} & a_{22} & a_{23} \\ a_{31} & a_{32} & a_{33} \end{bmatrix} \begin{Bmatrix} 0 \\ V_x \\ V_z \end{Bmatrix} \qquad (4.76)$$

Equation (4.76) indicates that ε_o', K_x', and K_z' are independent of y. Finally the resultant torque about the y-axis :

$$T = \oint p(s)\, q(s)\, ds \qquad (4.77)$$

where p(s) = perpendicular distance from the origin to the tangent at the point defined by s.

$A = \frac{1}{2} \oint p(s)ds$ = cross-sectional area of the tube

Substituting equation (4.67) in (4.77) will give:

$$T = \oint p(s)\left[q_o - \varepsilon_o' \int_o^s H_{11}ds + K_x' \int_o^s z\, H_{11}ds + K_z' \int_o^s x\, H_{11}ds\right]ds$$

Solving for q_o

$$q_o = \left(\frac{1}{2A}\right)\left[T + \varepsilon_o' \oint p(s)\int_o^s H_{11}ds\, ds - K_x' \oint p(s) \int_o^s z\, H_{11}ds\, ds - K_z' \oint p(s)\int_o^s x\, H_{11}ds\, ds\right] \qquad (4.78)$$

Let

$$a_4(s) = \oint p(s)\int_o^s H_{11}ds\, ds = \oint p(s)\, a_1(s)\, ds \qquad (4.79a)$$

$$a_5(s) = \oint p(s)\int_o^s z\, H_{11}ds\, ds = \oint p(s)\, a_2(s)\, ds \qquad (4.79b)$$

$$a_\sigma(s) = \oint p(s) \int_o^s x\, H_{11} ds\, ds = \oint p(s)\, a_3(s)\, ds \qquad (4.79c)$$

As ε_o', K_x', and K_z' are independent of y, the following statments can be deduced.

1. q(s) and q_o are independent of y as shown in equation (4.62)
2. q(s) and q_o depend on H_{11} but do not depend on H_{12} or H_{22}.
3. This dependence on H_{11} is on the function and not on the amplitude.

Integrals Q_1, Q_2, and Q_3 will be evaluated :

$$\begin{Bmatrix} Q_1 \\ Q_2 \\ Q_3 \end{Bmatrix} = \left[\begin{array}{c|c|c|c} \oint H_{12} ds & -\oint a_1(s) H_{12} ds & \oint a_2(s) H_{12} ds & \oint a_3(s) H_{12} ds \\ \hline \oint z\, H_{12} ds & -\oint z\, a_1(s) H_{12} ds & \oint z\, a_2(s) H_{12} ds & \oint z\, a_3(s) H_{12} ds \\ \hline \oint x\, H_{12} ds & -\oint x\, a_1(s) H_{12} ds & \oint x\, a_2(s) H_{12} ds & \oint x\, a_3(s) H_{12} ds \end{array}\right] \begin{Bmatrix} q_o \\ \varepsilon_o' \\ K_x' \\ K_z' \end{Bmatrix}$$

or

$$\{Q\} = [c]\,\{u\} \qquad (4.80)$$

The rate of twist in a single cell of a thin-walled beam, according to the classical theory, is related to the shear strains in the walls of the cell by the formula:

$$\frac{d\psi}{dy} = \frac{1}{2A} \oint \gamma_{ys}(s)\, ds \qquad (4.81)$$

The rate of twist is independent of the material and is based on geometric considerations. Substitution of equation (4.69) in (4.81) gives:

$$\frac{d\psi}{dy} = \frac{1}{2A} \oint \left[H_{12}(\varepsilon_o - z K_x - x K_z) + H_{22}\left[q_o - \varepsilon_o' \int_o^s H_{11} ds + K_x' \int_o^s z H_{11} ds + K_z' \int_o^s x H_{11} ds \right] \right] ds$$

or

$$\frac{d\psi}{dy} = \frac{1}{2A} \left[- \varepsilon_o c_{11} + K_x c_{21} + K_z c_{31} + q_o d_1 + \varepsilon_o' d_2 + K_x' d_3 + K_z' d_4 \right] \qquad (4.82)$$

where

$$c_{11} = \oint H_{12} ds \quad , \quad c_{21} = \oint z H_{12} ds \quad , \quad c_{31} = \oint x H_{12} ds$$

$$d_1 = \oint H_{22} ds \quad , \quad d_2 = - \oint a_1(s) H_{22} ds$$

$$d_3 = \oint a_2(s) H_{22} ds \quad , \quad d_4 = \oint a_3(s) H_{22} ds \qquad (4.83)$$

The rate of twist $\frac{d\psi}{dy}$ is generally a linear function of y because ε_o, K_x, K_z are linear functions of y, whereas q_o, ε_o', K_x', K_z' are constants. The average rate of twist over the length L will be as follows :

$$\frac{\psi(L) - \psi(0)}{L} = \frac{1}{2A} \left[- \bar{\varepsilon}_o c_{11} + \bar{K}_x c_{21} + \bar{K}_z c_{31} + q_o d_1 - \varepsilon_o' d_2 + K_x' d_3 + K_z' d_4 \right] \qquad (4.105)$$

where $\bar{\varepsilon}_o$, $\bar{K}_x$, $\bar{K}_z$ are average values of ε_o, K_x, K_z and obtained by replacing $M_x = \bar{M}_x = M_x (L/2)$ and $M_z = \bar{M}_z = M_z (L/2)$ into equation (4.73).

In another approach, the rate of twist can be computed by combining equations (4.75) and (4.80), eliminating ε_o, K_x, and K_z using equation (4.82), q_o using (4.78), and ε_o, K_x, and K_z using equation (4.76) :

$$\frac{d\psi}{dy} = \frac{1}{2A}\left[ST + (SA_R + D_R - C_R A_S C_S) A_S \begin{Bmatrix} 0 \\ V_z \\ V_x \end{Bmatrix} + C_R A_S \begin{Bmatrix} P \\ -M_x \\ -M_z \end{Bmatrix}\right] \quad (4.85)$$

where

A_S = [a] matrix of equation (4.75)

C_S = [c] matrix of equation (4.80) without first column

$A_R = [a_4 \quad -a_5 \quad -a_6]$

$C_R = [-c_{11} \quad c_{21} \quad c_{31}]$

$D_R = [d_2 \quad d_3 \quad d_4]$

$S = \frac{1}{2A}(d_1 - C_R A_S C_C)$

$C_C = [c_{11} \quad c_{21} \quad c_{31}]^T$

The average rate of twist over the span will be

$$\frac{\psi(L) - \psi(0)}{L} = \frac{1}{2A}\left[ST + (SA_R + D_R - C_R A_S C_S) A_S \begin{Bmatrix} 0 \\ V_z \\ V_x \end{Bmatrix} + C_R A_S \begin{Bmatrix} P \\ -\bar{M}_x \\ -\bar{M}_z \end{Bmatrix}\right] \quad (4.86)$$

In the case of thin-walled beams made of conventional isotropic materials, the rate of twist depends upon the

torque T and the shear forces V_x and V_z such that these quantities themselves are independent of y. This makes the shear centre a geometric property of the cross-section. But structures made of composite materials show dependence on P, M_x, and M_z as well. Since M_x and M_z vary along the span of the structure a shear centre in the usual sense does not exist. If the shear centre is redefined as that point through which a cross-sectional shear must pass so that the average rate of twist is zero when P, M_x, and M_z do not exist, only then can the shear centre be considered as a cross-sectional property.

4.6 CENTRE OF GRAVITY

The general principle for locating the centroid of an area is based on the method of determining the resultants of parallel force systems. In the case of a wing section made of glass fibre reinforced plastic, filled with polyurethene expanded foam, the scheme for computing the centroid is found to be relatively complicated. Two separate centroidal positions for a thin walled section and a solid foam section are computed. Application of the second condition of equilibrium then results in the exact position of the centre of gravity for both skin and foam.

$$\bar{x} = \frac{A_{skin}\,\rho_{skin}\,\bar{x}_{skin} + A_{solid}\,\rho_{solid}\,\bar{x}_{solid}}{\text{mass per unit length of the wing (skin + foam)}}$$

$$\bar{z} = \frac{A_{skin}\,\rho_{skin}\,\bar{y}_{skin} + A_{solid}\,\rho_{solid}\,\bar{y}_{solid}}{\text{mass per unit length of the wing (skin + foam)}}$$

(4.87)

4.7 MASS PER UNIT LENGTH

In the case of structures made of isotropic (conventional) materials, the density of the material is a constant quantity. Thus accurate predictions of mass per unit length for a particular structure is possible. But in the case of composite materials, the density depends upon the volume fraction of the fibre and the resin. (Manufacturing techniques play an important role in controlling the volume fraction of the constituent materials).

4.8 POLAR MASS MOMENT OF INERTIA

For an aerofoil section filled with foam the total polar mass moment of inertia will be the sum of the polar mass moment of inertia of the skin and that of the foam, as shown below.

$$I_p\Big|_{skin} = \rho_{skin}\left\{\left(I_{xx_{skin}} + I_{zz_{skin}}\right) + A_{skin}\, X_\alpha^2\right\} \qquad (4.88)$$

$$I_p\Big|_{sub} = \rho_{sub}\left\{\left(I_{xx_{sub}} + I_{zz_{sub}}\right) + A_{sub}\, X_\alpha^2\right\} \qquad (4.89)$$

$$I_p\Big|_{total} = I_p\Big|_{skin} + I_p\Big|_{sub} \qquad (4.90)$$

where

I_{xx} = second moment of area along the x-axis

I_{zz} = second moment of area along the z-axis

A_{skin} = area of the thin skin

A_{sub} = area subtended by the closed curve (profile of the aerofoil)

X_α = distance between the centre of gravity and the shear centre of the section

ρ_{skin} = density of the material of thin skin (GFRP)

ρ_{foam} = density of the foam filled in the wing section

4.9 COMPUTER PROGRAM

The development of computer codes for the theory discussed above was based on both BASIC and FORTRAN languages. The programmes have several versions that can run both on BBC and IBM compatible micro- or mini-computers as well as on a mainframe computer. The program consists of several subroutines that can be called by a main interface program. These subroutines have been written in such a way that the interface program can be structured to achieve any other desirable objective. The source codes for these subroutines as well as main interface programs are given in Appendix (C). A summary of the input and output parameters of these subroutines is given in Appendix (I).

These subroutines were combined in various ways to predict structural properties for a range of cross-sections with the capability to analyse structures made of conventional as well as composite materials.

4.9.1 SECTION

An interface program SECTION was written to predict static structural properties for isotropic structures. A flow chart for this program is given in Figure (4.8). Material properties such as Young's modulus of elasticity and shear modulus of rigidity together with wall thickness and cross-sectional details of the structure are entered as input into the program. The program can then predict the bending and torsional stiffness of the cross-section, mass per unit length, location of the centroid and the shear centre and the polar mass moment of inertia. An illustrative example with a sample run is given in Appendix (I).

4.9.2 KSTIF

A similar program KSTIF was developed to cater for sections made of composite materials. The program basically utilises the LAMINATE program discussed in Chapter (3) and SECTION as described in section (4.9.1) above. The program first evaluates the material equivalent elastic moduli and then computes the geometrical properties. In addition to bending and torsional stiffnesses, the coupled bending/torsion stiffness due to ply orientation is also evaluated. The program flow chart is shown in Figure (4.9). An illustrative example is given in Appendix (I).

4.10 EFFECT OF PLY ORIENTATION ON THE STIFFNESSES

The effect of ply orientation on the stiffnesses of a structure was studied. The cross-section of the structure chosen was an aerofoil shape. This parametric study was initially conducted on a single layer skin which can be extended to several layers. The computer program KSTIF.FOR was tailored in such a way that the ply orientation was automatically varied from zero to forty five degrees and various stiffnesses were computed. These stiffnesses were plotted against ply orientation and are shown in Figure (4.10). Finally the bending, torsional, and bending-torsional coupled stiffnesses were grouped together to obtain a dimensionless quantity ϕ given by :

$$\phi = \frac{K^2}{EI\ GJ} \qquad (4.91)$$

The nondimensional quantity ϕ was plotted against the ply orientation as shown in Figure (4.11). The effect of ply orientation on the moduli has already been discussed in Chapter (3) and it was found that by rotating the plies (ply angle is positive when rotated counter clock-wise)

Young's modulus of elasticity decreases while the shear modulus of rigidity increases. Hence a reduction of bending stiffness and an increase in the magnitude of torsional stiffness were found as anticipated. The interesting behaviour is that of the bending-torsional coupled stiffness, which reaches its maximum value when the ply angle is twenty two and a half degrees and disappears at forty five degrees. Similar behaviour was shown by the non-dimensional quantity ϕ when plotted against the ply orientation, see Figure (4.11).

4.11 CONCLUSIONS

Stiffness estimation of composite structures include evaluation of the laminate equivalent elastic constants and computation of the cross-sectional constants. The structure can be idealised as a solid beam, thin-walled beam or a large aspect ratio thin plate element. A suitable procedure of stiffness estimation is presented.

A general expression for the torsional stiffness of a multi-cell structure is derived which can be easily adopted for any number of cells.

The effect of ply orientation on the stiffnesses has been demonstrated. Bending stiffness decreased when the plies are at angles other than along the fibre direction and torsional stiffness increased as expected. In the case of woven materials this behaviour was exhibited for orientations up to 45^{o} and then it reversed. In the case of unidirectional materials the bending stiffness reached a minimum at 90^{o} and the torsional stiffness a maximum at that orientation. Bending-torsion coupled stiffness increased until $22\frac{1}{2}^{o}$. It then vanished at 45^{o}, where the bending stiffness was a minimum and the torsional stiffness was a maximum.

REFERENCES

1. Mansfield, E.H., "Flexural Vibrations of a Thin-Walled Cylinder of Rectangular Cross Section," R.A.E. The Aeronautical Quarterly, November 1958.

2. Housner, J.M. and Stein, M., "Flutter Analysis of Swept-Wing Subsonic Aircraft with Parameter Studies of Composite Wings," NASA TN D-7539, September 1974.

3. Weisshaar, T.A., "Structural Dynamic Tailoring of Advanced Composite Lifting Surfaces," Purdue University, Technical Report AAE-82-1, June 1982.

4. Weisshaar, T.A., "Divergence of Forward Swept Composite Wings," Journal of Aircraft, Vol. 17, No. 6, June 1980.

5. Mansfield, E.H. and Sobey, A.J., "The Fibre Composite Helicopter Blade, Part 1: Stiffness Properties, Part 2: Prospects for Aeroelastic Tailoring," Aeronautical Quarterly, May 1979, pp. 413-449.

6. Libove, C., "Stresses and Rate of Twist in Single-cell Thin-walled Beams with Anisotropic Walls," AIAA Journal, Vol. 26, No. 9, September, 1988.

7. Hong, Chang-Ho and Chopra, I., "Aeroelastic Stability Analysis of a Composite Rotor Blade," Journal of the American Helicopter Society, Vol. 30, No. 2, 1985.

8. Hong, Chang-Ho and Chopra, I., "Aeroelastic stability analysis of a composite bearingless rotor blade," Journal of the American Helicopter Society, Vol. 31, No. 4, October 1986.

9. Hodges, D.H. and Dowell, E.H., "Nonlinear Equations of Motions for the Elastic Bending and Torsion of Twisted Nonuniform Blades," NASA TN D-7818, December 1974.

10. Chandra, R., Temple, A.D., and Chopra, I., "Thin-Walled Composite Beams Under Bending, Torsional, Extensional Loads," Journal of Aircraft, Vol.27, No. 7, July 1990.

11. Smith, E.C. and Chopra, I., "Formulation and evaluation of an analytical model for composite box-beams," Journal of the American Helicopter Society, Vol. 28, No. 3, July 1991.

12. Eggenschwyler, A and Maillart, R.S., Bauzeitung, Proc. 2nd International Congr. Appl. Mech., Zürich, 1926, p. 434.

13. Blevins, R.D., Formulas for Natural Frequency and Mode Shape, Van Nostrand Reinhold, N.Y., 1979.

14. Weisshaar, T.A. and Foist, B. L., "Vibration Tailoring of Advanced Composite Lifting Surfaces," Journal of Aircraft, Vol. 22, No. 2, February 1985.

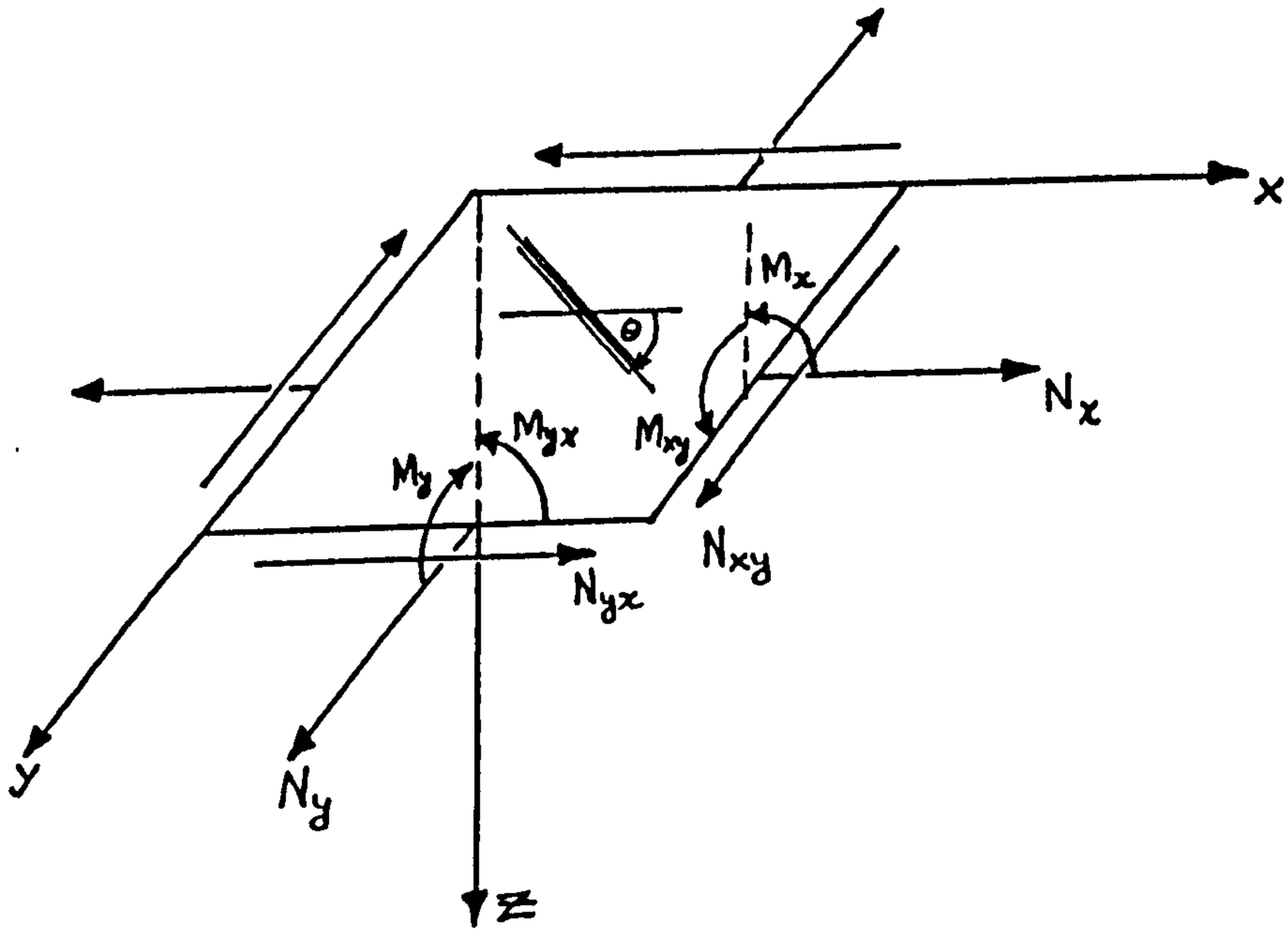

Figure 4.1(a) Orientation of axes for plate structure

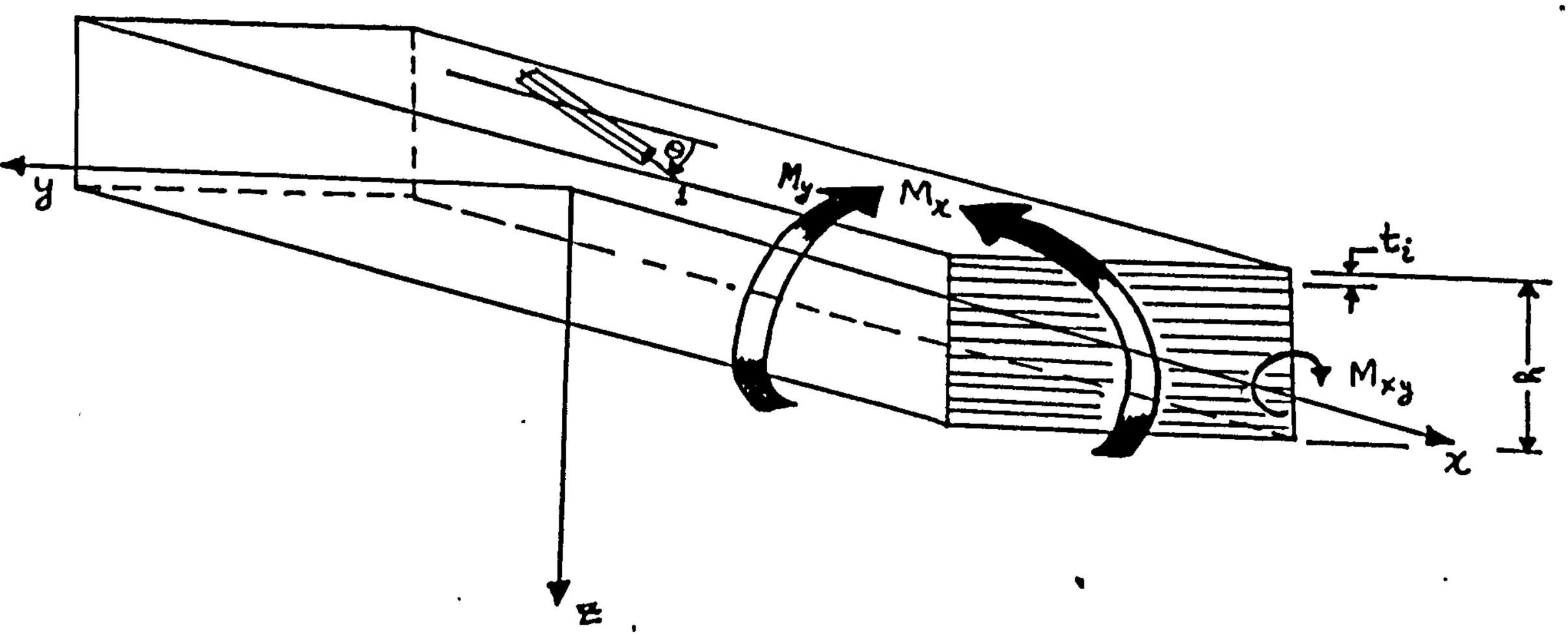

Figure 4.1(b) Orientation of axes for beam structure

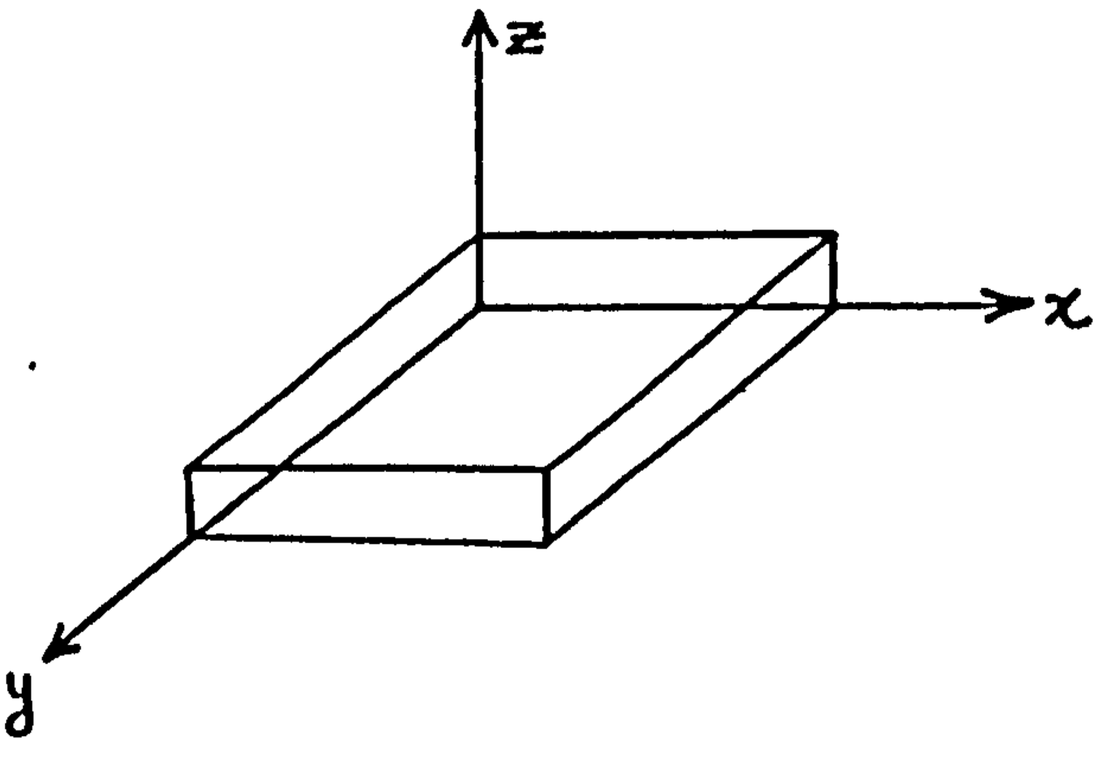

Figure 4.2(a) Co-ordinate system

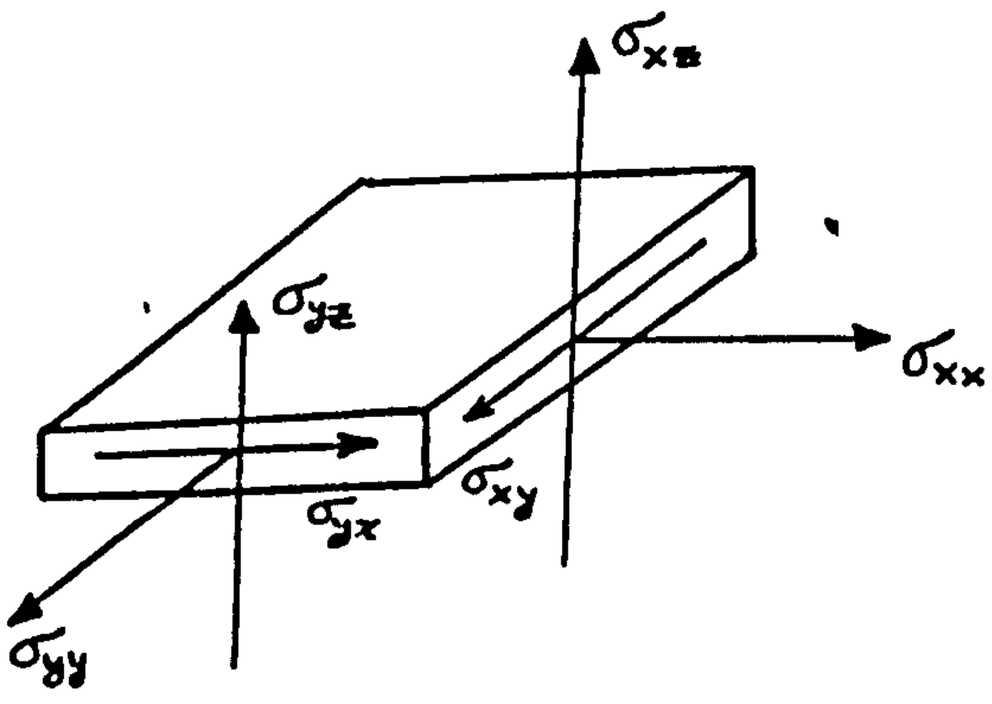

Figure 4.2(b) Stresses

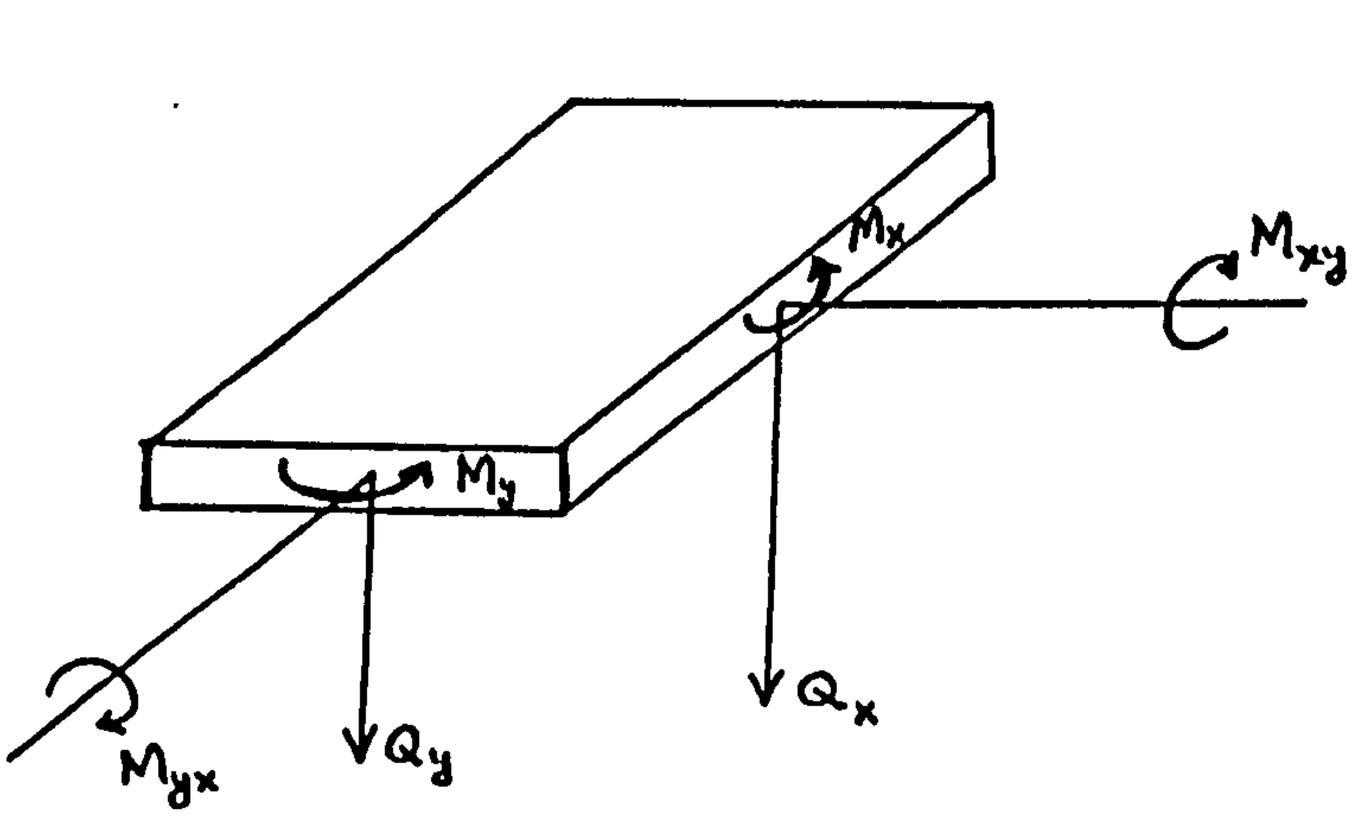

Figure 4.2(c) Resultant of forces and moments

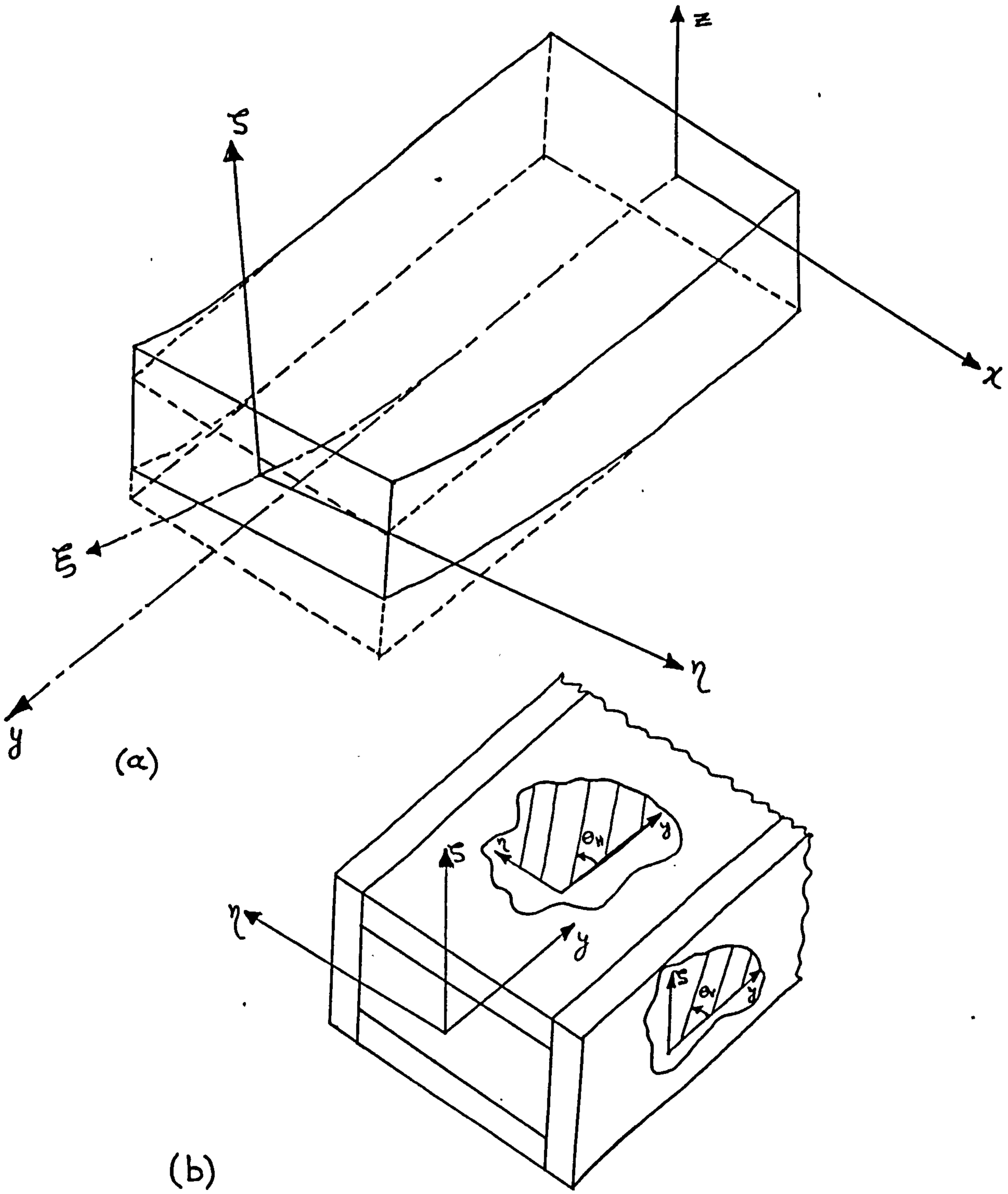

Figure 4.3(a) Boxbeam coordinates,
(b) Ply angle with reference axis

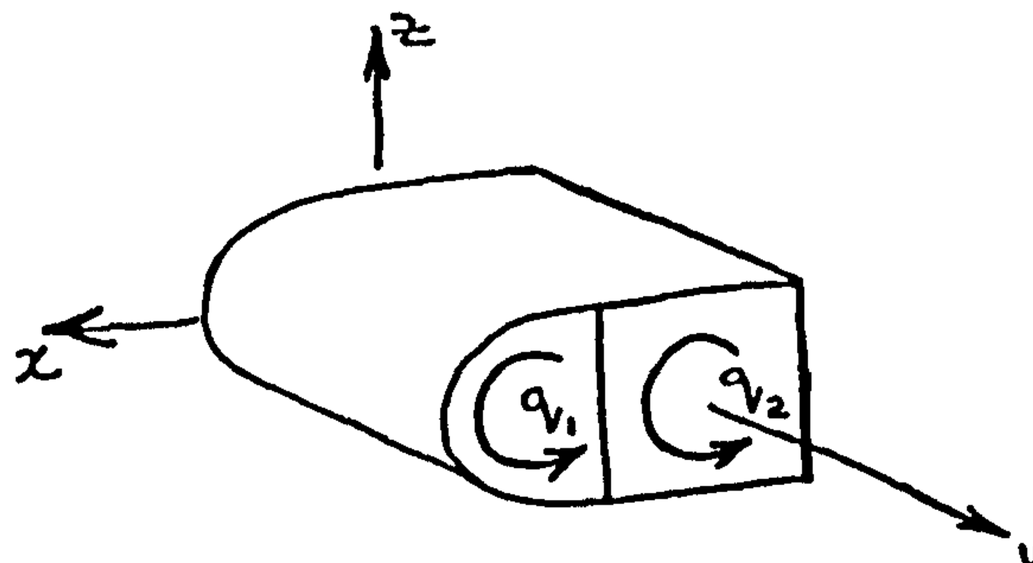

(a)

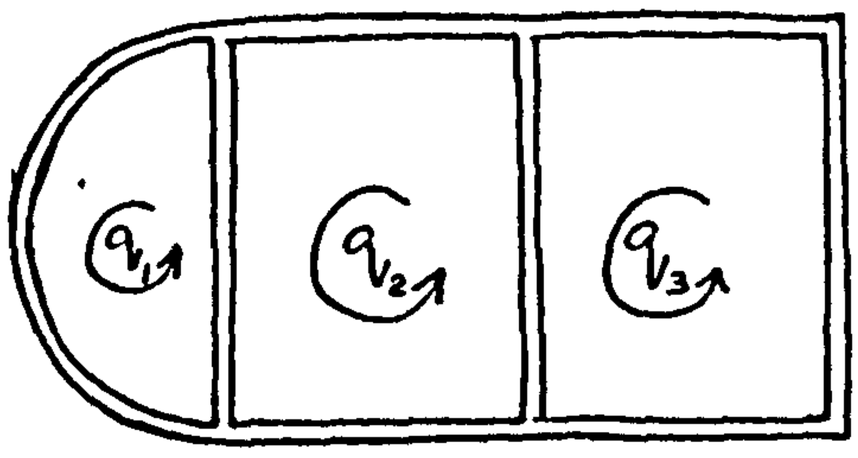

(b)

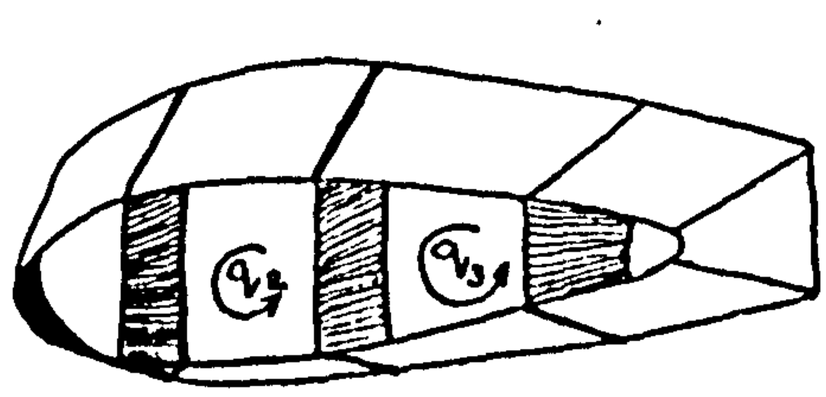

(c)

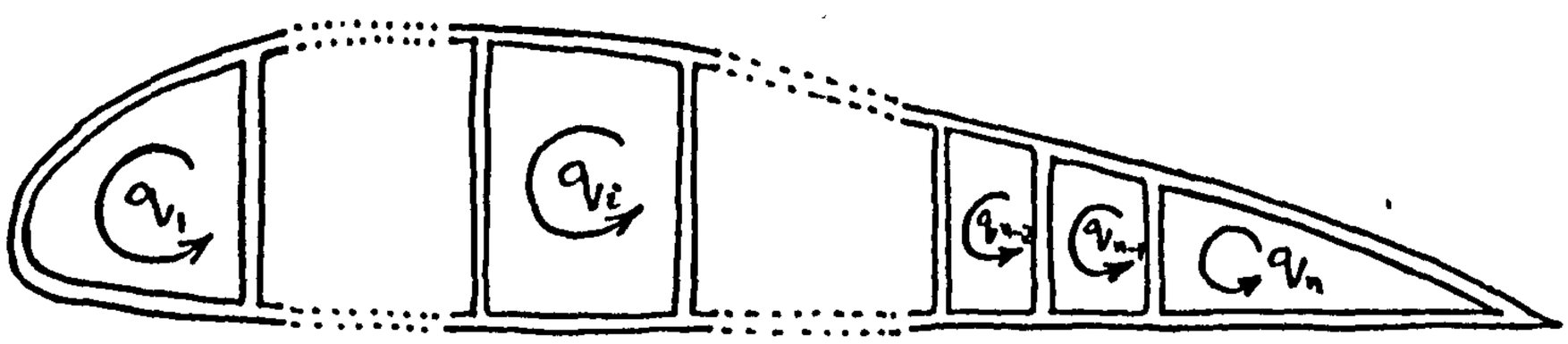

(d)

Figure 4.4 MULTI-CELL STRUCTURES

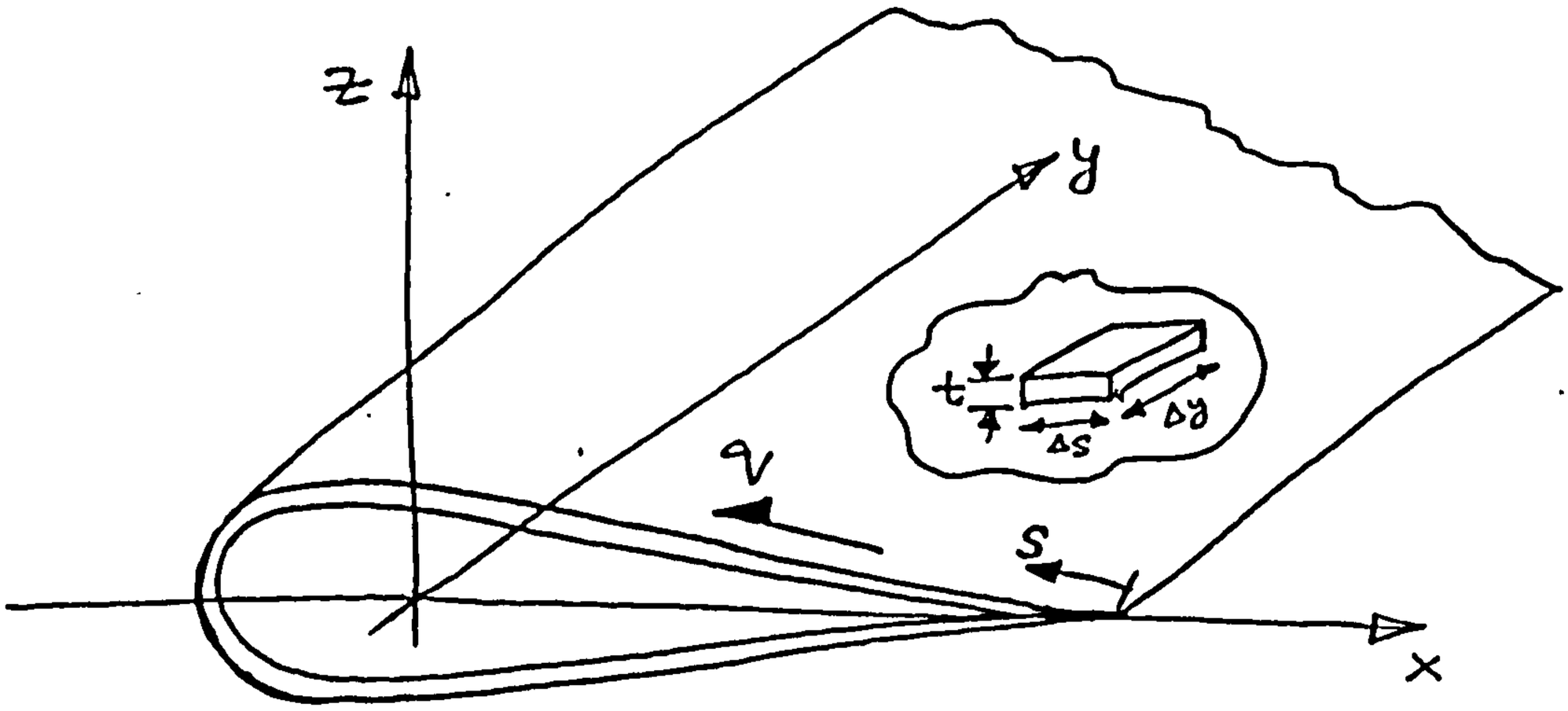

Figure 4.5 Co-ordinate system for closed section

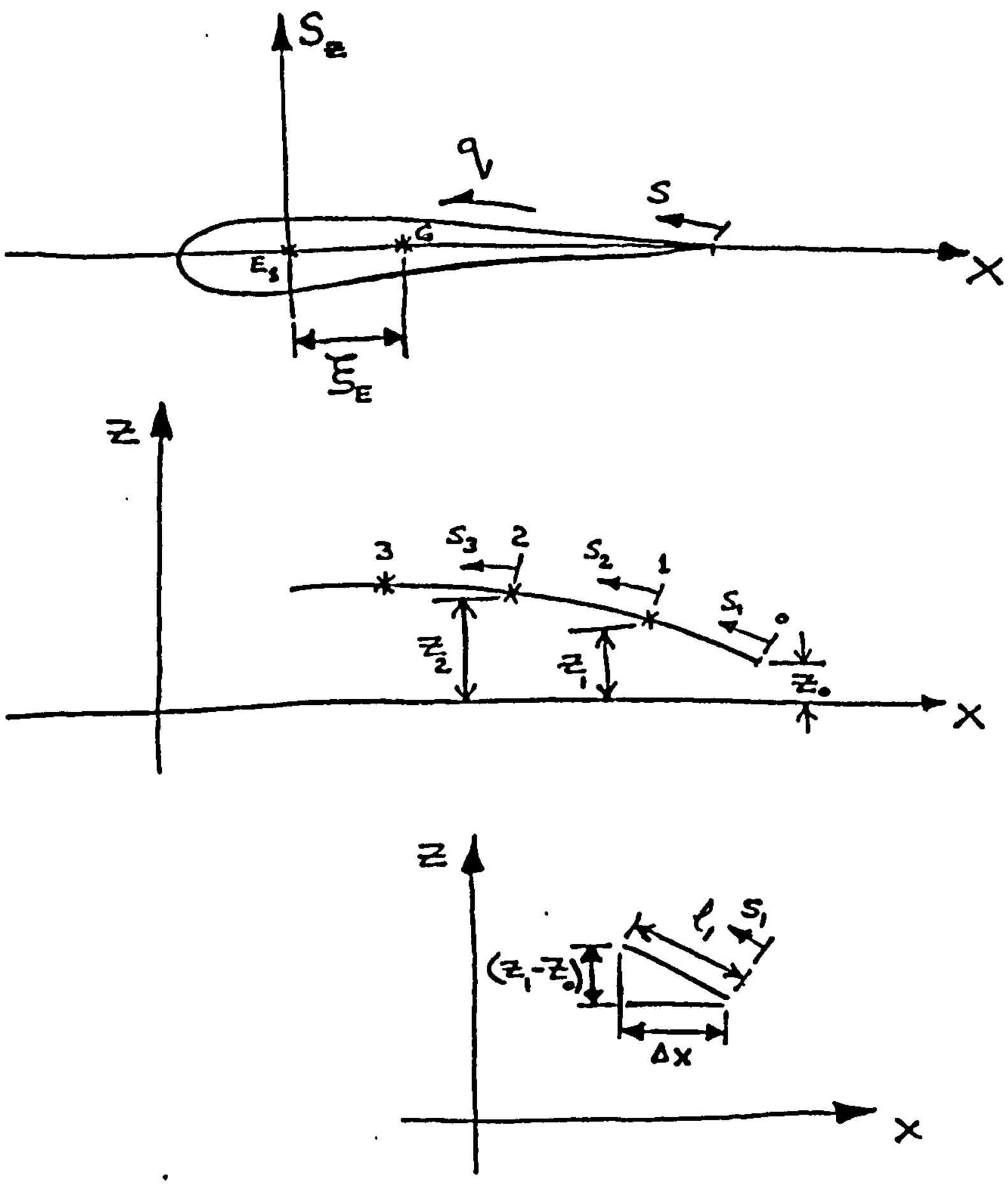

Figure 4.6 Segmentation of closed section

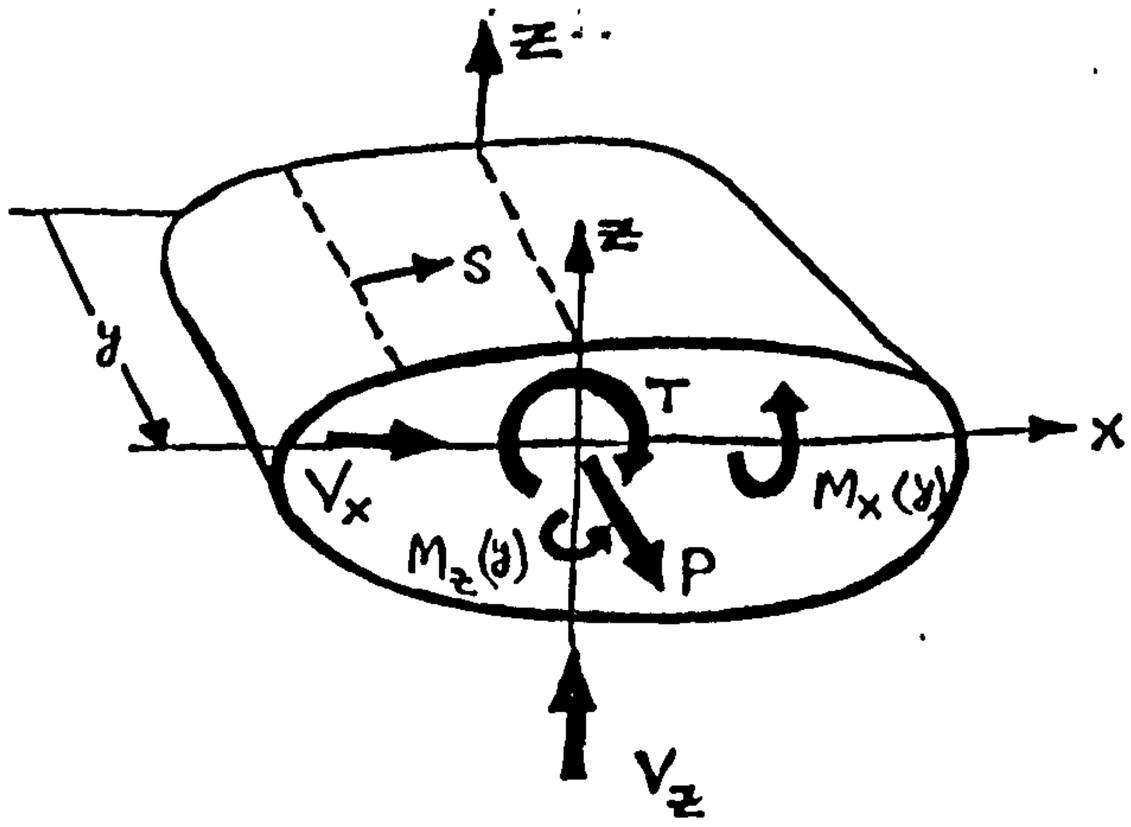

(α) SYSTEM OF COORDINATES AND LOADS

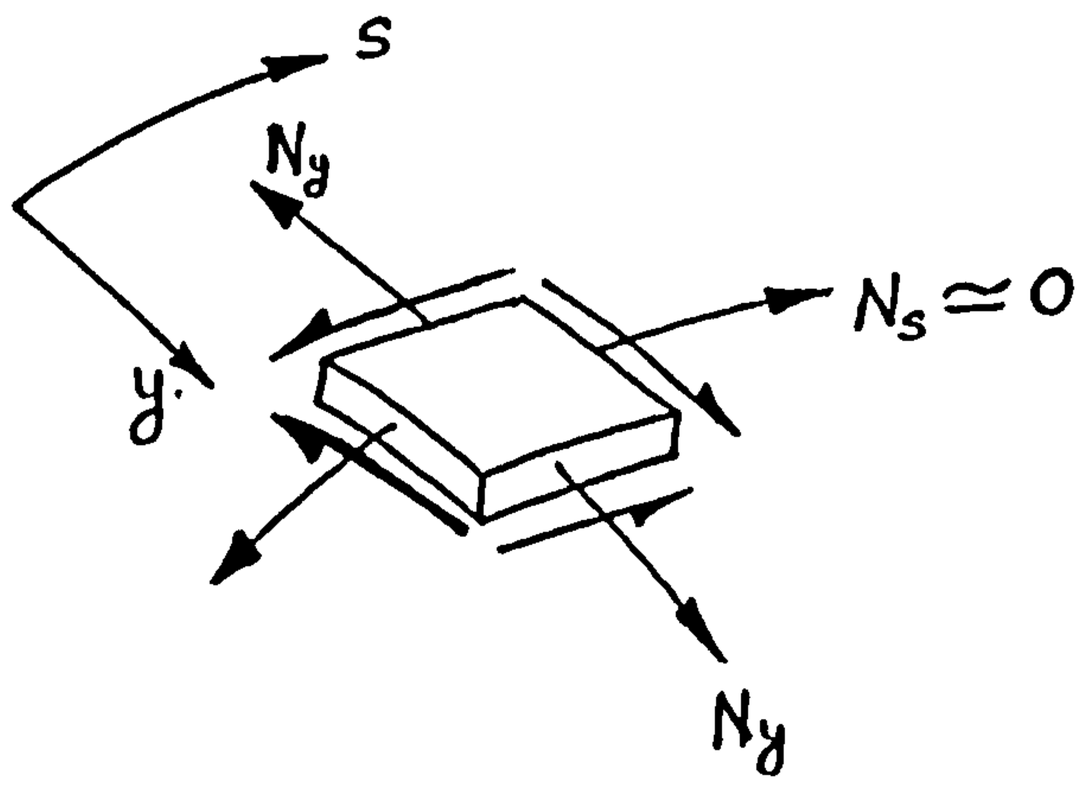

(b) STATE OF STRESS

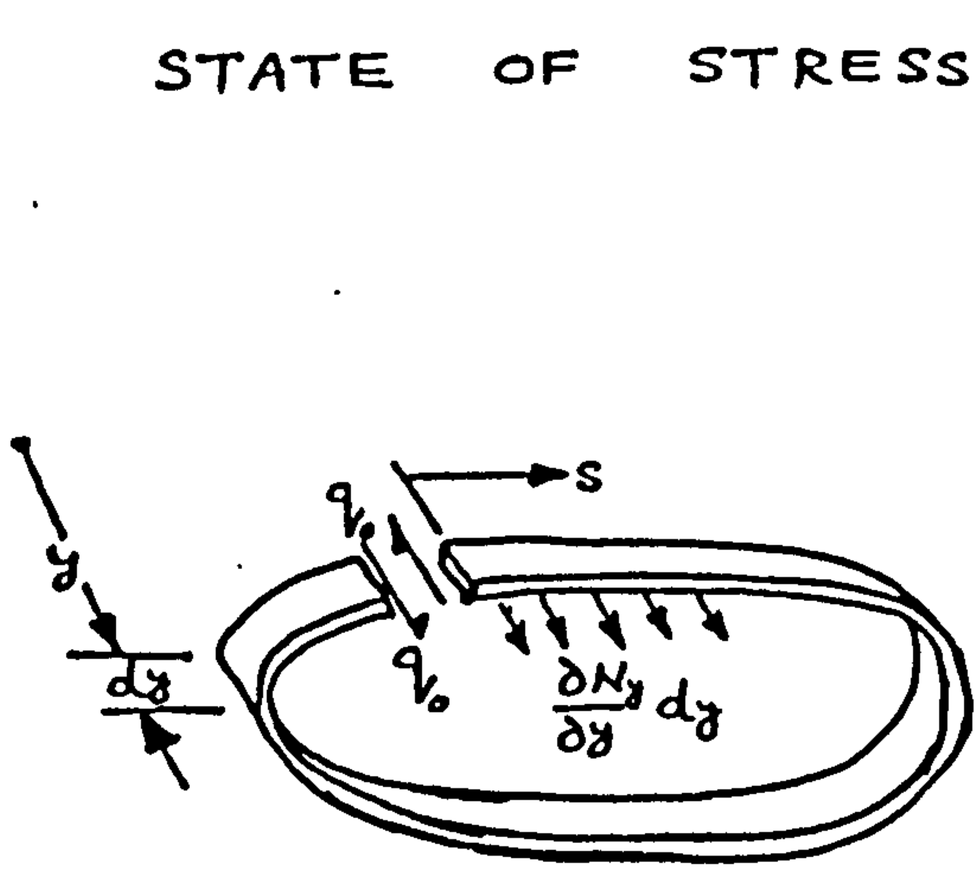

Figure 4.7 (C) SHEAR FLOW

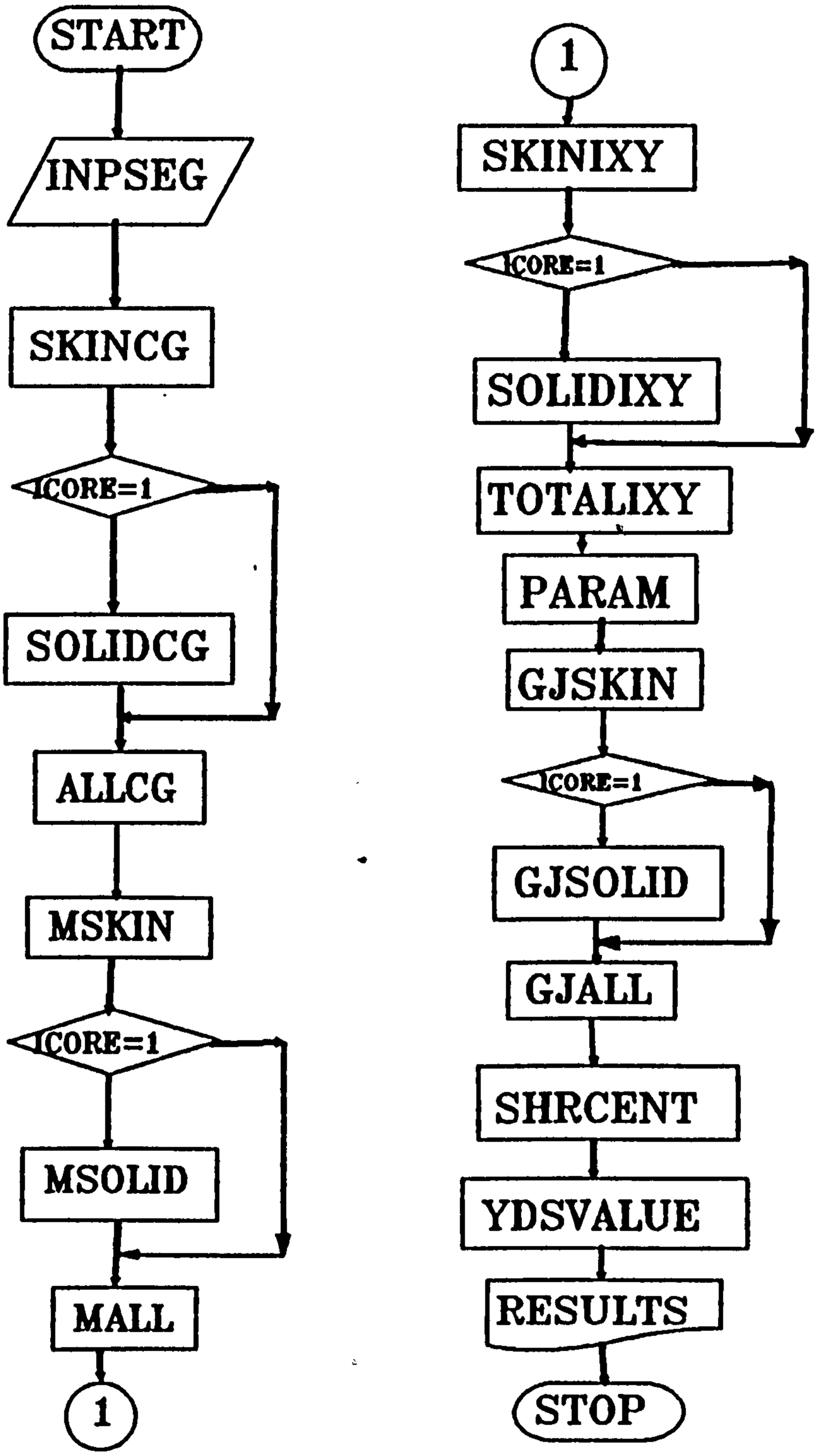

FIG. 4.8 FLOW CHART FOR COMPUTER PROGRAM "SECTION"

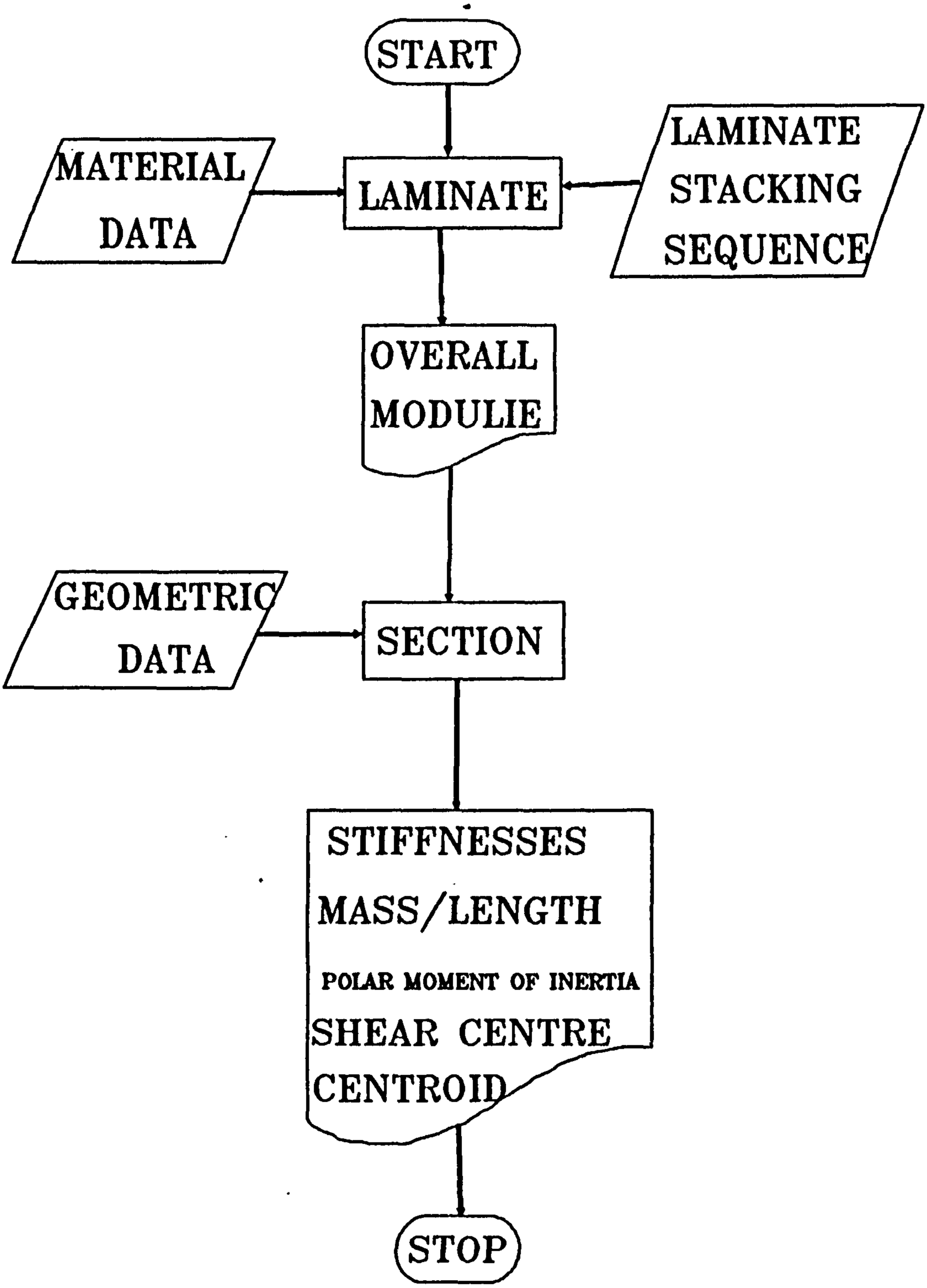

FIG. 4.9 FLOW CHART FOR COMPUTER PROGRAM "KSTIF"

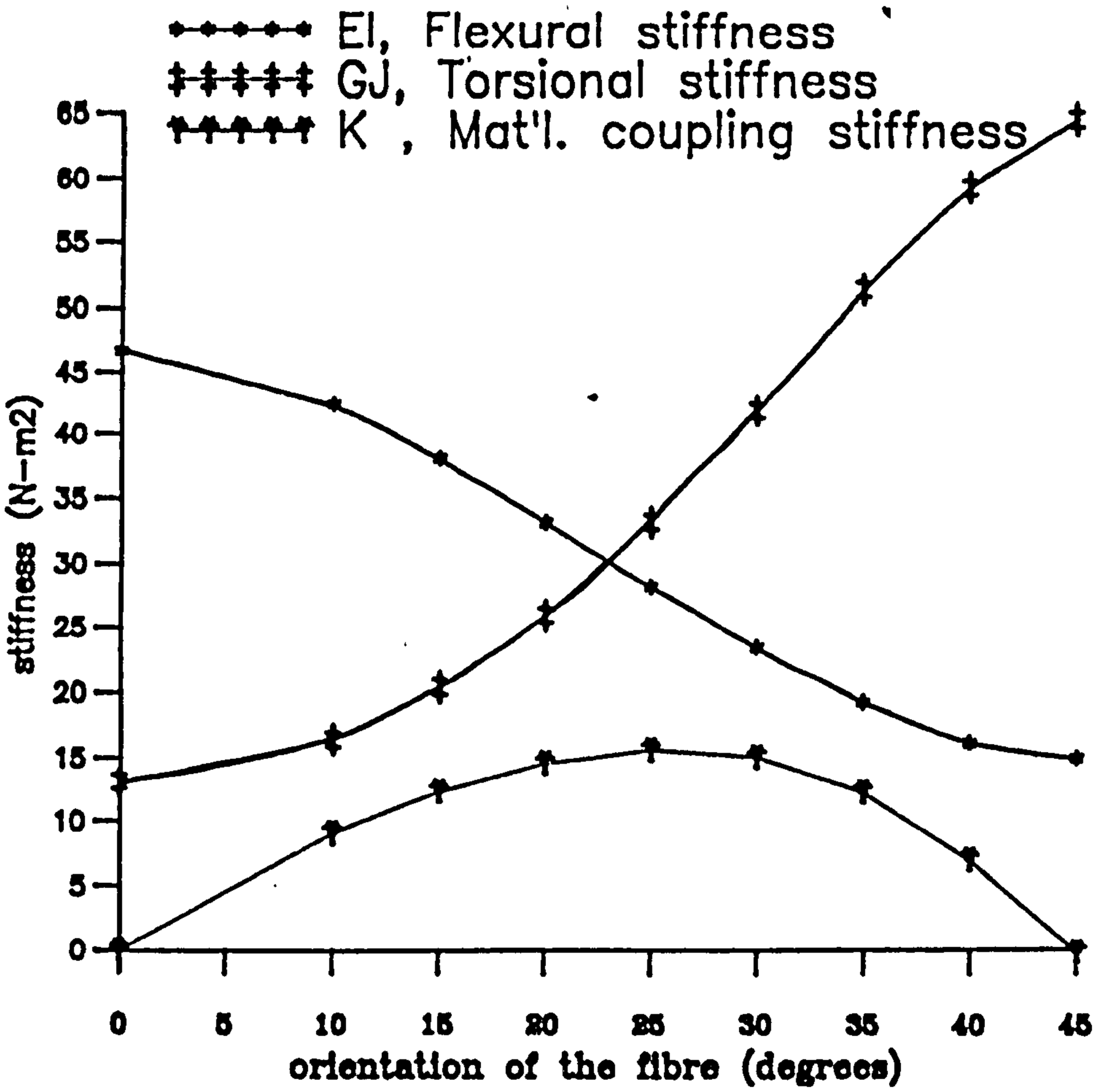

FOR WING W-DMS-7

FIG. 4.10 Effect of Fibre orientation on the Flexural, Torsional and Flexura/torsional coupled rigidities **(glass fibres in unsaturated polyester with 60% fibre volume fraction)**

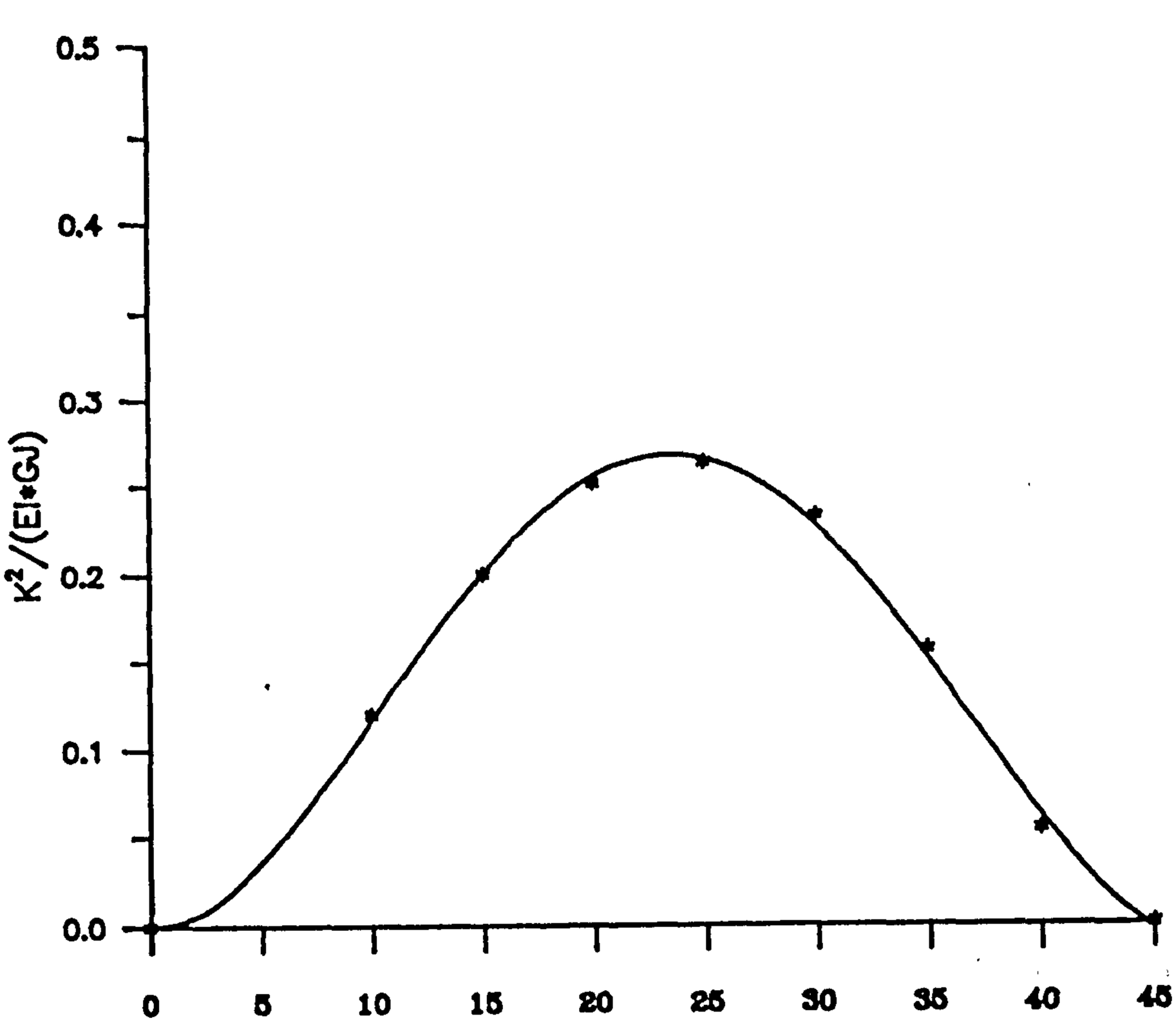

FOR WING W–DMS–7

FIG. 4.11 Effect of Fibre orientation on ϕ i.e. $K^2/(EI\ GJ)$ (glass fibres in unsaturated polyester with 60% fibre volume fraction)

CHAPTER : 5

STATIC STRUCTURAL PROPERTIES

5.1 INTRODUCTION

Experimental investigations of the static structural properties such as bending, torsional, bending-torsional coupling stiffnesses, mass distribution, polar mass moment of inertia, shear centre and centroid were carried out on beam and plate structures made of isotropic and anisotropic (composite) materials. In the case of composite structures, material tests were performed on standard specimens to establish their properties. Experiments on structures made of conventional (isotropic) materials were of dual purpose. First, these tests helped to validate the procedures adopted and components used in the experimental setup. Secondly, these tests served as a standard to compare results obtained from composite structures.

5.2 EXPERIMENTAL TECHNIQUES

A general description of experimental procedures adopted is first discussed. In order to determine bending, torsional, and bending-torsional coupled stiffnesses accurate measurement of transverse deflection and twist of the structure is vital. Several different techniques were employed to measure these displacements.

5.2.1 MECHANICAL

Simple dial gauges were used to measure the bending and torsional deflections of the loaded structures. Dial gauges are easy to use and do not require any additional equipment except stands with magnetic and relatively sturdy bases. The possible source of error due to the

common problem of stiction in dial gauges is overcome by using a spring loaded plunger. But some of the structures were so flexible that their stiffnesses were not greater than the stiffness of the spring used in the dial gauge. Therefore, part of the forces were absorbed in overcoming the stiffness of the spring resulting in an under estimated dial gauge reading and, hence, over estimated stiffnesses of the structure. Thus other techniques were used that could measure deflections remotely.

5.2.2 OPTICAL

An optical technique is a very familiar method for measuring deflections remotely. The deflection on the specimen is measured by the reflected back spot light or a laser beam focused on the mirrors attached to the test structure. In the set-up for this work, a cross-wire is observed on a scale (foot ruler) through the reflected rays from mirrors on the specimen by means of a telescope. The deflections are measured at more than one location in order to avoid end effects.

5.2.3 ELECTRICAL

Strain gauges were also used to measure the surface strains and subsequently the readings were decoded in terms of slope of the deflected beam and the angular deflection of the twisted structure. In the case of composite structures the size of the strain gauges has been of some concern. The non-homogeneous texture of composites require larger strain gauges so that the strains can be representative of the structure rather than local due to the fibres.

5.2.4 ACCELEROMETERS

Linear servo accelerometers that are originally used

in measurement of linear accelerations can be adopted to measure angular deflections. A brief description of linear servo accelerometers is given in Appendix (D). The mechanism and the circuit diagram of a linear servo accelerometer are shown in Figures (5.1) and (5.2).

5.3 EXPERIMENTAL PROCEDURE

In case of thin-walled open and closed section structures, the non-collinearity of the elastic axis (the locus of shear centres) and the centroidal axis made it necessary to establish the shear centre prior to the determination of the bending or torsional stiffnesses. (This was done to avoid elastic coupling which can occur if the transverse load is not applied at the shear centre.) But in the case of plate structures due to the collinearity of both the mass and elastic axes, this particular sequence was not essential. The tests were carried out in the following sequence in order to obtain maximum data from each specimen.

1. Manufacture of specimen
2. Specimen cut and trimmed to required dimensions
3. Various dimensions and weight are measured
4. Determination of the centre of gravity
5. Determination of polar mass moment of inertia
6. Root the specimen in Woods metal
7. Determination of the shear centre
8. Determination of the bending rigidity
9. Determination of the torsional rigidity
10. Evaluating the bending-torsional coupling rigidity

A variety of materials has been used in manufacturing various structures. Steps two and three are self explanatory. The centre of gravity of the structure

was found by supporting the structure spanwise on a sharp edge. The rest of the steps will be discussed separately in detail as follows.

5.4 MASS MOMENT OF INERTIA

An important structural property, the mass moment of inertia was found by two slightly different methods. The results obtained by the two methods were found to be in close agreement.

METHOD 1 : A very simple method was used to find the mass moment of inertia of the structure. Two small holes were drilled on either end of the structure and the specimen was suspended spanwise from a horizontal bracket as shown in Figure (5.3a). Then it was given a swing and the time for ten to fifteen oscillations was recorded. Thus the structure was treated as a compound pendulum as shown in Figure (5.3b). The time period of oscillation was then measured. The theory of the compound pendulum can be found in standard texts [1]. Using the equation of motion of the compound pendulum for small oscillations, an expression for the determination of polar mass moment of inertia was obtained as follows :

$$I_{po} = \frac{m\ g\ r\ T^2}{4\ \pi^2} + m\ (a^2 - 2\ a\ r) \qquad (5.1)$$

where I_{po} = mass moment of inertia about the shear centre
I_g = mass moment of inertia about centre of gravity
T = time period = $1/f$
f = frequency of oscillation
m = mass per unit length
g = acceleration due to gravity

r = distance between pivot point and centre of mass

a = distance between pivot point and shear centre

METHOD 2 : In the second method a mild steel rod of half an inch diameter was bolted to a horizontal wall bracket as shown in Figure (5.4). The other end of the bar was welded to a disc. A fixture was attached to the disc to hold the structure. The torsional rigidity of the bar was established experimentally. The mass moment of inertia of the disc was determined by twisting the disc and measuring the time period of oscillation of the disc on the rod in torsion. Then the test structure was attached to the fixture and the new time period of oscillations was recorded. The mass moment of inertia of the structure was determined using following expression [1].

$$\text{MOMENT OF INERTIA OF THE STRUCTURE} = \frac{GJ}{4\pi^2 \ell}\left\{T^2 - T_o^2\right\} \qquad (5.2)$$

where

T_o = time period of the oscillating disc

T = time period of the oscillating disc with structure

GJ = torsional rigidity of the rod

ℓ = length of the rod

5.5 SHEAR CENTRE

The structure was rooted in Woods-metal to form a cantilevered end condition. A light wooden attachment as shown in Figure (5.5) was made to fit the free end for the application of load on various structures. The cantilevered structure was firmly gripped in a vice on a L-shaped sturdy base specially made for this purpose.

The load was applied at different locations along the chord of the structure while torsional deflections of the structure were recorded using the various techniques mentioned earlier. The torsional deflections of the structure were measured near the root as well as near the tip. Then load positions were plotted against the difference between the two torsional deflections of the structure. The location for zero twist will be the shear centre for the cross-section of the structure.

5.6 STIFFNESS ESTIMATION

In the case of structures made of conventional (isotropic) materials, separate tests for the determination of bending rigidity and torsional rigidity can be conducted. Even elastically coupled structures can be carefully loaded at the shear centre to obtain transverse deflections when subjected to transverse bending loads and torsional displacements when twisted.

But for structures made of composite (anisotropic) materials this is not generally possible. The presence of material coupling requires the measurement of transverse and torsional deflections simultaneously when subjected to a transverse bending load or a torque. The results are treated together to evaluate bending, torsional, and bending-torsional coupled rigidities. The experimental set up is shown in Photographs (5.1), (5.2), (5.3). The displacements were measured by means of the various techniques mentioned above.

5.6.1 BENDING STIFFNESS OF ISOTROPIC STRUCTURES

When the structure is subjected to a transverse loading at the elastic axis, transverse deflection results due to bending moment and the distortion of the cross-section is produced by the variation of shear

stress over the depth of the beam.

Three sets of techniques were used in the determination of bending rigidity. The mathematical expressions pertaining to each type of technique are as follows :

5.6.1.1 DIAL GAUGES

Dial gauges were placed on the elastic axis along the span to measure the deflections due to the load applied at the tip of the wing. Using the Engineer's bending theory the deflection at various locations due to bending caused by a concentrated load at the tip of a cantilevered beam is given by the following expression [2].

$$\delta_B = \frac{P\ y^2}{6\ EI}\ (\ 3\ \ell - y\ ) \qquad (5.3)$$

and deflection due to shear

$$\delta_S = \frac{\alpha\ P\ y}{A\ G} \qquad (5.4)$$

therefore, total deflection is the sum of both δ_B and δ_S

$$\delta_T = \delta_B + \delta_S = \frac{P\ y^2}{6\ EI}(3\ \ell - y\ ) + \frac{\alpha\ P\ y}{A\ G} \qquad (5.5)$$

Hence the bending stiffness:

$$E\ I = \frac{y^2\ (3\ \ell - y)}{6\ \left\{\frac{\delta_T}{P} - \frac{\alpha\ y}{A\ G}\right\}} \qquad (5.6)$$

where

P = load applied at the tip (at the shear centre in to produce pure bending in the structure).

y = dial gauge location to calibrate the deflection

ℓ = length of the wing

α = shear coefficient

Deflections along the flexural axis (locus of the shear centres) were measured by a series of dial gauges with accuracy up to 0.01mm. These deflections were plotted against the loads (see Figure (5.7) for these plots from a typical test structure). The results for the experiments are discussed in sections (5.7) and (5.8).

5.6.1.2 STRAIN GAUGES

In the case of strain gauges, surface strains are measured when the structure is transversely loaded. The bending moment will cause stresses which will be tensile on the concave side and compressive on the convex side. Their magnitude will be maximum at the free surface of the structure. Strains developed due to these stresses are recorded by strain gauges. The bending rigidity of the structure can be determined by the following expression [s].

$$EI = \frac{p}{\varepsilon} \frac{h(c-y)}{2} \qquad (5.7)$$

where

EI = bending stiffness

$\frac{p}{\varepsilon}$ = slope of the load p to the surface strain ε

h = thickness of the beam

c = distance from root to the application of load

y = distance from root to the strain gauge

5.6.1.3 LINEAR SERVO ACCELEROMETER

A linear servo accelerometer measures the angular twist. It can be used in the case of bending rigidity determination to measure the slope of the deflected structure. If the load is applied at any point along the span other than at the tip, there will be two different types of slopes of the deformed structure. Therefore, the bending rigidity of the structure can be determined by

two sets of equations depending upon the location where the slope has been measured. In the case where the slope is measured between the root and the point of application of load, the bending rigidity is calculated by the following expression [8].

$$EI = \frac{P}{\theta} \frac{c^2}{2} \left[1 - \frac{(c - y)^2}{c^2}\right] \qquad (5.8)$$

In the case of the slope being measured at a location beyond the point of application of load, the following expression will be suitable [8].

$$EI = \frac{P}{\theta} \frac{c^2}{2} \qquad (5.9)$$

where

$\frac{P}{\theta}$ = slope of the load plotted against deflection

y = distance from root to the servo accelerometer

5.6.2 TORSIONAL STIFFNESS

A similar arrangement was made for measuring the torsional rigidity of the structures, (see Figure (5.6)). Angular deflections at two different locations were measured by optical and linear servo accelerometer techniques. The torque applied is proportional to the rate of twist with the torsional rigidity as the proportionality constant.

$$T = GJ \frac{d\theta}{dz} = GJ \frac{\theta}{\ell} \qquad (5.10)$$

where

θ = angle of twist over a length ℓ

GJ = torsional rigidity

T = applied torque

But applied torque on the structure is the product of load applied (P) and the moment arm (r) as shown in

Figure (5.6). The angular deflection in the structure using the optical technique will be :

$$\theta = \frac{\delta}{2R} \qquad (5.11)$$

where

δ = distance deflected in the telescope sight

R = distance between the scales and the mirrors on the structure.

Therefore,

$$GJ = 2\,\ell\,r\,R\,\frac{P}{\delta} \qquad (5.12)$$

where

$\frac{P}{\delta}$ = slope of the load plotted against the deflection.

(Results are discussed in sections (5.7) and (5.8)).

5.6.3 FLEXURAL, TORSIONAL, AND MATERIAL COUPLING RIGIDITIES OF COMPOSITE (ANISOTROPIC) STRUCTURES

The expressions pertaining to transverse deflection and twisting of the thin-walled beams due to transverse loading or torque (B.2.1) to (B.2.4) given by Chopra [4] (see in Appendix (B)) gave the following four equations :

$$EI = 0.5\left[\frac{P}{h}\right]_B (2\,\ell\,y - y^2) + K_{p\theta}\left[\frac{\psi}{h}\right]_B \qquad (5.13a)$$

$$GJ = K_{p\theta}\left[\frac{h}{\psi}\right]_B \qquad (5.13b)$$

$$EI = -K_{p\theta}\left[\frac{\psi}{h}\right]_T \qquad (5.13c)$$

$$GJ = \left[\frac{T}{\psi}\right]_T y - K_{p\theta}\left[\frac{h}{\psi}\right]_T \qquad (5.13d)$$

where

P = transverse loading

T = torque applied

h and ψ = transverse and torsional deflections

$\left(\frac{P}{h}\right)_B$ = slope of the load to the deflection during bending rigidity test

$\left(\frac{h}{\psi}\right)_B$ = slope of the deflection (transverse) to the twisting of the structure during bending test

$\left(\frac{T}{\psi}\right)_T$ = slope of the torque to the twist during torsional rigidity test

$\left(\frac{h}{\psi}\right)_T$ = slope of the deflection (transverse) to the twist during torsional rigidity test

K_{ps} = bending-torsional material coupling present in the symmetric laminates.

Comparing equations (5.13b) and (5.13c), a useful relation is obtained :

$$\left(\frac{\psi}{h}\right)_B = \phi \left(\frac{\psi}{h}\right)_T \qquad (5.14)$$

where $$\phi = \left[\frac{-K_{ps}^2}{EI\ GJ} \right]$$

which is a very important non-dimensional parameter and is a measure of bending-torsional coupling due to the stacking sequence of the composite material.

Comparing the expressions for EI and GJ obtained from the two types of loading, explicit expressions for EI, GJ, and K_{ps} are derived as follows:

$$EI = \left[- \frac{\left(\frac{T}{\psi}\right)_T \left(\frac{\psi}{h}\right)_B^2 \left(\frac{\psi}{h}\right)_T^2 Y}{\left(\frac{\psi}{h}\right)_B^2 - \left(\frac{\psi}{h}\right)_T^2} - \frac{\left(\frac{P}{h}\right)_B \left(\frac{\psi}{h}\right)_T^2 \frac{Y^2}{2}(2\ell - Y)}{\left(\frac{\psi}{h}\right)_B^2 - \left(\frac{\psi}{h}\right)_T^2} \right] \qquad (5.15a)$$

$$GJ = \left[- \frac{\left(\frac{T}{\psi}\right)_T \left(\frac{\psi}{h}\right)_T^2 Y}{\left(\frac{\psi}{h}\right)_B^2 - \left(\frac{\psi}{h}\right)_T^2} - \frac{\left(\frac{P}{h}\right)_B \frac{Y}{2}(2\ell - Y)}{\left(\frac{\psi}{h}\right)_B^2 - \left(\frac{\psi}{h}\right)_T^2} \right] \qquad (5.15b)$$

$$K_{ps} = \left[\frac{\left(\frac{T}{\psi}\right)_T \left(\frac{\psi}{h}\right)_B^2 \left(\frac{\psi}{h}\right)_T y}{\left(\frac{\psi}{h}\right)_B^2 - \left(\frac{\psi}{h}\right)_T^2} + \frac{\left(\frac{P}{h}\right)_B \left(\frac{\psi}{h}\right)_T \frac{y^2}{2}(2\ell - y)}{\left(\frac{\psi}{h}\right)_B^2 - \left(\frac{\psi}{h}\right)_T^2} \right] \quad (5.15c)$$

These expressions suggest that two kinds of measurements are required on the structure. The transverse and torsional deflections of the structure are measured when subjected to pure transverse loading and then to pure torque. Each type of loading will yield ratios between loading and corresponding deflection (i.e. transverse loading to the transverse deflection and torque to the twisting deformation), and the ratio of transverse and twisting deformation due to bending-torsional coupling of the material. Substituting these results in the above expressions will give the experimental measure of the flexural, torsional, and material coupling rigidities.

5.7 VALIDATION OF THE TEST TECHNIQUES

Tests were carried out on various structures made of conventional materials such as aluminium alloy in order to validate the test procedures adopted. The relative merits of various deflection measurement techniques were also assessed during these experiments.

The results are summarized in Tables (5.1) - (5.3). Material properties for aluminium alloy is given in Appendix (J). Tests carried out on three different specimens, a prismatic beam, a thin plate, and a thin-walled closed section with cantilevered end conditions are discussed in detail as follows :

5.7.1 BEAM ELEMENT

A bending rigidity test was performed on a cantilevered aluminium alloy prismatic beam with dimensions (25.7 mm x 9.8 mm). The results are given in Table (5.1). The test using strain gauges gave better results as compared to the linear servo accelerometers.

5.7.2 PLATE ELEMENT

A cantilevered thin aluminium alloy plate with dimensions (300 x 75 x 0.71 mm) was tested to establish its bending rigidity and torsional rigidity. The optical method was used to record the deflections due to the very flexible nature of the specimen. The results are given in Table (5.2). In both the bending and torsional rigidity tests, the experimentally observed figures were higher than the theoretical estimates. The error can be attributed to the end conditions and the method of application of the load. But the overall error levels were within engineering accuracy limits.

5.7.3 THIN-WALLED CLOSED SECTION

The torsional rigidity of a cantilevered aluminium thin-walled closed square section beam with dimensions of (50.8 x 1.35 mm) was determined using dial gauges and linear servo accelerometers. The results are summarized in Table (5.3). The method using an accelerometer as a torsional deflection measuring device gave better results compared with the dial gauges.

5.8 STRUCTURAL PROPERTIES OF COMPOSITE SECTIONS

5.8.1 FABRICATION OF SECTIONS

5.8.1.1 OPEN SECTIONS

Two piece metal moulds were made for the open sections. The prepreg GFRP sheets were cut to size with

the help of a template. The moulds were degreased and thoroughly cleaned. Then anti-stick spray was sprayed over the surfaces. The moulds were preheated to about $60^{o}C$ in an oven. The layers of composite material were carefully placed on top of each other. Air gaps were eliminated by means of a roller. Then the laid up material was cured according to the prescribed temperature and pressure as mentioned below. Tee-sections were prepared by joining two angle sections by means of epoxy glue.

5.8.1.2 CLOSED SECTIONS

The closed sections were made by a hand-lay-up technique. A wooden former was used to create the desired profile. Woven glass fibre cloth was cut to size. Then the cloth was flattened over wax paper sheets on a flat surface. The catalyst was added to the unsaturated polyester. After thorough mixing, it was spread over the cloth. When the resin reached the jelly state, another wax sheet was placed over the cloth and air bubbles were squeezed out. The laminate between the two wax paper sheets was later on wrapped around the wooden former to give it a profile. A moderate pressure was applied to keep the surface smooth and flat. After curing, both the top and bottom wax sheets were removed and the trailing edge was glued. Finally after curing it was trimmed to desired size.

5.8.2 PLATE STRUCTURES

Three composite plates with a lay-up sequence of $(0_8)_s$, $(\pm 30^{o})_s$, $(\pm 45^{o},0)_s$ were made from fibredux C920 unidirectional prepreg carbon fibre composite material. Fibredux C920 is a high toughness, general purpose epoxy prepreg with the fast curing capability of 60 minutes at

a temperature of 125° C or 5 minutes at a temperature of 160° C and at a pressure of 300 KN/m^2 [4]. A brief account of its material properties are given in Appendix (J). The plates were properly trimmed and were weighed. The span, chord and thickness dimensions were measured. Bending and torsional rigidity tests were carried out using a test rig as shown in Photograph (5.8).

There were six plies in each composite plate with dimensions as given in Table (5.4). The flexural moduli (laminate D-matrix) were caculated using the LAMINATE program and are tabulated in Table (5.5). Structural properties such as mass per unit length and the polar moment of inertia are presented in Table (5.6). The structural bending, torsional, and bending-torsional coupled rigidities are given in Table (5.7).

Results plotted in Figure (5.8) show good agreement between theoretical predictions and experimental results for flexural rigidity and coupled bending-torsional rigidity tests. The theoretical estimation of torsional rigidity for the zero degree case is well below the experimental figure. This is due to the reason that all the fibres are aligned with the longitudinal axis of the plate and in a torsional rigidity test the matrix resin will be primarily responsible for contributing to the torsional rigidity. However, the material property shear modulus of rigidity was established using a 45° laminated plate where the contribution of fibres was dominant as compared with resin.

5.8.3 THIN-WALLED OPEN SECTIONS

Three types of thin-walled open sections made of Fibredux 916G woven glass fibre prepreg composite were tested. Fibredux 916G is an epoxy prepreg with good adhesion to honeycomb and fire retarding capability with

good environmental resistance. A brief account of the material properties are given in Appendix (J). A cure cycle of 60 minutes at 120° C or 30 minutes at 130° C at a moderate pressure is recommended.

The choice of laminate lay-up was made in such a way that a decrease in bending stiffness and an increase in torsional stiffness was exhibited in the absence of coupled (bending-torsional) stiffness. This was necessary to avoid complications due to bending-torsional coupled stiffness of the structure.

(i) ANGLE SECTION

Four angle sections of zero degrees, $[0_2]_2$ and three of $[\pm 10^\circ]_2$, $[\pm 20^\circ]_2$ and $[\pm 45^\circ]_2$ each were made with sectional details as given in Table (5.8). Structural parameters such as mass per unit length and polar mass moment of inertia are tabulated in Table (5.9). Experimental results of flexural and torsional rigidities are compared with theoretical predictions in Table (5.10).

(ii) TEE SECTION

Four sections were prepared for zero degree lay-ups only. The sectional details are given in Table (5.11) and structural parameters such as mass per unit length and polar mass moment of inertia are given in Table (5.12). Structural rigidities are compared with the experimental results in Table (5.13).

(iii) CHANNEL SECTION

Four specially orthotropic zero degree lay-up specimens and other four generally orthotropic but symmetrically laminated channel sections of $[\pm 10^\circ]_2$, $[\pm 20^\circ]_2$, $[\pm 30^\circ]_2$ and $[\pm 45^\circ]_2$ lay-ups were manufactured.

The sectional details of these sections are given in Table (5.14). Structural parameters such as mass per unit length, polar mass moment of inertia, and shear centre locations along with structural rigidities are tabulated in Table (5.15).

Tests performed on composite thin-walled open sections yielded large disagreements between the predicted stiffnesses and the experimental results. There are several reasons for these errors. Effects of non-collinearity between the centroidal and elastic axes and warping already present even in sections made of isotropic materials makes the investigation complicated enough. In the case of composite materials, the bending-torsional coupling effect adds to this complexity. The three cross-sections discussed above appear in their order of complexity as follows.

In the case of bending rigidity tests, the percentage error for sections with a zero degree lay-up remained within engineering accuracy limits. But in the case of lay-ups other than zero degrees, the error increased. During the tests it was observed that when the load was applied at the shear centre (experimentally established in advance), the cross-section lost its shape near the mid-span and deviated from the closed space rigid diaphragm (CRSRD) assumption used in the development of the Engineer's bending theory. The other reason can be the effect of shear deformation which was ignored and which can be important for composite sections.

5.8.4 THIN-WALLED CLOSED SECTIONS

Thin-walled closed section composite beam structures were manufactured and tested for various static structural characteristics. The shape of the

cross-section was that of a NACA 0012 aerofoil with the ultimate aim to investigate aeroelastic behaviour of composite lifting surfaces. It was anticipated that these composite aerofoil shape sections would exhibit flutter in the wind tunnels at the City University. The wind tunnel speed and space limitations influenced the choice of material, number of layers, and ply orientation. A parametric study revealed that a single ply with zero degree ply orientation would be flexible enough to exhibit flutter within the available wind tunnel speed and space limits. Therefore, main attention was paid to a single ply with zero degree ply orientation structures. Later on, four other wings with 10, 20, 30, and 45 degrees ply orientation were manufactured and tested to observe the effect of ply orientation on stiffnesses and natural frequencies.

During bending rigidity tests some of the structures suffered from the Brazier-load-effect due to thin walls and some of the specimens were damaged during the test. Polystyrene or Polyurethene expanded foam filled sections were made to stop kinking or possible buckling of these structures. This increased the bending and torsional rigidities of the structure. The flutter speeds also increased due to the higher rigidities. The tests provided valuable experimental data about the static and dynamic properties of thin-walled closed section composite structures.

Hand laid up woven glass reinforced plastic was also used to prepare a specimen. The material properties for this are given in Appendix (J).

The dimensional details of thin-walled composite closed sections are given in Table (5.16). Structural parameters such as mass per unit length, location of the centroid, distance of the shear centre from the centroid

and polar mass moment of inertia with respect to the shear centre of these sections are compared with the experimental results in Tables (5.17) and (5.18).

Flexural and torsional rigidities of zero degree ply lay-up wings are compared with theoretical predictions in Table (5.19). Results for structures with other orientations having coupled flexural/torsional rigidities are compared in Table (5.20).

5.9 DISCUSSION OF RESULTS AND CONCLUSIONS

The experimental investigation of the static structural characteristics of structures made of isotropic or anisotropic (i.e. composite materials) was carried out with appreciably good results when compared with the theory. The tests covered thin-walled open and closed section beams and plates.

Experiments performed on composite plates showed large differences between theoretical predictions and experimental results in the torsional rigidity tests at zero degree lay-up. This can be attributed to an under-estimated value for the shear modulus of rigidity of the material. The results for other lay-ups agreed very well for the torsional rigidity test. In the case of the bending rigidity testing, the results were within engineering accuracy limits for the zero degree case but large errors were encountered for other lay-ups. One possible explanation is that the end conditions suppressed the chordwise curvature, affecting the twist deformation due to the D_{16} term of the compliance matrix. This effect will be zero in the case of the zero degree laminate but can be significant for the other lay-ups.

In the case of thin-walled open section structures, the disagreement between theoretical predictions and experimental results increased as the complexity of the

section increased. The effect of warping was found to be playing an important role as expected. These types of section require an improved mathematical model for further study.

Closed sections produced good results from torsional rigidity tests but in the case of flexural rigidity determination due to lack of control of the fibre volume fraction, large differences were encountered. A correction to this factor improved the overall status.

A summary of the percentage errors found between theoretical estimations and experimental results for different structures using a variety of measurement devices is given in Tables (5.21) - (5.24).

REFERENCES

1. Meriam, J.L. and Kraige, L.G., Engineering Mechanics, Vol 2 : Dynamics, John Wiley and Sons, 2nd edition, 1987.

2. Timoshenko, S., Strength of Materials, Part I : Elementary, Part II : Advanced, Van Nostrand Reinhold Company, 3rd edition, 1955.

3. Dally, J.W. and Riley, W.F., Experimental Stress Analysis, McGraw-Hill Book Company, 1965.

4. Ramesh, C., Stemple, A.D., and Chopra, I., "Thin-Walled Composite Beams Under Bending, Torsional, and Extensional Loads," Journal of Aircraft, Vol. 27, No. 7, July 1990, pp. 619-626.

Dimension : Width 25.7 mm , Thickness 9.8 mm		
Theoretically predicted bending rigidity : 141.1003 N-m^2		
Experimental results	(N-m^2)	Difference
Using Strain gauges	137.68	2.42 %
Using Linear servo acc.	130.58	7.46 %

TABLE : 5.1 Flexural rigidity results for prismatic bar

Dimension : Length 300 mm, Width 25.7 mm, Thickness 9.8 mm			
Rigidity Test	Theoretical (N-m^2)	Experimental (N-m^2)	% error
Bending	0.1541	0.16226	-5.29
Torsional	0.2357	0.23767	-0.84

TABLE : 5.2 Rigidity test results for plate structure

Width = Height = 50.8 mm , Thickness = 1.35 mm			
Torsional Rigidity Test	Theoretical (N-m^2)	Experimental (N-m^2)	
		Dial gauges	Linear Servo Accelerometer
Results	4778.47	3105.33	4406.11
% difference		35.01	7.79

TABLE : 5.3 Torsional rigidity results for square section

Lay-up	Thickness (mm)	Ply Thick (mm)	Chord (mm)	Length (mm)	Area (mm^2)
$[0_s]_s$	0.803	0.13383	73.5	291.0	59.0205
$[\pm 30]_s$	0.801	0.1335	74.0	291.0	59.274
$[\pm 45/0]_s$	0.804	0.1340	75.0	291.0	60.300

TABLE 5.4 Dimensions of composite plates

Lay-up	Flexural Moduli ... D-matrix (Nm)						Ratios	
	D_{11}	D_{12}	D_{16}	D_{22}	D_{26}	D_{66}	D_{16}/D_{11}	D_{16}/D_{66}
$[0_8]_s$	4.2251	0.0960	0.0	0.343	0.0	0.242	0.0	0.0
$[\pm^{+}_{+}30]_s$	2.6128	0.7355	0.5828	0.671	0.227	0.879	0.2230	0.6622
$[\pm^{+}45/0]_s$	1.549	0.928	0.436	1.404	0.436	1.074	0.2815	0.406

TABLE 5.5 Flexural moduli (D-matrix) of composite plates

Lay-up	Mass / length (Kg/m)			Moment of inertia
	Theo.	Exp.	% diff.	Theoretical (Kg-m)
$[0_8]_s$	0.0897	0.0868	3.23	$40.39 * 10^{-6}$
$[\pm^{+}_{+}30]_s$	0.09010	0.0859	4.66	$41.119 * 10^{-6}$
$[\pm^{+}45/0]_s$	0.09166	0.0906	1.16	$42.97 * 10^{-6}$

TABLE 5.6 Mass per unit length and moment of inertia of composite plates

Ply orientation		$[0_8]_s$	$[\pm^{+}_{+}30]_s$	$[\pm^{+}45, 0]_s$
Flexural Rigidity	Theory	0.31275	0.19334	0.1162
	Experiment	0.3043	0.1582	0.0972
	% Error	2.78	18.18	16.35
Torsion Rigidity	Theory	0.07103	0.26048	0.32212
	Experiment	0.1749	0.2435	0.3239
	% Error	-59.39	6.52	-0.55
Coupled Bending/ Torsion Rigidity	Theory	0.0	0.033596	0.06545
	Experiment	0.0	0.0284	0.0593
	% Error	0.0	15.36	9.40

TABLE 5.7 Rigidities of composite plates

Sp. No.	1	2	3	4	5	6	7
Orient.	Z E R O D E G R E E				10^{o}	20^{o}	45^{o}
SECTIONAL DETAILS							
a (mm)	30.00	31.00	31.50	31.00	30.00	31.00	31.00
b (mm)	30.00	31.00	31.00	31.50	30.00	31.00	31.00
h (mm)	42.00	44.00	44.50	45.00	44.00	44.00	44.00
t_a (mm)	0.907	0.953	0.838	0.990	1.070	1.074	1.163
t_b (mm)	0.921	0.909	0.946	0.993	1.071	1.074	1.163
ℓ (mm)	590.0	591.0	591.0	591.0	596.0	596.0	596.0

TABLE 5.8 Dimensions of composite thin-walled angle sections

Sp. No.	1	2	3	4	5	6	7
Orient.	Z E R O D E G R E E				10^{o}	20^{o}	45^{o}
STRUCTURAL PROPERTIES							
Mass per unit length - m (Kg/m)							
Theory	0.083	0.087	0.084	0.094	0.097	0.101	0.109
Exper.	0.0801	0.0844	0.0808	0.0909	0.0946	0.0979	0.1051
% Dif.	2.41	2.99	3.81	3.30	2.47	3.07	3.58
Mass Moment of Inertia - $I_{p\bullet}$ (Kg-m) * $10^{-\sigma}$							
Theory	24.89	27.87	27.34	30.60	29.10	32.35	34.92

TABLE 5.9 Structural parameters of composite angle sections

Sp. No.	1	2	3	4	5	6	7
Orient.	Z E R O D E G R E E				10^{o}	20^{o}	45^{o}
Flexural Rigidity - EI ($N-m^2$)							
Theory	197.16	215.67	213.3	237.0	243.55	228.08	212.80
Exper.	172.99	188.96	170.58	207.31	183.60	164.30	134.40
% Dif.	12.26	12.39	20.01	12.54	24.62	27.96	36.84
Torsional Rigidity - GJ ($N-m^2$)							
Theory	0.1069	0.1169	0.104	0.142	0.183	0.2035	0.3353
Exper.	0.1002	0.1178	0.1005	0.1347	0.1788	0.2034	0.3233
% Dif.	6.27	- 0.77	2.92	5.21	2.30	0.05	3.58

TABLE 5.10 Structural rigidities of composite angle sections

Ply Ang	Sp. No.	b (mm)	h (mm)	t_h (mm)	t_b (mm)	m (gm)	ℓ_t (mm)	ℓ_f (mm)
Zero Degree	1	64.0	32.0	1.955	0.901	130.5	588.0	568.0
	2	64.0	32.0	1.894	0.931	129.5	587.0	567.0
	3	63.0	32.0	1.806	0.971	130.5	591.0	571.0
	4	64.0	32.0	1.904	0.998	130.5	590.0	570.0

TABLE 5.11 Dimensions of composite thin-walled Tee sections

Sp. No.	STURCTURAL PROPERTIES			
	Mass / length			Mass Moment of Inertia (Theo.) Kg-m * 10^{-6}
	Theo.	Exp.	% dif	
1	0.170	0.2219	-30.5	57.89
2	0.169	0.2206	-30.5	57.88
3	0.168	0.2208	-31.4	56.37
4	0.176	0.2212	-25.7	60.10

TABLE 5.12 Structural parameters of composite Tee sections

Spec No.	Flexural Rigidity ($N-m^2$)			Torsional Rigidity ($N-m^2$)		
	Theo.	Exp.	% dif	Theo.	Exp.	% dif
1.	463.0	344.11	25.7	0.667	0.946	-41.8
2.	478.4	342.69	28.4	0.628	0.960	-52.9
3.	475.8	340.46	28.4	0.574	0.870	-51.6
4.	512.8	328.17	36.0	0.664	1.038	-56.3

TABLE 5.13 Structural rigidities of composite Tee sections

Sp.No.	1	2	3	4	5	6	7	8
Orien.	Z E R O D E G R E E				10^o	20^o	30^o	45^o
SECTIONAL DETAILS								
h (mm)	36.00	36.00	36.00	36.00	36.00	36.00	35.00	35.00
b (mm)	31.00	32.00	32.00	32.00	30.00	30.00	30.00	30.00
t_h (mm)	0.818	0.851	0.829	0.7917	0.820	0.790	0.801	0.800
t_b (mm)	1.646	1.588	1.513	1.584	1.380	1.520	1.550	1.720
ℓ (mm)	552.0	563.0	572.0	516.5	569.0	569.0	569.0	569.0

TABLE 5.14 Dimensions of composite thin-walled Channel sections

Sp.No.	1	2	3	4	5	6	7	8
Orien.	Z E R O D E G R E E				10^o	20^o	30^o	45^o
Mass per unit length - m (Kg/m)								
Theory	0.185	0.187	0.179	0.183	0.158	0.169	0.171	0.185
Exper.	0.1791	0.1879	0.1841	0.1844	0.1565	0.1650	0.1702	0.1800
% Dif.	3.18	-0.49	-2.85	-0.77	0.94	2.36	0.46	2.70
Mass Moment of Inertia - $I_{p\bullet}$ (Kg-m) * 10^{-4}								
Theory	1.667	1.767	1.691	1.739	1.338	1.432	1.437	1.563
Shear Centre - X_α (m)								
Theory	0.0228	0.0237	0.0237	0.0237	0.0219	0.0219	0.0220	0.0220
Exper.	0.0230	0.0232	0.0234	0.0233	0.0210	0.0224	0.0215	0.0224
% Dif.	-0.88	2.10	1.26	1.68	4.10	-2.29	2.27	-1.82
Flexural/Bending Rigidity - EI ($N-m^2$)								
Theory	852.3	852.1	813.5	844.7	690.2	704.8	622.8	636.0
Exper.	578.3	584.9	553.5	742.0	377.14	353.17	302.46	251.79
% Dif.	32.15	31.56	31.96	12.16	45.36	49.89	51.43	60.41
Torsional Rigidity - GJ ($N-m^2$)								
Theory	0.691	0.650	0.565	0.635	0.434	0.627	0.756	1.120
Exper.	0.9985	0.7803	0.9858	1.1867	0.828	1.0082	1.1442	1.189
% Dif.	-44.5	-20.1	-74.5	-86.8	-90.8	-60.7	-51.4	- 6.16

TABLE 5.15 Structural rigidities of composite Channel sections

Spc. No.	c (mm)	t_{skin} (mm)	A_{area} (mm^2)	A_{solid} (mm^2)	ℓ (mm)	W_{skin} (gm)	W_{total} (gm)
1.	114.0	0.548	128.782	1187.09	990.0	175.0	175.0
1A.	114.0	0.548	128.782	1187.09	585.0	175.0	175.0
2.	114.0	0.580	136.218	1189.17	955.0	207.4	312.4
3.	123.0	0.561	142.175	1279.50	853.0	226.7	290.0
3A.	115.0	0.561	134.851	1246.00	805.0	252.4	315.7
4.	117.0	0.576	140.146	1420.43	895.0	153.5	258.0
6.	130.0	0.541	146.017	1422.60	865.0	160.0	263.0
7.	118.0	0.473	114.169	1118.50	917.0	143.0	157.7
10^o	114.0	0.565	131.822	1114.00	969.0	169.0	169.0
20^o	114.0	0.546	127.389	1114.00	956.0	164.0	164.0
30^o	114.0	0.560	130.656	1114.00	960.0	167.0	167.0
45^o	114.0	0.551	128.556	1114.00	970.0	171.0	171.0

TABLE 5.16 Dimensions of thin-walled closed sections

Spc. No.	Centroid (mm)			Shear Centre (mm)		
	Theo.	Exp.	% diff	Theo.	Exp.	% diff
1.	55.817	58.00	- 3.91	-31.30	-38.00	-21.76
1A.	55.817	58.00	- 3.91	-32.22	-38.00	-17.94
2.	51.795	52.40	- 1.17	-32.22	-14.61	54.66
3.	54.965	55.10	- 0.25	-37.61	- 2.10	94.42
3A.	54.965	55.10	- 0.25	-28.21	-28.22	- 0.04
4.	51.709	55.50	- 7.33	-27.10	-20.50	24.35
6.	55.870	55.50	0.66	-34.37	-23.58	31.39
7.	56.136	56.00	0.24	-25.07	-29.49	-17.63
10^o	56.200	56.30	- 0.18	-28.22	-33.85	-19.95
20^o	56.200	56.30	- 0.18	-28.22	-33.37	-18.25
30^o	56.200	56.50	- 0.53	-28.22	-32.13	-13.86
45^o	56.200	56.00	0.36	-28.22	-33.19	-17.61

TABLE 5.17 Location of centroid and shear centre

Spc. No.	mass / length (Kg/m)			Mass moment inertia (Kgm)		
	Theo.	Exp.	% diff	Theo.	Exp.	% diff
1.	0.177	0.1767	- 0.13	0.000378	0.000461	-21.76
1A.	0.177	0.1767	- 0.13	0.000461	0.0007	-51.98
2.	0.335	0.3271	2.35	0.000415	0.000339	18.32
3.	0.354	0.340	3.96	0.000414	0.0006	-44.93
3A.	0.339	0.3922	-15.68	0.000611	0.000628	- 2.90
4.	0.288	0.2883	- 0.09	0.000527	0.000564	- 6.95
6.	0.304	0.3041	- 1.51	0.000482	0.000076	84.34
7.	0.178	0.172	3.37	0.00032	0.000547	-70.99
10^{o}	0.170	0.174	- 2.35	0.000331	0.000498	-50.45
20^{o}	0.165	0.172	- 3.64	0.000319	0.000512	-60.50
30^{o}	0.169	0.174	- 2.96	0.000327	0.000468	-43.12
45^{o}	0.166	0.176	- 6.02	0.000322	0.000504	-56.52

TABLE 5.18 Mass per unit length and polar mass moment of inertia of composite thin-walled closed sections

Sp. No.	Flexural Rigidity ($N-m^2$)			Torsional Rigidity ($N-m^2$)		
	Theo.	Exp.	% diff	Theo.	Exp.	% diff
1.	64.64	----	----	17.658	18.794	- 6.43
1A.	64.64	30.05	53.51	17.658	18.794	- 6.43
2.	64.43	69.66	- 4.52	40.025	41.874	- 4.62
3.	74.20	70.85	4.52	48.095	51.240	- 6.54
3A.	74.20	70.85	4.52	48.095	51.240	- 6.54
4.	99.69	86.30	13.43	39.285	37.489	4.57
6.	90.98	82.11	9.75	50.450	48.080	4.70
7.	55.19	52.16	5.49	30.109	28.161	6.47

TABLE 5.19 Flexural and torsional rigidity of zero degree lay-up thin-walled wing structures

Ply Ang.	Flexural Rigidity ($N-m^2$)			Torsional Rigidity ($N-m^2$)			Coupled Rigidity ($N-m^2$)		
	Theo.	Exp.	% diff	Theo.	Exp.	% diff	Theo.	Exp.	% diff
10^o	50.80	48.10	5.32	20.18	17.034	15.59	11.19	11.915	- 6.46
20^o	38.56	33.92	12.03	31.04	24.104	22.35	17.54	19.326	-10.21
30^o	27.92	25.78	7.67	51.30	53.984	- 5.23	18.45	17.477	5.29
45^o	17.38	16.98	2.30	74.64	78.167	- 4.73	0.0	0.0	0.0

TABLE 5.20 Flexural, torsional and coupled rigidities of generally orthotropic thin-walled wing structures

MATERIAL : ISOTROPIC (ALUMINUM)			
STRUCTURE	TEST	DEVICE	% Error
Beam (Pris. Bar)	Bending	Strain Gaug	2.42
		L. S. A.	7.46
Plate	Bending	Optical	- 5.29
	Torsion		- 0.84
Thin-walled Closed sec.	Torsion	Dial Gauge	35.01
		L. S. A.	7.79

TABLE 5.21 Error levels encountered in tests carried out on Aluminium structures

MATERIAL : COMPOSITE FIBREDUX C920			
TEST	PLY ORIENTATION		
	0	30	45
BENDING	2.78	18.18	16.35
TORSION	-59.39	6.52	- 0.55
BEND/TOR. COUPLED	0.0	15.36	9.40

TABLE 5.22 Error levels encountered in tests carried out on Composite plates

MATERIAL : ANISOTROPIC (COMPOSITES) FIBREDUX 916 G				
PLY ANGLE	TEST	PERCENTAGE ERRORS		
		ANGLE SEC.	TEE SEC.	CHANNEL SEC
0	Bending	14.30	29.63	26.96
	Torsion	3.41	-50.65	-56.48
10	Bending	24.62	----	45.36
	Torsion	2.30	----	-90.80
20	Bending	27.96	----	49.89
	Torsion	0.05	----	-60.70
30	Bending	----	----	51.43
	Torsion	----	----	-51.40
45	Bending	36.84	----	60.41
	Torsion	3.58	----	- 6.16

TABLE 5.23 Error levels encountered in tests carried out on composite thin-walled open sections using linear servo accelerometers

MATERIAL : ANISOTROPIC (COMPOSITES) GFRP			
PLY ANGLE	TEST (Percentage errors)		
	BENDING	TORSION	BEND/TOR.
0	36.45	- 1.42	---
10	5.32	15.59	- 6.46
20	12.03	22.35	- 10.21
30	7.67	- 5.23	5.29
45	2.30	- 4.73	---

TABLE 5.24 Error levels encountered in tests carried out on composite thin-walled closed sections using linear servo accelerometers

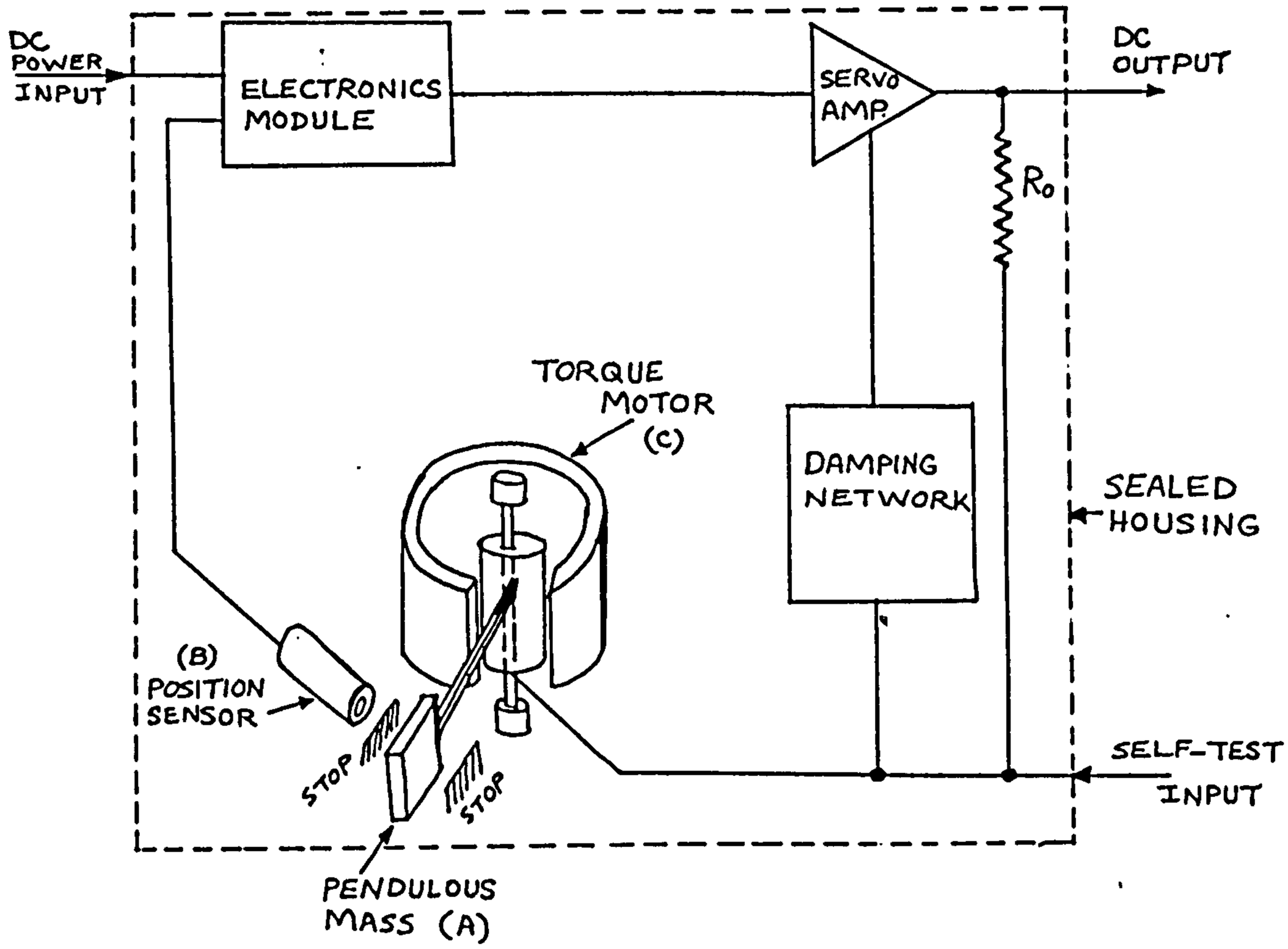

FIG. 5.1 LINEAR SERVO ACCELEROMETER

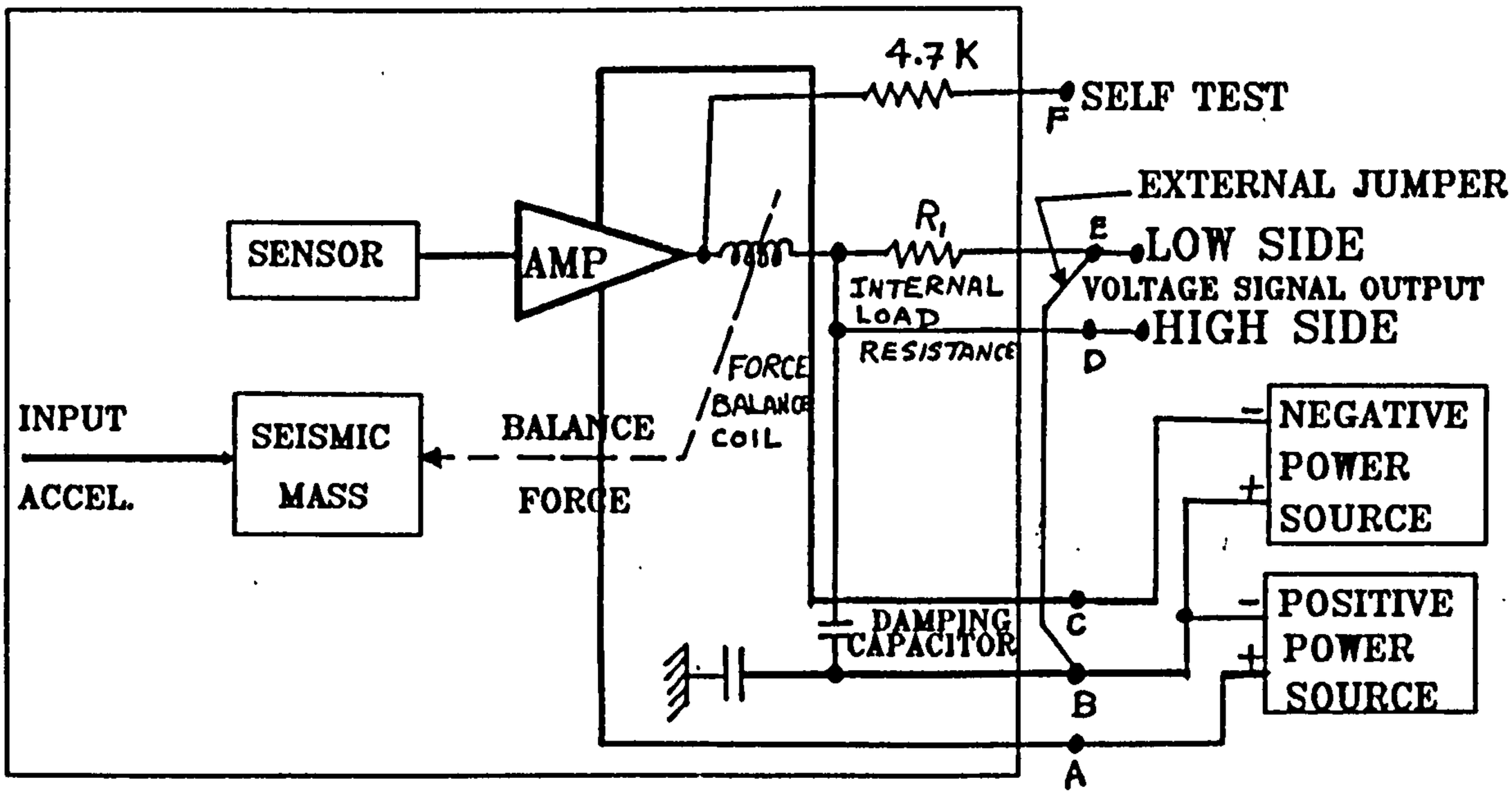

FIG. 5.2 CIRCUIT DIAGRAM

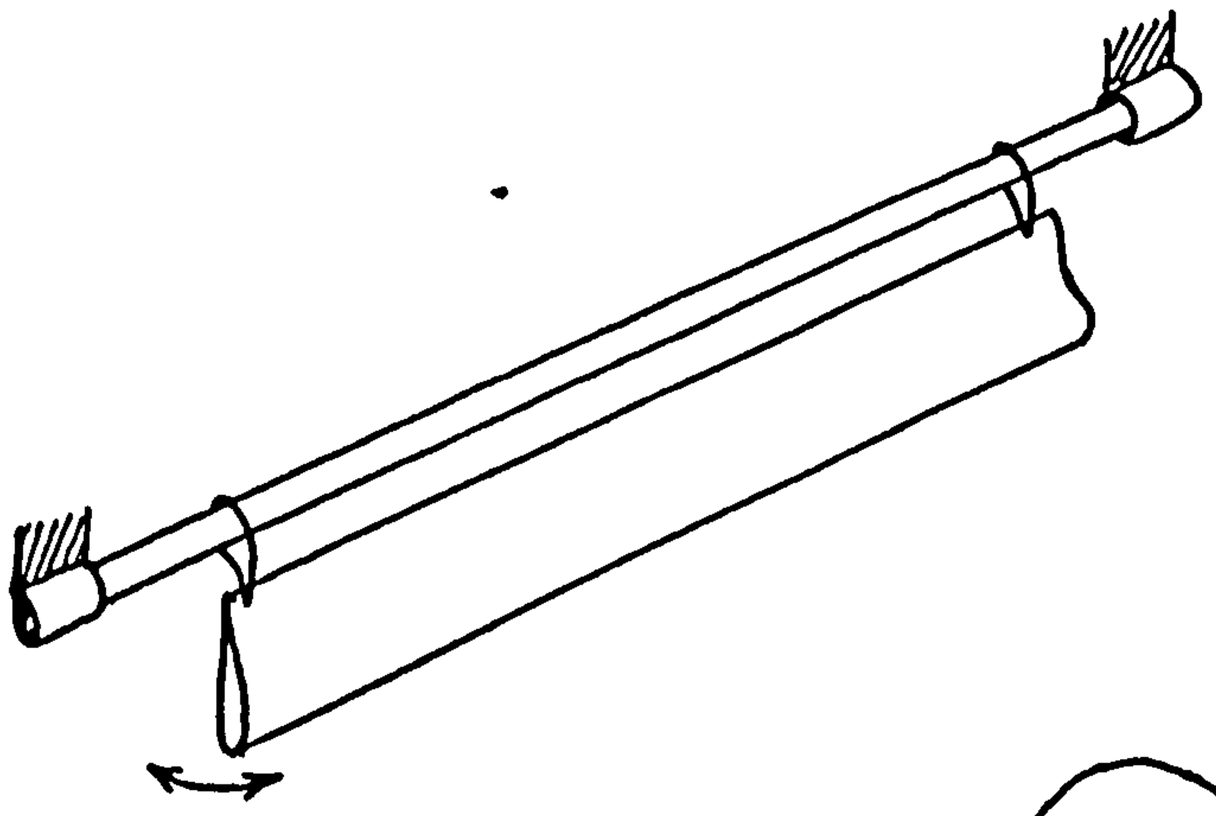

5.3(a) Schematic diagram

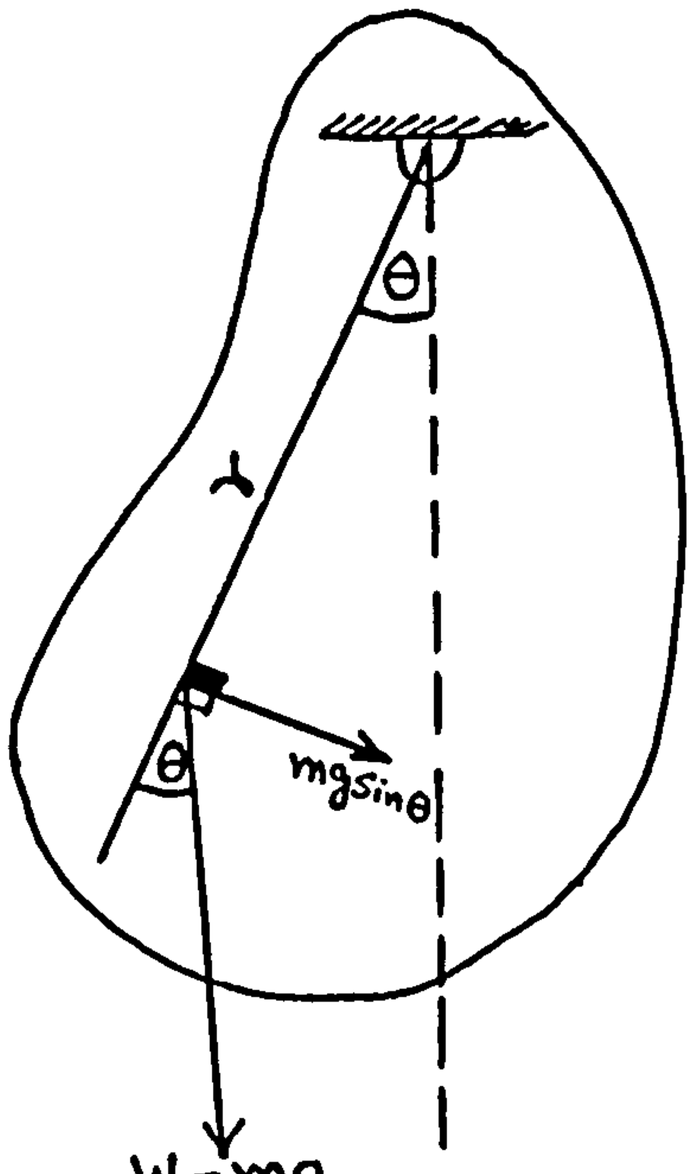

5.3(b) Free body diagram

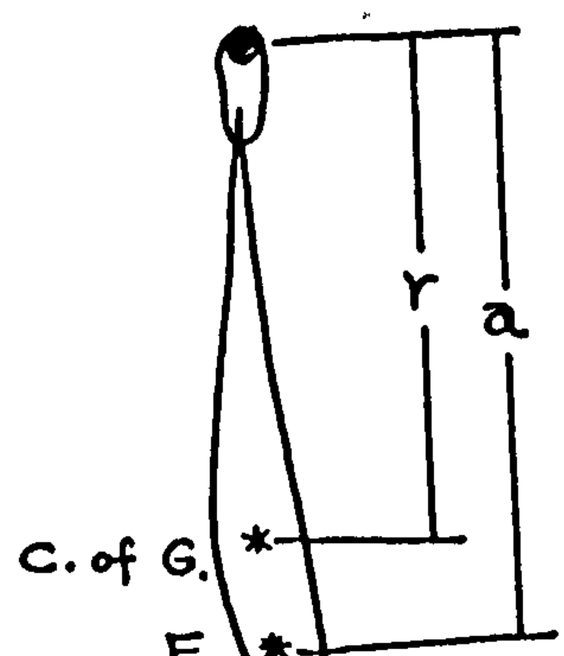

Figure 5.3 Polar mass moment of inertia test set up no. 1

Figure 5.4

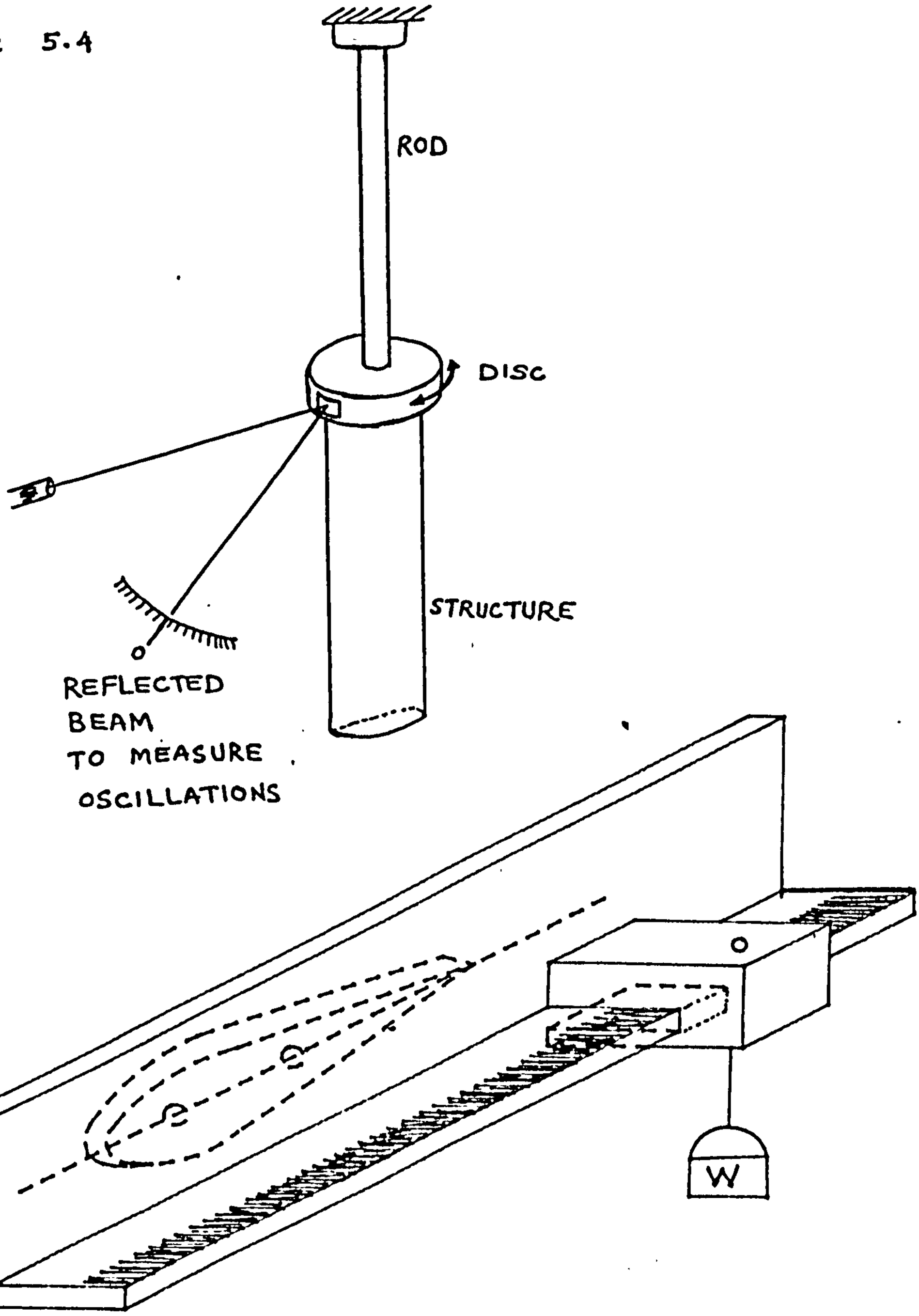

Figure 5.5 Loading arrangement for locating the shear centre

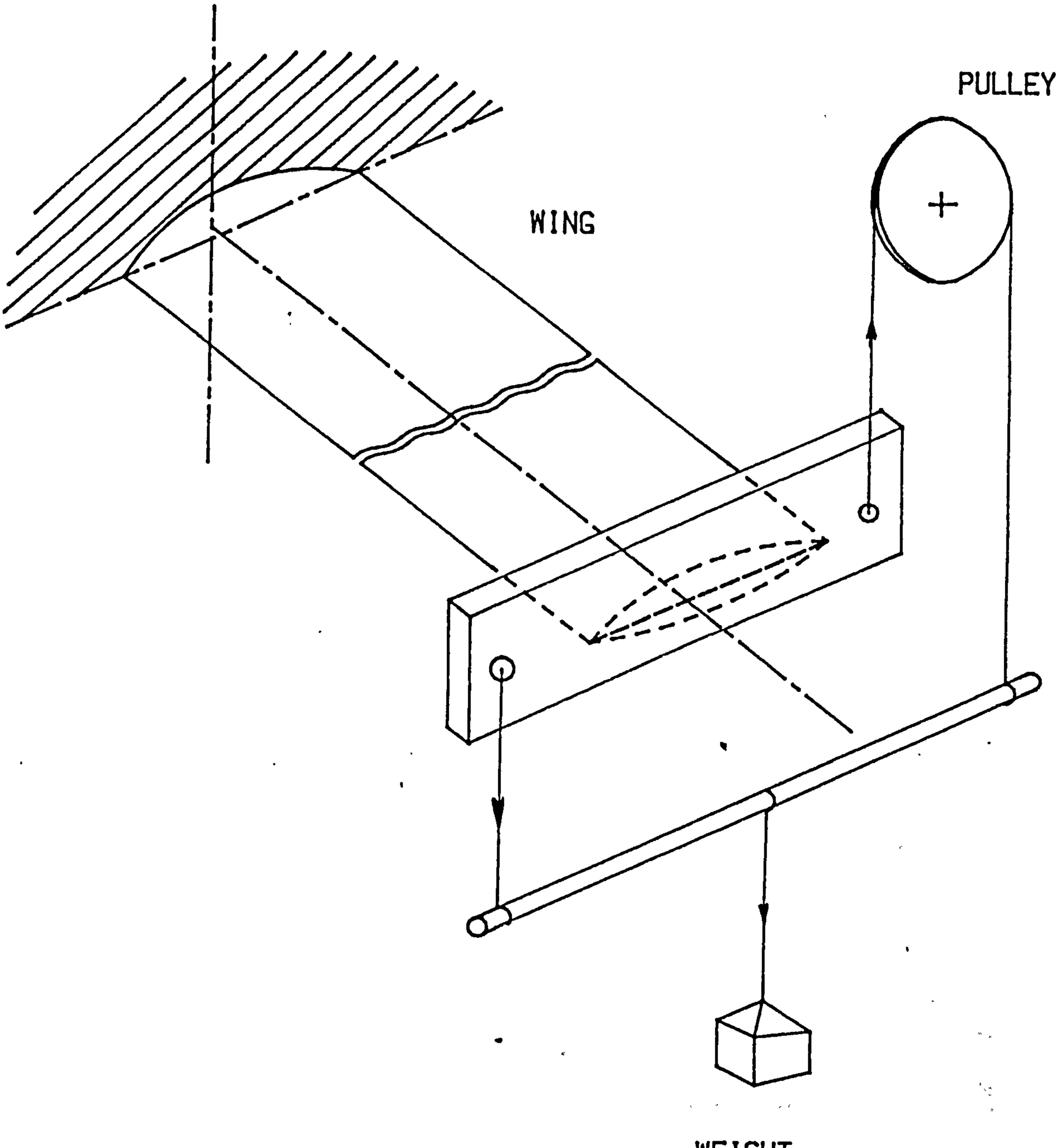

FIG. 5.6 Torsional Rigidity Test set-up

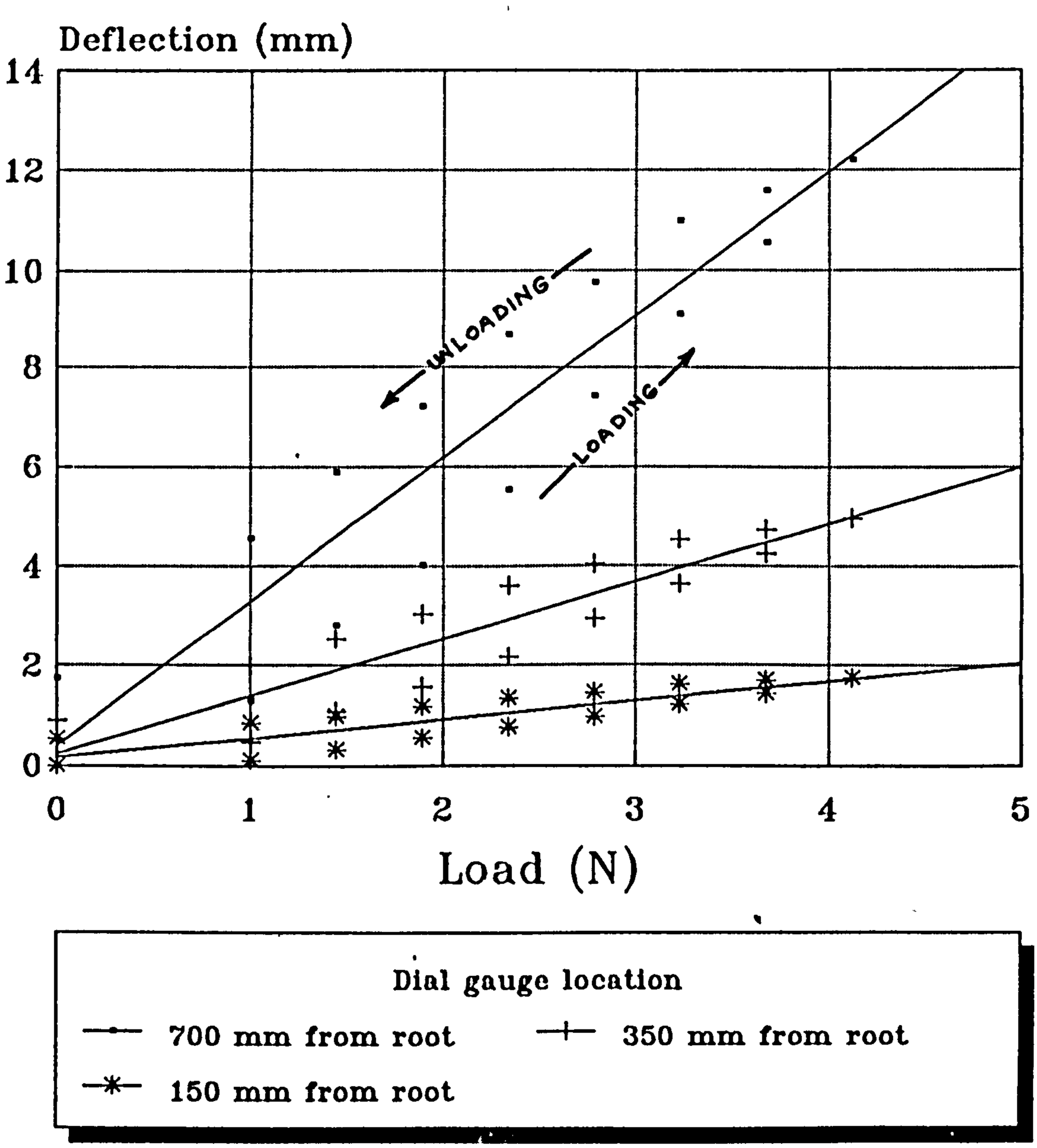

Figure 5.7 Bending rigidity test on a typical wing section

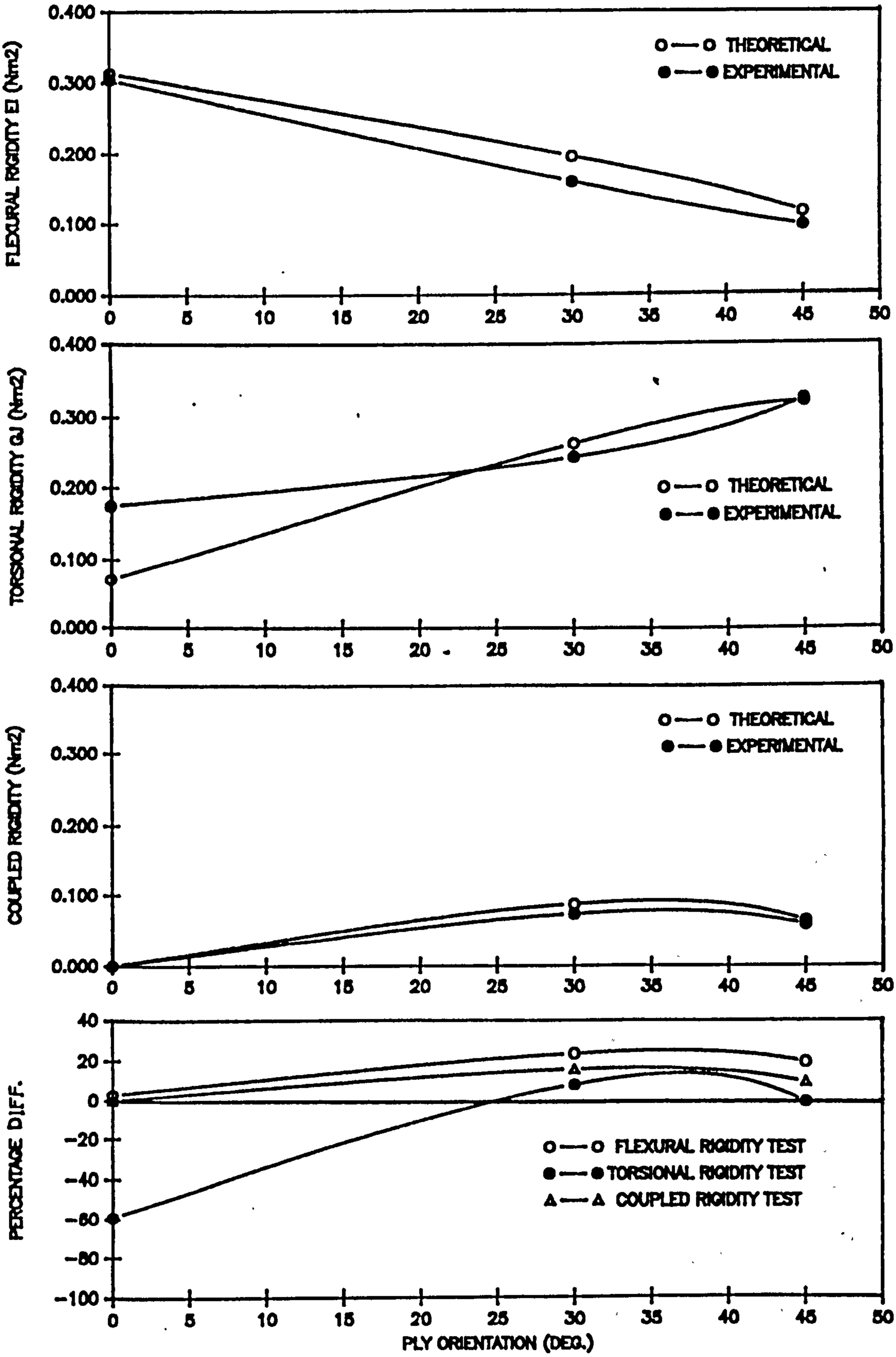

Figure 5.8 Comparison of theoretical predictions and experimental results for composite plates

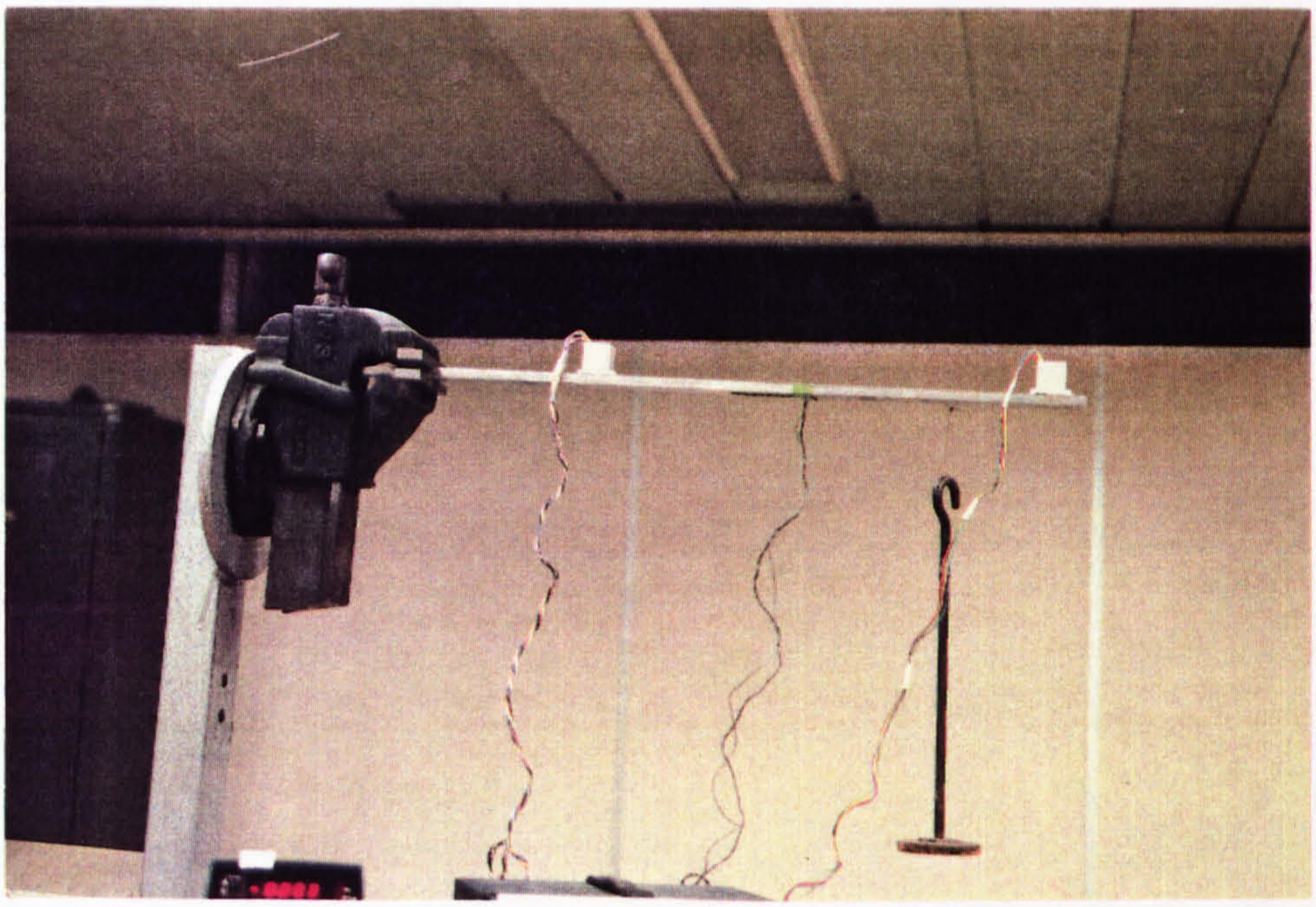

P 5.1 Bending test of aluminium prismatic bar

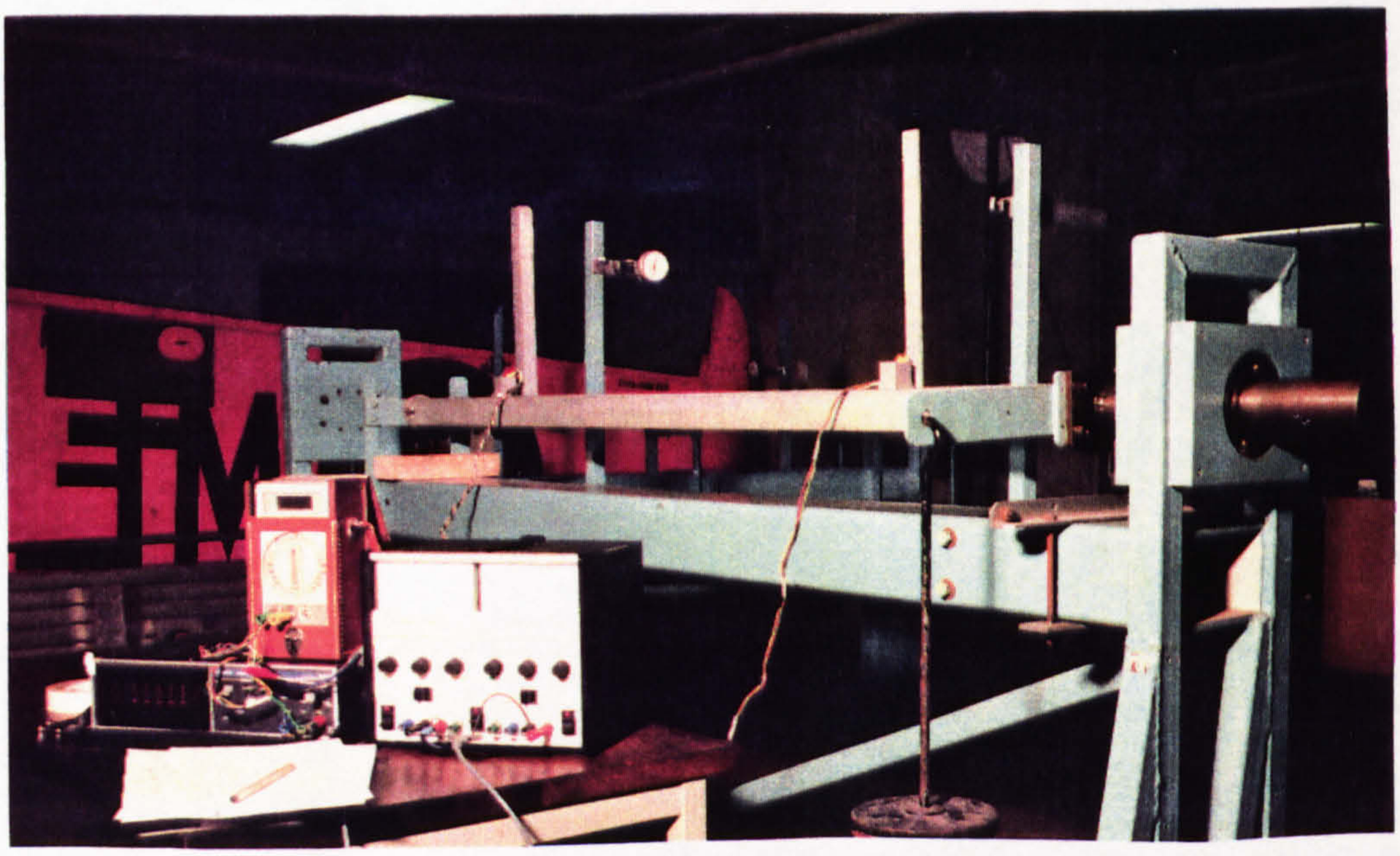

P 5.2 Torsion test of aluminium closed square section

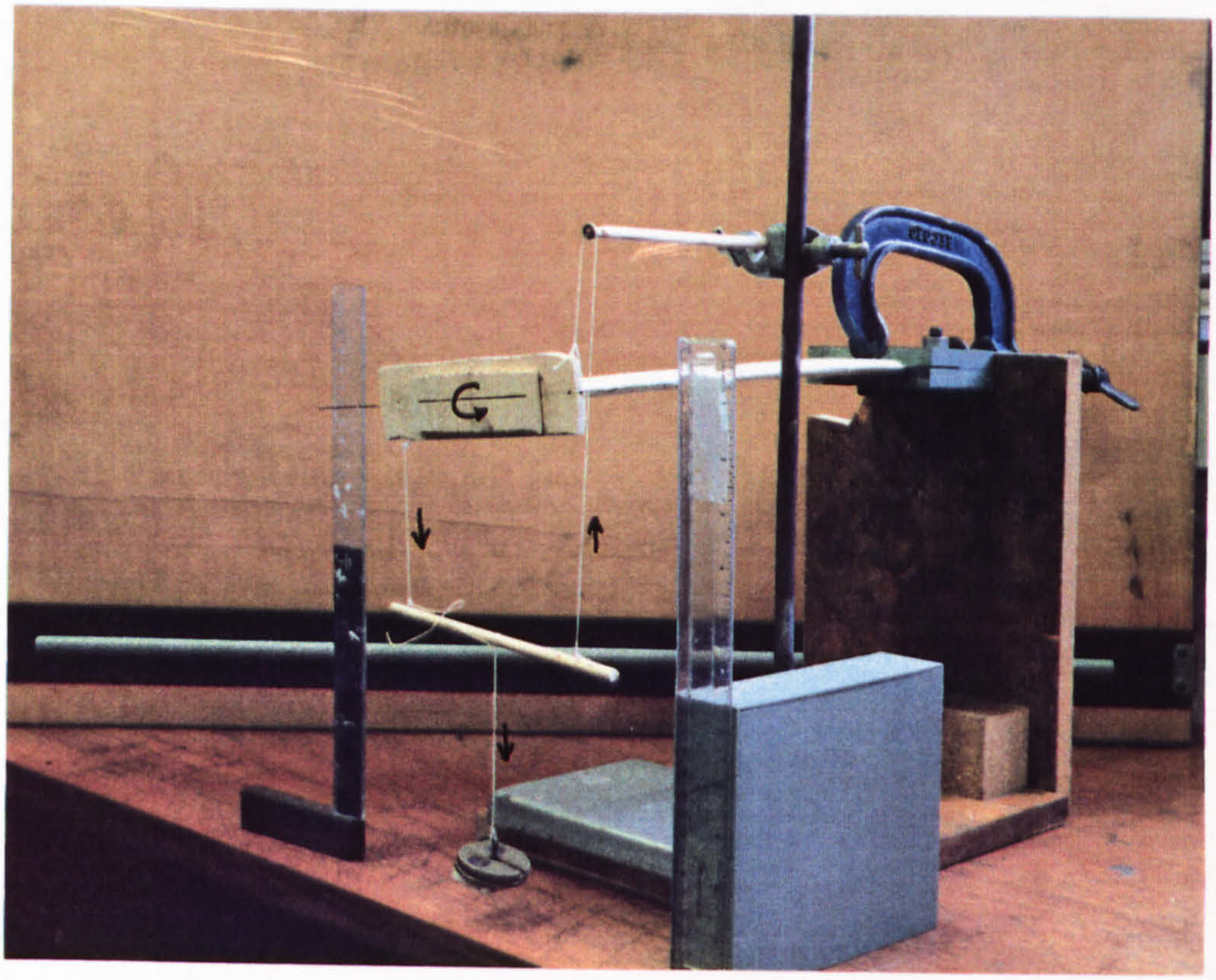

P 5.3 Torsion test set up for aluminium and composite plates

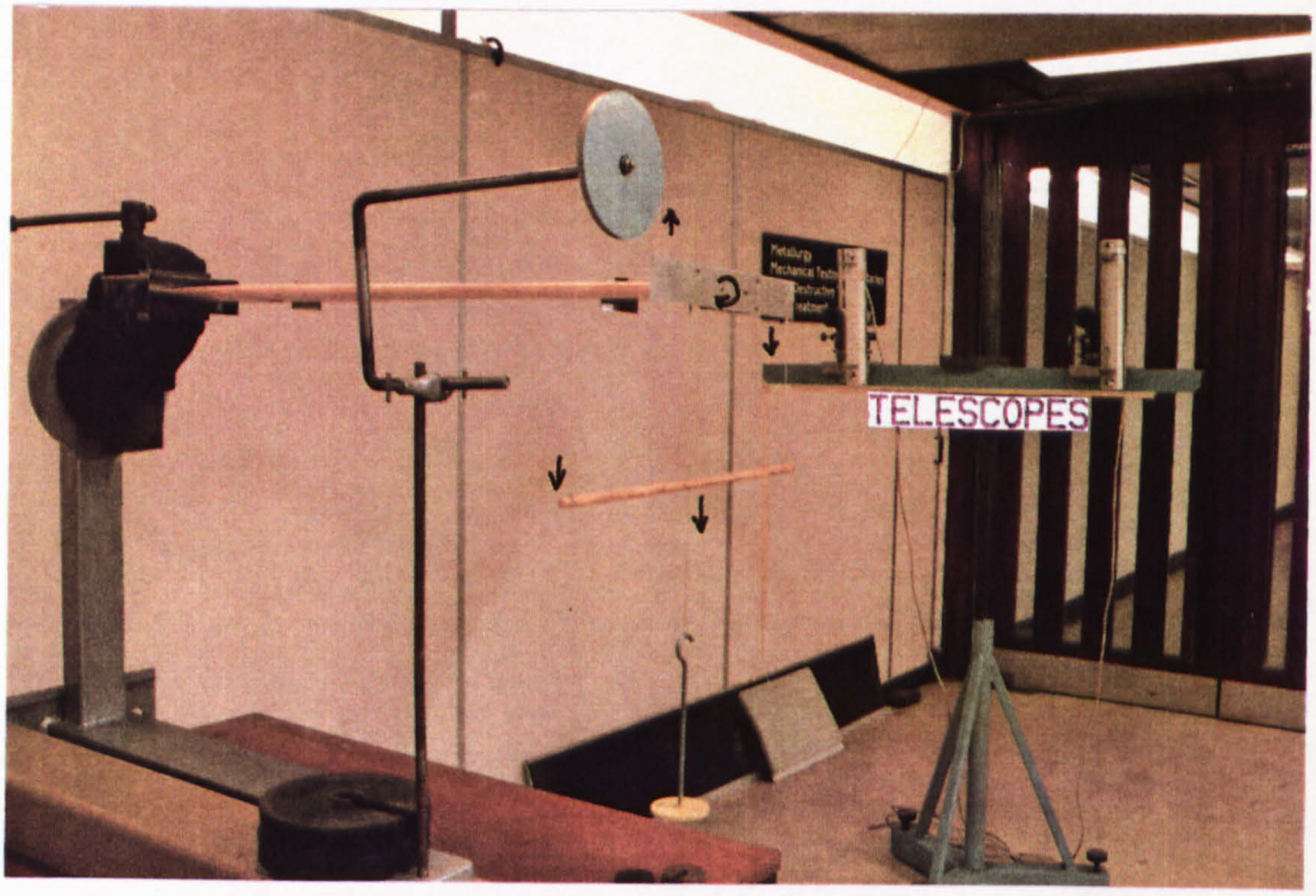

P 5.4 Torsion test set up for composite thin-walled wings

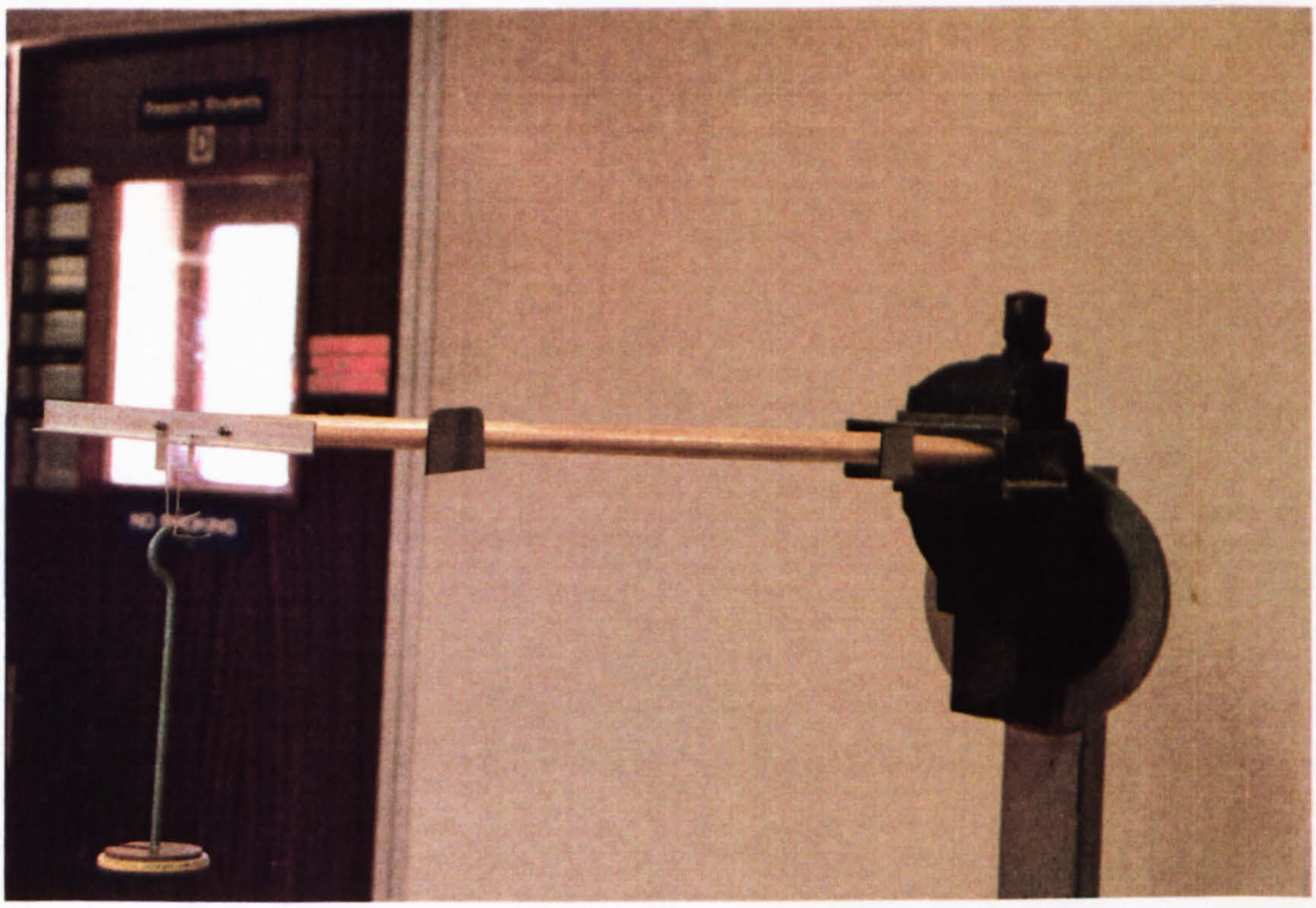

P 5.5 Chord wise moving load for shear centre determination

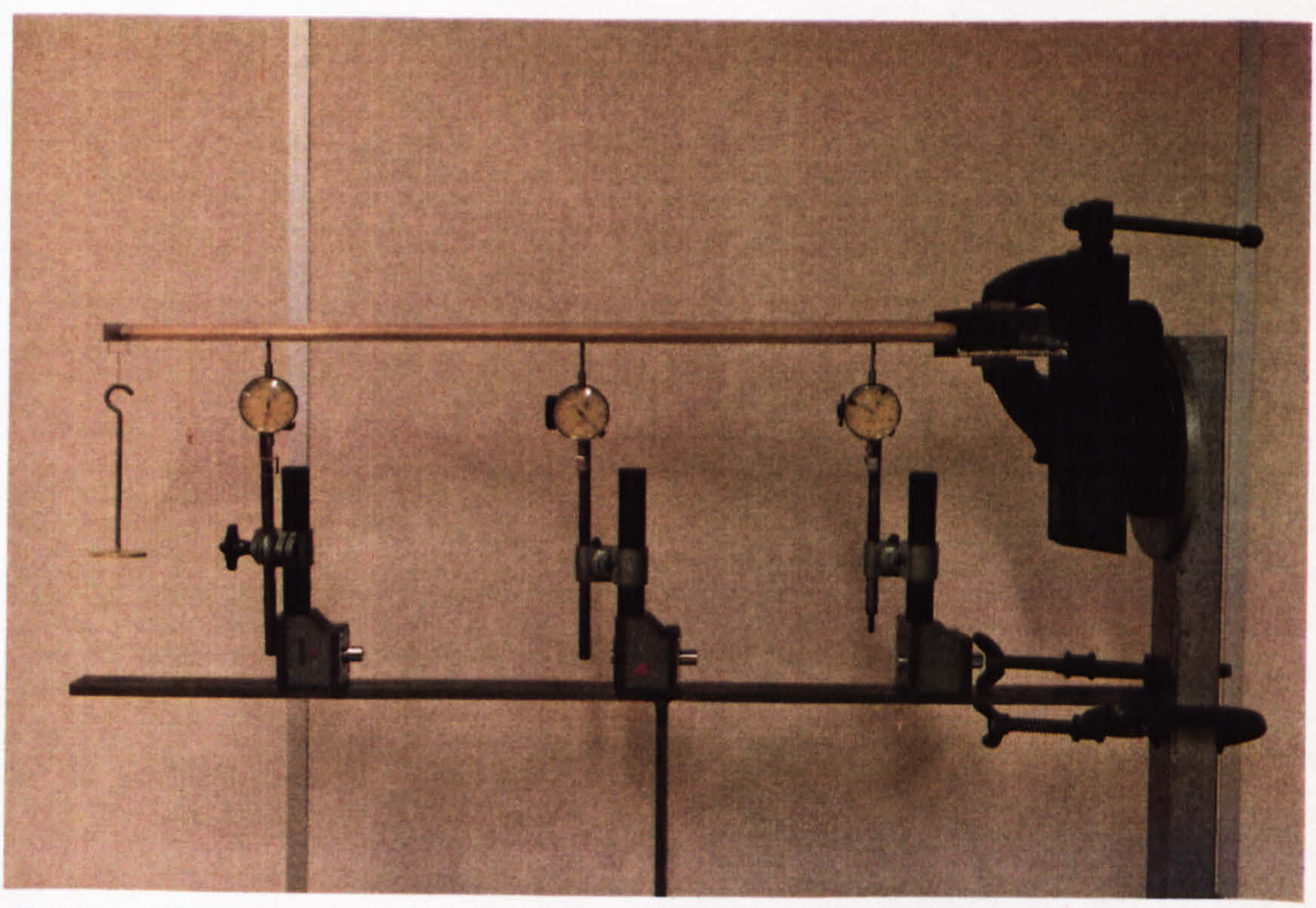

P 5.6 Bending rigidity test set up for composite thin-walled wings

CHAPTER : 6

DYNAMICS OF THIN-WALLED COMPOSITE STRUCTURES

6.1 INTRODUCTION

Dynamics refers to the study of relationships between forces and motion. The vibratory motion or simply natural vibration is an important kind of dynamic behaviour of a structure in which the system oscillates about a certain equilibrium position. The analysis and prediction of the dynamic behaviour of physical systems plays an important role in modern day engineering.

A summary of the structural elements that are used in structural idealization is presented with special reference to thin-walled composite beams. Choice of the dynamic stiffness matrix method is made after a brief description of various other discrete and approximate methods. The dynamic stiffness matrix is evaluated for the general case of a thin-walled anisotropic beam with non-collinear elastic and centroidal axes in the process of an axial load acting through the centroid. The degenerate cases of material coupling with and without the axial load are also discussed. Explicit stiffness expressions for the case of material coupling only are evaluated. Finally, computer programs to determine natural frequencies and mode shapes are described with a sample data file and result file.

6.2 STRUCTURAL IDEALIZATION

Due to the complexity of physical systems, structural parts are usually idealized as several individual components. Their physical properties which govern the dynamic behaviour of the system are sometimes determined experimentally. These characteristics help to construct a

mathematical model representing an idealization of the actual physical system. These mathematical models can be categorized as :

1. discrete-parameter systems, or lumped systems
2. distributed-parameter systems, or continuous systems

The former can be described by ordinary differential equations, whereas the latter is generally governed by partial differential equations and is comparatively difficult to analyse.

Furthermore, the components of a structure can be idealized as a bar, beam, plate, or a shell element. These idealized structures are then described by mathematical models. A summary of these mathematical models with their governing differential equation of motion is given below (in the order of complexity) :

6.2.1 BAR ELEMENT

$$c^2 \frac{\partial^2 v}{\partial y^2} - \frac{\partial^2 v}{\partial t^2} = 0 \qquad (6.2.1)$$

where

$c^2 = \frac{E}{\rho}$

E = modulus of elasticity

ρ = density of the material

v = displacement in the y direction

6.2.2 BEAM ELEMENT

(i) EULER BEAM (Euler-Bernoulli Beam)

$$\frac{\partial^2 h}{\partial y^2}\left[EI \frac{\partial^2 h}{\partial y^2}\right] + m \frac{\partial^2 h}{\partial t^2} = 0 \qquad (6.2.2)$$

where h is the transverse deflection

In the case of an external force per unit length f(y,t), the governing differential equation of motion will be :

$$\frac{\partial^2 h}{\partial y^2}\left[EI\ \frac{\partial^2 h}{\partial y^2}\right] + m\ \frac{\partial^2 h}{\partial t^2} = f(y,t) \qquad (6.2.3)$$

If the effect of rotary inertia is included we get

$$\frac{\partial^2 h}{\partial y^2}\left[EI\ \frac{\partial^2 h}{\partial y^2}\right] + m\ \frac{\partial^2 h}{\partial t^2} - \rho\ I\ \frac{\partial^4 h}{\partial y^2 \partial t^2} = 0 \qquad (6.2.4)$$

and with both rotary inertia and shear deformation

$$\frac{\partial^2 h}{\partial y^2}\left[EI\ \frac{\partial^2 h}{\partial y^2}\right] + m\ \frac{\partial^2 h}{\partial t^2} - \rho\ I\left[1 + \frac{E}{K'G}\right]\frac{\partial^4 h}{\partial y^2 \partial t^2} + \frac{\rho^2 I}{K'G}\ \frac{\partial^4 h}{\partial t^4} = 0 \qquad (6.2.5)$$

In the case of torsional vibration the differential equation is given by

$$-\ GJ\ \frac{\partial^2 \psi}{\partial y^2} - m\ r^2\ \frac{\partial^2 \psi}{\partial t^2} = 0 \qquad (6.2.6)$$

(ii) AXIALLY LOADED TIMOSHENKO BEAM

The differential equation of motion for a beam with shear deformation, rotary inertia, and axial load is given by :-

$$EI\ \frac{\partial^4 h}{\partial y^4} - \left[P - m\ \frac{\partial^2 h}{\partial t^2}\right] - \rho\ I\ \frac{\partial^4 h}{\partial y^2 \partial t^2} + \frac{E\ I}{K'GA}\ \frac{\partial^2}{\partial y^2}\left[P - m\ \frac{\partial^2 h}{\partial t^2}\right]$$

$$-\ \frac{\rho\ I}{K'GA}\ \frac{\partial^2}{\partial t^2}\left[P - m\ \frac{\partial^2 h}{\partial t^2}\right] = 0 \qquad (6.2.7)$$

(iii) BENDING - TORSION COUPLED BEAM

A beam with non-collinear elastic and centroidal axes has differential equations of motion as follows :

$$EI\ \frac{\partial^4 h}{\partial y^4} + m\ \frac{\partial^2 h}{\partial t^2} - m\ e\ \frac{\partial^2 \psi}{\partial t^2} = 0 \qquad (6.2.8)$$

$$GJ\ \frac{\partial^2 \psi}{\partial y^2} + m\ e\ \frac{\partial^2 h}{\partial t^2} - m\ r^2\ \frac{\partial^2 \psi}{\partial t^2} = 0 \qquad (6.2.9)$$

(iv) GENERALLY ORTHOTROPIC (COMPOSITE) THIN-WALLED BEAMS

These are beams with elastic and material coupling :

$$EI \frac{\partial^4 h}{\partial y^4} + K \frac{\partial^3 \psi}{\partial y^3} + m \frac{\partial^2 h}{\partial t^2} - m e \frac{\partial^2 \psi}{\partial t^2} = 0 \qquad (6.2.10)$$

$$K \frac{\partial^3 h}{\partial y^3} + GJ \frac{\partial^2 \psi}{\partial y^2} + m e \frac{\partial^2 h}{\partial t^2} - m r^2 \frac{\partial^2 \psi}{\partial t^2} = 0 \qquad (6.2.11)$$

where

ψ = Torsional deformation

EI = Bending/flexural rigidity

GJ = Torsional rigidity

m = Mass per unit length

I = Polar mass moment of inertia

r = Radius of gyration

P = Axial load

K = Shear deformation constant

e = Distance between the shear centre and centroid

K = Material bending/torsional coupling term.

6.2.3 PLATE ELEMENT (anisotropic)

$$\frac{\partial^4 h}{\partial y^4} - \omega^2 m \left(\frac{\ell^4}{D_{11}}\right) h + \left(\frac{2D_{16}\ell}{D_{11}}\right) \frac{\partial^3 \psi}{\partial y^3} = 0 \qquad (6.2.12)$$

$$- \left(\frac{D_{16}}{2\ D_{66}}\right) \frac{\partial^3 h}{\partial y^3} + \left(\frac{D_{11}\ c^2}{48\ D_{66}\ell^2}\right) \frac{\partial^4 \psi}{\partial y^4} - \frac{\partial^2 \psi}{\partial y^2} - \omega^2 \left(\frac{m\ c^2 \ell^2}{48\ D_{66}}\right) = 0 \qquad (6.2.13)$$

where

ω = circular frequency

D_{11}, D_{16}, and D_{66} = members of the D - matrix.

6.3 COUPLED VIBRATIONS

If a beam does not vibrate in a plane of symmetry, then the flexural vibrations will usually be coupled with torsional vibrations. This is due to the primary reason that the elastic axis is not coincident with the inertial axis. Although explicit dynamic stiffness expressions for the determination of uncoupled fundamental frequencies in bending and torsion are available in the literature, they are not applicable to the coupled vibrations. Frequent use of bending-torsion coupled beam elements have urged researchers to develop explicit and accurate means for the determination of coupled bending-torsion fundamental natural frequencies and mode shapes. Aircraft wings and other control surfaces with high aspect ratios generally fall under this category and are usually referred to as some form of VLASOV BEAM [1]. The coupled bending-torsion differential equations of motion are given in equations (6.2.8) and (6.2.9). In addition to the elastic coupling, structures made of generally orthotropic materials such as composites also display coupling between bending and torsional modes of vibration arising from the material properties. This aspect of dynamics of structures is discussed in this chapter.

6.4 SOLUTION TECHNIQUES

Exact modal solutions have been produced [3-5] for simple boundary conditions. Approximate solutions making use of discretization by either the lumped-mass method [6] or by assumed deformation shapes have been attempted. For the latter case, the Rayleigh-Ritz method [6,7], the Galerkin method [8,9], and the finite element method [10] have been investigated. Additional works based on approximate methods are by Engelbrecht [11] and Stacey [12]. These solution techniques are summarised in a block

diagram, Figure (6.1).

Most of the afore-mentioned methods are applicable to single-span beams (i.e. beams supported only at the ends), except the lumped-mass method [6]. An accurate method called the dynamic stiffness matrix approach [13-15] has been developed for vibration analysis of complex and multi-span structures. The dynamic stiffness matrix method is based on a single, frequency-dependent matrix, containing mass and stiffness properties of the element together. The method gives accurate results due to the application of exact member theory. The major advantage of this method is that it can be used for the determination of an unlimited number of frequencies. A single element can successfully determine any number of natural frequencies for a structure whereas in other approximate methods such as the Finite Element method, the number of elements chosen for the analysis puts severe limitations on the number of natural frequencies which can be determined with reasonable accuracy. A number of computer programs [16,17] based on the dynamic stiffness approach are available.

6.4.1 THE DYNAMIC STIFFNESS MATRIX METHOD

The dynamic stiffness matrix method is an accurate method using a single, frequency-dependent matrix called the dynamic stiffness matrix which includes both the mass and stiffness properties of the structure. Predictably, the use of exact member theory in the dynamic stiffness matrix approach gives accurate results. The governing differential equation of motion of the structure is directly solved to obtain the dynamic stiffness matrix. Thus the assumptions made, being within the limits of the differential equation, are less severe than required for assumed mode or lumped mass methods. A brief outline of the method as applied to the case of an elastically coupled structure is presented

below :

1. The differential equations of motion of the system are obtained by any suitable method. For example, in the case of an elastically coupled structure with non-collinear elastic and inertial axes two partial differential equations are formed.
2. The system of partial differential equations is solved as simultaneous differential equations.
3. The possible solutions will have n unknown coefficients where n corresponds to the degree of the differential equation. In order to solve this equation, n boundary conditions are required.
4. Substitution of the boundary conditions at both ends of the element will yield a matrix of order n x n relating deformations to the unknown coefficients mentioned in step 3.
5. Displacement equations are substituted into force and moment equations. Replacement of the boundary conditions at either end of the element will give another matrix of order n x n which relates forces and moments to the unknown constants.
6. The matrix of step 4 is inverted and multiplied with the matrix of step 5 which gives the dynamic stiffness matrix of order n x n. The resulting dynamic stiffness matrix relates the forces and displacements at the ends of the member.

6.5 THIN-WALLED COMPOSITE BEAMS

It has been mentioned in Chapter (4) that the thin-walled composite beams can be divided into two main categories, namely symmetric and antisymmetric. In a symmetric configuration, the ply lay-up is symmetrical about the mid-plane whereas in the case of an antisymmetric configuration, the ply lay-up is not symmetrical about the

mid-plane.

The symmetric lay-up beams can result in bending-twisting structural couplings as shown below (also see equation (4.7) of Chapter (4)).

$$\begin{Bmatrix} M_x \\ M_{xy} \end{Bmatrix} = \begin{bmatrix} K_{11} & K_{16} \\ K_{16} & K_{66} \end{bmatrix} \begin{Bmatrix} K_x \\ K_{xy} \end{Bmatrix} \qquad (6.5.1)$$

where K_{11} corresponds to flexural stiffness EI

K_{66} corresponds to torsional stiffness GJ

K_{16} corresponds to bending/torsional coupling stiffness K_a

The above equation can be written as

$$\begin{Bmatrix} M \\ T \end{Bmatrix} = \begin{bmatrix} EI & K_a \\ K_a & GJ \end{bmatrix} \begin{Bmatrix} w'' \\ \phi' \end{Bmatrix} \qquad (6.5.2)$$

where

M = bending moment = M_x

T = torque = M_{xy}

EI = effective bending stiffness

GJ = effective torsional stiffness

K_a = bending-twisting structural coupling

$w'' = \frac{d^2w}{dz^2}$ = bending curvature = K_x

$\phi' = \frac{d\phi}{dz}$ = twist derivative = K_{xy}

The antisymmetric lay-up beams can produce extension-twisting coupling [18] such that the twist and axial force are given by

$$\begin{Bmatrix} T \\ P \end{Bmatrix} = \begin{bmatrix} GJ & K_a \\ K_a & EA \end{bmatrix} \begin{Bmatrix} \phi' \\ u' \end{Bmatrix} \qquad (6.5.3)$$

where

P = axial force

K_α = extension/twisting structural coupling

$u' = \frac{du}{dz}$ = axial deflection derivative

The flexibility matrix for the symmetrically laminated cylindrical tube subjected to bending, torsion, and longitudinal tension is given by (also see equation (4.28) of Chapter (4)).

$$\left.\begin{aligned} \varepsilon_o &= F_{11}\, P \\ K_z &= F_{33}\, M_z \\ \begin{bmatrix} K_x \\ \tau \end{bmatrix} &= \begin{bmatrix} F_{22} & F_{24} \\ F_{24} & F_{44} \end{bmatrix} \begin{bmatrix} M_x \\ M_y \end{bmatrix} \end{aligned}\right\} \qquad (6.5.4)$$

The common feature of equations (6.5.1) to (6.5.4) is that the stiffness matrices describe the relationship between coupled bending-torsion and extension-torsion forces and their respective deformations.

6.6 EQUATIONS OF MOTION FOR THIN-WALLED CYLINDRICAL TUBES WITH ASYMMETRIC FIBRE LAY-UP

A thin-walled cylindrical beam with bending in only one plane e.g. an aircraft wing with no chordwise bending and torsion about the shear centre has been analysed by Mansfield and Sobey [19]. A similar approach is considered here. An axial load is also allowed to act through the shear centre. The theory is briefly summarised as follows.

The relation between bending moment and torque is given by (see equation (6.5.4))

$$\begin{bmatrix} K_x \\ \tau \end{bmatrix} = \begin{bmatrix} F_{22} & F_{24} \\ F_{24} & F_{44} \end{bmatrix} \begin{bmatrix} M_x \\ M_y \end{bmatrix} \qquad (6.6.1)$$

which can be rearranged by inverting the square matrix to give

$$\begin{bmatrix} M_x \\ M_y \end{bmatrix} = \begin{bmatrix} K_{22} & K_{24} \\ K_{24} & K_{44} \end{bmatrix} \begin{bmatrix} K_x \\ \tau \end{bmatrix} \qquad (6.6.2)$$

The strain energy in the beam of length ℓ is given by:

$$U = \frac{1}{2}\int_0^{\ell} \left\{ K_{22} \left(\frac{\partial^2 h}{\partial y^2} \right)^2 + 2\, K_{24} \frac{\partial^2 h}{\partial y^2} \frac{\partial \psi}{\partial y} + K_{44} \left(\frac{\partial \psi}{\partial y} \right)^2 \right\} dy \qquad (6.6.3)$$

The work done by a tensile load is given by (note that P can be negative when compressive)

$$W = -\frac{1}{2} P \int_0^{\ell} \left(\frac{\partial h}{\partial y} \right)^2 dy \qquad (6.6.4)$$

Therefore, the total potential energy is :

$$P.E. = U - W$$

$$= \frac{1}{2}\int_0^{\ell} \left\{ K_{22} \left(\frac{\partial^2 h}{\partial y^2} \right)^2 + 2\, K_{24} \frac{\partial^2 h}{\partial y^2} \frac{\partial \psi}{\partial y} + K_{44} \left(\frac{\partial \psi}{\partial y} \right)^2 + \frac{1}{2} P \left(\frac{\partial h}{\partial y} \right)^2 \right\} dy$$

or

$$= \frac{1}{2}\int_0^{\ell} \left\{ K_{22} \left(\frac{\partial^2 h}{\partial y^2} \right)^2 + 2\, K_{24} \frac{\partial^2 h}{\partial y^2} \frac{\partial \psi}{\partial y} + K_{44} \left(\frac{\partial \psi}{\partial y} \right)^2 - \frac{1}{2} P \left(\frac{\partial h}{\partial y} \right)^2 \right\} dy \qquad (6.6.5)$$

If a point (x,z) in the beam moves to the coordinates $(-z\psi, h+x\psi)$ for a given displacement h and rotation ψ, the time differentials will be

$$\left(-z \frac{\partial \psi}{\partial t} , \frac{\partial h}{\partial t} + x \frac{\partial \psi}{\partial t} \right)$$

Thus, the kinetic energy of the system is

$$T = \frac{1}{2}\int_0^{\ell} \iint_A \rho \left[\left(x^2 + z^2 \right) \left(\frac{\partial \psi}{\partial t} \right)^2 + 2\, x \left(\frac{\partial h}{\partial t} \right) \left(\frac{\partial \psi}{\partial t} \right) + \left(\frac{\partial h}{\partial t} \right)^2 \right] dA\, dy$$

Substituting the following relationships in the above expression

$m = \iint \rho \, dA$ = mass per unit length

$m\, r^2 = \iint \rho \, (x^2 + z^2) \, dA$ = mass polar moment of inertia

$m\, e = \iint \rho \, x \, dA$

the expression simplifies to

$$T = \frac{1}{2}\int_0^{\ell} m \left[r^2 \left(\frac{\partial \psi}{\partial t} \right)^2 + 2\, e \left(\frac{\partial h}{\partial t} \right)\left(\frac{\partial \psi}{\partial t} \right) + \left(\frac{\partial h}{\partial t} \right)^2 \right] dy \qquad (6.6.6)$$

The Lagrangian L is then given by:

$L = U - W - T$

$$L = \frac{1}{2} \int_0^{\ell} \left\{ K_{22} \left(\frac{\partial^2 h}{\partial y^2} \right)^2 + 2\, K_{24} \frac{\partial^2 h}{\partial y^2} \frac{\partial \psi}{\partial y} + K_{44} \left(\frac{\partial \psi}{\partial y} \right)^2 - P \left(\frac{\partial h}{\partial y} \right)^2 \right.$$

$$\left. - m \left[\left(\frac{\partial h}{\partial t} \right)^2 + 2\, e \left(\frac{\partial h}{\partial t} \right) \left(\frac{\partial \psi}{\partial t} \right) + r^2 \left(\frac{\partial \psi}{\partial t} \right)^2 \right] \right\} dy \qquad (6.6.7)$$

Using Hamilton's principle, the above will yield the following equations of motion :

$$P \frac{\partial^2 h}{\partial y^2} + K_{22} \frac{\partial^4 h}{\partial y^4} + K_{24} \frac{\partial^3 \psi}{\partial y^3} + m \frac{\partial^2 h}{\partial t^2} + m\, e \frac{\partial^2 \psi}{\partial t^2} = 0 \qquad (6.6.8)$$

and

$$- K_{24} \frac{\partial^3 h}{\partial y^3} - K_{44} \frac{\partial^2 \psi}{\partial y^2} + m\, e \frac{\partial^2 h}{\partial t^2} + m\, r^2 \frac{\partial^2 \psi}{\partial t^2} = 0 \qquad (6.6.9)$$

6.7 VIBRATION OF AXIALLY LOADED BEAMS WITH GEOMETRIC AND MATERIAL COUPLING

The vibration of axially loaded thin-walled composite beams with geometrical and material bending/torsional coupling is considered first. The dynamic stiffness matrix based on the equations of motion obtained in the previous section will be developed. The natural frequencies and mode shapes of the structure can be computed.

Substituting $EI = K'_{22}$, $GJ = K_{44}$, & $K = K_{24}$ in the equations of motion (6.6.8) and (6.6.9) :

$$EI\frac{\partial^4 h}{\partial y^4} + K\frac{\partial^3 \psi}{\partial y^3} + P\left[\frac{\partial^2 h}{\partial y^2} - e\frac{\partial^2 \psi}{\partial y^2}\right] + m\frac{\partial^2 h}{\partial t^2} - m\,e\frac{\partial^2 \psi}{\partial t^2} = 0 \qquad (6.7.1a)$$

$$K\frac{\partial^3 h}{\partial y^3} + GJ\frac{\partial^2 \psi}{\partial y^2} - P\left[e\frac{\partial^2 h}{\partial y^2} + r^2\frac{\partial^2 \psi}{\partial y^2}\right] + me\frac{\partial^2 h}{\partial t^2} - I_\alpha\frac{\partial^2 \psi}{\partial t^2} = 0 \qquad (6.7.1b)$$

The expressions for shear force, bending moment and torque are as follows :

Shear force :

$$S = \frac{\partial}{\partial y}(-P\,h - M_x) + P\,e\frac{\partial \psi}{\partial y} \qquad (6.7.2)$$

Bending moment:

$$M_x = EI\frac{\partial^2 h}{\partial y^2} + K\frac{\partial \psi}{\partial y} \qquad (6.7.3)$$

Torque:

$$T = GJ\frac{\partial \psi}{\partial y} + K\frac{\partial^2 h}{\partial y^2} + P\left[e\frac{\partial h}{\partial y} - r^2\frac{\partial \psi}{\partial y}\right] \qquad (6.7.4)$$

Let $h = H \sin(\omega t)$ and $\psi = \Psi \sin(\omega t)$

and $\xi = \frac{y}{\ell}$, so that $\frac{d\xi}{dy} = \frac{1}{\ell}$, $\frac{dh}{dy} = \frac{1}{\ell}\frac{dh}{d\xi}$

Substituting these relationships in the equation (6.7.1a) and simplifying:

$$D^4H + \frac{K\ell}{EI}D^3\Psi + \frac{P\ell^2}{EI}(D^2H - eD^2\Psi) - \left(\frac{m\omega^2\ell^4}{EI}\right)H + \left(\frac{m\omega^2\ell^4}{EI}\right)e\,\Psi = 0$$

Defining the following non-dimensional quantities

$$\bar{P} = \frac{P\ell^2}{EI} \quad , \quad \bar{K} = \frac{K\ell}{EI} \quad , \quad \bar{a} = \left(\frac{m\omega^2\ell^4}{EI}\right)$$

The above differential equation becomes

$$D^4 H + \bar{K} D^3 \Psi + \bar{P}(D^2 H - e D^2 \Psi) - \bar{a} H + \bar{a} e \Psi = 0 \qquad (6.7.5a)$$

Similarly equation (6.7.1b) will yield :

$$D^2\Psi + \bar{\bar{K}} D^3 H - \bar{\bar{P}}(-e D^2 H + r^2 D^2\Psi) - \bar{b} e H + \bar{b} r^2 \Psi = 0 \qquad (6.7.5b)$$

where

$$\bar{\bar{P}} = \frac{P}{GJ} \quad , \quad \bar{\bar{K}} = \frac{K}{\ell GJ}$$

$$\bar{b} = \left(\frac{m\omega^2\ell^2}{GJ}\right) \quad , \quad I_\alpha = m r^2$$

Rearranging equations (6.7.5a) and (6.7.5b)

$$\left(D^4 + \bar{P} D^2 - \bar{a}\right) H + \left(\bar{K} D^3 - \bar{P} e D^2 + e \bar{a}\right) \Psi = 0 \qquad (6.7.6a)$$

$$\left(\bar{\bar{K}} D^3 + \bar{\bar{P}} e D^2 - \bar{b} e\right) H + \left(D^2 - \bar{\bar{P}} r^2 D^2 + \bar{b} r^2\right) \Psi = 0 \qquad (6.7.6b)$$

Let

$$L_1 = \left[D^4 + \bar{P}\, D^2 - \bar{a}\right] \quad , \quad L_2 = \left[\bar{K} D^3 - \bar{P}\, e\, D^2 + e\, \bar{a}\right]$$

$$L_3 = \left[\bar{\bar{K}}\, D^3 + \bar{\bar{P}}\, e\, D^2 - \bar{b}\, e\right] \quad , \quad L_4 = \left[D^2 - \bar{\bar{P}}\, r^2\, D^2 + \bar{b}\, r^2\right]$$

The above pair of differential equations can be written as

$$L_1 H + L_2 \Psi = 0 \qquad (6.7.7a)$$

$$L_3 H + L_4 \Psi = 0 \qquad (6.7.7b)$$

Multiplying equation (6.7.7a) by L_4 and (6.7.7b) by L_2 and subtracting the first equation from the second will give

$$(L_1 L_4 - L_2 L_3)\, H = 0 \qquad (6.7.8)$$

Substituting corresponding quantities of L_1, L_2, L_3 & L_4 in the equation (6.7.8) and simplifying the end expression, we get

$$(D^6 + a\, D^4 + b\, D^2 + c)\, H = 0 \qquad (6.7.9)$$

where

$$a = \frac{\left[\bar{P} + \bar{b}\, r^2 + \bar{P}\, \bar{\bar{P}}\, (e^2 - r^2)\right]}{\Delta}$$

$$b = \frac{\left[(-\bar{P}\, \bar{b} - \bar{a}\, \bar{\bar{P}})(e^2 - r^2) - \bar{a}\right]}{\Delta}$$

$$c = \frac{\bar{a}\, \bar{b}\, (e^2 - r^2)}{\Delta} \quad , \quad \Delta = \left[1 - \bar{\bar{P}}\, r^2 - \frac{K^2}{EI\ GJ}\right]$$

The solution of equation (6.7.9) can be obtained by substituting

$$H = e^{p\zeta}$$

The equation will be

$$p^6 + a\ p^4 + b\ p^2 + c = 0 \qquad (6.7.10)$$

Substituting $\lambda = p^2$

$$\lambda^3 + a\ \lambda^2 + b\ \lambda + c = 0 \qquad (6.7.11)$$

Let $\lambda = x - \frac{a}{3}$

$$(x - \frac{a}{3})^3 + a\ (x - \frac{a}{3})^2 + b\ (x - \frac{a}{3}) + c = 0$$

After simplification we get

$$x^3 + (-\frac{a^3}{3} + b)\ x + (\frac{2}{27}\ a^3 - \frac{ab}{3} + c) = 0$$

Similarly

$$q = \frac{a^2}{3} - b \qquad \text{and} \qquad r = \frac{ab}{3} - \frac{2}{27}\ a^3 - c$$

The above cubic equation becomes

$$x^3 - q\ x - r = 0 \qquad (6.7.12)$$

If $27\ r^2 - 4\ q^2 < 0$

then all the three roots of the equation are real [20] as follows:

$$x_1 = 2\ (q/3)^{1/2} \cos\ (\phi/3) \qquad (6.7.13a)$$

$$x_2 = 2\ (q/3)^{1/2} \cos\ \left[(\pi-\phi)/3\right] \qquad (6.7.13b)$$

$$x_3 = 2\ (q/3)^{1/2} \cos\ \left[(\pi+\phi)/3\right] \qquad (6.7.13c)$$

where

$$\cos(\phi) = (3/q)^{3/2}\ (r/2)$$

since

$$\lambda = x - \frac{a}{3}$$

Therefore the roots α, β and γ will be

$$\alpha^2 = 2\,(q/3)^{1/2}\cos\,(\phi/3) - \frac{a}{3} \qquad (6.7.14a)$$

$$\beta^2 = 2\,(q/3)^{1/2}\cos\,\left[(\pi-\phi)/3)\right] + \frac{a}{3} \qquad (6.7.14b)$$

$$\gamma^2 = 2\,(q/3)^{1/2}\cos\,\left[(\pi+\phi)/3)\right] + \frac{a}{3} \qquad (6.7.14c)$$

Assuming a solution for real roots α, β and γ we have

$$H(\xi) = A_1\cosh(\alpha\xi) + A_2\sinh(\alpha\xi) + A_3\cos(\beta\xi) + A_4\sin(\beta\xi) + A_5\cos(\gamma\xi) + A_6\sin(\gamma\xi) \qquad (6.7.15a)$$

Simil arly

$$\Psi(\xi) = B_1\cosh(\alpha\xi) + B_2\sinh(\alpha\xi) + B_3\cos(\beta\xi) + B_4\sin(\beta\xi) + B_5\cos(\gamma\xi) + B_6\sin(\gamma\xi) \qquad (6.7.15b)$$

and the slope of the flexural axis of the beam is

$$\theta(\xi) = \frac{1}{\ell}\frac{\partial H}{\partial \xi} = \frac{1}{\ell}\left[\alpha A_1\sinh(\alpha\xi) + \alpha A_2\cosh(\alpha\xi) - \beta A_3\sin(\beta\xi) + \beta A_4\cos(\beta\xi) - \gamma A_5\sin(\gamma\xi) + \gamma A_6\cos(\gamma\xi)\right] \qquad (6.7.16)$$

For simplicity the following symbols will represent the corresponding quantities wherever they appear in the text.

$C_{h\alpha} = \cosh\,(\alpha\xi)$	$C_{h\beta} = \cosh\,(\beta\xi)$	$C_{h\gamma} = \cosh\,(\gamma\xi)$
$S_{h\alpha} = \sinh\,(\alpha\xi)$	$S_{h\beta} = \sinh\,(\beta\xi)$	$S_{h\gamma} = \sinh\,(\gamma\xi)$
$C_{\alpha} = \cos\,(\alpha\xi)$	$C_{\beta} = \cos\,(\beta\xi)$	$C_{\gamma} = \cos\,(\gamma\xi)$
$S_{\alpha} = \sin\,(\alpha\xi)$	$S_{\beta} = \sin\,(\beta\xi)$	$S_{\gamma} = \sin\,(\gamma\xi)$

Substitution of the higher derivatives of H and Ψ in to equation (6.7.5a) yields :

$$\left[\alpha^4 A_1 C_{h\alpha} + \alpha^4 A_2 S_{h\alpha} + \beta^4 A_3 C_\beta + \beta^4 A_4 S_\beta + \gamma^4 A_5 C_\gamma + \gamma^4 A_6 S_\gamma\right]$$

$$+ \bar{K}\left[\alpha^3 B_1 S_{h\alpha} + \alpha^3 B_2 C_{h\alpha} + \beta^3 B_3 S_\beta - \beta^3 B_4 C_\beta + \gamma^3 B_5 S_\gamma - \gamma^3 B_6 C_\gamma\right]$$

$$+ \bar{P}\left[\alpha^2 A_1 C_{h\alpha} + \alpha^2 A_2 S_{h\alpha} - \beta^2 A_3 C_\beta - \beta^2 A_4 S_\beta - \gamma^2 A_5 C_\gamma - \gamma^2 A_6 S_\gamma\right]$$

$$- e\bar{P}\left[\alpha^2 B_1 C_{h\alpha} + \alpha^2 B_2 S_{h\alpha} - \beta^2 B_3 C_\beta - \beta^2 B_4 S_\beta - \gamma^2 B_5 C_\gamma - \gamma^2 B_6 S_\gamma\right]$$

$$- \bar{a}\left[A_1 C_{h\alpha} + A_2 S_{h\alpha} + A_3 C_\beta + A_4 S_\beta + A_5 C_\gamma + A_6 S_\gamma\right]$$

$$+ e\bar{a}\left[B_1 C_{h\alpha} + B_2 S_{h\alpha} + B_3 C_\beta + B_4 S_\beta + B_5 C_\gamma + B_6 S_\gamma\right] = 0$$

Gathering terms with similar coefficients

$$\left[\alpha^4 A_1 + \bar{K}\,\alpha^3 B_2 + \bar{P}\,\alpha^2 A_1 - e\bar{P}\,\alpha^2 B_1 - \bar{a}\,A_1 + e\bar{a}\,B_1\right] C_{h\alpha}$$

$$+ \left[\alpha^4 A_2 + \bar{K}\,\alpha^3 B_1 + \bar{P}\,\alpha^2 A_2 - e\bar{P}\,\alpha^2 B_2 - \bar{a}\,A_2 + e\bar{a}\,B_2\right] S_{h\alpha}$$

$$+ \left[\beta^4 A_3 - \bar{K}\,\beta^3 B_4 - \bar{P}\,\beta^2 A_3 + e\bar{P}\,\beta^2 B_3 - \bar{a}\,A_3 + e\bar{a}\,B_3\right] C_\beta$$

$$+ \left[\beta^4 A_4 + \bar{K}\,\beta^3 B_3 - \bar{P}\,\beta^2 A_4 + e\bar{P}\,\beta^2 B_4 - \bar{a}\,A_4 + e\bar{a}\,B_4\right] S_\beta$$

$$+ \left[\gamma^4 A_5 - \bar{K}\,\gamma^3 B_6 - \bar{P}\,\gamma^2 A_5 + e\bar{P}\,\gamma^2 B_5 - \bar{a}\,A_5 + e\bar{a}\,B_5\right] C_\gamma$$

$$+ \left[\gamma^4 A_6 + \bar{K}\,\gamma^3 B_5 - \bar{P}\,\gamma^2 A_6 + e\bar{P}\,\gamma^2 B_6 - \bar{a}\,A_6 + e\bar{a}\,B_6\right] S_\gamma = 0$$

Let

$$K_\alpha = \bar{K}\,\alpha^3 \quad , \quad P_{\alpha 1} = \alpha^4 + \bar{P}\,\alpha^2 - \bar{a} \quad , \quad P_{\alpha 2} = e\,\bar{a} - e\,\bar{P}\,\alpha^2$$

$$K_\beta = \bar{K}\,\beta^3 \quad , \quad P_{\beta 1} = \beta^4 - \bar{P}\,\beta^2 - \bar{a} \quad , \quad P_{\beta 2} = e\,\bar{a} + e\,\bar{P}\,\beta^2$$

$$K_\gamma = \bar{K}\,\gamma^3 \quad , \quad P_{\gamma 1} = \gamma^4 - \bar{P}\,\gamma^2 - \bar{a} \quad , \quad P_{\gamma 2} = e\,\bar{a} + e\,\bar{P}\,\gamma^2$$

$$P_{k\alpha} = \frac{P_{\alpha 1}}{K_\alpha^2 - P_{\alpha 2}^2} \quad , \quad P_{k\beta} = \frac{P_{\beta 1}}{K_\beta^2 - P_{\beta 2}^2} \quad , \quad P_{k\gamma} = \frac{P_{\gamma 1}}{K_\gamma^2 - P_{\gamma 2}^2}$$

Equating coefficients of cosh, sinh, cos and sin of α, β and γ on both sides, the relations between A_{1-6} and B_{1-6} were found using the symbolic computing package DERIVE [27].

$$B_1 = P_{k\alpha}\,(A_1\,P_{\alpha 2} - A_2\,K_\alpha) \quad , \quad B_2 = P_{k\alpha}\,(A_2\,P_{\alpha 2} - A_1\,K_\alpha)$$

$$B_3 = -\,P_{k\beta}\,(A_3\,P_{\beta 2} + A_4\,K_\beta) \quad , \quad B_4 = -\,P_{k\beta}\,(A_4\,P_{\beta 2} - A_3\,K_\beta)$$

$$B_5 = -\,P_{k\gamma}\,(A_5\,P_{\gamma 2} + A_6\,K_\gamma) \quad , \quad B_6 = -\,P_{k\gamma}\,(A_6\,P_{\gamma 2} - A_5\,K_\gamma)$$

Therefore, equation (6.7.15) can be written as follows:

$$\begin{aligned}\Psi(\xi) = {} & \left[P_{k\alpha}\,(A_1\,P_{\alpha 2} - A_2\,K_\alpha)\right] C_{h\alpha} + \left[P_{k\alpha}\,(A_2\,P_{\alpha 2} - A_1\,K_\alpha)\right] S_{h\alpha} \\ & - \left[P_{k\beta}\,(A_3\,P_{\beta 2} + A_4\,K_\beta)\right] C_\beta - \left[P_{k\beta}\,(A_4\,P_{\beta 2} - A_3\,K_\beta)\right] S_\beta \\ & - \left[P_{k\gamma}\,(A_5\,P_{\gamma 2} + A_6\,K_\gamma)\right] C_\gamma - \left[P_{k\gamma}\,(A_6\,P_{\gamma 2} - A_5\,K_\gamma)\right] S_\gamma\end{aligned}$$

or in an alternate form as

$$\begin{aligned}\Psi(\xi) = {} & \left[P_{k\alpha}\,(P_{\alpha 2}\,C_{h\alpha} - K_\alpha S_{h\alpha})\right] A_1 + \left[P_{k\alpha}\,(P_{\alpha 2}\,S_{h\alpha} - K_\alpha C_{h\alpha})\right] A_2 \\ & - \left[P_{k\beta}\,(P_{\beta 2}\,C_\beta - K_\beta S_\beta)\right] A_3 - \left[P_{k\beta}\,(P_{\beta 2}\,S_\beta + K_\beta C_\beta)\right] A_4 \\ & - \left[P_{k\gamma}\,(P_{\gamma 2}\,C_\gamma - K_\gamma S_\gamma)\right] A_5 - \left[P_{k\gamma}\,(P_{\gamma 2}\,S_\gamma + K_\gamma C_\gamma)\right] A_6\end{aligned} \qquad (6.8.17)$$

Let the boundary conditions be such that H_1, Θ_1, Ψ_1 represent the vertical deflection, slope, and twist at $y = 0$ or $\xi = 0$ and H_2, Θ_2, Ψ_2 represent vertical deflection, slope and twist at $y = \ell$ or $\xi = 1$ respectively.

Therefore, in matrix form tranverse displacement, slope and twist for an element on both ends can be expressed as follows:

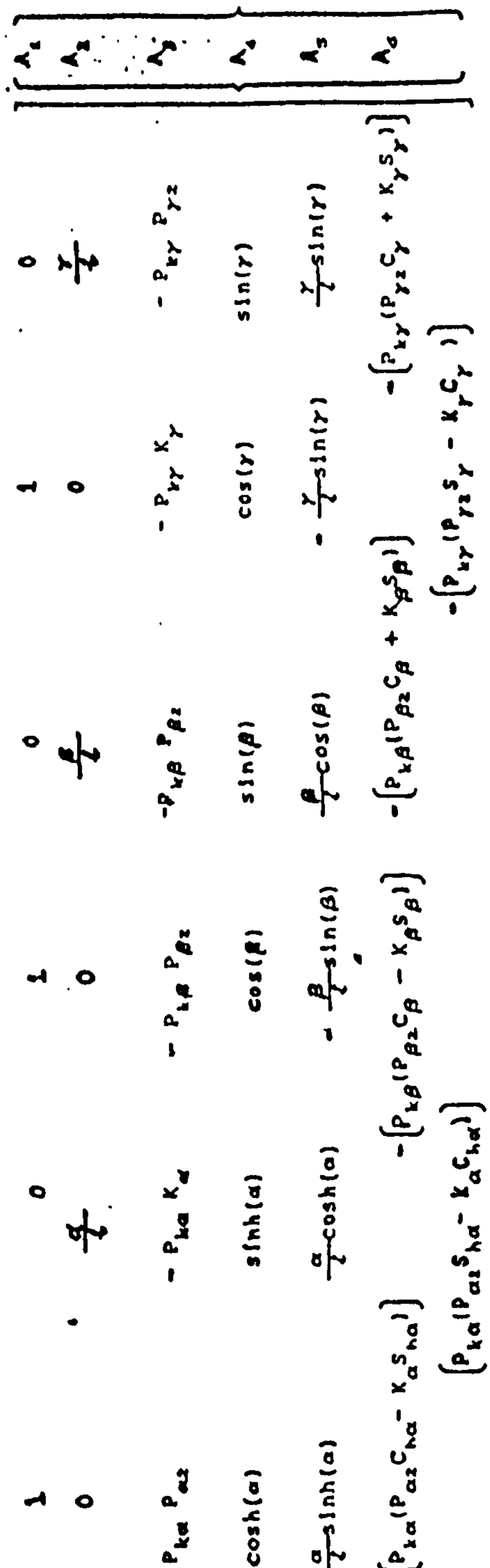

or simply

$$\{\underset{\sim}{U}\} = [\underset{\sim}{B}]\{\underset{\sim}{A}\} \qquad (6.7.18)$$

Now the expressions for shear force, bending moment and torque as given in equation (6.7.2) are evaluated as follows :

$$S = \frac{\partial}{\partial y}(-P\,h - M_x) + P\,e\,\frac{\partial \psi}{\partial y}$$

$$= -P\,\frac{\partial h}{\partial y} - \frac{\partial M_x}{\partial y} + P\,e\,\frac{\partial \psi}{\partial y}$$

where M_x is given by equation (6.7.3).

$$S = -P\,\frac{\partial h}{\partial y} - \frac{\partial}{\partial y}\left[EI\,\frac{\partial^2 h}{\partial y^2} + K\,\frac{\partial \psi}{\partial y}\right] + P\,e\,\frac{\partial \psi}{\partial y}$$

$$= -P\,\frac{\partial h}{\partial y} - EI\,\frac{\partial^3 h}{\partial y^3} + K\,\frac{\partial^2 \psi}{\partial y^2} + P\,e\,\frac{\partial \psi}{\partial y}$$

$$= -\frac{P}{\ell}\,\frac{\partial h}{\partial \xi} - \frac{EI}{\ell^3}\,\frac{\partial^3 h}{\partial \xi^3} + \frac{K}{\ell^2}\,\frac{\partial^2 \psi}{\partial \xi^2} + \frac{P\,e}{\ell}\,\frac{\partial \psi}{\partial \xi}$$

After substitution of the derivatives of h and ψ and necessary simplification we get :

$$S = \left\{-P\,\frac{\alpha}{\ell}\,S_{h\alpha} - EI\,\frac{\alpha^3}{\ell^3}\,S_{h\alpha} - K\,P_{k\alpha}\,\frac{\alpha^2}{\ell^2}\,(P_{\alpha 2}\,C_{h\alpha} - K_\alpha\,S_{h\alpha}) + P\,e\,P_{k\alpha}\,\frac{\alpha}{\ell}\,(P_{\alpha 2}\,S_{h\alpha} - K_\alpha\,C_{h\alpha})\right\} A_1$$

$$+ \left\{-P\,\frac{\alpha}{\ell}\,C_{h\alpha} - EI\,\frac{\alpha^3}{\ell^3}\,C_{h\alpha} - K\,P_{k\alpha}\,\frac{\alpha^2}{\ell^2}\,(P_{\alpha 2}\,S_{h\alpha} - K_\alpha\,C_{h\alpha}) + P\,e\,P_{k\alpha}\,\frac{\alpha}{\ell}\,(P_{\alpha 2}\,C_{h\alpha} - K_\alpha\,S_{h\alpha})\right\} A_2$$

$$+ \left\{+P\,\frac{\beta}{\ell}\,S_\beta - EI\,\frac{\beta^3}{\ell^3}\,S_\beta - K\,P_{k\beta}\,\frac{\beta^2}{\ell^2}\,(P_{\beta 2}\,C_\beta - K_\beta\,S_\beta)\right.$$

$$+ P\ e\ P_{k\beta}\ \frac{\beta}{\ell}\ (P_{\beta 2}\ S_\beta + K_\beta\ C_\beta)\Big\}\ A_3$$

$$+\ \Big\{-\ P\ \frac{\beta}{\ell}\ C_\beta + EI\ \frac{\beta^3}{\ell^3}\ C_\beta - K\ P_{k\beta}\ \frac{\beta^2}{\ell^2}\ (P_{\beta 2}\ S_\beta + K_\beta\ C_\beta)$$

$$- P\ e\ P_{k\beta}\ \frac{\beta}{\ell}\ (P_{\beta 2}\ C_\beta - K_\beta\ S_\beta)\Big\}\ A_4$$

$$+\ \Big\{+\ P\ \frac{\gamma}{\ell}\ S_\gamma - EI\ \frac{\gamma^3}{\ell^3}\ S_\gamma - K\ P_{k\gamma}\ \frac{\gamma^2}{\ell^2}\ (P_{\gamma 2}\ C_\gamma - K_\gamma\ S_\gamma)$$

$$+ P\ e\ P_{k\gamma}\ \frac{\gamma}{\ell}\ (P_{\gamma 2}\ S_\gamma + K_\gamma\ C_\gamma)\Big\}\ A_5$$

$$+\ \Big\{-\ P\ \frac{\gamma}{\ell}\ C_\gamma + EI\ \frac{\gamma^3}{\ell^3}\ C_\gamma - K\ P_{k\gamma}\ \frac{\gamma^2}{\ell^2}\ (P_{\gamma 2}\ S_\gamma + K_\gamma\ C_\gamma)$$

$$- P\ e\ P_{k\gamma}\ \frac{\gamma}{\ell}\ (P_{\gamma 2}\ C_\gamma - K_\gamma\ S_\gamma)\Big\}\ A_6$$

(6.7.19)

and

$$M_x = EI\ \frac{\partial^2 h}{\partial y^2} + K\ \frac{\partial \psi}{\partial y}$$

$$= \frac{EI}{\ell^2}\ \frac{\partial^2 h}{\partial \xi^2} + \frac{K}{\ell}\ \frac{\partial \psi}{\partial \xi}$$

$$= \Big\{\ EI\ \frac{\alpha^2}{\ell^2} C_{h\alpha} + K\ P_{k\alpha}\ \frac{\alpha}{\ell}\ \Big[P_{\alpha 2}\ S_{h\alpha} - K_\alpha\ C_{h\alpha}\Big]\Big\}\ A_1$$

$$+\ \Big\{\ EI\ \frac{\alpha^2}{\ell^2}\ S_{h\alpha} + K\ P_{k\alpha}\ \frac{\alpha}{\ell}\ \Big[P_{\alpha 2}\ C_{h\alpha} - K_\alpha\ S_{h\alpha}\Big]\Big\}\ A_2$$

$$+\ \Big\{-\ EI\ \frac{\beta^2}{\ell^2}\ C_\beta\ + K\ P_{k\beta}\ \frac{\beta}{\ell}\ \Big[P_{\beta 2}\ S_\beta\ + K_\beta\ C_\beta\ \Big]\Big\}\ A_3$$

$$+\ \Big\{-\ EI\ \frac{\beta^2}{\ell^2}\ S_\beta\ - K\ P_{k\beta}\ \frac{\beta}{\ell}\ \Big[P_{\beta 2}\ C_\beta\ - K_\beta\ S_\beta\ \Big]\Big\}\ A_4$$

$$+\ \Big\{-\ EI\ \frac{\gamma^2}{\ell^2}\ C_\gamma\ + K\ P_{k\gamma}\ \frac{\gamma}{\ell}\ \Big[P_{\gamma 2}\ S_\gamma\ + K_\gamma\ C_\gamma\ \Big]\Big\}\ A_5$$

$$+\ \Big\{-\ EI\ \frac{\gamma^2}{\ell^2}\ S_\gamma\ - K\ P_{k\gamma}\ \frac{\gamma}{\ell}\ \Big[P_{\gamma 2}\ C_\gamma\ - K_\gamma\ S_\gamma\ \Big]\Big\}\ A_6$$

(6.7.20)

and finally the torque from equation (6.7.4) is given by

$$T = GJ \frac{\partial \psi}{\partial y} + K \frac{\partial^2 h}{\partial y^2} + P \left[e \frac{\partial h}{\partial y} - r^2 \frac{\partial \psi}{\partial y} \right]$$

$$= \frac{GJ}{\ell} \frac{\partial \psi}{\partial \xi} + \frac{K}{\ell^2} \frac{\partial^2 h}{\partial \xi^2} + P \left[\frac{e}{\ell} \frac{\partial h}{\partial \xi} - \frac{r^2}{\ell} \frac{\partial \psi}{\partial \xi} \right]$$

$$= \left\{ K \frac{\alpha^2}{\ell^2} C_{h\alpha} + P e \frac{\alpha}{\ell} S_{h\alpha} + P_{k\alpha} \frac{\alpha}{\ell} (GJ - P r^2) \right.$$

$$\left. (P_{\alpha 2} S_{h\alpha} - K_\alpha C_{h\alpha}) \right\} A_1$$

$$+ \left\{ K \frac{\alpha^2}{\ell^2} S_{h\alpha} + P e \frac{\alpha}{\ell} C_{h\alpha} + P_{k\alpha} \frac{\alpha}{\ell} (GJ - P r^2) \right.$$

$$\left. (P_{\alpha 2} C_{h\alpha} - K_\alpha S_{h\alpha}) \right\} A_2$$

$$+ \left\{ - K \frac{\beta^2}{\ell^2} C_\beta - P e \frac{\beta}{\ell} S_\beta + P_{k\beta} \frac{\beta}{\ell} (GJ - P r^2) \right.$$

$$\left. (P_{\beta 2} S_\beta + K_\beta C_\beta) \right\} A_3$$

$$+ \left\{ - K \frac{\beta^2}{\ell^2} S_\beta + P e \frac{\beta}{\ell} C_\beta - P_{k\beta} \frac{\beta}{\ell} (GJ - P r^2) \right.$$

$$\left. (P_{\beta 2} C_\beta - K_\beta S_\beta) \right\} A_4$$

$$+ \left\{ - K \frac{\gamma^2}{\ell^2} C_\gamma - P e \frac{\gamma}{\ell} S_\gamma + P_{k\gamma} \frac{\gamma}{\ell} (GJ - P r^2) \right.$$

$$\left. (P_{\gamma 2} S_\gamma + K_\gamma C_\gamma) \right\} A_5$$

$$+ \left\{ - K \frac{\gamma^2}{\ell^2} S_\gamma + P e \frac{\gamma}{\ell} C_\gamma - P_{k\gamma} \frac{\gamma}{\ell} (GJ - P r^2) \right.$$

$$\left. (P_{\gamma 2} C_\gamma - K_\gamma S_\gamma) \right\} A_6 \qquad (6.7.21)$$

Adopting the following boundary conditions,

$y = 0$ or $\xi = 0$, $S = -S_1$, $M_x = -M_{x1}$, and $M_y = -M_{y1}$

$y = \ell$ or $\xi = 1$, $S = S_2$, $M_x = M_{x2}$, and $M_y = M_{y2}$

and after substituting these boundary conditions in equations (6.7.19) - (6.7.21) we get the following set of equations in the matrix form.

$$\begin{Bmatrix} S_1 \\ M_1 \\ T_1 \\ S_2 \\ M_2 \\ T_2 \end{Bmatrix} = \begin{bmatrix} D_{11} & D_{12} & D_{13} & D_{14} & D_{15} & D_{16} \\ D_{21} & D_{22} & D_{23} & D_{24} & D_{25} & D_{26} \\ D_{31} & D_{32} & D_{33} & D_{34} & D_{35} & D_{36} \\ D_{41} & D_{42} & D_{43} & D_{44} & D_{45} & D_{46} \\ D_{51} & D_{52} & D_{53} & D_{54} & D_{55} & D_{56} \\ D_{61} & D_{62} & D_{63} & D_{64} & D_{65} & D_{66} \end{bmatrix} \begin{Bmatrix} A_1 \\ A_2 \\ A_3 \\ A_4 \\ A_5 \\ A_6 \end{Bmatrix}$$

or

$$\{\underset{\sim}{F}\} = [\underset{\sim}{D}]\{\underset{\sim}{A}\} \qquad (6.7.22)$$

where

$$D_{11} = -\left(- K P_{k\alpha} \frac{\alpha^2}{\ell^2} P_{\alpha 2} - P e P_{k\alpha} \frac{\alpha}{\ell} K_{\alpha}\right)$$

$$D_{12} = -\left(- P \frac{\alpha}{\ell} - EI \frac{\alpha^3}{\ell^3} + K P_{k\alpha} \frac{\alpha^2}{\ell^2} K_{\alpha} + P e P_{k\alpha} \frac{\alpha}{\ell} P_{\alpha 2}\right)$$

$$D_{13} = -\left(- K P_{k\beta} \frac{\beta^2}{\ell^2} P_{\beta 2} + P e P_{k\beta} \frac{\beta}{\ell} K_{\beta}\right)$$

$$D_{14} = -\left(- P \frac{\beta}{\ell} + EI \frac{\beta^3}{\ell^3} - K P_{k\beta} \frac{\beta^2}{\ell^2} + K_{\beta} - P e P_{k\beta} \frac{\beta}{\ell} P_{\beta 2}\right)$$

$$D_{15} = -\left(- K P_{k\gamma} \frac{\gamma^2}{\ell^2} P_{\gamma 2} + P e P_{k\gamma} \frac{\gamma}{\ell} K_{\gamma}\right)$$

$$D_{16} = -\left(- P \frac{\gamma}{\ell} + EI \frac{\gamma^3}{\ell^3} - K P_{k\gamma} \frac{\gamma^2}{\ell^2} K_{\gamma} - P e P_{k\gamma} \frac{\gamma}{\ell} P_{\gamma 2}\right)$$

$$D_{21} = -\left(EI \frac{\alpha^2}{\ell^2} - K P_{k\alpha} \frac{\alpha}{\ell} K_{\alpha}\right)$$

$$D_{22} = -\left(K P_{k\alpha} \frac{\alpha}{\ell} P_{\alpha 2}\right)$$

$$D_{23} = -\left(- EI \frac{\beta^2}{\ell^2} + K P_{k\beta} \frac{\beta}{\ell} K_{\beta}\right)$$

$$D_{24} = - \left(- K \; P_{k\beta} \; \frac{\beta}{\ell} \; P_{\beta 2} \right)$$

$$D_{25} = - \left(- EI \; \frac{\gamma^2}{\ell^2} + K \; P_{k\gamma} \; \frac{\gamma}{\ell} \; K_{\gamma} \right)$$

$$D_{26} = - \left(- K \; P_{k\gamma} \; \frac{\gamma}{\ell} \; P_{\gamma 2} \right)$$

$$D_{31} = - \left(K \; \frac{\alpha^2}{\ell^2} - P_{k\alpha} \; \frac{\alpha}{\ell} \; (GJ - P \; r^2) \; K_{\alpha} \right)$$

$$D_{32} = - \left(P \; e \; \frac{\alpha}{\ell} + P_{k\alpha} \; \frac{\alpha}{\ell} \; (GJ - P \; r^2) \; P_{\alpha 2} \right)$$

$$D_{33} = - \left(- K \; \frac{\beta^2}{\ell^2} + P_{k\beta} \; \frac{\beta}{\ell} \; (GJ - P \; r^2) \; K_{\beta} \right)$$

$$D_{34} = - \left(P \; e \; \frac{\beta}{\ell} - P_{k\beta} \; \frac{\beta}{\ell} \; (GJ - P \; r^2) \; P_{\beta 2} \right)$$

$$D_{35} = - \left(- K \; \frac{\gamma^2}{\ell^2} + P_{k\gamma} \; \frac{\gamma}{\ell} \; (GJ - P \; r^2) \; K_{\gamma} \right)$$

$$D_{36} = - \left(P \; e \; \frac{\gamma}{\ell} - P_{k\gamma} \; \frac{\gamma}{\ell} \; (GJ - P \; r^2) \; P_{\gamma 2} \right)$$

$$D_{41} = - P \; \frac{\alpha}{\ell} \; S_{h\alpha} - EI \; \frac{\alpha^3}{\ell^3} \; S_{h\alpha} - K \; P_{k\alpha} \; \frac{\alpha^2}{\ell^2} \; (P_{\alpha 2} \; C_{h\alpha} - K_{\alpha} \; S_{h\alpha})$$

$$+ P \; e \; P_{k\alpha} \; \frac{\alpha}{\ell} \; (P_{\alpha 2} \; S_{h\alpha} - K_{\alpha} \; C_{h\alpha})$$

$$D_{42} = - P \; \frac{\alpha}{\ell} \; C_{h\alpha} - EI \; \frac{\alpha^3}{\ell^3} \; C_{h\alpha} - K \; P_{k\alpha} \; \frac{\alpha^2}{\ell^2} \; (P_{\alpha 2} \; S_{h\alpha} - K_{\alpha} \; C_{h\alpha})$$

$$+ P \; e \; P_{k\alpha} \; \frac{\alpha}{\ell} \; (P_{\alpha 2} \; C_{h\alpha} - K_{\alpha} \; S_{h\alpha})$$

$$D_{43} = P \; \frac{\beta}{\ell} \; S_{\beta} - EI \; \frac{\beta^3}{\ell^3} \; S_{\beta} - K \; P_{k\beta} \; \frac{\beta^2}{\ell^2} \; (P_{\beta 2} \; C_{\beta} - K_{\beta} \; S_{\beta})$$

$$+ P \; e \; P_{k\beta} \; \frac{\beta}{\ell} \; (P_{\beta 2} \; S_{\beta} + K_{\beta} \; C_{\beta})$$

$$D_{44} = - P \; \frac{\beta}{\ell} \; C_{\beta} + EI \; \frac{\beta^3}{\ell^3} \; C_{\beta} - K \; P_{k\beta} \; \frac{\beta^2}{\ell^2} \; (P_{\beta 2} \; S_{\beta} + K_{\beta} \; C_{\beta})$$

$$- P \; e \; P_{k\beta} \; \frac{\beta}{\ell} \; (P_{\beta 2} \; C_{\beta} - K_{\beta} \; S_{\beta})$$

$$D_{45} = P \frac{\gamma}{\ell} S_\gamma - EI \frac{\gamma^3}{\ell^3} S_\gamma - K P_{k\gamma} \frac{\gamma^2}{\ell^2} (P_{\gamma 2} C_\gamma - K_\gamma S_\gamma)$$

$$+ P e P_{k\gamma} \frac{\gamma}{\ell} (P_{\gamma 2} S_\gamma + K_\gamma C_\gamma)$$

$$D_{46} = - P \frac{\gamma}{\ell} C_\gamma + EI \frac{\gamma^3}{\ell^3} C_\gamma - K P_{k\gamma} \frac{\gamma^2}{\ell^2} (P_{\gamma 2} S_\gamma + K_\gamma C_\gamma)$$

$$- P e P_{k\gamma} \frac{\gamma}{\ell} (P_{\gamma 2} C_\gamma - K_\gamma S_\gamma)$$

$$D_{51} = EI \frac{\alpha^2}{\ell^2} C_{h\alpha} + K P_{k\alpha} \frac{\alpha}{\ell} \left[P_{\alpha 2} S_{h\alpha} - K_\alpha C_{h\alpha}\right]$$

$$D_{52} = EI \frac{\alpha^2}{\ell^2} S_{h\alpha} + K P_{k\alpha} \frac{\alpha}{\ell} \left[P_{\alpha 2} C_{h\alpha} - K_\alpha S_{h\alpha}\right]$$

$$D_{53} = - EI \frac{\beta^2}{\ell^2} C_\beta + K P_{k\beta} \frac{\beta}{\ell} \left[P_{\beta 2} S_\beta + K_\beta C_\beta\right]$$

$$D_{54} = - EI \frac{\beta^2}{\ell^2} S_\beta - K P_{k\beta} \frac{\beta}{\ell} \left[P_{\beta 2} C_\beta - K_\beta S_\beta\right]$$

$$D_{55} = - EI \frac{\gamma^2}{\ell^2} C_\gamma + K P_{k\gamma} \frac{\gamma}{\ell} \left[P_{\gamma 2} S_\gamma + K_\gamma C_\gamma\right]$$

$$D_{56} = - EI \frac{\gamma^2}{\ell^2} S_\gamma - K P_{k\gamma} \frac{\gamma}{\ell} \left[P_{\gamma 2} C_\gamma - K_\gamma S_\gamma\right]$$

$$D_{61} = K \frac{\alpha^2}{\ell^2} C_{h\alpha} + P e \frac{\alpha}{\ell} S_{h\alpha} + P_{k\alpha} \frac{\alpha}{\ell} (GJ - P r^2)$$

$$(P_{\alpha 2} S_{h\alpha} - K_\alpha C_{h\alpha})$$

$$D_{62} = K \frac{\alpha^2}{\ell^2} S_{h\alpha} + P e \frac{\alpha}{\ell} C_{h\alpha} + P_{k\alpha} \frac{\alpha}{\ell} (GJ - P r^2)$$

$$(P_{\alpha 2} C_{h\alpha} - K_\alpha S_{h\alpha})$$

$$D_{63} = - K \frac{\beta^2}{\ell^2} C_\beta - P e \frac{\beta}{\ell} S_\beta + P_{k\beta} \frac{\beta}{\ell} (GJ - P r^2)$$

$$(P_{\beta 2} S_\beta + K_\beta C_\beta)$$

$$D_{64} = - K \frac{\beta^2}{\ell^2} S_\beta + P e \frac{\beta}{\ell} C_\beta - P_{k\beta} \frac{\beta}{\ell} (GJ - P r^2)$$

$$(P_{\beta 2}\, C_\beta - K_\beta\, S_\beta)$$

$$D_{\alpha\beta} = - K \frac{\gamma^2}{\ell^2} C_\gamma - P\, e \frac{\gamma}{\ell} S_\gamma + P_{k\gamma} \frac{\gamma}{\ell} (GJ - P\, r^2)$$

$$(P_{\gamma 2}\, S_\gamma + K_\gamma\, C_\gamma)$$

$$D_{\alpha\alpha} = - K \frac{\gamma^2}{\ell^2} S_\gamma + P\, e \frac{\gamma}{\ell} C_\gamma - P_{k\gamma} \frac{\gamma}{\ell} (GJ - P\, r^2)$$

$$(P_{\gamma 2}\, C_\gamma - K_\gamma\, S_\gamma)$$

Finally equation (6.7.18) is substituted in equation (6.7.22) which leads to the determination of the dynamic stiffness matrix.

$$\{\underset{\sim}{F}\} = [\underset{\sim}{D}]\{\underset{\sim}{U}\}[\underset{\sim}{B}]^{-1} = [\underset{\sim}{K}]\{\underset{\sim}{U}\}$$

where $[\underset{\sim}{K}] = [\underset{\sim}{D}][\underset{\sim}{B}]^{-1}$ = Dynamic stiffness matrix

6.8 VIBRATION OF BEAMS WITH GEOMETRIC AND MATERIAL COUPLING

The generalized case discussed in section (6.7) has several degenerated cases. The derivations of dynamic stiffness matrices of these cases are discussed in detail in Appendix (K). Final results in the form of equations of motion along with B and D matrices are presented in this section. Both of these matrices are then used in obtaining the dynamic stiffness matrix, as described in the previous section.

EQUATIONS OF MOTION

$$EI\frac{\partial^4 h}{\partial y^4} + K \frac{\partial^3 \psi}{\partial y^3} + m \frac{\partial^2 h}{\partial t^2} - m\, e \frac{\partial^2 \psi}{\partial t^2} = 0 \qquad (6.8.1)$$

$$K \frac{\partial^3 h}{\partial y^3} + GJ \frac{\partial^2 \psi}{\partial y^2} + m\, e \frac{\partial^2 h}{\partial t^2} - I_\alpha \frac{\partial^2 \psi}{\partial t^2} = 0 \qquad (6.8.2)$$

The B - matrix is :-

$$\begin{bmatrix} 1 & 0 & 1 & 0 & 1 & 0 \\ 0 & \frac{\alpha}{\ell} & 0 & \frac{\beta}{\ell} & 0 & \frac{\gamma}{\ell} \\ e\,\bar{a}\,K_{\alpha 3} & -K_{\alpha}K_{\alpha 3} & e\,\bar{a}\,K_{\beta 3} & K_{\beta}K_{\beta 3} & e\,\bar{a}\,K_{\gamma 3} & K_{\gamma}K_{\gamma 3} \\ C_{h\alpha} & S_{h\alpha} & C_{\beta} & S_{\beta} & C_{\gamma} & S_{\gamma} \\ \frac{\alpha}{\ell}\,S_{h\alpha} & \frac{\alpha}{\ell}\,C_{h\alpha} & -\frac{\beta}{\ell}\,S_{\beta} & \frac{\beta}{\ell}\,C_{\beta} & -\frac{\gamma}{\ell}\,S_{\gamma} & \frac{\gamma}{\ell}\,C_{\gamma} \\ K_{\alpha 3}\mu_1 & K_{\alpha 3}\mu_2 & K_{\beta 3}\mu_3 & K_{\beta 3}\mu_4 & K_{\gamma 3}\mu_5 & K_{\gamma 3}\mu_6 \end{bmatrix} \qquad (6.8.3)$$

where

$$\mu_1 = e\,\bar{a}\,C_{h\alpha} - K_{\alpha}\,S_{h\alpha}$$
$$\mu_2 = e\,\bar{a}\,S_{h\alpha} - K_{\alpha}\,C_{h\alpha}$$
$$\mu_3 = e\,\bar{a}\,C_{\beta} - K_{\beta}\,S_{\beta}$$
$$\mu_4 = e\,\bar{a}\,S_{\beta} + K_{\beta}\,C_{\beta}$$
$$\mu_5 = e\,\bar{a}\,C_{\gamma} - K_{\gamma}\,S_{\gamma}$$
$$\mu_6 = e\,\bar{a}\,S_{\gamma} + K_{\gamma}\,C_{\gamma}$$

The D - matrix is :-

$$\begin{Bmatrix} S_1 \\ M_1 \\ T_1 \\ S_2 \\ M_2 \\ T_2 \end{Bmatrix} = \begin{bmatrix} D_{11} & D_{12} & D_{13} & D_{14} & D_{15} & D_{16} \\ D_{21} & D_{22} & D_{23} & D_{24} & D_{25} & D_{26} \\ D_{31} & D_{32} & D_{33} & D_{34} & D_{35} & D_{36} \\ D_{41} & D_{42} & D_{43} & D_{44} & D_{45} & D_{46} \\ D_{51} & D_{52} & D_{53} & D_{54} & D_{55} & D_{56} \\ D_{61} & D_{62} & D_{63} & D_{64} & D_{65} & D_{66} \end{bmatrix} \begin{Bmatrix} A_1 \\ A_2 \\ A_3 \\ A_4 \\ A_5 \\ A_6 \end{Bmatrix} \qquad (6.8.4)$$

where

$$D_{11} = - \left(K \; K_{\alpha 3} \frac{\alpha^2}{\ell^3} \; e \; \bar{a} \right) \cdot$$

$$D_{12} = - \left(- EI \; \frac{\alpha^3}{\ell^3} + K \; K_{\alpha 3} \frac{\alpha^2}{\ell^2} \; K_{\alpha} \right)$$

$$D_{13} = - \left(+ K \; K_{\beta 3} \frac{\beta^2}{\ell^2} \; e \; \bar{a} \right)$$

$$D_{14} = - \left(+ EI \; \frac{\beta^3}{\ell^3} + K \; K_{\beta 3} \frac{\beta^2}{\ell^2} \; K_{\beta} \right)$$

$$D_{15} = - \left(+ K \; K_{\gamma 3} \frac{\gamma^2}{\ell^2} \; e \; \bar{a} \right)$$

$$D_{16} = - \left(+ EI \; \frac{\gamma^3}{\ell^3} + K \; K_{\gamma 3} \frac{\gamma^2}{\ell^2} \; K_{\gamma} \right)$$

$$D_{21} = - \left(EI \; \frac{\alpha^2}{\ell^2} - K \; K_{\alpha 3} \frac{\alpha}{\ell} \; K_{\alpha} \right)$$

$$D_{22} = - \left(+ K \; K_{\alpha 3} \frac{\alpha}{\ell} \; e \; \bar{a} \right)$$

$$D_{23} = - \left(- EI \; \frac{\beta^2}{\ell^2} - K \; K_{\beta 3} \frac{\beta}{\ell} \; K_{\beta} \right)$$

$$D_{24} = - \left(+ K \; K_{\beta 3} \frac{\beta}{\ell} \; e \; \bar{a} \right)$$

$$D_{25} = - \left(- EI \; \frac{\gamma^2}{\ell^2} - K \; K_{\gamma 3} \frac{\gamma}{\ell} \; K_{\gamma} \right)$$

$$D_{26} = - \left(+ K \; K_{\gamma 3} \frac{\gamma}{\ell} \; e \; \bar{a} \right)$$

$$D_{31} = - \left(- GJ \; K_{\alpha 3} \frac{\alpha}{\ell} \; K_{\alpha} + K \; \frac{\alpha^2}{\ell^2} \right)$$

$$D_{32} = - \left(+ GJ \; K_{\alpha 3} \frac{\alpha}{\ell} \; e \; \bar{a} \right)$$

$$D_{33} = - \left(- GJ \; K_{\beta 3} \frac{\beta}{\ell} \; K_{\beta} - K \; \frac{\beta^2}{\ell^2} \right)$$

$$D_{34} = - \left(+ GJ \; K_{\beta 3} \frac{\beta}{\ell} \; e \; \bar{a} \right)$$

$$D_{35} = - \left(- GJ \; K_{\gamma 3} \frac{\gamma}{\ell} \; K_{\gamma} - K \; \frac{\gamma^2}{\ell^2} \right)$$

$$D_{36} = - \left[+ GJ\ K_{\gamma 3} \frac{\gamma}{\ell}\ e\ \bar{a} \right]$$

$$D_{41} = - EI\ \frac{\alpha^3}{\ell^3} \sinh(\alpha) - K\ K_{\alpha 3} \frac{\alpha^2}{\ell^2} \left[e\ \bar{a} \cosh(\alpha) - K_\alpha \sinh(\alpha) \right]$$

$$D_{42} = - EI\ \frac{\alpha^3}{\ell^3} \cosh(\alpha) - K\ K_{\alpha 3} \frac{\alpha^2}{\ell^2} \left[e\ \bar{a} \sinh(\alpha) - K_\alpha \cosh(\alpha) \right]$$

$$D_{43} = - EI\ \frac{\beta^3}{\ell^3} \sin(\beta) - K\ K_{\beta 3} \frac{\beta^2}{\ell^2} \left[- e\ \bar{a} \cos(\beta) + K_\beta \sin(\beta) \right]$$

$$D_{44} = + EI\ \frac{\beta^3}{\ell^3} \cos(\beta) - K\ K_{\beta 3} \frac{\beta^2}{\ell^2} \left[- e\ \bar{a} \sin(\beta) - K_\beta \cos(\beta) \right]$$

$$D_{45} = - EI\ \frac{\gamma^3}{\ell^3} \sin(\gamma) - K\ K_{\gamma 3} \frac{\gamma^2}{\ell^2} \left[- e\ \bar{a} \cos(\gamma) + K_\gamma \sin(\gamma) \right]$$

$$D_{46} = + EI\ \frac{\gamma^3}{\ell^3} \cos(\gamma) - K\ K_{\gamma 3} \frac{\gamma^2}{\ell^2} \left[- e\ \bar{a} \sin(\gamma) - K_\gamma \cos(\gamma) \right]$$

$$D_{51} = EI\ \frac{\alpha^2}{\ell^2} \cosh(\alpha) + K\ K_{\alpha 3} \frac{\alpha}{\ell} \left[e\ \bar{a} \sinh(\alpha) - K_\alpha \cosh(\alpha) \right]$$

$$D_{52} = EI\ \frac{\alpha^2}{\ell^2} \sinh(\alpha) + K\ K_{\alpha 3} \frac{\alpha}{\ell} \left[e\ \bar{a} \cosh(\alpha) - K_\alpha \sinh(\alpha) \right]$$

$$D_{53} = - EI\ \frac{\beta^2}{\ell^2} \cos(\beta) + K\ K_{\beta 3} \frac{\beta}{\ell} \left[- e\ \bar{a} \sin(\beta) - K_\beta \cos(\beta) \right]$$

$$D_{54} = - EI\ \frac{\beta^2}{\ell^2} \sin(\beta) + K\ K_{\beta 3} \frac{\beta}{\ell} \left[e\ \bar{a} \cos(\beta) - K_\beta \sin(\beta) \right]$$

$$D_{55} = - EI\ \frac{\gamma^2}{\ell^2} \cos(\gamma) + K\ K_{\gamma 3} \frac{\gamma}{\ell} \left[- e\ \bar{a} \sin(\gamma) - K_\gamma \cos(\gamma) \right]$$

$$D_{56} = - EI\ \frac{\gamma^2}{\ell^2} \sin(\gamma) + K\ K_{\gamma 3} \frac{\gamma}{\ell} \left[e\ \bar{a} \cos(\gamma) - K_\gamma \sin(\gamma) \right]$$

$$D_{61} = GJ\ K_{\alpha 3} \frac{\alpha}{\ell} \left[e\ \bar{a} \sinh(\alpha) - K_\alpha \cosh(\alpha) \right] + K\ \frac{\alpha^2}{\ell^2} \cosh(\alpha)$$

$$D_{62} = GJ\ K_{\alpha 3} \frac{\alpha}{\ell} \left[e\ \bar{a} \cosh(\alpha) - K_\alpha \sinh(\alpha) \right] + K\ \frac{\alpha^2}{\ell^2} \sinh(\alpha)$$

$$D_{63} = GJ\ K_{\beta 3} \frac{\beta}{\ell} \left[- e\ \bar{a} \sin(\beta) - K_\beta \cos(\beta) \right] - K\ \frac{\beta^2}{\ell^2} \cos(\beta)$$

$$D_{64} = GJ\ K_{\beta 3} \frac{\beta}{\ell} \left[e\ \bar{a} \cos(\beta) - K_\beta \sin(\beta) \right] - K\ \frac{\beta^2}{\ell^2} \sin(\beta)$$

$$D_{65} = GJ\ K_{\gamma 3} \frac{\gamma}{\ell} \left[- e\ \bar{a} \sin(\gamma) - K_\gamma \cos(\gamma) \right] - K\ \frac{\gamma^2}{\ell^2} \cos(\gamma)$$

$$D_{\alpha\alpha} = GJ\ K_{\gamma s}\frac{\gamma}{\ell}\left[\ e\ \bar{a}\ \cos(\gamma) - K_{\gamma}\sin(\gamma)\right] - K\ \frac{\gamma^2}{\ell^2}\ \sin\ (\gamma)$$

Finally the dynamic stiffness matrix is obtained by multiplying B and D matrices.

$$[\underset{\sim}{K}] = [\underset{\sim}{D}][\underset{\sim}{B}]^{-1} \qquad (6.8.5)$$

6.9 VIBRATION OF BEAMS WITH MATERIAL COUPLING

In section (6.8), the case of geometric and material coupling was analysed. Explicit expressions for the dynamic stiffness matrix with geometric coupling only has been derived by Banerjee [20]. In this section, final results will be presented in the form of equations of motion along with B and D matrices for thin-walled composite beams with material bending-torsion coupling only (see Appendix (K) for detail derivations). Doubly symmetrical sections and plates are good examples of such structures where material coupling can exist due to the laminate stacking sequence. The governing differential equations (6.8.1) and (6.8.2) are then reduce to the following forms.

EQUATIONS OF MOTION

$$EI\frac{\partial^4 h}{\partial y^4} + K\ \frac{\partial^3 \psi}{\partial y^3} + m\ \frac{\partial^2 h}{\partial t^2} = 0 \qquad (6.9.1)$$

$$K\ \frac{\partial^3 h}{\partial y^3} + GJ\ \frac{\partial^2 \psi}{\partial y^2} - I_{\alpha}\ \frac{\partial^2 \psi}{\partial t^2} = 0 \qquad (6.9.2)$$

The B - matrix is :-

$$\begin{bmatrix} 1 & 0 & 1 & 0 & 1 & 0 \\ 0 & \frac{\alpha}{\ell} & 0 & \frac{\beta}{\ell} & 0 & \frac{\gamma}{\ell} \\ 0 & K_\alpha & 0 & K_\beta & 0 & K_\gamma \\ C_{h\alpha} & S_{h\alpha} & C_\beta & S_\beta & C_\gamma & S_\gamma \\ \frac{\alpha}{\ell} S_{h\alpha} & \frac{\alpha}{\ell} C_{h\alpha} & -\frac{\beta}{\ell} S_\beta & \frac{\beta}{\ell} C_\beta & -\frac{\gamma}{\ell} S_\gamma & \frac{\gamma}{\ell} C_\gamma \\ K_\alpha S_{h\alpha} & K_{h\alpha} C_{h\alpha} & -K_\beta S_\beta & K_\beta C_\beta & -K_\gamma S_\gamma & K_\gamma C_\gamma \end{bmatrix} \quad (6.9.3)$$

The D - matrix is :-

$$\begin{bmatrix} 0 & -K_{\alpha a} & 0 & K_{\beta a} & 0 & K_{\gamma a} \\ K_{\alpha m} & 0 & K_{\beta m} & 0 & K_{\gamma m} & 0 \\ K_{\alpha t} & 0 & K_{\beta t} & 0 & K_{\gamma t} & 0 \\ -K_{\alpha a} S_{h\alpha} & -K_{\alpha a} C_{h\alpha} & -K_{\beta a} S_\beta & K_{\beta a} C_\beta & -K_{\gamma a} S_\gamma & K_{\gamma a} C_\gamma \\ K_{\alpha m} C_{h\alpha} & K_{\alpha m} S_{h\alpha} & -K_{\beta m} C_\beta & -K_{\beta m} S_\beta & -K_{\gamma m} C_\gamma & -K_{\gamma m} S_\gamma \\ K_{\alpha t} C_{h\alpha} & K_{\alpha t} S_{h\alpha} & -K_{\beta t} C_\beta & -K_{\beta t} S_\beta & -K_{\gamma t} C_\gamma & -K_{\gamma t} S_\gamma \end{bmatrix} \quad (6.9.4)$$

Finally the dynamic stiffness matrix will be computed by multiplying the D matrix with the inverse of the B matrix.

$$[\underset{\sim}{K}] = [\underset{\sim}{D}][\underset{\sim}{B}]^{-1} \quad (6.9.5)$$

6.10 COMPUTATION OF THE DYNAMIC STIFFNESS MATRIX

The dynamic stiffness matrix was computed by numerical techniques as well as by an analytical approach. Based on these methods, two FORTRAN subroutines were developed. The block of information common to both subroutines was the input of structural properties such as bending, torsional, and bending-torsional coupled stiffnesses, mass per unit length, polar mass moment of inertia, distance between the centroid and the shear centre, span of the structure, axial load applied, and frequency for which the matrix is desired. In the numerical approach, the B and D matrices were formed with the help of these structural parameters as discussed in sections (6.7), (6.8), and (6.9). Inversion of the B matrix was performed in two ways. A matrix inversion subroutine based on the Gauss elimination method was written to make the program self contained. However, the inversion subroutine based on this Gauss elimination method failed when the analysis for a box-beam structure or a plate structure was performed. (This was due to the fact that a diagonal term B_{33} was zero when geometric coupling did not exist). In such cases, a very small but not zero elastic coupling can be assumed (i.e. the value for B_{33}) and the above mentioned inversion subroutine is carried out. The other alternative was to use the NAG routine F01AAF [28], which is not based on the Gauss elimination method. Subsequently, the D matrix was multiplied by the inverted B matrix to obtain the dynamic stiffness matrix.

In the analytical approach, algebraic expressions of B and D matrices were symbolically processed by using REDUCE [29] (a symbolic computer package on the main-frame computer, for symbolic analysis of algebraic expressions). Explicit expressions for the dynamic stiffness matrix were thus obtained. The output obtained from REDUCE can be

further processed by GENTRAN (a package for obtaining a computer code in the FORTRAN language for analytical expressions). The output of REDUCE for the analytical expressions covered several hundred pages. Attempts were made to collect and condense various terms resulting in compact expressions for various elements of the dynamic stiffness matrix. The symmetric nature of the dynamic stiffness matrix reduces the labour to finding only 21 elements instead of 36. In the case of elastically coupled bending-torsional beams, this figure further reduces to 12 [20]. In the case of materially coupled structures, elements of the dynamic stiffness matrix were studied for a range of frequencies, as shown in Figure (6.2). A careful examination of these graphs indicated the need for only 13 independent quantities to define the stiffness elements.

6.11 DYNAMIC STIFFNESS MATRIX : EXPLICIT EXPRESSIONS FOR SYMMETRICALLY LAMINATED COMPOSITE STRUCTURES WITH MATERIAL BENDING-TORSIONAL COUPLING

Explicit expressions for the dynamic stiffness matrix of elastically coupled structure have already been evaluated by Banerjee [20]. Similar explicit expressions are presented here for materially bending-torsion coupled structures. The dynamic stiffness matrix obtained is a 6 x 6 matrix containing 36 elements. Due to symmetry, 21 elements are needed of which 13 elements are independent of each other. The elements of dynamic stiffness matrix are defined as follows :

$$K_{11} = \frac{\Phi_1}{\Delta} \quad , \quad K_{12} = \frac{\Phi_2}{\Delta} \quad , \quad K_{13} = \frac{\Phi_3}{\Delta}$$

$$K_{14} = \frac{\Phi_4}{\Delta} \quad , \quad K_{15} = \frac{\Phi_5}{\Delta} \quad , \quad K_{16} = \frac{\Phi_6}{\Delta}$$

$$K_{22} = \frac{\Phi_7}{\Delta} \quad , \quad K_{23} = \frac{\Phi_8}{\Delta} \quad , \quad K_{24} = - K_{15}$$

$$K_{25} = \frac{\Phi_9}{\Delta} \quad , \quad K_{26} = \frac{\Phi_{10}}{\Delta}$$

$$K_{33} = \frac{\Phi_{11}}{\Delta} \quad , \quad K_{34} = \frac{\Phi_{12}}{\Delta} \quad , \quad K_{35} = K_{26}$$

$$K_{36} = \frac{\Phi_{13}}{\Delta}$$

$$K_{44} = K_{11} \quad , \quad K_{45} = - K_{12} \quad , \quad K_{46} = - K_{13}$$

$$K_{55} = K_{22} \quad , \quad K_{56} = K_{23}$$

$$K_{66} = K_{33} \qquad (6.11.1)$$

where

$$\Delta = S_{h\alpha} \left[\alpha^2 \eta_1 + 2 \psi_2 \psi_3\right] - S_\beta \left[\beta^2 \eta_2 + 2 \psi_1 \psi_3\right] - S_\gamma \left[\gamma^2 \eta_3 + 2 \psi_1 \psi_2\right]$$
$$+ 2 \left\{\lambda_1 \left[\gamma S_\gamma (2 \omega_2 - \omega) - \nu_1\right]\right.$$
$$- \lambda_2 \left[\alpha S_{h\alpha} \omega - \nu_3\right]$$
$$\left. - \lambda_3 \left[\beta S_\beta (2 \omega_3 - \omega) - \nu_2\right]\right\} \qquad (6.11.2)$$

and Φ_1 to Φ_{13} are defined by the following expressions :

$$\Phi_1 = \alpha^2 S_{h\alpha} \phi_1 + \alpha S_{h\alpha} \zeta_1 \omega$$
$$+ \beta^2 S_\beta \phi_2 + \beta S_\beta \zeta_2 (\omega - 2 \omega_3)$$
$$+ \gamma^2 S_\gamma \phi_3 + \gamma S_\gamma \zeta_3 (\omega - 2 \omega_2)$$
$$+ C_{h\alpha} \Omega_1 + C_\beta \Omega_2 + C_\gamma \Omega_3 - 2 \Theta \qquad (6.11.3)$$

$$\Phi_2 = \ell \Big[K_{\alpha a}\, \sigma_1 - K_{\beta a}\, \sigma_2 - K_{\gamma a}\, \sigma_3 + \alpha\, \rho_1 + \beta\, \rho_2 + \gamma\, \rho_3 + K_\alpha\, z_1 + K_\beta\, z_2 + K_\gamma\, z_3 + \tau_1\, \varepsilon_1\, (C_\beta\, C_\gamma - 1) + \tau_2\, \varepsilon_2\, (C_{h\alpha} C_\gamma - 1) + \tau_3\, \varepsilon_3\, (C_{h\alpha} C_\beta - 1) \Big] \qquad (6.11.4)$$

$$\Phi_3 = - \Big[\alpha^2\, S_{h\alpha}\, Q_1 + \beta^2\, S_\beta\, Q_2 + \gamma^2\, S_\gamma\, Q_3 + \alpha\beta\, K_\gamma\, V_1 + \alpha\gamma\, K_\beta\, V_2 + \beta\gamma\, K_\alpha\, V_3 - \alpha\, \Sigma_1 + \beta\, \Sigma_2 + \gamma\, \Sigma_3 \Big] \qquad (6.11.5)$$

$$\Phi_4 = - \Big[\alpha^2\, S_{h\alpha} \left[K_{\beta a} \delta_3 + K_{\gamma a} \delta_2 \right] + \alpha\, S_{h\alpha}\, (\varepsilon_2 + \varepsilon_3)\, \omega + \beta^2\, S_\beta \left[K_{\alpha a} \delta_3 + K_{\gamma a} \delta_1 \right] + \beta\, S_\beta\, (\varepsilon_1 + \varepsilon_3)\, (\omega - 2\, \omega_3) + \gamma^2\, S_\gamma \left[K_{\alpha a} \delta_2 + K_{\beta a} \delta_1 \right] + \gamma\, S_\gamma\, (\varepsilon_1 + \varepsilon_2)\, (\omega - 2\, \omega_2) - 2 \left[K_{\alpha a} \psi_2 \psi_3 + K_{\beta a} \psi_1 \psi_3 + K_{\gamma a} \psi_1 \psi_2 \right] + \nu_1 (\varepsilon_1 + \varepsilon_2) + \nu_2 (\varepsilon_1 + \varepsilon_3) + \nu_3 (\varepsilon_2 + \varepsilon_3) \Big] \qquad (6.11.6)$$

$$\Phi_5 = - \ell \Big[- \alpha\, C_{h\alpha}\, (K_{\beta a} \delta_3 + K_{\gamma a} \delta_2) + K_\alpha\, C_{h\alpha} (K_{\beta a} \psi_3 + K_{\gamma a} \psi_2) + \beta\, C_\beta\, (K_{\alpha a} \delta_3 + K_{\gamma a} \delta_1) - K_\beta\, C_\beta\, (K_{\alpha a} \psi_3 + K_{\gamma a} \psi_1) + \gamma\, C_\gamma\, (K_{\alpha a} \delta_2 + K_{\beta a} \delta_1) - K_\gamma\, C_\gamma\, (K_{\alpha a} \psi_2 + K_{\beta a} \psi_1) - K_\alpha\, \dot{x}_1 + C_{h\alpha} \left\{ \varepsilon_2 (\omega_2 - \omega) + \varepsilon_3 (\omega_3 - \omega) \right\} + K_\beta\, x_2 + C_\beta \left\{ \varepsilon_1 (\omega_2 - \omega_3) + \varepsilon_3 (- \omega_3 + \omega) \right\}$$

$$+ K_\gamma x_3 + C_\gamma\left\{\varepsilon_1(-\omega_2+\omega_3) + \varepsilon_2(-\omega_2+\omega)\right\}\Big] \qquad (6.11.7)$$

$$\begin{aligned}\Phi_6 = -\Big[&\alpha^2 S_{h\alpha}\left[K_\gamma\,(C_\gamma K_{\beta a}-\varepsilon_3) + K_\beta\,(C_\beta K_{\gamma a}-\varepsilon_6)\right]\\
&+\beta^2 S_\beta\left[K_\gamma\,(C_\gamma K_{\alpha a}-\varepsilon_4) - K_\alpha\,(C_{h\alpha} K_{\gamma a}-\varepsilon_6)\right]\\
&+\gamma^2 S_\gamma\left[K_\beta\,(C_\beta K_{\alpha a}-\varepsilon_4) - K_\alpha\,(C_{h\alpha} K_{\beta a}-\varepsilon_5)\right]\\
&+\alpha C_{h\alpha}\left[K_{\beta a}\psi_3+K_{\gamma a}\psi_2\right] - \beta C_\beta\left[K_{\alpha a}\psi_3+K_{\gamma a}\psi_1\right] - \gamma C_\gamma\left[K_{\alpha a}\psi_2+K_{\beta a}\psi_1\right]\\
&+\alpha\beta K_\gamma\left[-\varepsilon_2(C_{h\alpha}-C_\gamma) - \varepsilon_1(C_\beta-C_\gamma)\right]\\
&+\alpha\gamma K_\beta\left[-\varepsilon_3(C_{h\alpha}-C_\beta) + \varepsilon_1(C_\beta-C_\gamma)\right]\\
&+\beta\gamma K_\alpha\left[+\varepsilon_2(C_{h\alpha}-C_\gamma) + \varepsilon_3(C_{h\alpha}-C_\beta)\right]\\
&-\alpha x_1+\beta x_2+\gamma x_3\Big] \qquad (6.11.8)\end{aligned}$$

$$\begin{aligned}\Phi_7 = \ell\Big[&S_\gamma J_1\left[\beta\delta_1 - K_\beta\psi_1\right] + S_{h\alpha} J_2\left[\gamma\delta_2 - K_\gamma\psi_2\right] + S_\beta J_3\left[\gamma\delta_1 - K_\gamma\psi_1\right]\\
&-(K_{\alpha m}+K_{\beta m})\,(S_{h\alpha} C_\beta\,\sigma_1 + S_\beta C_{h\alpha}\,\sigma_2)\\
&+(K_{\alpha m}+K_{\gamma m})\,(S_\gamma C_{h\alpha}\,\sigma_3)\\
&+C_{h\alpha}\Big\{\omega_3\left[3\lambda_2(K_{\alpha m}+K_{\beta m}) + 2\,(K_{\beta m}-K_{\gamma m})\right]\\
&+\omega_2\left[-3\lambda_2(K_{\alpha m}+K_{\beta m}) - 2\,(K_{\beta m}-K_{\gamma m})\right]\\
&+\tau_3\lambda_2\,(-2K_{\alpha m}-K_{\beta m}-K_{\gamma m})\Big\}\\
&-C_\beta\Big\{\omega_3\,(K_{\alpha m}+3K_{\beta m}-2K_{\gamma m}) + \omega_2(K_{\alpha m}+3K_{\beta m}-2K_{\gamma m})\end{aligned}$$

$$+ \tau_3 (K_{\beta m} - K_{\gamma m}) \Big\} \qquad (6.11.9)$$

$$\Phi_3 = \alpha^2 S_{h\alpha} S_\beta C_\gamma (K_{\beta m} - K_{\gamma m}) (K_\beta - K_\gamma)$$
$$+ \beta^2 S_\beta S_\gamma C_{h\alpha} (K_{\alpha m} + K_{\gamma m}) (K_\alpha - K_\gamma)$$
$$+ \gamma^2 S_\gamma S_\beta C_{h\alpha} (K_{\alpha m} + K_{\beta m}) (K_\alpha - K_\beta)$$
$$+ \alpha\beta K_\gamma \Big[C_{h\alpha} \Big[-\lambda_2 (K_{\alpha m} - K_{\beta m} + 2 K_{\gamma m}) + 2 (K_{\beta m} - K_{\gamma m})\Big]$$
$$- C_\beta (K_{\alpha m} + K_{\beta m}) + C_\gamma (K_{\alpha m} - K_{\beta m} + 2 K_{\gamma m})\Big]$$
$$+ \alpha\gamma K_\beta \Big[C_{h\alpha} \Big[-\lambda_2 (K_{\alpha m} + 2 K_{\beta m} - K_{\gamma m}) - 2 (K_{\beta m} - K_{\gamma m})\Big]$$
$$+ C_\beta (K_{\alpha m} + 2 K_{\beta m} - K_{\gamma m}) - C_\gamma (K_{\alpha m} + K_{\gamma m})\Big]$$
$$+ \beta\gamma K_\alpha \Big[C_{h\alpha} \Big[\lambda_2 (2 K_{\alpha m} + K_{\beta m} + K_{\gamma m})\Big]$$
$$- (C_\beta - C_\gamma) (K_{\beta m} - K_{\gamma m})\Big] \qquad (6.11.10)$$

$$\Phi_9 = -\ell \Big[(K_{\alpha m} + K_{\beta m}) \Big[\beta S_\gamma \delta_1 - K_\beta S_\gamma \psi_1 - S_{h\alpha} \sigma_1 + S_\beta \sigma_2\Big]$$
$$+ (K_{\beta m} - K_{\gamma m}) \Big[\gamma S_{h\alpha} \delta_2 - K_\gamma S_{h\alpha} \psi_2\Big]$$
$$+ (K_{\alpha m} + K_{\gamma m}) \Big[\gamma S_\beta \delta_1 - K_\gamma S_\beta \psi_1 + S_\gamma \sigma_3\Big]$$
$$+ \Big\{\omega_3 \Big[-K_{\alpha m} (\lambda_1 - 3\lambda_2 - \lambda_3) - K_{\beta m} (\lambda_1 - \lambda_2 - 3\lambda_3) + 2 K_{\gamma m} (\lambda_2 - \lambda_3)\Big]$$
$$+ \Big\{\omega_2 \Big[K_{\alpha m} (\lambda_1 - 3\lambda_2 - \lambda_3) + K_{\beta m} (\lambda_1 - \lambda_2 - 3\lambda_3) - 2 K_{\gamma m} (\lambda_2 - \lambda_3)\Big]$$
$$- \tau_3 \Big[2 K_{\alpha m} \lambda_2 - K_{\beta m} (\lambda_1 - \lambda_2 - \lambda_3) + K_{\gamma m} (\lambda_1 + \lambda_2 + \lambda_3)\Big]\Big]\Big] \qquad (6.11.11)$$

$$\Phi_{10} = \alpha^2 S_{h\alpha} (K_{\beta m} - K_{\gamma m}) (K_\gamma S_\beta - K_\beta S_\gamma)$$
$$+ \beta^2 S_\beta (K_{\alpha m} + K_{\gamma m}) (K_\gamma S_{h\alpha} - K_\alpha S_\gamma)$$
$$+ \gamma^2 S_\gamma (K_{\alpha m} + K_{\beta m}) (K_\beta S_{h\alpha} - K_\alpha S_\beta)$$
$$+ \alpha \beta K_\gamma \left\{K_{\alpha m}(\lambda_1 - \lambda_2 - \lambda_3) - K_{\beta m}(\lambda_1 - \lambda_2 + \lambda_3) - 2 K_{\gamma m}\lambda_1\right\}$$
$$- \alpha \gamma K_\beta \left\{K_{\alpha m}(\lambda_1 - \lambda_2 - \lambda_3) - 2 K_{\beta m}\lambda_3 + K_{\gamma m}(\lambda_1 - \lambda_2 + \lambda_3)\right\}$$
$$- \beta \gamma K_\alpha \left\{2 K_{\alpha m}\lambda_2 - K_{\beta m}(\lambda_1 - \lambda_2 - \lambda_3) + K_{\gamma m}(\lambda_1 + \lambda_2 - \lambda_3)\right\}$$
$$+ \alpha \left\{S_\beta \psi_3 (K_{\alpha m} + K_{\beta m}) + S_\gamma \psi_2 (K_{\alpha m} + K_{\gamma m})\right\}$$
$$- \beta \left\{S_{h\alpha}\psi_3 (K_{\alpha m} + K_{\beta m}) - S_\gamma \psi_1 (K_{\beta m} - K_{\gamma m})\right\}$$
$$- \gamma \left\{S_{h\alpha}\psi_2 (K_{\alpha m} + K_{\gamma m}) + S_\beta \psi_1 (K_{\beta m} - K_{\gamma m})\right\} \qquad (6.11.12)$$

$$\Phi_{11} = \alpha^2 S_{h\alpha}(K_\beta S_\gamma C_\beta - K_\gamma S_\beta C_\gamma) \zeta_1$$
$$- \beta^2 S_\beta (K_\alpha S_\gamma C_{h\alpha} - K_\gamma S_{h\alpha} C_\gamma) (\zeta_1 - \zeta_3)$$
$$+ \gamma^2 S_\gamma (K_\alpha S_\beta C_{h\alpha} - K_\beta S_{h\alpha} C_\beta) \zeta_3$$
$$+ \alpha \beta K_\gamma \left\{C_{h\alpha} \left[2 \zeta_1(\lambda_2 + 1) - \zeta_3\lambda_2\right] - C_\beta\zeta_3 - C_\gamma(2 \zeta_1 - \zeta_3)\right\}$$
$$+ \alpha \gamma K_\beta \left\{C_{h\alpha} \left[- \zeta_1(\lambda_2 + 2) - \zeta_3\lambda_2\right] - C_\beta(\zeta_1 + \zeta_3) + C_\gamma(\zeta_1 - \zeta_3)\right\}$$
$$+ \beta \gamma K_\alpha \left\{C_{h\alpha} (-\zeta_1 + 2 \zeta_3) \lambda_2 - C_\beta\zeta_1 + C_\gamma \zeta_1\right\}$$
$$- \alpha C_{h\alpha} \left[S_\beta \psi_3 \zeta_3 - S_\gamma \psi_2 (\zeta_1 - \zeta_3)\right]$$
$$+ \beta C_\beta \left[S_{h\alpha}\psi_3 \zeta_3 - S_\gamma \psi_1 \zeta_1\right]$$
$$+ \gamma C_\gamma \left[S_{h\alpha}\psi_2 (- \zeta_1 + \zeta_3) + S_\beta \psi_1 \zeta_1\right] \qquad (6.11.13)$$

$$\Phi_{12} = - \Big[\alpha\, S_{h\alpha}\, (C_\beta - C_\gamma)\, \zeta_1\, (\omega_3 - 2\,\omega_2 - \tau_3)$$

$$+ \beta\, S_\beta\, (C_{h\alpha} - C_\gamma)\, (\zeta_1 - \zeta_3)\, (3\,\omega_3 - 2\,\omega_2 - \tau_3)$$

$$+ \gamma\, S_\gamma\, (C_{h\alpha} - C_\beta)\, \zeta_3\, (\tau_3 - \omega_3)$$

$$+ C_{h\alpha}\, \Big[\zeta_3\, (\nu_1 + \nu_2) - \zeta_1 \nu_2\Big]$$

$$- C_\beta\, \Big[\zeta_3 \nu_1 - \zeta_1 \nu_3\Big]$$

$$- C_\gamma\, \Big[\zeta_3 \nu_2 - \zeta_1 (\nu_2 - \nu_3)\Big]\Big] \qquad (6.11.14)$$

$$\Phi_{13} = - \alpha^2\, S_{h\alpha}\, \Big[(K_\beta\, S_\gamma - K_\gamma\, S_\beta)\, \zeta_1\Big]$$

$$+ \beta^2\, S_\beta\, \Big[(K_\alpha\, S_\gamma + K_\gamma\, S_\alpha)\, (\zeta_1 - \zeta_3)\Big]$$

$$+ \gamma^2\, S_\gamma\, \Big[(K_\alpha\, S_\beta - K_\beta\, S_\alpha)\, \zeta_3\Big]$$

$$+ \alpha\, \beta\, K_\gamma\, \Big[-2\, \zeta_1\, \lambda_1 + \zeta_3\, (\lambda_1 + \lambda_2 - \lambda_3)\Big]$$

$$+ \alpha\, \gamma\, K_\beta\, \Big[\zeta_1 (\lambda_1 - \lambda_2 + \lambda_3) - \zeta_3\, (\lambda_1 - \lambda_2 - \lambda_3)\Big]$$

$$+ \beta\, \gamma\, K_\alpha\, \Big[\zeta_1 (\lambda_1 + \lambda_2 - \lambda_3) - 2\, \zeta_3\, \lambda_2\Big]$$

$$+ \alpha\, \Big[S_\beta\, \psi_3\, \zeta_3 + S_\gamma\, \psi_2\, (\zeta_3 - \zeta_1)\Big]$$

$$+ \beta\, \Big[S_{h\alpha} \psi_3\, \zeta_3 + S_\gamma\, \psi_2\, \zeta_1\Big]$$

$$- \gamma\, \Big[S_{h\alpha} \psi_2\, (\zeta_3 - \zeta_1) + S_\beta\, \psi_1\, \zeta_1\Big] \qquad (6.11.15)$$

where

α, β, γ = roots of the auxiliary equation (K.2.12) and are given by expression (K.2.14) (see Appendix (K2)).

For other quantities such as K_{α}, K_{β}, K_{γ}, $K_{\alpha e}$, $K_{\beta e}$, $K_{\gamma e}$, $K_{\alpha m}$, $K_{\beta m}$, $K_{\gamma m}$ and $K_{\alpha t}$, $K_{\beta t}$, $K_{\gamma t}$ see Appendix (K2).

$$S_{h\alpha} = \sinh(\alpha) \quad , \quad S_{\beta} = \sin(\beta) \quad , \quad S_{\gamma} = \sin(\gamma)$$

$$C_{h\alpha} = \cosh(\alpha) \quad , \quad C_{\beta} = \cos(\beta) \quad , \quad C_{\gamma} = \cos(\gamma)$$

$$\psi_1 = \alpha S_{h\alpha} K_{\alpha} \quad , \quad \psi_2 = \beta S_{\beta} K_{\beta} \quad , \quad \psi_3 = \gamma S_{\gamma} K_{\gamma}$$

$$\omega_1 = \alpha K_{\beta} K_{\gamma} \quad , \quad \omega_2 = \beta K_{\alpha} K_{\gamma} \quad , \quad \omega_3 = \gamma K_{\alpha} K_{\beta}$$

$$\delta_1 = S_{h\alpha} K_{\alpha}^2 \quad , \quad \delta_2 = S_{\beta} K_{\beta}^2 \quad , \quad \delta_3 = S_{\gamma} K_{\gamma}^2$$

$$\mu_1 = \alpha^2 S_{h\alpha} K_{\beta} K_{\gamma} \quad , \quad \mu_2 = \beta^2 S_{\beta} K_{\alpha} K_{\gamma} \quad , \quad \mu_3 = \gamma^2 S_{\gamma} K_{\alpha} K_{\beta}$$

$$\varepsilon_1 = K_{\alpha e} S_{h\alpha} \quad , \quad \varepsilon_2 = K_{\beta e} S_{\beta} \quad , \quad \varepsilon_3 = K_{\gamma e} S_{\gamma}$$

$$\varepsilon_4 = K_{\alpha e} C_{h\alpha} \quad , \quad \varepsilon_5 = K_{\beta e} C_{\beta} \quad , \quad \varepsilon_6 = K_{\gamma e} C_{\gamma}$$

$$\Omega_1 = \varepsilon_2 \nu_1 + \varepsilon_3 \nu_2 \quad , \quad \Omega_2 = \varepsilon_1 \nu_1 - \varepsilon_3 \nu_3 \quad , \quad \Omega_3 = \varepsilon_1 \nu_2 - \varepsilon_2 \nu_3$$

$$\zeta_1 = C_{\beta} \varepsilon_3 + C_{\gamma} \varepsilon_2 \quad , \quad \zeta_2 = C_{h\alpha} \varepsilon_3 + C_{\gamma} \varepsilon_1 \quad , \quad \zeta_3 = C_{h\alpha} \varepsilon_2 + C_{\beta} \varepsilon_1$$

$$\nu_1 = \alpha \beta \delta_3 \quad , \quad \nu_2 = \alpha \gamma \delta_2 \quad , \quad \nu_3 = \beta \gamma \delta_1$$

$$\sigma_1 = \beta \delta_3 + \gamma \delta_2 - K_{\beta} \psi_3 - K_{\gamma} \psi_2$$

$$\sigma_2 = \alpha \delta_3 - \gamma \delta_1 - K_{\alpha} \psi_3 + K_{\gamma} \psi_1$$

$$\sigma_3 = \alpha \delta_2 - \beta \delta_1 - K_{\alpha} \psi_2 + K_{\beta} \psi_1$$

$$\eta_1 = S_{\beta} \delta_3 + S_{\gamma} \delta_2 \quad , \quad \eta_2 = S_{h\alpha} \delta_3 - S_{\gamma} \delta_1 \quad , \quad \eta_3 = S_{h\alpha} \delta_2 - S_{\beta} \delta_1$$

$$\phi_1 = \delta_2\varepsilon_6 + \delta_3\varepsilon_5 \ , \ \phi_2 = \delta_1\varepsilon_6 + \delta_3\varepsilon_4 \ , \ \phi_3 = \delta_1\varepsilon_5 + \delta_2\varepsilon_4$$

$$\rho_1 = C_{h\alpha}\phi_1 + \eta_1\varepsilon_1 \ , \ \rho_2 = - C_\beta\phi_2 + \eta_2\varepsilon_2 \ , \ \rho_3 = - C_\gamma\phi_3 + \eta_3\varepsilon_3$$

$$\tau_1 = \omega_2 + \omega_3 - 2\,\omega \ , \ \tau_2 = \omega_2 - 2\,\omega_3 + \omega \ , \ \tau_3 = - 2\,\omega_2 + \omega_3 + \omega$$

$$x_1 = \psi_2\,\varepsilon_6 + \psi_3\,\varepsilon_5 \ , \ x_2 = \psi_1\,\varepsilon_6 + \psi_3\,\varepsilon_4 \ , \ x_3 = \psi_1\,\varepsilon_5 + \psi_2\,\varepsilon_4$$

$$y_1 = S_\beta\,\psi_3 + S_\gamma\,\psi_2 \ , \ y_2 = S_{h\alpha}\psi_3 - S_\gamma\,\psi_1 \ , \ y_3 = S_{h\alpha}\psi_2 - S_\beta\,\psi_1$$

$$z_1 = - C_{h\alpha}x_1 - \varepsilon_1\,y_1 \ , \ z_2 = C_\beta\,x_2 - \varepsilon_2\,y_2 \ , \ z_3 = C_\gamma\,x_2 - \varepsilon_3\,y_3$$

$$W_1 = C_\beta\,\varepsilon_6 + S_\gamma\,\varepsilon_2 - K_{\gamma a} \ , \ W_2 = S_\beta\,\varepsilon_3 + C_\gamma\,\varepsilon_5 - K_{\beta a}$$

$$W_3 = - S_{h\alpha}\varepsilon_3 + C_\gamma\,\varepsilon_4 - K_{\alpha a} \ , \ W_4 = - C_{h\alpha}\varepsilon_6 - S_\gamma\,\varepsilon_1 + K_{\gamma a}$$

$$W_5 = - S_{h\alpha}\varepsilon_2 + C_\beta\,\varepsilon_4 - K_{\alpha a} \ , \ W_6 = - C_{h\alpha}\varepsilon_5 - S_\beta\,\varepsilon_1 + K_{\beta a}$$

$$Q_1 = K_\beta\,W_1 + K_\gamma\,W_2 \ , \ Q_2 = K_\gamma\,W_3 + K_\alpha\,W_4 \ , \ Q_3 = K_\beta\,W_5 + K_\alpha\,W_6$$

$$\lambda_1 = C_\beta\,C_{h\alpha} - 1 \ , \ \lambda_2 = C_\beta\,C_\gamma - 1 \ , \ \lambda_3 = C_{h\alpha}\,C_\gamma - 1$$

$$V_1 = - 2\,\varepsilon_3\lambda_1 + \varepsilon_1\lambda_2 + \varepsilon_2\lambda_3$$

$$V_2 = \varepsilon_3\lambda_1 + \varepsilon_1\lambda_2 - 2\,\varepsilon_2\lambda_3$$

$$V_3 = \varepsilon_3\lambda_1 - 2\,\varepsilon_1\lambda_2 + \varepsilon_2\lambda_3$$

$$\Theta_1 = \psi_1\,\psi_2\,\varepsilon_6 \ , \ \Theta_2 = \psi_1\,\psi_3\,\varepsilon_5 \ , \ \Theta_3 = \psi_2\,\psi_3\,\varepsilon_4$$

$$\Theta = \Theta_1 + \Theta_2 + \Theta_3$$

$$\zeta_1 = K_{\beta t} - K_{\gamma t} \ , \ \zeta_2 = K_{\alpha t} + K_{\gamma t} \ , \ \zeta_3 = K_{\alpha t} + K_{\beta t}$$

$$\varphi_1 = K_{\beta m} + K_{\gamma m} \ , \ \varphi_2 = K_{\alpha m} + K_{\beta m} \ , \ \varphi_3 = K_{\beta m} - K_{\gamma m}$$

$$\Sigma_1 = \psi_3 K_{\beta a} + \psi_2 K_{\gamma a} + z_1 \ , \ \Sigma_2 = \psi_3 K_{\alpha a} + \psi_1 K_{\gamma a} - z_2 \ , \ \Sigma_3 = \psi_2 K_{\alpha a} + \psi_1 K_{\beta a} - z_3$$

$$J_1 = C_{h\alpha}\varphi_1 + C_\beta\varphi_3 \ , \ J_2 = C_\beta\,\varphi_2 - C_\gamma\varphi_1 \ , \ J_3 = C_{h\alpha}\varphi_2 - C_\gamma\varphi_3$$

6.12 APPLICATION OF THE DYNAMIC STIFFNESS MATRIX

The dynamic stiffness matrix developed in the previous sections can be utilized to solve free natural vibration problems of structures. A global dynamic stiffness matrix K_f of the final structure is formed by assembling the dynamic stiffness matrices of the individual members in the usual way. Natural frequencies of the structure are then determined by two independent methods as follows:

6.12.1 FREQUENCY-DETERMINANT PLOT TECHNIQUE

The Frequency-Determinant plot is a relatively easy and quick method for finding the natural frequencies of the structure. In this method, the value of the determinant of the dynamic stiffness matrix is calculated at each step by varying ω (frequency parameter). The value of the determinant is then plotted against the frequency. At a natural frequency of the structure the value of the determinant goes to zero.

There are however, numerous disadvantages in such a procedure. First, any natural frequencies corresponding to a constrained system with both ends clamped are not covered by this method. Second, structures having very close natural frequencies would require the step size for ω to be very small indeed. Finally, the value of the determinant may change sign not only by passing through zero but also via infinity.

The inversion of the B matrix, makes the determinant plot a discontinuous curve. When the value of the determinant changes sign by passing through the zero, the corresponding value of ω will be the natural frequency of the structure. In this case, the curve changes sign via infinity, the point generated by joining these two curves is a pole and does not represent a natural frequency.

6.12.2 WITTRICK - WILLIAMS ALGORITHM

The determinant of the dynamic stiffness matrix {K} is a highly irregular function of ω and any trial and error method, which involves computing $|K|$ and observing when it changes sign, may miss some roots. In order to solve this problem, an algorithm based on a theorem due to Lord Rayleigh [2] was suggested by Wittrick and Williams [21,22].

The Wittrick-Williams algorithm is briefly described as follows.

It has been established that j, the number of eigenvalues present in a range of frequency from zero to ω^* as the circular frequency of the structure ω is increased, is given by the expression :

$$j = j_o + s\{K_f\} \qquad (6.12.1)$$

where

j = number of natural frequencies of the structure exceeded by the trial frequency ω^*

j_o = number of natural frequencies exceeded by the trial frequency ω^* if constraints were imposed upon the structure so as to suppress all the nodal displacements

$= \sum j_m$

j_m = number of natural frequencies of a component member with its ends clamped, which have been exceeded by ω^*

K_f = the overall dynamic stiffness matrix (depending on the circular frequency of the structure ω) evaluated at $\omega = \omega^*$.

s { K_f } = number of negative elements on the leading diagonal of K_f^{Δ}

K_f^{Δ} = upper triangular matrix obtained by the application of Gauss elimination to K_f

The algorithm can be applied to systems with an infinite number of degrees of freedom, for which there is no comparable approach. The algorithm has been demonstrated in computer programs called BUNVIS [23] and CALFUN [24]. The same routine has been modified and combined with the subroutines DMCSN.FOR, DMCSE.FOR, and DMMECA.FOR in this work to develop VMECAS.FOR, for computation of the natural frequencies of structures with material and elastic coupling as well as an axial load at the centroid.

6.13 DEVELOPMENT OF COMPUTER PROGRAMS

Computer programs based on the theory discussed in sections (6.7) to (6.9) and section (6.11) were developed. A list of these programs along with brief description of each is given below.

1. DMCSN.FOR : Dynamic stiffness matrix for materially coupled structures (Numerical approach)
2. DMCSE.FOR : Dynamic stiffness matrix for materially coupled structures (Exact approach)
3. DMCS.FOR : Dynamic stiffness matrix for materially coupled structures (a combination of DMCSN.FOR and DMCSE.FOR programs)
4. DMMECA.FOR : Dynamic stiffness matrix for

materially and elastically coupled structures with axial load

5. VMECAS.FOR : Vibration of materially and elastically coupled with axially loaded structures

The common input statement of these programs consists of the following data as variables :

EI = Flexural or bending stiffness
GJ = Torsional stiffness
m = Mass per unit length
I = Polar mass moment of inertia per unit length about an axis through the shear centre
x_α or e = Distance between the centroid and shear centre (set to zero if not elastically coupled structure)
ℓ = Length of the structure
ω = Circular frequency
K = Bending-torsional coupled stiffness (set to zero if not materially coupled structure)
P = Axial load applied at the centroid (set to zero if not present)

(For example data files and result files of these programs, see Appendix (C)).

6.14 VALIDATION OF COMPUTER PROGRAM

The validation of computer program VMECAS.FOR was the next stage. Hollowell and Dugunji's [25] work on composite plates was selected to predict natural frequencies and mode shapes. Their work included comparison of theoretical predictions with experimental results. The authors [25] used a plate element in the structural idealization to predict natural frequencies and mode shapes. However, the

program VMECAS.FOR developed in this work uses beam element idealization. Plate structures can be idealized as beams when their aspect ratio exceeds a certain limit. A parametric study was therefore conducted to establish a figure for the aspect ratio at which a plate can be successfully idealized as a beam element. The material properties, thickness, and chord length of the plate were kept constant as given in Reference [25] and only the length of the structure was varied to obtain structures with different aspect ratios.

6.14.1 EFFECT OF ASPECT RATIO ON THE ACCURACY OF FREQUENCY AND MODE SHAPES OF A PLATE STRUCTURE

MATERIAL : Aluminium alloy

Young's Modulus of Elasticity = 68.9 GPa

Poisson's ratio = 0.3

Density = 2770.0 Kg/m^3

DIMENSIONS

Chord length = 76.0 mm

Thickness = 1.0 mm

END CONDITIONS : CANTILEVERED

Flexural stiffness EI = 0.436367 N m^2

Torsional stiffness GJ = 0.62826 N m^2

Mass per unit length m = 0.21052 Kg/m

Polar mass moment of inertia I_{po} = 1.01347 * 10^{-4} Kg-m

ASPECT RATIO : 1 to 5 in steps of 0.5

Length : 76 mm to 380 mm

(length increased in steps of 38 mm)

Sources of analysis :

1. LUSAS : A finite element package (see Appendix (L))

   Element used : QSL8 - thin shell element

   Description : A quadrilateral shell element for the analysis of shell structures with arbitrary geometry including multiple

junctions. The element can accommodate generally curved shell geometry with varying thicknesses and anisotropic materials may be specified. The formulation takes account of both membrane (in-plane) and flexural (out-of-plane) deformations and as required by thin shell theory, shearing deformations are excluded.

2. VMECAS.FOR : Program based on thin-walled composite beam element idealization.

Natural frequencies and mode shapes were calculated using LUSAS and VMECAS programs. The estimated natural frequencies along with the percentage difference between the results obtained by the two programs are tabulated for plates of aspect ratio 1.0 to 5.0 in Tables (6.1) to (6.5).

The results were further studied in the light of their normal mode shapes. The percentage difference between the results of the two estimates were plotted against the aspect ratio for natural frequencies with similar mode shapes as shown in Figure (6.3). For the first and second bending frequencies the difference is less than two percent for an aspect ratio of three. However, for the first and second torsional frequencies, the difference is about twelve percent for an aspect ratio of three. These large differences for the torsional modes can be attributed to the invalid assumption of having no chordwise bending. Moreover the structure exhibits combined spanwise and chordwise bending or spanwise bending accompanied with torsion. These complex modes are not calculated by the VMECAS.FOR program.

Therefore, for plate structures with aspect ratios greater than three, the VMECAS.FOR program will be able to predict bending frequencies within two percent accuracy whereas the torsional frequencies are likely to suffer from a difference of twelve percent as compared to predictions made by a finite element package.

6.14.2 COMPOSITE PLATES OF REFERENCE [25]

Orthotropic engineering constants for Hercules AS1/3501-6 uni-directional Graphite/Epoxy with approximately 60% fibre volume fraction are tabulated in Table (6.6) as per Reference [25], along with sectional parameters. The in-plane, on-axis lamina modulus components Q_{ij} were obtained from the orthotropic engineering constants. Flexural moduli for six different laminates were found by the LAMINATE program . These results were identical to Reference [25] and are shown in Table (6.7).

Hollowell and Dugunji [25] employed the Rayleigh-Ritz energy method to predict natural frequencies and mode shapes for these plates (see Appendix (E)). In the case of a cantilevered uniform rectangular plate, the governing equations are

$$\bar{w}'''' - \omega^2 m \left(\frac{\ell^4}{D_{11}}\right) \bar{w} + 2 \left(\frac{D_{16}\ell}{D_{11}}\right) \theta''' = 0 \qquad (6.14.1)$$

$$- \left(\frac{D_{16}}{2\ D_{66}}\right) \bar{w}''' + \left(\frac{D_{11}c^2}{48\ D_{66}\ell^2}\right) \theta'''' - \theta'' - \omega^2 \left(\frac{m\ c^2\ell^2}{48\ D_{66}}\right) \theta = 0 \qquad (6.14.2)$$

These two ordinary differential equations are coupled by the bending-twisting stiffness factor D_{16}. For the plates under discussion the stiffness ratios D_{16}/D_{11} and

D_{16}/D_{66} are negligibly small as shown in Table (6.7) and can be ignored.

This results in uncoupled bending and torsional equations and gives relatively simple expressions for computation of natural frequencies as follows:

$$\omega_{nB} = (k_{nB}/\ell^2)\sqrt{D11/m} \qquad (6.14.3)$$

$$\omega_{nT} = (K_{nT}/\ell^2)\sqrt{48D66R^2/\rho} \qquad (6.14.4)$$

where

k_{nB} = nth eigenvalue of the equation, subject to the boundary conditions on $\bar{w}$

K_{nT} = eigenvalue being function of β that can be obtained from Figures (2 & 3) or from Table 2 of Reference [26]. Its value approaches that for a long thin bar as the warping stiffness β goes to zero.

n = 1,2,3,.....

Natural frequencies were calculated by equations (6.14.3) and (6.14.4). In addition, natural frequencies and mode shapes for these plates were computed by CALFUN [24], LUSAS®, and VMECAS programs. The CALFUN computer program is briefly described in the following paragraphs whereas the other two programs LUSAS and VMECAS have already been discussed in a previous section.

CALFUN [24], a program for CAculation of Flutter speed Using Normal modes, is based on a Vlasov beam idealization. However, the program does not account for warping stiffness, rotary inertia, and material coupling and assumes that chordwise deformations do not exist.

The normal input to CALFUN includes bending rigidity (EI), torsional rigidity (GJ), mass per unit length (m), polar mass moment of inertia per unit length about the

elastic axis ($I_{p\bullet}$), distance between the elastic axis and the centroid (x_α), and the beam length. CALFUN computes natural frequencies and mode shapes for an aircraft wing.

In Reference [25], bending, torsional and coupled bending-torsional stiffnesses were not given. The plate stiffnesses were estimated using equation (4.18) of Chapter (4) as given below :

$$EI = D_{11}\, c \quad , \quad GJ = 4\, D_{66}\, c \quad , \quad K = 2\, D_{16}\, c \qquad (6.14.5)$$

where

D_{11}, D_{16} and D_{66} = elements of D matrix

c = chord length or width of the plate

These rigidities are given in Table (6.8).

A finite element package called LUSAS was used to establish natural frequencies of these orthotropic plates. These predictions are compared with test results and are tabulated in Tables (6.9a), (6.9b), and (6.9c).

Theoretical and experimental results shown in Tables (6.9a,b,c) are plotted against a non-dimensional quantity $\psi = \left(\frac{K^2}{EI\ GJ}\right)$ in Figure (6.4). The percentage differences between experimental results and theoretical estimation using different schemes of calculation are also plotted against ψ in Figure (6.5).

These plots reveal that large differences between experimental results and theoretical predictions will be encountered if the effect of material coupling is ignored as is the case in CALFUN and LUSAS. In Figure (6.6) results are compared only with VMECAS predictions. Good agreement exists for the first and second bending frequencies but in the case of the first torsional frequency, the deviation may be attributed to the fact that chordwise bending is ignored in the beam element

idealization. This fact is further investigated in the following paragraphs. Moreover, the normalised mode shapes of these materially coupled plates have been compared with corresponding mode shapes for assumed uncoupled plates in Figures (6.7) to (6.12). In the absence of material coupling, modes are either bending or torsional but in the presence of material coupling, modes can be identified as predominantly bending or predominantly torsional. That means for each frequency both kinds of mode are present, except that one type of mode can be relatively predominant in its amplitude as compared to the other.

Results published by Chuh Mei [10] and Garland [26] are selected to see how successfully frequencies and mode shapes can be predicted for thin-walled structures made of isotropic materials. Results for three channel sections are given in Table (6.10).

6.15 CONCLUSIONS

Dynamic stiffness matrices for thin-walled composite sections have been developed for three cases as follows:

1. Elastically and materially coupled beams with an axial load
2. Materially coupled beams with an axial load such as plates or doubly symmetrical sections
3. Materially coupled thin-walled beams

Explicit expressions for the dynamic stiffness matrix of the materially coupled case have been evaluated. This results in a substantial saving in computer time.

Computer programs have been developed to calculate these dynamic stiffness matrices from basic structural data. These programs have been combined with an

established algorithm [19] to predict the natural frequencies and mode shapes for elastically and materially coupled beams with an axial load.

A comparative study between CALFUN and VMECAS predictions with M.I.T. results revealed the importance of the material coupling term in the accurate computation of natural frequencies and mode shapes. As long as we are dealing with simple lay-ups, CALFUN is capable of accurately predicting the natural frequencies and mode shapes but as the layer sequence becomes more complex, a significant difference between theoretical predictions and experimental results appears. This suggests that analysing structures made of composite materials require inclusion of anisotropic characteristics in the program.

A parametric study of effect of aspect ratio on the accuracy of prediction of natural frequencies using beam element idealization has also been presented. It is found that for plate structures with aspect ratio greater than three, beam model idealization can predict frequencies within measurement accuracy.

REFERENCES

1. Vlasov, V.Z., "Thin Walled Elastic Rods," Moscow (1940), 2nd edition (1959). English translation published for U.S. Science Foundation Israel Program for Scientific Translations, Jerusalem (1961).

2. Lord Rayleigh 1977 Theory of Sound (2 vols.). N.Y.; Dover Publications, Second edt., 1945 reissue.

3. Goland, M., "The Flutter of a Uniform Cantilevered Wing," Journal of Applied Mechanics, Vol. 12, A-197-A-208, 1945.

4. Goland, M. and Luke, Y.L., "The Flutter of a Uniform Wing with Tip Weights," Journal of Applied Mechanics, Vol. 15, pp. 13-20, 1948.

5. Timoshenko, S.P. and Young, D.H., Vibration Problems in Engineering, Van Nostrand, third edition, New York, 1955, pp. 329-331 and 407-411.

6. Hurty, W.C. and Rubinstein, M.F., Dynamics of Structures, Prentice-Hall, Englewood Cliffs, New Jersey, 1964, pp. 161-166 and 222-225.

7. Bisplinghoff, R.L., Ashley, H., and Halfman, R.L., Aeroelasticity, Addison-Wesley, Reading, Massachusetts, 1955, pp. 105-206, 114 and 555-563.

8. Fung, Y.C., An Introduction to the Theory of Aeroelasticity, Dover Publication, New York, 1955, 1969 revised publication, pp. 52-55 and 198-201.

9. Rao, J.S. and Carnegie, W., "Solution of the equations

of motion of Coupled-bending bending torsion vibrations of turbine blades by the method of Ritz-Galerkin," International Journal of Mechanical Science, Vol. 12, 1970, pp. 875-882.

10. Mei, C., "Coupled Vibrations of Thin-walled Beams of Open Section Using the Finite Element Method," International Journal of Mechanical Science, Vol. 12, 1970, pp. 883-891.

11. Angelbrecht, "Coupled free vibration of a swept wing," Journal of Aeronautical Science, Vol. 18, 1951, pp. 329-338.

12. Stacey, J.A., "The Development of a Finite Element Aeroelastic Calculation Package and its Application to the Cranfield Aerobatic Aircraft-A1," M.Sc. Thesis, College of Aeronautics, Cranfield of Institute of Technology, 1976.

13. Williams, F.W. and Wittrick, W.H., "Efficient calculation of natural frequencies of certain marine structures," Int. J. Mech. Sci., Vol. 15, 1973, pp. 833-843.

14. Williams, F.W., "Computation of natural frequencies and initial buckling stresses of prismatic plate assemblies," J. Sound Vib., Vol. 21, 1972, pp. 87-106.

15. Banerjee, J.R. and Williams, F.W., "Exact Bernoulli-Euler dynamic stiffness matrix for a range of tapered beams," Int. J. numer. methods eng., Vol. 21, 1985, pp. 2289-2302.

16. Anderson, M.S., Stroud, W.J., Durling, B.J., and

Hennessy, K.W., "PASCO : Structural panel analysis and sizing code user manual," NASA Technical Memo 80182, 1980.

17. Anderson, M.S., Williams, F.W., Banerjee, J.R., Durling, B.J., Herstrom, C.L., Kennedy, D., and Warnaar, D.B., "User manual for BUNVIS-RG: An exact buckling and vibration program for lattice structures, with repetitive geometry and substructuring options," NASA Technical Memo 87669, 1986.

18. Chandra, R., Stemple, A.D., and Chopra, I., "Thin-Walled Composite Beams Under Bending, Torsional, and Extentional Loads," Journal of Aircraft, Vol. 27, No. 7, July 1990.

19. Mansfield, E.H. and Sobey, A.J., "The Fibre Composite Helicopter Blade, Part 1: Stiffness Properties, Part 2: Prospects for Aeroelastic Tailoring," Aeronautical Quarterly, May 1979.

20. Banerjee, J.R., "Coupled Bending-Torsional Dynamic Stiffness Matrix for Beam Elements," Int. J. for Num. methods in Eng., Vol. 28, pp. 1283-1298, 1989.

21. Wittrick, W.H. and Williams, F.W., "A general algorithm for computing natural frequencies of elastic structures," Quarterly Journal of Mechanics and Applied Mathematics, Vol. 24, pp. 263-284, 1971.

22. Williams, F.W. and Wittrick, W.H., "Exact buckling and frequency calculations surveyed," J. Struct. Eng. ASCE, Vol. 109, pp. 169-187, 1983.

23. Banerjee, J.R. and Williams, F.W., "User's guide to

the computer program BUNVIS (BUckling of Natural VIbrations of Space frames)", Departmental Report No. 5, Department of Civil Engineering and Building Technology, UMIST, 1982.

24. Banerjee, J.R., "Use and capability of CALFUN : A PROGRAM FOR CALCULATION OF FLUTTER SPEED USING NORMAL MODES," Proceedings Int. AMSE Conf. "Modeling & Simulation", Athens, June 27-29, 1984.

25. Hollowell, S.J. and Dugundji, J., "Aeroelastic Flutter and Divergence of Stiffness Coupled, Graphite/Epoxy Cantilevered Plates," Journal of Aircraft, Vol. 21, pp. 69-76, Jan. 1984.

26. Garland, C.F., "The Normal Modes of Vibrations of Beams having Noncollinear Elastic and Mass Axes," Presented at the Annual meeting, Philadelphia, Pa., December 4-8, 1939, of the American Society of Mechanical Engineers.

27. DERIVE, A Mathematical Assistant, Version 1.63, Copyright (c) 1988 by Soft Warehouse, Inc. Honolulu, Hawaii, U.S.A.

28. NAG Fortran Library Manual - Mark 13, NAG Ltd., Wilkinson House, Jordan Hill Road, Oxford, United Kingdom, OX2 8DR.

29. Hearn, A.C., "REDUCE User's Manual," The Rand Corporation, Santa Monica, CA 90406-2138, U.S.A., Version 3.3, July 1987.

Aspect Ratio	1.0			1.5		
	LUSAS (Hz)	VMECAS (Hz)	% Diff.	LUSAS (Hz)	VMECAS (Hz)	% Diff.
First Bending	143.861	139.484	3.04	63.660	61.993	2.62
First Torsion	351.278	258.994	26.27	213.995	172.662	19.31
Second Bending	871.194	874.126	-0.34	391.866	388.504	0.86

TABLE 6.1 Natural frequencies for plates (A.R. 1.0 & 1.5)

Aspect Ratio	2.0			2.5		
	LUSAS (Hz)	VMECAS (Hz)	% Diff.	LUSAS (Hz)	VMECAS (Hz)	% Diff.
First Bending	35.688	34.870	2.29	22.774	22.318	2.00
First Torsion	152.955	139.490	15.34	118.864	103.597	12.84
Second Bending	221.268	218.530	1.24	141.839	139.861	1.39

TABLE 6.2 Natural frequencies for plates (A.R. 2.0 & 2.5)

Aspect Ratio	3.0			3.5		
	LUSAS (Hz)	VMECAS (Hz)	% Diff.	LUSAS (Hz)	VMECAS (Hz)	% Diff.
First Bending	15.777	15.498	1.77	11.569	11.386	1.58
First Torsion	97.182	86.331	11.17	82.193	73.999	9.97
Second Bending	:98.534	97.126	1.43	72.374	71.358	1.40

TABLE 6.3 Natural frequencies for plates (A.R. 3.0 & 3.5)

Aspect Ratio	4.0			4.5		
	LUSAS (Hz)	VMECAS (Hz)	% Diff.	LUSAS (Hz)	VMECAS (Hz)	% Diff.
First Bending	8.843	8.718	1.42	6.979	6.888	1.30
First Torsion	71.215	64.748	9.08	62.880	57.554	8.47
Second Bending	55.382	54.633	1.35	43.731	43.167	1.29

TABLE 6.4 Natural frequencies for plates (A.R. 4.0 & 4.5)

Aspect Ratio	5.0		
	LUSAS (Hz)	VMECAS (Hz)	% Diff.
First Bending	5.646	5.579	1.18
First Torsion	56.210	51.799	7.85
Second Bending	35.400	34.965	1.23

TABLE 6.5 Natural frequencies for plates (A.R. 5.0)

MATERIAL PROPERTIES

Out-of-Plane loading

$E_l = 98.0 \times 10^9$ N/m^2

$E_t = 7.9 \times 10^9$ N/m^2

$\nu_{lt} = 0.28$

$G_{lt} = 5.6 \times 10^9$ N/m^2

Ply thickness = 0.134×10^{-3} m

Density = 1520.0 Kg/m^3

SECTIONAL PROPERTIES

Total length = 0.33 m

Effective length = 0.305 m

Chord length = 0.076 m

Aspect Ratio = 4

TABLE 6.6 Material and sectional properties of composite plates as given in reference [25], $V_f = 60\%$ (approx)

No.	Lay-up	Flexural Moduli. ...D-matrix (Nm)						Stiffness Ratios	
		D11	D12	D16	D22	D26	D66	D16/ D11	D16/ D66
1	$[0_2/90]_s$	4.125	0.096	0.0	0.49	0.0	0.243	0.0	0.0
2	$[\pm 45/0]_s$	1.55	0.928	0.437	1.404	0.437	1.075	0.28	0.407
3	$[45_2/0]_s$	1.55	0.928	0.946	1.404	0.946	1.075	0.61	0.88
4	$[-45_2/0]_s$	1.55	0.928	-.946	1.404	-.946	1.075	-0.61	-0.88
5	$[30_2/0]_s$	2.704	0.72	1.18	0.666	0.459	0.866	0.436	1.36
6	$[-30_2/0]_s$	2.704	0.72	-1.18	0.666	-.459	0.866	-0.436	-1.36

TABLE 6.7 Flexural moduli for composite plates

Lay-up	$[0_2/90]_s$	$[\pm 45/0]_s$	$[45_2/0]_s$	$[-45_2/0]_s$	$[30_2/0]_s$	$[-30_2/0]_s$
EI	0.3135	0.1178	0.1178	0.1178	0.2055	0.2055
GJ	0.074	0.327	0.327	0.327	0.263	0.263
K	0.0	0.06642	0.14379	-0.143792	0.17936	-0.17936

TABLE 6.8 Flexural, torsional, and coupled bending/torsional rigidities of composite plates

Lay-up	$[0_2/90]_s$	$[\pm 45/0]_s$	$[45_2/0]_s$	$[-45_2/0]_s$	$[30_2/0]_s$	$[-30_2/0]_s$
FIRST BENDING FREQUENCY (Hz)						
Exper.	11.10	6.1	4.8	4.8	6.0	6.0
THEORETICAL PREDICTIONS WITH PERCENTAGE DIFFERENCES						
Ref.25	10.70	5.7	4.6	4.6	6.0	6.0
% dif.	-3.74	-7.02	-4.35	- 4.35	0.0	0.0
CALFUN	11.025	6.775	6.775	6.775	8.95	8.95
% dif.	-0.68	9.96	29.15	29.15	32.96	32.96
LUSAS	9.405	7.690	7.380	7.380	7.999	7.999
% dif.	-18.02	20.68	34.96	34.96	24.99	24.99
VMECAS	11.052	6.3705	4.5972	4.5998	5.6585	5.6636
% dif.	- 0.43	4.25	- 4.41	- 4.35	- 6.04	- 5.94

TABLE 6.9a First bending frequency of composite plates

Lay-up	$[0_2/90]_s$	$[\pm 45/0]_s$	$[45_2/0]_s$	$[-45_2/0]_s$	$[30_2/0]_s$	$[-30_2/0]_s$
SECOND BENDING FREQUENCY (Hz)						
Exper.	69.0	38.0	30.0	30.0	36.0	36.0
THEORETICAL PREDICTIONS WITH PERCENTAGE DIFFERENCES						
Ref.25	67.0	37.0	32.0	32.0	41.0	41.0
% dif.	-2.99	-2.71	6.25	6.25	12.20	12.20
CALFUN	69.095	42.46	42.46	42.46	56.08	56.08
% dif.	0.13	10.50	29.34	29.34	35.80	35.80
LUSAS	58.74	48.15	45.83	45.83	46.48	46.48
% dif.	-17.47	21.07	34.54	34.54	22.54	22.54
VMECAS	69.259	39.774	28.376	28.391	34.095	34.117
% dif.	0.37	4.46	- 5.72	- 5.67	- 5.59	- 5.52

TABLE 6.9b Second bending frequency of composite plates

Lay-up	$[0_2/90]_s$	$[\pm 45/0]_s$	$[45_2/0]_s$	$[-45_2/0]_s$	$[30_2/0]_s$	$[-30_2/0]_s$
FIRST TORSIOANL FREQUENCY (Hz)						
Exper.	42.0	77.0	51.0	51.0	58.0	58.0
THEORETICAL PREDICTIONS WITH PERCENTAGE DIFFERENCES						
Ref.25	39.0	69.0	55.0	55.0	60.0	60.0
% dif.	-7.69	-11.59	7.27	7.27	3.33	3.33
CALFUN	33.302	70.08	70.08	70.08	62.87	62.87
% dif.	-26.12	- 9.88	27.22	27.22	7.74	7.74
LUSAS	38.47	64.69	46.14	46.14	49.95	49.95
% dif.	- 9.18	-19.03	-10.54	-10.54	-16.12	-16.12
VMECAS	33.325	70.239	70.039	70.034	64.301	64.290
% dif.	-26.03	- 9.63	27.18	27.18	9.80	9.78

TABLE 6.9c First torsional frequency of composite plates

REFERENCE	CHUH MEI [10]		GARLAND [26]
MATERIAL PROPERTIES			
Material	Aluminium alloy		cold-rolled steel
Modulus of Elasticity	E (Gpa)	69.0	207.0
Modulus of Rigidity	G (Gpa)	26.0	80.0
Poisson's ratio	ν	0.3	0.3
Density	ρ (Kg/m^3)	2720.0	7843.0
SECTIONAL PROPERTIES			
Section	channel		
b (mm)	19.05	25.4	25.4
h (mm)	12.7	12.7	12.7
t (mm)	0.635	0.635	0.635
ℓ (m)	1.016	1.016	1.016
STATIC PROPERTIES			
Flexural stiffness EI (N-m^2)	74.848	97.304	291.912
Torsional stiffness GJ (N-m^2)	0.11273	0.140912	0.43357
mass per unit lengt m/l (Kg/m)	0.08774	0.109677	0.316249
Polar mass moment of inertia $I_{p\bullet}$ (Kg-m)	$2.809*10^{-5}$	$6.386*10^{-5}$	$1.8414 * 10^{-4}$
Dist. bet. C. of G. and shear centre x_α (mm)	15.7098	21.87407	21.874
FREQUENCY (Hz) FIRST MODE			
Theory (Ref.)	12.8667	11.333	11.87
Finite element	12.633	11.433	----
Experimental	12.4167	10.667	11.833
CALFUN/VMECAS	11.855	9.926	11.932
LUSAS	12.8195	11.4652	------

TABLE 6.10 Natural frequencies of thin-walled open sections made of isotropic materials

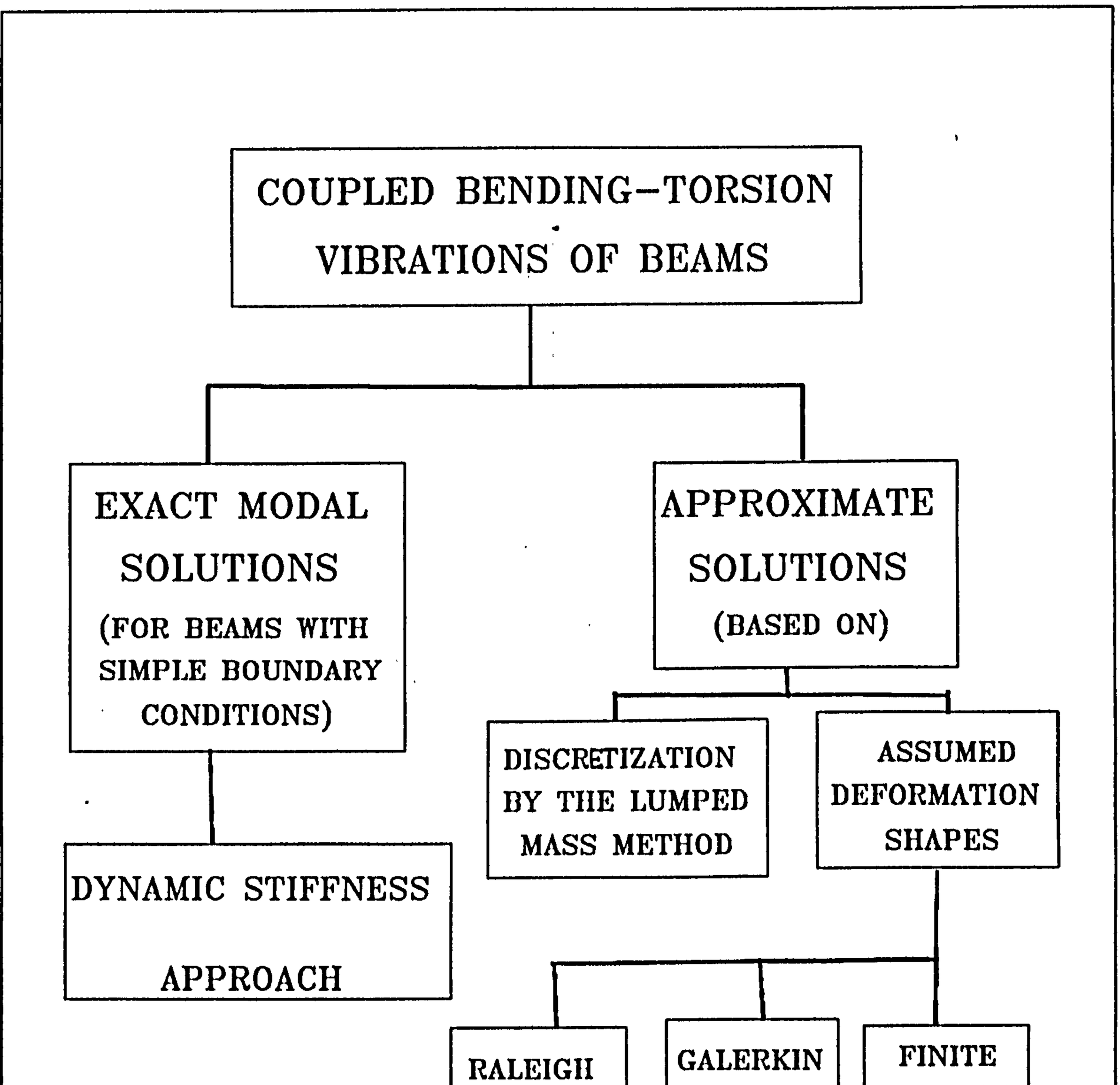

FIGURE 6.1 SOLUTION TECHNIQUES

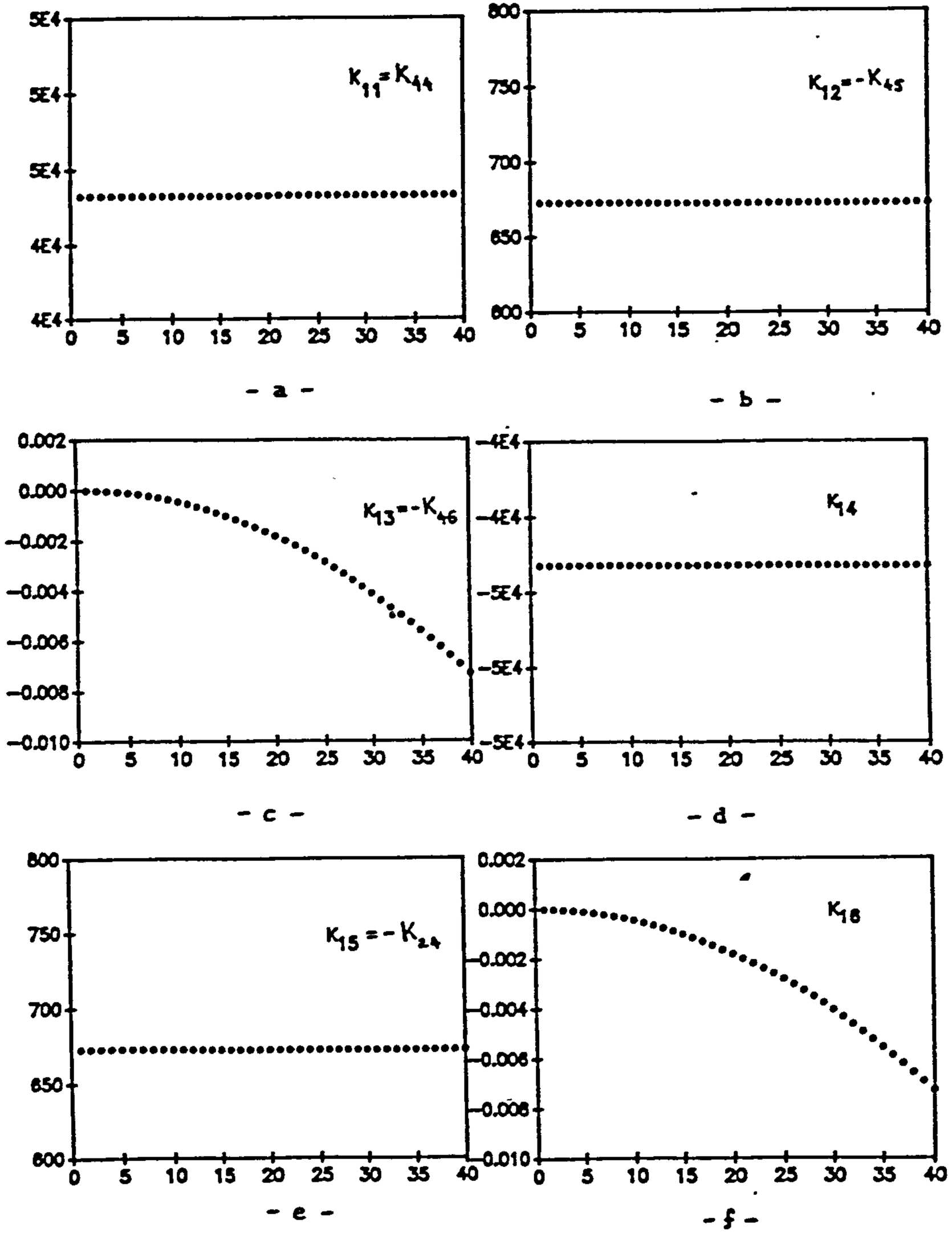

Figure 6.2 Elements of the dynamic stiffness matrix plotted against frequency (x-axis : rad/sec, y-axis : N/m)

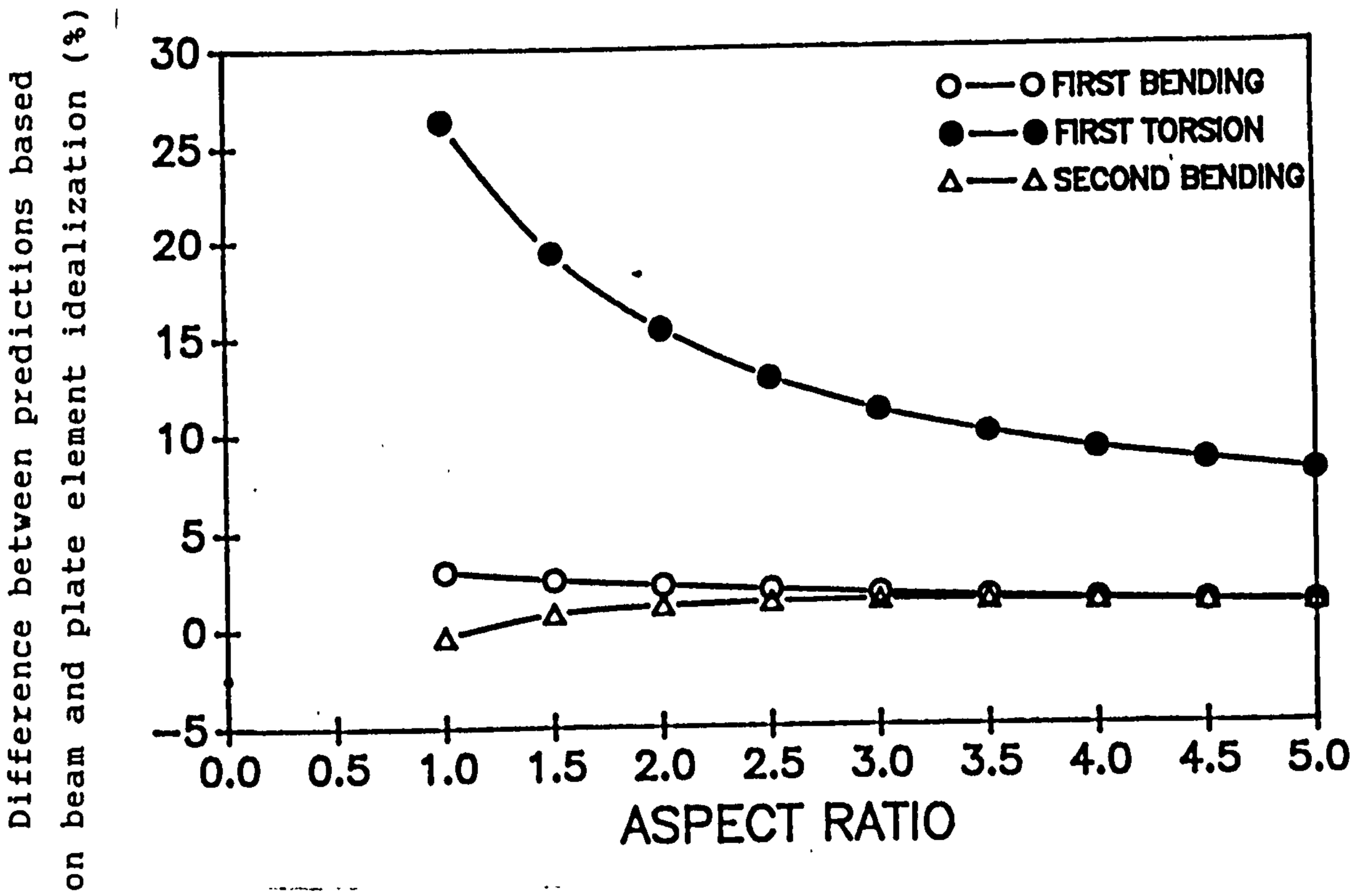

Figure 6.3 Effect of aspect ratio on the accuracy of calculation of natural frequencies of a plate structure using beam element idealization.

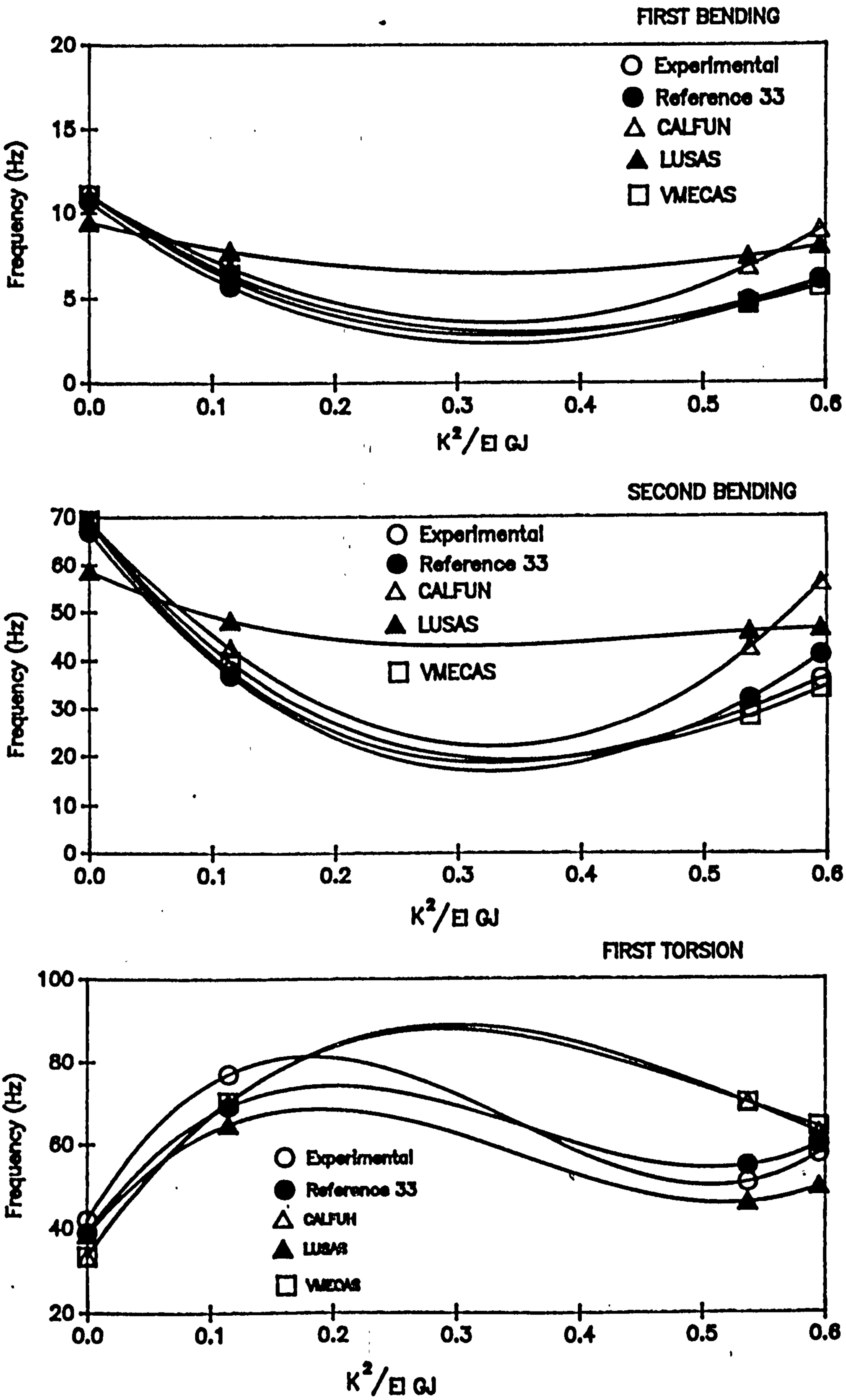

Figure 6.4 Effect of material coupling on the prediction of natural frequencies of carbon composite plates

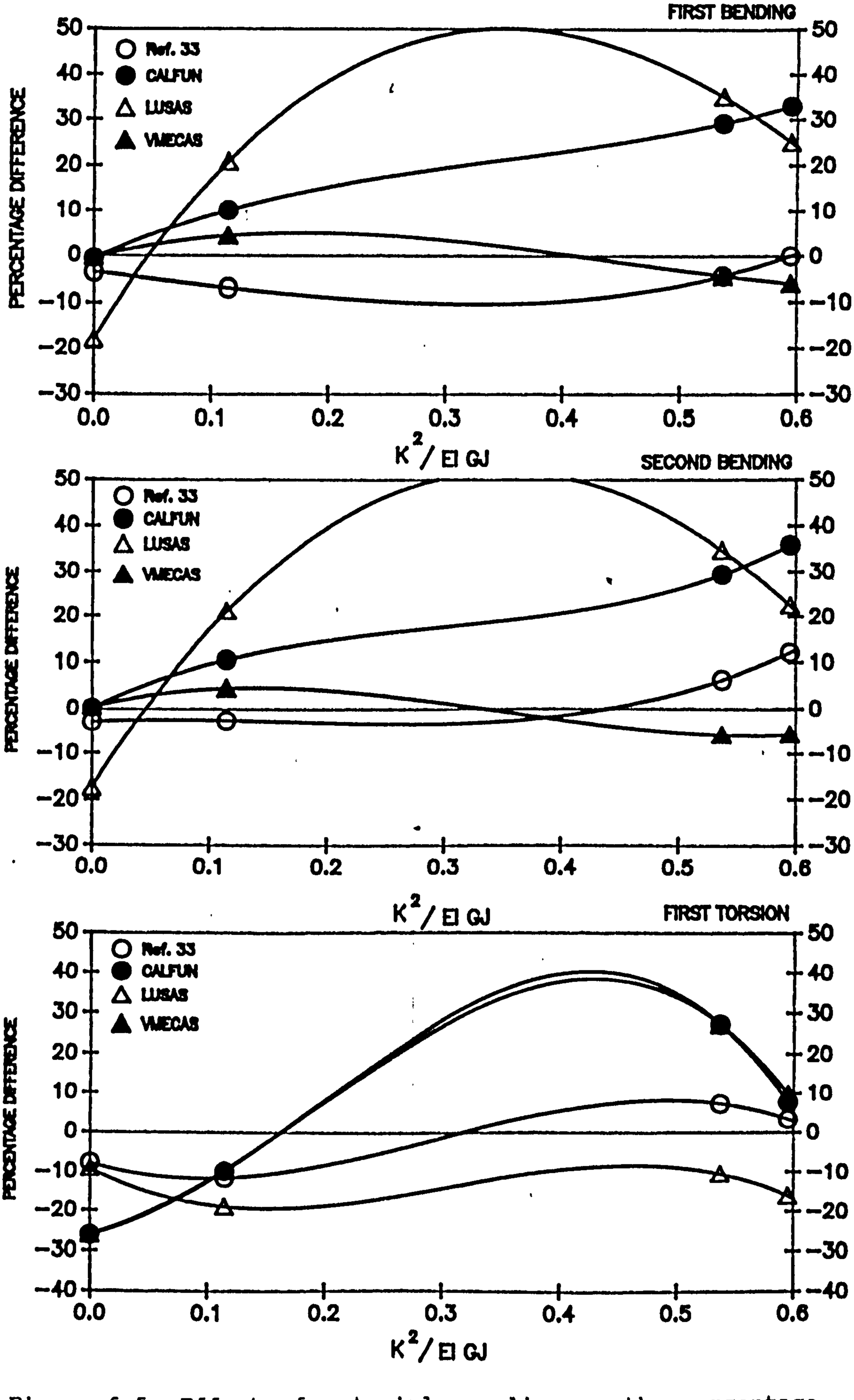

Figure 6.5 Effect of material coupling on the percentage error in prediction of natural frequencies of carbon composite plates

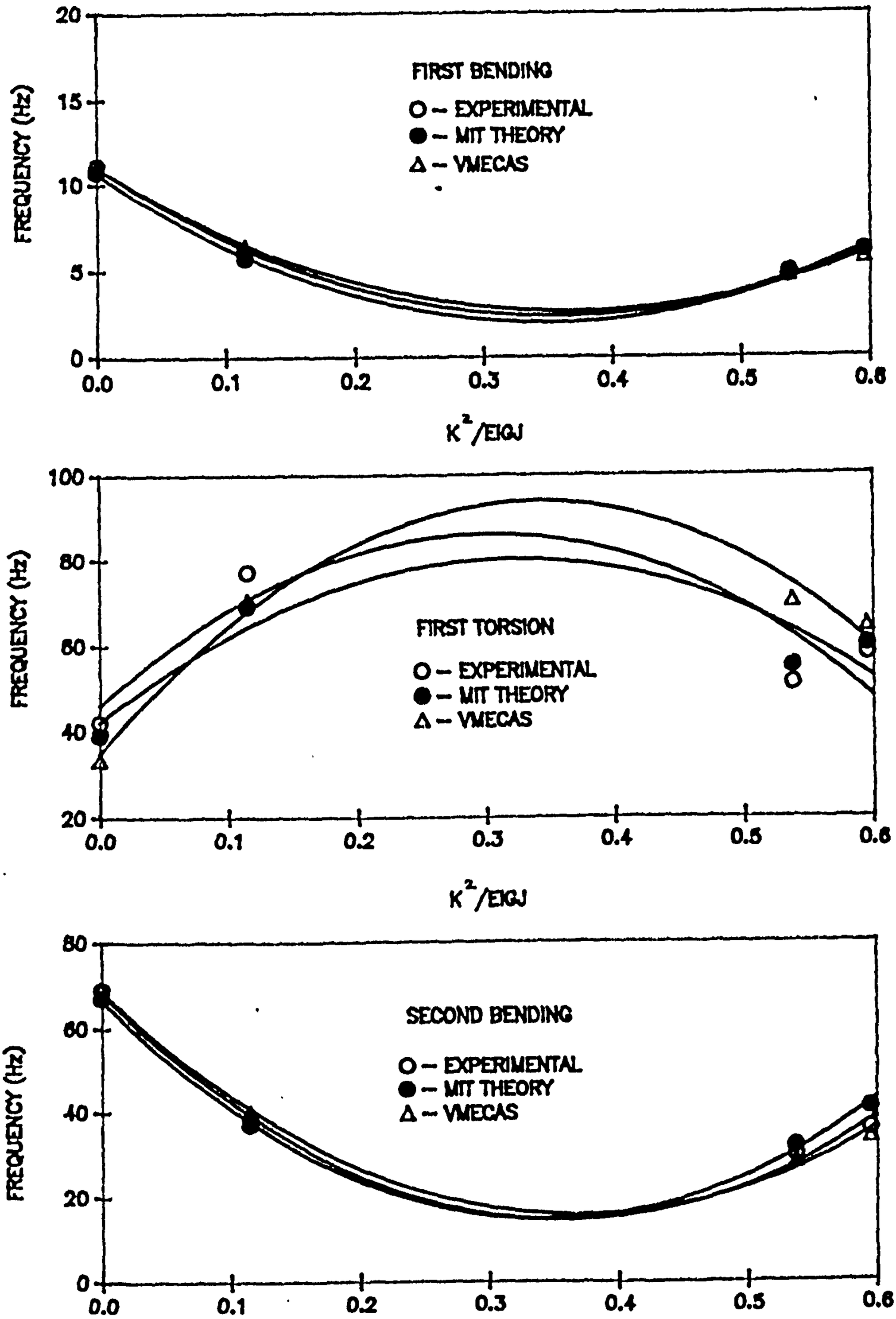

Figure 6.6 : Effect of material coupling on the prediction of frequency of Carbon composite plates

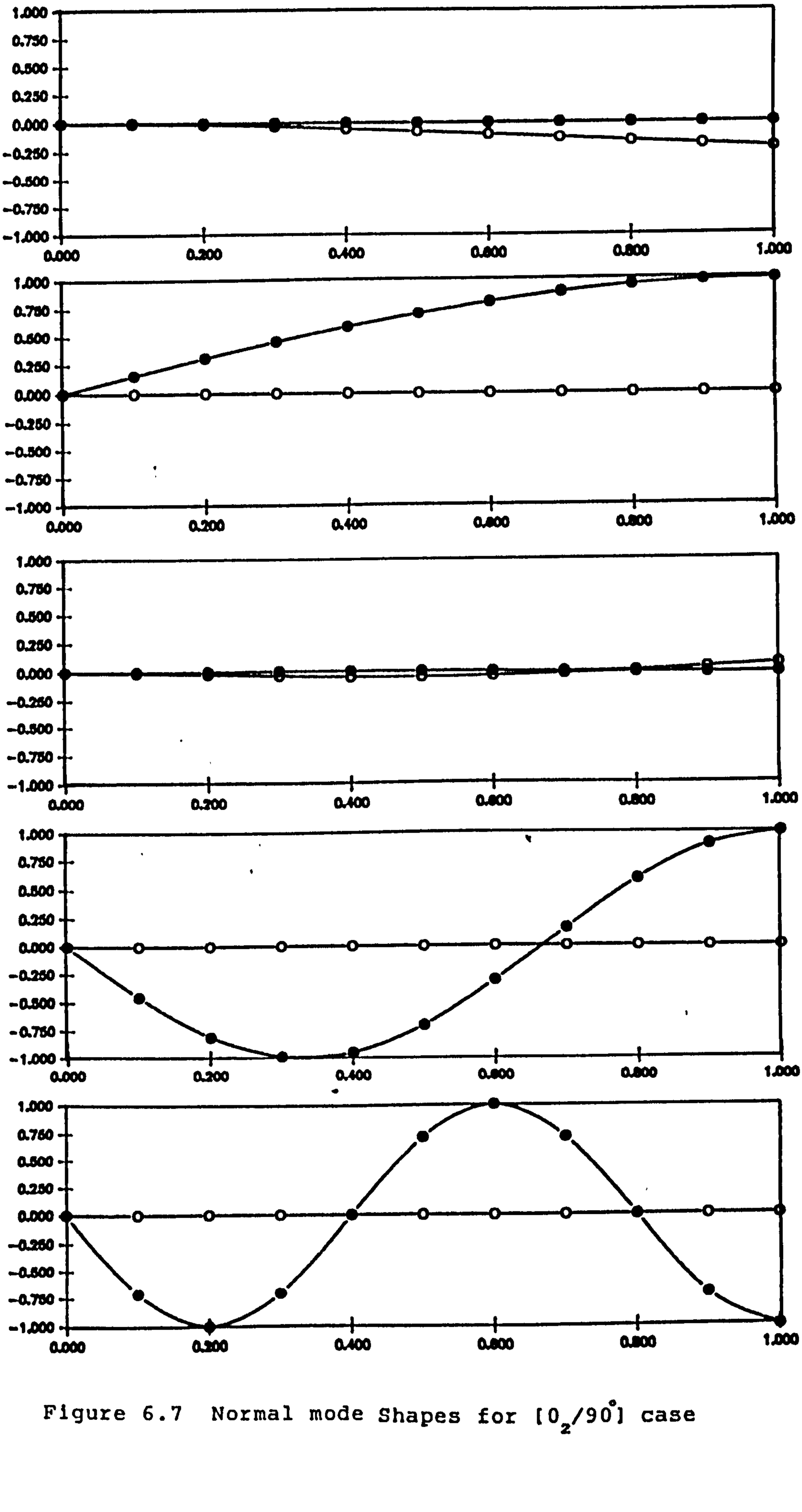

Figure 6.7 Normal mode Shapes for [$0_2/90^\circ$] case

Figure 6.8 Normal mode Shapes for [±45°/0] case

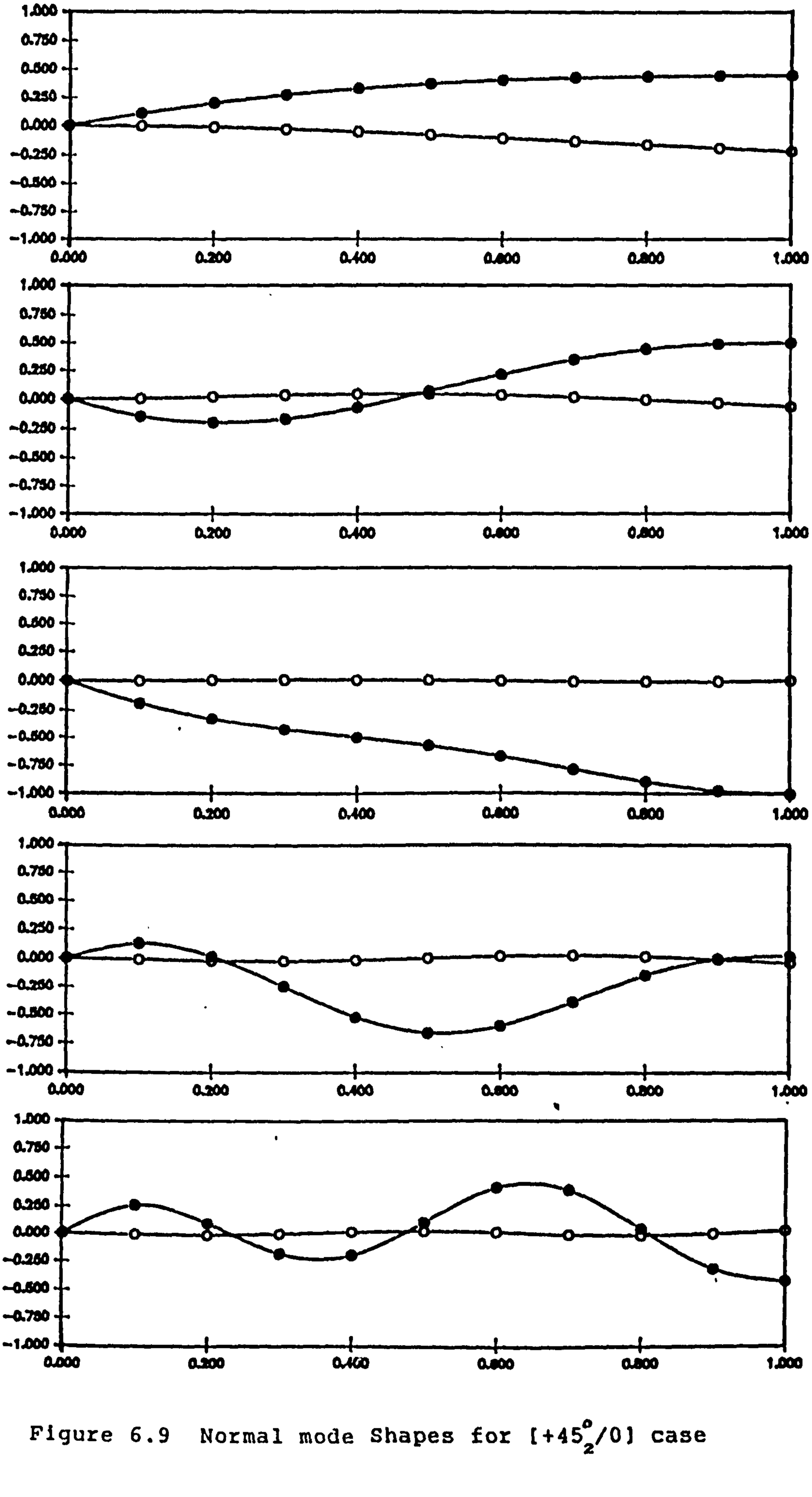

Figure 6.9 Normal mode Shapes for [+45$^{o}_{2}$/0] case

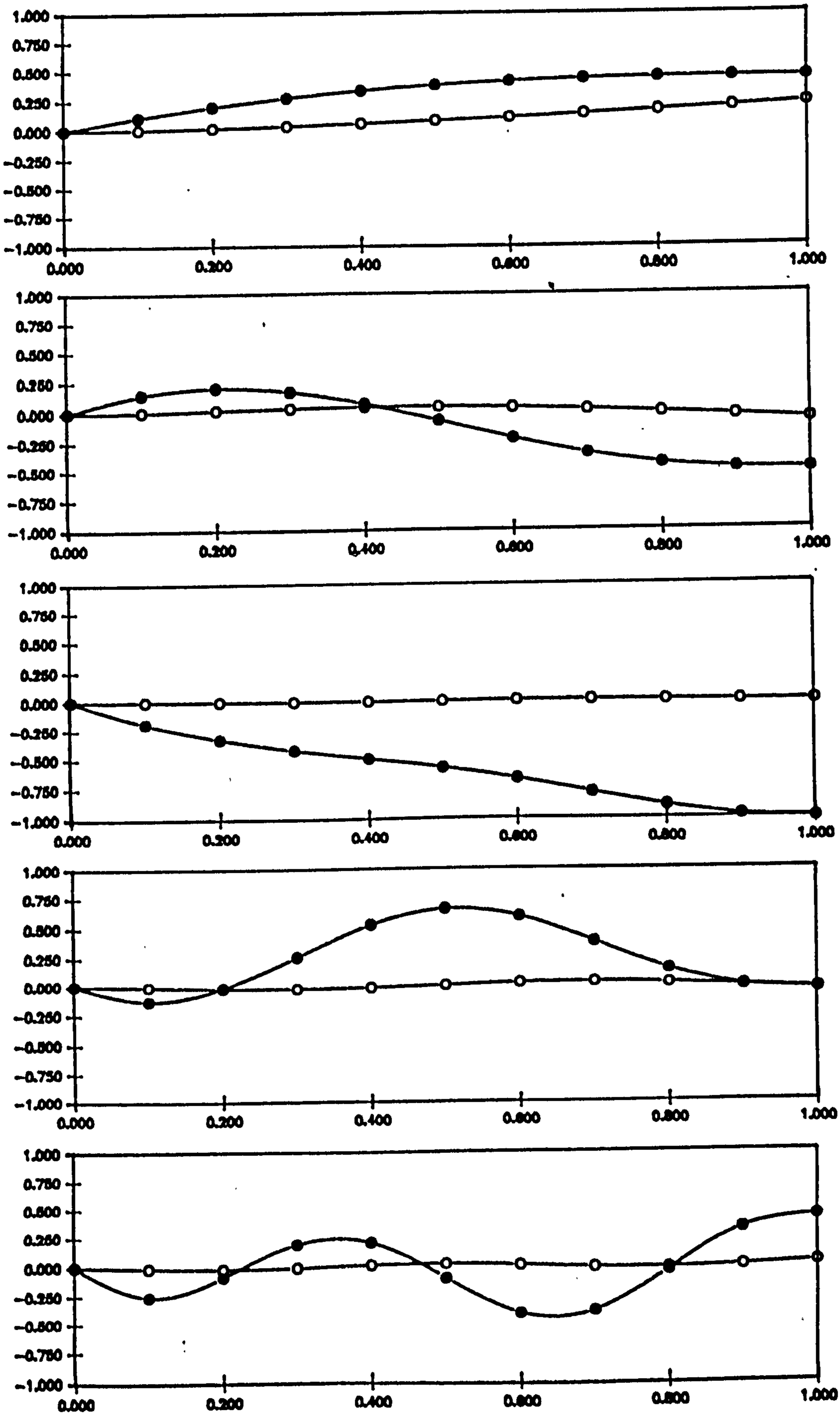

Figure 6.10 Normal mode Shapes for $[-45^{\circ}_{2}/0]$ case

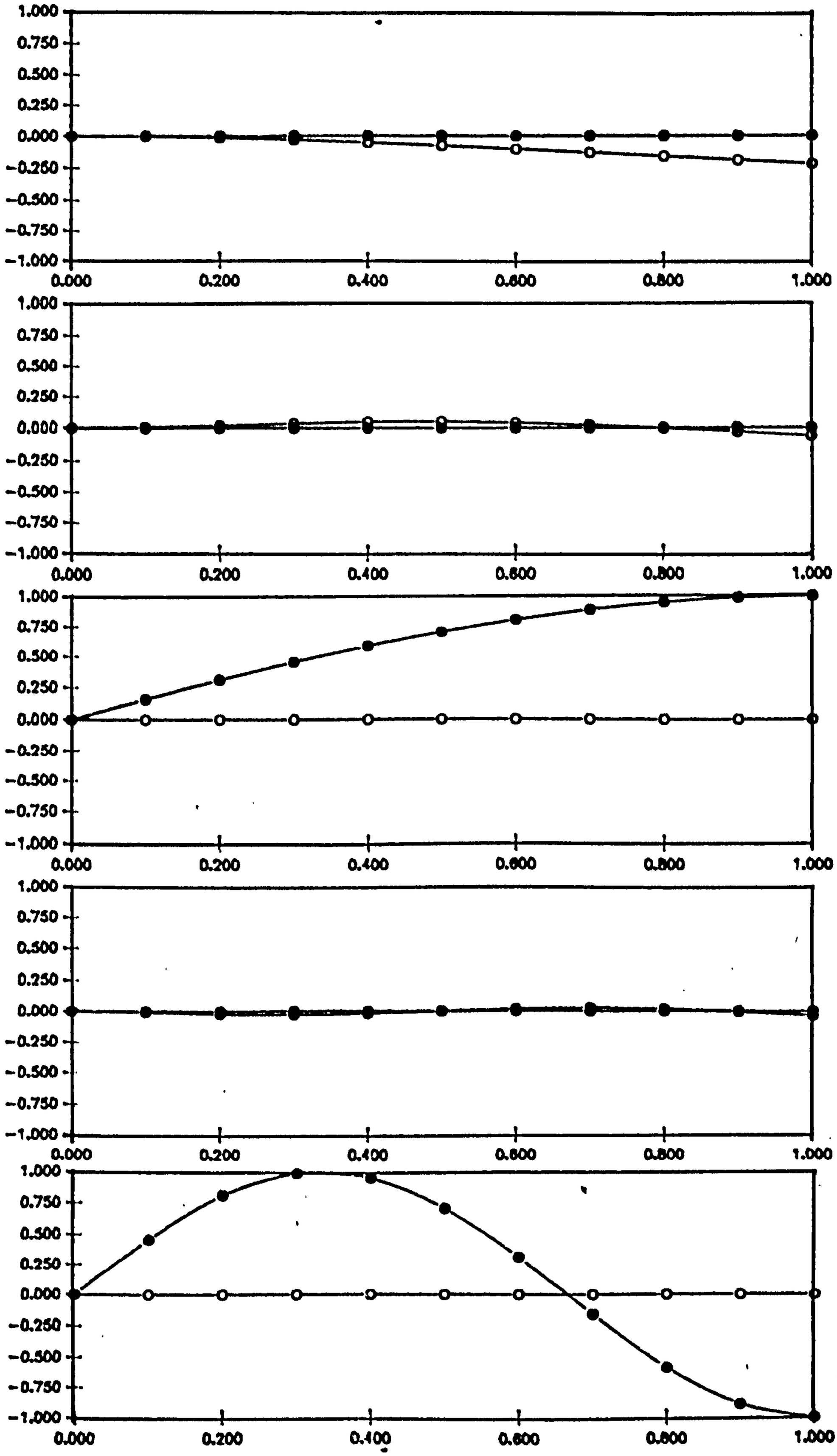

Figure 6.10a Normal mode Shapes for $[\pm 45^{\circ}/0]$, $[+45^{\circ}_2/0]$, and $[-45^{\circ}_2/0]$ cases assuming no material coupling

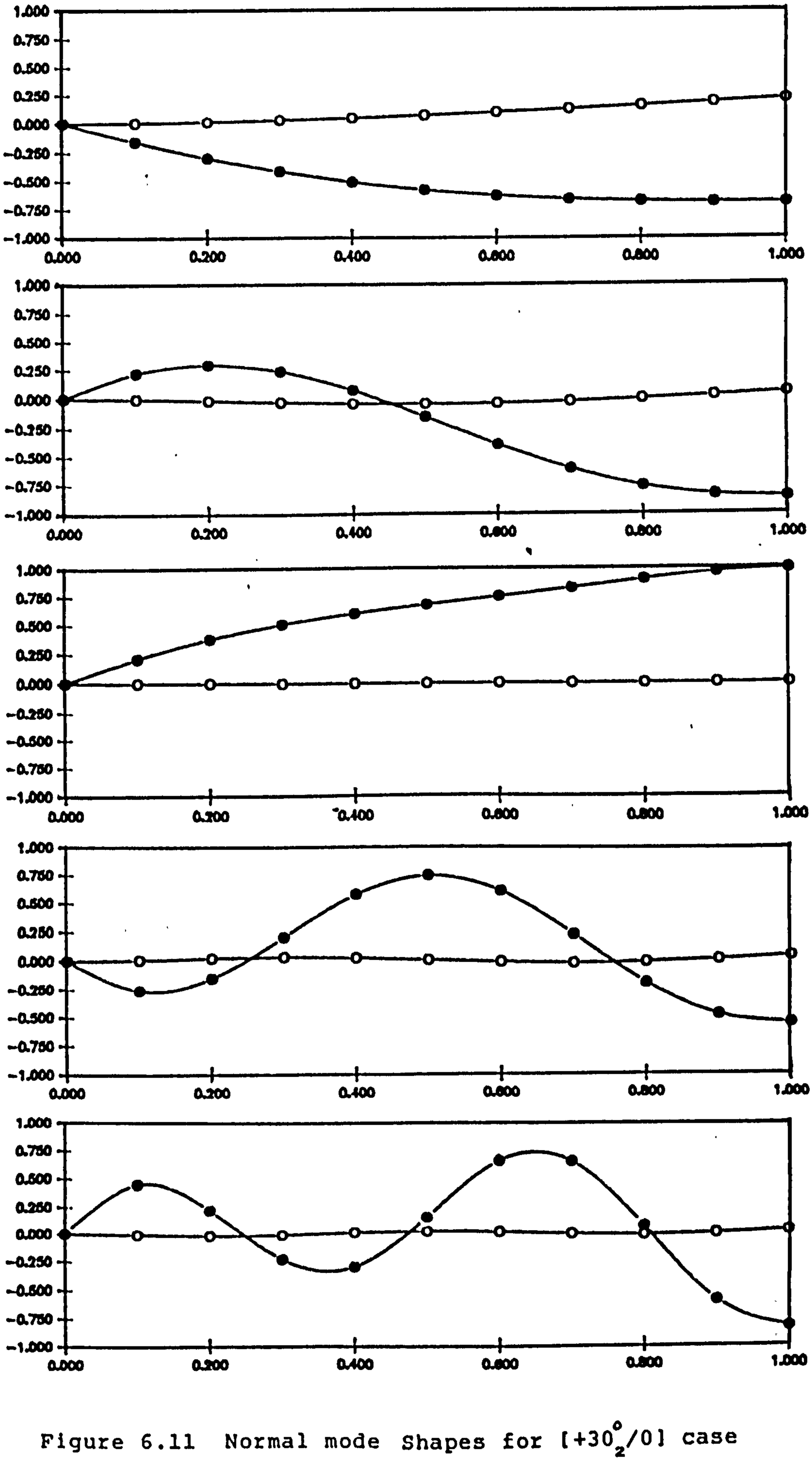

Figure 6.11 Normal mode Shapes for $[+30^{\circ}_{2}/0]$ case

Figure 6.12 Normal mode Shapes for $[-30^{\circ}_{2}/0]$ case

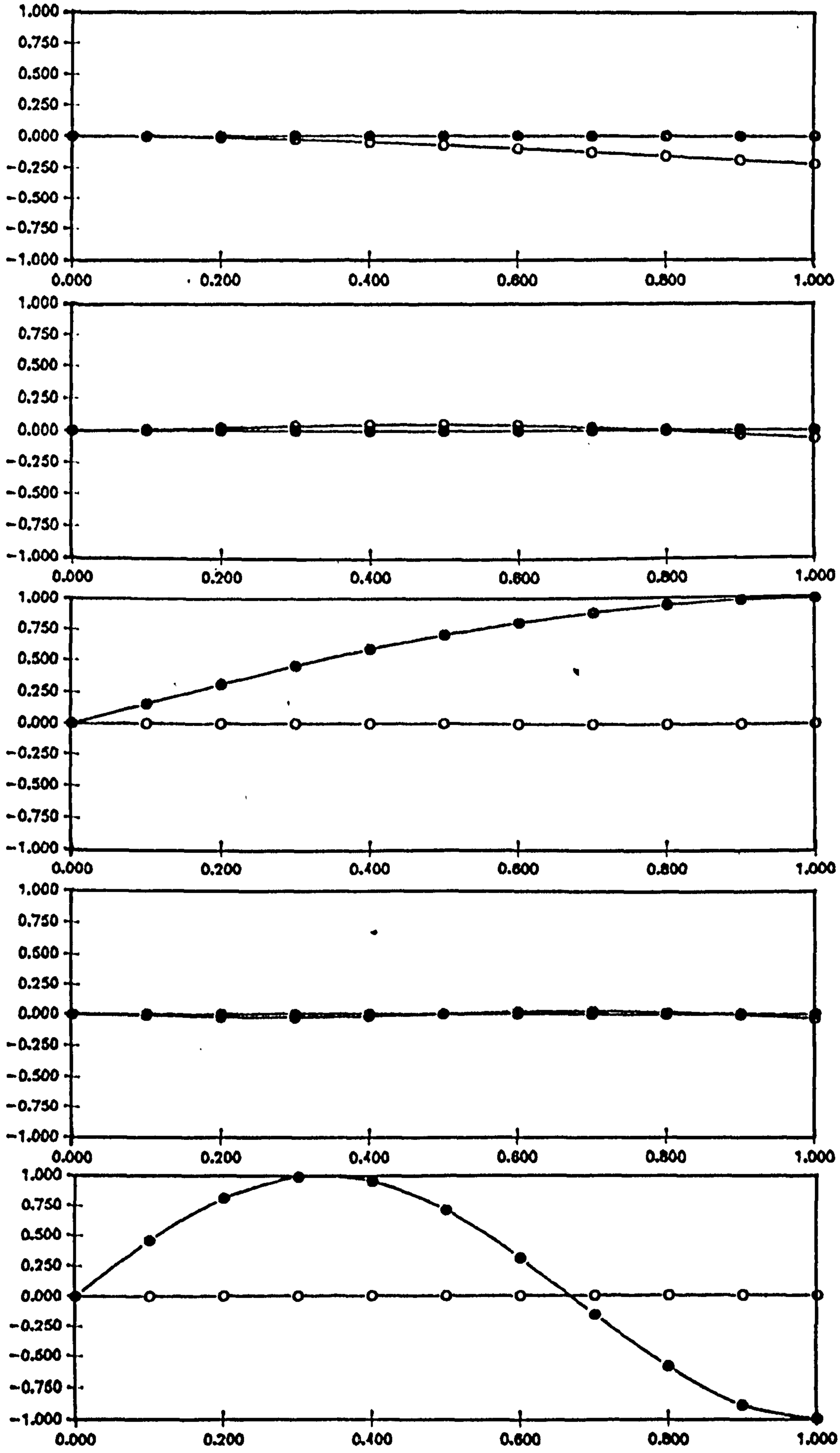

Figure 6.12a Normal mode Shapes for $[+30^{\circ}_{2}/0]$ and $[-30^{\circ}_{2}/0]$ cases assuming no material coupling

CHAPTER : 7

MODAL ANALYSIS OF COMPOSITE STRUCTURES

7.1 INTRODUCTION

Experimental observations pertaining to vibration and dynamics of a structure are usually made for two major reasons.

a. To determine the nature and extent of vibration response levels.
b. To verify theoretical models and predictions.

This chapter covers modal analysis performed on composite structures to verify a theoretical model and predictions based on it. Three types of structure, thin plate, thin-walled open section, and thin-walled closed section structures with cantilevered end conditions as discussed in Chapter 5 were tested. Theories concerning prediction of natural frequencies and mode shapes of these structures have already been discussed in Chapter (6). A brief historical review and application of modal testing will be followed by theory and measurement procedures. Validation of the testing technique is discussed before presenting the results on composite structures. A number of figures for power spectral density, frequency response and Bode plots are given for each case. The layout of the work in this chapter is shown in Figure (7.1).

7.2 MODAL ANALYSIS

Modal analysis or modal testing is the thorough integration of the theoretical basis of vibration, accurate measurement of vibration, and a realistic and

detailed data analysis. The philosophy of modal analysis or testing is described in Figure (7.2).

The usual trend in vibration studies is that systems each with a single-degree-of-freedom are used as building blocks to develop confidence and later on the knowledge is extended to multi-degree-freedom systems (see Figures (7.3)-(7.4)). The three major aspects of the measurement process that demand particular attention for the acquisition of high-quality data are shown in Figure (7.5).

The idea of modal testing was developed from 'Resonance Testing' and 'Mechanical Impedance Methods'. In 1947 Kennedy and Pancu [1] described methods for the accurate determination of natural frequencies and damping levels of aircraft structures. Bishop and Gladwell in 1963 [2] described the theory of resonance testing. Salter [3] proposed interpretation of measured data in a relatively non-analytical approach. Salter's method provided considerable understanding of the physical meaning of the vibration of the structure. By the 1970s, the introduction of transducers, electronics and digital analysers gave birth to the modern day modal testing procedures. There has been a considerable amount of work in this field since then. A bibliography can be found in Reference [4] and [5]. A notable contribution in book form has been made by Ewins [6] in the recent years.

7.3 EXPERIMENTAL PROCEDURE

Experiments were carried out on isotropic and composite structures with clamped-free (cantilevered) end conditions. Three different means of excitation were used as follows :

1. Electrodynamic or moving coil type shaker
2. Transient input by a hammer blow
3. Releasing the structure from a deformed position

A brief description of the apparatus used in each method of excitation will be discussed in the following paragraphs.

7.3.1 ELECTRODYNAMIC OR MOVING COIL TYPE SHAKER/VIBRATOR

Probably the most easily manoeuvrable type of excitation is the electrodynamic or moving coil type. It is driven, via a power amplifier, by an oscillator, which has continuously variable frequency and amplitudes ranges for both square and sinusoidal wave forms.

The vibrator selected for the vibration testing was the model 200 series, supplied by Ling Dynamics Systems Limited. These vibrators are miniature units for use in small scale vibration testing or as non-seismic pick-ups. They can be driven by any suitable oscillator/amplifier combination but in particular the Ling Dynamic Systems TPO 25 is recommended for this purpose. It has a light weight armature construction (an epoxy resin bonded coil wound on a laminated former). The top and bottom laminated spiders, vibrator body and a trunnion mounting, form the main parts of this model. The presence of a permanent magnet in the 200 series vibrators eliminates the requirement for a field power supply.

The electrodynamic shaker was connected to the structure with a thin stainless steel rod as shown in Photograph (7.1).

7.3.2 HAMMER OR IMPACTOR EXCITATION

Another popular method of excitation is through use of an impactor or hammer. It is a relatively simple means of a exciting the structure into vibration. The equipment consists of an impactor, with a set of different tips and heads which serve to extend the frequency and force level ranges for testing a variety of different structure.

A Kistler Type 9722 instrumented hammer was used, which incorporates a quartz force sensor. The hammer produces an analogue voltage which is proportional to the transient force transferred to the test object.

The motion of the structure is measured by means of accelerometers. The signals from the force transducer and accelerometers are compared by spectrum analyser to determine various dynamic characteristics such as compliance and mechanical impedance.

7.3.3 TRANSDUCERS TO MEASURE FORCE AND RESPONSE

The motion response of the structure can be in the form of displacement, velocity, or acceleration. Some of the structures had strain gauges for measuring static structural properties, therefore, a potentiometric circuit was used to record the dynamic strain. At a later date piezoelectric transducers were chosen to detect force and acceleration after giving due consideration to the following problems :

(a) interference of the device with the structure and

(b) adequate performance for the range of frequency and amplitude of the test.

The advantages and disadvantages of both methods are summarised as follows :

	ADVANTAGES	DISADVANTAGES
STRAIN GAUGE		
	1. Light weight	1. Expensive to make
	2. Any voltage amplifier can be used	2. Delicate
		3. Required on every structure
ACCELEROMETER		
	1. A single device can suffice for all the structure	1. May not be light enough to suit
	2. Easy to install	2. Requires a charge amplifier
	3. Short experiment preparation time	

7.3.4 SIGNAL PROCESSING

The mobility parameters were obtained by applying the following types of excitations to the structure.

(i) SINUSOIDAL EXCITATION

The structure was harmonically excited and the resulting harmonic response was measured. The frequency range was covered either by increasing the excitation frequency in small increments or sweeping throughout the range slowly but continuously, allowing quasi-steady conditions to be achieved.

(ii) TRANSIENT EXCITATION

A transient or impulsive (nonperiodic) excitation was also applied to the structure, hence, reducing labour involved in modal testing.

A fast Fourier transform spectrum analyser was used to process the time domain signal into the frequency domain. Frequency information was extracted from the response of the structure using statistical techniques as

described in Reference [6].

7.4 VALIDATION OF THE TEST TECHNIQUES USING STRUCTURES MADE OF CONVENTIONAL MATERIALS

In order to validate the test techniques adopted for the modal testing, structures made of conventional materials were tested to obtain their natural frequencies and mode shapes. The static structural properties of these structures were experimentally established and had been discussed in Chapter 5. The computer program VMECAS was generally used to predict the natural frequencies and mode shapes of these structures. The results are as follows :

7.4.1 BEAM ELEMENT

A cantilevered aluminium prismatic bar structure was tested with a length of 765 mm. The lowest three natural frequencies were predominantly of bending modes. Hence, only the bending stiffness of the structure was established experimentally as discussed in Table (5.1). The static structural properties of the structure were as follows:

Bending rigidity	EI_{xx}	$(N\text{-}m^2)$	141.10
Torsional rigidity	GJ	$(N\text{-}m^2)$	162.427
Mass per unit length	m/ℓ	(Kg/m)	0.680022
Polar mass moment of inertia	I_{po}	(Kg-m)	$4.287 * 10^{-5}$

Experimental results for the natural frequencies of the structure were compared with the theoretical predictions as shown in Table (7.1). The first natural frequency was estimated within 9 % of the experimental

value but for higher frequencies the discrepancies increased. The test was repeated for a shorter length of the same specimen. This time the free length was 637 mm. The first experimental frequency was found to be 19.0 Hz as compared to the theoretical prediction of 19.87 Hz with 4.4 % error.

The Bode plot and power spectral density (PSD) plot of the acceleration for the aluminium beam of 765.0 mm length are shown in Figures (7.8a,b). Figure (7.9a,b) shows the PSD of acceleration and plots of real and imaginary parts vs frequency for a beam of reduced length 637.0 mm. The theoretical normal mode shapes for the prismatic bar are given in Figure (7.10). Qualitative agreement was found between these theoretical predictions and the observed mode shapes when the structure was sinusoidally excited near the resonant frequencies.

The errors were expected due to following reasons:

1. Low resolution of the spectrum analyser
2. Flexible cantilevered end condition
3. Added mass of the exciter and transducer

In order to isolate the effect of end conditions on the experimental investigation of natural frequencies, a steel prismatic bar with free-free end conditions was tested. The agreement between theoretical and experimental results was found to be very good as shown in Table (7.2).

The dimensions and static structural properties of the steel prismatic bar were as follows :

b (mm) = 38.2	,	h (mm) = 9.6	,	ℓ (mm) = 1290.0	
Bending rigidity		EI_{xx}	($N-m^2$)	582.997	
Mass per unit length		m/ℓ	(Kg/m)	2.868	

7.4.2 PLATE STRUCTURE

An aluminium plate of 300mm x 75mm x 0.71 mm dimensions was tested. Structural parameters such as mass per unit length (spanwise) and polar mass moment of inertia used in estimating the natural frequencies are tabulated in Table (7.3) and an account of plate stiffnesses are given in Table (5.2).

Experimental results for natural frequencies of the aluminium plate are compared with the theoretical predictions in Table (7.4). The large discrepancies in bending frequencies suggest that bending rigidity has been overestimated. During the bending rigidity test it was observed that the plate deformed considerably within a very small range of loads. It is possible that whilst experiencing large deflections the structure deviated from the small deflection theory used in computing the bending stiffnesses. The added mass of the accelerometer can also result in a lower frequency as compared to the theoretical prediction when the additional mass is neglected.

Bode plots for the determination of mode shapes, using the magnitudes of the frequency response function for each modal frequency, are given in Figure (7.11). The calculated normal mode shapes are compared with the experimentally established ones in Figure (7.12). The modulus of acceleration response for the aluminium plate structure is plotted against frequency in Figure (7.13).

7.4.3 THIN-WALLED OPEN SECTION

An aluminium channel section was fabricated. Natural frequencies are given in Table (7.5) and normal mode shapes were estimated using the following structural data:

Dimensions of the channel section			
Width of the flanges	b	(mm) =	46.0
Height of the web	h	(mm) =	35.0
Thickness of web and flanges	t	(mm) =	0.702
Effective length	ℓ	(mm) =	559.0
Static structural properties			
Bending rigidity	EI_{xx}	($N-m^2$)	1535.577
Torsional rigidity	GJ	($N-m^2$)	0.388096
Mass per unit length	m/ℓ	(Kg/m)	0.239385
Polar mass moment of inertia	$I_{p\bullet}$	(Kg-m)	$4.457 * 10^{-4}$
Shear centre from centroid	X_{α}	(m)	0.03707

The modulus of acceleration response for the aluminium channel section is plotted against frequency in Figure (7.14).

7.4.4 DISCUSSION OF RESULTS

The validation programme for the test techniques using structures made of conventional materials such as steel and aluminium helped to establish the accuracy of the test techniques and the reliability of the equipment, and isolated various sources of errors. It was noticed that a rigid cantilevered end condition was necessary to obtain better agreement between theoretical and experimental results. Other effects like warping of the structure will also produce differences between the predicted and experimental results if the effect is not included in the theoretical model.

These results provided the possible sources of errors to be found when testing composite structures with similar boundary conditions. Therefore, the errors associated with the test technique can be isolated from the errors found in testing composite structures.

7.5 COMPOSITE PLATE STRUCTURE

The composite plates discussed in Chapter (5) were further tested to establish their natural frequencies and mode shapes. The dimensions of these composite plates are given in Table (5.4). Structural rigidities and other parameters are tabulated in Tables (5.5) and (5.6). Experimental results of natural frequencies are compared with the two sets of theoretical predictions based on theoretical and experimental static structural properties in Tables (7.6), (7.7), and (7.8) respectively.

The Bode plot and PSD plot for the acceleration and the modulus of acceleration response plot for plates with $[0_8]_s$, $[\bar{+}30^\circ]_s$, and $[\pm 45^\circ/0]_s$ stacking sequence are shown in Figures (7.15) and (7.16) respectively. Theoretical normal mode shapes are shown in Figure (7.17).

7.5.1 DISCUSSION OF RESULTS

The magnitude of the first natural frequency decreases as the ply orientation is changed from zero to 45 degrees. The dominantly bending mode shape characterized with the first natural frequency explains the reason for this behaviour. The bending stiffness of the structure decreases with increase in the ply orientation, therefore, the magnitude of the dominantly bending mode frequency decreases. The coupled mode shapes for plates with $[\bar{+}30^\circ]_s$ and $[\pm 45^\circ/0]_s$ stacking sequence are due to the presence of coupled bending-torsion stiffness parameter.

The normal mode shape for the second natural frequency is an uncoupled torsional mode for the $[0_8]_s$ case but a considerable degree of coupling between bending and torsional modes exists for composite plates with stacking sequence of $[\bar{+}30^\circ]_s$ and $[\pm 45^\circ/0]_s$. The magnitude of the frequency initially increases as the ply

orientation is changed from zero degree but later returns to its initial value for $[\pm 45^{\circ}/0]_s$ plate. This behaviour is similar to the trend exhibited by the coupled bending-torsion stiffness for a composite structure as explained in Chapter (5).

The third natural frequency is a second bending mode for the zero degree case. In the other two cases, an uncoupled first torsional mode is displayed. The magnitude of the natural frequency follows the trend similar to the second natural frequency except that it acquires a lower value for the $[\pm 45^{\circ}/0]_s$ case as compared to the zero degree case.

The differences between theoretical predictions and experimental results are summarized in Table (7.9). The superscript 1 refers to predictions of natural frequency using theoretical structural properties and superscript 2 represents the theoretical predictions based on experimental results of the structural static properties. The overall image of the experimental results improves after taking into account effects due to end conditions, additional mass of the accelerometer and deviation from the theoretical model adopted for prediction. The improved results showed an increase in the percentage difference between the theoretical predictions and experimental results with an increase in the magnitude of the coupled bending-torsion stiffness of the structure.

The effect of ply orientation on the percentage error in the prediction of natural frequencies based on both theoretical and experimental structural properties is shown in Figure (7.18). For each frequency three curves can be seen. The two long dashed curves are fitted to the individual percentage error data produced by comparing the experimental and the two theoretical predictions of natural frequencies based on theoretical and experimental

structural data. The solid line is an overall curve fitted to both the percentage error data produced by comparing the two sets of theoretical predictions and the experimental results.

For the first natural frequency the percentage error falls from 18% for aluminium and composite plates with ply lay-ups of 0^{o} and 45^{o} fibre orientations to a minimum average of 5% as the fibre orientation increases to 22^{o}. This is due to the magnitude of the bending-torsion coupling which is either zero or negligibly small for both $[0_s]_s$ and $[\pm 45/0]_s$ cases.

For the second natural frequency considerable disagreement exists for the zero degree case. This discrepancy can be attributed to the underestimated torsional stiffness of the plate.

In the case of the third natural frequency the error increases with the increasing degree of ply orientation and returns back to about 5% at 45^{o}. The study of the normal mode shapes shows that the third frequency represents a predominantly torsional mode.

7.6 THIN-WALLED OPEN SECTION COMPOSITE STRUCTURES

Three types of open thin-walled structures, namely tee, angle, and channel-sections were fabricated and tested for their structural properties as mentioned earlier in section (5.8.3). Their cross-sectional and static structural details were given in Tables (5.8) to (5.15). Natural frequencies and normal mode shapes for these structures were determined and are discussed in the following sub-sections.

7.6.1 ANGLE SECTION

The predicted natural frequencies and normal mode shapes were based on theoretical and experimental

structural properties. These results are given in Tables (7.10) to (7.16) for four zero degree specimens and three of 10, 20, and 45 degrees.

A representative Bode plot and power spectral density plot of acceleration response is shown in Figure (7.19). The frequency range is narrowed down to establish the frequency more accurately.

A representative plot of normal mode shapes for the first five natural frequencies is given in Figure (7.20).

7.6.2 TEE SECTION

Four specially orthotropic tee-sections of zero degree glass/epoxy structures were fabricated and tested for their structural properties as mentioned in Chapter (5). The sectional and structural characteristics are given in Tables (5.11) to (5.13). Natural frequencies and mode shapes are predicted based on these findings. Experimental results are compared with the two sets of predictions based on theoretical and structural characteristics of the section in Tables (7.17) to (7.20). Typical normal mode shapes for the first five frequencies of the zero degree lay-up tee section are given in Figure (7.21). Bode plot and power spectral density plot of acceleration response for a representative section are given in Figure (7.22).

7.6.3 CHANNEL SECTION

Four specially orthotropic i.e. zero degree lay-up channel sections and four generally orthotropic by symmetrically laminated channel sections of 10, 20, 30, and 45 degrees were fabricated and tested for their static and dynamic structural characteristics. The sectional and static structural properties are given in Tables (5.14) and (5.15) in Chapter (5).

The theoretical predictions of natural frequencies are compared with the experimental results in Tables (7.21) to (7.28). Figure (7.23) shows the Bode plot and power spectral density plot of acceleration response for a typical channel section.

7.6.4 DISCUSSION OF RESULTS

Preliminary examination of results obtained for open section composite structures give a very confusing picture. The error levels reduced with the higher order frequencies. This pattern of results was opposite to the test performed on an aluminium open section (channel section).

The natural frequencies were for predominantly torsional modes due to very low torsional rigidity, characteristic of open sections. Torsional mode frequencies are influenced by the torsional rigidity, mass per unit length and polar mass moment of inertia about the elastic axis. The former two quantities were experimentally established, whereas, the polar mass moment of inertia was theoretically calculated. An increase in polar mass moment of inertia, I_{po} will reduce the magnitude of torsional mode frequencies of open sections and vice versa. A closer examination of the composite open sections showed segregation of matrix material near the bends. The computation of polar mass moment of inertia used average wall thicknesses and did not account for the bulge near the bends. A higher value of polar mass moment of inertia reversed the trend of errors.

Another possible source of error was the theoretical model. Open sections are free to warp. The theoretical model used in predicting natural frequencies and normal mode shapes did not account for the strain energy

characterized with warping of the cross-section. The effect of this additional degree of deformation has already been observed in the prediction of structural rigidities in Chapter (5).

The error levels increased for other ply orientations similar to results obtained for composite plates.

7.7 THIN-WALLED CLOSED SECTION COMPOSITE STRUCTURES

Structural rigidities and other parameters such as mass per unit length, location of the centre of gravity, shear centre and polar mass moment of inertia for thin-walled closed section composite structures were experimentally found and compared with the theoretical predictions in Tables (5.17) to (5.20). These structures were further dynamically tested to establish their natural frequencies and mode shapes. Experimental results for zero degree ply orientation cases are compared with theoretical predictions in Tables (7.29) to (7.34).

Representative results of dynamic tests for these structures are given in Figures (7.24) and (7.25). These also include results obtained through an ultra-violet recorder.

In order to establish the mode shapes, the magnitude of the frequency response function and phase plots were obtained when the structure was struck with the hammer (impactor) at different locations spanwise and chordwise. For a representative case these measurements are given in Table (7.35). Mode shapes were determined by plotting the amplitude responses with the help of phase information for the respective natural frequencies.

Theoretical predictions about the normal mode shapes revealed their coupled bending and torsional deformations due to geometric and material coupling present in the structure. The relatively small chord made it difficult

to obtain enough information about the torsional modes by this method. The structure was excited using an electrodynamic shaker at resonant frequency and torsional modes were observed in stroboscopic light.

These experimental mode shapes are compared with theoretical results in Figure (7.26) and were found in good agreement with theoretical predictions.

The wings discussed above were of zero degree lay-up. In the case of other orientations the modulus of elasticity decreased and the shear modulus increased, resulting in lower bending rigidity and higher torsional rigidity. This led to a decrease in the bending mode frequency and an increase in the torsional mode frequency for structures without bending-torsion coupling rigidity.

In a parametric study discussed in Chapter (4), it was observed that bending-torsional coupling rigidity increased to a maximum at $22\frac{1}{2}^{o}$ from zero and returned to zero at 45^{o}. Material coupling rigidity, K, reduces the bending mode frequency to a minimum and increases the torsional mode frequency to a maximum at maximum K. It is also observed that in the presence of material coupling the bending mode frequency acquires a lower magnitude and the torsional mode frequency a greater value compared with the materially uncoupled case.

Therefore, four wings similar to W-DMS-7 with 10^{o}, 20^{o}, 30^{o}, and 45^{o} ply lay-up were manufactured and tested. Structural rigidities were established and are given in Table (5.20). Experimental results for natural frequencies are compared with the theoretical predictions in Tables (7.36) to (7.39).

7.7.1 DISCUSSION OF RESULTS

Experimental investigation of natural frequencies and normal mode shapes for closed section composite

thin-walled structures produced good agreement for the first two to three normal modes in the majority of the wings tested. An over estimated figure for the higher normal modes was the general trend displayed by all the specimens. In some cases inaccurate estimation of static structural properties resulted in large discrepancies between the theoretical predictions and experimental results.

The presence of elastic coupling due to non-collinearity of the elastic and centroidal axes and material bending-torsion coupling produced coupled mode shapes. The structure exhibited transverse deformations along with torsional displacements. Predominantly bending and torsional mode frequencies were observed when the structure was continuously excited with an electrodynamic shaker. In the case of predominantly torsional mode frequencies cross-sectional deformations were observed. The deformed cross-sectional geometry violated the Closed Space Rigid Diaphragm (CSRD) assumption and led to the possibility of another mode of vibration known as ovalisation. The deviation from the CSRD assumption and the presence of another mode of vibration can account for discrepancies between the theoretical predictions and experimental results. In most of the cases the mode shapes agreed with the theoretical predictions for the number of frequencies observed.

The first normal mode shape was found to be predominantly bending and the next two predominantly torsional in all the cases. The presence of coupled bending-torsion rigidity further increased the difference between the first bending mode and first torsional mode frequencies.

7.8 CONCLUSIONS

Tests with satisfactory results were performed on structures made of conventional materials such as aluminium and steel to validate the testing technique and to calibrate the equipment used.

Test were performed on three composite graphite fibre reinforced plastic plates. In the evaluation of fundamental frequencies, the validity of applying a beam-element idealization to various composite lay-ups was confirmed for low flexural coupling ratios D_{16}/D_{11} and D_{16}/D_{66}.

Composite thin-walled open sections with three different cross-sections were tested. Large discrepancies were found between theoretical predictions and experimental results. The investigation demanded a better theoretical model.

Natural frequencies and normal mode shapes for six wings of zero degree ply lay-up and four of 10, 20, 30, and 45 degrees ply lay-up were established. The error levels remained within 10 % for wings with specially orthotropic ply lay-ups. In the case of generally orthotropic ply lay-ups, deviations from theoretical predictions followed similar trends to those observed for composite plate structures.

REFERENCES

1. Kennedy, C.C. and Pancu, C.D.P., "Use of vectors in vibration measurement and analysis," J. Aero. Sci., Vol. 14, No. 11, 1947.

2. Bishop, R.E.D. and Gladwell, G.M.L., "An investigation into the theory of resonance testing," Proc. Roy. Soc. Phil. Trans. 255(A)241, 1963.

3. Salter, J.P., Steady state vibration, Kenneth Mason Press, 1969.

4. Allemang, R.J., "Experimental modal analysis bibliography," Proc. IMAC2, February 1984.

5. Mitchell, L.D., "Modal analysis bibliography - An update - 1980-1983," Proc. IMAC2, February 1984.

6. Ewins, D.J., Modal testing : Theory and practice, Research Study Press Ltd., John Wiley and Sons Inc., 1984.

FREQUENCY (Hz)	THEORETICAL (VMECAS)	EXPERIMENTAL	% DIFFERENCE
FIRST MODE	13.77	15.0	- 8.9
SECOND MODE	86.32	103.5	- 19.9
THIRD MODE	241.69	149.0	38.4

TABLE 7.1 Natural frequencies of a cantilevered aluminium prismatic bar with a free length of 765 mm.

FREQUENCY (Hz)	THEORETICAL	EXPERIMENTAL	% DIFFERENCE
FIRST MODE	30.50	30.5	0.0
SECOND MODE	84.09	84.0	0.1
THIRD MODE	164.85	165.0	- 0.1

TABLE 7.2 Natural frequencies of a steel prismatic bar with free-free end conditions

PARAMETER	UNITS	THEORETICAL	EXPERIMENTAL	% DIFFERENCE
Mass per unit length m/ℓ	Kg/m	0.143775	0.1397	2.83
Polar mass mome-nt of inertia	Kg-m	$6.74 * 10^{-5}$	-----	----

TABLE 7.3 Structural parameters of an aluminium plate

MODES	FREQUENCY (HZ)			
	THEORETICAL BASED ON		EXPERIMENTAL	% DIFF. (Exp.)
	THEORY	EXPERIMENT		
FIRST BENDING	6.437	6.7009	5.6	16.43
SECOND BENDING	40.3405	41.994	36.0	14.27
FIRST TORSION	49.2798	49.485	48.0	3.00
THIRD BENDING	112.954	117.584	------	----

TABLE 7.4 Natural frequencies of an aluminium plate

FREQUENCY (Hz)	THEORETICAL		EXPERIMENTAL	% DIFFERENCE (VMECAS)
	VMECAS	LUSAS		
FIRST MODE	39.483	48.247	42.5	- 7.64
SECOND MODE	92.336	137.01	97.5	- 5.59
THIRD MODE	145.120	137.01	146.0	- 0.61
FOURTH MODE	171.520	178.19	161.0	6.13
FIFTH MODE	197.910	195.58	196.0	0.97

TABLE 7.5 Natural frequencies of an aluminium channel section

FREQUENCY (Hz)	EXP.	PREDICTIONS BASED ON			
		THEORY	% DIFF.	EXP.	% DIFF.
1st. BENDING	10.00	12.3389	18.96	12.373	19.18
1st. TORSION	38.06	36.027	- 5.64	56.533	32.68
2nd. BENDING	78.00	77.324	- 0.87	77.541	- 0.59

TABLE 7.6 Natural frequencies of composite plate $[0_3]_s$

FREQUENCY (Hz)	EXP.	PREDICTIONS BASED ON			
		THEORY	% DIFF.	EXP.	% DIFF.
1st. Mode	8.00	8.9239	10.35	8.3144	3.78
2nd. Mode	48.00	55.027	12.77	51.44	6.69
3rd. Mode	83.00	69.258	-19.84	66.769	-24.31

TABLE 7.7 Natural frequencies of composite plate $[\pm 30^{\circ}]_s$

FREQUENCY (Hz)	EXP.	PREDICTIONS BASED ON			
		THEORY	% DIFF.	EXP.	% DIFF.
1st. Mode	5.44	6.9979	22.26	6.4482	15.64
2nd. Mode	37.50	43.676	14.14	40.281	6.90
3rd. Mode	70.70	74.574	5.19	74.725	5.39

TABLE 7.8 Natural frequencies of composite plate $[\pm 45^{\circ}/0]_s$

PLY OREINTATION		Aluminium	$[0_3]_s$	$[\pm 30]_s$	$[\pm 45/0]_s$
FIRST MODE	EXPERI.	5.60	10.00	8.00	5.44
	THEORY[1]	6.437	12.338	8.9239	6.9979
	% DIFF.	13.00	18.96	10.35	22.26
	THEORY[2]	6.7009	12.373	8.3144	6.4482
	% DIFF.	16.43	19.18	3.78	15.64
SECOND MODE	EXPERI.	36.00	38.06	48.00	37.50
	THEORY[1]	40.3405	36.027	55.027	43.676
	% DIFF.	10.76	-5.64	12.77	14.14
	THEORY[2]	41.994	56.533	51.44	40.281
	% DIFF.	14.27	32.68	6.69	6.90
THIRD MODE	EXPERI.	48.00	78.00	68.59	70.70
	THEORY[1]	49.2798	77.324	69.258	74.574
	% DIFF.	2.60	- 0.87	- 19.84	5.19
	THEORY[2]	49.485	77.541	66.769	74.725
	% DIFF.	3.00	- 0.59	- 24.31	5.39

TABLE 7.9 Percentage difference in plate vibration tests

FREQUENCY (Hz)	EXP.	PREDICTIONS BASED ON			
		THEORY	% DIFF.	EXP.	% DIFF.
1st. TORSION	22.0	27.12	18.88	26.26	16.22
2nd. TORSION	77.0	79.67	3.35	77.02	0.03
3rd. TORSION	131.0	138.53	5.46	134.05	2.30

TABLE 7.10 Natural frequencies of angle section No. 1

FREQUENCY (Hz)	EXP.	PREDICTIONS BASED ON THEORY	% DIFF.	EXP.	% DIFF.
1st. TORSION	23.0	26.80	14.18	26.83	14.28
2nd. TORSION	75.5	79.16	4.62	78.67	4.03
3rd. TORSION	131.0	136.74	4.20	137.12	4.46

TABLE 7.11 Natural frequencies of angle section No. 2

FREQUENCY (Hz)	EXP.	PREDICTIONS BASED ON THEORY	% DIFF.	EXP.	% DIFF.
1st. TORSION	22.0	25.59	14.03	25.09	12.32
2nd. TORSION	73.0	75.89	3.81	73.89	1.20
3rd. TORSION	129.0	130.25	0.96	129.92	- 0.84

TABLE 7.12 Natural frequencies of angle section No. 3

FREQUENCY (Hz)	EXP.	PREDICTIONS BASED ON THEORY	% DIFF.	EXP.	% DIFF.
1st. TORSION	22.0	28.12	21.76	27.37	19.62
2nd. TORSION	72.0	82.63	12.86	80.10	10.11
3rd. TORSION	126.0	143.68	12.31	139.91	9.94

TABLE 7.13 Natural frequencies of angle section No. 4

FREQUENCY (Hz)	EXP.	PREDICTIONS BASED ON THEORY	% DIFF.	EXP.	% DIFF.
1st. TORSION	29.0	32.15	9.80	31.50	7.94
2nd. TORSION	89.0	91.05	2.25	84.33	- 5.54
3rd. TORSION	182.0	165.55	- 9.94	163.39	-11.39

TABLE 7.14 Natural frequencies of angle section No. 5

FREQUENCY (Hz)	EXP.	PREDICTIONS BASED ON THEORY	% DIFF.	EXP.	% DIFF.
1st. TORSION	30.0	32.09	6.51	31.68	5.30
2nd. TORSION	85.5	88.23	3.09	79.44	- 7.63
3rd. TORSION	190.0	165.50	-14.80	165.12	-15.07

TABLE 7.15 Natural frequencies of angle section No. 6

FREQUENCY (Hz)	EXP.	PREDICTIONS BASED ON THEORY	% DIFF.	EXP.	% DIFF.
1st. TORSION	32.0	38.41	16.68	36.40	12.08
2nd. TORSION	83.5	89.03	6.21	74.79	-11.65
3rd. TORSION	192.0	203.46	5.63	198.74	3.39

TABLE 7.16 Natural frequencies of angle section No. 7

FREQUENCY (Hz)	EXP.	PREDICTIONS BASED ON THEORY	% DIFF.	EXP.	% DIFF.
1st. TORSION	38.0	45.42	16.34	48.77	22.08
2nd. TORSION	123.0	106.34	-15.67	94.50	-30.16
3rd. TORSION	149.56	145.23	- 2.98	169.85	11.95
4th TORSION	210.0	234.88	10.59	275.43	23.76
5th TORSION	302.5	330.05	8.35	390.89	22.61

TABLE 7.17 Natural frequencies of tee section No. 1

FREQUENCY (Hz)	EXP.	PREDICTIONS BASED ON THEORY	% DIFF.	EXP.	% DIFF.
1st. TORSION	38.0	44.54	14.68	49.73	23.59
2nd. TORSION	87.0	105.70	17.69	91.33	4.74
3rd. TORSION	122.0	140.85	13.38	107.78	-13.19
4th TORSION	205.0	228.62	10.33	278.56	26.41
5th TORSION	287.5	320.99	10.43	394.81	27.18

TABLE 7.18 Natural frequencies of tee section No. 2

FREQUENCY (Hz)	EXP.	PREDICTIONS BASED ON THEORY	% DIFF.	EXP.	% DIFF.
1st. TORSION	38.0	45.42	16.34	48.77	22.08
2nd. TORSION	123.0	106.34	-15.67	94.50	-30.16
3rd. TORSION	149.56	145.23	- 2.98	169.85	11.95
4th TORSION	210.0	234.88	10.59	275.43	23.76
5th TORSION	302.5	330.05	8.35	390.89	22.61

TABLE 7.19 Natural frequencies of tee section No. 3

FREQUENCY (Hz)	EXP.	PREDICTIONS BASED ON THEORY	% DIFF.	EXP.	% DIFF.
1st. TORSION	38.0	45.42	16.34	48.77	22.08
2nd. TORSION	123.0	106.34	-15.67	94.50	-30.16
3rd. TORSION	149.56	145.23	- 2.98	169.85	11.95
4th TORSION	210.0	234.88	10.59	275.43	23.76
5th TORSION	302.5	330.05	8.35	390.89	22.61

TABLE 7.20 Natural frequencies of tee section No. 4

FREQUENCY (Hz)	EXP.	PREDICTIONS BASED ON THEORY	% DIFF.	EXP.	% DIFF.
1st. TORSION	38.5	28.73	-34.01	34.01	-13.20
2nd. TORSION	73.0	86.11	15.23	101.22	27.88
3rd. TORSION	111.0	145.23	23.57	166.64	33.39
4th TORSION	164.0	194.79	15.81	176.50	7.08

TABLE 7.21 Natural frequencies of channel section No. 1

FREQUENCY (Hz)	EXP.	PREDICTIONS BASED ON THEORY	% DIFF.	EXP.	% DIFF.
1st. TORSION	27.0	26.56	- 1.66	28.81	6.28
2nd. TORSION	50.0	79.60	37.19	86.05	41.89
3rd. TORSION	136.0	134.18	- 1.36	145.95	6.82
4th TORSION	164.0	185.43	11.56	158.59	- 3.41

TABLE 7.22 Natural frequencies of channel section No. 2

FREQUENCY (Hz)	EXP.	PREDICTIONS BASED ON THEORY	% DIFF.	EXP.	% DIFF.
1st. TORSION	27.0	24.93	- 8.30	32.21	16.18
2nd. TORSION	53.0	74.75	29.10	95.73	44.64
3rd. TORSION	156.0	125.90	- 23.91	156.69	0.44
4th TORSION	160.0	175.06	8.60	167.66	4.57

TABLE 7.23 Natural frequencies of channel section No. 3

FREQUENCY (Hz)	EXP.	PREDICTIONS BASED ON THEORY	% DIFF.	EXP.	% DIFF.
1st. TORSION	28.0	28.91	3.51	39.02	28.24
2nd. TORSION	52.0	86.70	40.02	116.56	55.39
3rd. TORSION	104.0	145.83	28.68	197.77	47.41
4th TORSION	160.0	203.66		215.16	

TABLE 7.24 Natural frequencies of channel section No. 4

FREQUENCY (Hz)	THEORY	EXPT.	% DIFF.
1st. TORSION	24.709	33.0	-33.55
2nd. TORSION	74.071	97.0	-30.96
3rd. TORSION	124.71	134.5	- 7.85
4th TORSION	172.23	172.0	0.13

TABLE 7.25 Natural frequencies of channel section No. 5

FREQUENCY (Hz)	THEORY	EXPT.	% DIFF.
1st. TORSION	28.556	35.0	-22.60
2nd. TORSION	85.490	100.5	-17.56
3rd. TORSION	144.58	141.5	2.13
4th TORSION	175.01	183.0	- 4.57

TABLE 7.26 Natural frequencies of channel section No. 6

FREQUENCY (Hz)	THEORY	EXPT.	% DIFF.
1st. TORSION	31.075	36.5	-17.46
2nd. TORSION	92.788	100.0	- 7.77
3rd. TORSION	157.38	135.0	14.22
4th TORSION	169.30	194.0	-14.59

TABLE 7.27 Natural frequencies of channel section No. 7

FREQUENCY (Hz)	THEORY	EXPT.	% DIFF.
1st. TORSION	35.862	35.0	2.40
2nd. TORSION	106.28	94.5	11.08
3rd. TORSION	166.36	131.0	21.26
4th TORSION	185.86	189.0	- 1.69

TABLE 7.28 Natural frequencies of channel section No. 8

NORMAL MODE NUMBER	FREQUENCIES (Hz) ℓ_{free} = 585 mm		
	THEORETICAL	EXPERIMENTAL	% DIFF.
FIRST	20.977	19.5	7.04
SECOND	85.69	84.0	1.97
THIRD	129.33	150.0	-15.98
FOURTH	247.66	192.0	22.47

TABLE 7.29 Natural frequencies for composite wing W-DMS-1A

NORMAL MODE NUMBER	FREQUENCIES (Hz) ℓ_{free} = 850 mm		
	THEORETICAL	EXPERIMENTAL	% DIFF.
FIRST	11.29	11.0	2.57
SECOND	70.12	66.0	5.88
THIRD	116.67	122.0	- 4.57
FOURTH	194.23	176.0	9.38
FIFTH	350.43	315.0	10.09

TABLE 7.30 Natural frequencies for composite wing W-DMS-2

NORMAL MODE NUMBER	FREQUENCIES (Hz) ℓ_{free} = 800 mm		
	THEORETICAL	EXPERIMENTAL	% DIFF.
FIRST	12.621	12.0	4.92
SECOND	79.070	68.0	14.00
THIRD	91.464	117.0	-27.92
FOURTH	221.340	136.0	38.56

TABLE 7.31 Natural frequencies for composite wing W-DMS-3

NORMAL MODE NUMBER	FREQUENCIES (Hz) ℓ_{free} = 698 mm		
	THEORETICAL	EXPERIMENTAL	% DIFF.
FIRST	15.356	17.5	-13.96
SECOND	92.324	96.0	- 3.98
THIRD	148.358	162.0	- 9.20
FOURTH	247.318	240.0	2.96

TABLE 7.32 Natural frequencies for composite wing W-DMS-3A

NORMAL MODE NUMBER	FREQUENCIES (Hz) ℓ_{free} = 796 mm		
	THEORETICAL	EXPERIMENTAL	% DIFF.
FIRST	15.224	14.5	4.76
SECOND	86.360	81.0	6.21
THIRD	100.134	131.0	-30.82
FOURTH	239.351	212.0	11.43
FIFTH	296.408	375.0	-26.52

TABLE 7.33 Natural frequencies for composite wing W-DMS-4

NORMAL MODE NUMBER	FREQUENCIES (Hz) ℓ_{free} = 797 mm		
	THEORETICAL	EXPERIMENTAL	% DIFF.
FIRST	15.248	14.0	8.19
SECOND	79.883	70.0	12.37
THIRD	98.448	92.0	6.55
FOURTH	223.495	150.0	32.88

TABLE 7.34 Natural frequencies for composite wing W-DMS-7

Location of the hit as percentage of beam length		FREQUENCY -- (Hz)			
		1st	2nd	3rd	4th
		17.5	96.0	162.0	240.0
0	Amp.	1.369	5.781	1.304	10.170
	Phs.	-169	71	- 29	- 80
25	Amp.	5.485	31.43	4.872	30.42
	Phs.	-178	41	- 37	- 90
50	Amp.	17.57	53.06	1.61	5.184
	Phs.	-170	42	90	19
75	Amp.	29.87	22.25	3.537	35.52
	Phs.	-169	45	161	70
100	Amp.	38.83	60.18	0.7365	30.85
	Phs.	- 45	- 98	148	- 145

TABLE 7.35 Amplitude and phase for the first five frequencies of wing W-DMS-3A

NORMAL MODE NUMBER	FREQUENCIES (Hz) ℓ_{free} = 800 mm		
	THEORETICAL	EXPERIMENTAL	% DIFF.
FIRST	14.618	14.0	4.23
SECOND	80.127	64.0	20.13
THIRD	110.820	96.0	13.37
FOURTH	211.800	170.0	19.74

TABLE 7.36 Natural frequencies for composite wing with 10^{o} ply lay-up

NORMAL MODE NUMBER	FREQUENCIES (Hz) ℓ_{free} = 800 mm		
	THEORETICAL	EXPERIMENTAL	% DIFF.
FIRST	11.970	9.5	20.64
SECOND	71.755	54.5	24.05
THIRD	128.440	89.5	30.32
FOURTH	192.370	141.0	26.70

TABLE 7.37 Natural frequencies for composite wing with 20^{o} ply lay-up

NORMAL MODE NUMBER	FREQUENCIES (Hz) ℓ_{free} = 800 mm		
	THEORETICAL	EXPERIMENTAL	% DIFF.
FIRST	10.291	10.0	2.83
SECOND	63.494	59.5	6.29
THIRD	160.290	135.0	15.78
FOURTH	174.500	162.5	6.88

TABLE 7.38 Natural frequencies for composite wing with 30^{o} ply lay-up

NORMAL MODE NUMBER	FREQUENCIES (Hz) ℓ_{free} = 800 mm		
	THEORETICAL	EXPERIMENTAL	% DIFF.
FIRST	8.941	8.5	4.93
SECOND	55.799	53.5	4.12
THIRD	155.020	147.5	4.85
FOURTH	196.710	159.0	19.17

TABLE 7.39 Natural frequencies for composite wing with 45^{o} ply lay-up

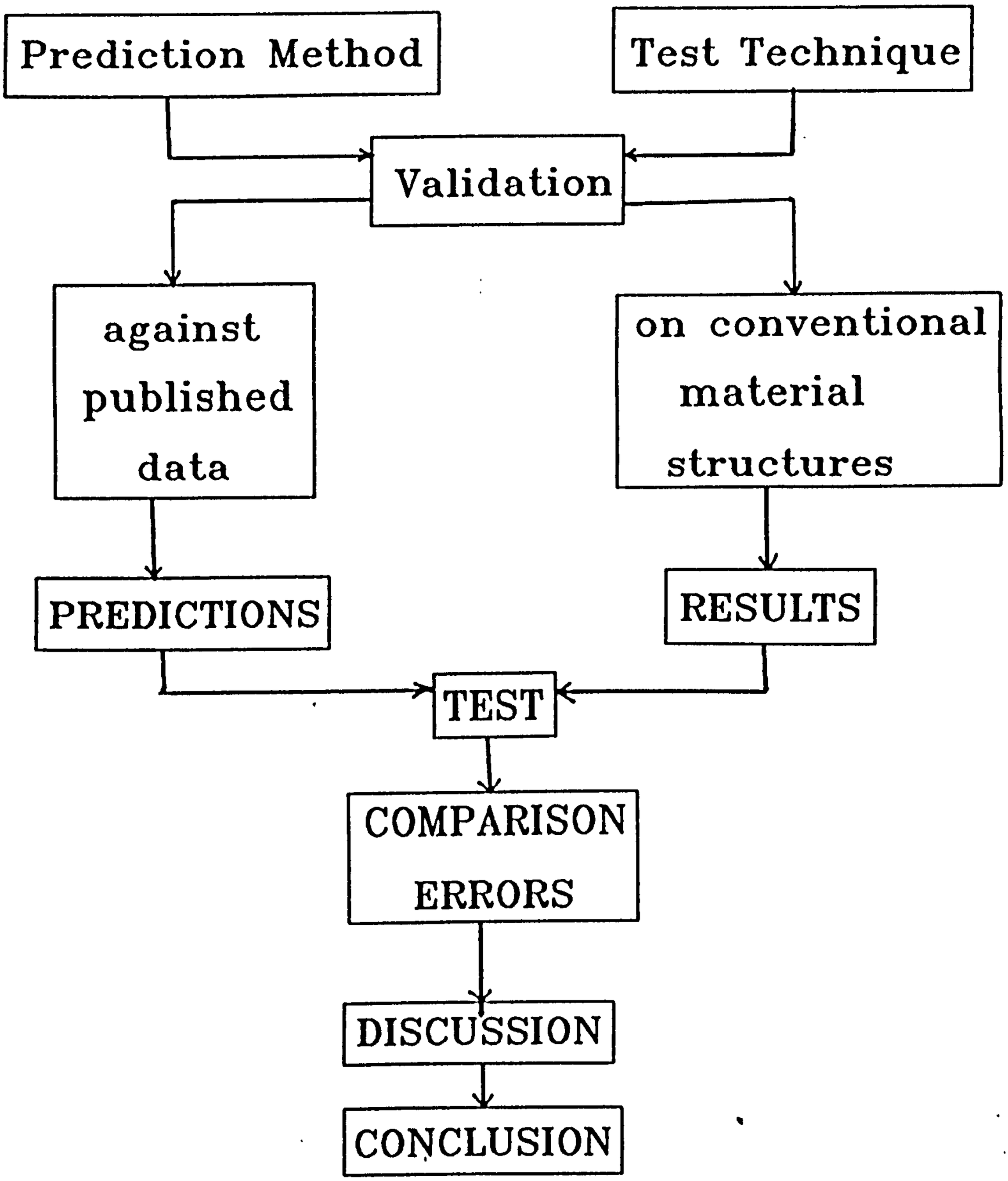

Figure 7.1 : Lay-out of Chapter 7

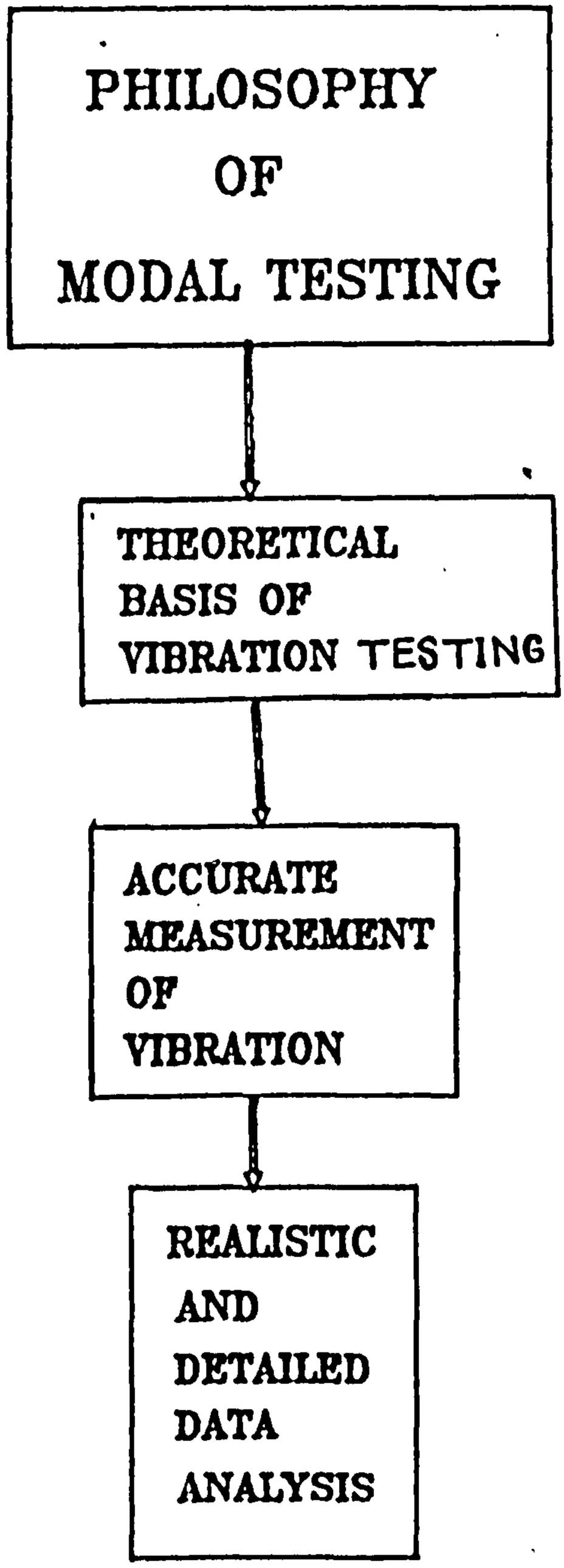

Figure 7.2 Philosophy of Modal Testing

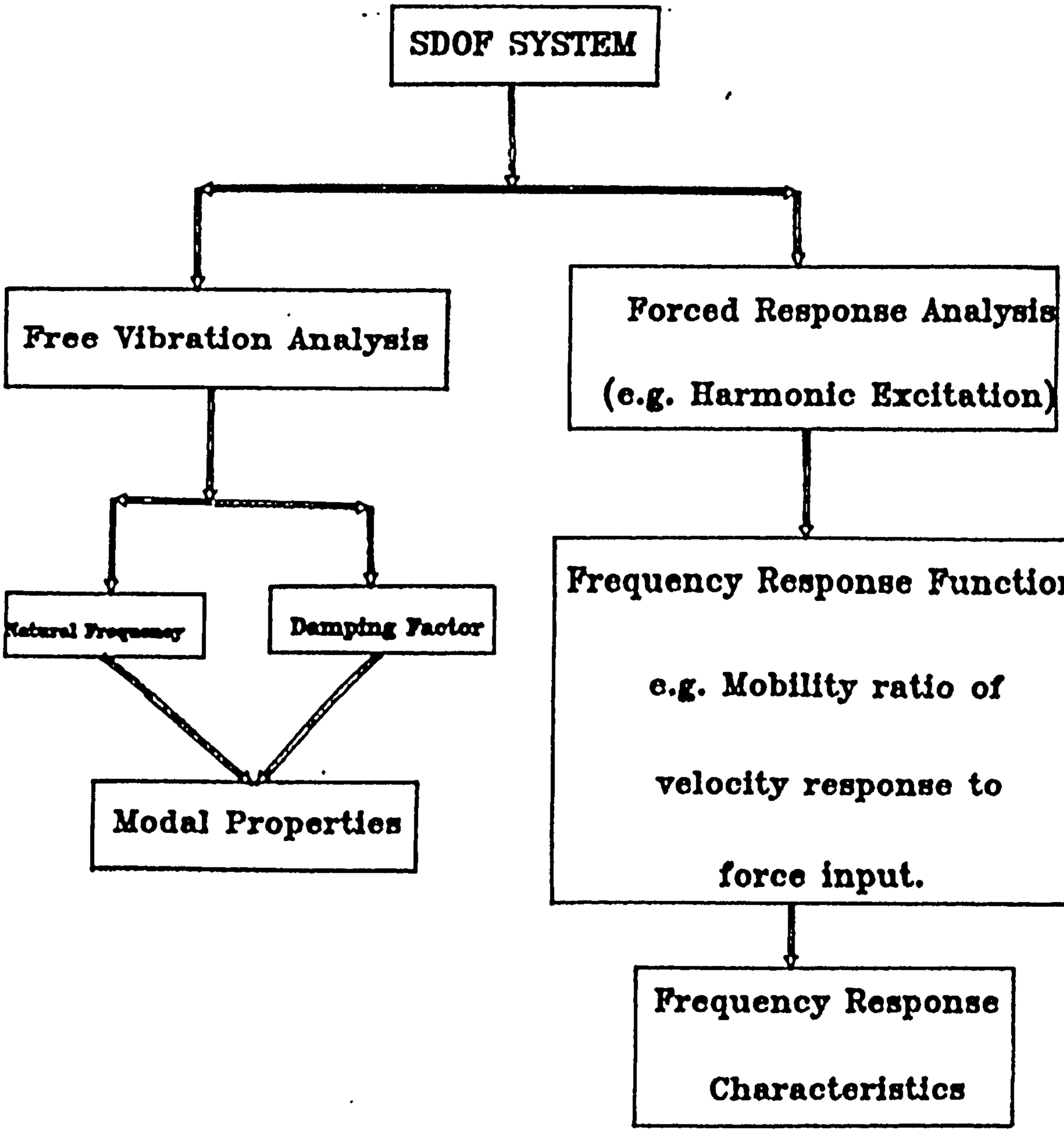

Figure 7.3 Single Degree of Freedom Systems

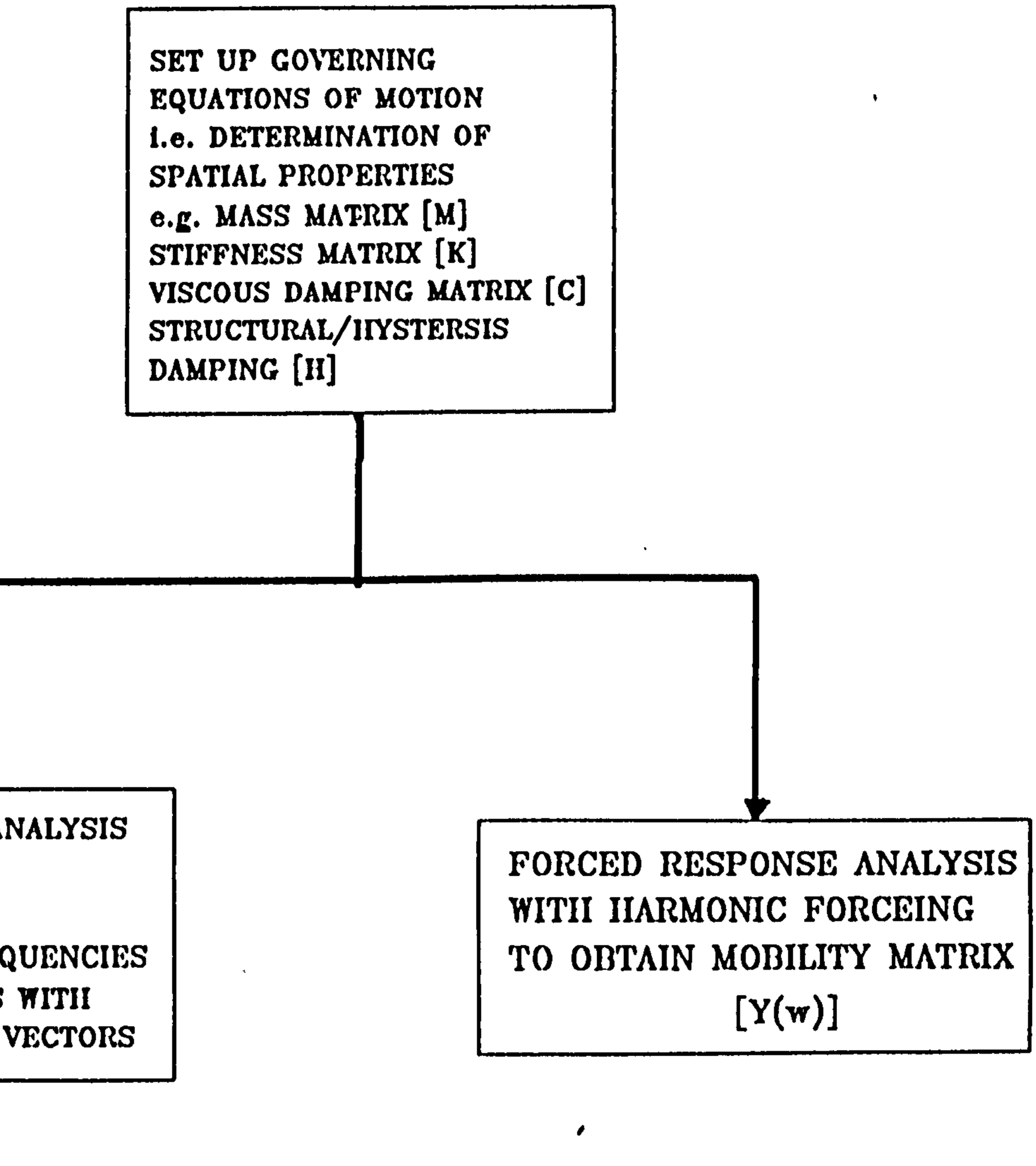

Figure 7.4 Multi - Degree of Freedom System
Vibration Analysis

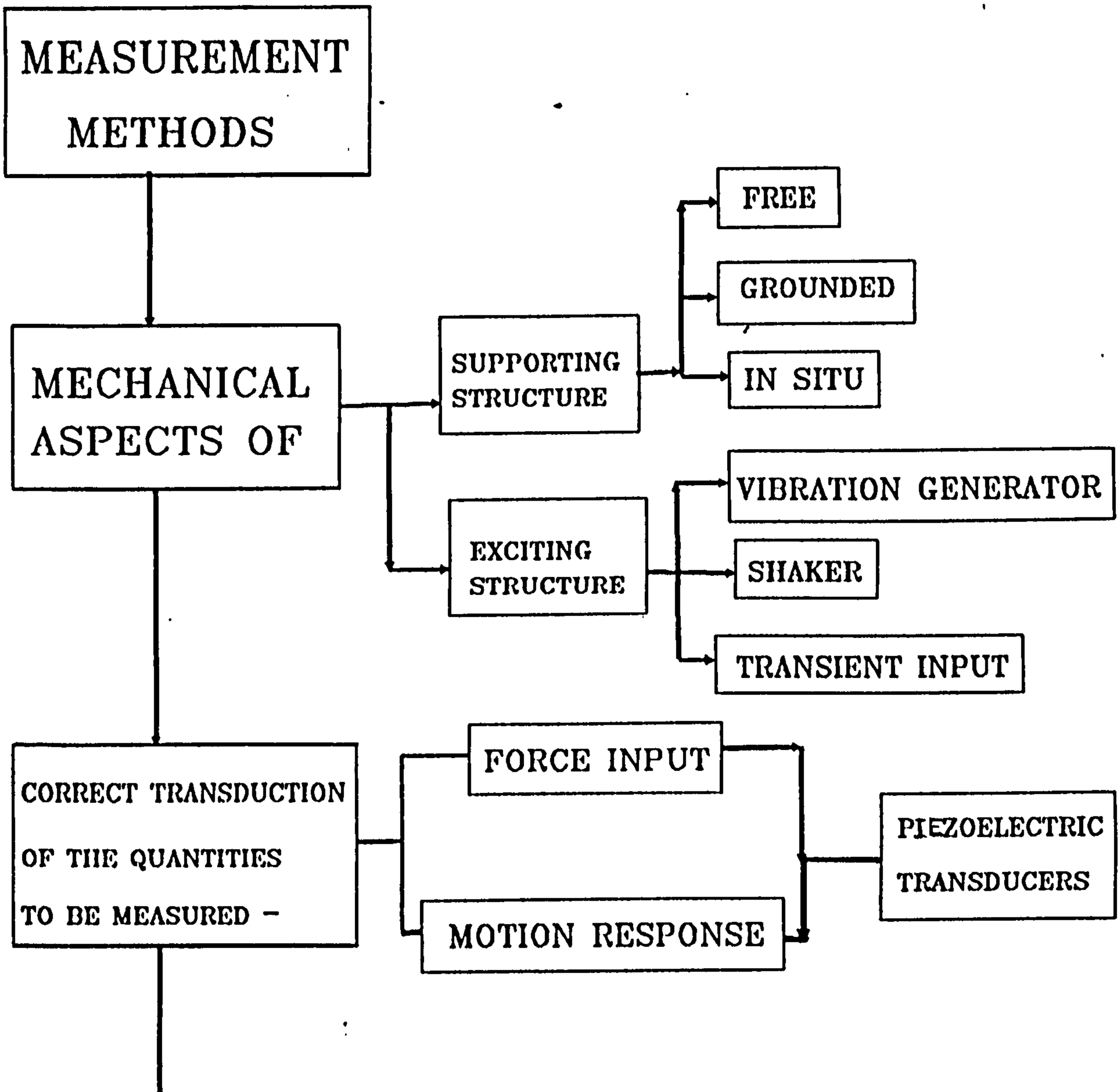
MEASUREMENT METHODS
MECHANICAL ASPECTS OF
SUPPORTING STRUCTURE
FREE
GROUNDED
IN SITU
EXCITING STRUCTURE
VIBRATION GENERATOR
SHAKER
TRANSIENT INPUT
CORRECT TRANSDUCTION OF THE QUANTITIES TO BE MEASURED -
FORCE INPUT
MOTION RESPONSE
PIEZOELECTRIC TRANSDUCERS
SIGNAL PROCESSING CORRESPONDING TO THE TYPE OF TEST

Figure 7.5

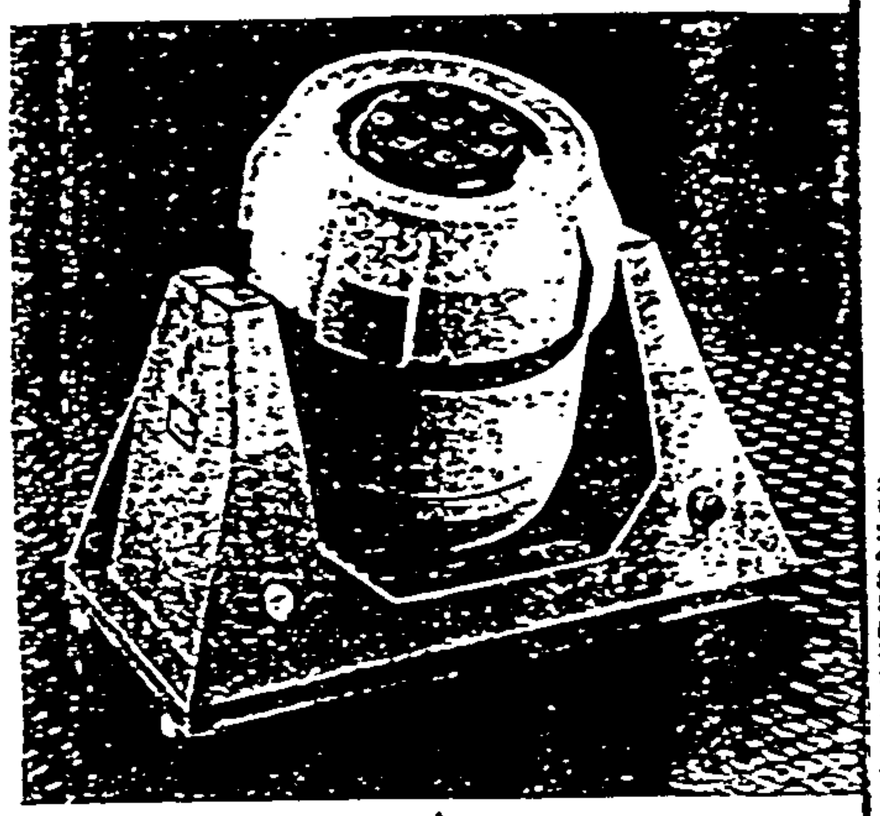

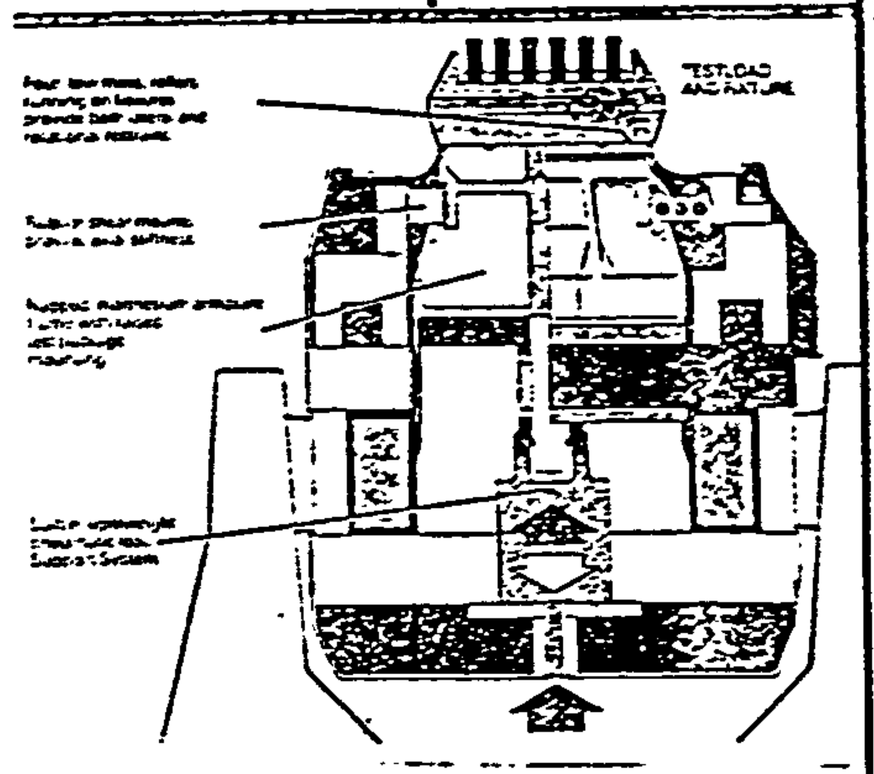

Fig. 7.6a Electrodynamic shaker

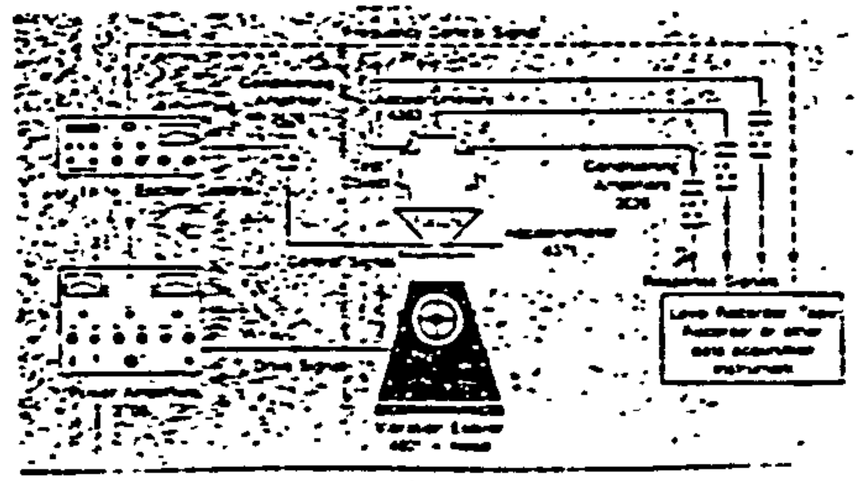

Fig. 7.6b Vibration testing using shaker

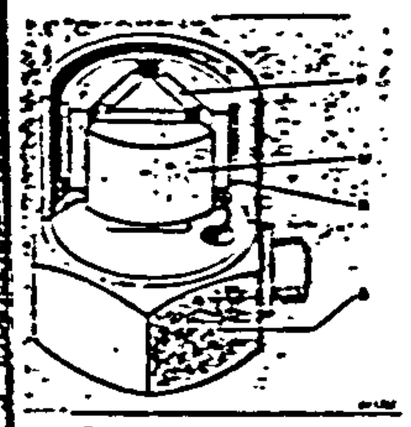

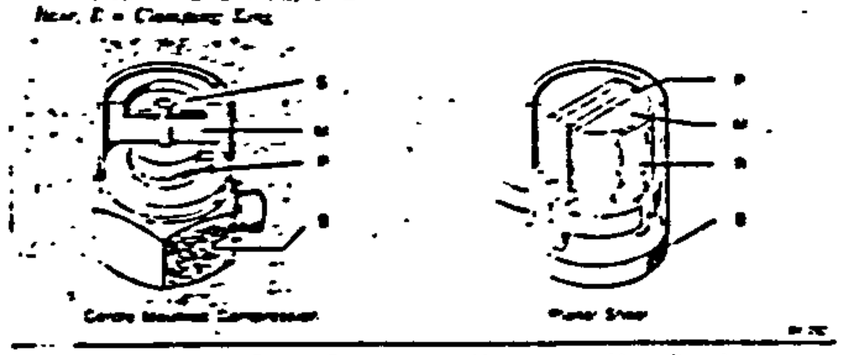

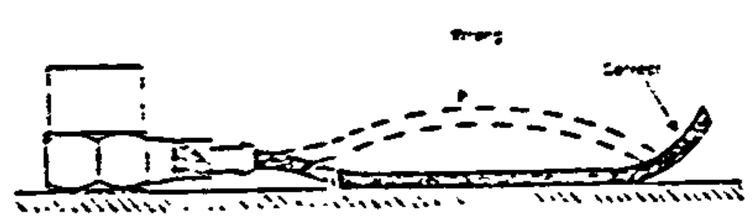

Fig. 7.6c Accelerometer

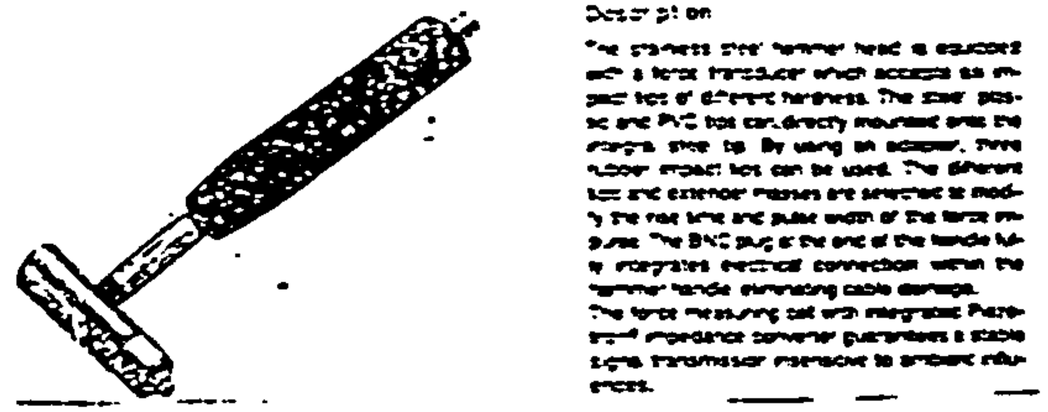

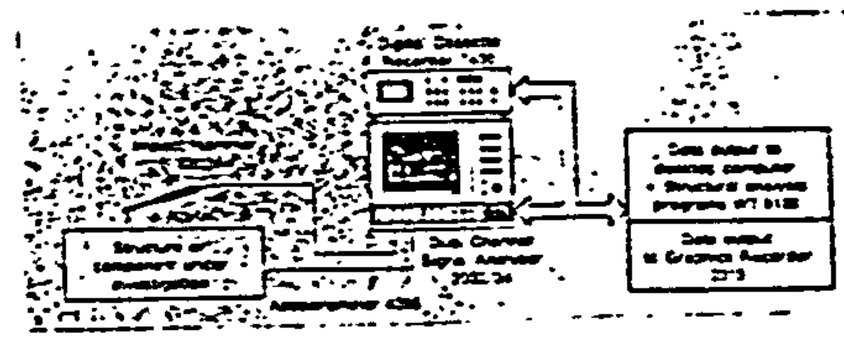

Impulse Hammer Measuring Kit

Fig. 7.6d Vibration testing using a hammer

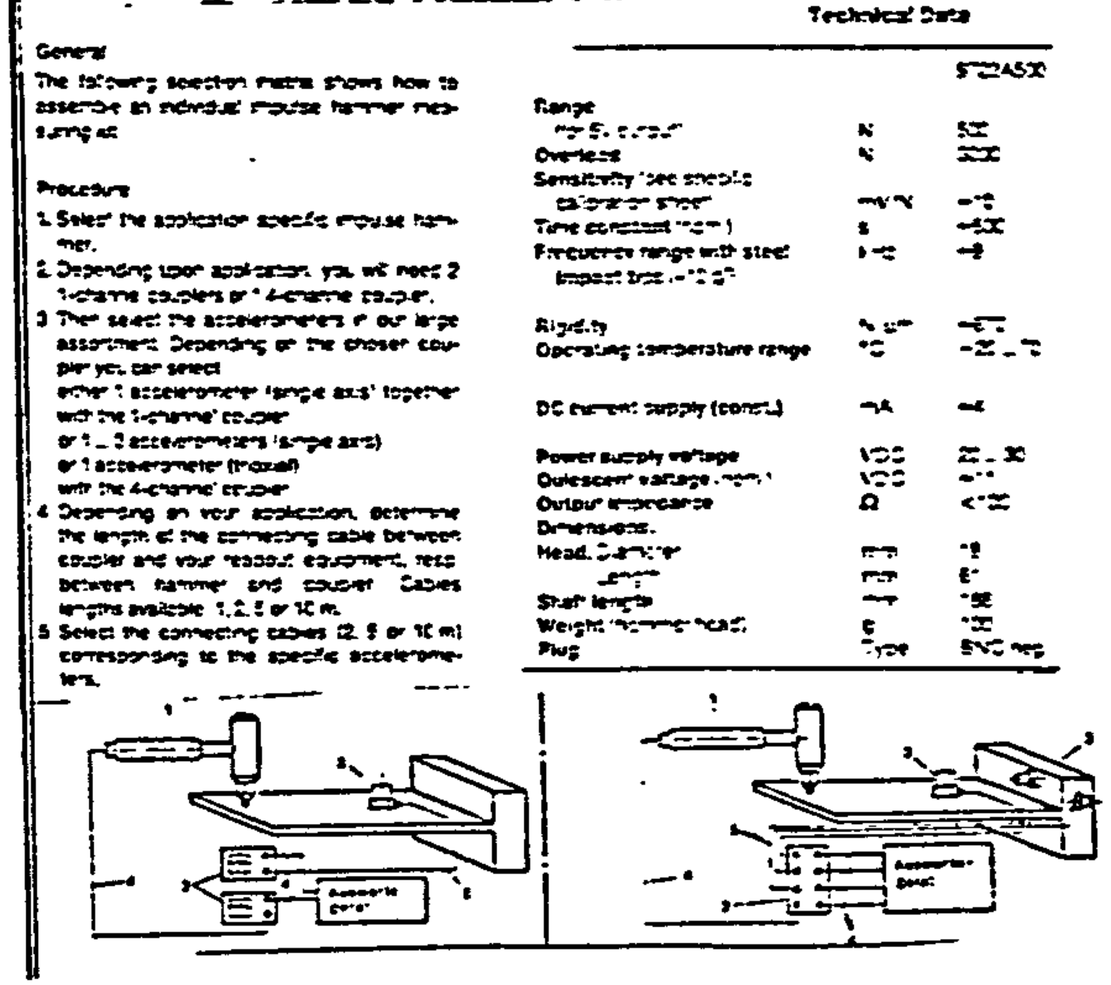

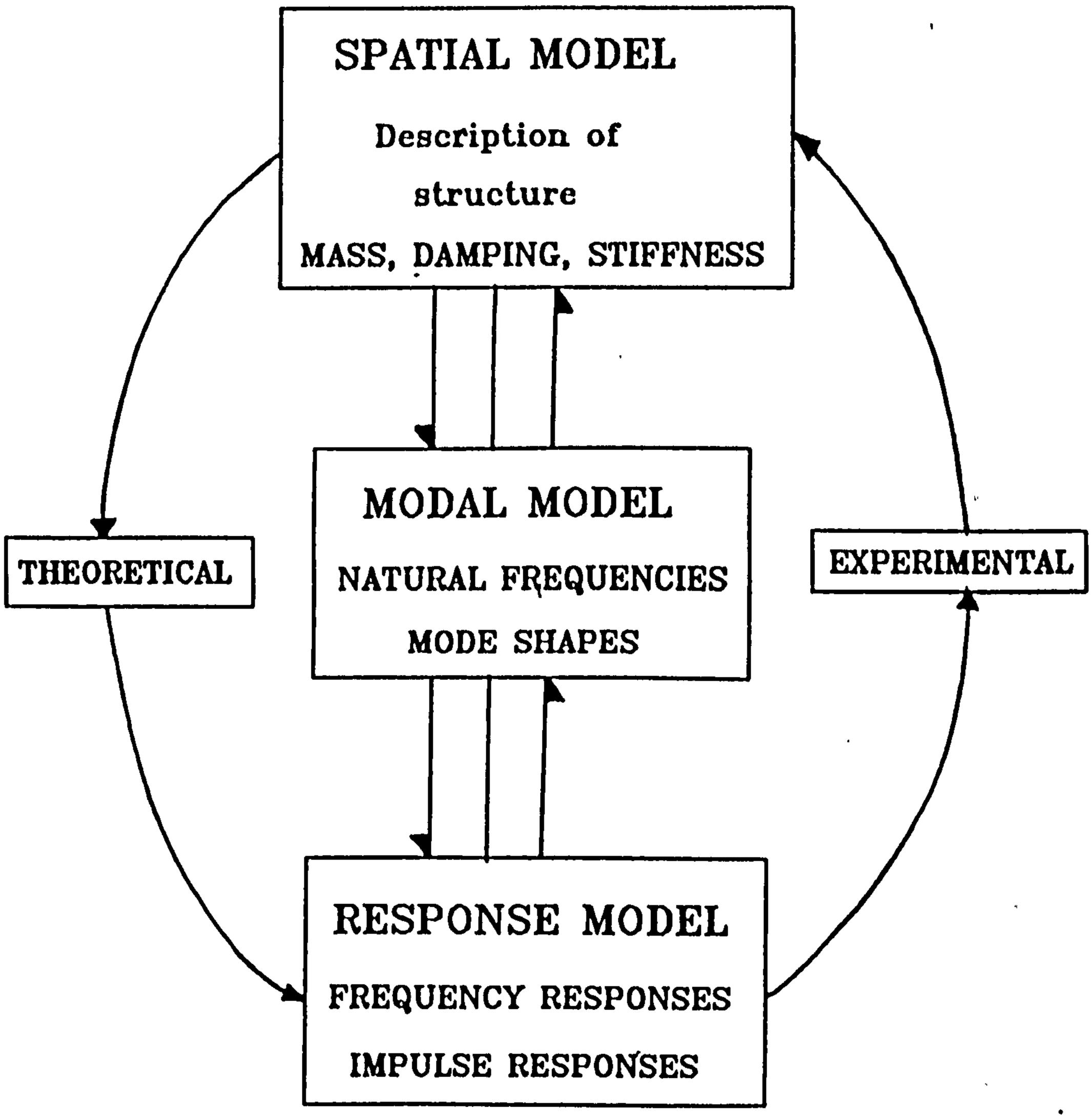

Figure 7.7 Routes to vibration analysis

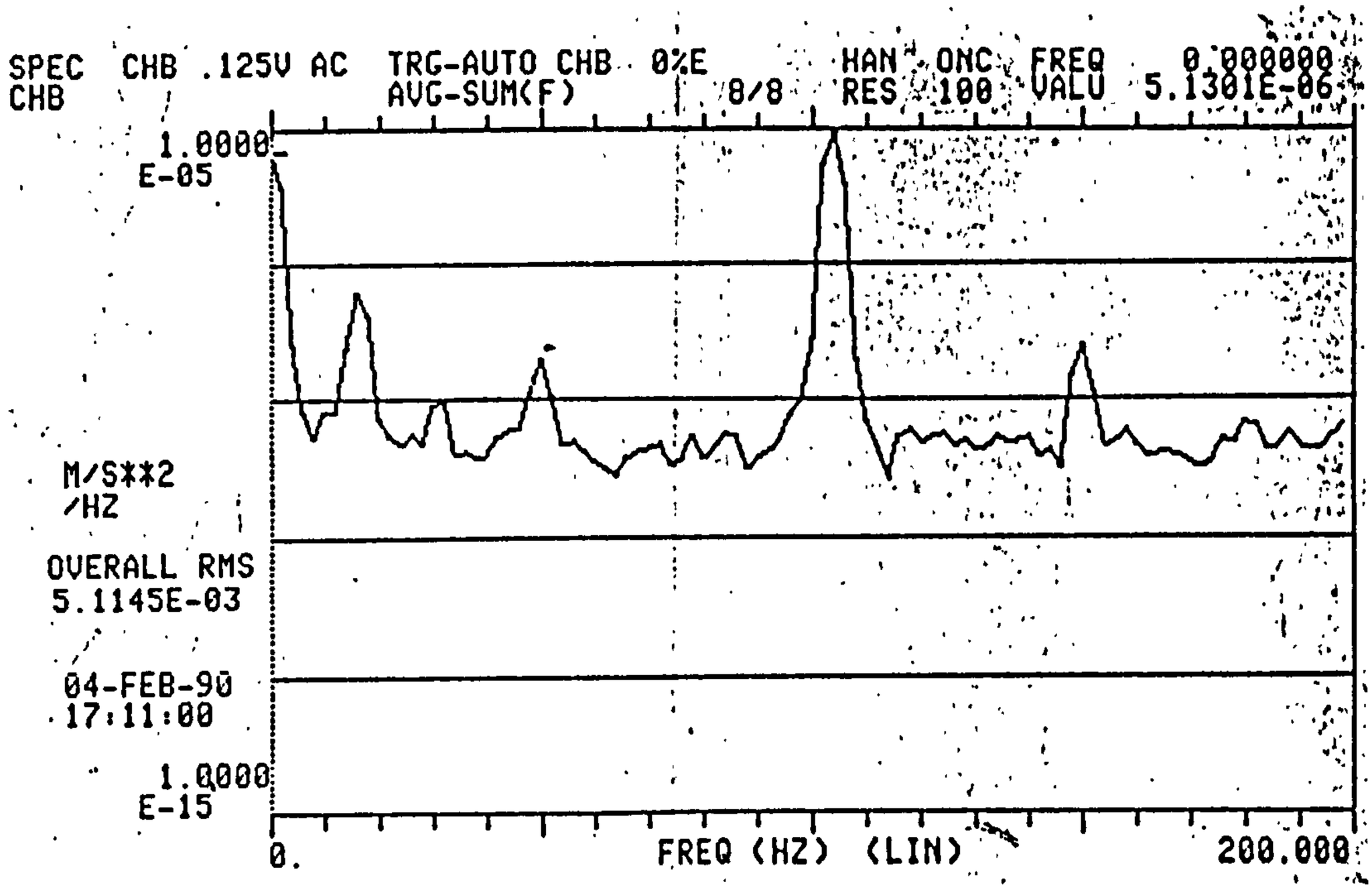

Fig. 7.8a Power spectral density of acceleration response plot (Aluminum Prismatic bar)

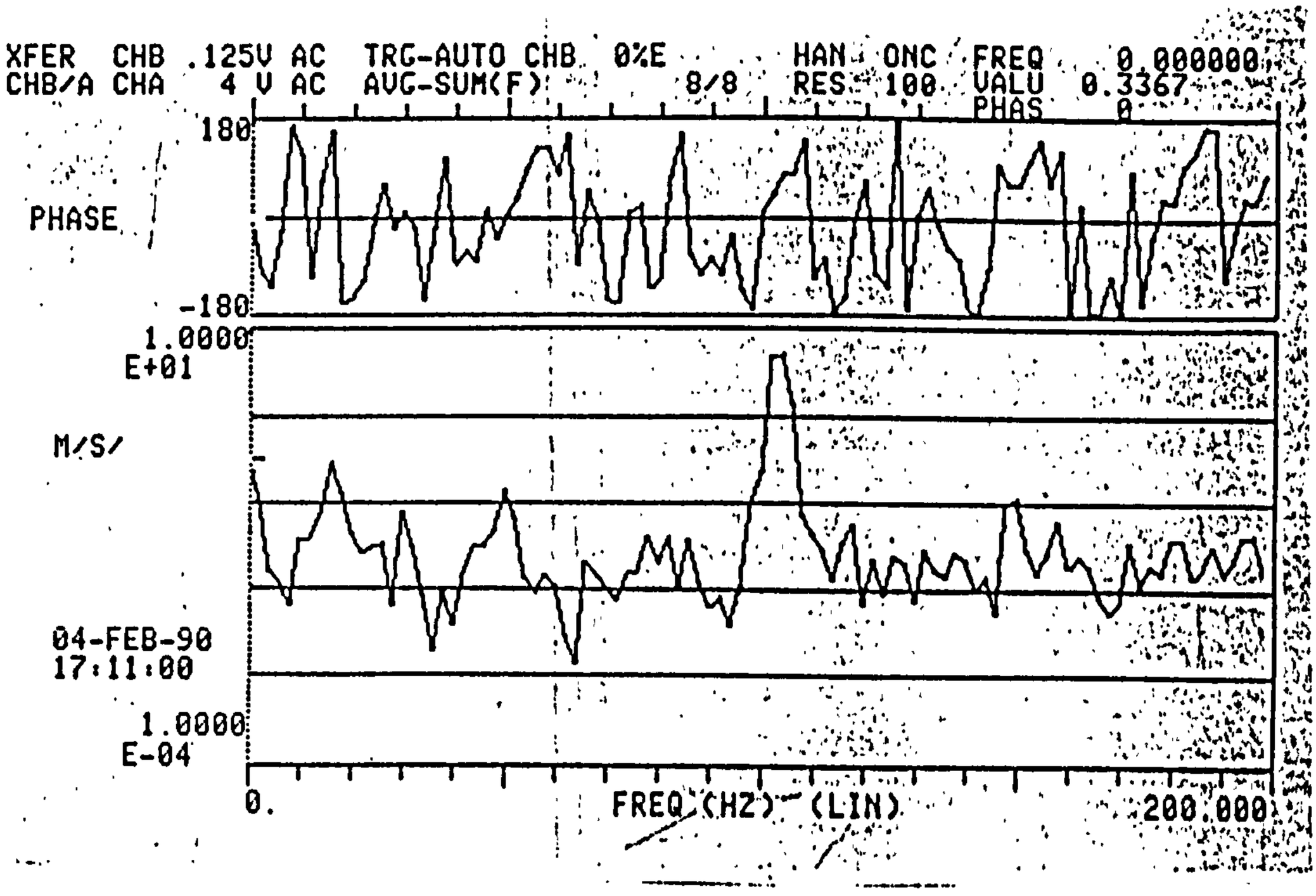

Fig. 7.8b Frequency Response and Phase plot (Aluminum Prismatic bar)

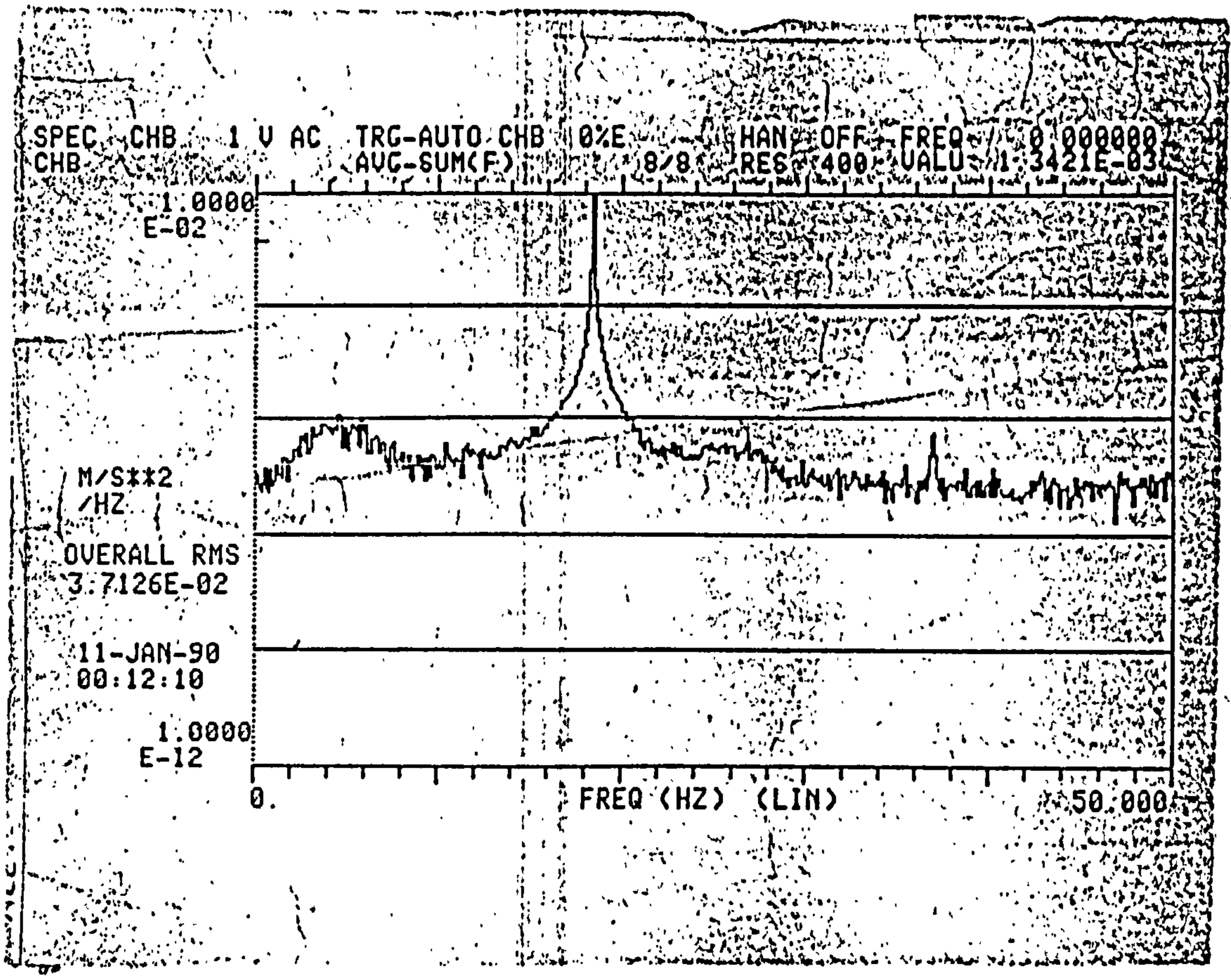

Fig. 7.9 a Power Spectral Density plot (acc. resp.)
(Aluminum Prismatic bar)

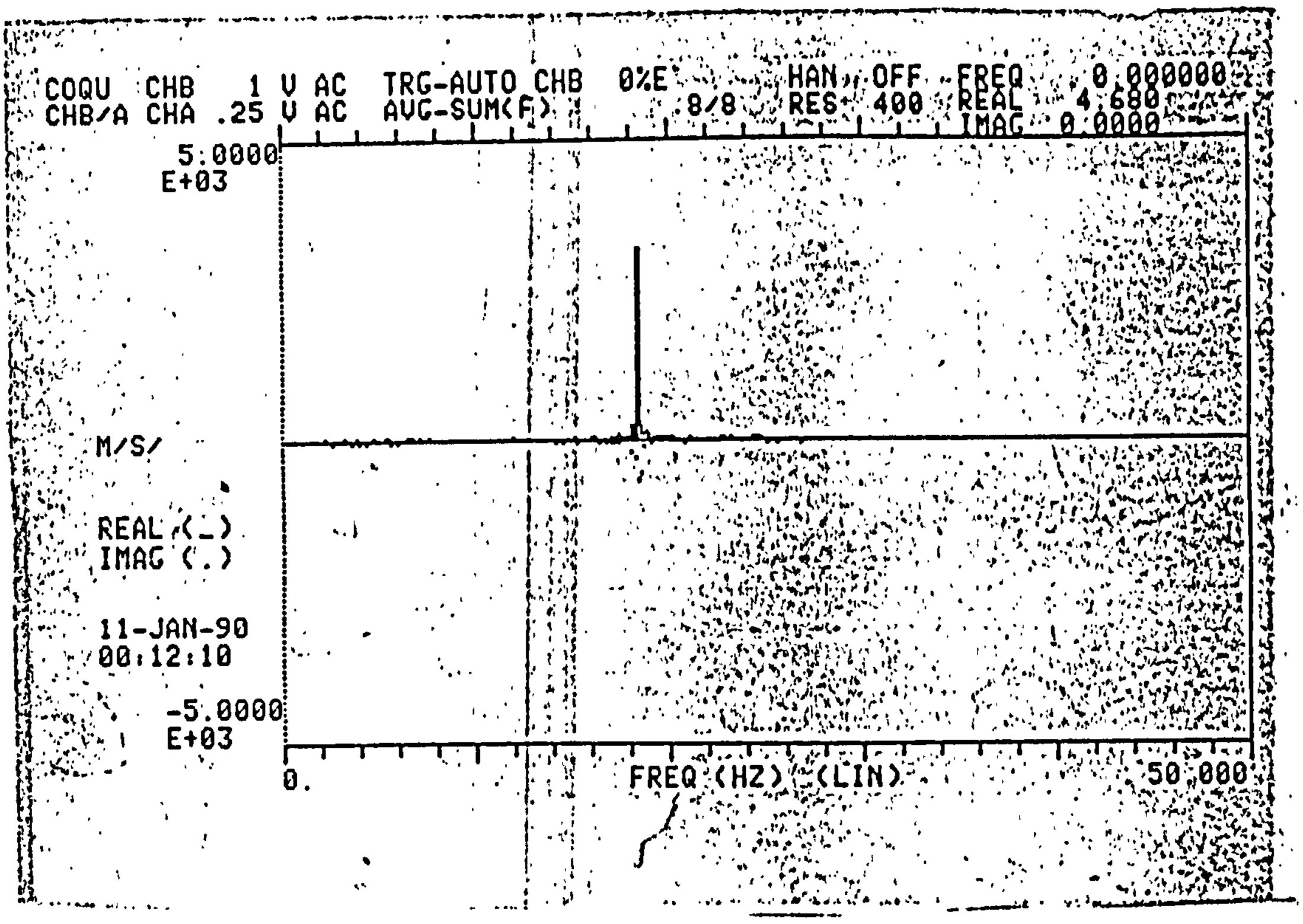

Fig. 7.9 b Real and Imaginary parts plotted against frequency
(Aluminum Prismatic bar)

Figure 7.10 Normal mode shapes for aluminium prismatic bar structure

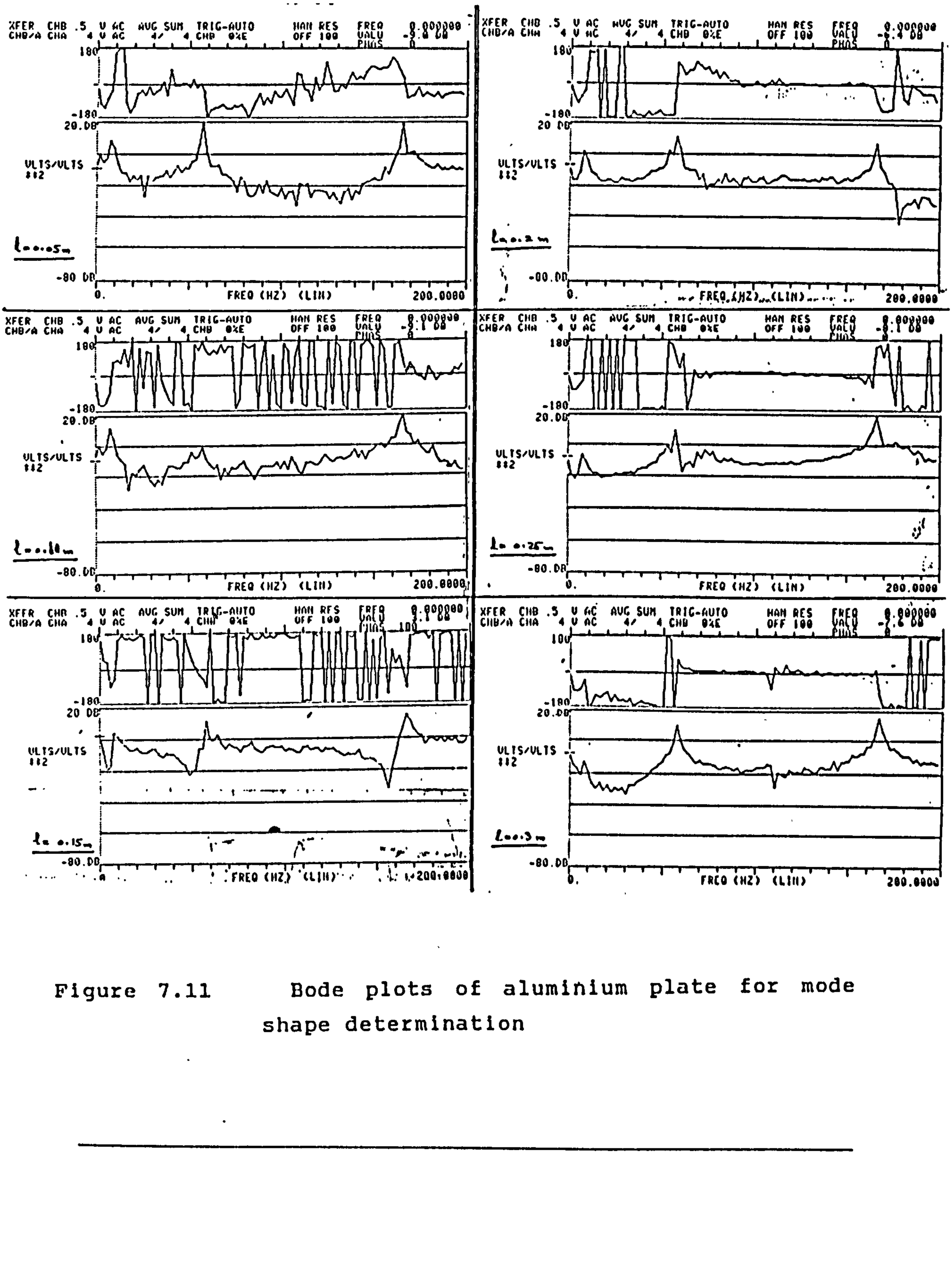

Figure 7.11 Bode plots of aluminium plate for mode shape determination

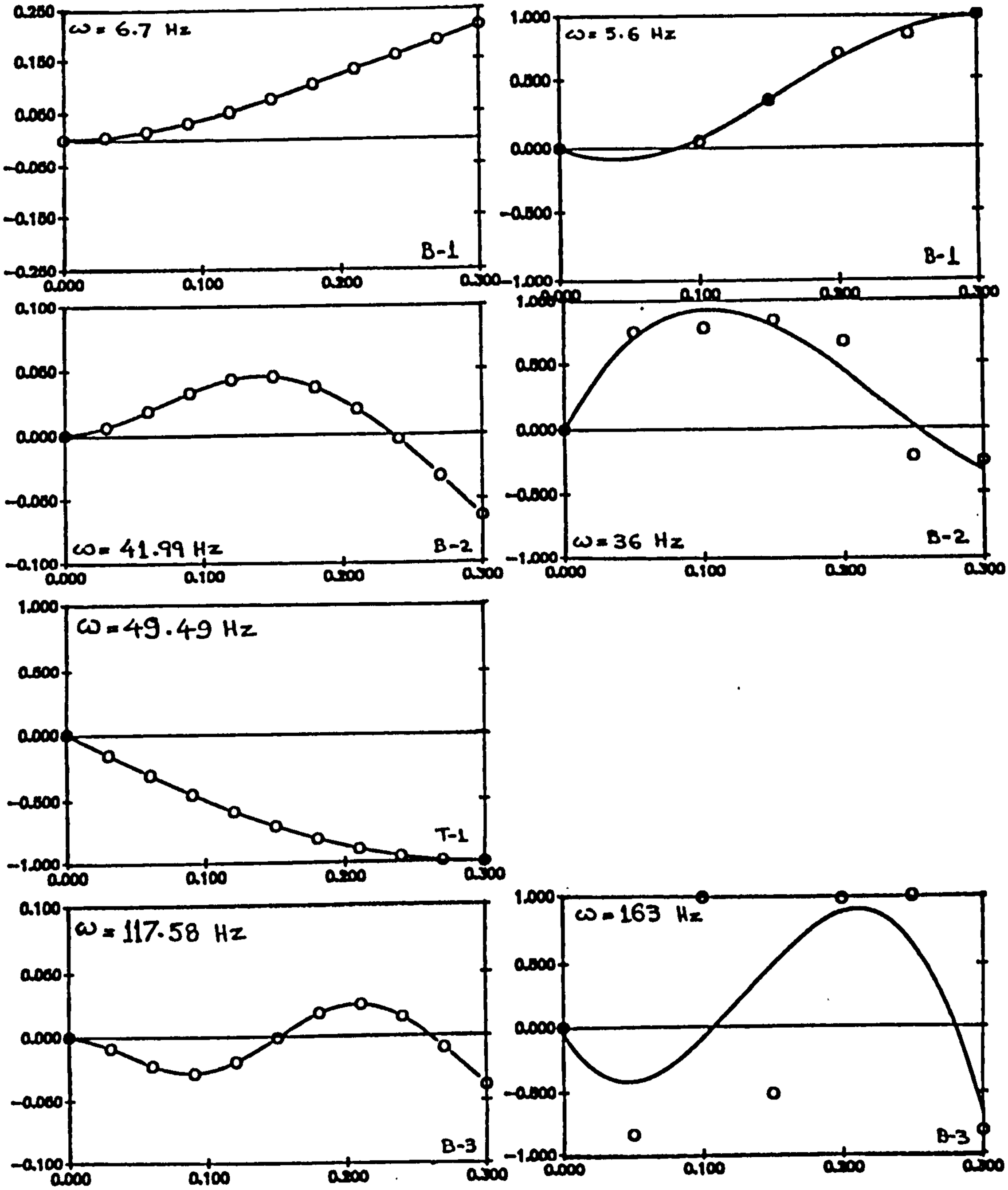

THEORETICAL EXPERIMENTAL

Figure 7.12 Comparison of theoretical and experimental normal mode shapes for the aluminium plate structure
x - axis : length (m)
y - axis : nondimensionalised vertical displacement

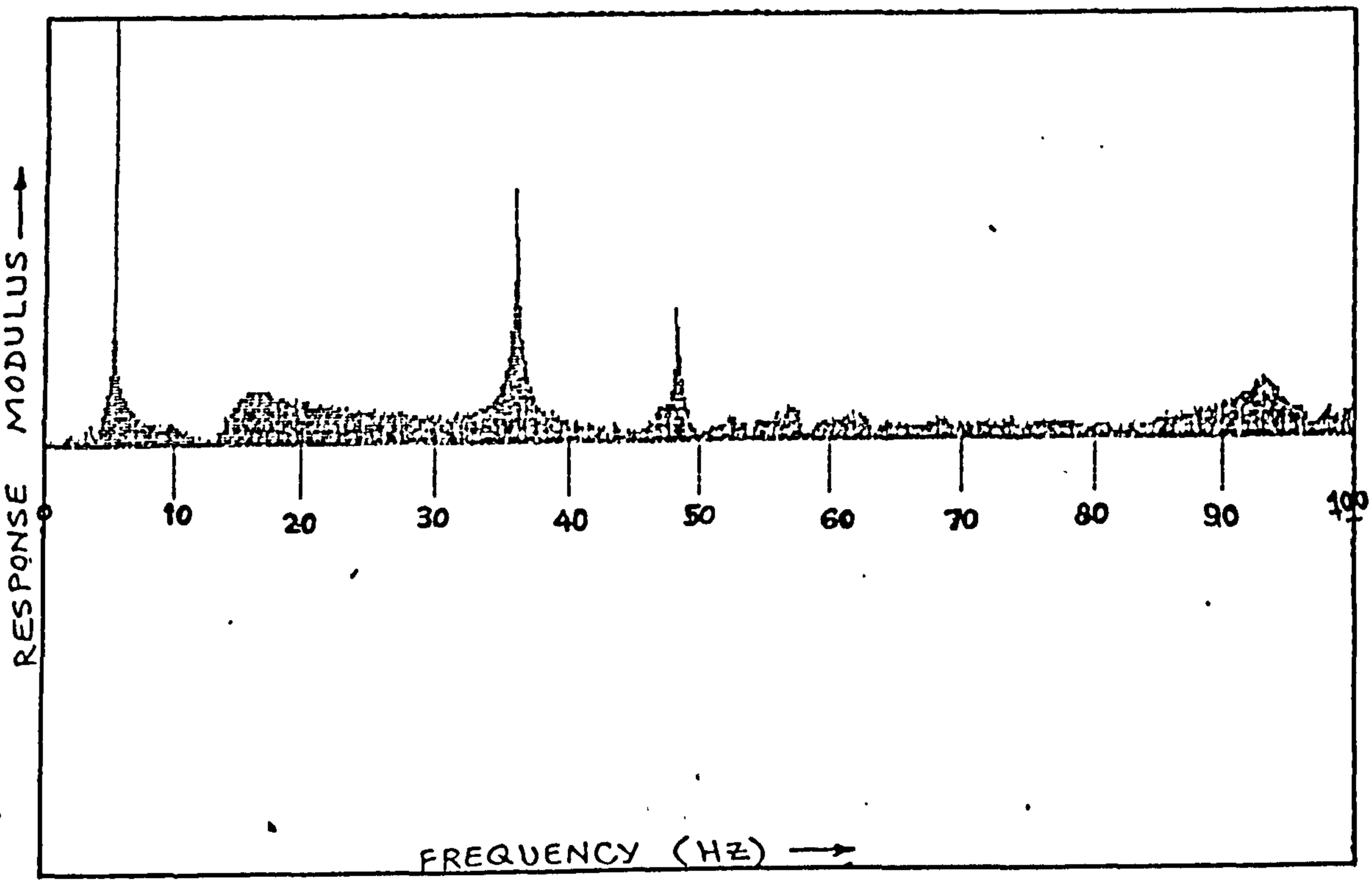

Figure 7.13 Modulus of acceleration response vs frequency of aluminium plate

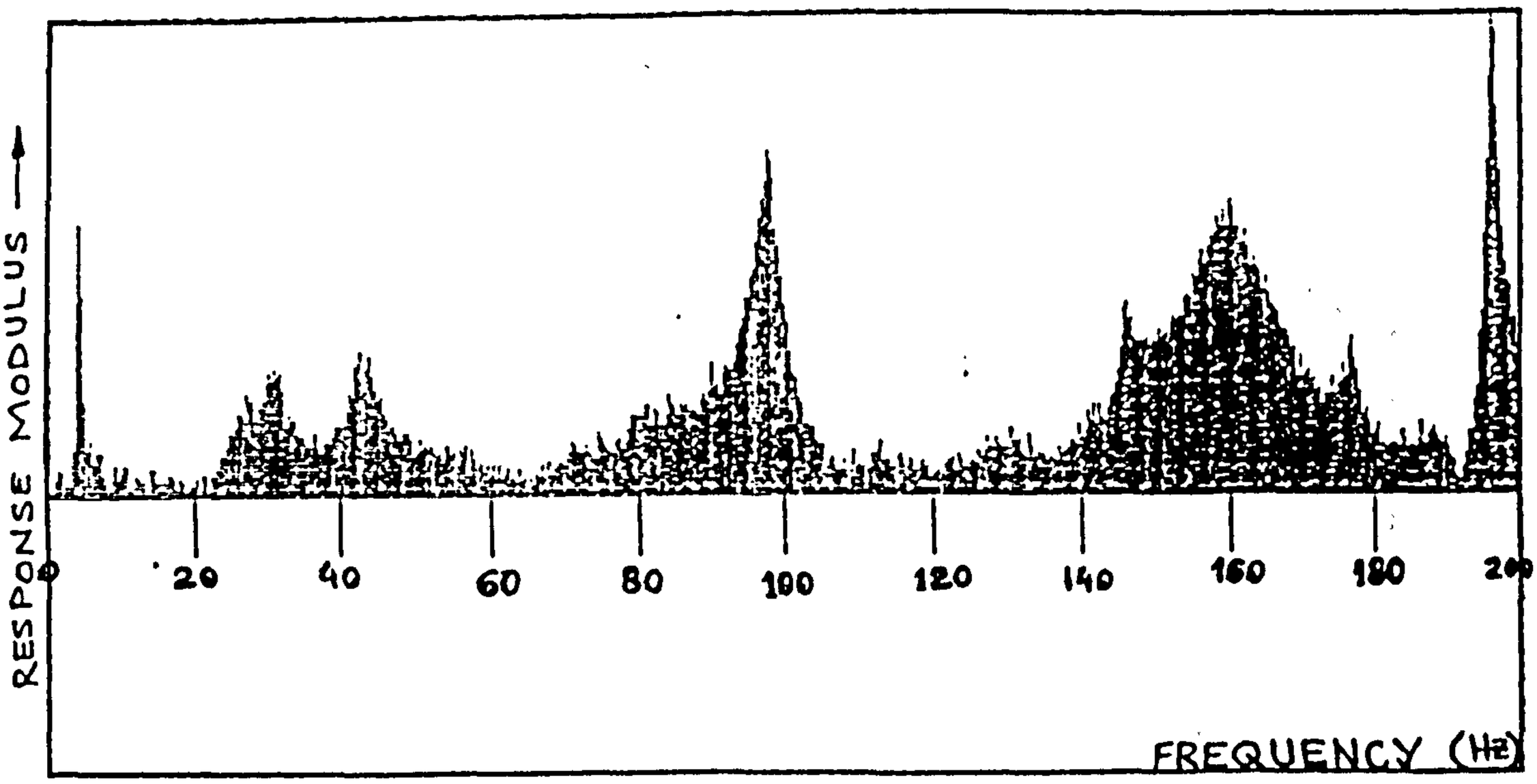

Figure 7.14 Modulus of acceleration response vs frequency of aluminium channel section

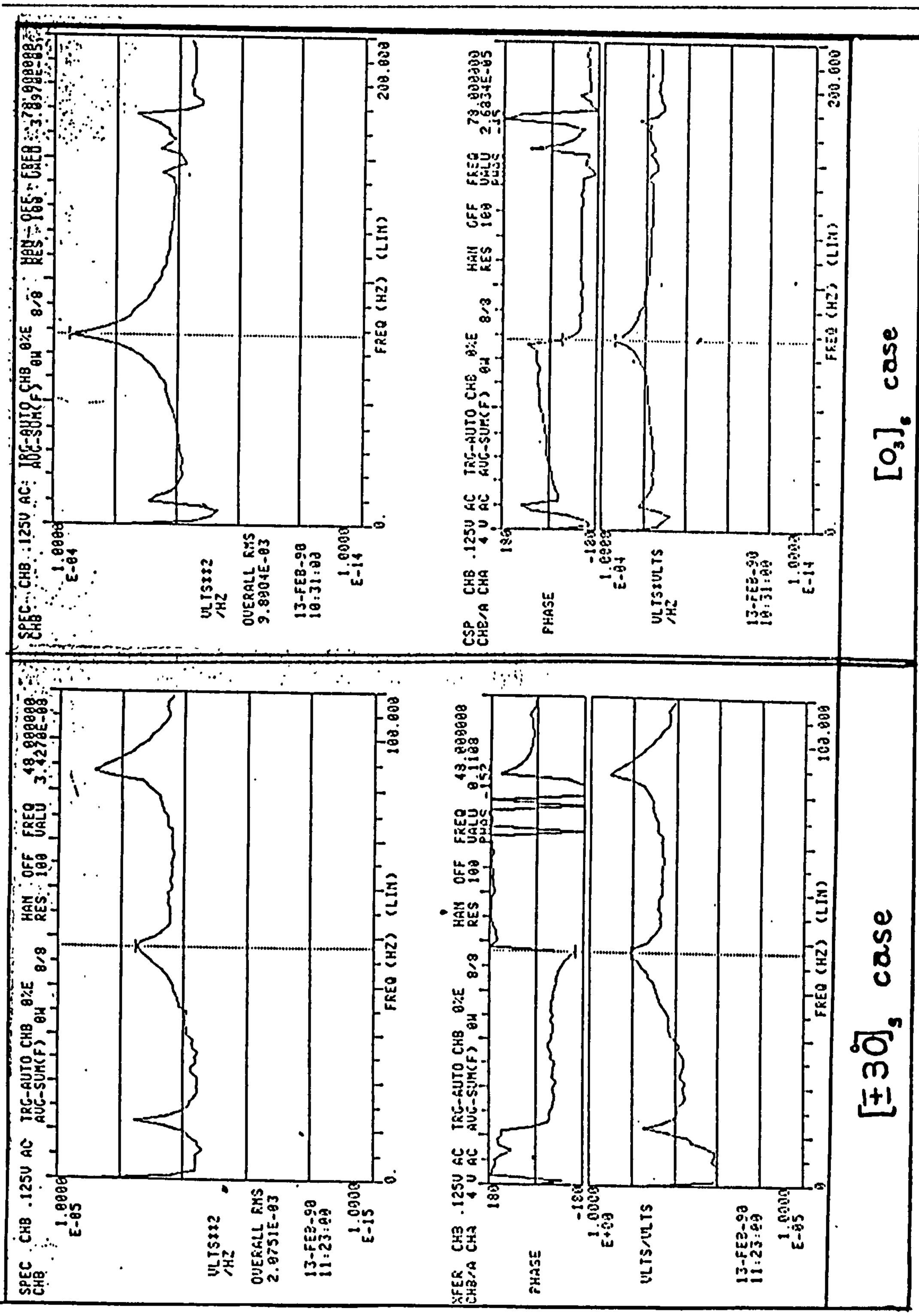

Figure 7.15 Power spectral density plot of acceleration response and Bode plots for composite plates

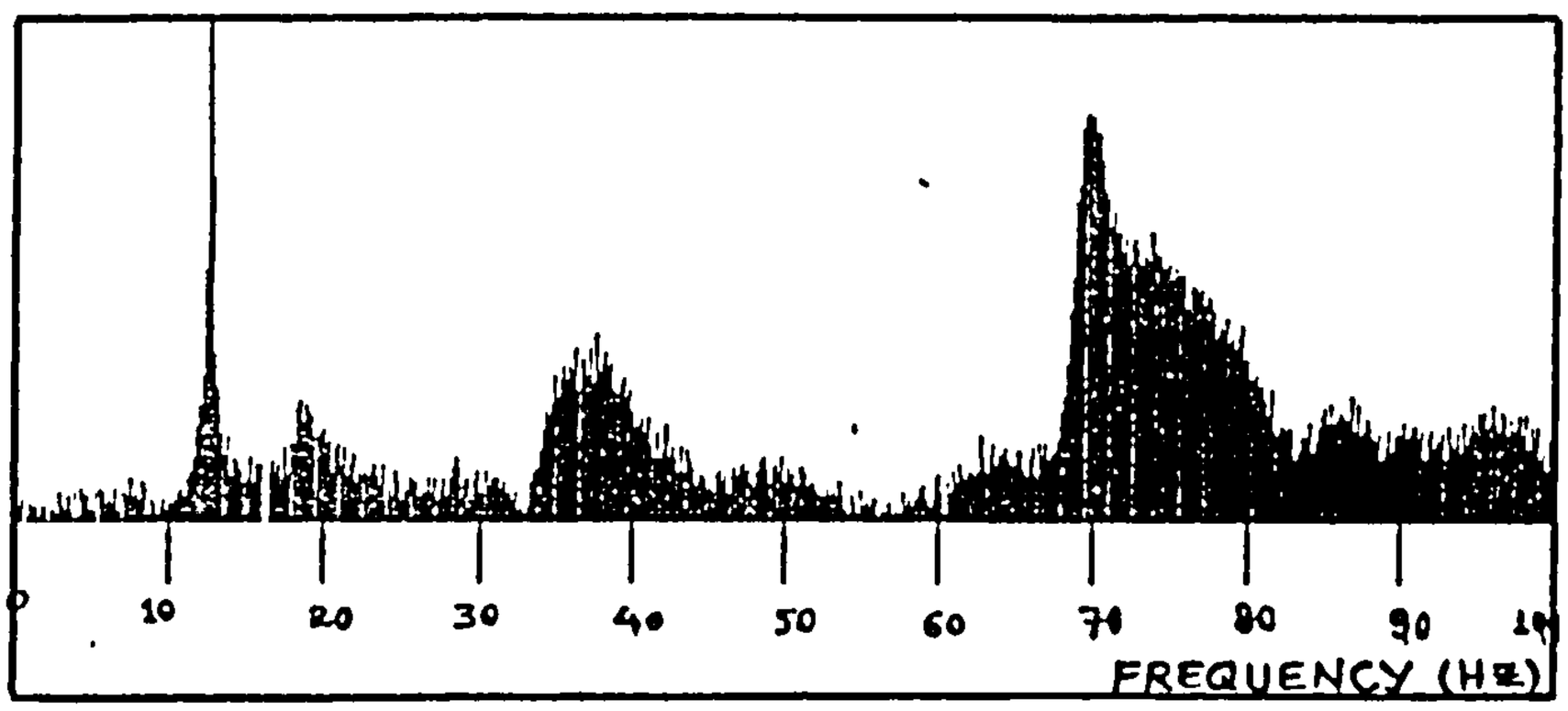

Figure 7.16(a) Modulus of acceleration response vs frequency plot for composite plate of $[0_6]$ case

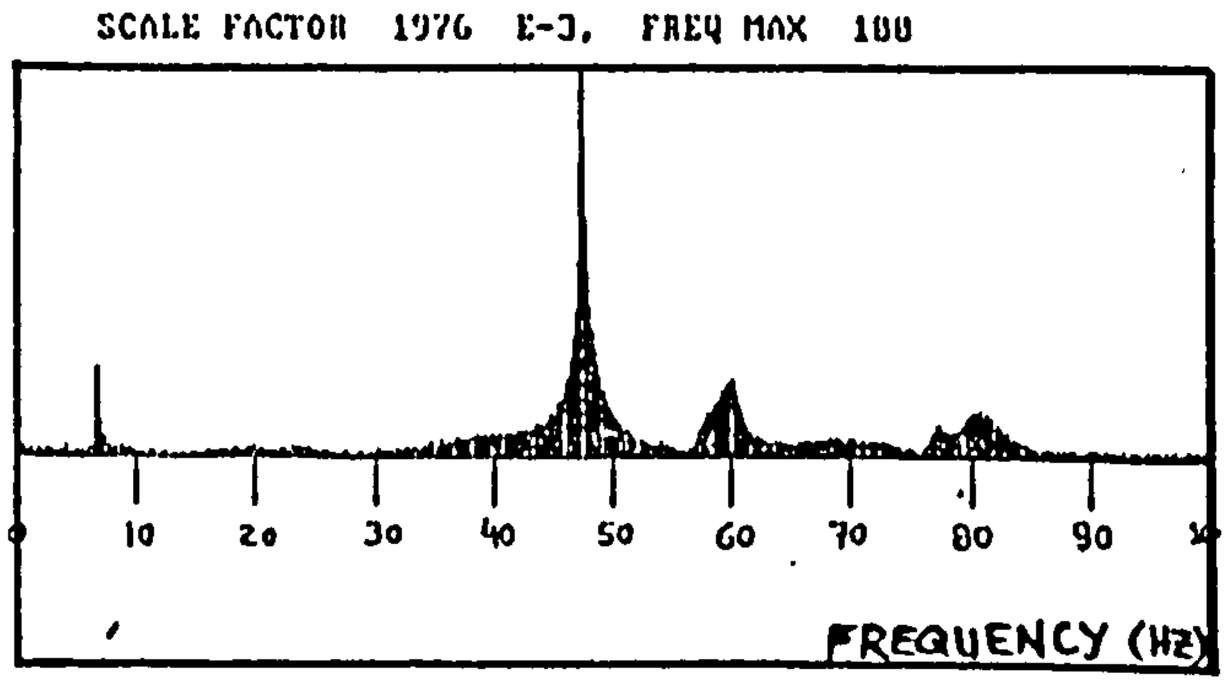

Figure 7.16(b) Modulus of acceleration response vs frequency plot for composite plate of $[\pm 30^{\circ}]_s$ case

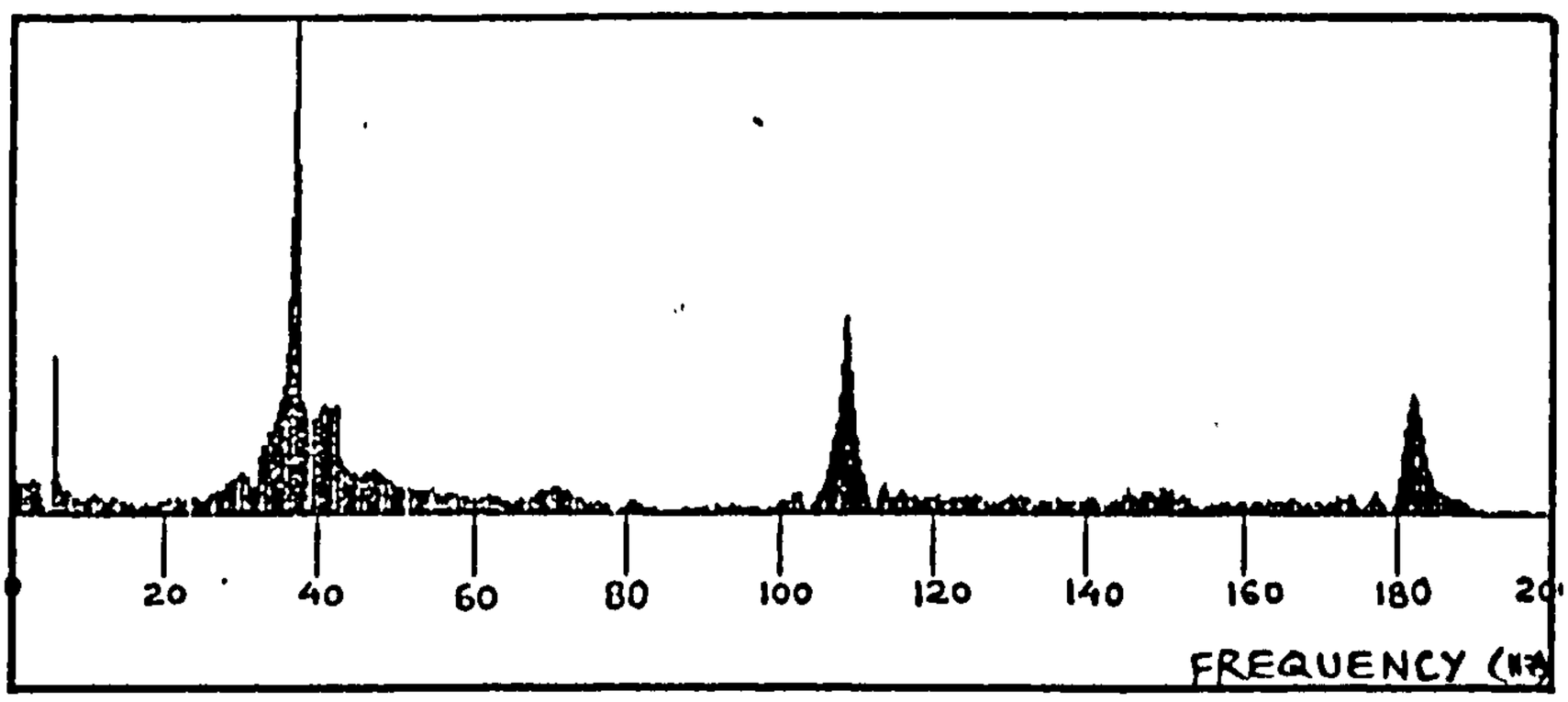

Figure 7.16(c) Modulus of acceleration response vs frequency plot for composite plate of $[\pm 45^{\circ}/0]_s$ case

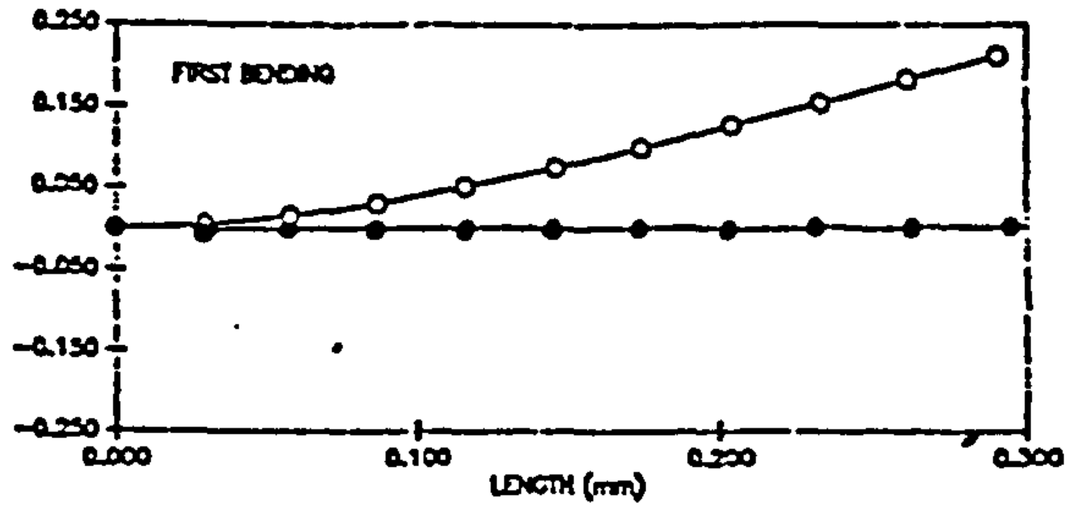

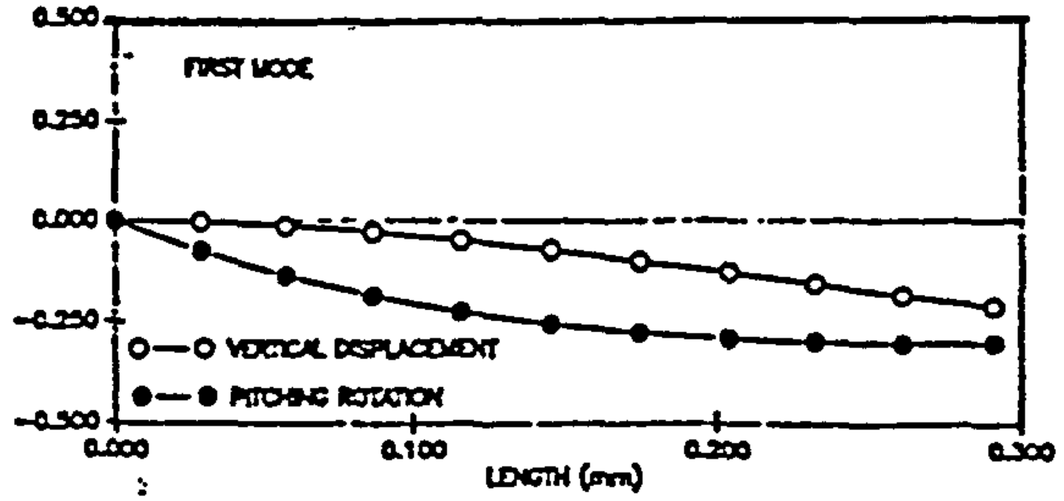

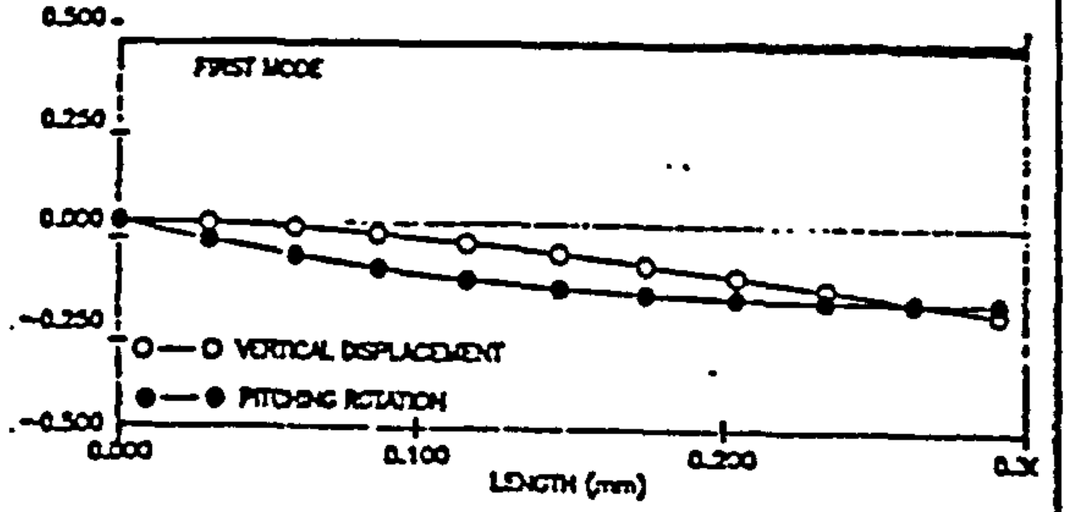

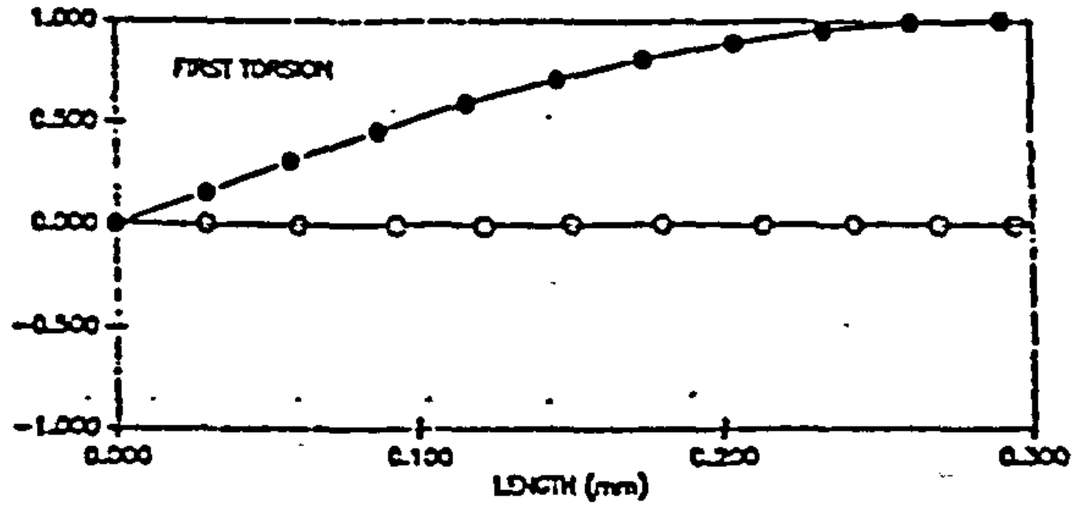

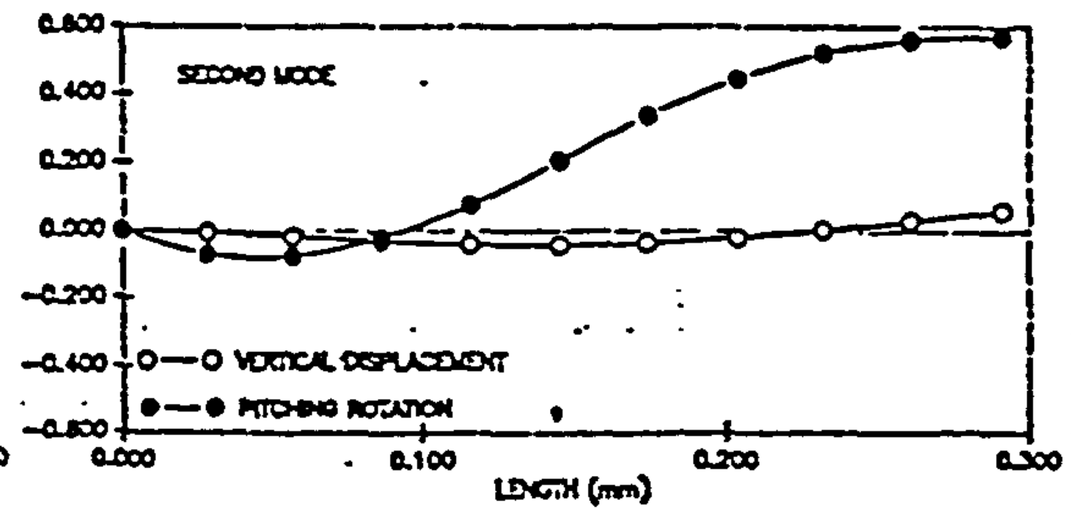

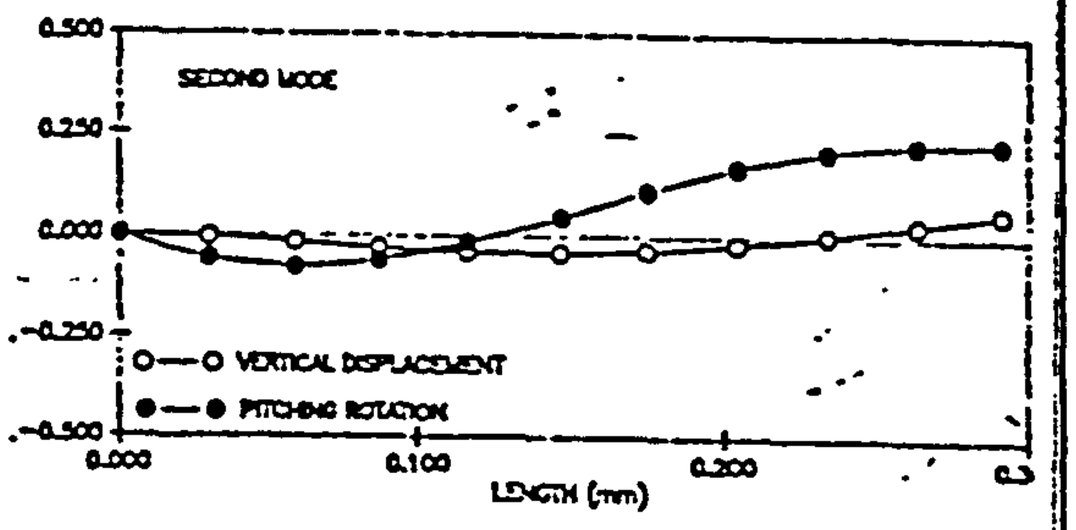

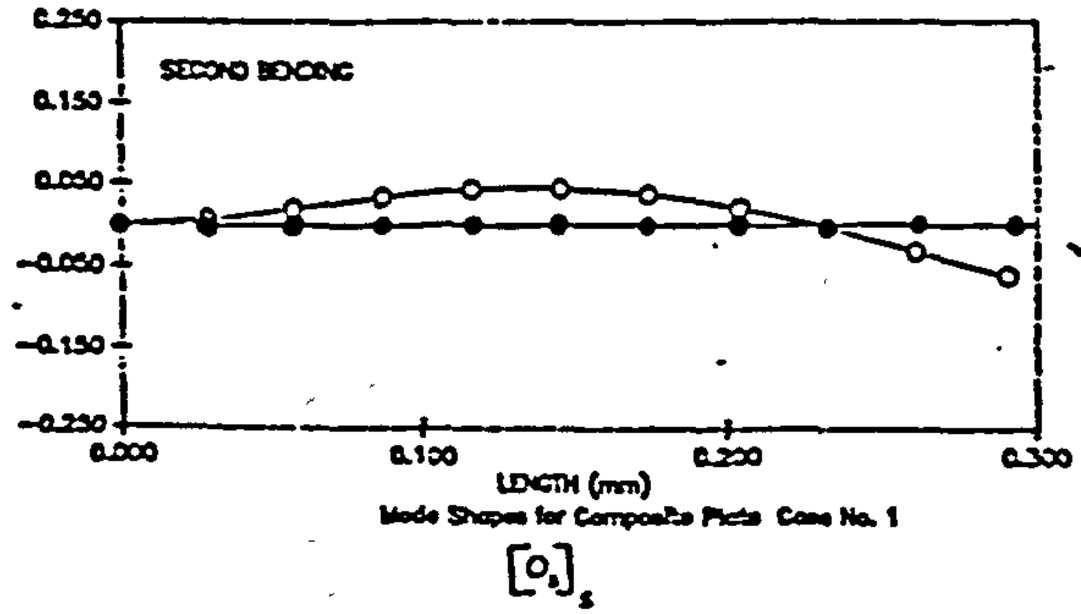

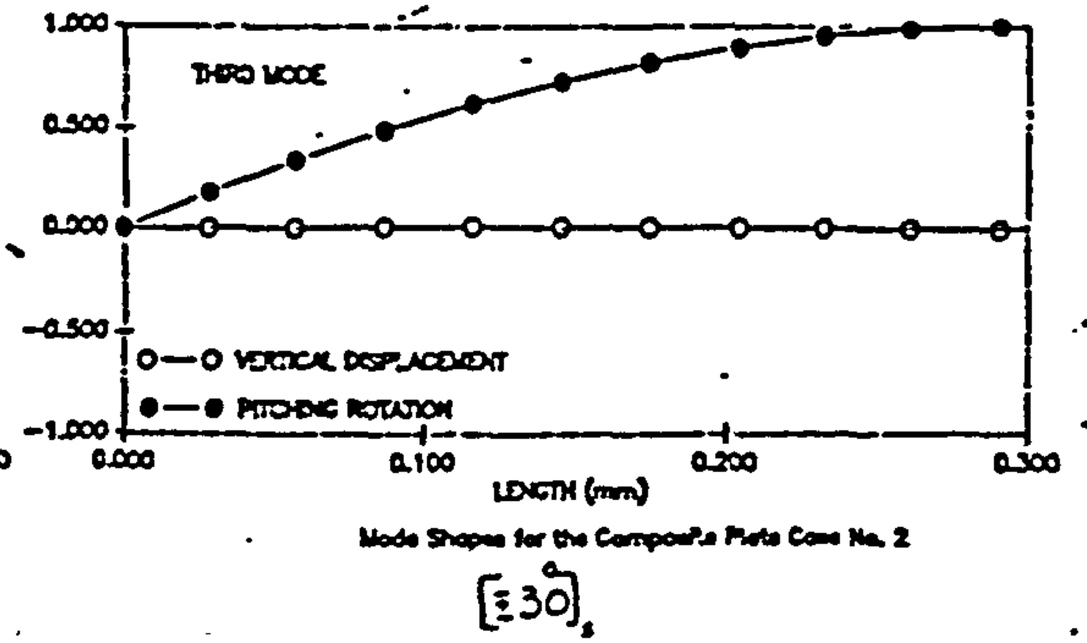

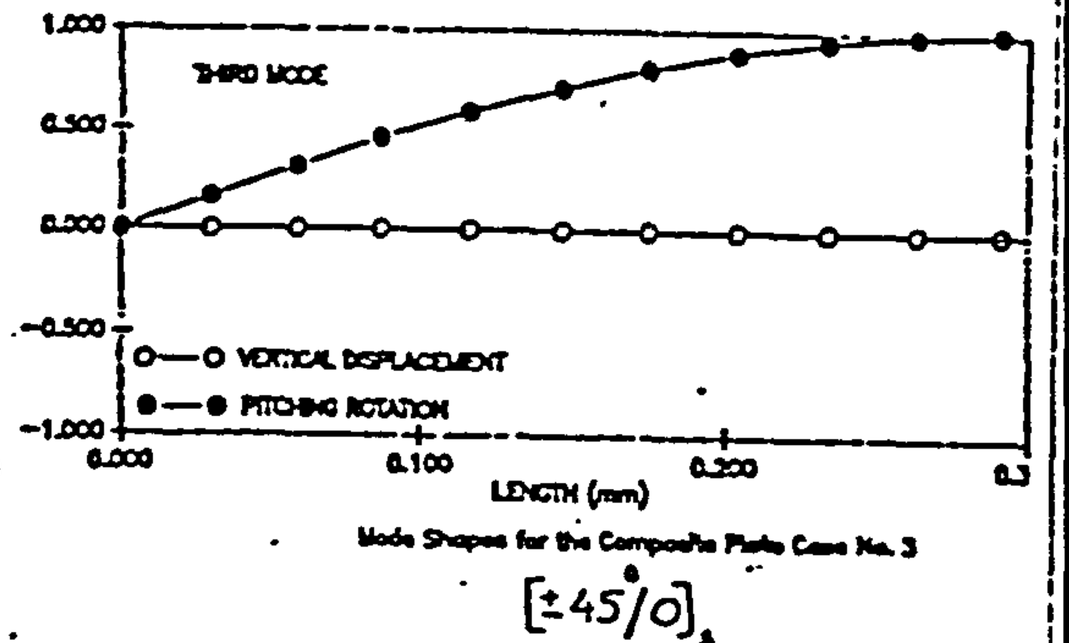

Figure 7.17 Normal mode shapes for composite plates $[0_3]_s$, $[\pm 30]_s$, $[\pm 45/0]_s$

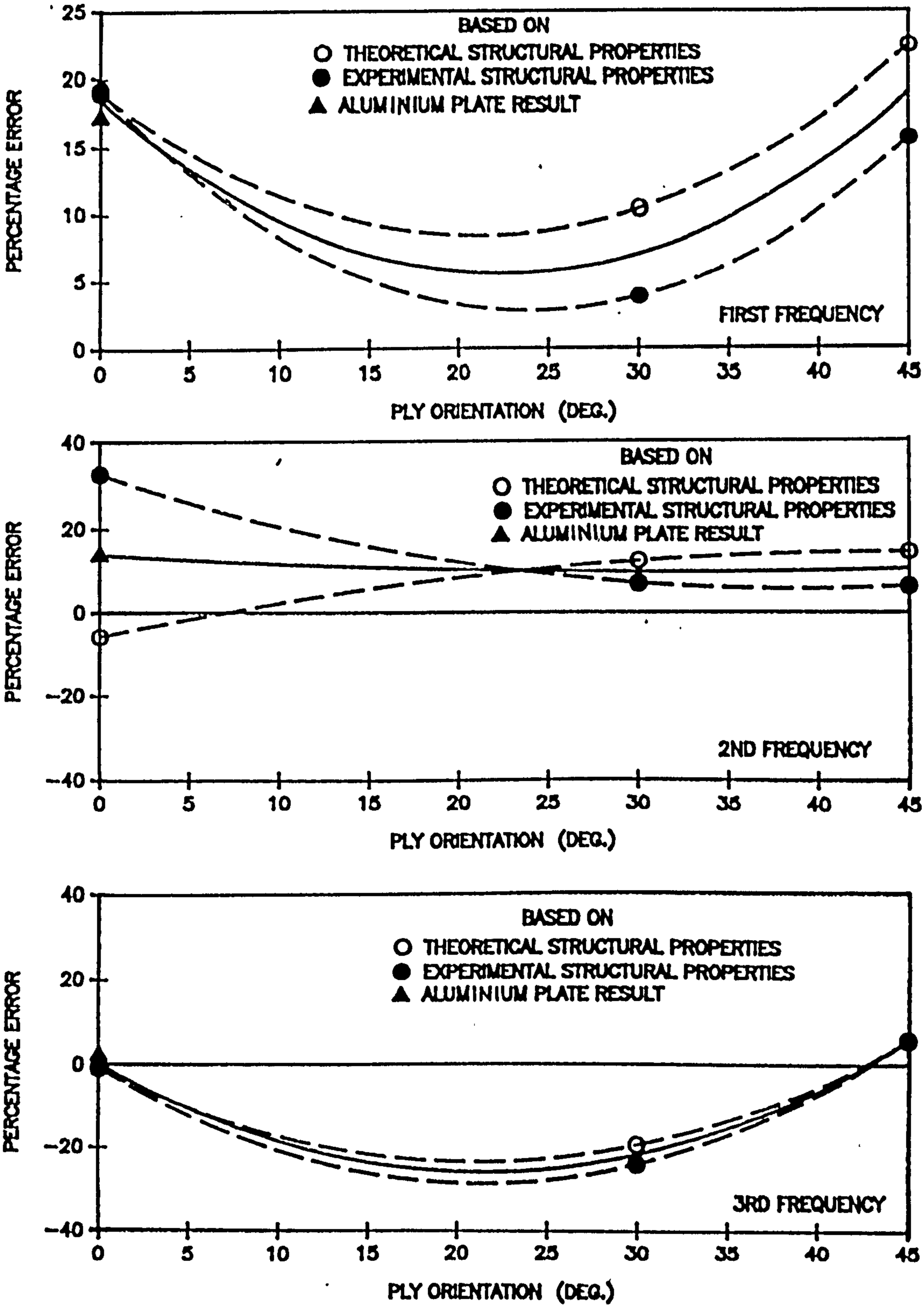

FIG. 7.18 Effect of Ply orientation on the percentage error in prediction of natural frequencies based on theoretical and experimental structural properties

ANGLE NO. 3

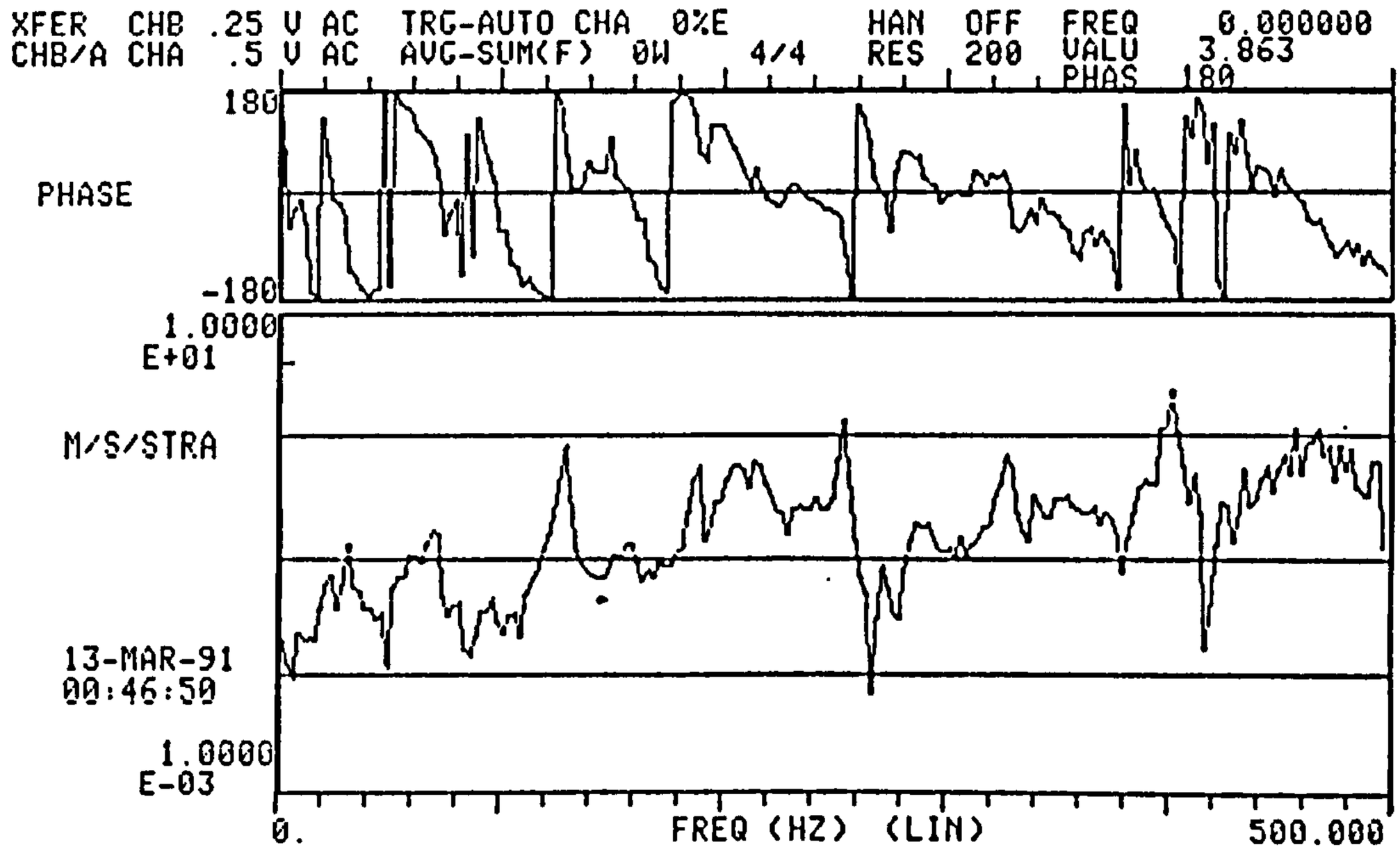

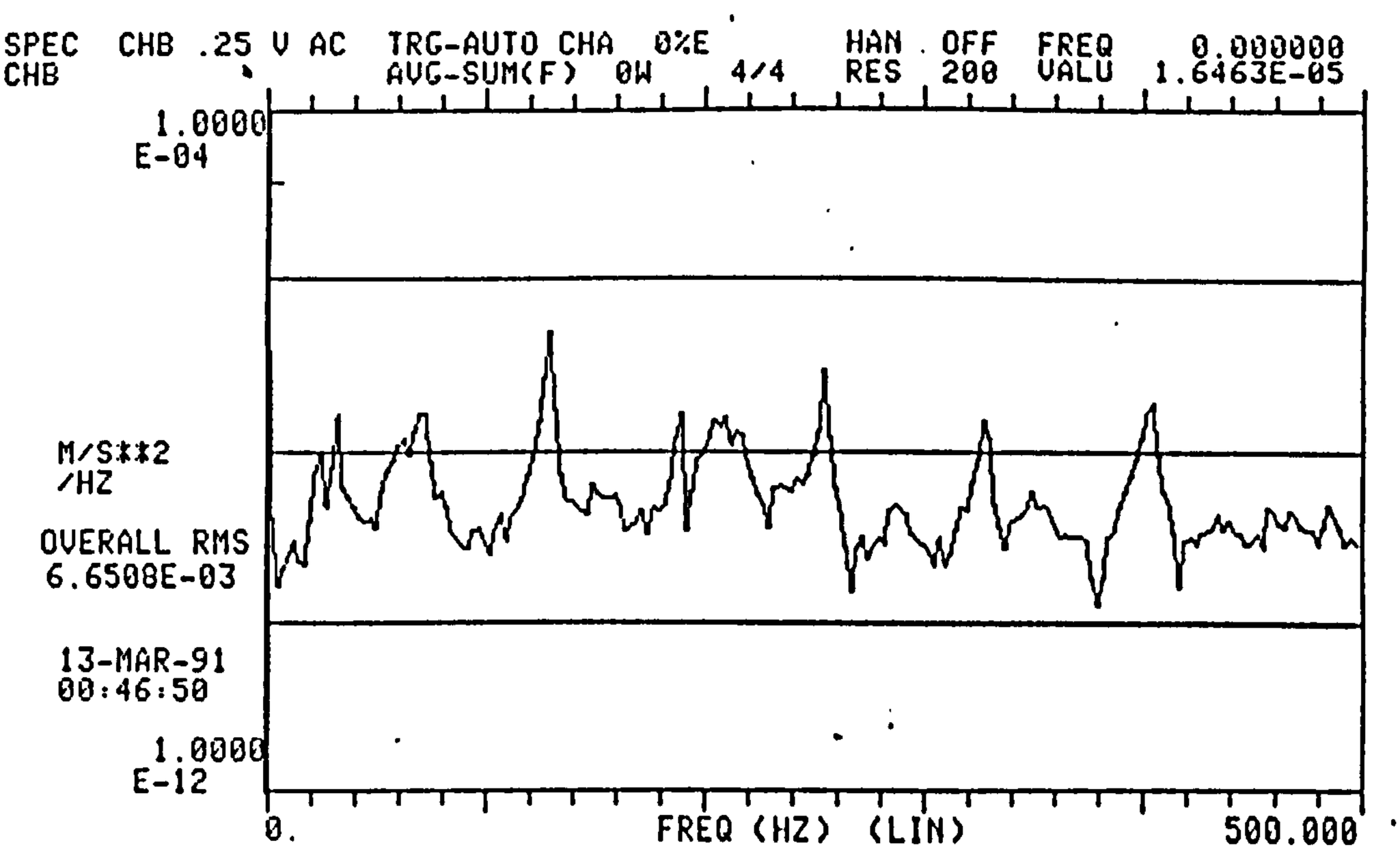

Figure 7.19 Bode plot and PSD of acceleration response plot for a typical angle section

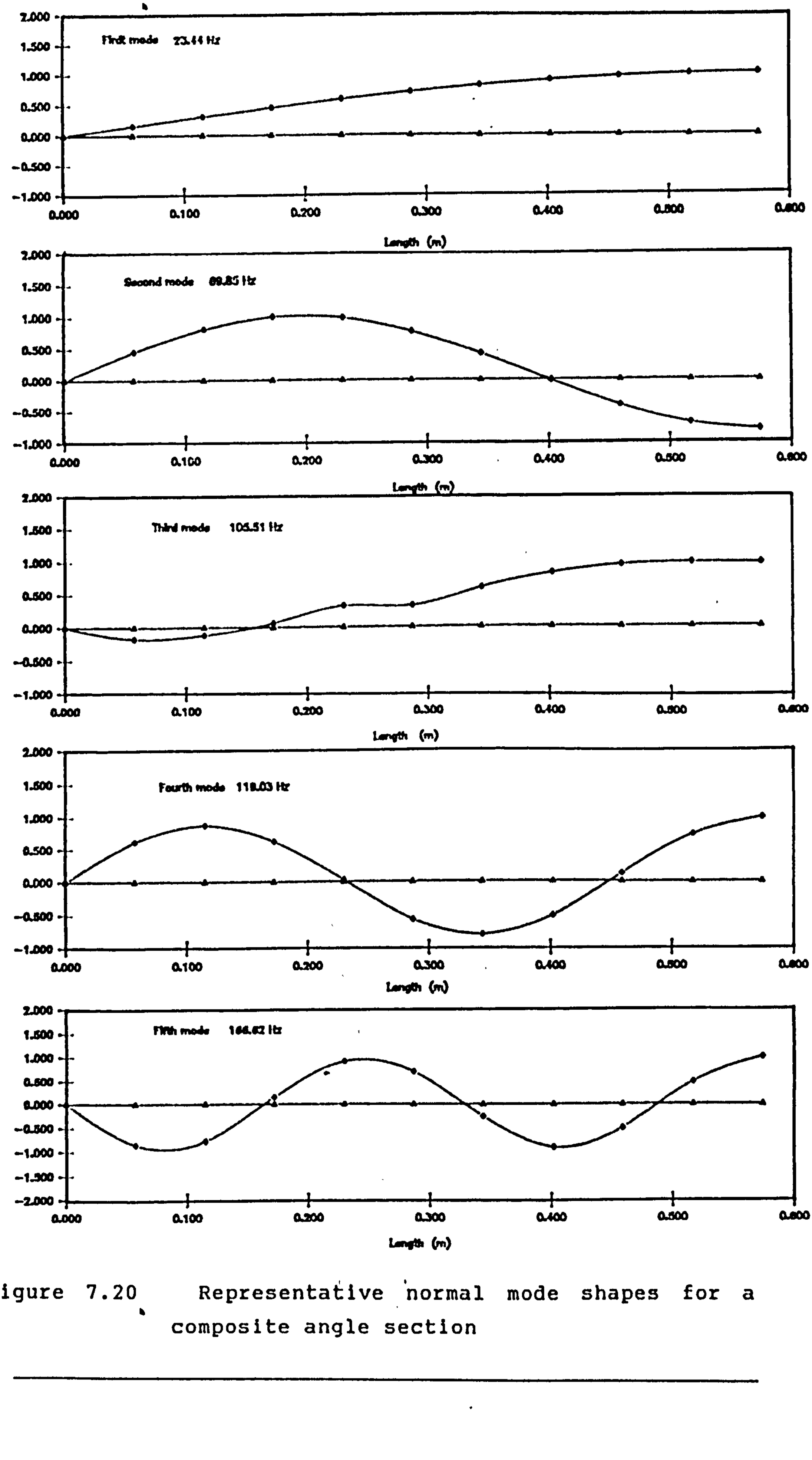

Figure 7.20 Representative normal mode shapes for a composite angle section

Figure 7.21 Representative normal mode shapes for a composite tee section

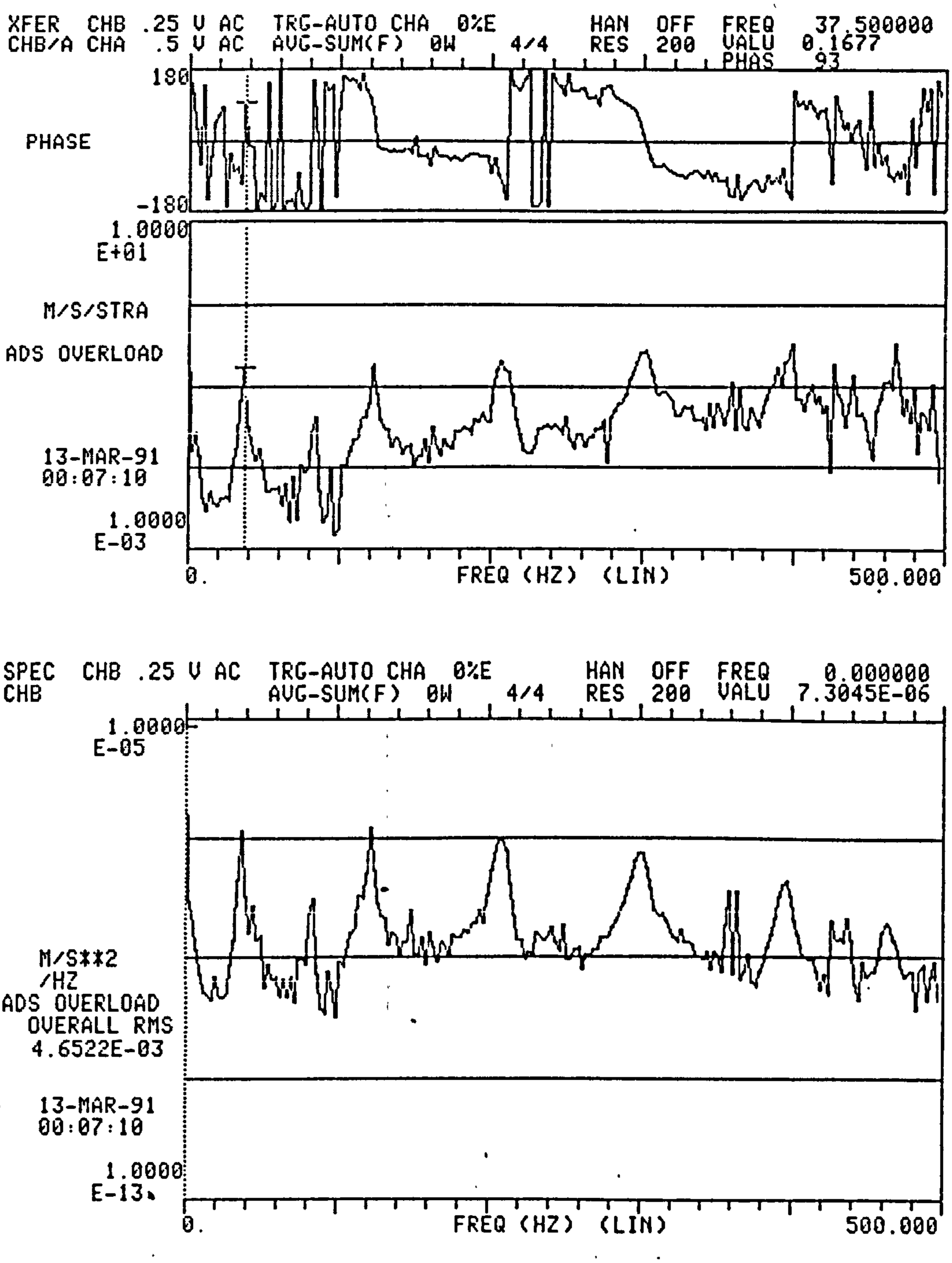

Figure 7.22 Bode plot and PSD of acceleration response plot for a typical tee section

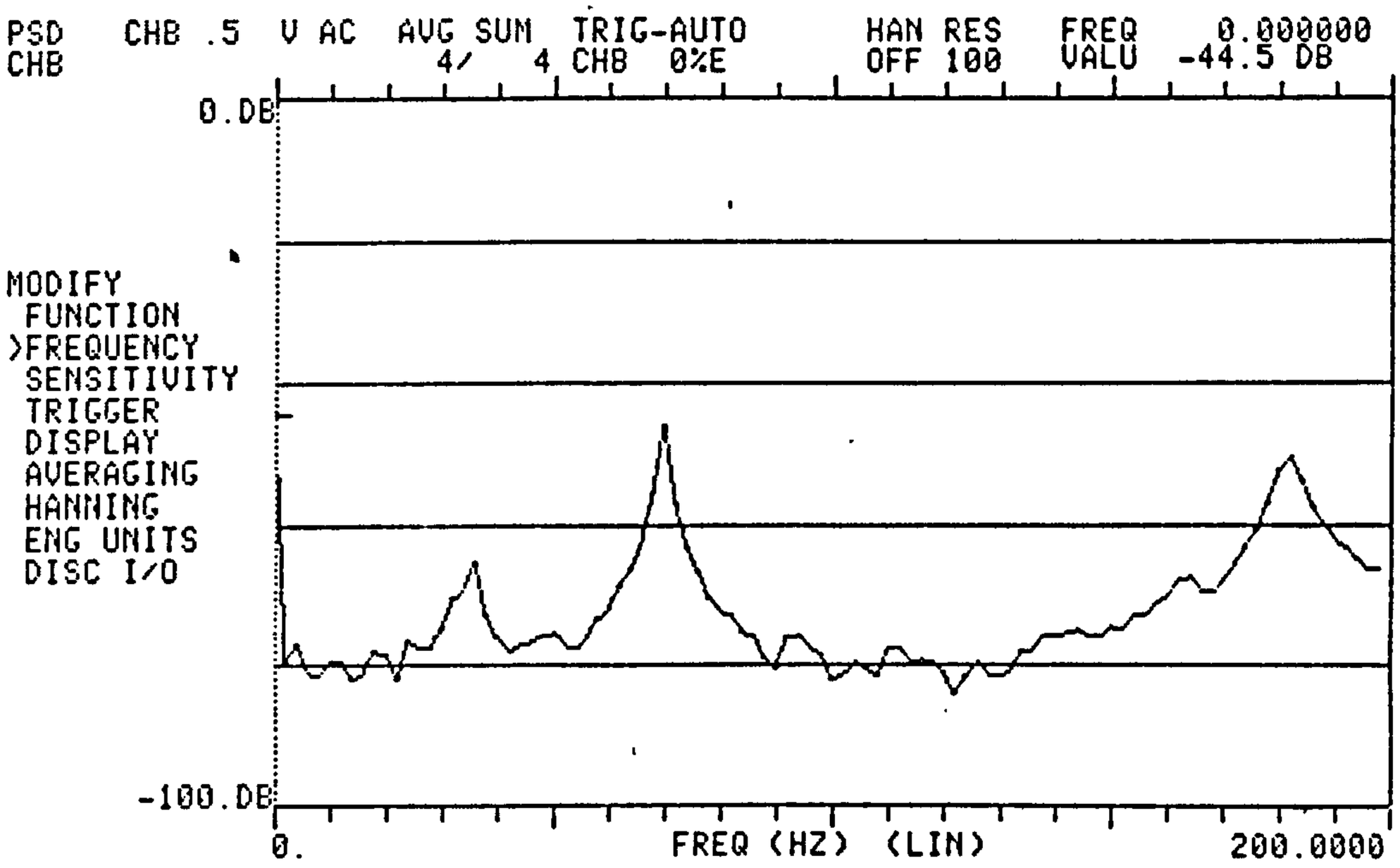

Figure 7.23(a) Power spectral density of acceleration response plot for a typical composite channel section

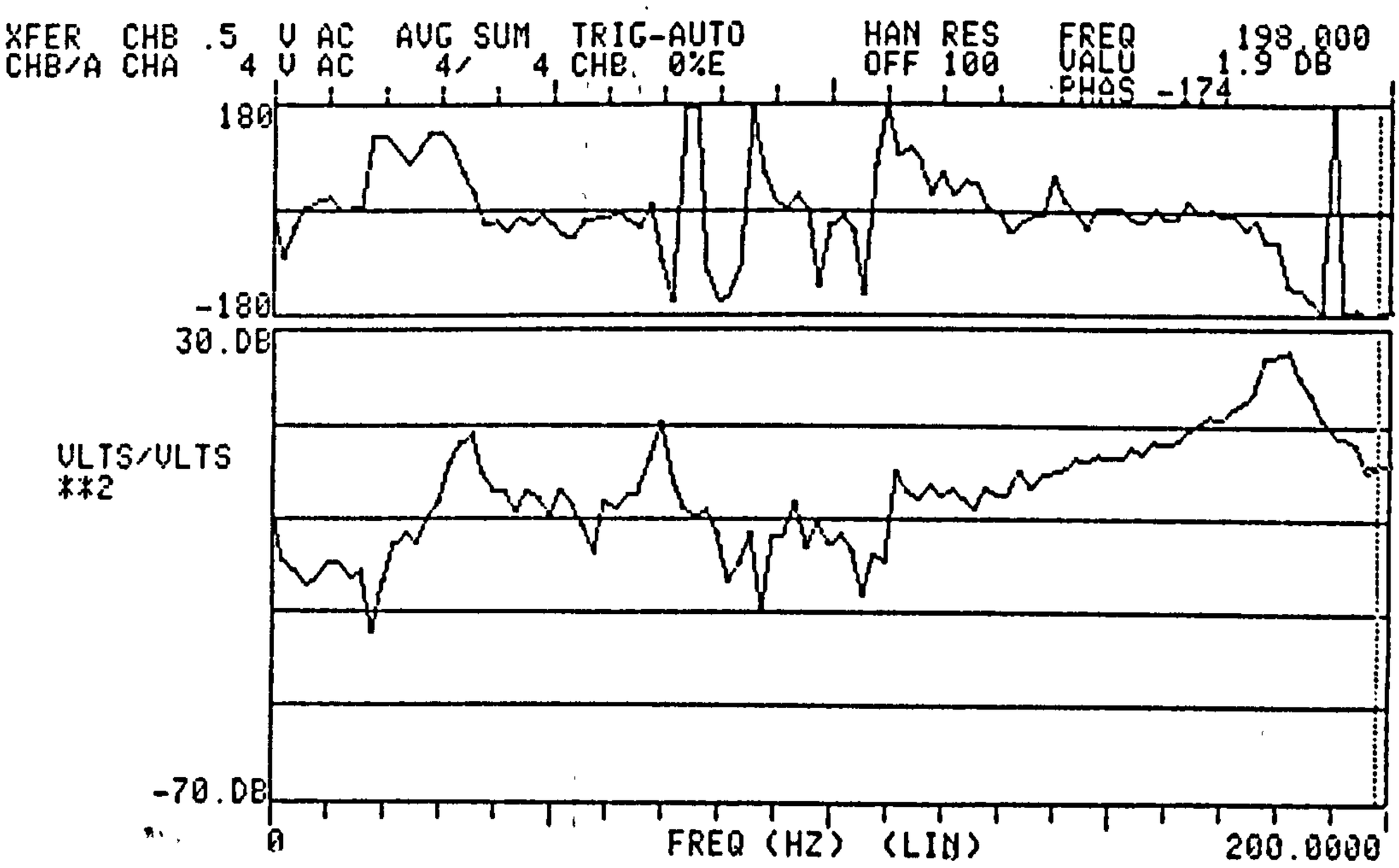

Figure 7.23(b) Bode plot for a typical composite channel section

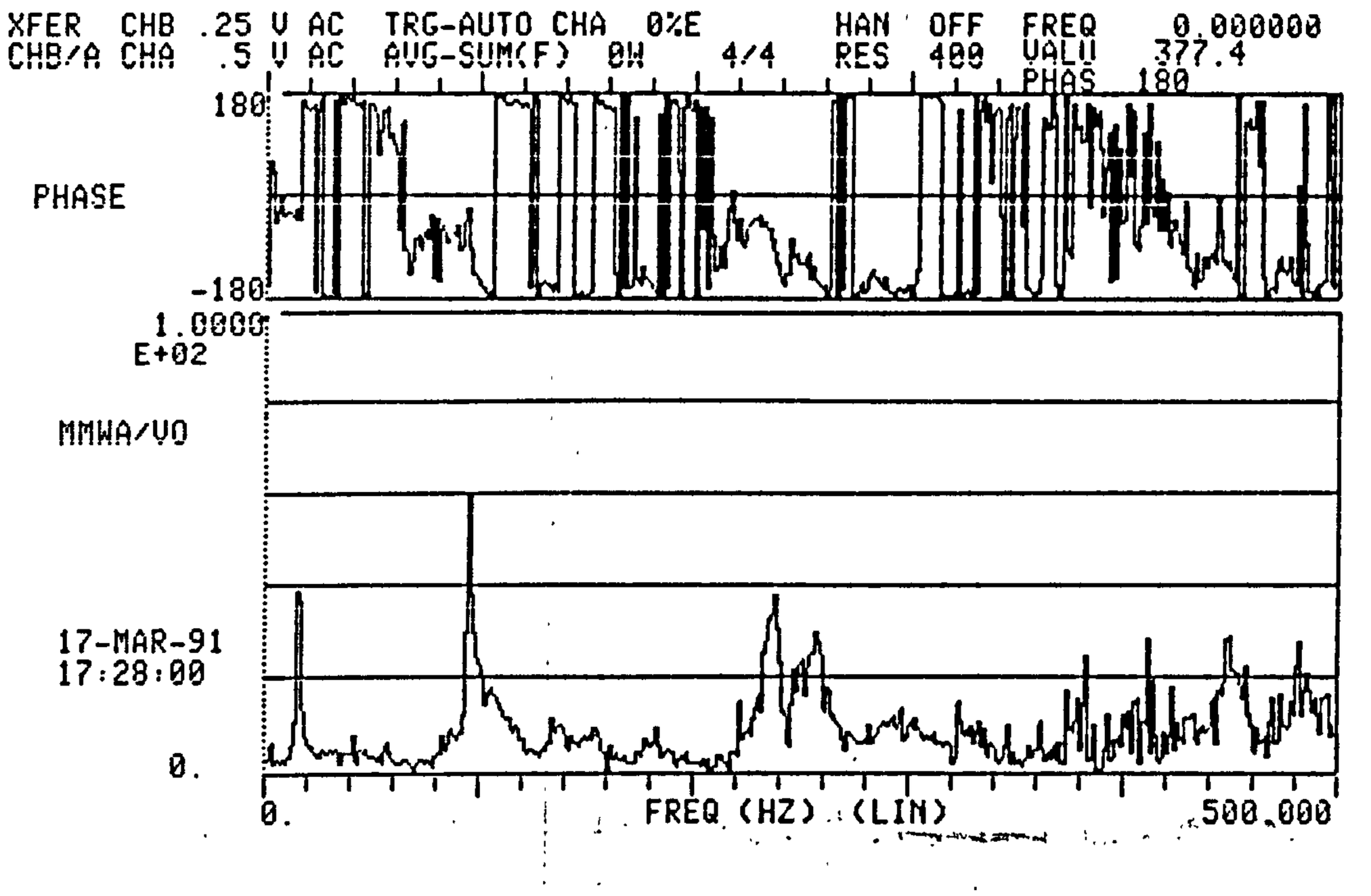

Figure **7.24a** Frequency Response plot for W-DMS-3A wing when excited at the tip

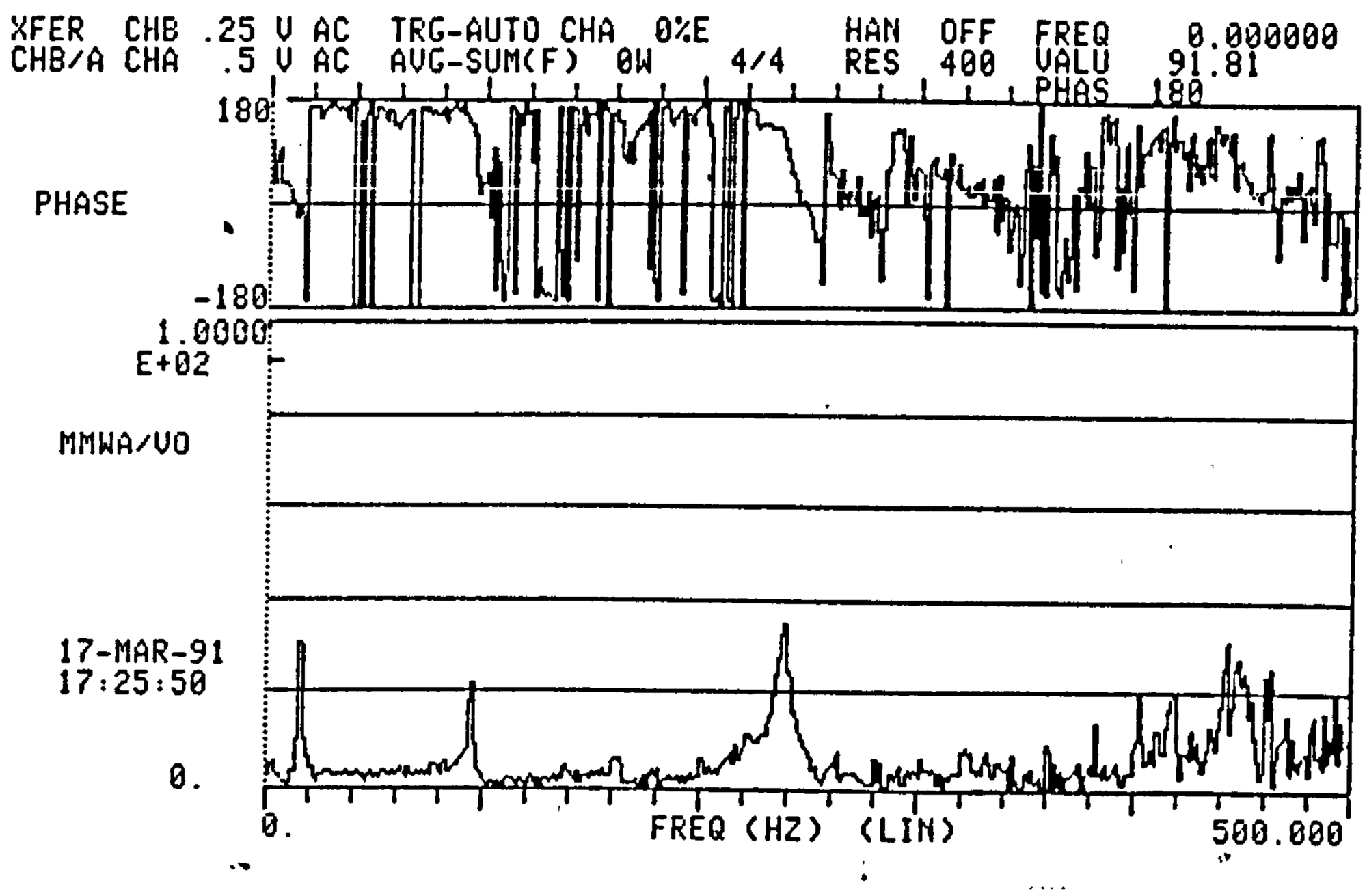

Figure **7.24b** Frequency Response plot for W-DMS-3A wing when excited at 3/4 of the length from the root.

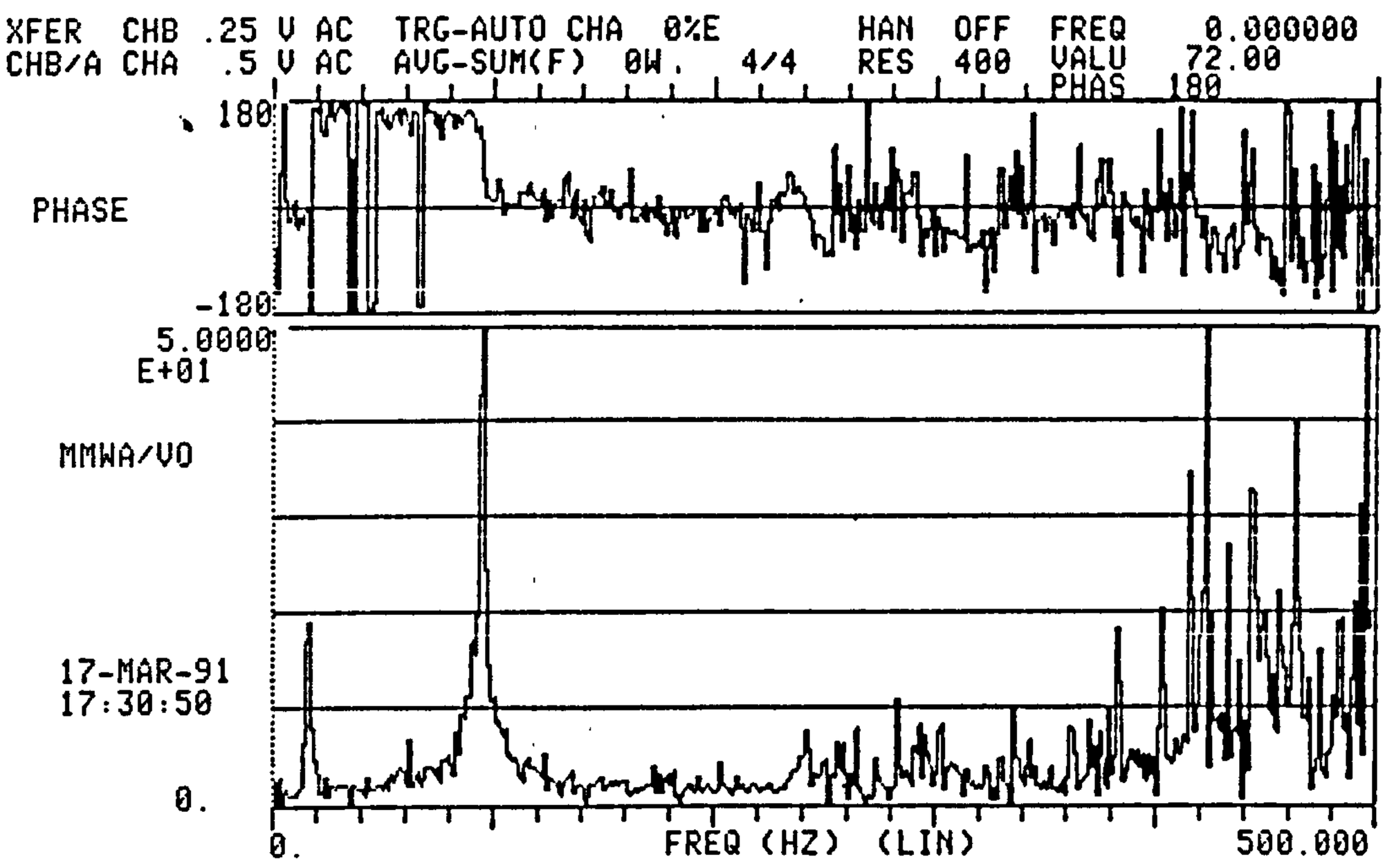

Figure **7.24c** Frequency Response plot for W-DMS-3A wing when excited at 1/2 of the length from the root.

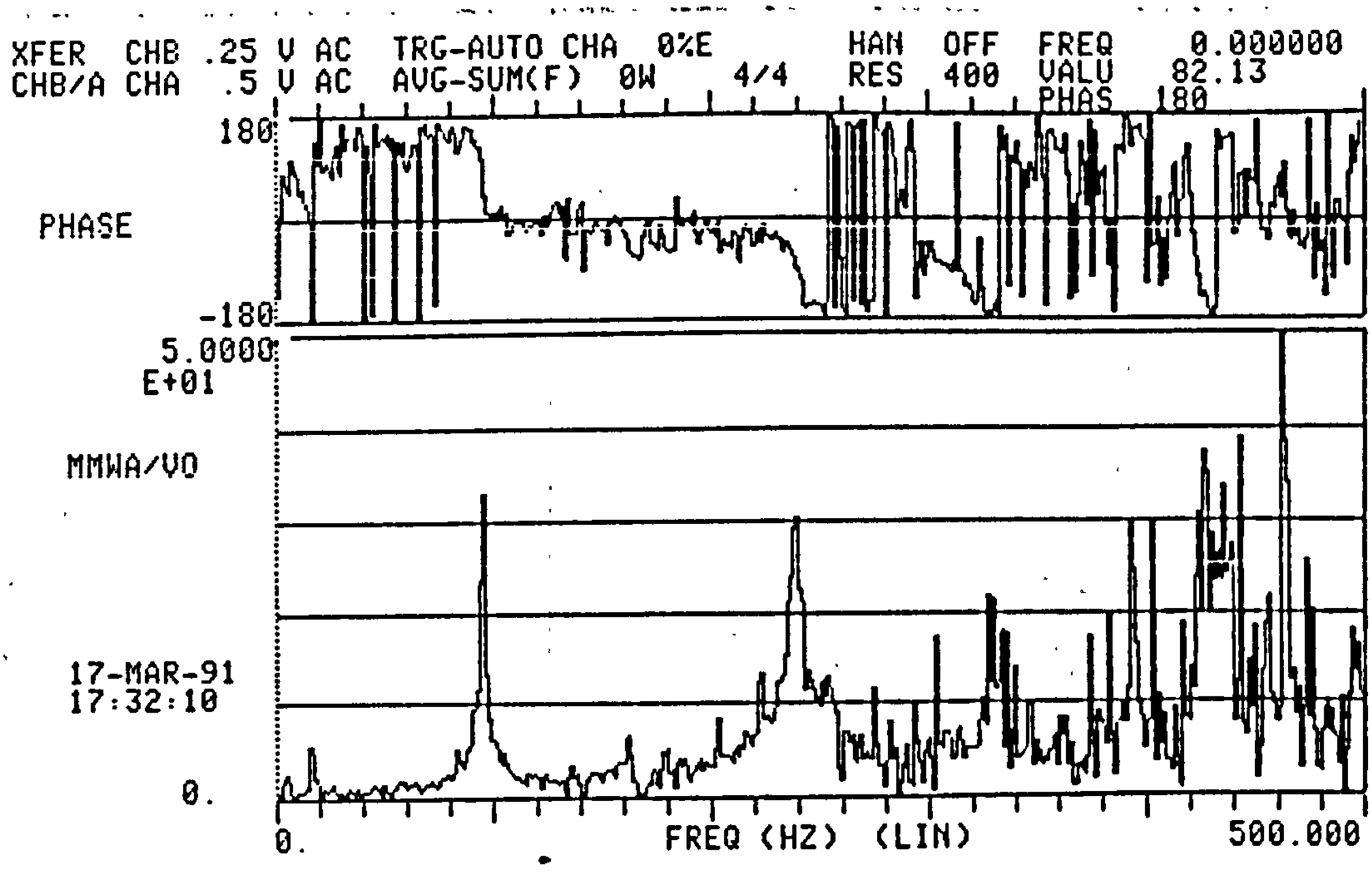

Figure **7.24d** Frequency Response plot for W-DMS-3A wing when excited at 1/4 of the length from the root.

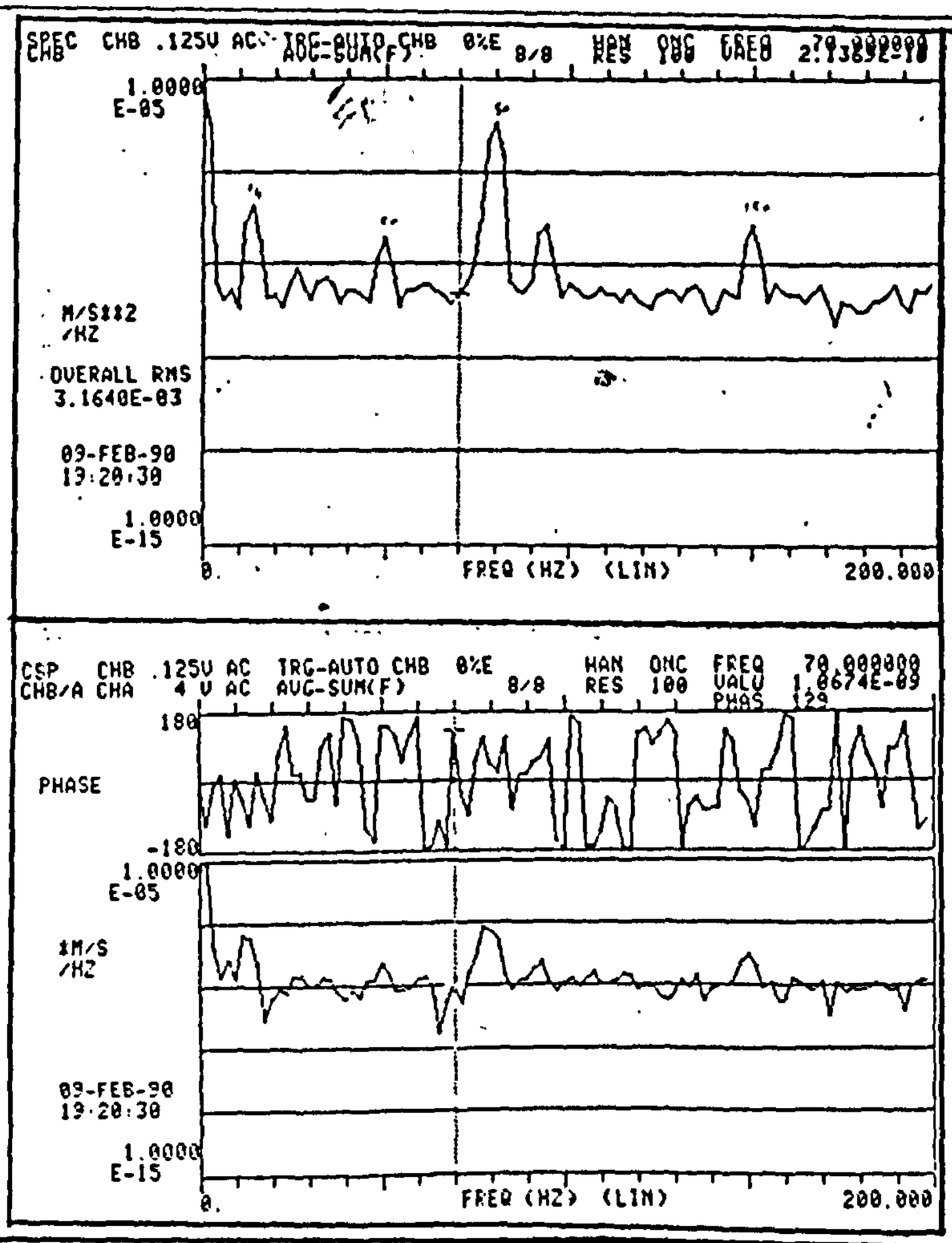

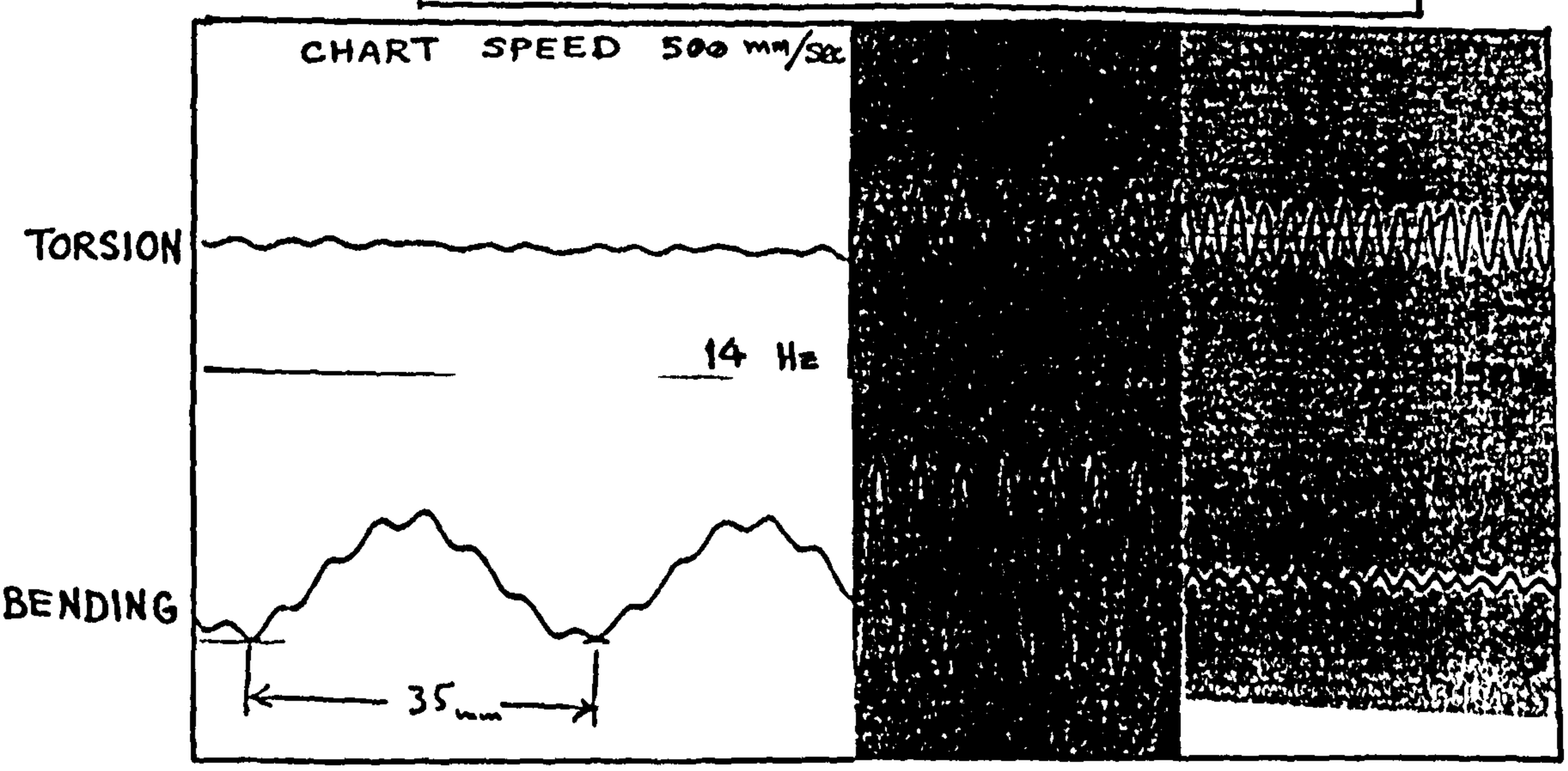

Figure 7.25 PSD of acceleration response plot and Bode plot with ultra-violet recorder traces for W-DMS-4 composite wing

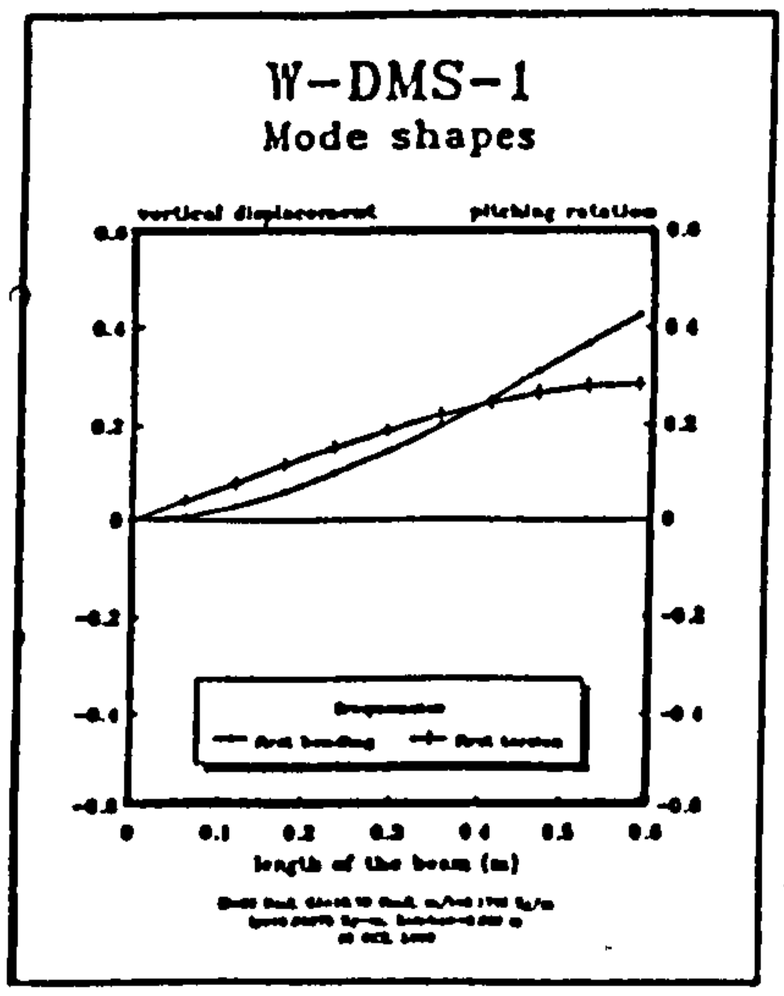

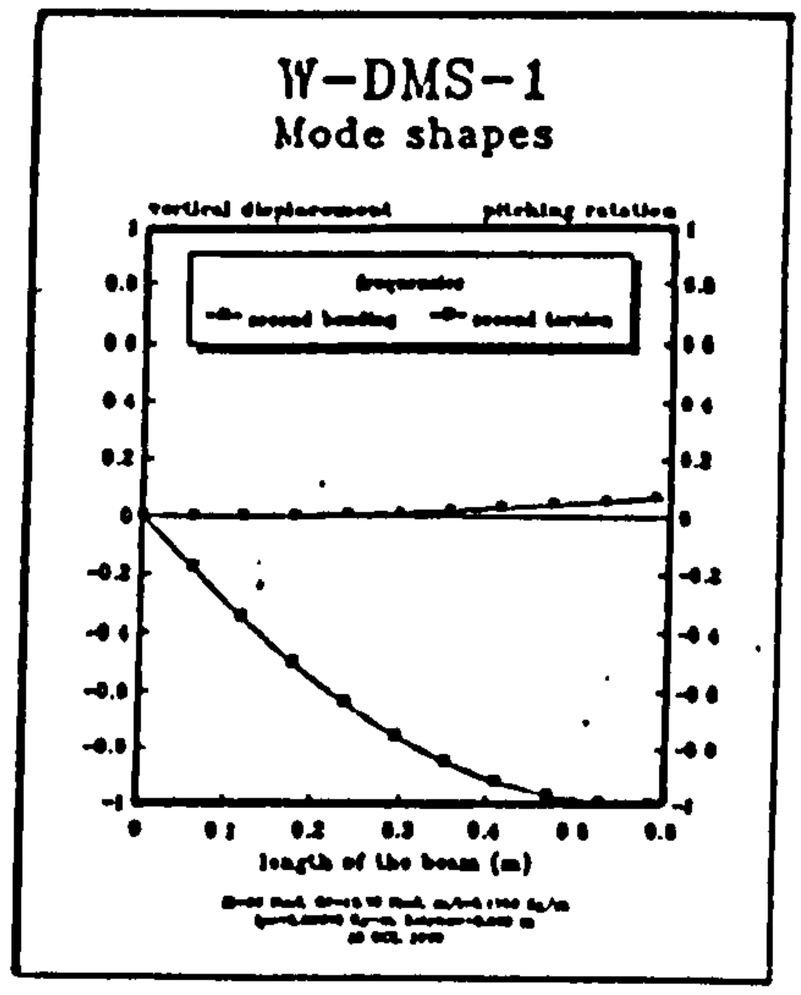

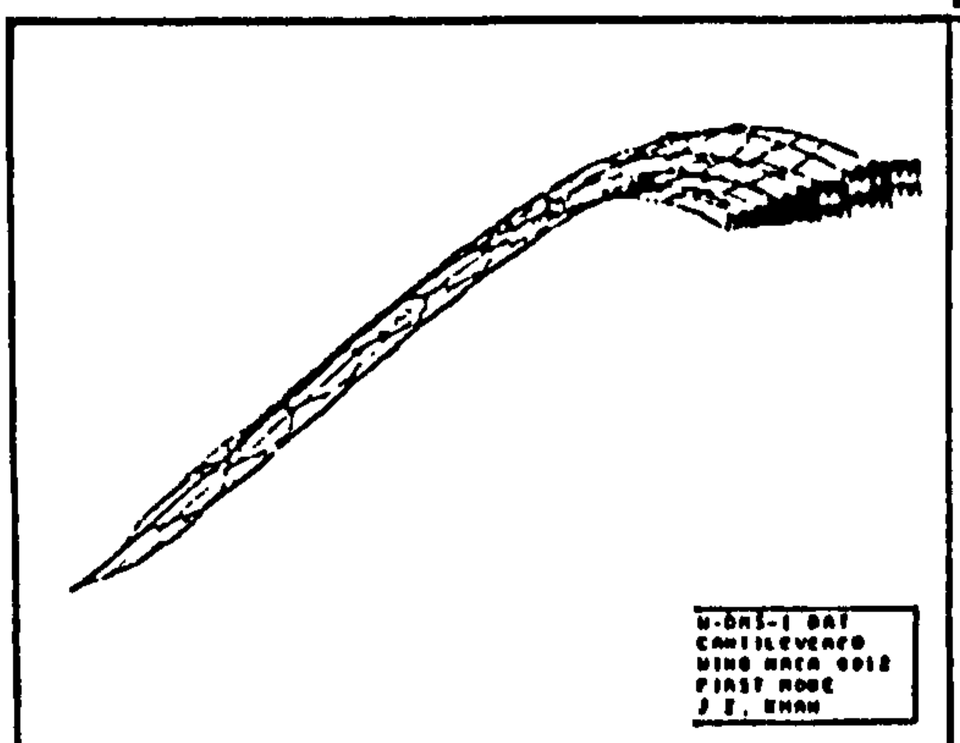

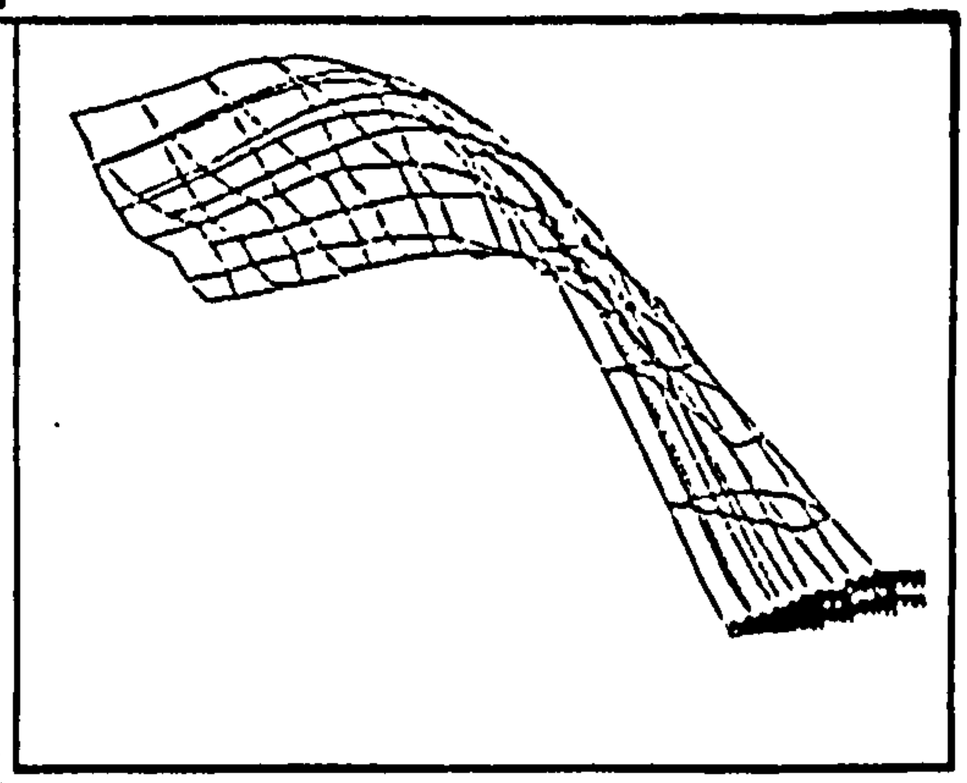

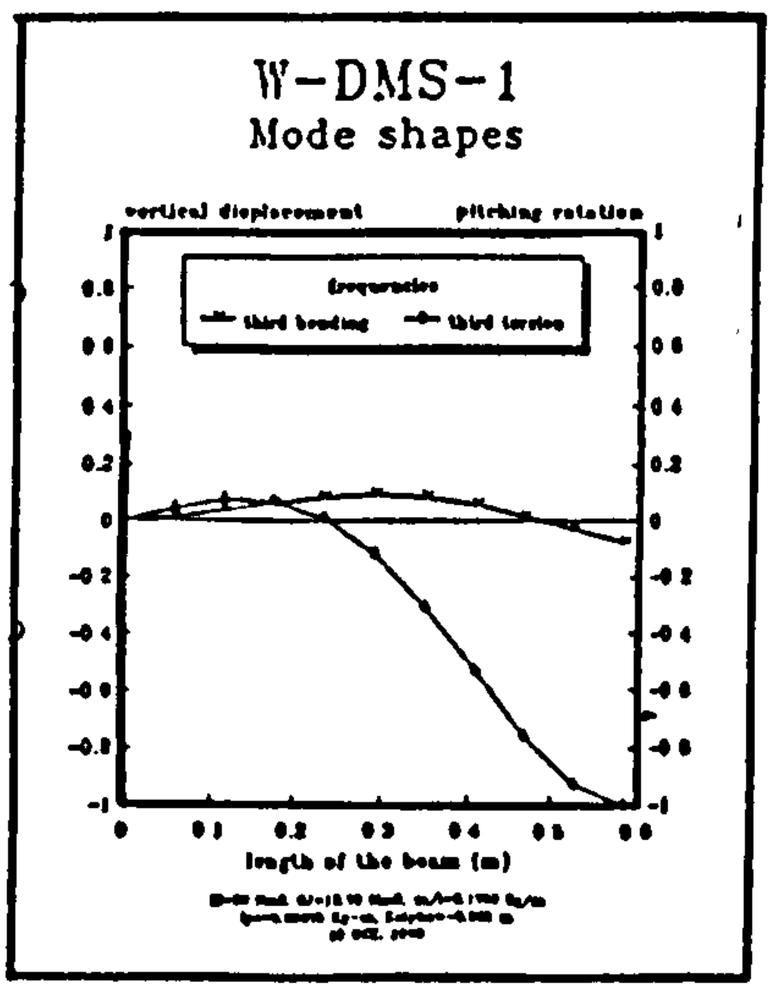

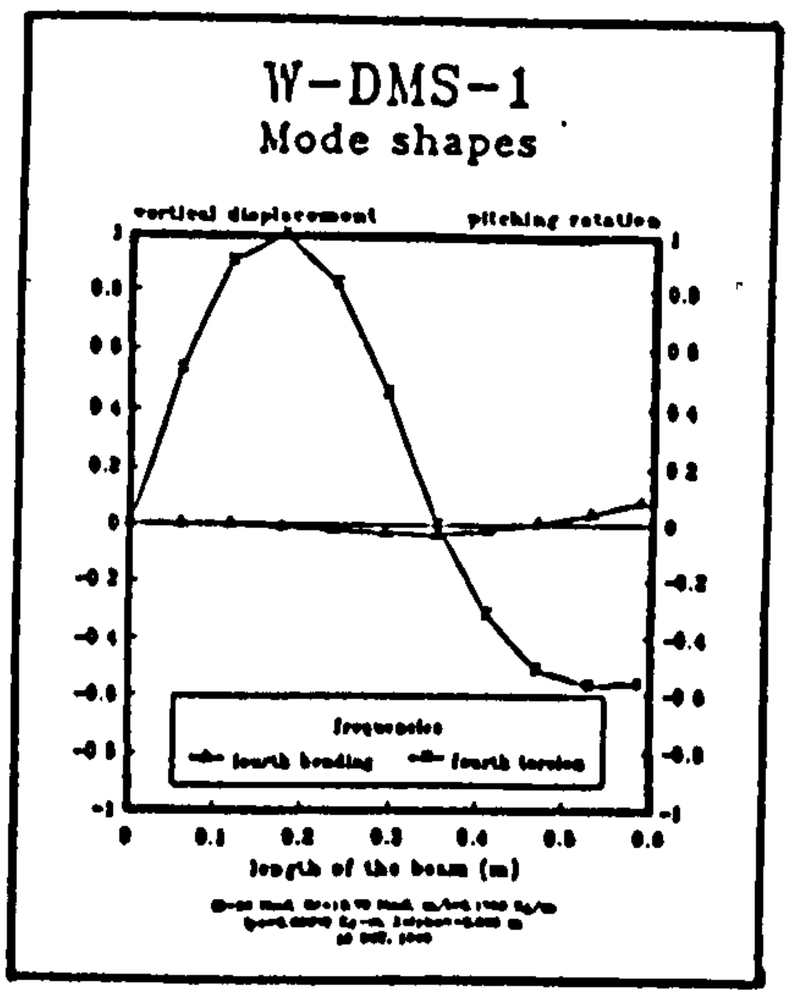

: Figure 7.26 Representative normal mode shapes for thin-walled composite closed sections compared with experimental results

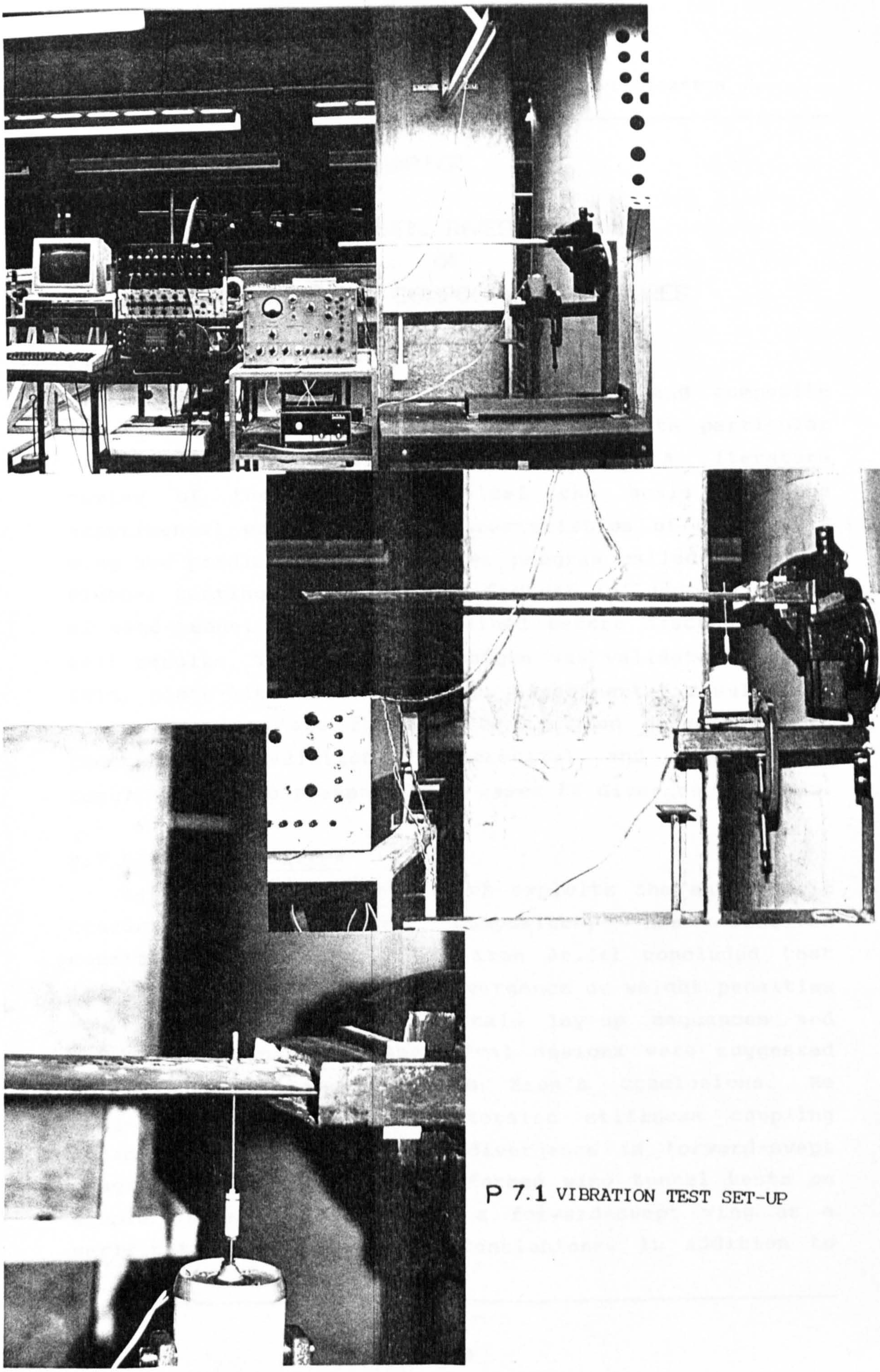

P 7.1 VIBRATION TEST SET-UP

CHAPTER : 8

AEROELASTIC INVESTIGATION OF METALLIC AND COMPOSITE STRUCTURES

8.1 INTRODUCTION

Aeroelastic investigation of metallic and composite thin plate like structures is discussed with particular reference to the phenomenon of flutter. A literature review of the subject provided the basis for the experimental work. Flutter characteristics of a complete wing are predicted by a computer program called CALFUN-C. Flutter testing techniques and factors influencing choice of wind-tunnel model are explained before discussing the test results. The testing technique was validated using a thin, plate-like aluminium wing. Experimental results for composite wings are found to be in good agreement with theoretical predictions. Theoretical and experimental results are also presented for cases of divergence speeds.

8.2 LITERATURE REVIEW

Aeroelastic tailoring, which exploits the anisotropic character of advanced composites, has received considerable attention since Kron Jr.[1] concluded that forward-swept wings without divergence or weight penalties may be possible through certain lay-up sequences and material combinations. Analytical designs were suggested by Weisshaar [2,3] based on Kron's conclusions. He suggested that the bending-torsion stiffness coupling could be useful to overcome divergence in forward-swept wings. Sherrer et al. [4] performed wind tunnel tests on simple plate like models of a forward-swept wing as a verification of Weisshaar's conclusions. In addition to

this, he also showed that the prevailing analytical techniques for prediction of divergence dynamic pressures were adequate for the majority of the test conditions. Wilkinson and Rauch [5] of Grumman Aircraft and Ellis et al. [6] of Rockwell North American Aircraft provided additional information on specific forward-swept wing model designs, (more exhaustive discussion on these efforts can be found in Ref. [7]), whereas Weisshaar et al. [8] explored the inclusion of rigid body freedoms.

Hollowell and Dugundji [9] provided useful experimental data on aeroelastic tailoring of graphite/epoxy cantilevered plates. The effect of bending-torsion stiffness coupling on divergence and flutter velocities of unswept lifting surfaces in incompressible flow was described. Furthermore, Landsberger and Dugundji [10] analytically and experimentally investigated the aeroelastic deflections, divergence and flutter behaviour of both unswept and 30° forward-swept rectangular, graphite/epoxy, cantilevered plate-type wings, with various amounts of bending-torsion stiffness coupling.

8.3 COMPUTER PROGRAM CALFUN-C

In the light of the current literature survey, a theoretical and experimental programme of investigation was prepared. The first step necessary was to predict the static structural properties of composite plates used in reference [9]. To confirm these predictions there were two options. First, to calculate natural frequencies and mode shapes based on these predictions and compare them with the published results. Secondly, to manufacture similar plates and experimentally test them. Later on the second option was modified and a different type of laminate stacking sequence was selected. In this way the second

option became second stage of the investigation.

A computer program called CALFUN which is a self-contained program for calculation of flutter speed using normal modes [11] was available as a source of predictions. The program utilizes the minimum amount of data and predicts the flutter speed and the associated mode shape of a high aspect ratio slender wing aircraft using normal modes and unsteady aerodynamics in two dimensional flow.

A comparative study between CALFUN and M.I.T. results revealed useful facts about the use of CALFUN. As long as we are dealing with simple lay-ups the program is capable of accurately predicting the frequencies and flutter characteristics. As the layer sequence becomes more complex, a significant drift appears which requires inclusion of anisotropic characteristics in the program for analysing the composite structures. CALFUN was modified to account for composite wing flutter analysis by including VMECAS as a subroutine. The modified version is called CALFUN-C and it can analyse composite wings with material coupling terms; it can also handle an axial load passing through centroid (approach includes aeroelastic behaviour of a helicopter rotor blade).

In order to validate the applicability of the program, the relatively simple approach would have been to compare the results with the already published data of reference [9]. The available experimental results were backed by the Rayleigh-Ritz energy method applied to the plate structural element. The material properties were directly transformed into flexural moduli per unit length which were subsequently used as the main structural parameters to control the dynamic and aeroelastic behaviour of the structure. Obviously this was an adequate approach, keeping in view the simple geometrical nature of the plate

structures. However, in our scheme of analysis the expected inputs are flexural, torsional and bending-torsion coupling stiffnesses that will influence the behaviour of the structure along with other properties such as mass per unit length, polar mass moment of inertia per unit length, etc. The derivation of structural properties of these plates has already been discussed in Chapter (5). Natural frequencies and normal mode shapes of these plates have been covered in Chapter (6). CALFUN and CALFUN-C computer programs were used to predict flutter speeds and flutter frequencies for these plates. The results obtained are compared with the theoretical and experimental results given in references [9,10] as shown in Tables (8.1) and (8.2).

The percentage differences shown in Tables (8.1) and (8.2) are based on comparisons between CALFUN and CALFUN-C and reference [9]. The experimental values are taken from reference [9]. A flutter test was not possible on the plate with $[\pm 45^{\circ}/0]_s$ lay-up due to the maximum wind tunnel speed limitation. In the case of the $[-45^{\circ}_2/0]_s$ and $[-30^{\circ}_2/0]_s$, plates divergence was experienced because the divergence speed was less than that of the flutter. Comparison of these percentage differences not only demonstrates the capability of the computer program CALFUN-C, but also shows the need for inclusion of material coupling term K in any aeroelastic computations. Otherwise the predicted flutter speed may be dangerously overestimated.

8.4 FLUTTER TESTING

8.4.1 FLIGHT FLUTTER TESTING

Due to the catastrophic nature of the flutter and difficulties inherent in the instrumentation and test

procedure a direct confirmation of the predicted flutter speed and frequency had not been possible in general. However, under the supervision of experienced personnel well acquainted with relatively modern techniques, flight flutter testing has contributed a lot to flight safety measures. During a flight flutter experiment an aircraft may fly near the critical speed range without expeariencing flutter provided it is not disturbed by gust or turbulence in the air. In such circumstances the test becomes extremely dangerous.

There are many methods of flight flutter testing. Two of the well known methods that have been used with some success are discussed as follows:

1. During a flight flutter test, the lifting surface is excited by means of an electrodynamic shaker and the peak response is measured as a function of air speed. The resonant frequency is determined by varying the shaker frequency at each air speed. As the flutter speed is approached a modal damping decreases so the flutter speed can be extrapolated. Nowadays, flight flutter testing based on this method has become more reliable due to the use of modern equipment giving better performance in the region of resonant frequencies.
2. In another flight flutter testing technique the modal rates of decay are determined after the structure has been deflected by either gust or rapid deflection of the control surface or by other means as a function of air speed. As the critical flutter speed is approached one of the rates of decay diminishes. Thus a plot of modal rates of decay versus airspeed can help extrapolate critical flutter speed.

Both these methods have the primary objective of determining flutter speed by extrapolating from test results determined at sub-critical flutter speeds. However, the approach adopted for these two methods have two basic shortcomings. First, the actual flutter speed may be approached rather suddenly and hence not safely; second, the critical speed determined by extrapolating from test results represents a single item to compare against a single calculated item. It would be of practical value if correlation could be demonstrated between damped sub-critical oscillations obtained by test and predicted decay or damping determined by some theory. In the following section one method of correlating theory and experiment at sub-critical speeds is given.

8.4.2 CORRELATION OF THEORY AND TEST AT SUBCRITICAL SPEEDS

The typical flutter stability determinant, evaluated for a given flutter parameter 1/k i.e. the reciprocal of the reduced frequency k, and set equal to zero, results in a polynomial, the complex roots of which have the following form [23] :

$$Z = X + i\,Y = (1 + i\,g)\left[\frac{\omega_\alpha}{\omega}\right]^2 \qquad (8.4.1)$$

where g = damping coefficient required for flutter at the frequency ω

ω_α = torsional mode frequency (Hz)

$X = \left[\frac{\omega_\alpha}{\omega}\right]^2$

and the critical flutter velocity is given by:

$$v\ (m/s) = 5.291 * 10^{-4}\ \omega_\alpha\ b_r\ \frac{1/k}{\sqrt{X}} \qquad (8.4.2)$$

where

b_r = reference semichord in metres

$1/k$ = dimensionless flutter parameter

$= v / b_r \omega$

$g = Y / X$

In investigating a particular flutter mode, the damping coefficient g versus v/ω_α is plotted using a given set of 1/k values to present the flutter characteristics of the aeroplane in question. It is assumed that the motion of the system is neither damped nor diverging, but simple harmonic. The motion below the critical flutter speed is assumed to be damped. In this case the harmonic motion $e^{i\omega_1 t}$ has to be modified by a typical damping factor $e^{-\lambda t}$ so that it can be represented by the following expression :

$$e^{i\omega_1 t}\, e^{-\lambda t} = e^{i\omega_1 + \lambda t} \qquad (8.4.3)$$

This is similar to the case when a complex value is assigned to the flutter frequency i.e. :

$$\omega = \omega_1 + i\,\lambda \qquad (8.4.4)$$

This is applicable if the elements of the determinant are equally treated under the assumption. Each element of the flutter stability determinant is formed by the combination of aerodynamic and mechanical terms. As far as the mechanical and noncirculatory aerodynamic terms are concerned, the assignment of a complex ω is no problem. However, in the circulatory aerodynamic terms, the Theodorsen function $C(k) = F(1/k) + iG(1/k)$ is developed on the assumption that the aerofoil motion is harmonic i.e. ω is real. For such terms the assumption of a damped

oscillatory motion is incorrect. However, the presence of aerofoil oscillations (even though with a damped motion) assures that the approximation of C(k) based on harmonic hypothesis is correct [28].

The two unknowns chosen in the solution of the flutter determinant are g and ω (see equation (8.4.1)). The choice of g is arbitrary and this choice can be replaced with several other physical parameters such as frequency ratio, etc. If now the frequency $\omega = (\omega_1 + i\lambda)$ is allowed to be complex i.e. damped motion is assumed, then the frequency ω_1 and the rate of decay λ may be chosen as the unknowns. The actual value g_a is replaced for g, which is obtained from the ground vibration test. The characteristic flutter stability polynomial will then have the form as follows [25]:

$$Z = (1 + i\,g)\left[\frac{\omega_\alpha}{\omega}\right]^2$$

$$= (1 + i\,g_a)\left[\frac{\omega_\alpha}{(\omega_1 + i\lambda)}\right]^2 \qquad (8.4.5)$$

Therefore,

$$(\omega_1 + i\,\lambda) = \omega\sqrt{\frac{1 + ig_a}{1 + ig}} \cong \omega\,\frac{1 + ig_a/2}{1 + ig/2}$$

$$\cong \frac{\omega\left\{1 + (i/2)(g_a - g) + g_a g/4\right\}}{1 + g^2/4}$$

$$\cong \omega\left[1 + \frac{i}{2}(g_a - g)\right] \qquad (8.4.6)$$

Since usually g and g_a are less than 0.1,

$$\omega_1 = \omega = \frac{\omega_\alpha}{\sqrt{X}}$$

and

$$\lambda = \frac{\omega}{2} (g_a - g) = \frac{\omega_\alpha}{2\sqrt{X}} (g_a - g) \qquad (8.4.7)$$

The oscillatory frequency ω_1 can be predicted with these approximations and this should follow a mechanical disturbance of the aerofoil at any speed until the critical flutter speed is achieved. The decay component λ which is proportional to the logarithmic decrement of the damped oscillatory motion is expected to be below the critical flutter speed.

8.4.3 SUMMARY

The following steps are followed in the vectorial analysis of flight flutter test results.

1. Obtain the usual characteristic roots, $Z = X + iY$ for a given $1/k$.

2. Compute $g = Y / X$

3. Compute $v = 5.291 * 10^{-4} \omega_\alpha b_r \frac{1/k}{\sqrt{X}}$

4. Compute the flutter frequency which is the frequency chosen for the frequency of damped oscillation :

$$\omega = \frac{\omega_\alpha}{\sqrt{X}} = \omega_1$$

5. Obtain the g_a from ground vibration test.

6. Calculate $\lambda = \frac{\omega_\alpha}{2\sqrt{X}} (g_a - g)$

7. Plot g against v / ω_α, which is the standard format for the g-v curve.

8. Plot λ against v.

9. Plot $\pm e^{-\lambda t}$ as the envelope of a sinusoidal wave of frequency ω_1.

The predicted decay characteristics for the subcritical flutter speed of the lifting surface (plots of steps 7 to 9) are compared with test results over a range of velocities.

A more rigorous analysis on similar lines can be found in reference [42].

8.4.4 TEST PROCEDURE

The test is carried out in the following manner :

1. Records of the oscillatory characteristics of a lifting surface by giving a force impulse at a given air speed v_t are taken.
2. The oscillatory frequency ω is obtained from the test records.
3. The damping ratio λ_t is determined from the logarithmic decrement of the test oscillations :

$$\lambda_t = \frac{1}{2\pi} \log_e \frac{A_i}{A_{i+1}} \qquad (8.4.8)$$

where A_i = maximum amplitude of the ith wave
(Test measurements are taken after the forcing function is removed)

4. λ_t is plotted against v_t.

8.4.5 COMPARISON OF FLIGHT FLUTTER TEST METHODS

Goland and Luke [19] have also discussed theoretically the question of oscillation modes of a wing at sub-critical flutter speeds. Their method [19] is based on a better approximation of Wagner's lift growth function. This is achieved by a complete decay study, independent of the flutter analysis. But the advantage of above mentioned technique is that it utilizes the results already obtained

in the usual flutter analysis. Their results indicate that resonance testing, as compared with the study of decaying transients, gives safer results in flight flutter testing. The reasoning behind this lies in the specific results which they obtained on their theoretical examples. These results showed that the rate of decay of the flight mode (which was later to develop into the critical mode at flutter) actually increased with air speed until 85% of the flutter speed and then rapidly decreased to zero at the critical flutter speed.

8.5 FLUTTER MODEL

8.5.1 MODEL DESIGN

An aircraft wing deflects under its own weight and also under aerodynamic loadings when the aircraft is in flight. The aerodynamic loading changes as the wing deforms, leading to further deformation of the wing. It is the interaction of the elastic forces of the wing with aerodynamic and inertia forces that leads to the oscillatory phenomenon known as flutter. Failure can occur very soon after the onset of flutter, hence the study of this aeroelastic problem is very important.

Wind tunnel models are used to help in the analysis of wing flutter for both conventional and unconventional designs.

Flutter models are built to establish flutter speed and frequency in the wind tunnel with probably two different objectives in mind. The most common one is to scale a full size aircraft and establish the flutter characteristics so as to achieve confidence in the already designed structure. Secondly the use of advanced types of computing techniques based on complex theoretical models have necessitated wind tunnel flutter tests. Thus

fabricated, a flutter model with reasonable structural characteristics subjected to the wind tunnel tests strengthens the researcher's belief in the theoretical model. In other words the process of 'successful flutter prediction involves choice of a theoretical model for structural properties, aerodynamic theory for aerodynamic derivatives and validation of the eventual programme by wind tunnel flutter tests and flight flutter tests.

(i) FIRST CATEGORY

In the first category of flutter models, the model is designed to represent the full scale wing by using certain scale relationships discussed in section (8.5.2); the full scale aeroelastic characteristics are then derived, using the same relationships, from the model characteristics.

There are several design alternatives to make a flutter model representing a full scale wing. The most obvious method is the one in which the full scale structure is simply scaled down and reproduced. This model can be prepared from the same material as the aircraft wing or from other different materials. It is appreciated that the model will have the required scaled stiffness by virtue of the fact that its structure is similar to that of the aircraft wing. Since the model is very much smaller than the full scale wing, all the material thicknesses would also have to be similarly scaled down. This condition generally makes it impractical to use the same material as used in the aircraft wing for the manufacture of the model. In order to obtain a material thickness that can be used, a material with much reduced Young's modulus of elasticity E, will have to be used. The above mentioned model will be difficult to manufacture and hence it will be very costly. Furthermore, the situation is different if the model is used for high speed tests. In contrast when

this is the case, only the above method of construction is suitable [14].

(ii) SECOND CATEGORY

The second category of flutter models (that was of prime interest in this work) is built on the same lines, except that the motives are slightly different. Besides other restraints discussed above under the sub-heading of similarity parameters, the construction of flutter model is greatly influenced by the theoretical model to be adopted for flutter prediction. An accurate flutter prediction depends upon the theoretical model representing the structural and aerodynamic aspects of the model. The main core of the lifting surface may be representing a prismatic beam, a thin plate, a box beam or even an arbitrary shape thin walled structure that not only provides the basic stiffnesses but also the aerodynamic profile. Since the theoretical details for each of these idealized elements are quite different from each other it is necessary to identify the structural details of the main core. This will not only affect the static structural properties but also the natural frequencies and the normal mode shapes, resulting in an unrealistic aerodynamic distribution on the deformed surface. Furthermore the aspect ratio, nature and degree of sweep, etc., demands more complex aerodynamic theories to predict the aerodynamic distribution on the lifting surface. Thus in this category of flutter testing, the models have to comply with the theoretical model chosen for prediction of flutter characteristics.

The wing model to be designed and built is for use in the return circuit, open jet wind tunnel T3 at The City University. It is a low speed wind tunnel that can run at a maximum speed of 56.0 m/s.

8.5.2 SIMILARITY PARAMETERS

The properties of an aircraft wing that are to be represented by a model may be listed as:

a) Linear dimension
b) Aerodynamic shape
c) Distribution of stiffness
d) Distribution of mass
e) Distribution of inertia
f) Structural damping

The properties of the testing media are:

g) Density, viscosity and ratio of specific heats
h) Velocity
i) Mach number

and the static external forces may be regarded as:

j) Type of support
k) Acceleration due to gravity

Having decided on the design of the model, it is necessary to scale down the aircraft wing data in order to represent the wing by the model. Similarity parameters for the case where the aircraft structure is simulated by a different type of structure in the model are discussed in Reference [15].

The proper scaling of model characteristics is important in constructing flutter models. Since the model geometric scale ratio changes other parameters, it is usually fixed by a consideration of wind tunnel limitations.

1. The maximum model span should not exceed 80 % of the tunnel width in order to avoid excessive blocking or wall interference. This gives the ratio $\frac{b_M}{b_A}$ [16]. The subscripts M and A refers to model and full scale aircraft respectively whereas the quantity b can be any linear dimension for example wing span.
2. Other parameters such as model scale stiffness, mass distribution, bending, torsional, and coupled bending-torsion stiffnesses should be duplicated.
3. The mass or weight ratio should be :

$$\frac{\left(\frac{m}{\pi\rho b^2}\right)_M}{\left(\frac{m}{\pi\rho b^2}\right)_A} = 1 \qquad (8.5.1)$$

$$\frac{m_M}{m_A} = \frac{\rho_M \; b_M^2}{\rho_A \; b_A^2} \qquad (8.5.2)$$

where m = mass per unit length

ρ_M = wind tunnel operating density

ρ_A = flight density of full-scale aircraft

Then the total mass or weight ratio will be :

$$\frac{M_M}{M_A} = \frac{\rho_M}{\rho_A} \left(\frac{b_M}{b_A}\right)^3 \qquad (8.5.3)$$

4. The frequency ratio should be :

$$\frac{\left(\frac{V}{b\omega}\right)_M}{\left(\frac{V}{b\omega}\right)_A} = 1 \qquad \text{or} \qquad \left(\frac{V}{b\omega}\right)_M = \left(\frac{V}{b\omega}\right)_A \qquad (8.5.4)$$

5. The velocity ratio should be :

$$\frac{V_M}{V_A} = \sqrt{\frac{b_M}{b_A}} \qquad (8.5.5)$$

6. The static moment scale ratio should be :

$$\frac{S_M}{S_A} = \frac{\rho_M}{\rho_A}\left[\frac{b_M}{b_A}\right]^4 \qquad (8.5.6)$$

7. The weight moment of inertia ratio should be :

$$\frac{I_M}{I_A} = \frac{\rho_M}{\rho_A}\left[\frac{b_M}{b_A}\right]^5 \qquad (8.5.7)$$

8. The stiffness ratio should be :

$$\frac{\text{Model stiffness}}{\text{Aeroplane stiffness}} = \frac{\rho_M}{\rho_A}\left[\frac{V_M}{V_A}\right]^2\left[\frac{b_M}{b_A}\right]^4 \qquad (8.5.8)$$

The similarity parameters given above may not be satisfied simultaneously but these ratios provide the guide lines for the wind tunnel flutter model design. Once the model is ready, it is given a vibration test to establish true frequencies.

8.6 PLATE LIKE FLUTTER MODELS

The requirement of thin wings for faster aeroplanes justifies the aeroelastic analysis of thin plate-like structures (the investigation of which could have been

otherwise misunderstood for just academic interest). It has been already mentioned in Chapter (6) that a special degenerated case of a thin-walled beam is a doubly symmetrical structure with no elastic coupling behaviour. Box-beams and plates (for aspect ratios greater than 3.5) are some examples. Hence it was hoped that the program for aeroelastic analysis based on thin-walled beam elements can be safely applied to thin-plate like lifting surfaces made of conventional (isotropic) or composite (generally orthotropic) materials.

An aluminium and three composite plates were prepared. Polystyrene foam fairings were glued to these plates to generate the aerodynamic effects.

The structural and modal properties of these thin plate-like wings were established as discussed in Chapter (5) and (7).

The sub-critical flutter speed behaviour was observed by obtaining Bode plots at frequent intervals of wind tunnel speed. These plates were flexible enough to sustain vibrations with large amplitudes without suffering plastic deformations, thus providing considerable ease in doing the experiment and recording the necessary data. A video film was prepared to record the event.

8.6.1 ALUMINIUM PLATE LIKE AEROELASTIC MODEL

Experimental aeroelastic investigations were made on similar lines to those mentioned in Reference [9]. Two objectives were set forth. Firstly, to acquire a feel for the phenomenon and secondly to validate the experimental technique. Moreover the accuracy of CALFUN was also investigated in predicting flutter speed and frequency of thin plate-like wings.

The dimensional details of the aluminium plate-like wing are given in Table (8.3) with various structural

properties tabulated in Table (8.4).

The dynamic and aeroelastic test results are given in Table (8.5).

The aeroelastic predictions showed that in the unswept configuration the wing would suffer from divergence prior to flutter. Therefore, this wing was studied for 10° and 20° sweep angles. Sweeping backwards cured the problem of divergence, and the results given in Table (8.6) were obtained.

It was observed that for conventional materials (isotropic), the results are reasonably within engineering accuracy. A parametric study showed that, at moderate sweep angles (up to 25° sweep back) the magnitude of flutter speed initially drops and then sharply increases with sweep angle. The magnitude of this drop in flutter speed greatly depends on the ratio of rigidities. This will be more obvious, on comparing the possible drop in the case of various lay-ups of composite plates.

Power spectral density plots of acceleration response for an aluminum wing with 10° sweep angle at various sub-critical flutter speeds are shown in Figure (8.1). An obvious and singular peak of flutter frequency appeared on approaching the critical flutter speed as explained.

8.6.2 COMPOSITE PLATE LIKE AEROELASTIC MODELS

Three graphite/epoxy composite plates with $[0]_{8}$, $[\pm 30^{\circ}]_{s}$ and $[\pm 45^{\circ}/0]_{s}$ ply lay-up sequence were tested. The dimensional details for composite plates are given in Table (5.4). The various structural parameters and structural rigidities are given in Tables (5.6) and (5.7) respectively. Results of natural frequencies are given in Tables (7.6) to (7.8). Flutter test results are compared with theoretical predictions in Tables (8.7) and (8.8).

8.6.3 DISCUSSION OF RESULTS

Power spectral density plots for composite $[0_6]$, $[\pm 30^\circ]_s$ and $[\pm 45^\circ/0]_s$ cases with 0° and 20° swept back configurations at sub-critical speeds are shown in Figures (8.2) to (8.5). The appearance of a singular peak at the flutter frequency and the disappearance of the neighbouring first bending mode and first torsional mode frequencies are clearly exhibited by these plots. Turbulence present in the wind tunnel gives enough excitation to the wing so that the accelerometer signal is picked up for further analysis. It also presents the problem of noise in the signal and can be seen in the plots. It was noted in earlier flutter tests conducted by other investigators that it was necessary to externally excite the structure at the critical flutter speed to initiate the flutter. The tests reported here did not require any such initial excitation and may be due to the presence of some degree of turbulence in the wind tunnel.

The effect of ply orientation on the flutter speed and frequency predictions in terms of percentage differences between theoretical and experimental results is plotted in Figures (8.6) and (8.7). The probable reasons for the discrepancies are discussed as follows :

1. It was observed that the flutter speed is not a single discrete value but in fact is a critical band of velocities. It has a lower and an upper limit. With increasing airspeed, flutter may not be triggered when reached at the lower flutter speed limit. But as the speed is lowered from the upper limit gradually the lower limit can be established. All this requires a very fine control on the airspeed. During the experiment it was observed that precise control over the wind tunnel speed was not possible. Therefore, it was difficult to

precisely locate the lower limit of the critical flutter speed.

2. The computer program predicted the flutter speed and frequency by using strip theory to model the aerodynamic distribution. This theory assumes a value of 2π for the lift-curve slope of the wing. The finite aspect ratio and deviation from the actual profile result in a lower value, and provide a valid source of error.
3. An error in the estimation of structural properties will give rise to wrong natural frequencies and normal mode shapes. The aerodynamic distribution is calculated corresponding to these mode shapes. Therefore, flutter calculations will directly suffer from these structural properties estimations.
4. It was pointed out both in Chapter (6) and (7) that ignoring chordwise deformations may have been the cause of the poor estimation of the torsional modes. This effect may also produce errors in the flutter calculations. However, results for the 20° swept configuration are within engineering accuracy.

The effect of ply orientation on flutter speed and frequency observed in Tables (8.1) and (8.2) is graphically shown in Figures (8.8) and (8.9). These plots clearly demonstrate the need and success of CALFUN-C computer program. The predictions of flutter speed and frequency can be very misleading, if the material coupling term is ignored in the calculations.

8.7 CONCLUSIONS

The validity of using generally orthotropic Vlasov beam model for composite plate-like wings in the flutter

predictions is confirmed. Furthermore, the validity of strip theory in flutter calculations is also confirmed for the wings tested. Various reasons are discussed for the probable sources of discrepancies between experimental results and theoretical predictions.

The flutter tests conducted has been recorded on a VHS format video tape. The film contains a short description of the testing facility and covers short clips of the various tests performed on aluminium and composite plate-like wings.

REFERENCES

1. Kron, J. Jr., "Divergence Elimination with Advanced Composites," AIAA Paper 75-1009, 1975.

2. Weisshaar, T.A., "The influence of Aeroelasticity on Swept Composite Wings," AFWAL-TR-80-3137, November 1980.

3. Weisshaar, T.A., "Aeroelastic Tailoring of Forward Swept Composite Wings," Journal of Aircraft, Vol. 18, August 1981, pp. 669-676.

4. Sherrer, V.C., Hertz, T.J., and Shirk, M.H., "Wind Tunnel Demonstration of Aeroelastic Tailoring Applied to Forward Swept Wings," Journal of Aircraft, Vol. 18, November 1981, pp. 976-983.

5. Wilkinson, K. and Rauch, F., "Predicted and Measured Divergence Speeds of an Advanced Composite Forward Swept Wing Model," AFWAL-TR-80-3059, July 1980.

6. Ellis, J.W., Dobbs, S.K., and Miller, G.D., "Structural Design and Wind Tunnel Testing of a Forward Swept Fighter Wing," AFWAL-TR-80-3073, July 1980.

7. Hertz, T.J., Shirk, M.H., Ricketts, R.H., and Weisshaar, T.A., "On the Track of Practical Forward Swept Wings," Astronautics Aeronautics, Vol. 20, January 1982, pp. 40-53.

8. Weisshaar, T.A., Zeiler, T.A., Hertz, T.J., and Shirk, M.H., "Flutter of Forward Swept Wings, Analyses and Tests," Proceedings of the 23rd AIAA/ASME/ASCE/AHS Structures, Structural Dynamics, and Material Conference, New Orleans, La., May 1982, pp. 111-121.

9. Hollowell, S.J. and Dugundji, J., "Aeroelastic Flutter and Divergence of Stiffness Coupled, Graphite/Epoxy Cantilevered Plates," Journal of Aircraft, Vol. 21, January 1984, pp. 69-76.

10. Landsberger, B.J. and Dugundji, J., "Experimental Aeroelastic Behavior of Unswept and Forward-Swept Cantilevered Graphite/Epoxy Wings," Journal of Aircraft, Vol. 22, August 1985, pp. 679-686.

11. Loring, S.J., "Use of Generalized Coordinates in Flutter Analysis," SAE Journal (Transactions), Vol. 52, No. 4, April 1944, pp. 113-132.

12. Broadbent, E.G. and Hartley, E.V., "Vectorial Analysis of Flight Flutter Test Results," R.A.E. Tech. Note Struct. 233, 18th of February, 1958, pp 1347-1370.

13. Goland, M. and Luke, Y.L., "A Study of the Bending-Torsion Aeroelastic Modes for Aircraft Wings," J. Aeronaut. Sci., July 1949.

14. Windsor, E.P.L., "The use of Flexible Models in Aeroelastic research," Von Karman Institute for Fluid Dynamics, Course Note 43, May 1964.

15. Templeton, H., "Models for Aeroelastic Investigation," R.A.E. Technical Note No. Structures 179, November 1955.

16. Wassermann, L.S. and Mykytow, W.J., "Wind tunnel Flutter tests," Manual on Aeroelasticity, Vol. IV, A.G.A.R.D.

17. Rauscher, M., "Report on the Suitability of Various

Materials and Methods of Construction of Wind Tunnel Flutter Models," MIT Aeroelastic Research Lab. Rept. 1.0, to Bureau of Aeronautics, U.S. Navy, June 1942.

18. Bergen, W.B., "Experimental Investigations in Aircraft Dynamics," Journal of Aeronautical Sciences, October 1943.

19. Von Doenhoff, A. and Stivers, NACA Report No. 824, 1945.

20. Rosenbaum, R. and Scanlan, R.H., "A Note on Flight Flutter Testing," Journal of Aeronautical Sciences, June 1948.

21. Beckley, L.E. and Rauscher, M., "The Design of Sectional Type Flutter and Dynamic Models of Aircraft Structures," MIT Aeroelastic Research Lab. Rept. to Bureau of Aeronautics, U.S. Navy, Contract Noa(s) 7493, 1948.

22. Schwartz, M.D. and Wrisley, D.L., "Investigation of Flight Flutter Testing Techniques," Paper, Inst. Aero. Sci. (N.Y.), January 1951.

23. Bisplinghoff, R.L., Ashley, H. and Halfman, R.L., Aeroelasticity, Addison-Wesley Publishing Co. Inc. 1957.

24. Rae, W.H. and Pope, A., Low-speed wind tunnel testing, 2nd Edt. John Wiley & Sons, 1984.

25. Fung, Y.C., An Introduction to the Theory of Aeroelasticity, Dover Publications, Inc., New York, 1969.

26. Kinnaman, E.B., "Flutter Analysis of Complex Airplanes by Experimental Methods," J. Aeronaut. Sci. 19, pp.

577-584, 1952.

27. Lambourne, N.C., "An Experimental Investigation on the Flutter Characteristics of a Model Flying Wing," Aeronaut. Research Council R. & M. 2626, 1952.

28. Theodorsen, T., "General Theory of Aerodynamic Instability and the Mechanism of Flutter," NACA TR 496, 1934.

29. Felt, L.R. and Kehoe, M.W., "Flight Flutter Testing at Ames-Dryden," 16th annual symposium proceedings of the society of flight test engineers, 1985.

30. Norton, W.J., "Limit-cycle Oscillation and Flight Flutter Testing," 21st annual symposium proceedings of the society of flight test engineers, 1990.

No.	Lay-up	Flutter Speed (m/s)						
		THEORETICAL			EXP.	% age difference		
		CALFUN (1)	CALFUN-C (2)	Ref.9 (3)	Ref.9	(1)	(2)	(3)
1	$[0_2/90^\circ]_s$	17.6		21.0	25.0	-42.05		-19.05
2	$[\pm 45^\circ/0]_s$	39.5	37.25	39.0	>32.0	---	---	---
3	$[45^\circ_2/0]_s$	39.5	31.00	27.8	28.0	29.11	9.68	- 3.70
4	$[-45^\circ_2/0]_s$	39.5	42.75	27.8	Div. 12.5	---	---	---
5	$[30^\circ_2/0]_s$	35.0	26.50	27.8	27.0	22.86	- 1.89	2.88
6	$[-30^\circ_2/0]_s$	35.0	43.00	30.0	Div. 11.7	---	---	---

TABLE 8.1 Flutter speeds of composite plates
(see Tables (6.6)-(6.9) for dimensions, static and dynamic details)

No.	Lay-up	Flutter Frequency (Hz)						
		THEORETICAL			EXP.	% age difference		
		CALFUN (1)	CALFUN-C (2)	Ref.9 (3)	Ref.9	(1)	(2)	(3)
1	$[0_2/90^\circ]_s$	21.5		25.0	29.0	-34.90		-16.00
2	$[\pm 45^\circ/0]_s$	41.5	34.22	39.0	---	---	---	---
3	$[45^\circ_2/0]_s$	41.5	25.47	28.0	24.0	42.20	5.77	14.29
4	$[-45^\circ_2/0]_s$	41.5	35.30	27.0	Div.	---	---	---
5	$[30^\circ_2/0]_s$	36.0	27.57	31.0	28.0	22.20	- 1.55	9.68
6	$[-30^\circ_2/0]_s$	36.0	35.59	29.0	Div.	---	---	---

TABLE 8.2 Flutter frequencies of composite plates

MATERIAL : ALUMINIUM		
Span	= 300	mm
Chord length	= 75	mm
Thickness	= 0.71	mm
Cross sectional area	= 53.25 x 10^{-6}	m^2

TABLE 8.3 Dimensions of aluminium plate-like wing

PARAMETER	UNITS	THEORETICAL	EXPERIMENTAL	% DIF.
Mass per unit length	Kg/m	0.143775	0.1397	2.83
Bending rigidity EI	Nm^2	0.1541	0.16226	-5.29
Torsional rigidity GJ	Nm^2	0.2357	0.23767	-0.84
Polar moment of inertia I_p	Kg-m	6.74 x 10^{-5}	----	----

TABLE 8.4 Structural parameters of aluminium plate-like wing

NORMAL MODE SHAPE	UNITS	THEORETICAL PREDICTIONS USING CALFUN		EXP.	% DIFF.
		using calculated data	using measured data		
First Bending	Hz	6.437	6.7009	5.54	17.32
Second Bending	Hz	40.3405	41.994	36.122	13.98
First Torsion	Hz	49.2798	49.485	48.199	2.60
Third Bending	Hz	112.954	117.584	------	-----
Second Torsion	Hz	147.840	148.456	------	-----
Divergence Speed	m/s	34.546	34.690	39.91	-14.32
Flutter Speed	m/s	33.60	33.40	Diverged before flutter	
Flutter Freq.	Hz	26.66	27.30		

TABLE 8.5 Dynamic and aeroelastic results of aluminium plate-like wing

Sweep back	FLUTTER SPEED (m/s)			FLUTTER FREQUENCY (Hz)		
	THEO. (CALFUN)	EXPT.	% DIFF.	THEO. (CALFUN)	EXPT.	% DIFF.
Unswept	33.40	Diverged	------	27.30	---	----
10°	32.26	38.87	-20.49	26.26	29.0	-10.43
20°	30.95	27.80	10.18	24.35	22.75	6.57

TABLE 8.6 Flutter test results for aluminium plate-like wing with unswept and swept configurations

Lay-up	Sweep Angle	Flutter Speed (m/s)				
		Exp.	Theo.1	% diff	Theo.2	% diff
$[0_s]_s$	0°	33.80	18.25	-85.21	29.50	-14.58
	20°	32.83	30.30	- 8.35	32.37	- 1.43
$[\pm 30^\circ]_s$	0°	41.59	33.50	-24.15	32.00	-30.00
	20°	38.52	35.80	- 7.60	35.20	- 9.44
$[\pm 45^\circ/0]_s$	0°	48.06	38.50	-24.83	39.00	-23.23
	20°	40.06	39.40	- 1.68	39.44	- 1.55

TABLE 8.7 Flutter speed of composite thin plate-like wings

Lay-up	Sweep Angle	Flutter Frequency (Hz)				
		Exp.	Theo.1	% diff	Theo.2	% diff
$[0_s]_s$	0°	38.74	23.40	-65.56	34.30	-12.95
	20°	38.50	36.29	- 6.09	38.04	- 1.21
$[\pm 30^\circ]_s$	0°	38.67	37.40	- 3.40	37.50	- 3.12
	20°	41.70	39.47	- 5.65	39.65	- 5.17
$[\pm 45^\circ/0]_s$	0°	61.91	37.45	-65.31	47.27	-30.97
	20°	35.00	37.56	6.82	36.17	3.24

TABLE 8.8 Flutter frequency of composite thin plate-like wings

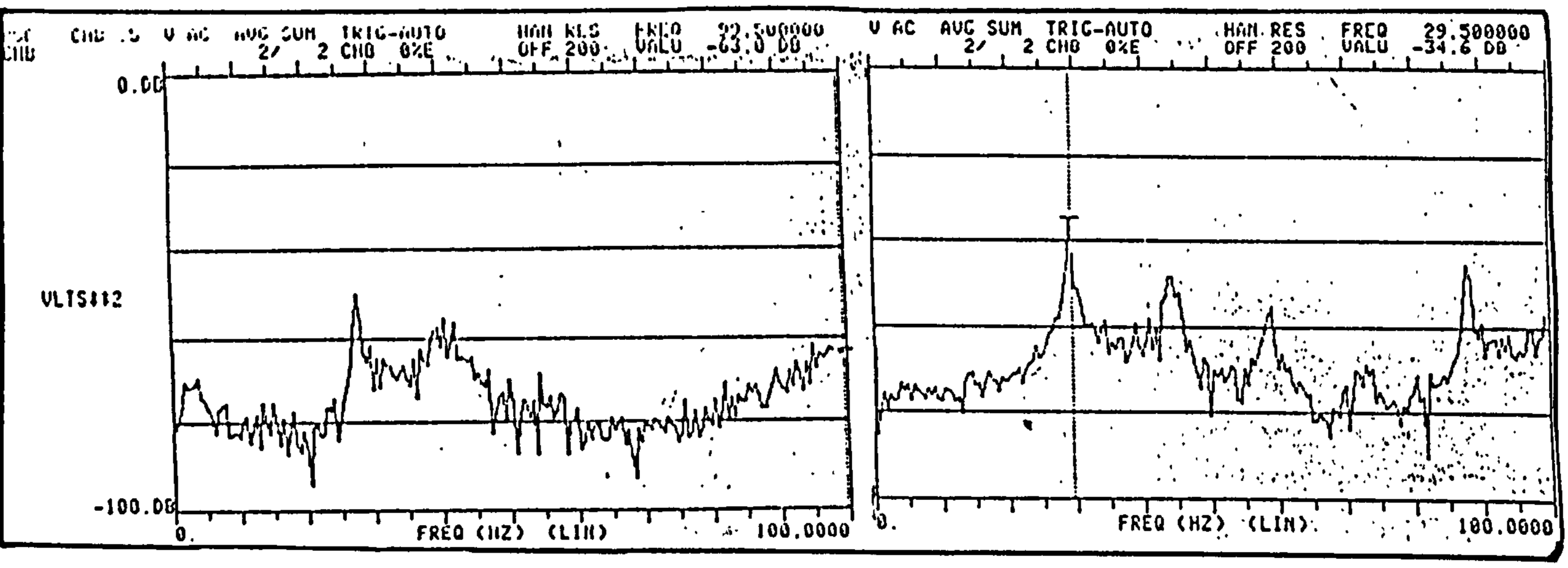

—(i)— —(ii)—

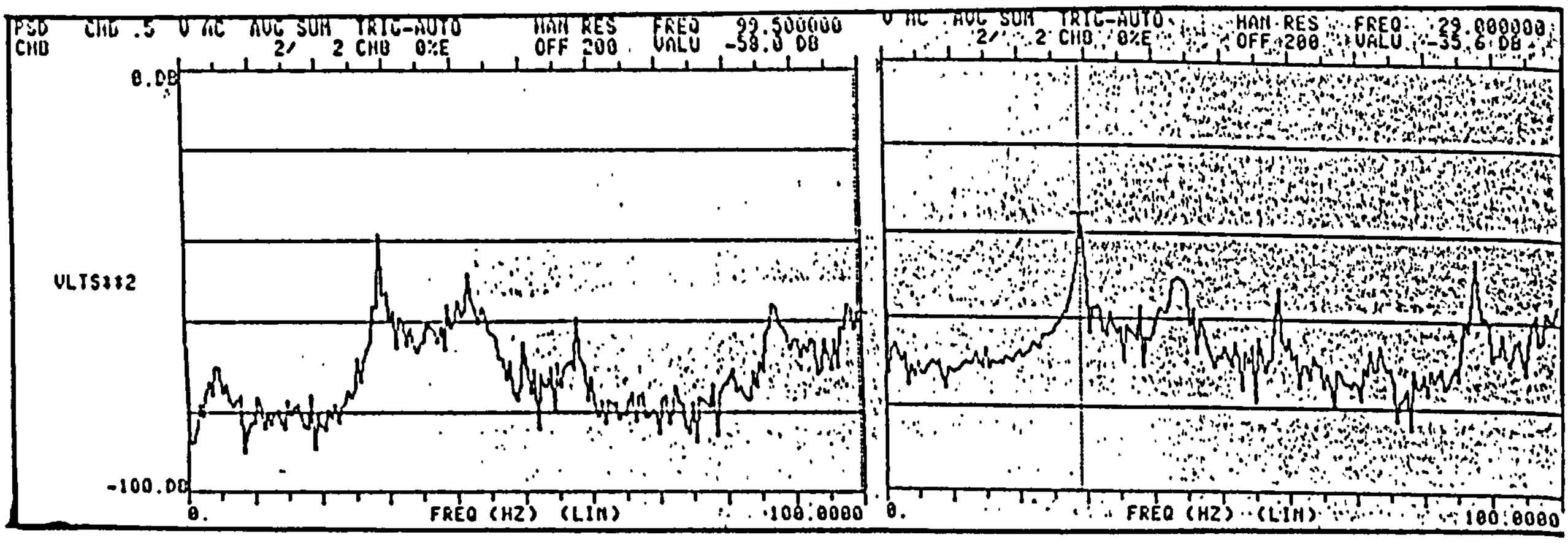

—(iii)— —(iv)—

Figure 8.1 PSD of acceleration response plots for aluminium wing 10^{o} sweep at (i) 35.81 m/s , (ii) 37.104 m/s (iii) 38.19 m/s , (iv) 38.87 m/s

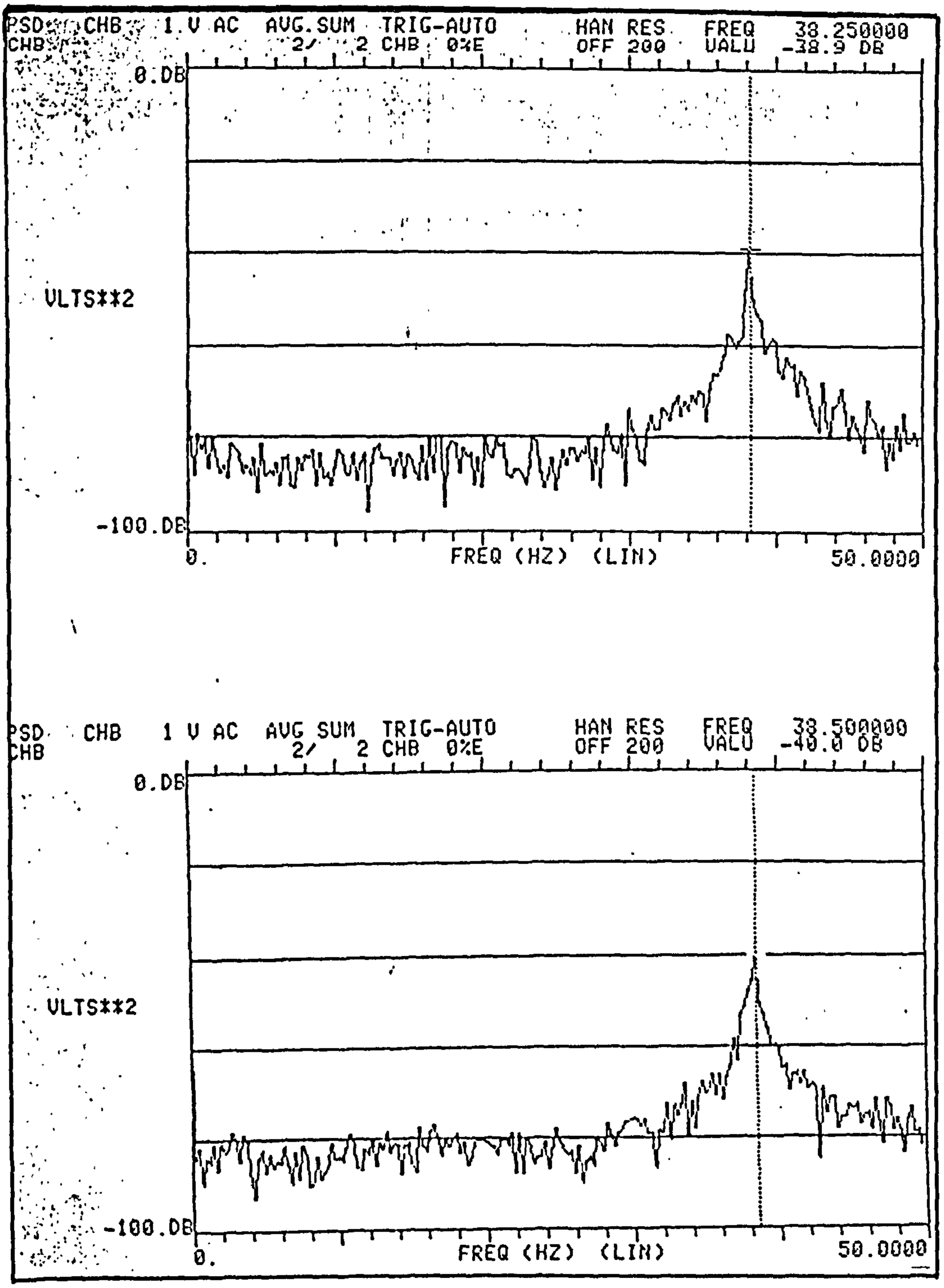

Figure 8.2 PSD of acceleration response plots for zero degree composite plate with 20^{o} sweep

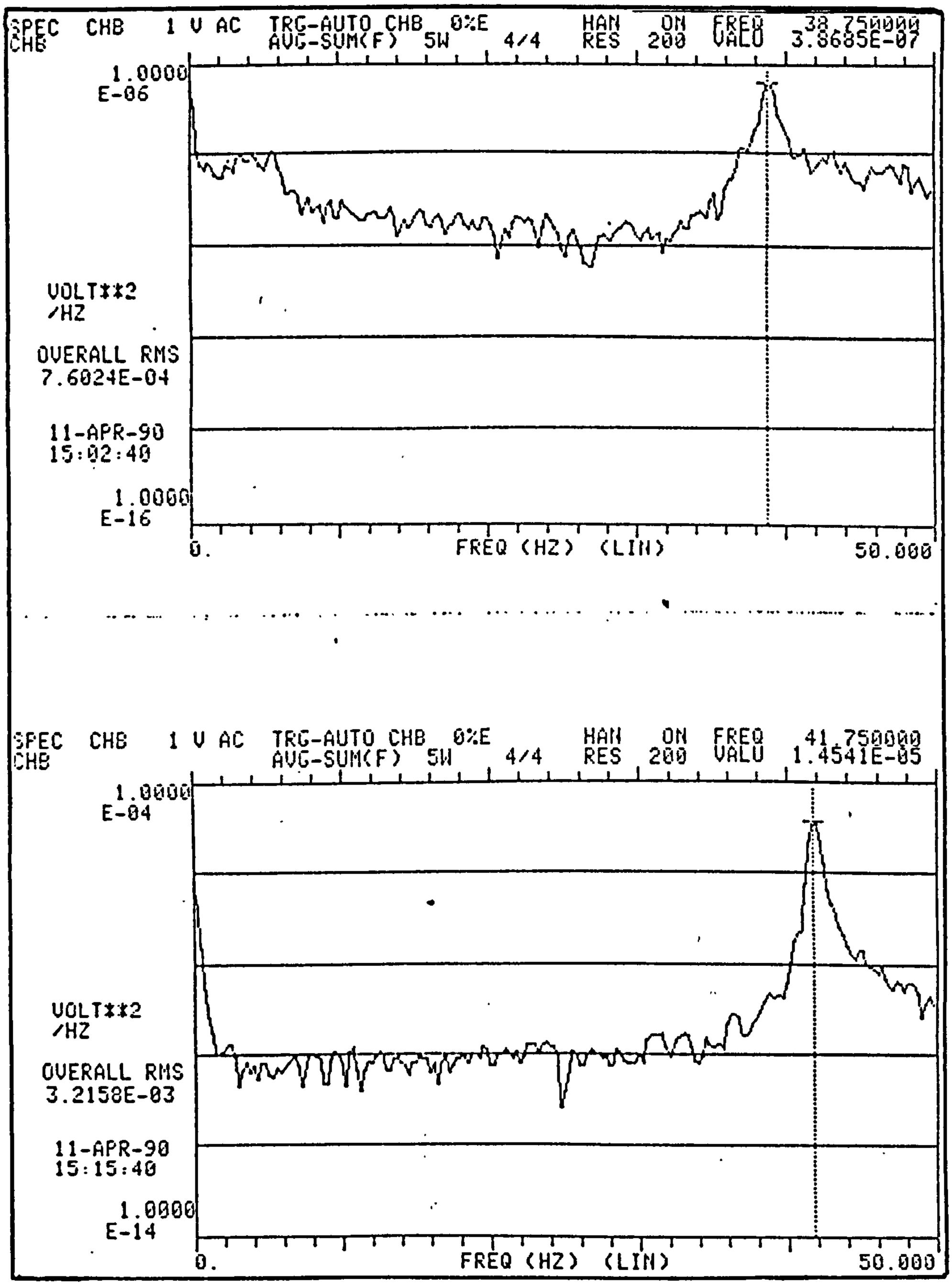

Figure 8.3 PSD of acceleration response plots for $[\pm 30^{\circ}]_s$ composite wing with 0° and 20° sweep

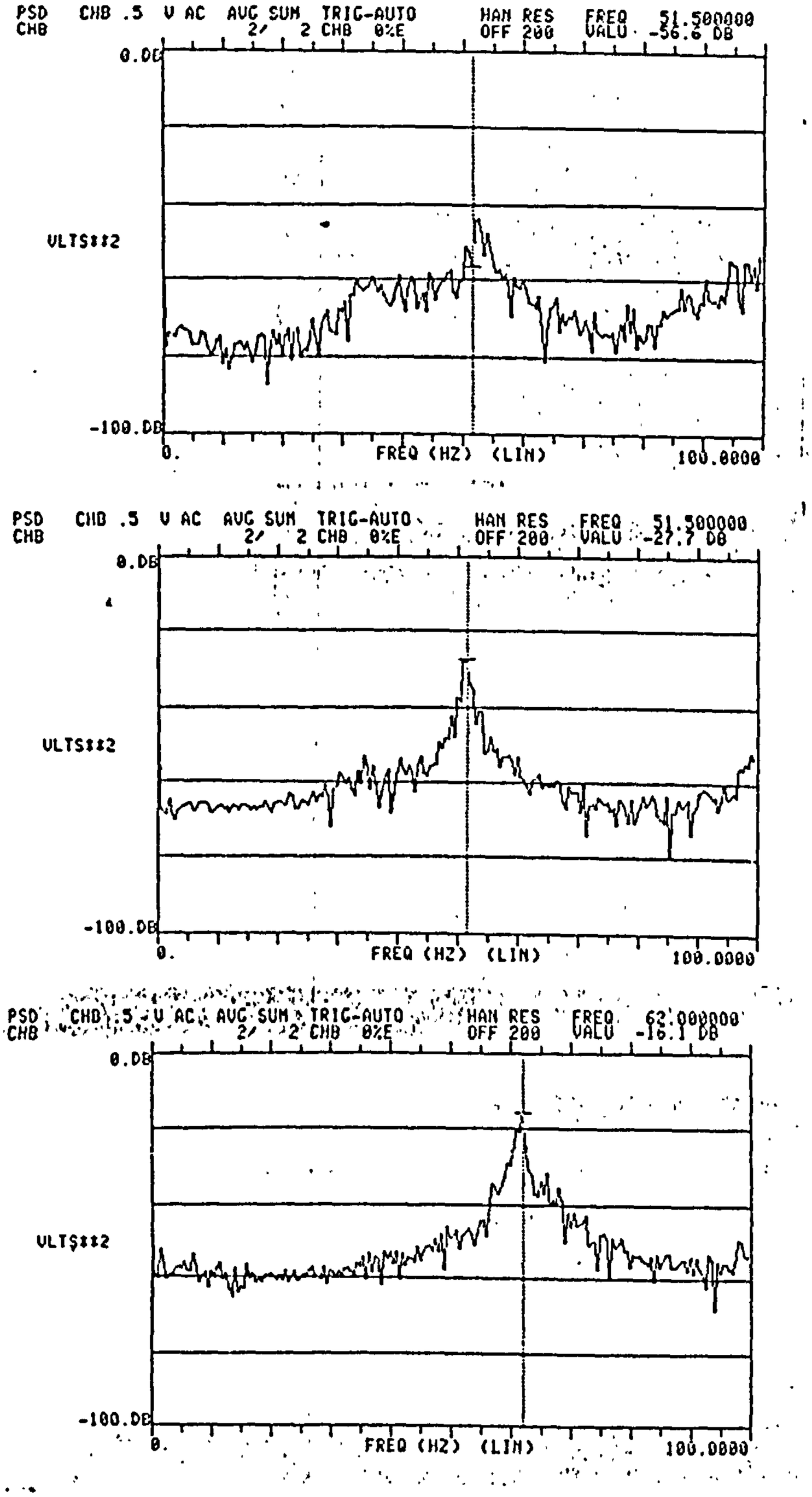

Figure 8.4 PSD of acceleration response plots for $[\pm 45^{\circ}/0]_s$ composite wing with 0° sweep (i) 40.23 m/s, (ii) 43.83 m/s (iii) 47.22 m/s

Text cut off in original

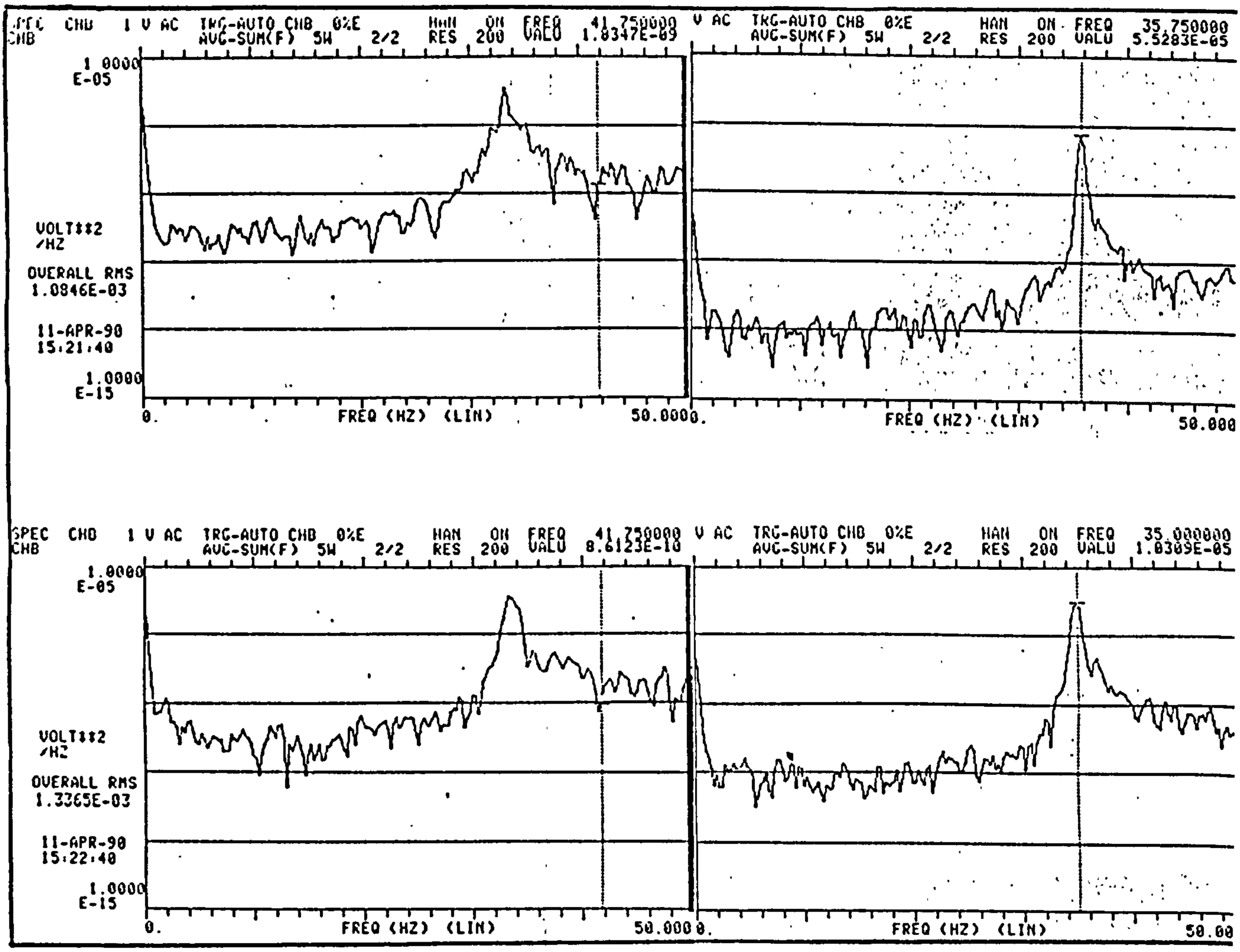

Figure 8.5 PSD of acceleration response plots for $[\pm 45^{\circ}/0]_s$ composite wing with 20^{o} sweep at various pre-critical flutter speeds

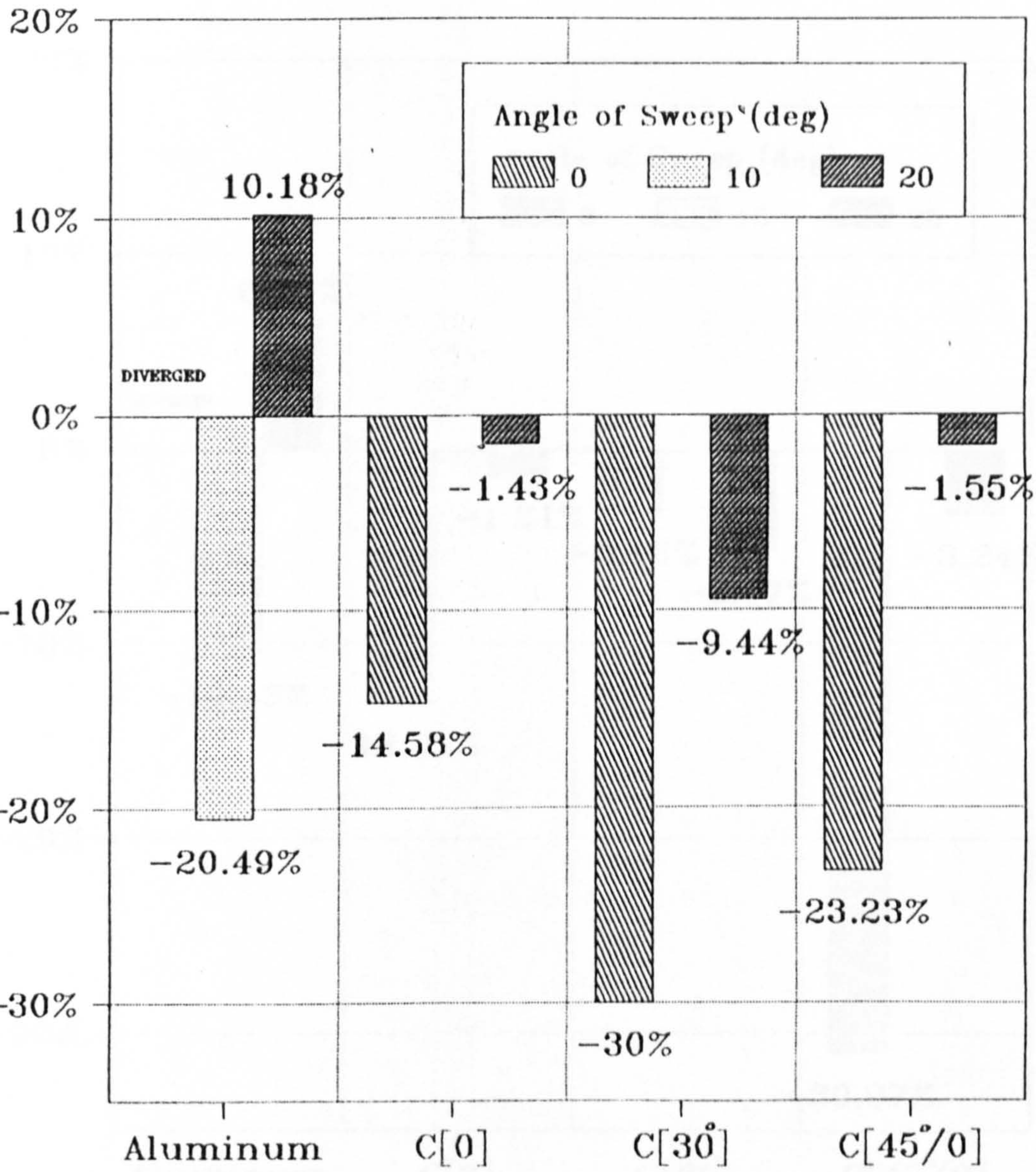

Graphite/Epoxy composite plates with three different lay-up sequence are [0]-6 plies, [+-+30°]s, and [+-45°/0]s

Figure 8.6 Effect of ply orientation on prediction of flutter speed

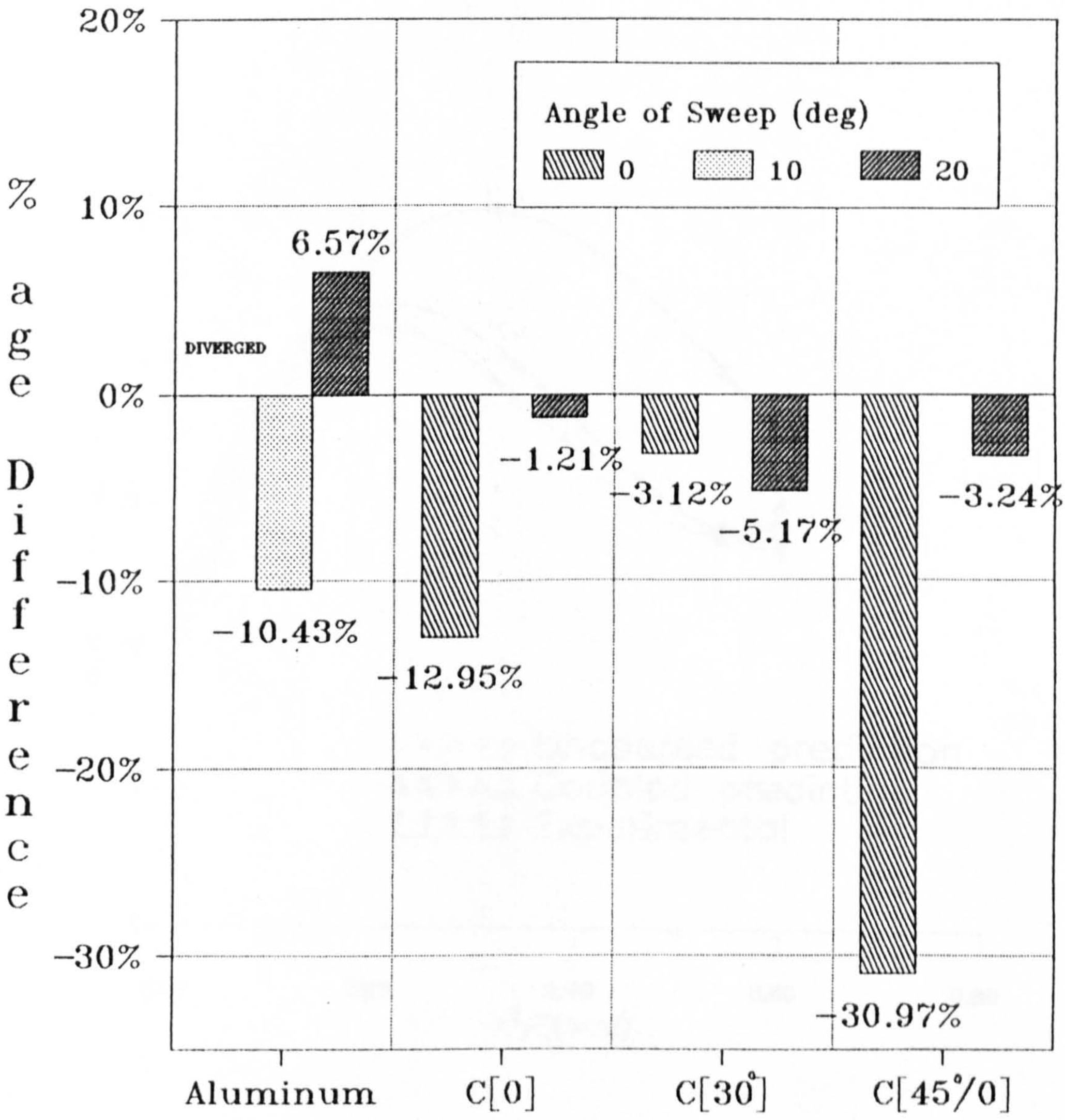

Graphite/Epoxy composite plates with three different lay-up sequence are [0]-6 plies, [+−+30°]s, and [+−45°/0]s

Figure 8.7 Effect of ply orientation on prediction of flutter frequency

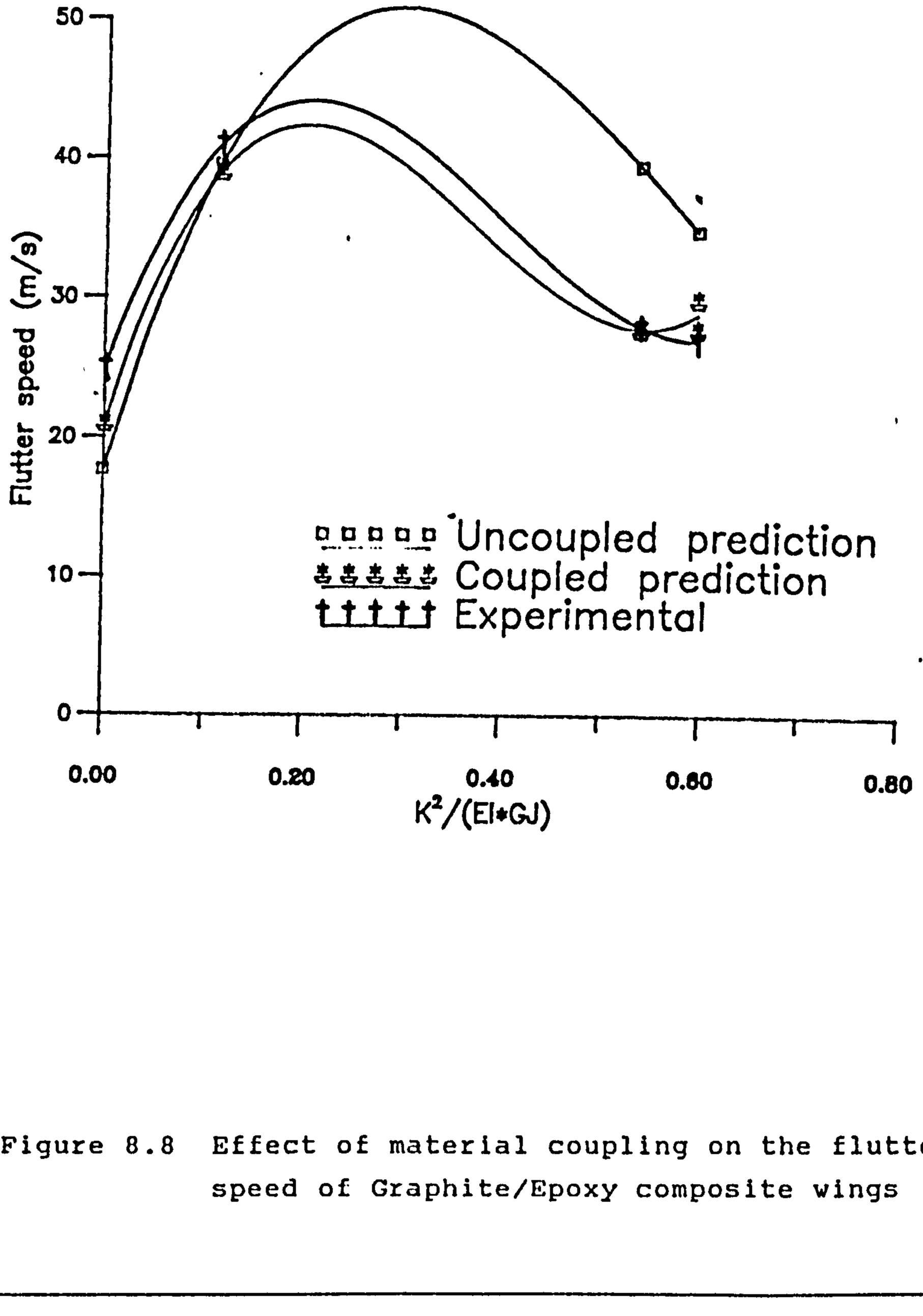

Figure 8.8 Effect of material coupling on the flutter speed of Graphite/Epoxy composite wings

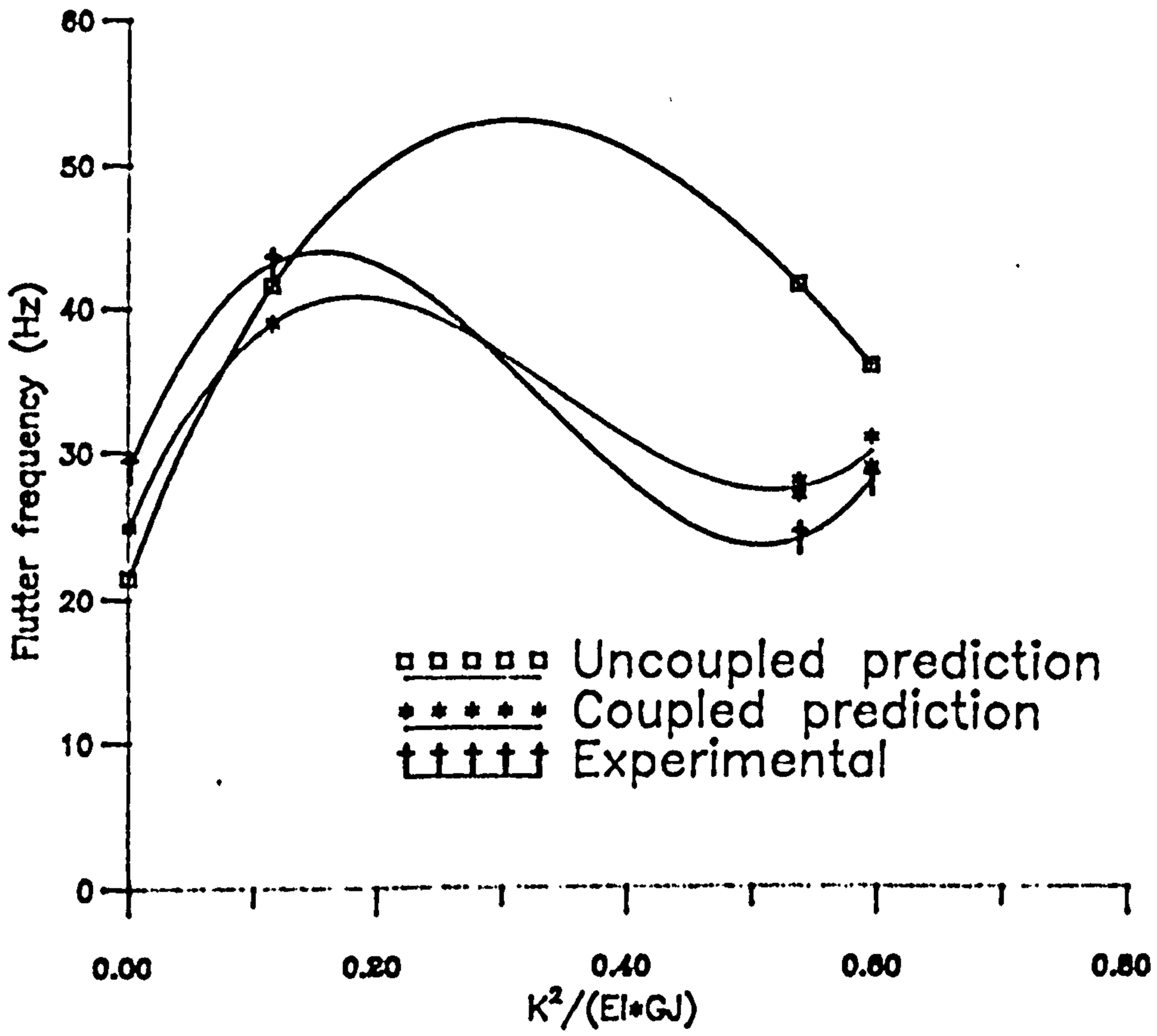

Figure 8.9 Effect of material coupling on the flutter frequency of Graphite/Epoxy composite wings

CHAPTER : 9

AEROELASTIC INVESTIGATION OF THIN-WALLED CLOSED SECTION COMPOSITE WING STRUCTURES

9.1 INTRODUCTION

The lack of published information on aeroelastic testing of thin-walled closed section composite wings (with or without spars and ribs) led to the selection of this topic. Thin-walled closed section composite wing structures were manufactured from glass fibre reinforced plastic and unsaturated isophathalic resin using the hand-lay-up technique. The dimensional details of the wings were estimated using the maximum wind tunnel speed and dimensions of the working section as independent parameters. The lift-curve slope value for the wings was determined experimentally. Aeroelastic investigation of these composite wings included study of sub-critical speed behaviour, stall flutter, and determination of divergence speed. The results showed good agreement between experimental results and theoretical predictions.

9.2 MATERIAL

Glass fibre reinforced plastic, chemically known as calcium-alumina borosilicate glass with an alkali content of less than one percent, (commonly known as 'E - glass') and unsaturated isophathalic resin was used in manufacturing thin-walled closed section composite wings.

The main feature that helped in the selection of this material was its ease in manufacturing intricate shapes due to room temperature curing cycle, (preferably about 18^{o}- 20^{o} C). The requirement of a flexible structure with low Young's modulus of elasticity was another reason to choose this material. The hand-lay-up technique was found

suitable and relatively economical. However, this may have the problem of inconsistency in maintaining the relative volume fraction of fibre and resin during the manufacture. The complexity of the problem was reduced by using woven cloth.

9.2.1 MATERIAL PROPERTIES

The material properties were experimentally established by performing tensile tests on a specially orthotropic specimen to obtain E_1 and E_2 (Young's moduli along and across the fibre directions), and the Poisson's ratios ν_{12}, ν_{21}. The tensile test was conducted on a 45^{o} laminated specimen to determine the shear modulus G_{12}.

A plate of 4 plies with symmetric lay-up was prepared and strips of various suitable dimensions were cut along the fibre direction and at 45-degrees. Aluminium grip pads were glued to the specimen. Strain gauges of half inch length were found suitable to cover a large number of fibres and to give a representative measure of strain produced in the specimen. The experimentally established material properties are given in appendix (J).

9.3 THIN-WALLED COMPOSITE WINGS

9.3 1 CONSTRUCTION OF WINGS

The cross-sectional profile of the closed thin-walled structure was selected to be an aerofoil shape. A wooden wing of about 100mm chord length of NACA 0012 profile was readily available in the department, which was used as a core or wooden former. Woven cloth was cut to size (usually a piece of 950 X 250 mm of GFRP woven cloth). The cloth was laid on a wax sheet of paper over a flat surface. The cloth was marked with a centre line. In the case of wings other than zero degree lay up, the sheet

was cut into two halves. A suitable quantity of unsaturated isophathalic resin was mixed with the accelerator. The resin was gently spread over the GFRP cloth and was left for a while to polymerize. Another sheet of wax paper was placed over it and was placed under a flat surface with moderate pressure for some time. While the resin was still in a jelly state, the leading edge of the wooden wing core was aligned with the centre line of the cloth (in the case of other than zero degree ply lay up, a lap joint of the two pieces of cloth was made at the leading edge). Then the semi-cured cloth was wrapped around the former and was left for full cure with a moderate pressure to retain the desired shape. The trailing edges were glued with Redox 410 glue and the wing was trimmed to desired sizes of chord and span.

In early experiments, Brazier-load effect was experienced i.e. kinking of the thin walls occurred as the structure was transversely loaded. This problem was solved by filling Polyurethene expanded foam into the cavity of the wing. This technique proved successful because the section no longer collapsed on transverse loading and retained its geometry on being twisted for torsional rigidity and shear centre tests. In other cases, an F-board (honey-comb) spar was longitudinally glued to the skin to improve the structural bending rigidity, see Photographs (9.1) and (9.2).

9.3.2 SECTIONAL DETAILS

The trimmed wing with its final size was given a code number. It was then weighed and various dimensions such as chord and span lengths were measured [see Table (5.16)]. The thickness of the skin varied considerably which is typical of the hand-lay-up technique. Therefore, several measurements of the thickness of the skin were

made at various locations in order to obtain a good average.

Impressions of the profile resulting on both sides of the wing were taken on paper. The contour was divided into several small straight segments. The co-ordinates of these segments were then measured from the chord line. Some of the wings were filled with foam and tested.

Structural rigidities and other parameters such as mass per unit length, location of the centre of gravity, shear centre and polar mass moment of inertia for these sections were experimentally found and compared with the theoretical predictions as shown in Tables (5.17) - (5.20). Finally tests were carried out for dynamic behaviour. Results for natural frequencies and normal mode shapes are given in Tables (7.29) to (7.39).

9.4 EFFECT OF MATERIAL COUPLING ON FLUTTER SPEED

The flutter speed is sensitive to the difference between the frequencies of the two coupled modes causing the flutter (the influence of material coupling on bending and torsional frequency has been discussed in Chapter (7.7)). In light of the above, two distinct situations may arise, namely the torsional mode frequency being greater than the bending mode frequency and the bending mode frequency being greater than the torsional mode frequency. In the former case omission of material coupling from the theoretical model gives a conservative estimate of the flutter speed due to overestimated bending and underestimated torsional mode frequencies. However, for structures with a bending frequency greater than the torsional frequency, omission of material coupling rigidity will dangerously over-estimate the critical flutter speed.

These facts were important in designing the composite

wings for wind-tunnel flutter tests because of the practical limitations on tunnel speed. Theoretical analysis showed that material coupling increased the flutter speed with ply orientation because the first torsional mode frequency was greater than the first bending mode frequency. Consequently, the lowest design flutter speed was achieved using zero degree ply orientation (see Chapter (8) for details).

In an attempt to understand the aeroelastic behaviour of these thin-walled closed sections (i.e. composite wings) only two areas namely, flutter (binary i.e. bending-torsion flutter) and divergence were studied intensively. The presence of material bending-torsion coupling similar to elastic coupling, (due to non-coaxial centroidal and elastic axes,) which plays an important role in changing the aeroelastic characteristics of a lifting surface was also accounted for.

Experimental investigation of the aeroelastic behaviour of thin-walled composite wings was thus carried out with the following results.

9.5 EXPERIMENTAL RESULTS

9.5.1 WING W-DMS-1

During determination of flexural rigidity, the composite wing specimen suffered from the Brazier load effect. The lower skin of the wing collapsed inwardly near the root resulting in permanent damage. Therefore, it was not possible to conduct any dynamic tests to establish the natural frequencies and the mode shapes. The flutter speed of the specimen was estimated to be 72.0 m/s based on available static structural properties which was above the maximum attainable speed of the wind-tunnel.

9.5.2 WING W-DMS-1A

The damaged portion near the root was removed, the wing was re-rooted and the structure was tested again to determine its bending rigidity. The estimated flutter speed increased to 80.0 m/s due to a decrease in aspect ratio. In the light of these results the task was divided into three stages.

1. To manufacture at least two more similar structures in order to obtain an average of the structural properties.
2. The flutter speed can be reduced by minimizing the difference between the predominantly bending mode and predominantly torsional mode frequencies. This can be achieved by increasing the bending rigidity and polar mass moment of inertia, and by decreasing the mass per unit length and torsional rigidity. Thus the wing section was filled with polyurethene expanded foam which increased the bending rigidity, polar mass moment of inertia as well as torsional rigidity and mass per unit length.
3. The third possibility was to mechanically destabilize the wing by opening its trailing edge in an attempt to reduce the torsional rigidity and increase the distance between the centroide and the shear centre. This will also increase the value of the polar moment of inertia.

9.5.3 WING W-DMS-1B

The structural properties obtained after splitting the trailing edge of the wing are as follows :

$GJ = 0.01725$ N-m^2, $X_\alpha = 135.4$ mm , $I_{p_\bullet} = 0.00344455$ kg-m

The sharp decrease in torsional rigidity required an

estimation of divergence speed using equation (9.1) prior to flutter testing.

$$V_d = \sqrt{\frac{\pi^2 \, GJ}{2 \, \rho (ec)^2 s^2} \left(\frac{\partial C_l}{\partial \alpha}\right)} \qquad (9.1)$$

where

ρ_{air} = 1.225 kg/m^3

s = span or length of the wing = 0.585 m

$\left(\frac{\partial C_l}{\partial \alpha}\right)$ = lift-curve-slope value = 2 π (assumed)

ec = distance between the aerodynamic centre and the shear centre = 0.1081 m

The predicted divergence speed was 1.66 m/s. The wing lost its shape because of the erratic flapping of the two surfaces. A double sided adhesive tape was used to keep the trailing edges together. The new shear centre was 8.5mm behind the aerodynamic centre. The divergence speed was calculated to be 21.15 m/s, ignoring any increase in the torsional rigidtiy, as compared to the experimental value of 24.0 m/s with a difference of 13.5% , probably due to a nominal increase in torsional rigidity.

9.5.4 WING W-DMS-2

The next wing was filled with a light and hard core foam (expanded polyurethene) to stop the local kinking due to the Brazier-load-effect and to retain the shape during bending or torsion of the structure. The flutter check list suggested an increase in bending rigidity and decrease in torsional rigidity to reduce the flutter speed by decreasing the difference between the bending and torsional mode frequencies. The bending rigidity improved but at the expense of added torsional stiffness, mass per unit length and polar mass moment of inertia. These changes were contrary to each other.

TORSIONAL RIGIDITY ESTIMATIONS OF FOAM FILLED WINGS

The prediction of various properties of a foam filled section was made by assuming linear summation of the contributions made by the two materials. For example in case of bending, it was assumed that the total resistance offered in deflecting the structure to the applied load will be the sum of bending stiffness of the skin section plus the bending stiffness of the foam section. Similarly in the case of torsion the structure is assumed to be acting like a pair of helical springs with two different stiffnesses wound one over another. In the case of an applied torque, the skin section first offers the resistance and then the foam packed inside it contributes to the torsional rigidity. Table (9.1) compares the torsional rigidity of a skin section with that of a foam filled section.

The estimated flutter speed and frequency were 106 m/s and 74.48 Hz respectively, still beyond the wind tunnel airspeed limit. The results of the static and dynamic tests were in close agreement with the theoretical predictions.

9.5.5 WING W-DMS-3

An extended flap-like trailing edge was produced when both the top and bottom skins were glued together. The extended flap was removed to increase the aspect ratio (approximately 14) and to reduce the mass per unit length of the wing. The flutter speed and frequency were estimated to be 107 m/s and 50.45 Hz respectively. A wind tunnel test was conducted to study the sub-critical flutter behaviour of the wing. The large amplitude flapping motion damaged the tip of the wing where it was restrained by a fishing line to avoid any possible divergence. The removal of damaged tip reduced the aspect

ratio and increased the flutter speed to 152 m/s.

9.5.6 WING W-DMS-4

Another wing identical to W-DMS-3 was constructed with an estimated flutter speed of 100.0 m/s and flutter frequency of 59.68 Hz. The possibility of putting a steel strip of (3.3 mm diameter) near the trailing edge was considered to move the centroid to its extreme position near the trailing edge with an increase in the elastic coupling. This reduced the flutter speed to 96.3 m/s. That still did not solve the problem. So it was further used in determining the lift-curve slope value.

LIFT-CURVE SLOPE VALUE

CALFUN (computer program used for the prediction of flutter speed and frequency) utilizes strip theory to calculate the aerodynamic distribution over the wing. Strip theory assumes a lift-curve slope value of 2π for an infinite wing in incompressible flow conditions (see Appendix (F) for theory). The finite aspect ratio and profile resulting from the hand-lay-up technique will result in a lower lift-curve slope value. An experiment was set up to determine the lift-curve slope value for the composite wings (see Photographs (9.3) and (9.4)). The lift-curve slope value for the three dimensional composite wing was estimated using a computer program as given in Appendix (C).

The test was carried out at three different speeds 15.59, 21.78 and 24.20 m/s and their Reynolds numbers were $1.249*10^5$, $1.745*10^5$ and $1.939*10^5$ respectively. The coefficient of lift was plotted against the angle of attack for each run as shown in Figure (9.1). The experimental results are compared with the theoretical predictions in Table (9.2).

The value of the lift-curve slope given in reference [1] is for steady conditions and does not necessarily correspond to the slope obtained in transient conditions when the boundary layer has insufficient time to fully develop at each lift coefficient. The presence of some degree of turbulence in the wind tunnel can be one of the many reasons for this large error.

The inexact profile of the wing and surface roughness alter the aerodynamic distribution and the coefficient of lift corresponding to a certain angle of incidence, giving a smaller lift-curve slope value.

The scale effect is negligible for a wing thickness to chord ratio less than 12% . During construction the eventual thickness sometimes exceeded this figure, resulting in a smaller value of the lift-curve slope.

9.5.7 WING W-DMS-7

The wing was filled with polystyrene foam, usually used as packing material. It was selected due to its low density (approximately 27.32 kg/m^3 found experimentally).

The wing was split at the elastic axis on the lower side as the leading edge faces the oncoming wind. The torsional rigidity reduced to a small value of 0.011391 $N-m^2$. The divergence speed was predicted to be 7.88 m/s. The tip of the wing was loosely held with a fishing line for safety reasons. The wind tunnel speed was gradually increased. The wing experienced stall flutter (stall flutter is defined as flutter of a lifting surface in which the aerofoil sections are in stalled flow during at least part of each cycle of oscillation) before the predicted divergence speed of 9.0 m/s.

9.5.8 WING W-DMS-12

A wing similar to W-DMS-7 was constructed with a

spar, placed inside the hollow wing along the elastic axis. An initial investigation into the dynamic behaviour of the wing revealed a well distinguished single peak for the first frequency of 10.5 Hz. Two peaks of 58.5 Hz, and 63.0 Hz gave the indication of a second frequency in that range. The peak for the third frequency was very flat and unclear as shown in Figure (9.2).

The wing was held in a specially built fixture in the wind tunnel. The airspeed was gradually increased and by means of an accelerometer attached to the wing the magnitude of the frequency response function was recorded at different speeds as shown in Figure (9.3). As the airspeed was increased the second frequency, which was a torsional mode, disappeared. The third frequency peak was now well distinguished at 123 Hz. As the speed was further increased, the amplitude of first frequency decreased and another frequency at about 190 Hz appeared. But soon a single peak appeared at 20 m/s airspeed of approximately 120 Hz. A further increase in airspeed increased the magnitude of this single peak. The airspeed was increased to its maximum safe limit of 44.6 m/s without experiencing flutter. The limitations of the spectrum analyser made it difficult to obtain a quantitative measure with enough resolution to represent these quantities in a graphical form.

The wing exhibited sub-critical flutter behaviour similar to the flutter tests conducted on aluminium and composite plates as shown in Chapter (8). The modal damping of predominantly bending and torsional mode frequencies increased with increase in airspeed except in the case of flutter the damping ratio of the dynamic aeroelastic mode passed through zero. The magnitude of the frequency response function for the flutter frequency was initially reduced and then remained constant for the

rest of the experiment. The wind tunnel speed limitations made it difficult to observe total loss of modal damping characteristic of the critical flutter speed.

The glued trailing edge produced a cambered airfoil instead of the NACA 0012. Therefore, high lift forces were developed and the wing showed tip divergence within the elastic range of the material. It was highly dangerous due to strength limitations of the structure.

9.5.9 WINGS WITH GENERALLY ORTHOTROPIC LAY-UP

Wings with a generally orthotropic lay-up had high flutter speeds as discussed in section (9.4). These wings were constructed to study their static and dynamic behaviour. The theoretical estimates of flutter speed and frequency for 10^{o}, 20^{o}, 30^{o}, and 45^{o} ply lay-up is given in Table (9.4).

9.6 CONCLUSIONS

The aeroelastic behaviour of thin-walled closed section composite wings with elastic bending-torsion coupling was investigated. The wind tunnel speed limitations did not allow the performance of a binary (bending-torsion) flutter test. However, a stall flutter test was carried out successfully. Other aeroelastic phenomena such as divergence and sub-critical flutter tests on composite wings were also carried out. Divergence tests yielded good agreement between experimental results and theoretical predictions.

REFERENCES

1. Glauert, H., The Elements of Airfoil and Airscrew Theory, Cambridge University Press, London, 1926.

Without foam :			
GJ (Theo.)	17.17	N m^2	
GJ (Exp.)	21.474	N m^2	(with two mirrors)
Percent diff.	25 %		
GJ (Exp.)	20.93	N m^2	(with one mirror)
Percent diff.	22 %		
With foam :			
G for the foam	0.275	GPa	
GJ (Theo.)	40.025	N m^2	
GJ (Exp.)	41.874	N m^2	
Percent diff.	- 4.6 %		

Table 9.1 Torsional rigidity test summary for foam filled wings

Lift-curve slope value per degree (per radian)		% diff
Theoretical (strip theory)	0.10966 (6.283)	
Experimental value for NACA 0012 (see Ref. [1])	0.105 (6.016)	4.25
Average experimental value	0.082978 (4.754)	24.33

Table 9.2 Lift-curve slope value for a composite wing

FLUTTER	WING NUMBER						
	1	1A	2	3	3A	4	7
SPEED m/s	72.0	80.0	106.0	107.0	152.0	100.0	80.0
$FREQUENCY_{Hz}$	59.83	67.80	74.48	50.45	102.65	59.68	62.39

Table 9.3 Summary of the estimated flutter speed and frequency for composite wings with zero degree lay up

FLUTTER	WING LAY-UP IN DEGREES			
	10	20	30	45
SPEED m/s	75.0	96.0	122.0	146.0
$FREQUENCY_{Hz}$	66.05	74.00	101.22	123.35

Table 9.4 Summary of the estimated flutter speed and frequency for composite wings with generally orthotropic lay-up

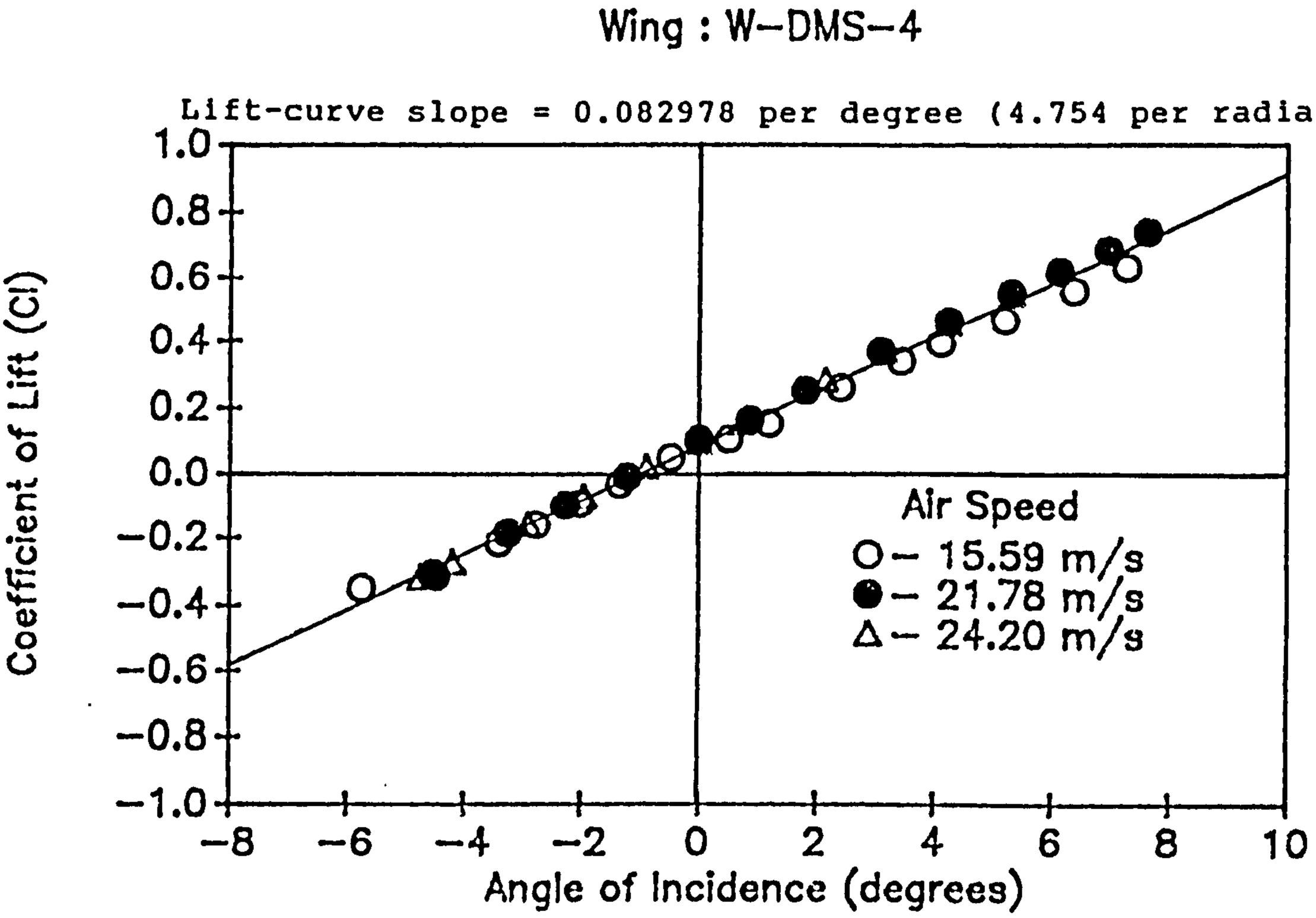

Figure 9.1 Lift-curve slope for wing W-DMS-4

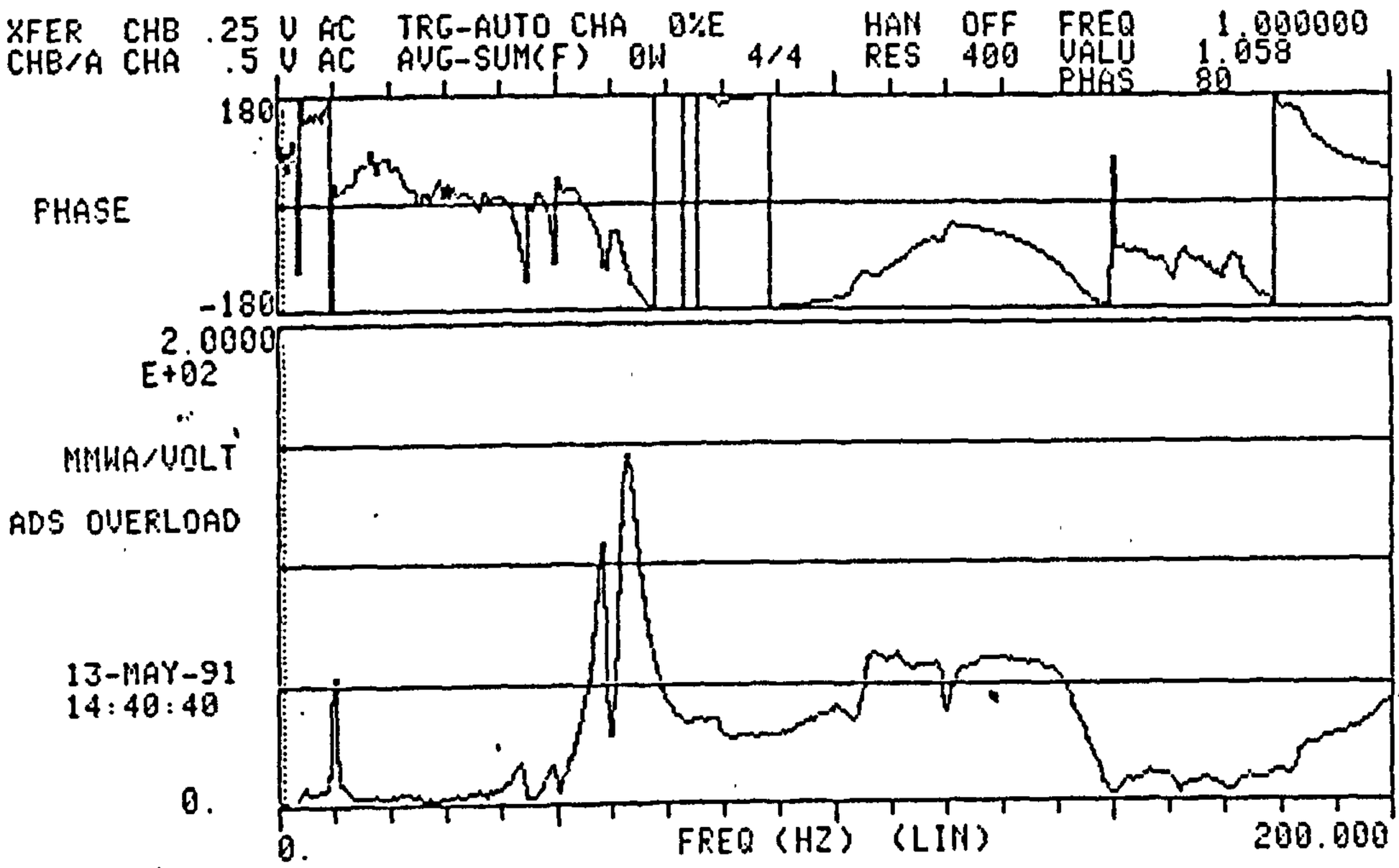

Figure 9.2a Frequency response and phase plots for W-DMS-12 before the wind tunnel test

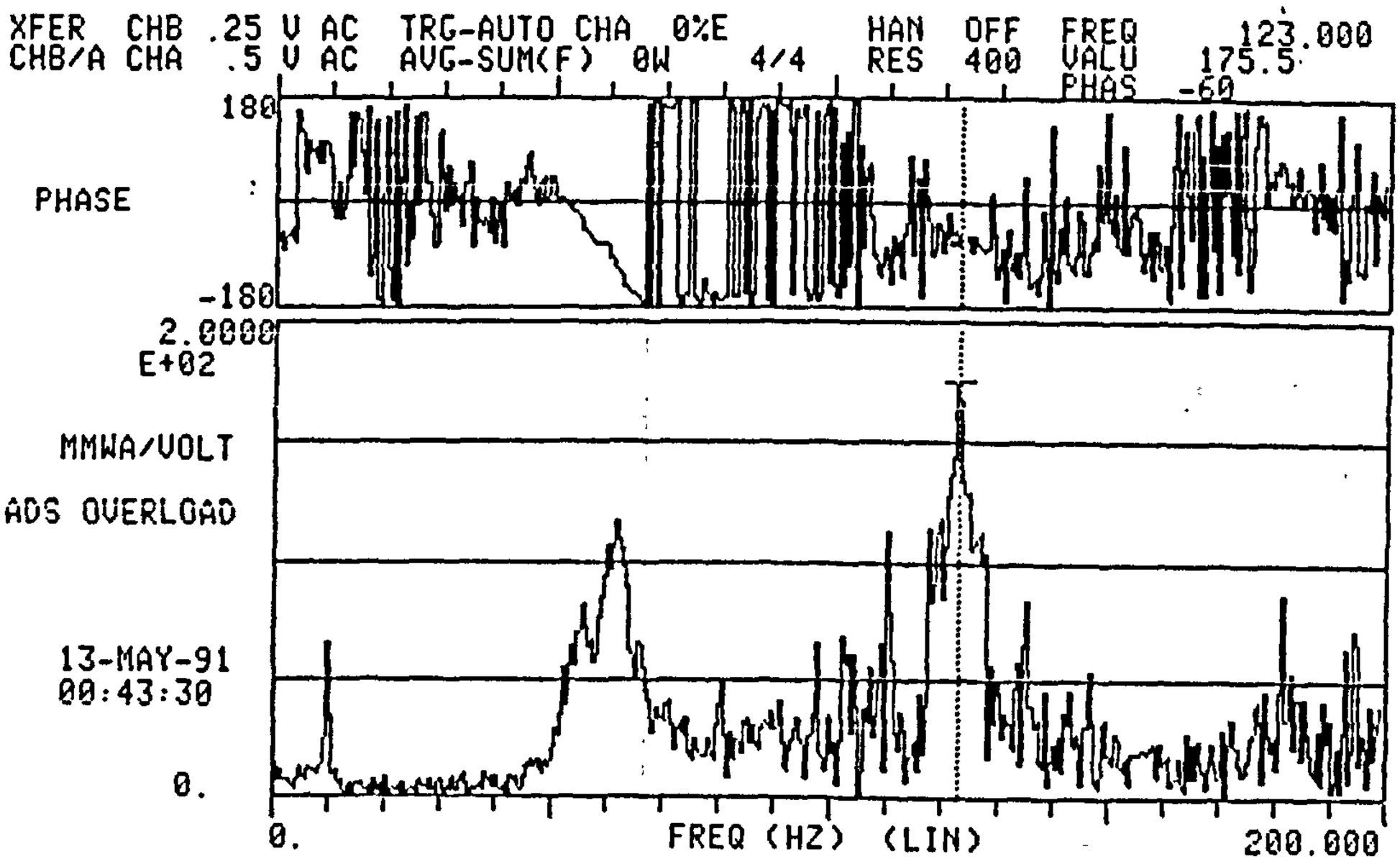

Figure 9.2a Frequency response and phase plots for W-DMS-12 after the wind tunnel test

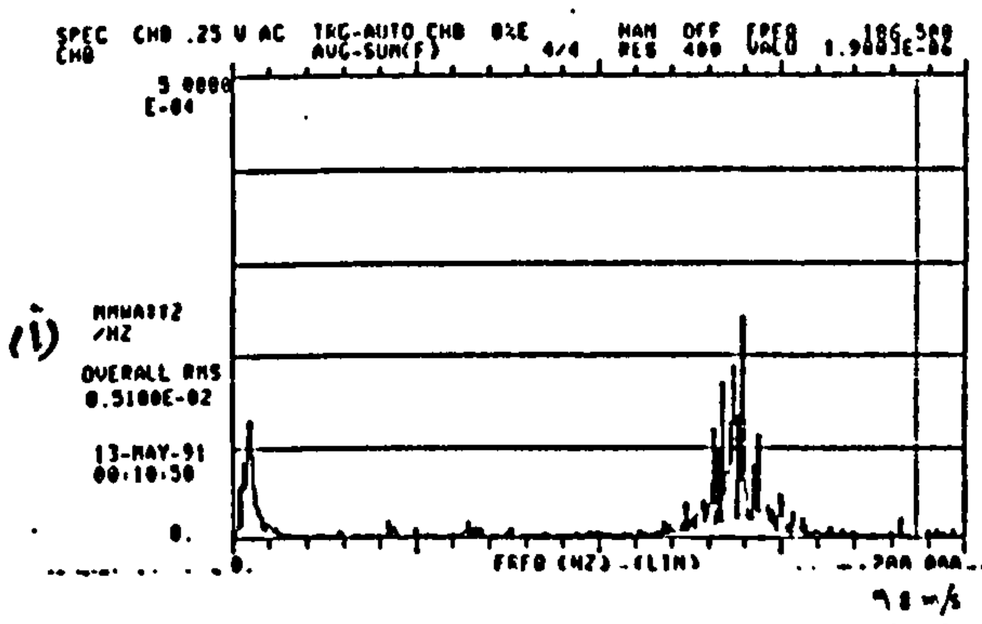

(i) 9.8 m/s

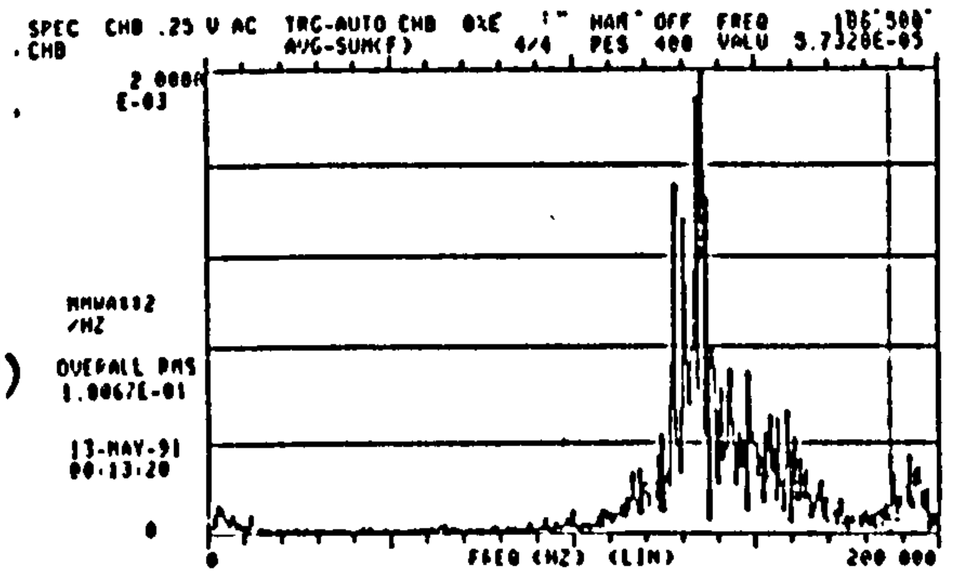

(ii) 15.3 m/s

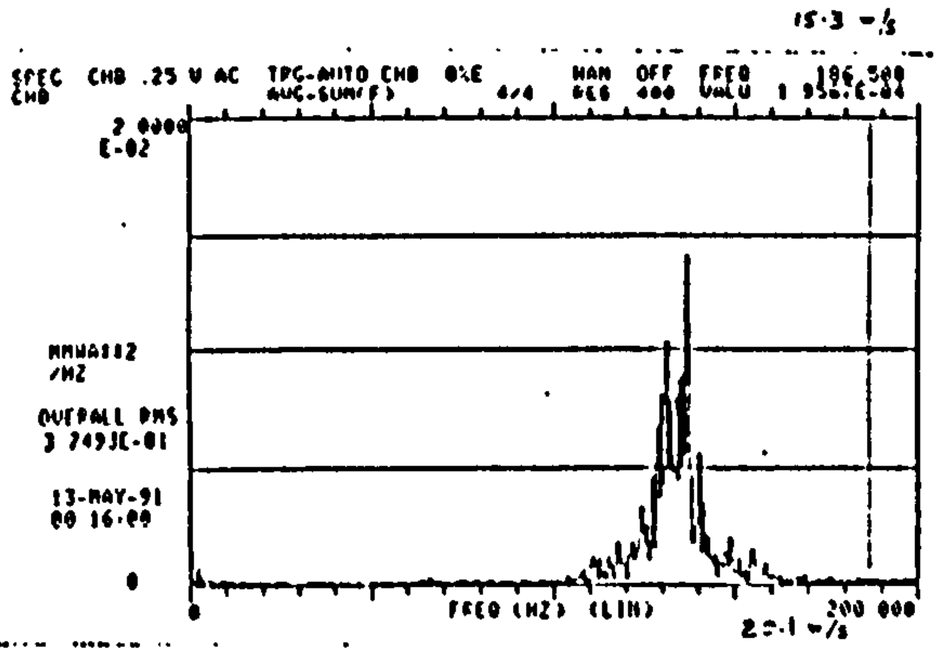

(iii) 20.1 m/s

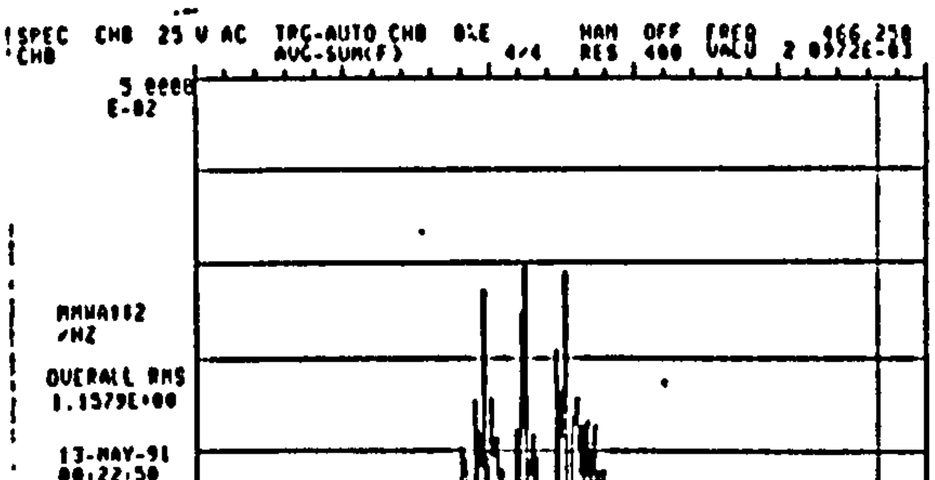

(vii) 30.0 m/s

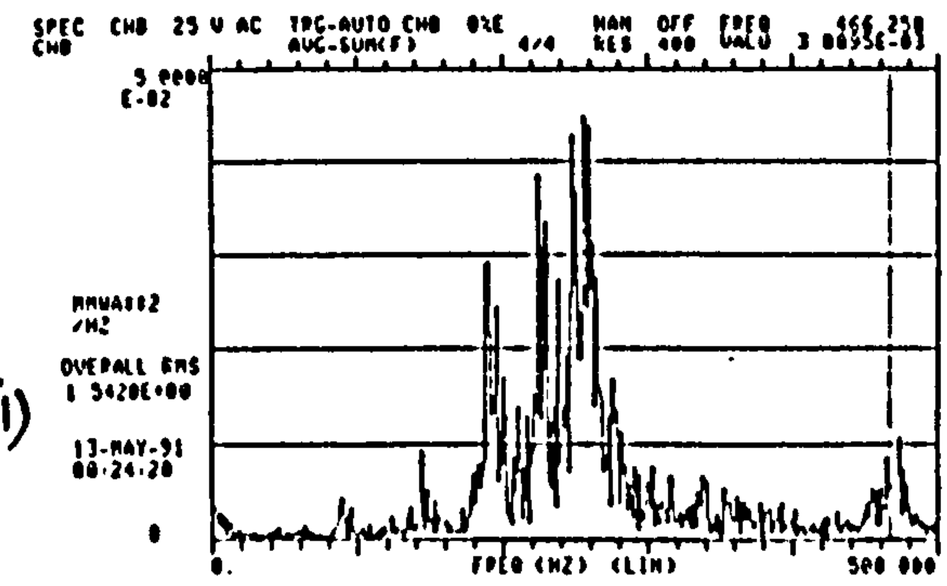

(viii) 32.5 m/s

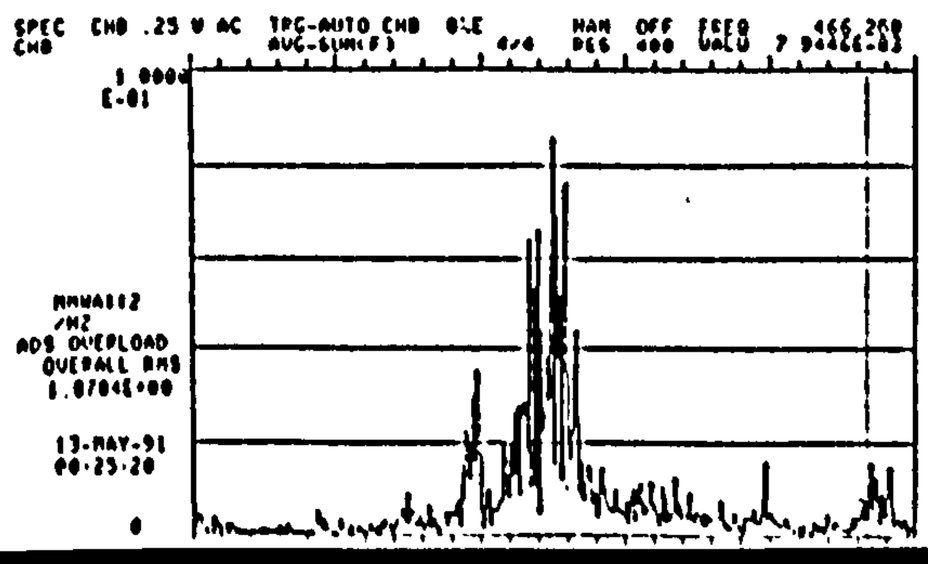

(ix) 34.0 m/s

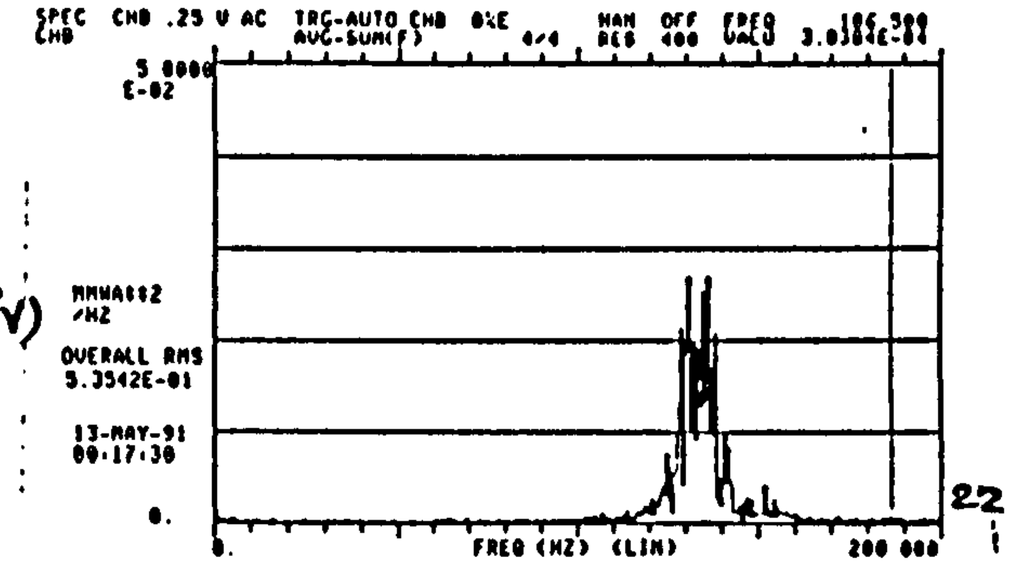

(iv) 22

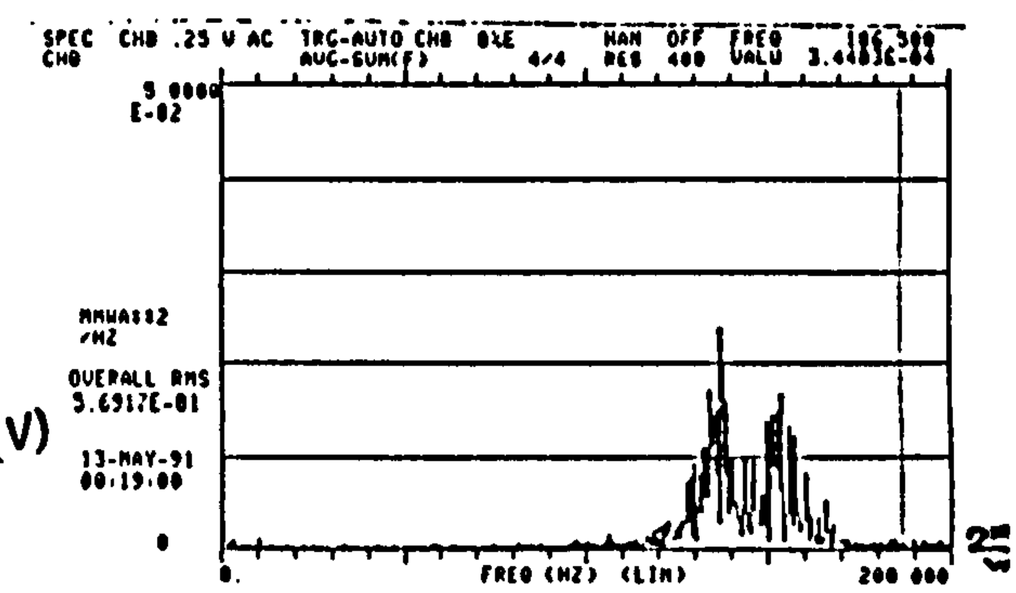

(v) 25

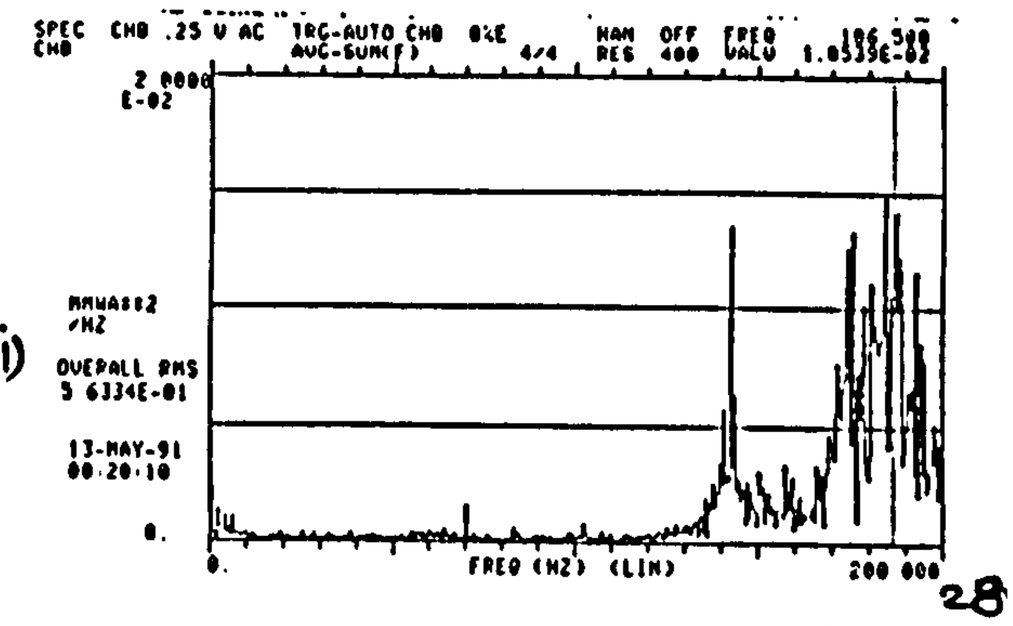

(vi) 28

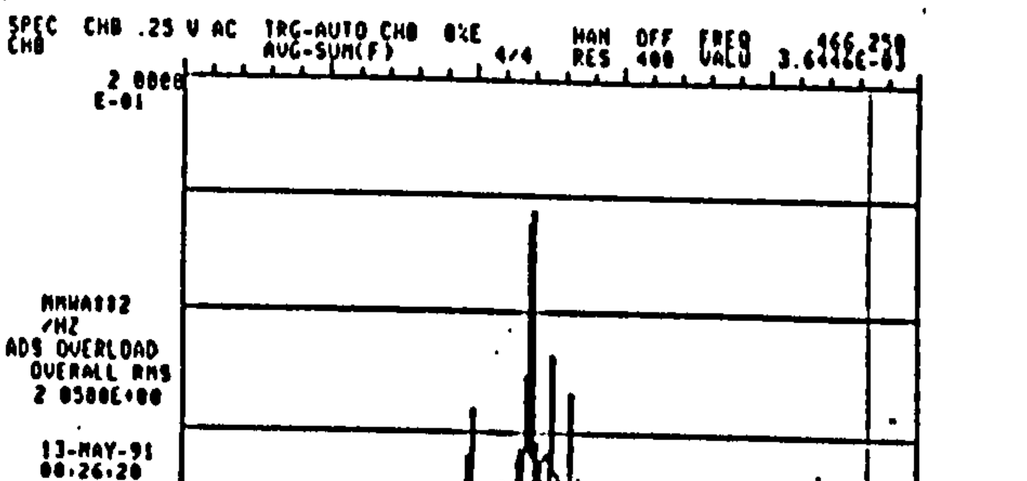

(x) 36.8

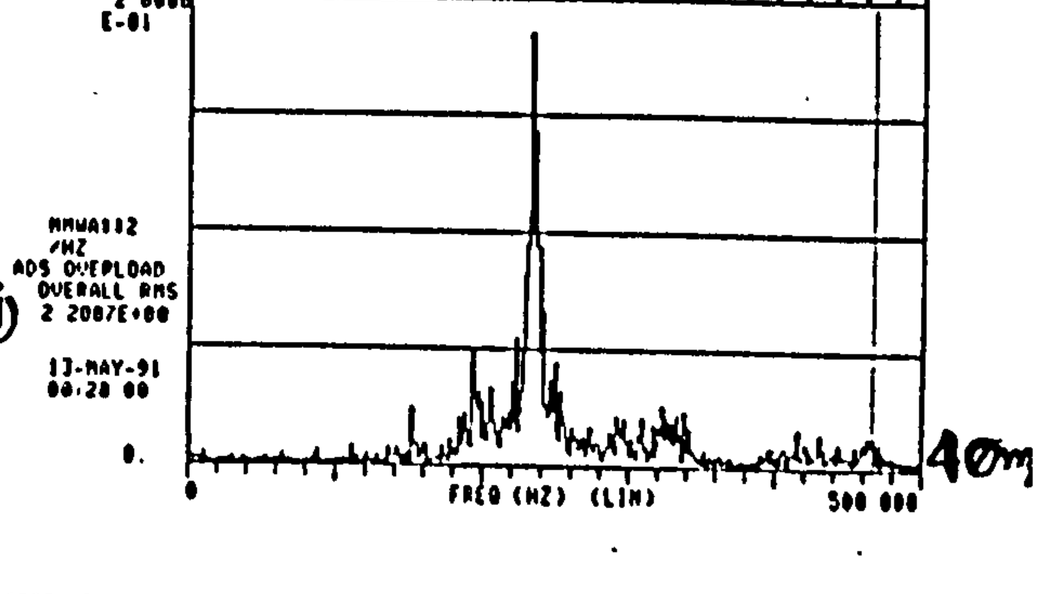

(xi) 40m

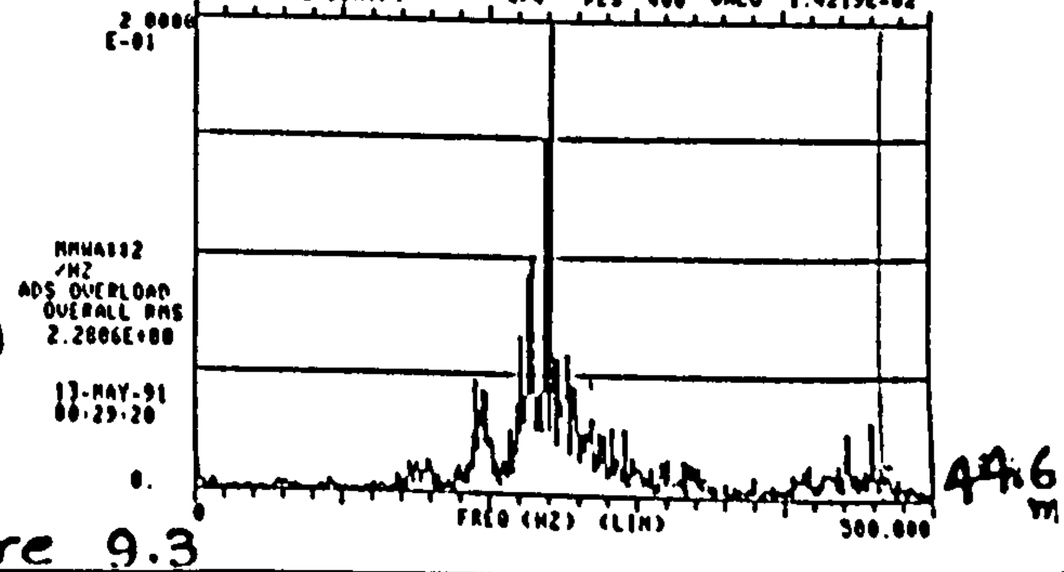

(xii) 44.6 m

Figure 9.3

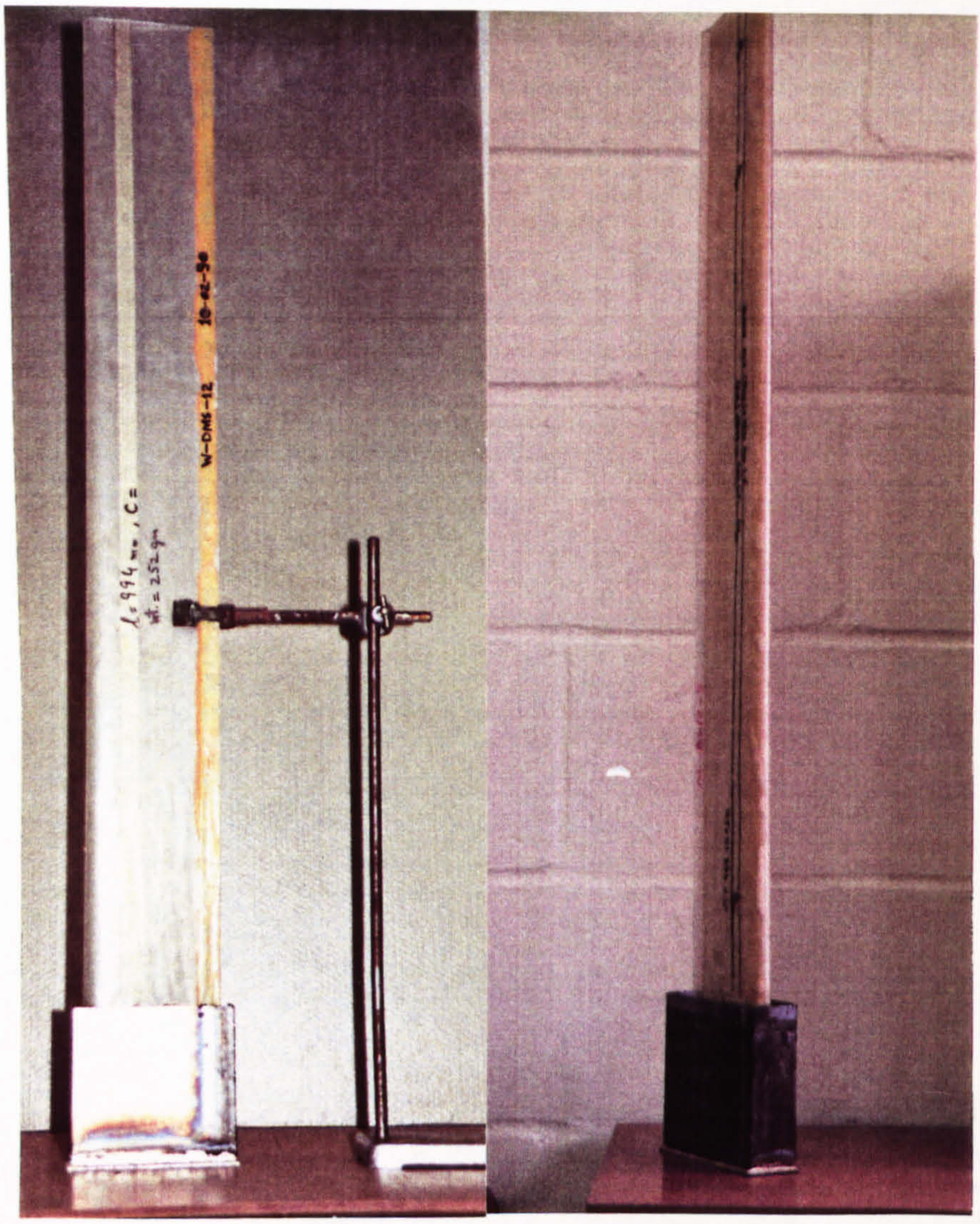

P 9.1 Composite wings (i) with F-board spar, (ii) foam filled

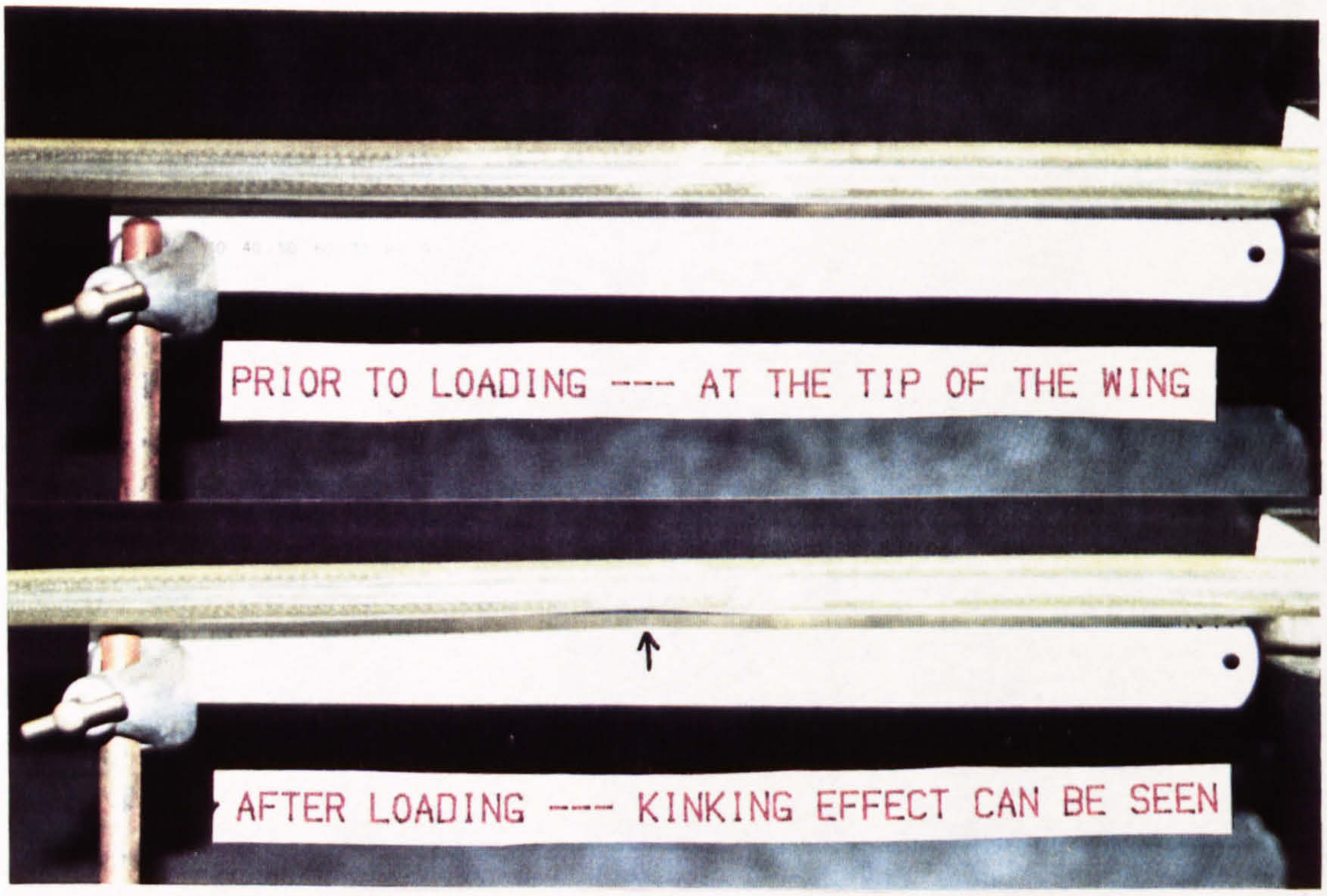

P. 9.2 Brazier-Load effect (found during bending rigidity test)

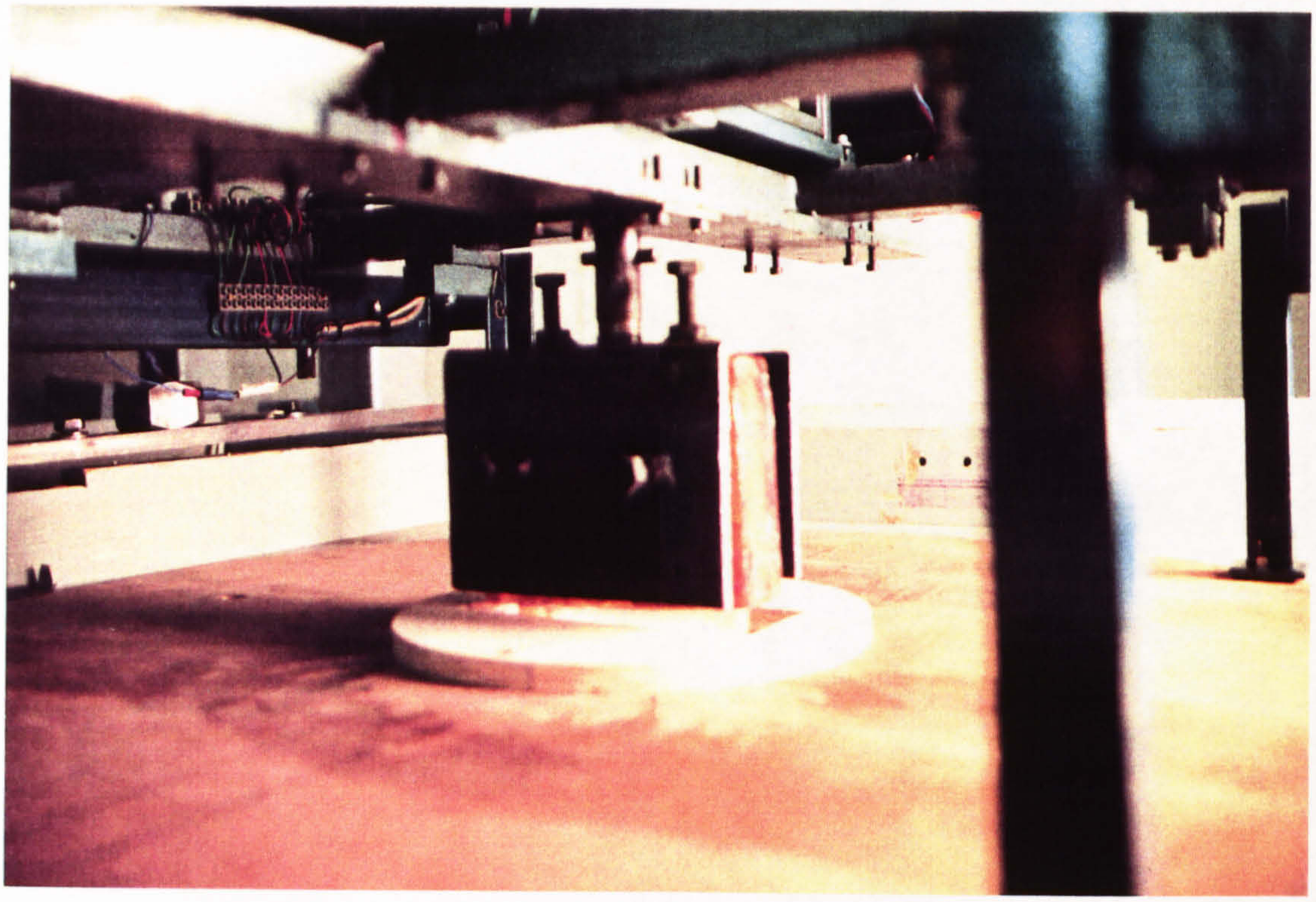

P 9.3 Wing attachment to the wind tunnel balance

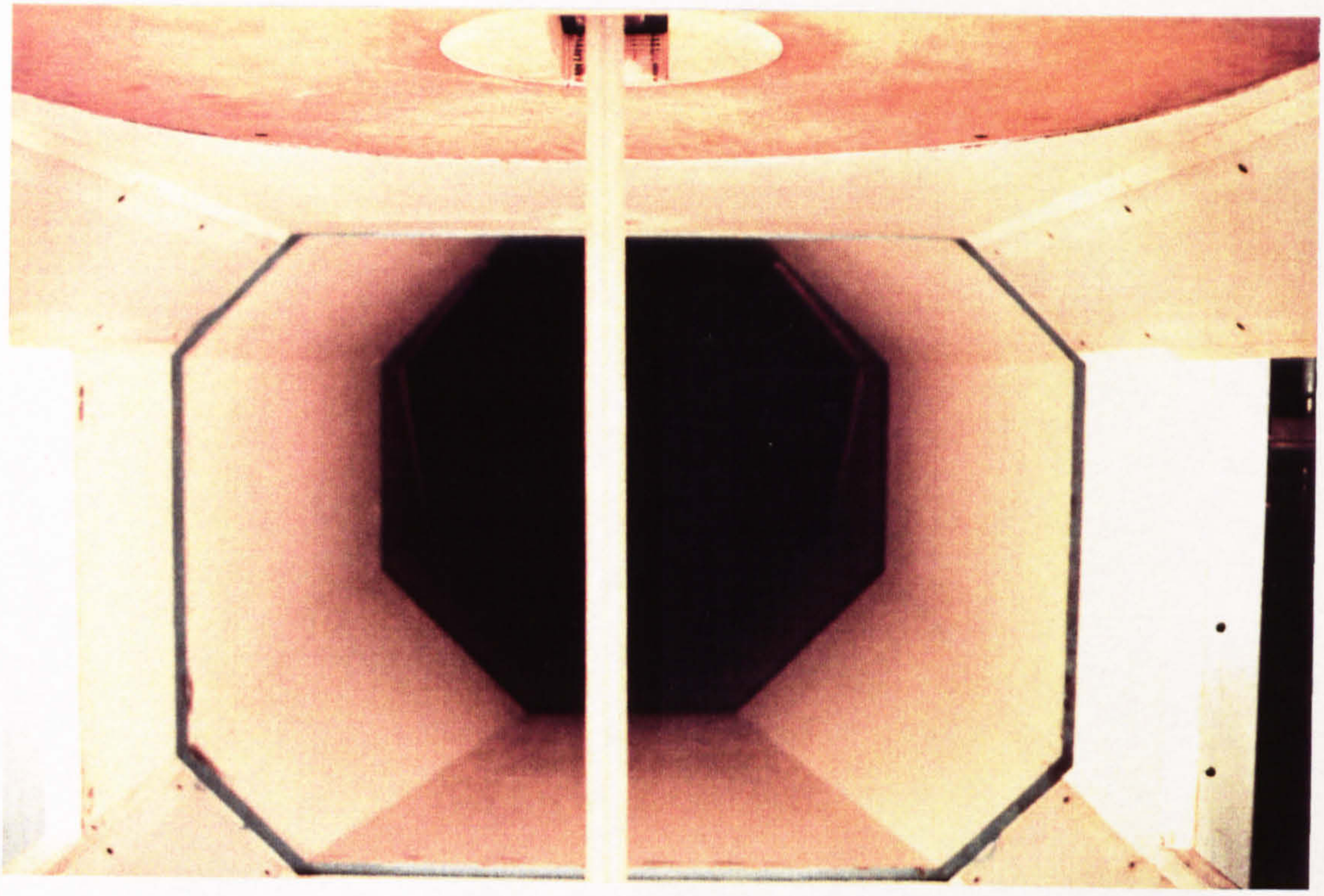

P 9.4 Wing in the wind tunnel

CHAPTER : 10

10.1 PRINCIPAL CONCLUSIONS

An investigation into the static, dynamic, and aeroelastic behaviour of thin-walled composite structures with application to aircraft wings has been carried out with the following general conclusions :-

A survey of the work done by the pioneers of aeroelasticity and their successors from the earlier days to the late eighties has been presented. Their efforts have helped a lot to make accurate predictions and eliminate adverse aeroelastic effects especially in the case of aircraft flutter.

The difficulties faced by the earlier investigators were greatly reduced by the introduction of computer techniques such as finite element analysis, etc. Symbolic computing facilities have made it possible to obtain explicit and exact closed form solutions for many aeroelastic problems.

A laminate can be designed to exhibit a desired set of deformations, in which the plate bending stiffness matrix [D] plays a vital role. The bending and torsional deformations are elastically uncoupled if members in the third row and column of the (D) matrix are absent. However, in the case of a fully populated D-matrix (which occurs with a general arbitrary fibre lay-up) bending and torsional deformations are coupled together. The magnitude and sign of D_{16} and D_{66} determines the direction and the extent of this coupling. Symmetrically laid-up laminates subjected to bending moments or torques can display coupled transverse displacement and twist, while antisymmetrically laid-up laminates subjected to torque or normal loads (tension or compression) can exhibit coupled

deformations by twisting as well as longitudinal displacement. Quantitative analysis has been carried out in detail to predict such behaviour of laminated composite beams and plates.

The ratio of Young's modulus in the fibre direction to the shear modulus (E/G), plays an important role in establishing these properties when the orientation of the fibres are changed. As the ply orientation varies, materials with larger (E/G) ratios will produce greater changes in the laminate equivalent elastic moduli. This quality will eventually help in making choice of the material for a particular application.

A suitable procedure of stiffness estimation for composite structures with various types of cross-sectional details is presented.

A general expression for the torsional rigidity of multi-cell structure is derived which can be easily adopted for any number of cells.

The effect of ply orientation on the stiffnesses has been demonstrated. Flexural rigidity is reduced when the plies are at angles other than its principal (or fibre) axis whereas the torsional rigidity is increased as expected. This trend followed up to 45^{o} ply angle with the principal or fibre axis and then the trend reversed. Flexural/torsional coupled rigidity increased until the ply angle was 22^{o}. It then vanished at 45^{o}, where bending rigidity was at a minimum and torsional rigidity was at a maximum.

The experimental investigation of static characteristics of structures made of isotropic or anisotropic (i.e. composite materials) was carried out with satisfactorily good results when compared with their theoretical values. The tests covered beams, plates, thin-walled open and closed section composite and metal

structures.

Experiments performed on composite plates showed large discrepancies in torsional rigidity tests for zero degree lay-ups. This was possibly due to the difference in material property between results obtained through the tests carried out on the specimen with 45^{o} lay-up and the original structure with all the fibres along the span. The results for other lay-ups agreed very well for the torsional rigidity test. In the case of a bending rigidity test, the results were within normal engineering accuracy limits for the zero degree case but large errors were encountered for other lay-ups. One possible explanation is that the end fittings suppressed the chordwise curvature, affecting the twist deformation due to the D_{16} term of the compliance matrix. This effect will be zero in the case of zero degree laminate but can be significant for other lay-ups.

In the case of thin-walled open section structures, the agreement between theoretical predictions and experimental results got worse as the complexity of the section increased. The effect of warping was found to be playing an important role as expected. This type of section requires an improved mathematical model for further study.

Closed sections produced good results for torsional rigidity tests but in the case of flexural rigidity tests, large differences were encountered. This was probably due to lack of control on the volume fraction. A correction to this factor improved the overall status.

Dynamic stiffness matrices for axially loaded thin-walled composite sections with elastic and material coupling (bending-torsional) were developed. The following degenerated cases were also investigated :

1. Materially coupled beams along with an axial load (e.g. plates or doubly symmetrical sections such as box beam)
2. Materially coupled thin-walled beams
3. Explicit expressions for dynamic stiffness matrix for the materially coupled case

Computer programs have been developed to calculate the dynamic stiffness matrices from basic structural data. These programs were then combined with the codes of an established algorithm to compute the natural frequencies and mode shapes for such beams.

The effect of material coupling (bending-torsional) on the natural frequencies and normal mode shapes was studied, and the results were compared with the predictions obtained when not accounting for the coupling effect.

A parametric study on the effect of aspect ratio on the accurate prediction of natural frequencies using beam element idealization has also been presented. It is found that for plate structures with aspect ratios greater than three, beam model idealization can predict frequencies within measurement accuracy.

Tests with satisfactory results were performed on structures made of conventional materials such as aluminium and steel to validate the testing technique and to calibrate the equipment used.

Tests were performed on three composite graphite fibre reinforced plastic plates. In the evaluation of fundamental frequencies, the validity of applying a beam-element idealization to various composite lay-ups was confirmed for low flexural coupling ratio's involving the terms D_{16}/D_{11} and D_{16}/D_{66}.

Composite thin-walled open sections with three

different cross-sections were tested. Large discrepancies were found between theoretical predictions and experimental results. The investigation prompted the need for a better theoretical model.

Natural frequencies and mode shapes for six zero degree ply lay-up wings and four with 10, 20, 30, and 45 degrees ply lay-ups were established. The average difference between theoretical predictions and experimental results remained within 10% for wings with specially orthotropic ply lay-ups. In the case of generally orthotropic ply lay-ups, deviation from theoretical predictions followed similar trends as observed for composite plate structures.

The validity of using a generally orthotropic Vlasov's beam model for composite plate flutter predictions is confirmed. Furthermore, the validity of "Strip Theory" for high aspect ratio wings in flutter calculations is also confirmed for the wings tested. Various reasons are discussed which may be the probable sources of discrepancies between experimental results and theoretical predictions.

The aeroelastic behaviour of thin-walled closed section composite wings with elastic bending-torsion coupling was investigated. The wind tunnel speed limitations did not allow the performance of a binary (bending-torsion) flutter test. However, a stall flutter test was carried out successfully. Other aeroelastic phenomena such as divergence and sub-critical flutter tests on composite wings were also carried out with satisfactory results. The lift-curve slope values for these wings were also established experimentally.

10.2 FURTHER WORK

The investigation discussed in this thesis has shown

that interesting areas for further research should include:

(i) The development of a formulation for estimating the static structural properties such as bending, torsional, and bending/torsional coupled rigidities of thin-walled open section composite structures.

(ii) The development of a computer program to interface the various analysis programs developed during this work, i.e. optimizing a composite structure for minimum weight with static, dynamic and aeroelastic constraints.

(iii) The subroutine already developed for the dynamic analysis of composite structures can be incorporated into computer programs that can investigate the response analysis of an aircraft to gusts and turbulence. In this way the aeroelastic tailoring concept can be extended to produce passive structures to counter these undesirable effects.

(iv) At the moment aerodynamic tailoring and active control are being investigated independently. Efforts should be made to merge them into one design tool in future.

(v) The introduction of non-conventional materials in the manufacture of modern aeroplanes needs a lot of investigation into the aeroelastic behaviour of structures made of these materials. The use of fibrous materials in acquiring passive means of overcoming aeroelastic problems is still another fertile area of research. The progress in the field of passive control

technology in suppression of flutter depends on the derivation of relatively simple nonlinear models and on the proposal for new algorithms for the calculation of the coupling between flow and structure .

(vi) Large space structures represent another potential area of aeroelastic tailoring research. The repetitive lattice arrangement of a number of space structures form an anisotropic design. The passive control system of these space structures can be enhanced by achieving passive modal control through tailoring the orientations of the structural members.

APPENDIX : A

A.1 MANSFIELD THIN-WALLED RECTANGULAR CROSS-SECTION [1]

The effective flexural rigidity EI for cylindrical rectangular cross-section with significant shear lag and shear deflection is given by :

$$EI_{effective} = E\ h^2 \left[\frac{(F + F_s)\ \psi_1 + \left[\frac{h\ t_v}{6}\right] \psi_2}{1 + \left[\frac{F + F_s}{h\ t_v}\right] \psi_3} \right] \qquad (A.1.1)$$

A.2 HOUSNER AND STEIN BOX BEAM MODEL [2]

The equivalent bending and torsional stiffnesses of a box beam with thin laminated composite balanced ply cover sheets forming the upper and lower surfaces of the wing are given as follows :

$$EI = EI_o - (B_{22})^2 / A_{22} \qquad (A.2.1)$$

$$GJ = GJ_o - (B_{33})^2 / A_{22} \qquad (A.2.2)$$

$$K = K_o - B_{22}B_{33} / A_{22} \qquad (A.2.3)$$

where

$$EI_o = \bar{b} \left[\sum_{l=1}^{N} \bar{Q}_{22}(l)\ \beta_l \right] \qquad (A.2.4)$$

$$GJ_o = \bar{b} \left[\sum_{l=1}^{N} 4\ \bar{Q}_{66}(l)\ \beta_l \right] \qquad (A.2.5)$$

$$K_o = \bar{b} \left[\sum_{l=1}^{N} 2\ \bar{Q}_{26}(l)\ \beta_l \right] \qquad (A.2.6)$$

$$A_{22} = \bar{b} \left[\sum_{l=1}^{N} \bar{Q}_{22}(l)\ t_l \right] \qquad (A.2.7)$$

$$B_{22} = \bar{b} \left[\sum_{l=1}^{N} \bar{Q}_{22}(l) \ \delta_l \right] \qquad (A.2.8)$$

$$B_{99} = 2 \ \bar{b} \left[\sum_{l=1}^{N} \bar{Q}_{26}(l) \ \delta_l \right] \qquad (A.2.9)$$

Classical Euler-Bernoulli beam deformation assumptions were used in the analysis.

REFERENCES

1. Mansfield, E.H., "Flexural Vibrations of a Thin-Walled Cylinder of Rectangular Cross Section," R.A.E. The Aeronautical Quarterly, November 1958.

2. Housner, J.M. and Stein, M., "Flutter Analysis of Swept-Wing Subsonic Aircraft with Parameter Studies of Composite Wings," NASA TN D-7539, September 1974.

APPENDIX : B

B.1 THIN-WALLED CONTOUR ANALYSIS [1]

Mansfield and Sobey [1], analysed the composite thin-walled cylindrical tube composed of an arbitrary lay-up of fibre composite plies. Expressions were derived for the coupled torsional, extensional and flexural stiffnesses for linear displacements.

For a mirror-wise cylindrical tube subjected to torsion, bending and longitudinal tension using cylindrical coordinates and in the absence of circumferencial stresses and strains in the structure i.e. $N_s = 0$ and $\varepsilon_s = 0$, equations (3.1a,b) of Chapter (3):

$$\begin{Bmatrix} N_y \\ N_{ys} \end{Bmatrix} = \begin{bmatrix} A_{11} & A_{13} \\ A_{13} & A_{33} \end{bmatrix} \begin{Bmatrix} \varepsilon_y \\ \gamma_{ys} \end{Bmatrix} \qquad (B.1.1)$$

or

$$\begin{Bmatrix} \varepsilon_y \\ \gamma_{ys} \end{Bmatrix} = \begin{bmatrix} A_{11} & A_{13} \\ A_{13} & A_{33} \end{bmatrix}^{-1} \begin{Bmatrix} N_y \\ N_{ys} \end{Bmatrix} = \begin{bmatrix} A^*_{11} & A^*_{13} \\ A^*_{13} & A^*_{33} \end{bmatrix} \begin{Bmatrix} N_y \\ N_{ys} \end{Bmatrix} \qquad (B.1.2)$$

or

$$\begin{Bmatrix} N_y \\ \gamma_{ys} \end{Bmatrix} = \begin{bmatrix} \left(H_{11} = \dfrac{1}{A^*_{11}}\right) & -\left(H_{12} = \dfrac{A^*_{13}}{A^*_{11}}\right) \\ \left(H_{12} = \dfrac{A^*_{13}}{A^*_{11}}\right) & \left(H_{22} = A^*_{33} - \dfrac{A^{*2}_{13}}{A^*_{11}}\right) \end{bmatrix} \begin{Bmatrix} \varepsilon_y \\ N_{ys} \end{Bmatrix} \qquad (B.1.3)$$

and the resultant tensile load P in the cylinder is :

$$P = \varepsilon_o \oint H_{11}\, ds - N_{ys} \oint H_{21}\, ds \qquad (B.1.4)$$

Similarly the bending moment about the x-axis is :

$$M_x = K_x \oint z^2 H_{11}\, ds - N_{ys} \oint z\, H_{21}\, ds \qquad (B.1.5)$$

and the chordwise moment about the z-axis is :

$$M_z = K_z \oint x^2 H_{11}\, ds + N_{yo} \oint x H_{21}\, ds \qquad (B.1.6)$$

Finally the resultant torque about the y-axis is :

$$M_y = 2 N_{yo} \oint p\, ds \qquad (B.1.7)$$

where $A = \oint p\, ds$ = cross sectional area of the tube

p = perpendicular distance from the origin to the tangent at s.

Combining equations (B.1.4) to (B.1.7) in a matrix form:

$$\begin{Bmatrix} \varepsilon_o \\ K_x \\ K_z \\ \tau \end{Bmatrix} = \begin{bmatrix} F_{11} & 0 & 0 & F_{14} \\ 0 & F_{22} & 0 & F_{24} \\ 0 & 0 & F_{33} & F_{34} \\ F_{14} & F_{24} & F_{34} & F_{44} \end{bmatrix} \begin{Bmatrix} P \\ M_x \\ M_z \\ M_y \end{Bmatrix} \qquad (B.1.8)$$

where

$$\left.\begin{aligned} F_{11} &= \frac{1}{\oint H_{11} ds}, & F_{14} = F_{41} &= \frac{\oint H_{21} ds}{2A \oint H_{11} ds} \\ F_{22} &= \frac{1}{\oint z^2 H_{11} ds}, & F_{24} = F_{42} &= \frac{\oint z H_{21} ds}{2A \oint z^2 H_{11} ds} \\ F_{33} &= \frac{1}{\oint x^2 H_{11} ds}, & F_{34} = F_{43} &= \frac{-\oint x H_{21} ds}{2A \oint x^2 H_{11} ds} \\ F_{44} &= \frac{1}{4A^2} \left[\oint H_{22} ds + \frac{\left[\oint H_{21} ds\right]^2}{\oint H_{11} ds} + \frac{\left[\oint x H_{21} ds\right]^2}{\oint x^2 H_{11} ds} + \frac{\left[\oint z H_{21} ds\right]^2}{\oint z^2 H_{11} ds} \right] \end{aligned}\right\} \qquad (B.1.9)$$

Equation (B.1.8) gives the flexibility matrix for the general cylindrical tube subjected to bending, torsion, and longitudinal tension. For mirror-wise tubes equation (B.1.8) uncouples to give the stiffness matrix for a symmetrically laminated thin-walled structure with bending-torsional coupling.

$$\left.\begin{aligned} \varepsilon_o &= F_{11}\, P \\ K_z &= F_{33}\, M_z \\ \begin{bmatrix} K_x \\ \tau \end{bmatrix} &= \begin{bmatrix} F_{22} & F_{24} \\ F_{24} & F_{44} \end{bmatrix} \begin{bmatrix} M_x \\ M_y \end{bmatrix} \end{aligned}\right\} \qquad \text{(B.1.20)}$$

B.2 COMPOSITE BOX BEAM [2]

Hong and Chopra [2] developed a nonlinear analysis for thin-walled composite beams undergoing transverse bending (flap and lag) and torsion and axial deflections based on the nonlinear strain displacement relations of Hodges and Dowell [9]. A simple analytical expression was given for the cross-section warping, while effects of transverse shear were neglected. Extensive investigations in the behaviour of structural coupling terms due to ply orientations were made.

In the case of a uniform cantilevered symmetric thin-walled beam subjected to tip load P, the transverse deflection and twist in the structure is given by :

$$h_B = \frac{P\,(2\,\ell\,x - x^2)}{2(EI - K_{pa}^2 / GJ)} \qquad \text{(B.2.1)}$$

$$\psi_B = \frac{P\,(2\,\ell\,x - x^2)}{2(EI - K_{pa}^2 / GJ)}\, K_{pa}/GJ \qquad \text{(B.2.2)}$$

In the case of a uniform cantilevered symmetric thin-walled beam subjected to a tip torsional load T, the transverse deflection and twist in the structure is given by :

$$h_T = \frac{T\,x}{(GJ - K_{ps}^2 / EI)} K_{ps}/EI \qquad (B.2.3)$$

$$\psi_T = \frac{T\,x}{(GJ - K_{ps}^2 / EI)} \qquad (B.2.4)$$

The subscripts s and t denote the transverse and torsional deflections due to bending and torsional loads respectively.

STIFFNESS COEFFICIENTS : EI, GJ, K_{ps}

$$EI = \sum_{k=1}^{N} \int\int_{1,2} \bar{C}_{11}^{(k)} \zeta^2 \, d\eta \, d\zeta + \sum_{l=1}^{M} \int\int_{3,4} \bar{C}_{11}^{(l)} \zeta^2 \, d\eta \, d\zeta \qquad (B.2.5)$$

$$GJ = \sum_{k=1}^{N} \int\int_{1,2} \bar{C}_{\sigma\sigma}^{(k)} \zeta^2 \, d\eta \, d\zeta + \sum_{l=1}^{M} \int\int_{3,4} \bar{C}_{\sigma\sigma}^{(l)} \hat{\eta}^2 \, d\eta \, d\zeta \qquad (B.2.6)$$

$$K_{ps} = \sum_{k=1}^{N} \int\int_{1,2} \bar{C}_{1\sigma}^{(k)} \hat{\zeta} \, \zeta \, d\eta \, d\zeta \qquad (B.2.7)$$

where 1 and 2 represent top and bottom of the box and 3, 4 represent the left and right sides of the laminated box beam.

$$\bar{C}_{11} = \bar{Q}_{11} - \bar{Q}_{12}^2 / \bar{Q}_{22} \qquad (B.2.8)$$

$$\bar{C}_{1\sigma} = \bar{Q}_{1\sigma} - \bar{Q}_{12}\,\bar{Q}_{2\sigma} / \bar{Q}_{22} \qquad (B.2.9)$$

$$\bar{C}_{\sigma\sigma} = \bar{Q}_{\sigma\sigma} - \bar{Q}_{2\sigma}^2 / \bar{Q}_{22} \qquad (B.2.10)$$

where

$\bar{Q}$ = stiffness matrix of the kth lamina in x-η or x-ζ plan

N and M = number of plies in laminate 1 or 2 and 3 or 4

REFERENCES

1. Mansfield, E.H. and Sobey, A.J., "The Fibre Composite Helicopter Blade, Part 1: Stiffness Properties, Part 2: Prospects for Aeroelastic Tailoring," Aeronautical Quarterly, May 1979, pp. 413-449.

2. Hong, Chang-Ho and Chopra, I., "Aeroelastic Stability Analysis of a Composite Rotor Blade," Journal of the American Helicopter Society, Vol. 30, No. 2, 1985.

3. Hodges, D.H. and Dowell, E.H., "Nonlinear Equations of Motion for the Elastic Bending and Torsion of Twisted Nonuniform Blades," NASA TN D-7818, December 1974.

APPENDIX : C

COMPUTER PROGRAMS

A floppy disc is provided containing the following computer programs written in FORTRAN language.

1. CONTENT.DOC
2. SECTION.FOR
3. KSTIF.FOR
4. DMCS.FOR = (DMCSE.FOR + DMCSN.FOR)
5. DMMECA.FOR
6. VMECAS.FOR
7. LIFCUR.FOR

The 'CONTENT.DOC' file explains further about the compilation requirements of these Fortran files. Each program is supported by a data file and a result file.

APPENDIX : D

LINEAR SERVO ACCELEROMETER

Servo accelerometers are DC-operated closed-loop force balance transducers for the measurement of acceleration. They are more stable and accurate than open-loop accelerometers by several orders of magnitude. In closed-loop force balance accelerometers, undesirable characteristics such as sensitivity to supply voltage, nonlinearity in the acceleration-to-position pickoff, and high thermal coefficients of scale factor and zero shift are negligible.

Typical applications of servo accelerometers are in high reliability guidance systems, monitoring and controlling decelerations in mass transit systems and to check slopes and gradients. For the last twenty years, high reliability for such critical applications has been a significant feature of these inertial devices.

The A200 series linear servo accelerometer measures vector acceleration with high accuracy using the closed-loop torque balance principle. The pendulous mass (A) as shown in Figure (5.1), develops a torque proportional to the product of its mass unbalance and the applied acceleration [1]. The movement of mass (A) is detected by the position sensor (B) whose output signal is applied to an electronic amplifier. The output current from the servo amplifier is applied to torque motor (C), which then develops a torque exactly equal to, but directly opposed to, the initial torque from the pendulous mass (A). Thus mass (A) stops moving, assuming a position minutely differing from its zero 'g' position. The current through the torque motor is accurately proportional to input acceleration, and when passed through a stable resistor (Ro), an accurately proportional output voltage

is developed. The system is damped by means of a phase advancing network within the integrated thick film module. The A200 series servo operation can be checked for proper servo operation (self-test) by applying an independent current input to the torque motor. By adjusting the parameters of the servo amplifier and related electronic networks, the operating characteristics of a servo accelerometer can be changed or modified to suit a particular application. This same flexibility gives rise to a variety of optional features in some models.

The device was set up according to the circuit diagram shown in Figure (5.2). A steady ∓ 15 volts DC supply was plugged into a common junction box. The output voltage was measured by a digital volt meter. When the servo accelerometer is placed on an absolutely horizontal flat surface, the output voltage is zero. For a ∓ 90 degrees tilt angle the maximum output is ∓ 5 volts. Due to the availability of very accurate digital volt meters with high resolutions, it is possible to measure even a hundredth of a degree. An additional advantage is the extreme light weight of the device.

REFERENCE

1. Schaevitz, "Linear and Angular Servo Accelerometers", Technical bulletin 4501E.

APPENDIX : E

COMPOSITE PLATE VIBRATION [1]

The Rayleigh-Ritz energy method (due to its simplicity and relative ease of application) was employed to analyse free vibrations, flutter and divergence by approximating plate deflections. The wing was considered as a rectangular cantilevered flat plate with uniform thickness. A five term deflection equation was chosen to approximate the plate deflection for the first and second bending, first and second torsion and first chordwise vibration modes [1]. Jensen et al.[2,3] showed that the last two terms were important to obtain accurate approximations for the first three vibration modes. Therefore, in terms of generalized coordinates, the deflection equation is

$$w = \sum_{i=1}^{5} \gamma_i(x,y)\ q_i(t) \qquad (E.1)$$

where w = lateral deflection

$\gamma_i(x,y)$ = the non-dimensional deflection or mode shape of the ith mode and can be written as

$= \phi_i(x)\ \psi_i(y)$ $\quad (i=1,2,3,4,5)$

ϕ = single-dimension mode shape in x direction

ψ = single-dimension mode shape in y direction

The mode shapes assumed were as follows

$\phi_1(x)$ = first cantilever beam mode

$\phi_2(x)$ = second cantilever beam mode

$\phi_3(x) = \sin(\pi x/2\ell)$, $\phi_4(x) = \sin(3\pi x/2\ell)$

$\phi_5(x) = \frac{x}{\ell}(1-x/\ell)$

$\psi_1(y) = 1$; $\psi_2(y) = 1$

$\psi_3(y) = y/c$, $\psi_4(y) = y/c$

$\psi_3(y) = [4(y/c)^2 - \ell/3]$

and

$q_i(t)$ = generalized displacement of the ith mode, such that all of the modes satisfy the geometric boundary conditions for a cantilevered plate. It has the units of length and is a function of time.

In the case of a symmetric anisotropic laminated plate, the strain energy is [4]

$$U = \frac{1}{2}\int_0^{\ell}\int_{-c/2}^{c/2}\left[D_{11}\left(\frac{\partial^2 w}{\partial x^2}\right)^2 + 2\,D_{12}\left(\frac{\partial^2 w}{\partial x^2}\right)\left(\frac{\partial^2 w}{\partial y^2}\right) + D_{22}\left(\frac{\partial^2 w}{\partial y^2}\right)^2 + 4\,D_{16}\left(\frac{\partial^2 w}{\partial x^2}\right)\left(\frac{\partial^2 w}{\partial x\partial y}\right) + 4\,D_{26}\left(\frac{\partial^2 w}{\partial y^2}\right)\left(\frac{\partial^2 w}{\partial x\partial y}\right) + 4\,D_{66}\left(\frac{\partial^2 w}{\partial x\partial y}\right)^2\right] dy\,dx \qquad (E.2)$$

Taking the partial derivative of the deflection equation (E.1), we can write equation (E.2) in summation notation as follows

$$U = \frac{1}{2}\sum_{i=1}^{3}\sum_{j=1}^{3} K_{ij}\,q_i\,q_j \qquad (E.3)$$

where

k_{ij} = element of a symmetric 5 x 5 matrix

$$= \int_0^{\ell}\int_{-c/2}^{c/2}\left[D_{11}\left(\frac{\partial^2\gamma_i}{\partial x^2}\right)\left(\frac{\partial^2\gamma_j}{\partial x^2}\right) + D_{22}\left(\frac{\partial^2\gamma_i}{\partial y^2}\right)\left(\frac{\partial^2\gamma_j}{\partial y^2}\right) + 4\,D_{66}\left(\frac{\partial^2\gamma_i}{\partial x\partial y}\right)\left(\frac{\partial^2\gamma_j}{\partial x\partial y}\right) + D_{12}\left\{\left(\frac{\partial^2\gamma_i}{\partial x^2}\right)\left(\frac{\partial^2\gamma_j}{\partial y^2}\right) + \left(\frac{\partial^2\gamma_i}{\partial y^2}\right)\left(\frac{\partial^2\gamma_j}{\partial x^2}\right)\right\} + 2\,D_{16}\left\{\left(\frac{\partial^2\gamma_i}{\partial x^2}\right)\left(\frac{\partial^2\gamma_j}{\partial xy}\right) + \left(\frac{\partial^2\gamma_i}{\partial xy}\right)\left(\frac{\partial^2\gamma_j}{\partial x^2}\right)\right\} + 2\,D_{26}\left\{\left(\frac{\partial^2\gamma_i}{\partial y^2}\right)\left(\frac{\partial^2\gamma_j}{\partial xy}\right) + \left(\frac{\partial^2\gamma_i}{\partial xy}\right)\left(\frac{\partial^2\gamma_j}{\partial y^2}\right)\right\}\right] dy\,dx \qquad (E.4)$$

APPENDIX : E

The kinetic energy for the plate is

$$T = \frac{1}{2} \int_0^{\ell} \int_{-c/2}^{c/2} m \left[\frac{\partial w}{\partial t}\right]^2 dy\, dx \qquad (E.5)$$

where $m = \rho_a t_a$

$= $ mass per unit area

ρ_a = density of the graphite/epoxy

t_a = total plate thickness

Rewriting in summation notation

$$T = \frac{1}{2} \sum_{i=1}^{5} \sum_{j=1}^{5} M_{ij}\, q_i\, q_j \qquad (E.6)$$

where M_{ij} = is an element of 5 x 5 matrix

$$= \int_0^{\ell} \int_{-c/2}^{c/2} \gamma_i\, m\, \gamma_j\, dy\, dx \qquad (E.7)$$

Similarly the variation in external work can be written as

$$\delta W_e = \int_0^{\ell} \int_{-c/2}^{c/2} \Delta p_z\, \delta w\, dy\, dx \qquad (E.8)$$

where

Δp_z = distributed lateral load per unit area

The above expression in summation notation can be written as follows:

$$\delta W_e = \sum_{i=1}^{5} Q_i\, \delta q_i \qquad (E.9)$$

where

Q_i = generalized force

$$= \int_0^{\ell} \int_{-c/2}^{c/2} \Delta p_z\, \gamma_i\, dy\, dx \qquad (E.10)$$

Lagrange's equation provides the relationship between work and energy, and is a statement of Hamilton's energy principle. This is in fact the basis of the Rayleigh-Ritz method.

$$\frac{d}{dt}\left(\frac{\partial T}{\partial \dot{q}_i}\right) - \frac{\partial T}{\partial q_i} + \frac{\partial U}{\partial q_i} = Q_i \qquad (E.11)$$

Substituting the respective quantities in the Lagrange's equation, five equations of motion are obtained. In matrix form these can be expressed as

$$[M]\ddot{\underset{\sim}{q}} + [K]\underset{\sim}{q} = \underset{\sim}{Q} \qquad (i,j = 1,2,....,5) \qquad (E.12)$$

where [M] = diagonal mass matrix

[K] = symmetric stiffness matrix

Their details can be seen in ref.[9].

In order to observe the function of coupling D-matrix terms we go back to Hamiltons's principle and assume a solution

$$w(t) = w \sin \omega t \qquad (E.13)$$

and suitable substitutions yield

$$\delta \int\int \frac{1}{2} \left[D_{11}\left(\frac{\partial^2 w}{\partial x^2}\right)^2 + 2\, D_{12} \left(\frac{\partial^2 w}{\partial x^2}\right)\left(\frac{\partial^2 w}{\partial y^2}\right) + D_{22}\left(\frac{\partial^2 w}{\partial y^2}\right)^2 \right.$$

$$+ 4\, D_{16} \left(\frac{\partial^2 w}{\partial x^2}\right)\left(\frac{\partial^2 w}{\partial x \partial y}\right) + 4\, D_{26} \left(\frac{\partial^2 w}{\partial y^2}\right)\left(\frac{\partial^2 w}{\partial x \partial y}\right)$$

$$\left. + 4\, D_{66} \left(\frac{\partial^2 w}{\partial x \partial y}\right)^2 - \omega^2 m\, w^2 \right] dA = 0 \qquad (E.14)$$

In the case of a uniform rectangular plate clamped at x=0, the governing equations are

$$\bar{w}'''' - \omega^2\, m \left[\frac{\ell^2}{D_{11}}\right] \bar{w} + \left[\frac{2\, D_{16}\, \ell}{D_{11}}\right] \theta''' = 0 \qquad (E.15)$$

$$- \left[\frac{D_{16}}{2D_{66}}\right] \bar{w}''' + \left[\frac{c^2 D_{11}}{48 D_{66} \ell^2}\right] \theta'''' - \theta'' - \omega^2 m \left[\frac{c^2 \ell^2}{48 D_{66}}\right] \theta = 0 \qquad (E.16)$$

These two ordinary differential equations are coupled by the bending-twisting stiffness factor D_{16}. In the case of negligibly small stiffness ratios D_{16}/D_{11} and D_{16}/D_{66}, they can be ignored. This results in uncoupled bending and

torsion equations and eventually yields relatively simple solutions

$$\bar{w}'''' - \omega^2 \, m \left[\frac{\ell^2}{D_{11}}\right] \bar{w} = 0 \qquad \text{(E.17)}$$

which is identical to the equation of transverse vibration of a bar

$$\bar{w}'''' - \omega^2 \, \rho_a A \, \ell^4 / \, E \, I \, \bar{w} = 0 \qquad \text{(E.18)}$$

Comparing equations (E.17) and (E.18) shows that

$$\rho_a A \; / \; EI = m \; / \; D_{11} \qquad \text{(E.19)}$$

Therefore,

$$EI = \rho_a A \; D_{11} / \; m = \rho_a A \; D_{11} / \; \rho_a t \; = D_{11} \; c \qquad \text{(E.20)}$$

since $A = c \; t_a$

resulting in the following expression for natural bending frequencies,

$$\omega_{nB} = (k_{nB}/\ell^2)\sqrt{D_{11}/m} \qquad (n = 1,2,3,....) \qquad \text{(E.21)}$$

where k_{nB} = nth eigenvalue of the equation, subject to the boundary conditions on $\bar{w}$

The second equation (E.16) is reduced to :

$$\left[\frac{c^2 D_{11}}{48 D_{66} \ell^2}\right] \theta'''' - \theta'' - \omega^2 m \left[\frac{c^2 \ell^2}{48 D_{66}}\right] \theta = 0 \qquad \text{(E.22)}$$

Equation (E.22) still contains terms that represent warping stiffness, St. Venant torsion stiffness ($4D_{66}c = GJ$ for an isotropic plate) and the torsional polar inertia about y = 0 respectively.

Substitute $R = \ell/c$ and $\beta = \dfrac{D_{11}}{48 D_{66}} R^2$

where β represents the influence of warping stiffness and depends upon the aspect ratio and ratio of bending to torsion stiffness

$$K_T^2 = \omega^2 \rho \frac{\ell^4}{48 D_{\theta\theta}} R^2$$

so the equation becomes

$$\beta \theta'''' - \theta'' - K_T^2 \theta = 0 \qquad (E.23)$$

Finally the frequencies are given by the expression

$$\omega_{nT} = (K_{nT}/\ell^2) \sqrt{48 D_{\theta\theta}} R^2/\rho \qquad (E.24)$$

where K_{nT} is the nth eigenvalue and is a function of β as described in reference [5]. The value of β approaches that for a long thin bar as the warping stiffness β goes to zero.

This can be compared with the expression for the torsional frequencies of a prismatic bar made of isotropic material,

$$\omega_n = K_n \sqrt{GJ/\ell^2 I}_p \qquad (E.25)$$

The natural frequencies for composite plates were predicted using equations (E.21) and (E.25).

REFERENCES

1. Hollowell, S.J. and Dugunji, J., "Aeroelastic Flutter and Divergence of Stiffness Coupled, Graphite/Epoxy Cantilevered Plates," Journal of Aircraft, Vol. 21, Jan. 1984, pp. 69-76.

2. Jensen, D.W., "Natural Vibration of Cantilevered Graphite/Epoxy Plates with Bending-Torsion Coupling," M.S. Thesis, M.I.T. Department of Aeronautics and Astronautics, Cambridge, Mass., August 1981.

3. Jensen, D.W., Crawley, E.F., and Dugundji, J., "Vibration of Cantilevered Graphite/Epoxy Plates with Bending-Torsion Coupling," Journal of Reinforced Plastics and Composites, Vol. 1, July 1982, pp. 254-269.

4. Ashton, J.E. and Whitney, J.M., Theory of Laminated Plates, Technomic Publishing Co., Stamford, Conn., 1970.

5. Crawley, E.F. and Dugundji, J., "Frequency Determination and Non-dimensionalization for Composite Cantilevered Plates," Journal of Sound and Vibration, Vol. 72(1), 1980, pp. 1-10.

APPENDIX : F
LIFT-CURVE SLOPE

THEORY

The lift-curve slope of an infinite wing in an incompressible flow condition is equal to 2π per radian and is denoted by a_o. If the compressibility effects are expressed in terms of Mach number M, then for an aerofoil section with subsonic speed (M<1), the change in lift-curve slope value is given by Glauert's formula [1].

$$a_o' = \frac{1}{\sqrt{1-M^2}}\, a_o \quad \text{(for 2-dimensional wing section)} \qquad \text{(F.1)}$$

The effect of finite span is then approximated by the following expression

$$a' = \frac{a_o'}{1 + a_o' \frac{1+\tau}{\pi\, AR}} = \frac{a_o}{\sqrt{1-M^2} + a_o \frac{1+\tau}{\pi\, AR}} \qquad \text{(F.2)}$$

where

AR = aspect ratio

$= \frac{b^2}{S}$.

b = wing-span from tip to tip

S = wing area

The above expression is valid for an unswept, subsonic wing with moderate aspect ratio (AR) and symmetric loading, where τ is Glauert's correction factor for nonelliptic plan form wings.

In the case of small aspect ratio, equation (F.2) gives :

$$a' = \frac{a_o'}{\sqrt{1 + \left(\frac{a_o'}{\pi\, AR}\right)} + a_o'\left(\frac{1+\tau}{\pi\, AR}\right)} \qquad \text{(F.3)}$$

In the case of swept wings :

$$(a_o)_{swept} = a_o \cos \Lambda \quad \text{(incompressible, infinite span)} \qquad (F.4)$$

where a_o is the lift-curve slope of the airfoil section normal to the leading edge.

For subsonic, infinite span :

$$(a_o')_{swept} = \frac{(a_o)_{swept}}{\sqrt{1-M^2\cos^2\Lambda}} \qquad (F.5)$$

For finite aspect ratio and symmetric loading :

$$(a')_{swept} = \frac{(a_o')_{swept}}{\sqrt{1 + \left[\frac{(a_o')_{swept}}{\pi\ AR}\right]^2} + (a_o')_{swept}\left[\frac{1+\tau}{\pi\ AR}\right]} \qquad (F.3)$$

If wing is tapered, the sweep angle Λ should be measured along the quarter chord line.

REFERENCE

1. Glauert, H., The Elements of Aerofoil and Airscrew Theory, Cambridge University Press, London, 1926.

APPENDIX : G

G.1 FLEXURAL OR BENDING RIGIDITY

When a thin walled unsymmetrical section like an arbitrary profile of an aerofoil is subjected to a transverse loading both horizontal and vertical components of deflection occur. For the vertical component of deflection :

$$\frac{d^2z}{dy^2} = - \frac{\bar{M}_x}{EI_{xx}} \qquad (G.1)$$

For a cantilevered beam with a concentrated load P at the tip, the bending moment is given by :

$$M_x = - P (l - y) \qquad (G.2)$$

Therefore,

$$EI \frac{d^2z}{dy^2} = P (l - y) \qquad (G.3)$$

$$EI \frac{dz}{dy} = P (l y - \frac{y^2}{2}) + A \qquad (G.4)$$

$$EI z = P (l \frac{y^2}{2} - \frac{y^3}{6}) + A y + B \qquad (G.5)$$

where the boundary conditions are,

$$\text{at } y = 0 ; \frac{dz}{dy} = 0 \rightarrow A = 0 \qquad (G.6a)$$

$$\text{at } y = 0 ; z = 0 \rightarrow B = 0 \qquad (G.6b)$$

Therefore,

$$EI z = P \frac{y^2}{6} (3 l - y) \qquad (G.7)$$

$$EI = \frac{y^2}{6} (3 l - y) (\frac{P}{z}) \qquad (G.8)$$

G.2 TORSION OF BEAMS

In 1784, Coulomb [1] developed the exact solution for the torsional problem of a circular shaft by assuming that the cross-sections of the bar remain plane and rotate without any distortion during twist. Later on Navier

applied the same theory to noncircular cross-sections by making same assumptions and came up with erroneous results, in 1864 [2].

Saint-Venant proposed corrections in solving the problem of torsion of bars with couples applied at the ends [3], by employing a semi-inverse method. Initially, he made certain assumptions to the deformation of the twisted bar and showed that these can satisfy equilibrium equations :

$$\frac{\partial \sigma x}{\partial x} + \frac{\partial \tau xy}{\partial y} + \frac{\partial \tau xz}{\partial z} + X = o \qquad \text{(G.9a)}$$

$$\frac{\partial \sigma y}{\partial y} + \frac{\partial \tau xy}{\partial x} + \frac{\partial \tau yz}{\partial z} + Y = o \qquad \text{(G.9b)}$$

$$\frac{\partial \sigma z}{\partial z} + \frac{\partial \tau xz}{\partial x} + \frac{\partial \tau yz}{\partial y} + Z = o \qquad \text{(G.9c)}$$

with the boundary conditions

$$\bar{X} = \sigma_x \ell + \tau_{xy} m + \tau_{xz} n \qquad \text{(G.10a)}$$

$$\bar{Y} = \sigma_y m + \tau_{yz} n + \tau_{xy} \ell \qquad \text{(G.10b)}$$

$$\bar{Z} = \sigma_z n + \tau_{xz} \ell + \tau_{yz} m \qquad \text{(G.10c)}$$

The assumptions are checked by the uniqueness of the solution of the elasticity equations. This provides an exact solution of the torsion problem, provided the torques on the ends are applied as shear stresses in exactly the same way as desired by the solution itself.

When a uniform bar of any cross-section is twisted by couples applied at the ends, Saint-Venant assumed that the deformation in the twisted shaft is due to :

1. Rotation of the cross-section as in the case of a circular section and
2. Warping of the cross-section, which is the same for all the sections.

The displacements corresponding to rotation of cross-section are

$$u = -\theta_z . y \qquad v = \theta_z . x \qquad (G.11)$$

where

θ_z = angle of rotation at a distance z from the origin

The warping of the cross-section is defined by a function ψ

$$w = \theta\, \psi(x,y) \qquad (G.12)$$

Components of strain can be computed by substituting the assumed displacements in the displacement strain relations. This will give

$$\varepsilon_x = \varepsilon_y = \varepsilon_z = \gamma_{xy} = 0 \qquad (G.13a)$$

$$\gamma_{xz} = \frac{\partial w}{\partial x} + \frac{\partial u}{\partial z} = \theta \left(\frac{\partial \psi}{\partial x} - y \right) \qquad (G.13b)$$

$$\gamma_{yz} = \frac{\partial w}{\partial y} + \frac{\partial v}{\partial z} = \theta \left(\frac{\partial \psi}{\partial y} + x \right) \qquad (G.13c)$$

The corresponding stress components will be

$$\sigma_x = \sigma_y = \sigma_z = \tau_{xy} = 0 \qquad (G.14a)$$

$$\tau_{xz} = G\,\theta \left(\frac{\partial \psi}{\partial x} - y \right) \qquad (G.14b)$$

$$\tau_{yz} = G\,\theta \left(\frac{\partial \psi}{\partial y} + x \right) \qquad (G.14c)$$

In accordance with the assumptions laid down regarding displacements corresponding to rotation and warping of the cross-section, the normal stresses acting between the longitudinal fibres of the shaft or in the longitudinal direction of those fibres, will not exist. Moreover, there will be no distortion in the planes of cross-sections, as ε_x, ε_y and γ_{xy} are zero. Therefore, at each point pure shear defined by τ_{xz} and τ_{yz} exists. Next we have to determine the function $\psi(x,y)$, due to warping of the cross-section, such that the equations of equilibrium are satisfied.

Substituting the above mentioned stress components in the equations of equilibrium and neglecting the body

forces, we come to the conclusion that the function ψ must satisfy the following equation

$$\frac{\partial^2 \psi}{\partial x^2} + \frac{\partial^2 \psi}{\partial y^2} = 0 \qquad \text{(G.15)}$$

The accuracy of the Saint-Venant theory is that of the order of the Engineer's bending theory. Basically what the theory says is that solid sections resist torque by offering a shear stress distribution. This concept may be equally valid for thin-walled closed sections, but in the case of a concentrated torque or a built-in end a substantial amount of axial constraint stress-system may also contribute to the overall torsional stiffness. In general, the angle of twist of a uniform bar of length ℓ with unconstrained ends under a torque T is

$$\theta = \frac{T\ \ell}{G\ J} \qquad \text{(G.16)}$$

where

J = torsion constant of the cross-section

GJ = torsional stiffness/rigidity of the bar

G.3 SHEAR CENTRE OF A CLOSED SECTION

General stress, strain and displacement relationships for an element (δs * δy * t) of a closed or open tube are deduced from considering that the element is maintained in equilibrium by a system of direct and shear stresses. The direct stress σ_y is produced by bending moments or by bending action of shear loads. The shear stresses τ_{sy}, τ_{ys} are due to shear and/or torsion of a closed tube or shear of an open tube. The hoop stress σ_s is usually zero but may be present in closed tubes due to internal pressure. If t is assumed to be constant over the length δs then $\tau_{ys} = \tau_{sy} = \tau$. But it is convenient to work in terms of shear flow q, i.e. shear force per unit length

$$q = \tau\ t \qquad \text{(G.17)}$$

which is regarded as being positive in the direction of increasing s.

For equilibrium of the element in the y-direction and neglecting body forces, we have

$$\frac{\partial q}{\partial s} + t \frac{\partial \sigma_y}{\partial y} = 0 \qquad \text{(G.18)}$$

Similarly for equilibrium in the s direction

$$\frac{\partial q}{\partial y} + t \frac{\partial \sigma_s}{\partial s} = 0 \qquad \text{(G.19)}$$

Hoop stresses for the present investigation are absent. So we are left with the following expressions.

$$\frac{\partial q}{\partial s} + t \frac{\partial \sigma_y}{\partial y} = 0 \qquad \text{(G.20)}$$

$$\frac{\partial q}{\partial y} = 0 \qquad \text{(G.21)}$$

The second expression above suggests that the shear flow in the y-direction is constant. The direct stresses are obtained with reasonable accuracy from the Engineer's theory of bending as follows :

$$\sigma_y = \left(\frac{M_z I_{xx} - M_x I_{xz}}{I_{xx} I_{zz} - I_{xz}^2} \right) x + \left(\frac{M_x I_{zz} - M_z I_{xz}}{I_{xx} I_{zz} - I_{xz}^2} \right) z \qquad \text{(G.22)}$$

or in a more concise form

$$\sigma_y = \frac{\bar{M}_x}{I_{xx}} z + \frac{\bar{M}_z}{I_{zz}} x \qquad \text{(G.23)}$$

where

$$\bar{M}_x = \frac{M_x - M_z I_{xz} / I_{zz}}{1 - I_{xz}^2 / I_{xx} I_{zz}} \quad , \quad \bar{M}_z = \frac{M_z - M_x I_{xz} / I_{xx}}{1 - I_{xz}^2 / I_{xx} I_{zz}} \qquad \text{(G.24)}$$

Consequently,

$$\frac{\partial \sigma_y}{\partial y} = \frac{\bar{S}_z}{I_{xx}} z + \frac{\bar{S}_x}{I_{zz}} x \qquad \text{(G.25)}$$

for a beam with a cross-section that is uniform along its length. The value for σy is entered into expression (G.20) and is integrated over the limits zero to s.

$$\int_o^s \frac{\partial q}{\partial s}\, ds = - \frac{\bar{S}_z}{I_{xx}} \int_o^s t\, z\, ds - \frac{\bar{S}_x}{I_{zz}} \int_o^s t\, x\, ds \qquad (G.26)$$

where

$$\bar{S}_z = \frac{S_z}{1 - I_{xz}^2 / I_{xx} I_{zz}}, \quad \bar{S}_x = \frac{- S_z I_{xz} / I_{xx}}{1 - I_{xz}^2 / I_{xx} I_{zz}}$$

Choosing an origin for s where the shear flow has the unknown value q_{so} and integrating equation (G.26) gives

$$q_s = - \frac{\bar{S}_z}{I_{xx}} \int_o^s t\, z\, ds - \frac{\bar{S}_x}{I_{zz}} \int_o^s t\, x\, ds + q_{so} \qquad (G.27)$$

In the case of open tubes, q_{so} will be zero, because we can take the origin for s at the open edge of the tube. Then q=o when s=o and equation (G.27) becomes

$$q_s = - \frac{\bar{S}_z}{I_{xx}} \int_o^s t\, z\, ds - \frac{\bar{S}_x}{I_{zz}} \int_o^s t\, x\, ds \qquad (G.28)$$

which represents the basic shear, q_b for an open tube. Comparing equations (G.27) and (G.28) :

$$q_s = q_b + q_{so} \qquad (G.29)$$

We obtain q_b by supposing that the closed tube section is cut at some convenient point thereby producing an open tube. The shear flow distribution along this open tube is given by

$$q_b = - \frac{\bar{S}_z}{I_{xx}} \int_o t\, z\, ds - \frac{\bar{S}_x}{I_{zz}} \int_o t\, x\, ds \qquad (G.30)$$

and

$$q_{so} = - \frac{\oint \frac{q_b}{G\,t}\, ds}{\oint \frac{1}{G\,t}\, ds} = - \frac{\oint q_b\, ds}{\oint ds} \qquad (G.31)$$

APPENDIX : H

USER INSTRUCTIONS FOR LAMINATE PROGRAM

Input to the program is made in the following manner.

1. The material data in the form of E_1, E_2, G_{12}, and ν_{12} are entered for different materials.
2. Laminate data in the form of total number of plies and their individual thickness, orientation and material number are entered.
3. Load data in the form of normal loads, moments, etc. are entered. The program can cater for the temperature changes.

The flow diagram of the analysis is given in Figure (3.1) and the results are printed in the following manner.

1. Q - matrix corresponding to the material.
2. Q - matrix corresponding to ply.
3. A, B, and D - matrices corresponding to over all laminate.
4. A, B, and D - inverse matrices.
5. Overall modulie are computed for the given laminate

AN EXAMPLE RUN OF THE LAMINATE PROGRAM

```
            ************    DATA FILE    ************
1
150.0 8.0 5.0 0.333
1
8
0.25   45.0 1
0.25  -45.0 1
0.25   90.0 1
0.25    0.0 1
0.25   90.0 1
0.25  -45.0 1
0.25   45.0 1
```

```
            **************    RESULT FILE    **************
PROGRAMME : LAMINAT.F
OBJECTIVE : TO ANALYSE SYM. & ANTI-SYM. LAMINATES
          : EQUIVALENT ELASTIC CONSTANTS CALCULATION
INPUT     : E1, E2, G12, PR12
          : NUMBER OF PLIES
          : PLY THICKNESS, PLY ORIENTATION
TOTAL NUMBER OF MATERIALS
E1            E2            G12           PR12
-----------(GPa)---------------
 150.00000     8.00000     5.00000     0.33300
Q MATRIX  (GPa)
 150.89239      2.67985      0.00000
   2.67985      8.04759      0.00000
   0.00000      0.00000      5.00000
NUMBER OF LAMIANTES
  1
NUMBER OF PLIES
  8
PLY NO.   MATERIAL    PLY THICK.    PLY ORIENTATION
                        (mm)            (deg.)
(Enter only material, ply thickness and orientation)
 1   1    0.25000     45.00000
 2   1    0.25000    -45.00000
 3   1    0.25000     90.00000
 4   1    0.25000      0.00000
 5   1    0.25000      0.00000
 6   1    0.25000     90.00000
 7   1    0.25000    -45.00000
 8   1    0.25000     45.00000
Q BAR MATRIX MEMBERS  (GPa)
  QB11          QB12          QB13          QB22          QB23          QB33
46.07492      36.07492      35.71120      46.07492      35.71120      38.39507
46.07492      36.07492     -35.71120      46.07492     -35.71120      38.39507
 8.04759       2.67985       0.00000     150.89239       0.00000       5.00000
```

```
150.89239     2.67985     0.00000     8.04759     0.00000     5.00000
150.89239     2.67985     0.00000     8.04759     0.00000     5.00000
  8.04759     2.67985     0.00000   150.89239     0.00000     5.00000
 46.07492    36.07492   -35.71120    46.07492   -35.71120    38.39507
 46.07492    36.07492    35.71120    46.07492    35.71120    38.39507
A MATRIX       (MN/m)
 125.54491    20.71731     0.00000
  43.75477   120.54491     0.00000
  18.03746    23.03746    24.19754
B MATRIX
  83.67380    25.38698    11.15975
  74.05283   227.41030    11.15975
  47.32560    59.82560    28.79470
D MATRIX       (Nm)
  32.87521    12.97712     5.57987
  28.02327    38.05301     5.57987
  16.87602    20.62602    13.84718
A INVERSE MATRIX      (m/GN)
   8.47278    -1.45616     0.00000
  -3.07541     8.82421     0.00000
  -3.38786    -7.31570    41.32652
B - INVERSE MATRIX
  15.44836    -0.16648    -5.92269
  -4.21423     4.94200    -0.28206
 -16.63446    -9.99417    45.04887
D - INVERSE MATRIX     (1/KNm)
  43.96467    -6.89686   -14.93688
 -31.37220    38.54447    -2.89014
  -6.85085   -49.00835    94.72596
EX          EY          GXY
---------(GPa)-----------
MEMBRANE MODE
  59.01253    56.66227    12.09877
BENDING  MODE
  34.11831    38.91609    15.83515
```

APPENDIX : I

LIST OF SUBROUTINES USED IN COMPUTER PROGRAMS : SECTION & KSITF

SUBROUTINE	INPUT	DESCRIPTION
INPSEG	NSEG,NT,ICORE,E,G,T,X,Y, RHOFIB,RHOFOAM	To enter material and geometric properties
SKINCG	NSEG,E,T,X,Y,SKXB,SKYB, ASKIN,AL	To calculate the cent. of gravity for skin
SOLIDCG	NSEG,X,Y,SOXB,SOYB, ASOLID	To calculate the cent. of gravity for foam
ALLCG	RHOFIB,RHOFOAM,ASKIN, ASOLID,SKXB,SKYB,SOXB, SOYB,AMALL,AXB,AYB	To calculate the over--all centre of gravity
MSKIN	RHOFIB,ASKIN,AMSKIN	To calculate m/ℓ of skin structure
MSOLID	RHOFOAM,ASOLID,AMSOLID	To calculate m/ℓ of packed foam
MALL	RHOFIB,RHOFOAM,ASKIN, ASOLID,AMALL	To calculate overall mass per unit length
SKINIXY	NSEG,E,T,X,Y,AL,AXB,AYB, SKIXX,SKIYY,SKIXY, SKEIXX,SKEIYY,SKEIXY	To calculate second moment of inertia and stiffness of the skin
SOLIDIXY	NSEG,E,T,X,Y,AL,AXB,AYB, SOIXX,SOIYY,SOIXY, SOEIXX,SOEIYY,SOEIXY	To calculate second moment of inertia and stiff. of packed foam
PARAM	NSEG,AL,G,T,DELTA,PARA	Calculate parametric length of the section
GJSKIN	ASOLID,DELTA,GJ	Calculate the tors. rigidity of the sec.
SHRCENT	NSEG,NT,X,Y,T,AL,AXB,AYB SKIXX,SKIYY,SKIXY,ES	To calculate the shear centre of the skin sec
YDSVALUE	NSEG,X,Y,AL,YDS,Y2DS	Calculate first & 2nd-moment of inertia

These subroutines were combined in various ways to predict structural properties of a range of cross sections with the capability to analyse structures made of conventional as well as composite materials.

EXAMPLE RUN

```
PROGRAM      : SECTION
DATE         : 16 JAN. 1990
NAME OF THE DATA FILE :  W-DMS-7
MATERIAL PROPERTIES :
E     GPa      18.620
G     GPa       1.338
DENSITY OF GLASS FIBRE    Kg/m**3    1291.873
DENSITY OF FOAM           Kg/m**3      27.320
GEOMETRICAL PROPERTIES :
CHORD LENGTH    (mm)     118.0
**********************************************************
                R E S U L T S
**********************************************************
TOTAL SKIN AREA      (mm**2)       120.711
TOTAL SOLID AREA     (mm**2)      1121.000
TOTAL PARMETER       (mm)          241.422
LOCATION OF C. G. FOR SKIN ONLY      (mm)     58.210     0.028
LOCATION OF C. G. FOR FOAM ONLY      (mm)     46.127     0.050
LOCATION OF C. G. FOR OVERALL SEC.   (mm)     56.227     0.032
DIST. BETWEEN C. G. AND SHEAR CENTRE (mm)   - 31.445
MASS PER UNIT LENGTH (SKIN)          (Kg/m)    0.156
MASS PER UNIT LENGTH (FOAM)          (Kg/m)    0.031
MASS PER UNIT LENGTH (ALL)           (Kg/m)    0.187
SECOND MOMENT OF AREA (SKIN) ABOUT X-AXIS   (mm**4)    3444.286
SECOND MOMENT OF AREA (SKIN) ABOUT Y-AXIS   (mm**4)    144419.701
SECOND MOMENT OF AREA (SKIN) ABOUT XY-AXIS  (mm**4)    692.992
SECOND MOMENT OF AREA (FOAM) ABOUT X-AXIS   (mm**4)    14570.478
SECOND MOMENT OF AREA (FOAM) ABOUT Y-AXIS   (mm**4)    856927.574
```

SECOND MOMENT OF AREA (FOAM) ABOUT XY-AXIS (mm^4) 151502.312
SECOND MOMENT OF AREA (ALL) ABOUT X-AXIS (mm^4) 18014.765
SECOND MOMENT OF AREA (ALL) ABOUT Y-AXIS (mm^4) 1001347.274
SECOND MOMENT OF AREA (ALL) ABOUT XY-AXIS (mm^4) 150809.321
POLAR MASS MOMENT OF INERTIA (Kg-m) 3.99308E-4
EI_x ($N\ m^2$) 64.133
EI_z ($N\ m^2$) 2689.095
EI_{xz} ($N\ m^2$) 12.904
GJ ($N\ m^2$) 13.925

EXAMPLE RUN

PROGRAM : KSTIF.FOR
SUBROUTINE : LAMINAT.F
OBJECTIVE : TO ANALYSE SYM. & ANTI-SYM. LAMINATES
INPUT : E1, E2, G12, PR12
: NUMBER OF PLIES
: PLY THICKNESS, PLY ORIENTATION

E1	E2	G12	PR12
2.35000E+01	2.35000E+01	4.00000E+00	1.30000E-01

NUMBER OF LAMIANTES
1
NUMBER OF PLIES
4

PLY NO.	PLY THICKNESS	PLY ORIENTATION
1	3.80000E-01	2.00000E+01
2	3.80000E-01	-2.00000E+01
3	3.80000E-01	-2.00000E+01
4	3.80000E-01	2.00000E+01

Q MATRIX (GPa)

2.39040E+01	3.10752E+00	0.00000E+00
3.10752E+00	2.39040E+01	0.00000E+00
0.00000E+00	0.00000E+00	4.00000E+00

Q BAR MATRIX FOR PLY NO. 1

```
   2.12604E+01   5.75111E+00   3.15051E+00
   5.75111E+00   2.12604E+01  -3.15051E+00
   3.15051E+00  -3.15051E+00   6.64359E+00
Q BAR MATRIX        FOR PLY NO. 2
   2.12604E+01   5.75111E+00  -3.15051E+00
   5.75111E+00   2.12604E+01   3.15051E+00
  -3.15051E+00   3.15051E+00   6.64359E+00
Q BAR MATRIX        FOR PLY NO. 3
   2.12604E+01   5.75111E+00  -3.15051E+00
   5.75111E+00   2.12604E+01   3.15051E+00
  -3.15051E+00   3.15051E+00   6.64359E+00
Q BAR MATRIX        FOR PLY NO. 4
   2.12604E+01   5.75111E+00   3.15051E+00
   5.75111E+00   2.12604E+01  -3.15051E+00
   3.15051E+00  -3.15051E+00   6.64359E+00
A MATRIX      (MN/m)
   3.23158E+01 8.74169E+00 0.00000E+00
   8.74169E+00 3.23158E+01 0.00000E+00
   0.00000E+00 0.00000E+00 1.00983E+01
B MATRIX
============ NOT PRESENT DUE TO SYMMETRIC LAY-UP =======
D MATRIX      (Nm)
   6.22187E+00   1.68307E+00   6.91500E-01
   1.68307E+00   6.22187E+00  -6.91500E-01
   6.91500E-01  -6.91500E-01   1.94425E+00
A - INVERSE MATRIX      (m/GN)
   3.33878E+01 -9.03167E+00   0.00000E+00
  -9.03167E+00   3.33878E+01   0.00000E+00
   0.00000E+00   0.00000E+00   9.90269E+01
B - INVERSE MATRIX
============ NOT PRESENT DUE TO SYMMETRIC LAY-UP =======
D - INVERSE MATRIX
   1.86803E+02 -6.02992E+01 -8.78851E+01
  -6.02992E+01   1.86803E+02   8.78851E+01
  -8.78851E+01   8.78851E+01   5.76852E+02
```

EX	EZ	GXZ
1.97047E+01	1.97047E+01	6.64359E+00

H11	H21	H22
2.99511E-02	0.0	9.90269E+01

SUBROUTINE : SECTION.F

ENTER NUMBER OF SKIN SEGMENTS

4

ENTER NUMBER OF SEGMENTS ABOVE THE LINE OF SYMMETRY

2

ENTER DENSITY FOR FIBRE AND FOAM (Kg/m^3)

(If it is not foam filled then just put it zero)

1800.0 0.0

E -------- ($N\ m^2$)	G ------	Thickness (mm)	X - coord (mm)	Y-coord (mm)
19.7046588	6.643594	1.52	15.00	8.00
19.7046588	6.643594	1.52	0.00	0.00
19.7046588	6.643594	1.52	15.00	-8.00
19.7046588	6.643594	1.52	9.00	0.00

CENTRE OF GRAVITY : X - coord Z - coord (mm)

9.16667 0.00

MASS PER UNIT LENGTH (Kg/m) : 0.147744

AREA OF THE SECTION (mm^2) : 82.08

SECOND AREA MOMENT (mm^4) :

I_{xx}	I_{zz}	I_{xz}
1.751040	1.447800	0.00

BENDING RIGIDITY TORSIONAL RIGIDITY ($N\ m^2$)

34.5036 21.112

THE SHEAR CENTRE (mm)

-32.90

YDS	Y2DS	(mm^4)
216.00	1152.00	

EIX	EIZ	GJ ($N\ m^2$)
34.5036	28.5284	21.112

K22	K24	K44
34.5036	0.00	21.112

APPENDIX : J

MATERIAL PROPERTIES

ALUMINIUM

Modulus of Elasticity	68.9 GPa
Shear modulus of rigidity	26.5 GPa
Poisson's ratio	0.3
Density	2700.0 Kg/m^3

FIBREDUX C920 UNIDIRECTIONAL PREPREG CARBON FIBRE COMPOSITE

PROPERTY	UNITS	C920
E_ℓ	GPa	98.00
E_t	GPa	7.90
$G_{\ell t}$	GPa	5.60
$\nu_{\ell t}$	---	0.28
ρ	Kg/m^3	1520

MATERIAL : 916G WOVEN GLASS FIBRE REINFORCED PLASTIC

PROPERTY	UNITS	916G
E_ℓ	GPa	23.50
E_t	GPa	23.50
$G_{\ell t}$	GPa	7.00
$\nu_{\ell t}$	---	0.13
ρ	Kg/m^3	1410.00

MATERIAL : WOVEN GLASS REINFORCED PLASTIC

PROPERTY	UNITS	WOVEN-GRP
E_ℓ	GPa	18.63
E_t	GPa	18.63
$G_{\ell t}$	GPa	1.376
$\nu_{\ell t}$	---	0.13

APPENDIX : K

DYNAMIC STIFFNESS MATRICES OF DEGENERATED CASES

K.1 VIBRATION OF BEAMS WITH GEOMETRIC AND MATERIAL COUPLING

In case of a thin-walled symmetrically laminated composite beam with the elastic axis not coinciding with the centroidal axis and no axial load applied, the equations of motion (6.6.8) and (6.6.9) are reduced to the following expressions.

$$EI\frac{\partial^4 h}{\partial y^4} + K\frac{\partial^3 \psi}{\partial y^3} + m\frac{\partial^2 h}{\partial t^2} - m\,e\frac{\partial^2 \psi}{\partial t^2} = 0 \qquad (K.1.1)$$

$$K\frac{\partial^3 h}{\partial y^3} + GJ\frac{\partial^2 \psi}{\partial y^2} + m\,e\frac{\partial^2 h}{\partial t^2} - I_\alpha\frac{\partial^2 \psi}{\partial t^2} = 0 \qquad (K.1.2)$$

and the shear force:

$$S = -EI\,h''' - K\,\psi'' \qquad (K.1.3)$$

bending moment:

$$M = EI\,h'' + K\,\psi' \qquad (K.1.4)$$

torque:

$$T = GJ\,\psi' + K\,h'' \qquad (K.1.5)$$

Let

$$h = H\sin(\omega t) \quad , \quad \psi = \Psi\sin(\omega t)$$

$$\zeta = \frac{y}{\ell} \quad , \quad \frac{d\zeta}{dy} = \frac{1}{\ell} \qquad (K.1.6)$$

$$\frac{dh}{dy} = \frac{1}{\ell}\frac{dh}{d\zeta} \quad ,\text{etc.}$$

Substituting relations (K.1.6) into (K.1.1) and simplifying gives:

$$D^4H + \bar{K}\,D^3\Psi - \bar{a}\,H + \bar{a}\,e\,\Psi = 0 \qquad (K.1.7)$$

where

$$\bar{a} = \left[\frac{m\omega^2 \ell^4}{EI}\right]$$

$$\bar{K} = \frac{K\ \ell}{EI}$$

Similarly from equation (K.1.2):

$$\bar{\bar{K}}\ D^3H + D^2\Psi - \bar{b}\ e\ H + \bar{b}\ r^2\ \Psi = 0 \qquad \text{(K.1.8)}$$

where

$$\bar{b} = \left[\frac{m\omega^2 \ell^2}{GJ}\right] \quad , \quad I_\alpha = m\ r^2 \quad , \quad \bar{\bar{K}} = \frac{K}{\ell\ GJ}$$

Rearranging equations (K.1.7) and (K.1.8)

$$\left[D^4 - \bar{a}\ \right] H + \left[\ \bar{K}\ D^3 + \bar{a}\ e\right] \Psi = 0 \qquad \text{(K.1.9)}$$

$$\left[\ \bar{\bar{K}}\ D^3 - \bar{b}\ e\ \right] H + \left[D^2 + \bar{b}\ r^2\right] \Psi = 0 \qquad \text{(K.1.10)}$$

Let

$$L_1 = \left[D^4 - \bar{a}\ \right] \quad , \quad L_2 = \left[\ \bar{K}\ D^3 + \bar{a}\ e\right]$$

$$L_3 = \left[\ \bar{\bar{K}}\ D^3 - \bar{b}\ e\ \right] \quad , \quad L_4 = \left[D^2 + \bar{b}\ r^2\right]$$

Equations (K.1.9) and (K.1.10) give :

$$L_1\ H + L_2\ \Psi = 0 \qquad \times L_4 \rightarrow \quad L_1L_4\ H + L_2L_4\ \Psi = 0$$

$$L_3\ H + L_4\ \Psi = 0 \qquad \times L_2 \rightarrow \quad L_3L_2\ H + L_4L_2\ \Psi = 0$$

Subtracting the first expression from the second and substituting corresponding values of L_1, L_4, L_2 & L_3 :

$$\left[\left[D^4 - \bar{a}\ \right]\left[D^2 + \bar{b}\ r^2\right] - \left[\ \bar{K}\ D^3 + \bar{a}\ e\right]\left[\ \bar{\bar{K}}\ D^3 - \bar{b}\ e\ \right]\right] H = 0$$

Let

$$\Delta = \left(1-\frac{K^2}{EI\ GJ}\right)$$

$$a = \frac{\bar{b}\ r^2}{\Delta} \quad , \quad b = \frac{-\ \bar{a}}{\Delta} \quad , \quad c = \frac{-\ \bar{a}\ \bar{b}\ (r^2-\ e^2)}{\Delta}$$

Therefore,

$$(D^6+\ a\ D^4+\ b\ D^2+\ c)\ H = 0 \qquad (K.1.11)$$

Let $H = e^{p\zeta}$

The auxiliary equation can be

$$p^6+\ a\ p^4+\ b\ p^2+\ c = 0 \qquad (K.1.12)$$

Substituting $\lambda = p^2$.

$$\lambda^3+\ a\ \lambda^2+\ b\ \lambda\ +\ c = 0 \qquad (K.1.13)$$

Let $\lambda = x - \frac{a}{3}$

$$(x - \frac{a}{3})^3+\ a\ (x - \frac{a}{3})^2+\ b\ (x - \frac{a}{3})\ +\ c = 0$$

After simplification we get

$$x^3+\ (-\ \frac{a^3}{3}\ +\ b)\ x\ +\ (\frac{2}{27}\ a^3-\ \frac{ab}{3}\ +\ c)\ =\ 0$$

Let $q = \frac{a^2}{3} - b$

$$r = \frac{ab}{3} - \frac{2}{27}\ a^3-\ c$$

Therefore,

$$x^3-\ q\ x\ -\ r\ =\ 0$$

If $27\ r^2-\ 4\ q^2 < 0$

then all the three roots of the equation are real as follows:

$$x_1 = 2\,(q/3)^{1/2}\cos\,(\phi/3)$$

$$x_2 = 2\,(q/3)^{1/2}\cos\,\left[(\pi-\phi)/3\right]$$

$$x_3 = 2\,(q/3)^{1/2}\cos\,\left[(\pi+\phi)/3\right]$$

where

$$\cos(\phi) = (3/q)^{3/2}\,(r/2)$$

Since

$$\lambda = x - \frac{a}{3}$$

therefore, the roots α, β and γ will be

$$\left.\begin{aligned}
\alpha^2 &= 2\,(q/3)^{1/2}\cos\,(\phi/3) - \frac{a}{3}\\
\beta^2 &= 2\,(q/3)^{1/2}\cos\,\left[(\pi-\phi)/3\right] + \frac{a}{3}\\
\gamma^2 &= 2\,(q/3)^{1/2}\cos\,\left[(\pi+\phi)/3\right] + \frac{a}{3}
\end{aligned}\right\} \qquad \text{(K.1.14)}$$

Assuming a solution for real roots α, β and γ we have

$$H(\zeta) = A_1\cosh(\alpha\zeta) + A_2\sinh(\alpha\zeta) + A_3\cos(\beta\zeta) + A_4\sin(\beta\zeta) + A_5\cos(\gamma\zeta) + A_6\sin(\gamma\zeta) \qquad \text{(K.1.15)}$$

Similarly

$$\Psi(\zeta) = B_1\cosh(\alpha\zeta) + B_2\sinh(\alpha\zeta) + B_3\cos(\beta\zeta) + B_4\sin(\beta\zeta) + B_5\cos(\gamma\zeta) + B_6\sin(\gamma\zeta) \qquad \text{(K.1.16)}$$

and the slope of the deflected structure is

$$\Theta(\zeta) = \frac{1}{\ell}\frac{\partial H}{\partial \zeta}$$

$$= \frac{1}{\ell}\left[\alpha A_1 \sinh(\alpha\zeta) + \alpha A_2 \cosh(\alpha\zeta) - \beta A_3 \sin(\beta\zeta) + \beta A_4 \cos(\beta\zeta) - \gamma A_5 \sin(\gamma\zeta) + \gamma A_6 \cos(\gamma\zeta)\right] \quad \text{(K.1.17)}$$

Let

$$S_{h\alpha} = \sinh(\alpha\zeta), \quad C_{h\alpha} = \cosh(\alpha\zeta)$$
$$S_{\beta} = \sin(\beta\zeta), \quad C_{\beta} = \cos(\beta\zeta)$$
$$S_{\gamma} = \sin(\gamma\zeta), \quad C_{\gamma} = \cos(\gamma\zeta)$$

Substituting the higher derivatives of both H and Ψ into equation (K.1.7) and equating coefficients of cosh, sinh, cos and sin of α, β and γ to zero, the relations between A_{1-6} and B_{1-6} were found using DERIVE (a package to handle symbolic computation).

$$\Psi(\zeta) = \left[K_{\alpha 3}\left(e\ \bar{a}\ C_{h\alpha} - K_{\alpha}\ S_{h\alpha}\right)A_1 + K_{\alpha 3}\left(e\ \bar{a}\ S_{h\alpha} - K_{\alpha}\ C_{h\alpha}\right)A_2\right.$$
$$+ K_{\beta 3}\left(e\ \bar{a}\ C_{\beta} - K_{\alpha}\ S_{\beta}\right)A_3 + K_{\beta 3}\left(e\ \bar{a}\ S_{\beta} + K_{\alpha}\ C_{\beta}\right)A_4$$
$$\left. + K_{\alpha 3}\left(e\ \bar{a}\ C_{\gamma} - K_{\alpha}\ S_{\gamma}\right)A_5 + K_{\gamma 3}\left(e\ \bar{a}\ S_{\gamma} + K_{\alpha}\ C_{\gamma}\right)A_6\right] \quad \text{(K.1.18)}$$

where

$$K_{\alpha} = \bar{K}\ \alpha^3, \quad K_{\alpha 1} = \bar{a}\ e^2 - K_{\alpha}^2, \quad K_{\alpha 2} = \bar{a} - \alpha^4, \quad K_{\alpha 3} = \frac{K_{\alpha 2}}{K_{\alpha 1}}$$

$$K_{\beta} = \bar{K}\ \beta^3, \quad K_{\beta 1} = \bar{a}\ e^2 - K_{\beta}^2, \quad K_{\beta 2} = \bar{a} - \beta^4, \quad K_{\beta 3} = \frac{K_{\beta 2}}{K_{\beta 1}}$$

$$K_{\gamma} = \bar{K}\ \gamma^3, \quad K_{\gamma 1} = \bar{a}\ e^2 - K_{\gamma}^2, \quad K_{\gamma 2} = \bar{a} - \gamma^4, \quad K_{\gamma 3} = \frac{K_{\gamma 2}}{K_{\gamma 1}}$$

Assuming the following boundary conditions :

$$H = H_1,\ \Theta = \Theta_1,\ \Psi = \Psi_1 \quad \text{at} \quad \zeta = 0 \quad \text{or} \quad y = 0$$
$$H = H_2,\ \Theta = \Theta_2,\ \Psi = \Psi_2 \quad \text{at} \quad \zeta = 1 \quad \text{or} \quad y = \ell$$

Therefore, in matrix form we have

$$\begin{Bmatrix} H_1 \\ \theta_1 \\ \Psi_1 \\ H_2 \\ \theta_2 \\ \Psi_2 \end{Bmatrix} = \begin{bmatrix} 1 & 0 & 1 & 0 & 1 & 0 \\ 0 & \frac{\alpha}{\ell} & 0 & \frac{\beta}{\ell} & 0 & \frac{\gamma}{\ell} \\ e\,\bar{a}\,K_{\alpha s} & -K_\alpha K_{\alpha s} & e\,\bar{a}\,K_{\beta s} & K_\beta K_{\beta s} & e\,\bar{a}\,K_{\gamma s} & K_\gamma K_{\gamma s} \\ C_\alpha & S_\alpha & C_\beta & S_\beta & C_\gamma & S_\gamma \\ \frac{\alpha}{\ell} S_\alpha & \frac{\alpha}{\ell} C_\alpha & -\frac{\beta}{\ell} S_\beta & \frac{\beta}{\ell} C_\beta & -\frac{\gamma}{\ell} S_\gamma & \frac{\gamma}{\ell} C_\gamma \\ K_{\alpha s}\mu_1 & K_{\alpha s}\mu_2 & K_{\beta s}\mu_3 & K_{\beta s}\mu_4 & K_{\gamma s}\mu_5 & K_{\gamma s}\mu_6 \end{bmatrix} \begin{Bmatrix} A_1 \\ A_2 \\ A_3 \\ A_4 \\ A_5 \\ A_6 \end{Bmatrix} \tag{6.8.3}$$

where

$$\mu_1 = e\,\bar{a}\,C_{h\alpha} - K_\alpha S_{h\alpha}$$
$$\mu_2 = e\,\bar{a}\,S_{h\alpha} - K_\alpha C_{h\alpha}$$
$$\mu_3 = e\,\bar{a}\,C_\beta - K_\beta S_\beta$$
$$\mu_4 = e\,\bar{a}\,S_\beta + K_\beta C_\beta$$
$$\mu_5 = e\,\bar{a}\,C_\gamma - K_\gamma S_\gamma$$
$$\mu_6 = e\,\bar{a}\,S_\gamma + K_\gamma C_\gamma$$

or simply

$$\{\underset{\sim}{U}\} = [\underset{\sim}{B}]\{\underset{\sim}{A}\} \tag{K.1.19}$$

Now the expressions for shear force , bending moment and torque are evaluated.

The shear force of equation (K.1.3) becomes :

$$S = -EI\,h''' - K\,\psi''$$

$$= \left[- EI \frac{\alpha^3}{\ell^3} \sinh(\alpha) - K K_{\alpha s} \frac{\alpha^2}{\ell^2} \left[e \bar{a} \cosh(\alpha) - K_\alpha \sinh(\alpha) \right] \right] A_1$$

$$+ \left[- EI \frac{\alpha^3}{\ell^3} \cosh(\alpha) - K K_{\alpha s} \frac{\alpha^2}{\ell^2} \left[e \bar{a} \sinh(\alpha) - K_\alpha \cosh(\alpha) \right] \right] A_2$$

$$+ \left[- EI \frac{\beta^3}{\ell^3} \sin(\beta) - K K_{\beta s} \frac{\beta^2}{\ell^2} \left[- e \bar{a} \cos(\beta) + K_\beta \sin(\beta) \right] \right] A_3$$

$$+ \left[+ EI \frac{\beta^3}{\ell^3} \cos(\beta) - K K_{\beta s} \frac{\beta^2}{\ell^2} \left[- e \bar{a} \sin(\beta) - K_\beta \cos(\beta) \right] \right] A_4$$

$$+ \left[- EI \frac{\gamma^3}{\ell^3} \sin(\gamma) - K K_{\gamma s} \frac{\gamma^2}{\ell^2} \left[- e \bar{a} \cos(\gamma) + K_\gamma \sin(\gamma) \right] \right] A_5$$

$$+ \left[+ EI \frac{\gamma^3}{\ell^3} \cos(\gamma) - K K_{\gamma s} \frac{\gamma^2}{\ell^2} \left[- e \bar{a} \sin(\gamma) - K_\gamma \cos(\gamma) \right] \right] A_6 \quad \text{(K.1.20)}$$

The bending moment as given in equation (K.1.4) becomes :

$$M = EI\, h'' + K\, \psi'$$

$$= \left[EI \frac{\alpha^2}{\ell^2} \cosh(\alpha) + K K_{\alpha s} \frac{\alpha}{\ell} \left[e \bar{a} \sinh(\alpha) - K_\alpha \cosh(\alpha) \right] \right] A_1$$

$$+ \left[EI \frac{\alpha^2}{\ell^2} \sinh(\alpha) + K K_{\alpha s} \frac{\alpha}{\ell} \left[e \bar{a} \cosh(\alpha) - K_\alpha \sinh(\alpha) \right] \right] A_2$$

$$+ \left[- EI \frac{\beta^2}{\ell^2} \cos(\beta) + K K_{\beta s} \frac{\beta}{\ell} \left[- e \bar{a} \sin(\beta) - K_\beta \cos(\beta) \right] \right] A_3$$

$$+ \left[- EI \frac{\beta^2}{\ell^2} \sin(\beta) + K K_{\beta s} \frac{\beta}{\ell} \left[e \bar{a} \cos(\beta) - K_\beta \sin(\beta) \right] \right] A_4$$

$$+ \left[- EI \frac{\gamma^2}{\ell^2} \cos(\gamma) + K K_{\gamma s} \frac{\gamma}{\ell} \left[- e \bar{a} \sin(\gamma) - K_\gamma \cos(\gamma) \right] \right] A_5$$

$$+ \left[- EI \frac{\gamma^2}{\ell^2} \sin(\gamma) + K K_{\gamma s} \frac{\gamma}{\ell} \left[e \bar{a} \cos(\gamma) - K_\gamma \sin(\gamma) \right] \right] A_6 \quad \text{(K.1.21)}$$

and finally torque from equation (K.1.5) becomes :

$$T = GJ\, \psi' + K\, h''$$

$$= \left[GJ\, K_{\alpha s} \frac{\alpha}{\ell} \left[e \bar{a} \sinh(\alpha) - K_\alpha \cosh(\alpha) \right] + K \frac{\alpha^2}{\ell^2} \cosh(\alpha) \right] A_1$$

$$+ \left[GJ\, K_{\alpha s} \frac{\alpha}{\ell} \left[e \bar{a} \cosh(\alpha) - K_\alpha \sinh(\alpha) \right] + K \frac{\alpha^2}{\ell^2} \sinh(\alpha) \right] A_2$$

$$+ \left[GJ\, K_{\beta s} \frac{\beta}{\ell} \left[- e \bar{a} \sin(\beta) - K_\beta \cos(\beta) \right] - K \frac{\beta^2}{\ell^2} \cos(\beta) \right] A_3$$

$$+ \left[GJ\, K_{\beta s} \frac{\beta}{\ell} \left[e \bar{a} \cos(\beta) - K_\beta \sin(\beta) \right] - K \frac{\beta^2}{\ell^2} \sin(\beta) \right] A_4$$

$$+\left[GJ\ K_{\gamma s}\frac{\gamma}{\ell}\left(-\ e\ \bar{a}\ \sin(\gamma)\ -\ K_{\gamma}\cos(\gamma)\right)\ -\ K\ \frac{\gamma^2}{\ell^2}\cos\ (\gamma)\right]A_5$$

$$+\left[GJ\ K_{\gamma s}\frac{\gamma}{\ell}\left(\ \ e\ \bar{a}\ \cos(\gamma)\ -\ K_{\gamma}\sin(\gamma)\right)-\ K\ \frac{\gamma^2}{\ell^2}\sin\ (\gamma)\right]A_6 \qquad (K.1.22)$$

Assuming the following boundary conditions,

$S = -S_1$, $M_x = -M_{x1}$, $M_z = -M_{z1}$ at $\xi = 0$ or $y = 0$

$S = S_2$, $M_x = M_{x2}$, $M_z = M_{z2}$ at $\xi = 1$ or $y = \ell$

Therefore, expressions for the shear force, bending moment and torque can be expressed in matrix form as follows :

$$\begin{Bmatrix} S_1 \\ M_1 \\ T_1 \\ S_2 \\ M_2 \\ T_2 \end{Bmatrix} = \begin{bmatrix} D_{11} & D_{12} & D_{13} & D_{14} & D_{15} & D_{16} \\ D_{21} & D_{22} & D_{23} & D_{24} & D_{25} & D_{26} \\ D_{31} & D_{32} & D_{33} & D_{34} & D_{35} & D_{36} \\ D_{41} & D_{42} & D_{43} & D_{44} & D_{45} & D_{46} \\ D_{51} & D_{52} & D_{53} & D_{54} & D_{55} & D_{56} \\ D_{61} & D_{62} & D_{63} & D_{64} & D_{65} & D_{66} \end{bmatrix} \begin{Bmatrix} A_1 \\ A_2 \\ A_3 \\ A_4 \\ A_5 \\ A_6 \end{Bmatrix}$$

or

$$\{F\} = [\underset{\sim}{D}]\{A\} \qquad (K.1.23)$$

where

$$D_{11} = -\left(-\ K\ K_{\alpha s}\frac{\alpha^2}{\ell^2}\ e\ \bar{a}\ \right)$$

$$D_{12} = -\left(-\ EI\ \frac{\alpha^3}{\ell^3}\ +\ K\ K_{\alpha s}\frac{\alpha^2}{\ell^2}\ K_{\alpha}\ \right)$$

$$D_{13} = -\left(+\ K\ K_{\beta s}\frac{\beta^2}{\ell^2}\ e\ \bar{a}\ \right)$$

$$D_{14} = -\left(+\ EI\ \frac{\beta^3}{\ell^3}\ +\ K\ K_{\beta s}\frac{\beta^2}{\ell^2}\ K_{\beta}\ \right)$$

$$D_{15} = -\left(+\ K\ K_{\gamma s}\frac{\gamma^2}{\ell^2}\ e\ \bar{a}\ \right)$$

$$D_{16} = -\left(+\ EI\ \frac{\gamma^3}{\ell^3}\ +\ K\ K_{\gamma s}\frac{\gamma^2}{\ell^2}\ K_{\gamma}\ \right)$$

APPENDIX : K

$$D_{21} = - \left(EI \frac{\alpha^2}{\ell^2} - K K_{\alpha 3} \frac{\alpha}{\ell} K_{\alpha} \right)$$

$$D_{22} = - \left(+ K K_{\alpha 3} \frac{\alpha}{\ell} e \bar{a} \right)$$

$$D_{23} = - \left(- EI \frac{\beta^2}{\ell^2} - K K_{\beta 3} \frac{\beta}{\ell} K_{\beta} \right)$$

$$D_{24} = - \left(+ K K_{\beta 3} \frac{\beta}{\ell} e \bar{a} \right)$$

$$D_{25} = - \left(- EI \frac{\gamma^2}{\ell^2} - K K_{\gamma 3} \frac{\gamma}{\ell} K_{\gamma} \right)$$

$$D_{26} = - \left(+ K K_{\gamma 3} \frac{\gamma}{\ell} e \bar{a} \right)$$

$$D_{31} = - \left(- GJ K_{\alpha 3} \frac{\alpha}{\ell} K_{\alpha} + K \frac{\alpha^2}{\ell^2} \right)$$

$$D_{32} = - \left(+ GJ K_{\alpha 3} \frac{\alpha}{\ell} e \bar{a} \right)$$

$$D_{33} = - \left(- GJ K_{\beta 3} \frac{\beta}{\ell} K_{\beta} - K \frac{\beta^2}{\ell^2} \right)$$

$$D_{34} = - \left(+ GJ K_{\beta 3} \frac{\beta}{\ell} e \bar{a} \right)$$

$$D_{35} = - \left(- GJ K_{\gamma 3} \frac{\gamma}{\ell} K_{\gamma} - K \frac{\gamma^2}{\ell^2} \right)$$

$$D_{36} = - \left(+ GJ K_{\gamma 3} \frac{\gamma}{\ell} e \bar{a} \right)$$

$$D_{41} = - EI \frac{\alpha^3}{\ell^3} \sinh(\alpha) - K K_{\alpha 3} \frac{\alpha^2}{\ell^2} \left[e \bar{a} \cosh(\alpha) - K_{\alpha} \sinh(\alpha) \right]$$

$$D_{42} = - EI \frac{\alpha^3}{\ell^3} \cosh(\alpha) - K K_{\alpha 3} \frac{\alpha^2}{\ell^2} \left[e \bar{a} \sinh(\alpha) - K_{\alpha} \cosh(\alpha) \right]$$

$$D_{43} = - EI \frac{\beta^3}{\ell^3} \sin(\beta) - K K_{\beta 3} \frac{\beta^2}{\ell^2} \left[- e \bar{a} \cos(\beta) + K_{\beta} \sin(\beta) \right]$$

$$D_{44} = + EI \frac{\beta^3}{\ell^3} \cos(\beta) - K K_{\beta 3} \frac{\beta^2}{\ell^2} \left[- e \bar{a} \sin(\beta) - K_{\beta} \cos(\beta) \right]$$

$$D_{45} = - EI \frac{\gamma^3}{\ell^3} \sin(\gamma) - K K_{\gamma 3} \frac{\gamma^2}{\ell^2} \left[- e \bar{a} \cos(\gamma) + K_{\gamma} \sin(\gamma) \right]$$

$$D_{46} = + EI \frac{\gamma^3}{\ell^3} \cos(\gamma) - K K_{\gamma 3} \frac{\gamma^2}{\ell^2} \left[- e \bar{a} \sin(\gamma) - K_{\gamma} \cos(\gamma) \right]$$

$$D_{51} = EI \frac{\alpha^2}{\ell^2} \cosh(\alpha) + K K_{\alpha 3} \frac{\alpha}{\ell} \left[e \bar{a} \sinh(\alpha) - K_{\alpha} \cosh(\alpha) \right]$$

$$D_{52} = EI \frac{\alpha^2}{\ell^2} \sinh(\alpha) + K K_{\alpha 3} \frac{\alpha}{\ell} \left[e \bar{a} \cosh(\alpha) - K_{\alpha} \sinh(\alpha) \right]$$

$$D_{53} = - EI \frac{\beta^2}{\ell^2} \cos(\beta) + K K_{\beta 3} \frac{\beta}{\ell} \left[- e \bar{a} \sin(\beta) - K_{\beta} \cos(\beta) \right]$$

$$D_{54} = - EI \frac{\beta^2}{\ell^2} \sin(\beta) + K K_{\beta 3} \frac{\beta}{\ell} \left[e \bar{a} \cos(\beta) - K_{\beta} \sin(\beta) \right]$$

$$D_{55} = - EI \frac{\gamma^2}{\ell^2} \cos(\gamma) + K K_{\gamma 3} \frac{\gamma}{\ell} \left[- e \bar{a} \sin(\gamma) - K_{\gamma} \cos(\gamma) \right]$$

$$D_{56} = - EI \frac{\gamma^2}{\ell^2} \sin(\gamma) + K K_{\gamma 3} \frac{\gamma}{\ell} \left[e \bar{a} \cos(\gamma) - K_{\gamma} \sin(\gamma) \right]$$

$$D_{61} = GJ K_{\alpha 3} \frac{\alpha}{\ell} \left[e \bar{a} \sinh(\alpha) - K_{\alpha} \cosh(\alpha) \right] + K \frac{\alpha^2}{\ell^2} \cosh(\alpha)$$

$$D_{62} = GJ K_{\alpha 3} \frac{\alpha}{\ell} \left[e \bar{a} \cosh(\alpha) - K_{\alpha} \sinh(\alpha) \right] + K \frac{\alpha^2}{\ell^2} \sinh(\alpha)$$

$$D_{63} = GJ K_{\beta 3} \frac{\beta}{\ell} \left[- e \bar{a} \sin(\beta) - K_{\beta} \cos(\beta) \right] - K \frac{\beta^2}{\ell^2} \cos(\beta)$$

$$D_{64} = GJ K_{\beta 3} \frac{\beta}{\ell} \left[e \bar{a} \cos(\beta) - K_{\beta} \sin(\beta) \right] - K \frac{\beta^2}{\ell^2} \sin(\beta)$$

$$D_{65} = GJ K_{\gamma 3} \frac{\gamma}{\ell} \left[- e \bar{a} \sin(\gamma) - K_{\gamma} \cos(\gamma) \right] - K \frac{\gamma^2}{\ell^2} \cos(\gamma)$$

$$D_{66} = GJ K_{\gamma 3} \frac{\gamma}{\ell} \left[e \bar{a} \cos(\gamma) - K_{\gamma} \sin(\gamma) \right] - K \frac{\gamma^2}{\ell^2} \sin(\gamma)$$

Substituting equation (K.1.18) in equation (K.1.23) gives :

$$\{A\} = [\underset{\sim}{B}]^{-1}\{U\}$$

$$\{F\} = [\underset{\sim}{D}] [\underset{\sim}{B}]^{-1}\{U\}$$

$$= [\underset{\sim}{K}]\{U\} \qquad (K.1.24)$$

where

$[\underset{\sim}{K}] = [\underset{\sim}{D}][\underset{\sim}{B}]^{-1}$ = the dynamic stiffness matrix

K.2 VIBRATION OF BEAMS WITH MATERIAL COUPLING

In section (K.1), structures with geometric and material coupling were analysed. Symmetrically laminated composite beams with doubly symmetrical cross sections and plates present structures with material bending/torsional coupling only. In the case of such structures, the governing differential equations (K.1.1) and (K.1.2) are reduced to the following expressions.

$$EI\frac{\partial^4 h}{\partial y^4} + K\frac{\partial^3 \psi}{\partial y^3} + m\frac{\partial^2 h}{\partial t^2} = 0 \qquad (K.2.1)$$

$$K\frac{\partial^3 h}{\partial y^3} + GJ\frac{\partial^2 \psi}{\partial y^2} - I_\alpha\frac{\partial^2 \psi}{\partial t^2} = 0 \qquad (K.2.2)$$

For this special case with material coupling only the expressions for shear force, bending moment, and torque are given as follows :

Shear force :

$$S = -EI\,h''' - K\,\psi'' \qquad (K.2.3)$$

Bending moment :

$$M = EI\,h'' + K\,\psi' \qquad (K.2.4)$$

Torque :

$$T = GJ\,\psi' + K\,h'' \qquad (K.2.5)$$

Letting

$$h = H\sin(\omega t) \quad , \quad \psi = \Psi\sin(\omega t)$$

$$\zeta = \frac{y}{\ell} \quad , \quad \frac{d\zeta}{dy} = \frac{1}{\ell} \qquad (K.2.6)$$

$$\frac{dh}{dy} = \frac{1}{\ell}\frac{dh}{d\zeta} \quad ,\text{etc.}$$

Substituting relations (K.2.6) into (K.2.1) and simplifying gives:

$$D^4H + \bar{K}\,D^3\Psi - \bar{a}\,H = 0 \qquad (K.2.7)$$

where

$$\bar{a} = \left(\frac{m\omega^2\ell^4}{EI}\right)$$

$$\bar{K} = \frac{K\,\ell}{EI}$$

Similarly from equation (K.2.2):

$$\bar{K}\,D^3H + D^2\Psi + \bar{b}\,r^2\,\Psi = 0 \qquad (K.2.8)$$

where

$$\bar{b} = \left\{\frac{m\omega^2 \ell^2}{GJ}\right\} \quad , \quad I_\alpha = m\, r^2 \quad , \quad \bar{\bar{K}} = \frac{K}{\ell\, GJ}$$

Rearranging equations (K.2.7) and (K.2.8)

$$\left(D^4 - \bar{a}\right) H + \left(\bar{K}\, D^2\right) \Psi = 0 \qquad \text{(K.2.9)}$$

$$\left(\bar{\bar{K}}\, D^2\right) H + \left(D^2 + \bar{b}\, r^2\right) \Psi = 0 \qquad \text{(K.2.10)}$$

Let

$$L_1 = \left(D^4 - \bar{a}\right) \quad , \quad L_2 = \left(\bar{K}\, D^2\right)$$

$$L_3 = \left(\bar{\bar{K}}\, D^2\right) \quad , \quad L_4 = \left(D^2 + \bar{b}\, r^2\right)$$

Equations (K.2.9) and (K.2.10) give :

$$L_1 H + L_2 \Psi = 0 \quad \times L_4 \Rightarrow L_1 L_4 H + L_2 L_4 \Psi = 0$$

$$L_3 H + L_4 \Psi = 0 \quad \times L_2 \Rightarrow L_3 L_2 H + L_4 L_2 \Psi = 0$$

Subtracting the first expression from the second:

$$(L_1 L_4 - L_2 L_3)\, H = 0$$

By substituting corresponding values of L_1, L_4, L_2 & L_3 :

$$\left[\left(D^4 - \bar{a}\right)\left(D^2 + \bar{b}\, r^2\right) - \left(\bar{K}\, D^2\right)\left(\bar{\bar{K}}\, D^2\right)\right] H = 0$$

Let

$$\Delta = \left(1 - \frac{K^2}{EI\ GJ}\right)$$

$$a = \frac{\bar{b}\, r^2}{\Delta} \quad , \quad b = \frac{-\bar{a}}{\Delta} \quad , \quad c = \frac{-\bar{a}\,\bar{b}\, r^2}{\Delta}$$

Therefore

$$\left(D^6 + a\, D^4 + b\, D^2 + c\right) H = 0 \qquad \text{(K.2.11)}$$

Let $H = e^{px}$

The auxiliary equation will be

$$p^3 + a\,p^4 + b\,p^2 + c = 0 \qquad (K.2.12)$$

Substituting $\lambda = p^2$

$$\lambda^3 + a\,\lambda^2 + b\,\lambda + c = 0 \qquad (K.2.13)$$

Let $$\lambda = x - \frac{a}{3}$$

$$(x - \frac{a}{3})^3 + a\,(x - \frac{a}{3})^2 + b\,(x - \frac{a}{3}) + c = 0$$

After simplification we get

$$x^3 + (-\frac{a^3}{3} + b)\,x + (\frac{2}{27}\,a^3 - \frac{ab}{3} + c) = 0$$

Let $$q = \frac{a^2}{3} - b$$

$$r = \frac{ab}{3} - \frac{2}{27}\,a^3 - c$$

Therefore

$$x^3 - q\,x - r = 0$$

If $$27\,r^2 - 4\,q^3 < 0$$

then all the three roots of the equation are real as follows :

$$x_1 = 2\,(q/3)^{1/2} \cos\,(\phi/3)$$

$$x_2 = 2\,(q/3)^{1/2} \cos\,\left[(\pi-\phi)/3\right]$$

$$x_3 = 2\,(q/3)^{1/2} \cos\,\left[(\pi+\phi)/3\right]$$

where

$$\cos(\phi) = (3/q)^{3/2} (r/2)$$

Since

$$\lambda = x - \frac{a}{3}$$

so the roots α, β and γ will be

$$\left.\begin{aligned} \alpha^2 &= 2\,(q/3)^{1/2} \cos\,(\phi/3) - \frac{a}{3} \\ \beta^2 &= 2\,(q/3)^{1/2} \cos\,\left[(\pi-\phi)/3\right] + \frac{a}{3} \\ \gamma^2 &= 2\,(q/3)^{1/2} \cos\,\left[(\pi+\phi)/3\right] + \frac{a}{3} \end{aligned}\right\} \qquad \text{(K.2.14)}$$

Assuming a solution for real roots α, β and γ, the amplitudes of bending deflection and torsional rotation are given by;

$$H(\zeta) = A_1\cosh(\alpha\zeta) + A_2\sinh(\alpha\zeta) + A_3\cos(\beta\zeta) + A_4\sin(\beta\zeta) + A_5\cos(\gamma\zeta) + A_6\sin(\gamma\zeta) \qquad \text{(K.2.15)}$$

Similarly

$$\Psi(\zeta) = B_1\cosh(\alpha\zeta) + B_2\sinh(\alpha\zeta) + B_3\cos(\beta\zeta) + B_4\sin(\beta\zeta) + B_5\cos(\gamma\zeta) + B_6\sin(\gamma\zeta) \qquad \text{(K.2.16)}$$

and the slope of the deflected structure is

$$\theta(\zeta) = \frac{1}{\ell}\frac{\partial H}{\partial \zeta} = \frac{1}{\ell}\left[\alpha A_1\sinh(\alpha\zeta) + \alpha A_2\cosh(\alpha\zeta) - \beta A_3\sin(\beta\zeta) + \beta A_4\cos(\beta\zeta) - \gamma A_5\sin(\gamma\zeta) + \gamma A_6\cos(\gamma\zeta)\right] \qquad \text{(K.2.17)}$$

Let

$$S_{h\alpha} = \sinh(\alpha\zeta), \quad C_{h\alpha} = \cosh(\alpha\zeta)$$
$$S_{\beta} = \sin(\beta\zeta), \quad C_{\beta} = \cos(\beta\zeta)$$
$$S_{\gamma} = \sin(\gamma\zeta), \quad C_{\gamma} = \cos(\gamma\zeta)$$

Substituting the derivatives of both H and Ψ in equation (K.2.7) and equating coefficients of cosh, sinh, cos and sin of α, β and γ to zero, the relations between $A_{1-\sigma}$ and $B_{1-\sigma}$ are found as follows :

$$B_1 = K_\alpha A_2 \quad , \quad B_2 = K_\alpha A_1$$
$$B_3 = K_\beta A_4 \quad , \quad B_4 = - K_\beta A_3$$
$$B_5 = K_\gamma A_6 \quad , \quad B_6 = - K_\gamma A_5$$

where

$$K_\alpha = \frac{\bar{a} - \alpha^4}{\bar{K}\ \alpha^3} \quad , \quad K_\beta = \frac{\bar{a} - \beta^4}{\bar{K}\ \beta^3} \quad , \quad K_\gamma = \frac{\bar{a} - \gamma^4}{\bar{K}\ \gamma^3}$$

Therefore, the expression for torsional rotation in equation (K.2.16) can be written as

$$\Psi(\xi) = K_\alpha A_1 S_{h\alpha} + K_\alpha A_2 C_{h\alpha} - K_\beta A_3 S_\beta + K_\beta A_4 C_\beta - K_\gamma A_5 S_\gamma + K_\beta A_6 C_\gamma \qquad (K.2.18)$$

Assuming the following boundary conditions :

$$H = H_1,\ \Theta = \Theta_1,\ \Psi = \Psi_1 \quad \text{at} \quad \xi = 0 \quad \text{or} \quad y = 0$$
$$H = H_2,\ \Theta = \Theta_2,\ \Psi = \Psi_2 \quad \text{at} \quad \xi = 1 \quad \text{or} \quad y = \ell$$

We have in matrix form

$$\begin{Bmatrix} H_1 \\ \Theta_1 \\ \Psi_1 \\ H_2 \\ \Theta_2 \\ \Psi_2 \end{Bmatrix} = \left[\begin{array}{cccccc} 1 & 0 & 1 & 0 & 1 & 0 \\ 0 & \frac{\alpha}{\ell} & 0 & \frac{\beta}{\ell} & 0 & \frac{\gamma}{\ell} \\ 0 & K_\alpha & 0 & K_\beta & 0 & K_\gamma \\ C_{h\alpha} & S_{h\alpha} & C_\beta & S_\beta & C_\gamma & S_\gamma \\ \frac{\alpha}{\ell} S_{h\alpha} & \frac{\alpha}{\ell} C_{h\alpha} & -\frac{\beta}{\ell} S_\beta & \frac{\beta}{\ell} C_\beta & -\frac{\gamma}{\ell} S_\gamma & \frac{\gamma}{\ell} C_\gamma \\ K_\alpha S_{h\alpha} & K_{h\alpha} C_{h\alpha} & - K_\beta S_\beta & K_\beta C_\beta & - K_\gamma S_\gamma & K_\gamma C_\gamma \end{array}\right] \begin{Bmatrix} A_1 \\ A_2 \\ A_3 \\ A_4 \\ A_5 \\ A_6 \end{Bmatrix}$$

or simply in matrix notation

$$\{U\} = [\underset{\sim}{B}]\{A\} \qquad (K.2.19)$$

Now the expressions for shear force, bending moment and torque are evaluated. On substituting the expressions for h and ψ in equation (K.2.3) we get the following expression for the shear force :

$$S = -EI\ h''' - K\ \psi''$$

$$= -K_{\alpha m}S_{h\alpha}A_1 - K_{\alpha m}C_{h\alpha}A_2 - K_{\beta m}S_{\beta}A_3 + K_{\beta m}C_{\beta}A_4 - K_{\gamma m}S_{\gamma}A_5 + K_{\gamma m}C_{\gamma}A_6 \qquad (K.2.20)$$

where

$$K_{\alpha m} = \left[EI\ \frac{\alpha^3}{\ell^3} + K\ K_{\alpha}\frac{\alpha^2}{\ell^2}\right] = \frac{\alpha}{\ell}K_{\alpha m}$$

$$K_{\beta m} = \left[EI\ \frac{\beta^3}{\ell^3} + K\ K_{\beta}\frac{\beta^2}{\ell^2}\right] = \frac{\beta}{\ell}K_{\beta m}$$

$$K_{\gamma m} = \left[EI\ \frac{\gamma^3}{\ell^3} + K\ K_{\gamma}\frac{\gamma^2}{\ell^2}\right] = \frac{\gamma}{\ell}K_{\gamma m}$$

The bending moment as given in equation (K.2.4) becomes :

$$M = EI\ h'' + K\ \psi'$$

$$= K_{\alpha m}C_{h\alpha}A_1 + K_{\alpha m}S_{h\alpha}A_2 - K_{\beta m}C_{\beta}A_3 - K_{\beta m}S_{\beta}A_4 - K_{\gamma m}C_{\gamma}A_5 - K_{\gamma m}S_{\gamma}A_6 \qquad (K.2.21)$$

where

$$K_{\alpha m} = \left[EI\ \frac{\alpha^2}{\ell^2} + K\ K_{\alpha}\frac{\alpha}{\ell}\right]$$

$$K_{\beta m} = \left[EI\ \frac{\beta^2}{\ell^2} + K\ K_{\beta}\frac{\beta}{\ell}\right]$$

$$K_{\gamma m} = \left[EI\ \frac{\gamma^2}{\ell^2} + K\ K_{\gamma}\frac{\gamma}{\ell}\right]$$

and finally the torque from equation (K.2.5) becomes :

$$T = GJ\ \psi' + K\ h''$$

$$= K_{\alpha t}C_{h\alpha}A_1 + K_{\alpha t}S_{h\alpha}A_2 - K_{\beta t}C_{\beta}A_3 - K_{\beta t}S_{\beta}A_4 - K_{\gamma t}C_{\gamma}A_5 - K_{\gamma t}S_{\gamma}A_6 \qquad (K.2.22)$$

where

$$K_{\alpha t} = \left[GJ\, K_{\alpha} \frac{\alpha}{\ell} + K \frac{\alpha^2}{\ell^2} \right]$$

$$K_{\beta t} = \left[GJ\, K_{\beta} \frac{\beta}{\ell} + K \frac{\beta^2}{\ell^2} \right]$$

$$K_{\gamma t} = \left[GJ\, K_{\gamma} \frac{\gamma}{\ell} + K \frac{\gamma^2}{\ell^2} \right]$$

Assuming the following boundary conditions,

$$S = -S_1,\ M_x = -M_{x1},\ M_z = -M_{z1} \quad \text{at} \quad \xi = 0 \quad \text{or} \quad y = 0$$

$$S = S_2,\ M_x = M_{x2},\ M_z = M_{z2} \quad \text{at} \quad \xi = 1 \quad \text{or} \quad y = \ell$$

Therefore, we have the shear force, bending moment and torque expressed in the matrix form as follows :

$$\begin{Bmatrix} S_1 \\ M_1 \\ T_1 \\ S_2 \\ M_2 \\ T_2 \end{Bmatrix} = \begin{bmatrix} 0 & -K_{\alpha m} & 0 & K_{\beta m} & 0 & K_{\gamma m} \\ K_{\alpha m} & 0 & -K_{\beta m} & 0 & -K_{\gamma m} & 0 \\ K_{\alpha t} & 0 & -K_{\beta t} & 0 & -K_{\gamma t} & 0 \\ -K_{\alpha m} S_{h\alpha} & -K_{\alpha m} C_{h\alpha} & -K_{\beta m} S_{\beta} & K_{\beta m} C_{\beta} & -K_{\gamma m} S_{\gamma} & K_{\gamma m} C_{\gamma} \\ K_{\alpha m} C_{h\alpha} & K_{\alpha m} S_{h\alpha} & -K_{\beta m} C_{\beta} & -K_{\beta m} S_{\beta} & -K_{\gamma m} C_{\gamma} & -K_{\gamma m} S_{\gamma} \\ K_{\alpha t} C_{h\alpha} & K_{\alpha t} S_{h\alpha} & -K_{\beta t} C_{\beta} & -K_{\beta t} S_{\beta} & -K_{\gamma t} C_{\gamma} & -K_{\gamma t} S_{\gamma} \end{bmatrix} \begin{Bmatrix} A_1 \\ A_2 \\ A_3 \\ A_4 \\ A_5 \\ A_6 \end{Bmatrix}$$

or simply

$$\{F\} = [\underset{\sim}{D}]\{A\} \qquad \text{(K.2.23)}$$

But $\{A\} = [\underset{\sim}{B}]^{-1}\{U\}$

therefore

$$\{F\} = [\underset{\sim}{D}][\underset{\sim}{B}]^{-1}\{U\}$$

$$= [\underset{\sim}{K}]\{U\}$$

where $[\underset{\sim}{K}] = [\underset{\sim}{D}][\underset{\sim}{B}]^{-1}$ = is the required dynamic stiffness matrix

APPENDIX : L

LUSAS : FINITE ELEMENT COMPUTER PROGRAM

LUSAS [1] is a general purpose engineering analysis system which incorporates facilities for linear and nonlinear static analysis, step by step dynamic analysis, eigenvalue extraction, linear buckling and steady and transient field (thermal) analysis. The system is based on the finite element displacement method of analysis and contains a comprehensive range of elements and solution procedures for the analysis of most types of engineering structure. The element library includes elements for the analysis of trusses, frames, grillages, membrane structures, plates, thick and thin shells, axisymmetric solids and general solids. Several types of element may be used to idealise different parts of a structure providing nodal freedoms match.

The system contains a wide range of both linear and nonlinear material types (constitutive models) which cover most engineering materials. The support node conditions may be either restrained completely or free. They can also be restrained with a prescribed displacement or restrained by means of a spring. The load types available are similarly wide ranging and include point loads, constant body forces, centrifugal forces, surface pressures, temperature and uniformly distributed loads.

The eigenvalue extraction solution procedure adopted is the subspace iteration method which incorporates the existing frontal solution algorithm. This allows large problems to be solved efficiently on an element-by-element basis without the need to reduce the problem size.

The standard eigen-problem may be expressed as

$$K \phi = \lambda \phi \qquad (L.1)$$

where K is the global stiffness matrix

λ is the vector of eigenvalues

ϕ is the vector of corresponding eigenvectors

In vibration analysis the standard eigen-problem may be expressed as

$$K \phi = \lambda M \phi \qquad (L.2)$$

where M is the global mass matrix

λ are the vibration frequencies (rad/sec) squared, ω^2

ϕ is the eigenvector

The mass matrices for each element are consistent mass matrices although lumped masses may be input as an option. In general the element mass matrices are formed as

$$M = \int_v N^T \rho N \, dv \qquad (L.3)$$

where ρ is the density

N is the element shape function

To evaluate the accuracy of the solution, error norms on each eigenvalue are output. The Sturm sequence check is also available to ensure that the lowest n eigenvalues have been found.

In order to compute the natural frequencies of the structure, the following formula should be applied to the eigenvalues output from LUSAS.

$$f \text{ (Hz)} = \frac{\sqrt{\omega^2}}{2\pi} \qquad (L.4)$$

where $\omega^2 = \lambda$ (output eigenvalues).

REFERENCE

1. LUSAS, Finite Element Analysis Ltd., 25 Holborn Viaduct, London EC1A 2BP, U.K.